DISSERTATION

HYDRAULIC EFFECTS OF BIOFILMS ON THE DESIGN AND OPERATION OF WASTEWATER FORCEMAINS

Submitted by

Christopher T. Michalos

Department of Civil and Environmental Engineering

In partial fulfillment of the requirements

For the Degree of Doctor of Philosophy

Colorado State University

Fort Collins, Colorado

Fall 2016

Doctoral Committee:

Advisor: Christopher I. Thornton

Neil S. Grigg
Pierre Y. Julien
John D. Williams

ABSTRACT

HYDRAULIC EFFECTS OF BIOFILMS ON THE DESIGN AND OPERATION OF WASTEWATER FORCEMAINS

The impact of biofouling on wastewater forcemains is generally not accounted for in current design practice and little information is available in literature regarding the effect of wastewater biofilms on forcemain hydraulics. In practice, many engineers select a clean water, new pipe roughness factor, to perform hydraulic calculations which may lead to under-sizing wastewater lift station pumps. Forcemains have to cope with a particularly challenging task; they have to ensure that solids contained in the wastewater (sand, gravel, organics) are readily transported along with the wastewater. Forcemain design standards generally recommend a velocity of 2.0 ft/s (0.6 m/s) to prevent deposition of solids and a velocity of 3.5 ft/s (1.1 m/s) to re-suspend solids that may have settled. To further complicate forcemain design and operation; wastewater lift station pumps generally operate intermittently which requires remobilization of any material that may have settled while the pumps remain idle. Therefore, forcemains must be designed to be self-cleaning in order to prevent solids deposition which could cause increased sulfide production leading to corrosion and odor issues; loss of capacity through a reduction of cross sectional area; or even blockage at low points, or at the toe of an adversely sloped pipe leading to costly removal.

The goal of this research is to identify short-comings in current forcemain design practice by 1) evaluating the hydraulic effect of biofilms on the absolute roughness (k_s) of forcemains; 2) evaluating the hydraulic effect of biofilms on Hazen-Williams C factor; and 3) determine critical velocity required for sediment transport, air clearing, self-cleansing, and optimal diameter of forcemains, which are not identified in forcemain design standards.

Operational data were collected and evaluated for 20 municipal wastewater forcemains located in the United States. Data from previous studies, academic research, reports, and published papers were used to supplement and support research findings. A total of 415 data points obtained from 68 forcemain systems ranging from 3- to 66 inches in diameter were evaluated as part of this research. Results of the hydraulic

analysis determined that 44% of the systems evaluated were operating at velocities between 2- and 3.5 ft/s and 16% of systems were operating at velocities less than 2 ft/s; indicating that these systems are over designed and do not provide sufficient velocity to re-suspend solids promoting sedimentation.

The hydraulic effect of biofilms on forcemain flow resistance was evaluated and determined that k_s and C factor varied with forcemain velocity. Calculated values of k_s ranged from approximately 35 mm to 0.01 mm, with larger values occurring at velocities less than 1 m/s (3.3 ft/s). The upper range of k_s values are orders of magnitude larger than the standard clean water, new pipe k_s value found in literature. C factor results ranged from approximately 30 to 150; approximately 60% of forcemain systems evaluated are operating at C factors less than 100, which is much lower than the recommended values of 130 – 150, depending on pipe material. Results suggest that biofilms effect forcemains in a similar manner regardless of pipe diameter, material, or age. Although velocity was determined to be the principle factor affecting k_s and C factor; a comparison of the C factor results to k_s results show that C factor is dependent upon both velocity and diameter. Equations were developed to estimate k_s and C factor and should be utilized along with the Colebrook-White / Darcy-Weisbach and Hazen-Williams equations to estimate the friction headloss for forcemains.

The required design velocity for self-cleansing, sediment transport, air clearing, and economical diameter ranges from approximately 4- to 11 ft/s, depending on diameter. Selecting a design velocity between 2 ft/s (0.6 m/s) and 3.5 ft/s (1.1 m/s) may not be appropriate and the minimum design velocity should be selected upon either the self-cleansing velocity or economical pipe sizing. Although each system should be evaluated to determine the correct minimum design velocity based upon the proposed system properties, these results indicate that the minimum forcemain design velocity should be at least 5 ft/s (1.5 m/s).

TABLE OF CONTENTS

LIST OF TABLES

LIST OF FIGURES

LIST OF SYMBOLS

A	=	area (ft^2, m^2)
c_f	=	local drag coefficient
C	=	Hazen-Williams coefficient
C	=	Hazen-Williams (adjusted coefficient)
C_D	=	particle drag coefficient
C_f	=	friction coefficient
C_o	=	initial or reference factor
C_u	=	constant (US Customary Units, SI Units)
d	=	diameter (ft, m)
d_s	=	particle diameter (in., mm)
dS	=	sulfide concentration
$d[S]/dt$	=	sulfide production rate
dt	=	detention time
D	=	diameter, inside diameter (ft, m)
e/D or ε/d	=	relative roughness
f	=	friction factor
g	=	acceleration due to gravity (ft/s^2, m/s^2)
G	=	particle specific gravity
h_f	=	head loss due to friction (ft, m)
h_l	=	head loss (ft, m)
k	=	von Kármán constant
k_s	=	absolute roughness height of the pipe wall applied with consistent units as the pipe diameter
k_s/D	=	ratio of the sand grain size to the pipe diameter
k_t	=	absolute roughness after t years
K_u	=	unit coefficient (US Customary Units, SI Units)
L	=	length, pipe length (ft, m)
P	=	pressure
P/γ	=	pressure head (ft, m)
Q	=	discharge (cfs, m^3/s)
R	=	hydraulic radius (ft, m)
R_e	=	Reynolds number
R_{ep}	=	particle Reynolds number
S	=	friction slope (ft/ft, m/m)
t	=	time (years)
T	=	temperature (°C, °F)
u_s	=	structure uniformity factor
U	=	average velocity in the pipe (ft/s, m/s)
U_*	=	friction velocity, also known as the shear velocity (ft/s, m/s)
U^*_{sus}	=	suspension shear velocity (ft/s, m/s)
v	=	velocity (ft/s, m/s)

v_o	=	initial velocity (ft/s, m/s)
V	=	velocity (ft/s, m/s)
$V^2/2g$	=	velocity head (ft, m)
Z	=	elevation head (ft, m)
α	=	growth factor (mm/year)
α	=	forcemain angle from horizontal
δ	=	viscous sublayer thickness (ft, m)
γ	=	unit weight of the fluid
Δh_l	=	change in head loss
μ	=	dynamic viscosity (lbf-s/ft^2, N-s/m^2)
ν	=	kinematic viscosity (ft^2/s, m^2/s)
ρ	=	fluid density (slugs/ft^3, kg/m^3)
τ_o	=	shear stress (lb/ft^2, kg/m-s^2)
τ_c	=	critical shear stress (lb/ft^2, kg/m-s^2)
τ^*	=	shields parameter
τ_c^*	=	critical shields parameter
τ_{co}^*	=	critical shields number
τ_{sus}^*	=	dimensionless shear stress for particle suspension
τ_c	=	critical shear stress (lb/ft^2, kg/m-s^2)
τ_c	=	critical shear stress (lb/ft^2, kg/m-s^2)
ϕ	=	particle angle of repose
μ_c	=	tan ϕ
ω_o	=	fall velocity of particle

LIST OF ACRONYMS

ASCE	American Society of Civil Engineers
Avg	average
AC	asbestos cement pipe
AWWA	American Water Works Association
AWWARF	American Water Works Association Research Foundation
BOD	biochemical oxygen demand
BOD_5	five day biochemical oxygen demand
CI, CIP	cast iron pipe
CCP	concrete cylinder pipe
COD	chemical oxygen demand
D-W	Darcy-Weisbach
DI, DIP	Ductile Iron Pipe
DIPRA	Ductile Iron Pipe Research Association
DO	dissolved oxygen
DOC	dissolved organic carbon
EPA	U.S. Environmental Protection Agency
FOGs	fats, oils, and grease
HRT	hydraulic retention time
HGL	hydraulic grade line
HDPE	high-density polyethylene
H_2S	hydrogen sulfide
ID	inside diameter
LCC	life cycle cost
LSI	Langelier Saturation Index
MOP	manual of practice
Max	maximum
Min	minimum
N	Nitrogen
P	Phosphorus
PCCP	pre-stressed concrete cylinder pipe
PE	polyethylene
PVC	polyvinyl chloride
RCP	reinforced concrete pipe
SCADA	Supervisory Control and Data Acquisition
SI	International System of Units
SS	suspended solids
TEB	total error band
TOC	total organic carbon
TDS	total dissolved solids
TS	total solids
U.K.	United Kingdom
uPVC	Unplasticized Polyvinyl Chloride

US	United States
VFD	variable frequency drive
WEF	Water Environment Federation
WERF	Water Environment Research Foundation

1 Introduction

The determination of energy losses caused by pipe friction is important for analysis and design of pipeline systems. An accurate estimate of friction loss is critical to pipeline sizing and can have a significant impact on hydraulic calculations and pump selection. Increased hydraulic roughness reduces hydraulic capacity and increases operation and maintenance costs. Pipe friction is a complex phenomenon and questionable friction calculations are surprisingly common. Pipeline flow resistance is influenced by flow velocity, interior diameter, surface roughness of pipe and/or lining materials, water temperature, and service water.

Chemical or biological processes within the service water also influences friction loss. Biologically active water such as raw water, recycled water, and wastewater will form biofilms that attach to the pipe wall and can dramatically increase head loss. Biofilms and Biofouling can occur due to any combination of bacteria, algae, fungi, and invertebrate organisms in raw water; bacteria and biological nutrients in recycled water; and bacteria, biological nutrients, sediments, and grease in wastewater. Biofouling effects hydraulic performance reducing capacity and is generally not included in current design practice.

Proper selection of roughness factors are required to ensure a pipeline systems ability to convey the design flow. Although both water and wastewater pipelines are subjected to biofilms and biofouling, the hydraulic effect of biofilms on the design and operation of wastewater forcemains are the primary focus of this research. In addition, forcemains are required to transport grit and are subjected to grease and gas accumulation which could also affect the design and operation of forcemains.

In-service operational data were collected and evaluated for 20 municipal wastewater forcemains located in the United States to determine the hydraulic effect of biofilms on forcemains. Data from previous studies, academic research, reports, and published papers were used to supplement and support research findings. The presented research improves current knowledge of wastewater forcemain flow resistance and results will provide engineers with a design guide for selecting and applying hydraulic roughness factors to optimize the design of lift station/forcemain systems.

1.1 Research Objectives

The goal of this research is to identify short-comings in current forcemain design practice through expanded evaluation of the findings by HR Wallingford identified in Report *SR 641 - Flow resistance of wastewater pumping mains: improved design through better data* in order to improve hydraulic design methodologies of forcemains. Key objectives to achieve this goal are as follows:

- Evaluate the hydraulic effect of biofilms on absolute roughness (k_s);
- Evaluate the hydraulic effect of biofilms on Hazen-Williams C factor; and
- Estimate critical velocity required for sediment transport, air clearing, self-cleansing and optimal diameters of forcemains, which are not identified in forcemain design standards.

1.2 Dissertation Organization

The work presented in this dissertation is organized into nine chapters. Brief descriptions of the contents of each chapter are provided below.

- Chapter 2: Literature Review provides a brief overview of the principles of pipeline design, theory of roughness, roughness coefficients, modern pipe materials, types of service water affected by biofilms, and problems associated with biofouling of pipelines.
- Chapter 3: Data Collection and Analysis Methodology describes the types of data required for the research, sources of data, assumptions, and methodology utilized for analysis of the data.
- Chapter 4: Wastewater Lift Station / Forcemain Systems describes typical forcemain systems within the United States, composition of wastewater, and provides a description of the data collected for the research.
- Chapter 5: Hydraulic Analysis and Results presents the results of hydraulic calculations. Calculated results for absolute roughens and C factor were screened against pipe diameter, material, pipe age, and shear stress to determine the hydraulic effect of biofilms on forcemains. An uncertainty analysis was conducted to evaluate the effect of changes in temperature, pipe length, internal diameter, flowrate, and headloss on the results of the hydraulic calculations to

determine the validity of the calculations given that data was not field collected and the analysis relied on operational data collected from a utility's SCADA system.

- Chapter 6: Lift Station and Forcemain Operation and Maintenance reviews operational issues associated with forcemains including grit/sediment transport, air clearing, and sulfide generation. Pumping cycles of the lift station/forcemain systems collected as part of this research were evaluated to determine if the frequency and duration of pumping influenced the results of the hydraulic calculations. In addition, the calculated performance of the pumps were compared to the design duty point to determine if the increased headloss as a results of biofilms affect the annual operational costs of the pumps.
- Chapter 7: Prediction of Roughness Factors defines the methodology used to develop equations to predict absolute roughens and C factor given the forcemain velocity.
- Chapter 8: Implementation of Results utilizes the predictive equations developed in Chapter 7 to evaluate optimal pipeline sizing and to define design velocities required for grit/sediment transport and air clearing in forcemains considering adverse pipe deflections which occur as the forcemain undulates to follow the topography along the pipeline alignment.
- Chapter 9: Conclusions and Recommendations provides a summary of the results, forcemain design recommendations, research limitations, and recommendations for further work.

2 Literature Review

2.1 Pipeline Design

Factors that should be considered during pipeline design include discharge (proposed and future); head loss; operating and surge pressures; and dynamic forces and stresses acting on the pipe material. The head loss for a given discharge relates to flow efficiency. Pipeline design should balance the economics of pipeline construction, operation and maintenance costs, as well as, satisfy future design flows. The service life could be greater than 50 years for municipal pipelines in which the selected diameter may be initially oversized to allow for some growth in flow with time. The optimum pipe size will yield the least present worth of capital and operation costs for the desired discharge as shown in Figure 2.1.

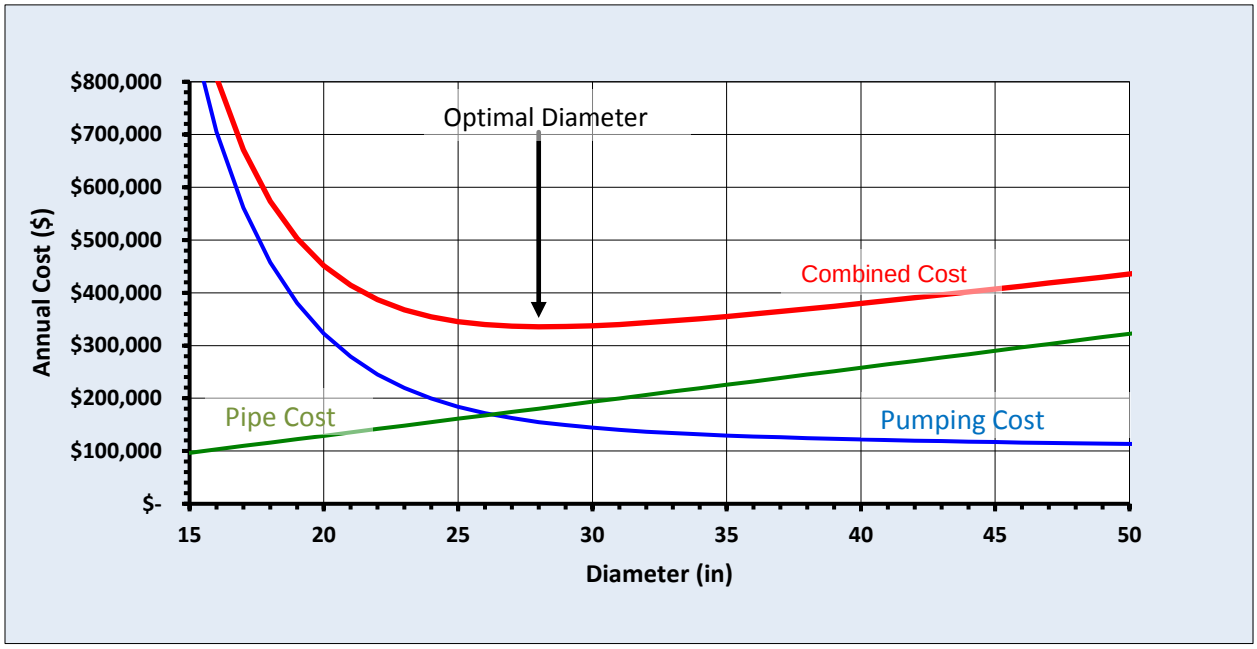

Figure 2.1: Selection of Optimum Pipe Diameter

Therefore, accurate calculations of head loss taking into account how service water impacts performance is important for both new pipe as well as the future pipe conditions. However, the calculation of friction loss can only produce accurate results if the correct roughness factor is applied for hydraulic calculations. Selection of conservative roughness values may be warranted, but when conservatism is

added on top of conservatism, the selected pipe diameter would likely be oversized which could lead to deposition of solids, water-quality issues, and excessive capital cost.

2.2 Flow in Closed Conduits

A brief historical review of major contributions in the development of pipe flow theories, along with current design practice and the corresponding application limitations, are summarized in this section. Table 2.1 identifies the chronological development of pipe flow theories.

Table 2.1: Chronological Development of Pipe Flow Theories

Date	Name	Contribution
1839 – 1841	Hagen and Poiseuille	Laminar flow equation
1850	Darcy and Weisbach	Turbulent flow equation
1884	Reynolds	Distinction between laminar and turbulent flow and Reynolds number
1913	Blasius	Friction factor equation for smooth pipe
1914	Stanton and Pannell	Experimental values of friction factor for smooth pipes
1930	Nikuradse	Experimental values of friction factor for artificially roughened pipes
1930s	Prandtl and von Kármán	Equation for rough and smooth friction factors
1937 – 1939	Colebrook and White	Experimental values of the friction factor for commercial pipes and the transition formula
1944	Moody	The Moody diagram for commercial pipes
1958	Ackers	The hydraulic research station charts and tables for the design of pipes and channels
1972 – 1975	Barr	Direct solution of the Colebrook-White equation
1976	Swamee and Jain	Direct solution of the Colebrook-White equation

The development of pipe flow theory generally includes three major concepts, including 1) the distinction between laminar and turbulent flow; 2) the distinction between rough and smooth pipes; and 3) the distinction between artificially roughened pipes and commercial pipes.

The Colebrook-White equation transition formula represents the culmination of all the previous work, and can be applied to any fluid in any pipe operating under turbulent flow conditions. The later contributions of Moody (1944), Ackers (1958), Barr (1972), and Swamee and Jain (1976) are mainly concerned with the practical application of the Colebrook-White equation (Chadwick et al. 2004). In addition, many other researchers have provided explicit equations to approximate the Colebrook-White equation; these efforts will be discussed in more detail in the following section.

Reynolds' experiments demonstrated that there were two kinds of flow, laminar and turbulent. He found that transition from laminar to turbulent flow occurred at a critical velocity for a given pipe and fluid (Chadwick et al. 2004). Expressing his results as a dimensionless parameter (R_e), Reynolds found that laminar flow always occurred when $R_e \leq 2{,}000$ and that turbulent flow always occurred for $R_e \geq 4{,}000$. For R_e between 2,000 and 4,000, he found that the flow could be either laminar or turbulent and termed this the transition region. Although the exact values taken to limit the range of R_e vary with author and application, they are often accepted as identified above. The Reynolds Number (R_e) is calculated by Equation 2.1.

$$R_e = \frac{\rho V D}{\mu} = \frac{VD}{\nu} \tag{2.1}$$

where ρ = fluid density (slugs/ft^3, kg/m^3); V = velocity (ft/s, m/s); D = diameter (ft, m); μ = dynamic viscosity (lb$_f$-s/ft^2, N-s/m^2); and ν = kinematic viscosity (ft^2/s, m^2/s). Considering that turbulent flow occurs at $R_e \geq 4{,}000$, the corresponding velocity and discharge were determined for standard diameters ranging from 0.25- to 96 in. at $R_e = 4{,}000$ and are presented in Table 2.2.

Table 2.2: Velocity and Discharge at $R_e = 4{,}000$

Nominal Diameter (in.)	Velocity (ft/s)	Discharge (cfs)
0.25	2.337	0.001
0.5	1.168	0.002
1	0.584	0.003
2	0.292	0.006
4	0.146	0.013
6	0.097	0.019
8	0.073	0.025
10	0.058	0.032
12	0.049	0.038
16	0.037	0.051
20	0.029	0.064
24	0.024	0.076
30	0.019	0.096
36	0.016	0.115
48	0.012	0.153
60	0.010	0.191
72	0.008	0.229
84	0.007	0.268
96	0.006	0.306

Most municipal pipelines are ≥ 6 inches in diameter and designed with a minimum velocity of 2 ft/s (0.6 m/s) to prevent sedimentation and minimum velocity of 2 to 3 ft/s (0.6 to 0.9 m/s) to remove air. As presented in Table 2.2, laminar flow is generally not experienced in pipeline operation and the vast majority of flows in closed-conduit systems are turbulent; therefore, the focus of this research will be in the turbulent flow regime. Municipal pipelines are generally designed with a maximum velocity of 10 to 12 ft/s (3.1 to 3.7 m/s) to minimize the potential of lining erosion and to minimize energy input in order to optimize pipe size. Therefore, it is desirable to determine the discharge and R_e for velocities equal to 12 ft/s (3.7 m/s) in order to define the maximum flow characteristics of municipal pipelines. As presented in Table 2.3, R_e ranges from $2x10^4$ to $3x10^6$ for 0.25- to 96 in. diameter pipelines.

Table 2.3: Discharge and R_e for Velocity = 12 ft/s at T = 60 °F

Nominal Diameter (in.)	Discharge (cfs)	R_e
0.25	0.004	2.1E+04
0.5	0.016	4.1E+04
1	0.065	8.2E+04
2	0.262	1.6E+05
4	1.047	3.3E+05
6	2.356	4.9E+05
8	4.189	6.6E+05
10	6.545	8.2E+05
12	9.425	9.9E+05
16	16.755	1.3E+06
20	26.180	1.6E+06
24	37.699	2.0E+06
30	58.905	2.5E+06
36	84.823	3.0E+06
48	150.8	3.9E+06
60	235.6	4.9E+06
72	339.3	5.9E+06
84	461.8	6.9E+06
96	603.2	7.9E+06

2.3 Darcy-Weisbach Equation

Darcy and Weisbach developed an equation to describe the friction head loss (h_f), or loss of energy resulting from flow in closed conduits in a wide variety of applications. The Darcy-Weisbach equation, shown as Equation 2.2, has the advantage of incorporating a dimensionless friction factor that describes the

effects of material roughness along the interior surface of the pipe wall and flow regime on retarding the flow.

$$h_f = f\frac{L}{D}\frac{V^2}{2g} \tag{2.2}$$

where h_f = head loss due to friction (ft, m); f = a dimensionless friction factor; L = length (ft, m); D = inside diameter (ft, m); V = velocity (ft/s, m/s); and g = acceleration due to gravity (ft/s^2, m/s^2). As seen from the Darcy-Weisbach equation, the head loss is directly proportional to the length of the pipeline and friction factor. Therefore, the longer the fluid must travel and the rougher the conduit, the greater the energy loss. The equation also relates the diameter inversely to the head loss. In addition, as the pipe diameter increases, the effects of shear stress on the pipe wall are reduced.

Nikuradse made a major contribution to the theory of pipe flow by objectively differentiating between smooth and rough turbulence in pipes. He carried out a series of painstaking experiments where smooth pipe walls were artificially roughened by sticking uniform sand grains onto the pipe wall measuring the friction factor and velocity distributions at various Reynolds numbers and determined that the friction factor varied based upon the relative roughness of the pipe, which is the ratio of the sand grain size to the pipe diameter (k_s/D). By using different diameter pipe and sand grains of different sizes, he produced a set of experimental results of f and R_e for a range of relative roughness of 1/30 to 1/1014. He plotted the results as log f vs. log R_e for each value of k_s/D, as shown in Figure 2.2, which shows that there are five regions of flow.

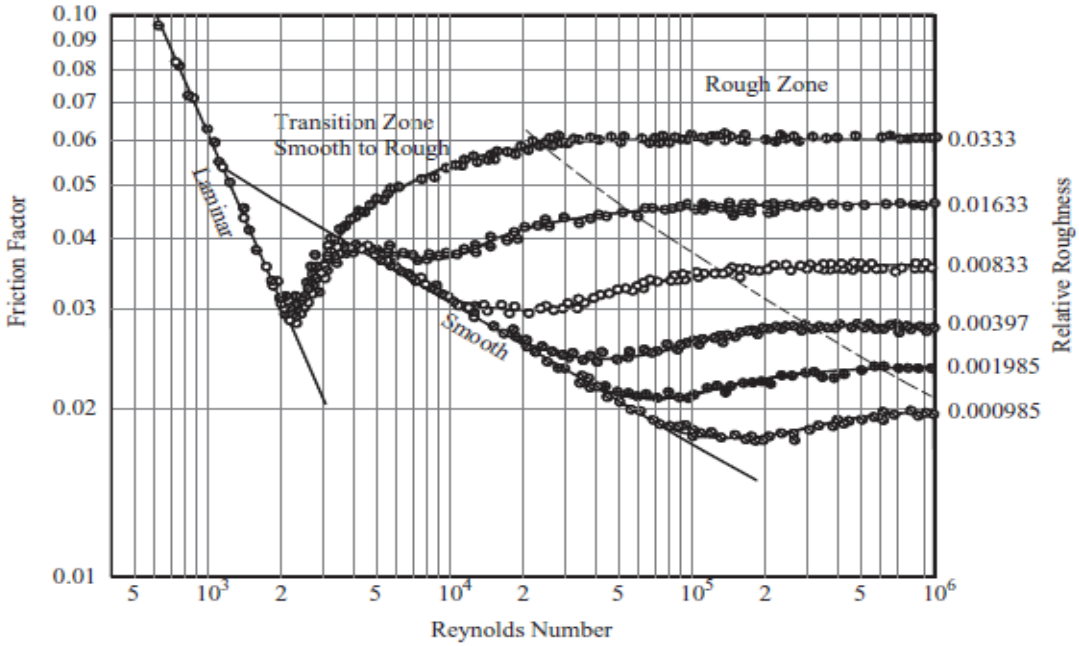

Figure 2.2: Nikuradse Experimental Data Plotted as f vs. R_e (Rennels and Hudson 2012)

Based upon Nikuradse's experiments, Prandtl and von Kármán established the following empirical formulas for estimating the friction factor in turbulent pipe flows:

Smooth Pipe ($k/d \approx 0$):

$$\frac{1}{\sqrt{f}} = -2\log\left(\frac{2.51}{R_e\sqrt{f}}\right) \tag{2.3}$$

Rough Pipe ($k/d \gg 0$):

$$\frac{1}{\sqrt{f}} = -2\log\left(\frac{k/_D}{R_e\sqrt{f}}\right) \tag{2.4}$$

Although Prandtl and von Kármán provided the framework for a pipe friction theory, the results were not directly useful to engineers since they applied to artificially roughened pipes. The roughness of commercial pipes are both uneven in size and spacing and, therefore, do not necessarily correspond to the results of the Nikuradse's experiments.

Colebrook and White made two major contributions to the development and application of pipe friction theory. First, they conducted experiments to determine the effect of non-uniform roughness found

on commercial pipe. As a result of these experiments, they discovered that the *f* vs. R_e curves exhibited a gradual change from smooth to rough turbulence in the turbulent transition region in contrast to Nikuradse's results. In which, they were able to determine an effective roughness size for commercial pipes and publish a list of k_s values applicable to commercial pipe. Their second major contribution included combining the Prandtl and von Kármán smooth and rough laws (Equations 2.3 and 2.4, respectively) into the Colebrook-White equation, which gave predicted results very close to the observed transitional behavior of commercial pipes and is applicable to the entire turbulent region for commercial pipe using an effective roughness value determined experimentally for each pipe material type. The Colebrook-White equation is generally the accepted design formula for turbulent friction. Both logarithmic forms of the Colebrook-White equation are presented as Equations 2.5a and 2.5b.

$$\frac{1}{\sqrt{f}} = -2\log\left(\frac{k_s}{3.7D} + \frac{2.51}{R_e\sqrt{f}}\right) \tag{2.5a}$$

$$\frac{1}{\sqrt{f}} = -0.88\ln\left(\frac{k_s}{3.7D} + \frac{2.51}{R_e\sqrt{f}}\right) \tag{2.5b}$$

where k_s = the absolute roughness height of the pipe wall applied with consistent units as the pipe diameter. At first, the Colebrook-White equation was not widely used by engineers because it is an implicit equation that requires a trial-and-error solution. Since the Colebrook-White equation is implicit and difficult to solve by hand, Moody developed a chart plotting the results of the Colebrook-White equation. This chart, known as the Moody diagram (Figure 2.3), is probably the most famous and useful figure in fluid mechanics. It provides the ability to determine the friction factor based upon the relative roughness and Reynolds number and can be used for circular and noncircular pipe flows as well as open channel flows and has a reported accuracy of ±15% for design calculations (White 1998). The Moody Diagram, shown as Figure 2.3, graphically shows the laminar, transition zone, smooth pipe flow, and rough and smooth turbulent flow regimes. As shown in Figure 2.3, as R_e decreases, *f* approaches the smooth line curve. This can be explained by the presence of the laminar sub layer along the pipe wall that decreases in thickness as the R_e increases.

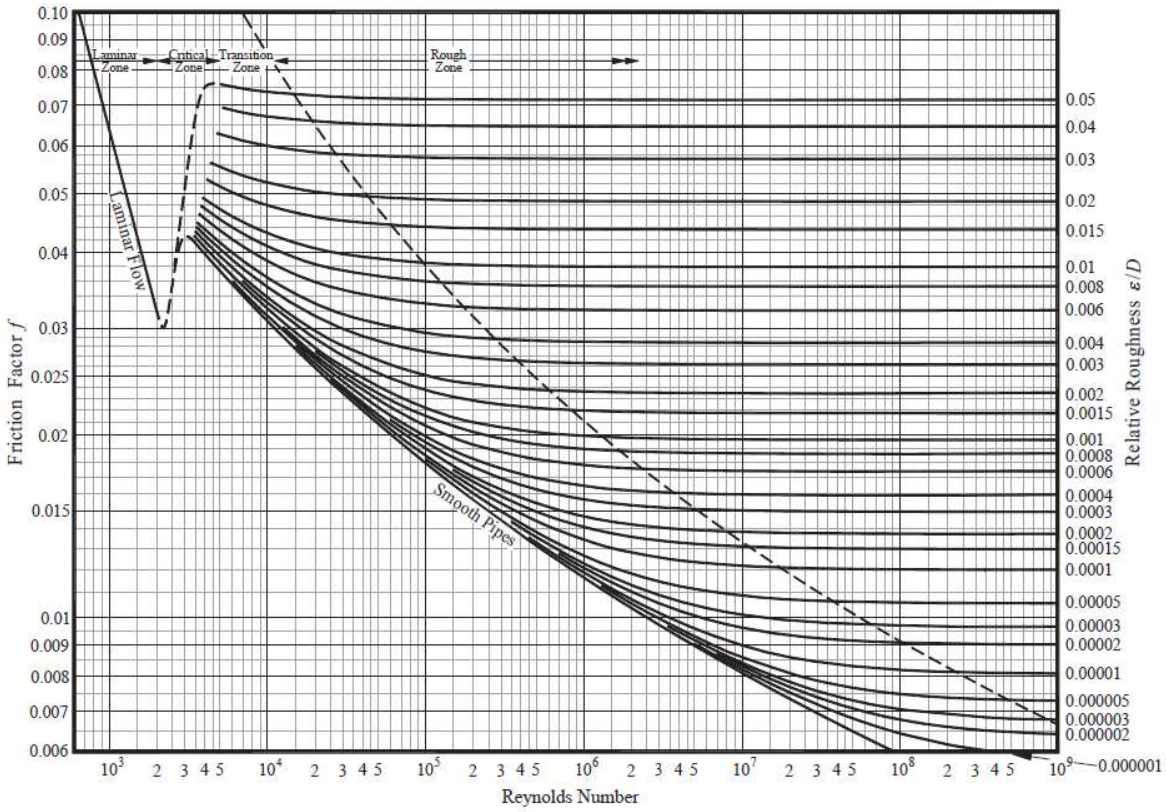

Figure 2.3: Moody Diagram (Rennels and Hudson 2012)

Ackers (1958) presented discharge (Q), diameter (D), and friction head loss (h_f) in a series of charts for various k_s values, providing engineers a simple methodology for applying the Colebrook-White equation. As previously noted, k_s is the absolute roughness for commercial pipe. Typical values for k_s are presented in Table 2.4. Numerous values, or ranges of k_s values, are provided in the published literature, this variability can lead to calculation errors. It should be noted that the relative roughness, k_s/D, or sometimes referred to as ε/d or e/D, is dimensionless; it is also important to note that the application of the absolute roughness values and the inside diameter are in the same units when applying to friction factor equations, such as the Colebrook-White equation.

Table 2.4: Typical Absolute Roughness Values, k_s New Pipe (Rennels and Hudson (2012))

	US Customary Units		SI Units
Pipe or Lining Material	e (in.)	ε (ft)	e or ε (mm) (m x 10^3)
Asbestos cement	0.000096	0.000008	0.0024
Carbon steel, commercial	0.0018	0.00015	0.045
Concrete, smoothed	0.012	0.0010	0.30
Concrete, ordinary	0.040	0.0033	1.0
Concrete, coarse	0.12	0.010	3.0
Glass tube	0.000060	0.0000050	0.0015
Iron, cast, uncoated	0.0102	0.00085	0.26
Iron, cast, asphalted	0.0048	0.00040	0.12
Iron, cast, cement-lined	0.000096	0.000008	0.0024
Iron, cast, bituminous-lined	0.000096	0.000008	0.0024
Iron, cast, centrifugally-spun	0.00012	0.000010	0.030
Iron, galvanized	0.0060	0.00050	0.15
Iron, wrought	0.0022	0.00018	0.060
Fiberglass	0.00020	0.000010	0.005
PVC and plastic	0.000060 – 0.00024	0.0000005 – 0.000020	0.0015 – 0.0060
Stainless steel, commercial	0.0018	0.00015	0.045
Steel, riveted	0.036 – 0.36	0.0030 – 0.030	0.90 – 9.0
Tubing, drawn (aluminum, brass, copper, lead, etc.)	0.000060	0.0000050	0.0015
Wood stave	0.0072 – 0.036	0.00060 – 0.0030	0.18 – 0.90

It is widely accepted that the Darcy-Weisbach equation, with the Colebrook-White equation for calculating the friction coefficient, is a highly accurate pipe-water flow equation (Liou 1998, Christensen 2000). The Colebrook-White equation has become the accepted standard for testing single-phase friction factor correlations in turbulent regimes (Fang et al. 2011). However, application of the Colebrook-White equation can be cumbersome to use. Because of this, numerous authors such as Barr (1972, 1981) and Swamee and Jain (1976) have tried to establish explicit approximations of the Colebrook-White equation. These explicit equations are generally accurate to within ±2% of Colebrook-White, which is considered acceptable for practical engineering applications.

The more common explicit approximations of the Colebrook-White equation, along with their identified limitations and reported accuracies, are provided in Appendix A. Assuming that the Colebrook-White equation provides the most accurate estimate of the friction factor, each explicit equation was compared against the Colebrook-White equation to determine relative accuracy given the following constraints that cover the general operational ranges found in municipal pipelines:

- velocity less than 18 ft/s (5.5 m/s);
- $R_e \geq 4{,}000$ (turbulent flow);
- water at 60°F ($\nu = 1.22 \times 10^{-5}$ ft^2/s), 15.6°C ($\nu = 1.11 \times 10^{-6}$ m^2/s);
- inside diameter of 6, 12, 24, 36, and 60 in (152.4, 304.8, 609.6, 914.4, and 1524 mm); and
- k_s/D of 0.0001, 0.001, and 0.015 (representing very smooth pipe, smooth pipe, and rough pipe).

Although municipal pipelines are generally designed with a maximum velocity of 12 ft/s (3.7 m/s) to minimize potential erosion of cement mortar linings and to minimize energy input to optimize pipe size, the comparison of explicit friction factor equations were evaluated for R_e values corresponding to velocity < 18 ft/s (5.5 m/s) to determine relative error at higher velocities.

In addition, the analysis was focused within this range because expected data received for this research will be within this range. The results of this analysis are presented in Table 2.5 and show that other than the equations developed by Round (1980), Moody (1947), and Wood (1966), the explicit equations provide an average accuracy within 1% of the Colebrook-White equation. Table 2.5 also ranks each equation based upon the calculated accuracy relative to the Colebrook-White equation.

Additional analysis was performed to further identify potential limitations in applying the explicit approximations to the Colebrook-White equation to identify relative accuracies across multiple flow rates and diameters. This analysis was performed using all explicit equations based upon the following assumptions:

- velocity less than 18 ft/s (5.5 m/s);
- minimum $R_e = 4{,}000$ (turbulent flow);
- water at 60°F ($\nu = 1.22 \times 10^{-5}$ ft^2/s), 15.6°C ($\nu = 1.11 \times 10^{-6}$ m^2/s);
- inside diameters of 6, 12, 24, 36, and 60 in.; and
- k_s of 0.0018 in. (0.045 mm) representing carbon steel pipe.

Results are provided in Figures B.1 to B.5 (Appendix B) for fairly smooth pipe. For clarity, results from less accurate equations were not presented in the figures.

Table 2.5: Summary of Explicit Equations to Approximate the Colebrook-White Equation

Rank	Author	Δf % (Compared to Colebrook-White)									Notes
		k_s/D = 0.0001			k_s/D = 0.001			k_s/D = 0.015			
		Min	Max	Avg	Min	Max	Avg	Min	Max	Avg	
1	Zigrang and Sylvester (1982)	-0.10	0.06	-0.03	-0.03	0.06	0.00	0.00	0.03	0.01	Very accurate, long equation, easy to apply
2	Romeo et al. (2002)	0.00	0.16	0.04	-0.03	0.15	-0.01	-0.06	0.05	-0.05	Very accurate, long equation, difficult to apply
3	Barr (1981)	-0.38	0.04	-0.01	-0.51	0.05	-0.03	-0.10	0.12	-0.05	Very accurate, easy to apply
4	Sonnad and Goudar (2006)	0.11	1.01	0.23	0.01	0.98	0.08	0.01	0.61	0.02	Very accurate, long equation, difficult to apply
5	Haaland (1983)	-1.37	1.21	-0.98	-1.25	0.77	-0.19	0.04	0.44	0.20	Very accurate, easy to apply, tends to under-predict f
6	Chen (1979)	0.64	4.64	1.34	0.03	4.22	0.29	-0.05	1.15	-0.03	Accurate, difficult to apply, over-predicts f, accuracy increases for R_e > 100,000 and larger k_s/D values, should not be applied to small k_s/D and low R_e
7	Jain (1976)	-0.48	1.54	0.23	0.25	1.81	0.45	-0.06	3.15	0.09	Accurate, easy to apply
8	Churchill (1977)	-0.33	1.76	0.32	0.31	2.02	0.52	0.03	3.11	0.18	Accurate, difficult to apply
9	Swamee and Jain (1976)	-0.39	1.67	0.31	0.35	1.94	0.55	0.08	3.31	0.24	Accurate, easy to apply, slightly conservative when $V \geq 3$ ft/s
10	Churchill (1973)	-0.31	1.80	0.35	0.35	2.07	0.56	0.09	3.38	0.24	Accurate, easy to apply
11	Manadilli (1997)	0.06	0.69	0.59	0.37	1.09	0.63	0.09	2.46	0.24	Accurate, easy to apply
12	Ghanbari et al. (2011)	0.53	1.04	0.96	0.49	1.09	0.89	-0.59	0.33	-0.51	Accurate, easy to apply
13	Round (1980)	-1.84	4.99	2.64	-0.79	4.61	3.83	-2.73	-2.25	-2.63	Inaccurate, easy to apply
14	Wood (1966)	-0.26	6.26	4.21	-0.77	5.39	4.93	-3.90	1.83	1.68	Inaccurate, easy to apply
15	Moody (1947)	-11.29	-8.45	-9.76	-8.76	-5.65	-6.13	-11.29	-11.94	-11.98	Inaccurate, easy to apply

As presented in Figures B.1 to B.5, most empirical relationships provide a calculated accuracy to within ±1% of the friction factor (*f*) relative to the Colebrook-White equation. Zigrang and Sylvester (1982), Barr (1981), Sonnad and Goudar (2006), and Romeo et al. (2002) provide very accurate results. Equations developed by Jain (1976), Swamee and Jain (1976), and Churchill (1973, 1977) also provide good results with accuracies within ±0.5% of *f* as determined from Colebrook-White. Haaland (1983) is also fairly accurate, but tends to under-predict *f* compared to Colebrook-White.

Although, each explicit equation closely approximates the Colebrook-White equation, it should be noted that the Colebrook-White equation provides 3 to 5% error when compared to the actual experimental data. Therefore, exact matching of the *f* predicted by the Colebrook-White equation may not be necessary (Bhave and Gupta 2006).

Since the Swamee and Jain (1976) equation is one of the easiest explicit equations to apply, provides an accuracy to within 0.5%, and produces estimates of *f* that are slightly conservative; the Swamee-Jain equation is recommended to calculate Darcy *f* if the Colebrook-White equation cannot be utilized. The Swamee-Jain equation is presented as Equation 2.6.

$$f = \frac{0.25}{\left[\log\left(\frac{k_S}{3.7D}+\frac{5.74}{R_e^{0.9}}\right)\right]^2} \tag{2.6}$$

2.4 Hazen-Williams Equation

In addition to the Darcy-Weisbach equation, both the Hazen-Williams and the Manning equation have also been used to calculate head loss in closed conduits. The Hazen-Williams equation is the most popular in the United States, whereas the Darcy-Weisbach equation is preferred in Europe and academia. Based upon this literature review, Manning's equation is generally used for open-channel flow, but is also applicable to fully turbulent closed-conduit flow; is seldom used in practice; and is not as accurate in calculating head loss closed conduits and, therefore, will not be discussed further.

The Hazen-Williams equation has been used for many years in water supply engineering and became popular because it is an easy to use, well-documented, explicit equation, based upon field testing

of existing pipes in service. However, it is only applicable to water at standard temperature within a limited diameter and velocity range that generally applies to the intermediate zone of the Moody diagram. The original form of the Hazen-Williams equation is presented as Equation 2.7.

$$V = K_u C R^{0.63} S^{0.54} \tag{2.7}$$

where V = velocity (ft/s, m/s); K_u = a unit coefficient (K_u = 1.318 US Customary Units, 0.849 for SI Units); C = the Hazen-Williams coefficient; R = hydraulic radius (ft, m); and S = friction slope (ft/ft, m/m). Since $h_l = S/L$, $R = A/P = D/4$ for pipes flowing full, and $Q = VA$ (A = area (ft^2, m^2)); the equation can be rearranged to calculate head loss (h_l) as shown as Equation 2.8.

$$h_l = \frac{K_u Q^{1.852} L}{C^{1.852} D^{4.87}} \tag{2.8}$$

where h_l = head loss (ft, m); K_u = a unit coefficient (K_u = 4.72 US Customary Units, 10.65 for SI Units); Q = discharge (cfs, m^3/s); L = pipe length (ft, m); and D = diameter (ft, m). Typical values of C factors for new pipes conveying clean water are provided in Table 2.6. These values were obtained from fluid mechanics textbooks and handbooks and are generally provided with little to no guidance or background information as to how to select or apply the C factor. Therefore, the engineer assumes that the C factor is a constant and applicable to all diameters, velocities, and service water. In addition, the literature generally provides numerous values, or ranges of C factors, this variability can lead to calculation errors.

Table 2.6: Typical C Factors for New Pipe C with Clean Water

Pipe Material	Typical C	Range
PVC, HDPE	140	135 – 150
Cement mortar lined ductile iron or steel	140	120 – 145
New cast iron or welded steel (unlined)	120	100 – 140
Concrete	120	130 – 140

Chin (2000) indicated that the Hazen-Williams equation is applicable to the flow of water at 16˚C (60.8˚F) in pipes with diameters between 50 mm (2 in.) and 1,850 mm (72 in.), and flow velocities less than 3 m/s (10 ft/s). However, most literature indicates that the Hazen-Williams equation is most accurate for

water at a standard temperature (68°F), with a typical pipe size of 24-in. (0.6-m) diameter, and a velocity of 3.28 ft/s (1 m/s).

Applying the Hazen-Williams equation to very cold or hot water, or unusually high or low velocities, can result in significant errors. The formula becomes increasing inaccurate as R_e deviates from $5x10^5$. In addition, field testing has shown that *C* varies with pipe diameter as well as pipe material type, although a single value of *C* for each pipe material is generally presented in the literature (Table 2.6). Many authors have shown that the Hazen-Williams *C* factor has a strong R_e dependence and is mostly applicable to where the pipe is relatively smooth and in the early part of the transition to rough flow. Jain (1976) has shown that an error of up to 39% can be expected in the evaluation of the velocity by the Hazen-Williams equation over a wide range of diameters and friction slopes (head loss). Lamont (1954) indicated that the Hazen-Williams equation should not be applied to the rough turbulent flow region and when *C* factors are less than 100. The Hazen-Williams equation is generally not recommended, since the roughness coefficient (*C*) is strictly limited to a particular flow condition, pipe size, and water temperature; and application outside this range can lead to significant errors (Liou 1998).

As can be seen from Equation 2.7, *C* is not dimensionless. It has units and is, therefore, a function of other parameters. From a theoretical standpoint, the *C* factor of a pipe should vary with the flow velocity under turbulent conditions. Jain (1976) proposed a formula to determine the *C* factor, incorporating kinematic viscosity, absolute roughness, diameter, and velocity. In addition, Liou (1998) determined that the *C* factor was a function of R_e, k_s, *D*, and kinematic viscosity (ν) and he developed an equation to calculate the C factor directly based upon these parameters. These relationships are provided as Equations 2.9 and 2.10.

Jain (1976):

$$C = \frac{17.25\left[1.14 - 2\log\left(\frac{k_S}{D} + \frac{6.74x10^{-4}}{(VD)^{0.9}}\right)\right]^{1.08}}{(VD)^{0.081}} \quad (2.9)$$

Liou (1998):

$$C = C_u f^{-0.54} R_e^{0.06} \left(\frac{k_s}{D}\right)^{0.01} k_s^{-0.01} \nu^{-0.08} \tag{2.10}$$

where C_u = 17.22 in US Customary Units and 14.07 in SI Units. Figure 2.4 illustrates how the *C* factor varies with diameter, applying Equation 2.8 assuming water at 68˚F and a velocity of 3 ft/s for pipe ranging from 4 to 84 in. (101.6 to 2133.6 mm) in diameter. As seen in Figure 2.4, *C* factors increase between 10 and 40% as diameter increases. Misapplying the *C* factor could, therefore, provide a significant error in head-loss calculations.

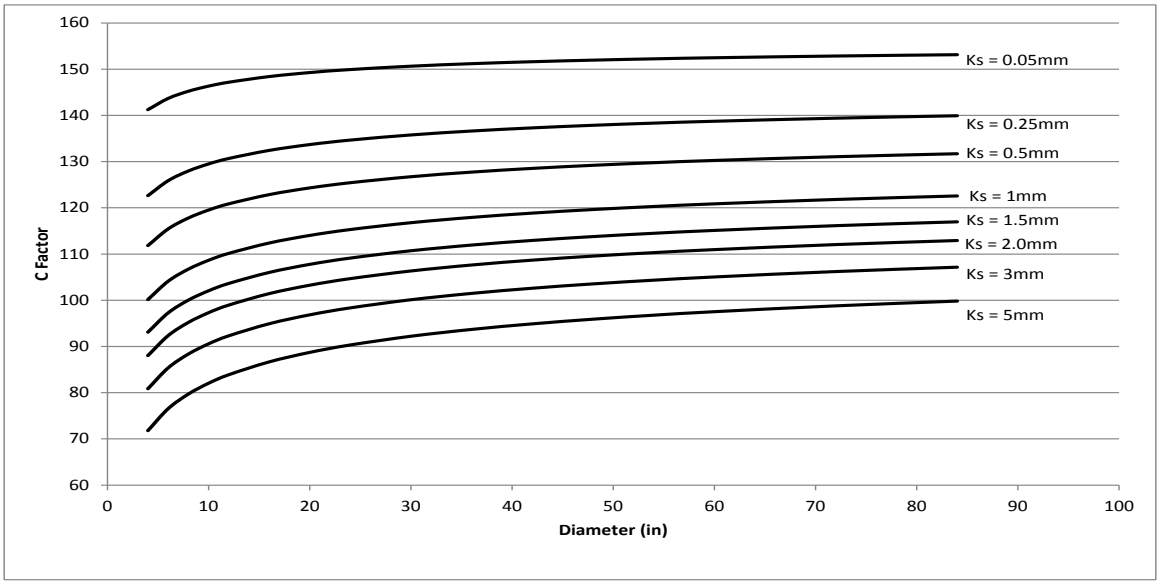

Figure 2.4: Comparison of Calculated *C* Factor to Diameter

Despite the limitations identified above, the range of applicability falls into the general range of use for most municipal water conveyance systems. Christensen (2000) reported that the Hazen-Williams formula yields relatively accurate results near the smooth flow turbulent regime. For smooth pipes ($k_s \leq$ 0.028 mm) the relative error was determined to be ±8% and increases to ±40% for rough pipes ($k_s \geq$ 1.52 mm). If a *C* factor is provided along with the appropriate testing data, then Equation 2.11 can be used to adjust the *C* factor for different velocities, but the effects of this correction are usually minimal. A two-fold increase in the flow velocity correlates to an apparent 5% decrease in the roughness factor. The difference is usually within the error range for the roughness estimate in the first place, so most engineers

assume the *C* factor remains constant regardless of flow (Walski 1984). However, if *C* factor tests are done at very high velocities (>10 ft/s (3 m/s)), then a significant error can result when the resulting *C*-factors are used to predict head loss at low velocities.

$$C = C_o \left(\frac{V_o}{V}\right)^{0.081} \tag{2.11}$$

where C = Hazen-Williams (adjusted coefficient), C_o = initial or reference C factor; v_o = initial velocity (ft/s, m/s); and v = velocity (ft/s, m/s). Over the years, a significant database of *C* factors has been developed based upon field tests. However, *C* factors found in the literature for various pipe materials generally are not accompanied with the relevant background testing information such as, velocity, diameter, water temperature, and service water, for which the *C* factors were determined in order to apply Equation 2.11. Therefore, this information should be reported with any test results so the results can be modified according to the application.

2.5 Comparison of Darcy-Weisbach and Hazen-Williams Equations

A comparison between the Hazen-Williams C factors and Darcy-Weisbach friction factors are plotted on a Moody diagram in Figure 2.5. It shows equivalent values of friction factor, *f* vs. R_e for Hazen-Williams C factors ranging from 80 to 160. The water is assumed to be 15˚C (59˚F). By equating friction slope ($S = h_l/L$) to both the Darcy-Weisbach and Hazen-Williams equations, solving for *f* and introducing the R_e to eliminate *Q*, the friction factor (*f*) can be calculated for a given *C* factor using Equation 2.12. Conversely, the equivalent *C* factor can be converted if the friction factor is known using Equation 2.13.

$$f = \frac{1014.2}{C^{1.852} R^{0.148} D^{0.0184}} \tag{2.12}$$

$$C = \frac{42.118}{f^{0.541} R^{0.0757} D^{0.010}} \tag{2.13}$$

where *D* is in meters. Similar expressions can be utilized for US Customary Units. If either the friction factor (*f*) or Hazen-Williams *C* factor is known for a given discharge, the other factor can be converted using Equation 2.14a (SI) or Equation 2.14b (Metric).

$$0.0827f = \frac{10.7D^{0.13}}{C^{1.85}Q^{0.15}} \quad \text{(SI Units)} \tag{2.14a}$$

$$0.252f = \frac{4.73D^{0.13}}{C^{1.85}Q^{0.15}} \quad \text{(US Customary Units)} \tag{2.14b}$$

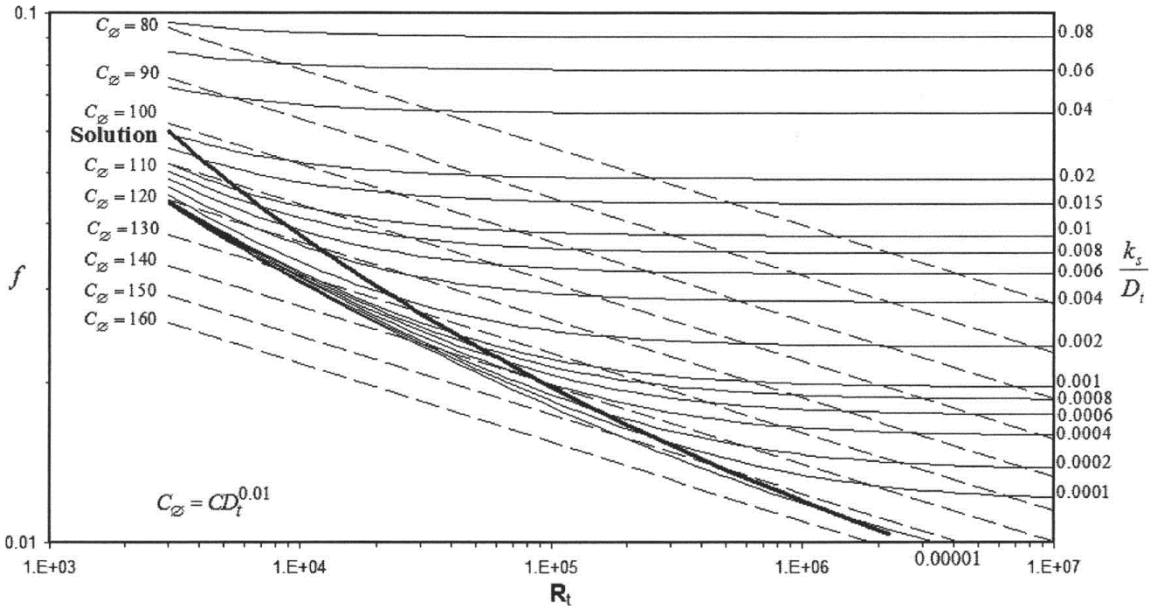

Figure 2.5: Comparison of Darcy *f* and *C* Factor Plotted on the Moody Diagram (Travis and Mays 2007)

Based upon a review of Equation 2.12, *f* is strongly dependent upon pipe diameter. As shown in Figure 2.5, *C* factors greater than approximately 152 plot below the smooth pipe law developed by Prandtl and von Kármán for all R_e. Although several theoretical limitations have been identified for using the Hazen-Williams equation, both the Darcy-Weisbach (using Colebrook-White) and the Hazen-Williams equations should be compared, 1) to identify potential errors and 2) to develop guidelines for application of the Hazen-Williams equation, assuming that the Darcy-Weisbach equation provides the most accurate calculation for head loss. An analysis was performed assuming water is conveyed in an unlined carbon steel pipe (k_s = 0.0018 in.) to determine if the relative error associated with using the Hazen-Williams equation is significant, considering variation in temperature, diameter, and *C* factor.

The relative errors associated with changes in temperature for *C* factors of 130 and 140 are presented in Figure 2.6 and show increasing errors associated with temperatures deviating from 68°F (20°C).

Figure 2.7 shows that increased error is introduced with increasing diameter. Figure 2.8 shows the effect of changes in *C* factors. In each case, the results show that errors can be as much as 30%, with the least error occurring when *C* = 145. However, it should be noted that a *C* factor of 100 to 140 would be selected for unlined steel pipe based upon Table 2.6, thus increasing the potential error when utilizing the Hazen-Williams equation.

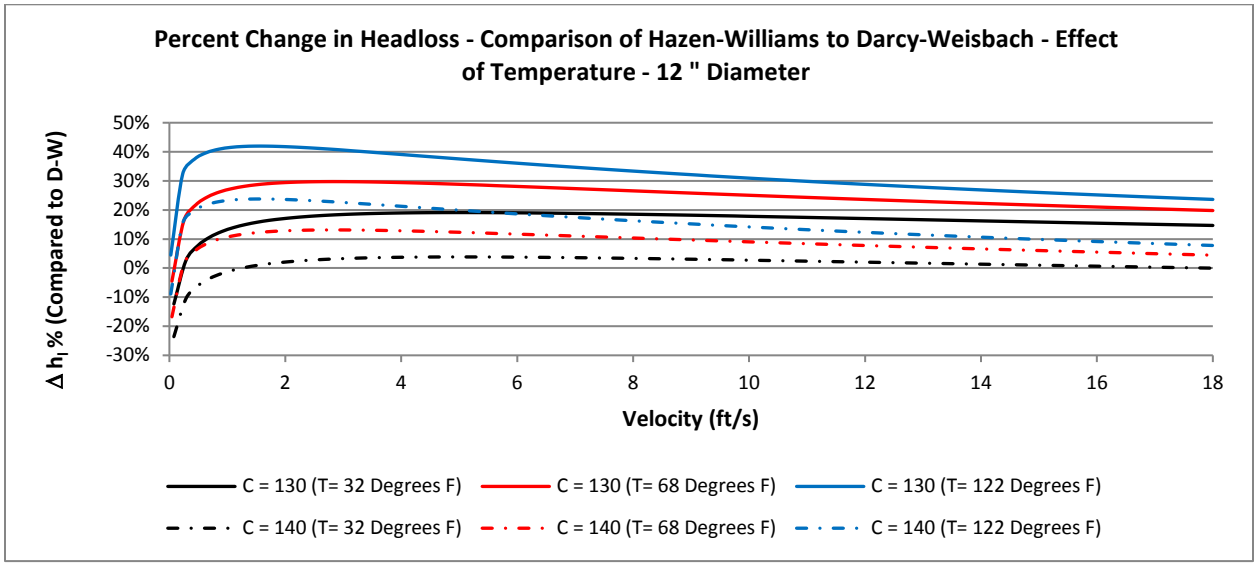

Figure 2.6: Percent Change in Head Loss – Comparison of Hazen-Williams Equation to Darcy-Weisbach (D-W) – Effect of Temperature

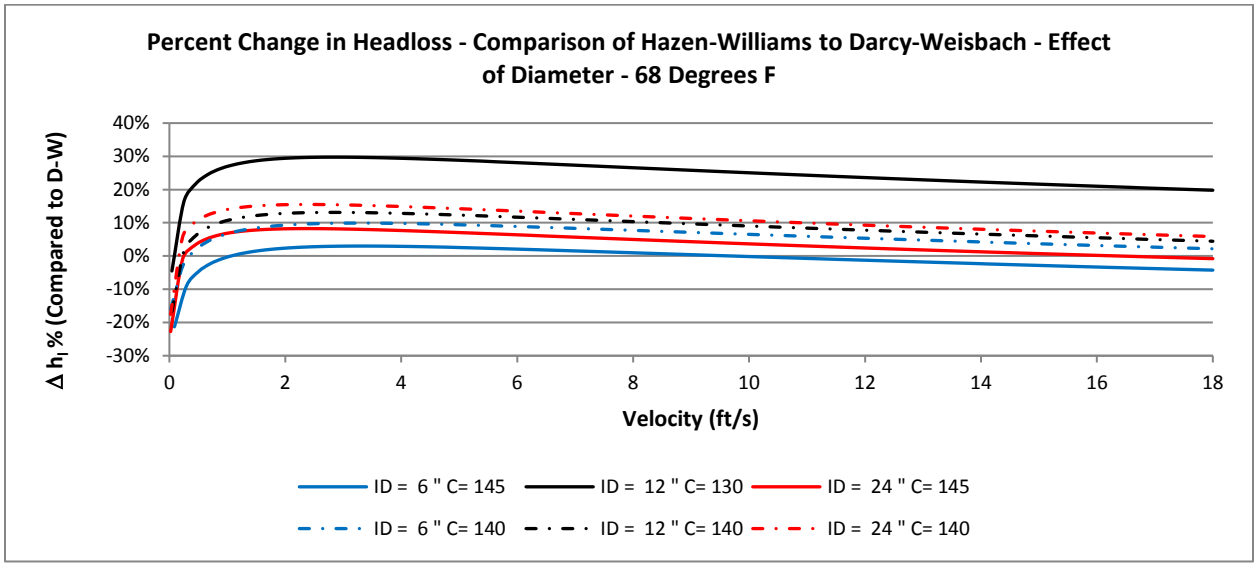

Figure 2.7: Percent Change in Head Loss – Comparison of Hazen-Williams Equation to Darcy-Weisbach – Effect of Diameter

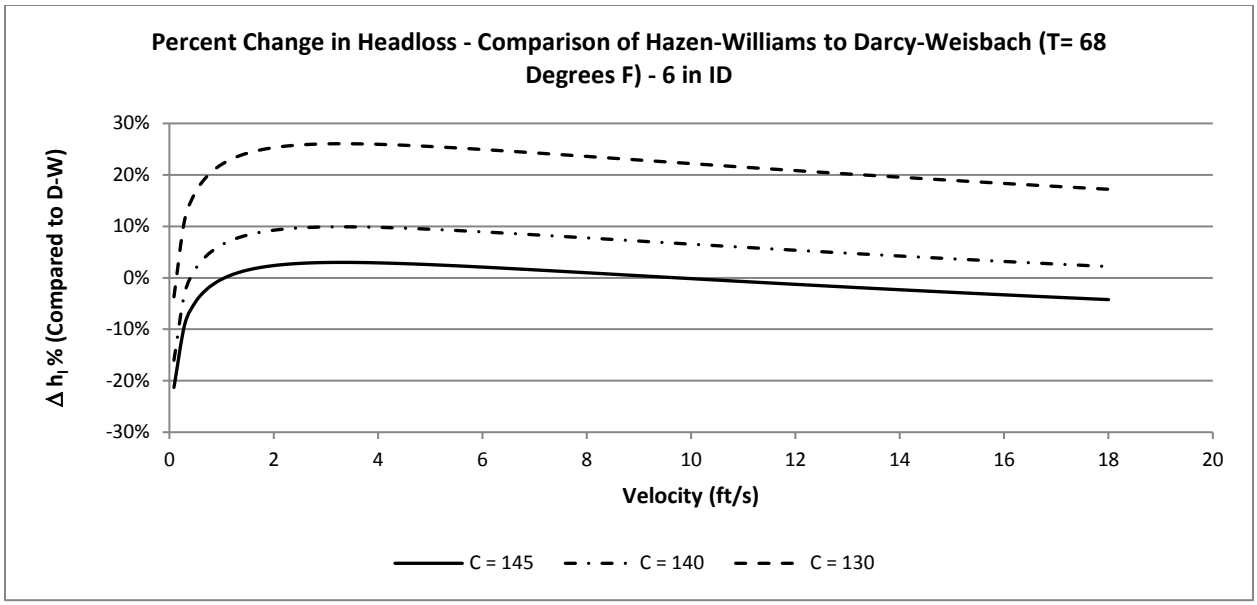

Figure 2.8: Percent Change in Head Loss – Comparison of Hazen-Williams Equation to Darcy-Weisbach – Effect of C Factor

Utilizing the results presented in Figures 2.6 to 2.8, system curves were developed in order to determine the significance of the identified errors for variation of temperature, diameter, and *C* factor. A system curve provides a chart of the head loss against the discharge or velocity. System curves were developed for a pipe length of 1,000 ft and *C* factors of 130 and 140. Considering that the relative percent change in head loss is the same regardless of pipe length, the results for a pipe length of 100 ft are not presented because the difference in calculated head loss was approximately 0.5 ft (0.152 m) at 10 ft/s (3 m/s) and would be considered within reasonable error for the calculation. However, as shown in Figures 2.9 to 2.12, the relative change in calculated head loss was moderate for a pipe length of 1,000 ft, (304.8 m) but would be significant for a length of 10,000 ft (3,048 m). Another observation from the system curve comparison is that using the Hazen-Williams equation tends to over-predict the head loss, which could lead to costly decisions to increase pipe diameter to reduce head loss or providing a larger pump to overcome perceived additional energy input requirements. Even though using the Hazen-Williams equation over-predicts the head loss, using a *C* factor of 140 provides a head loss within acceptable accuracy to the Darcy-Weisbach equation, despite the apparent relative errors provided in Figures 2.6 to 2.8.

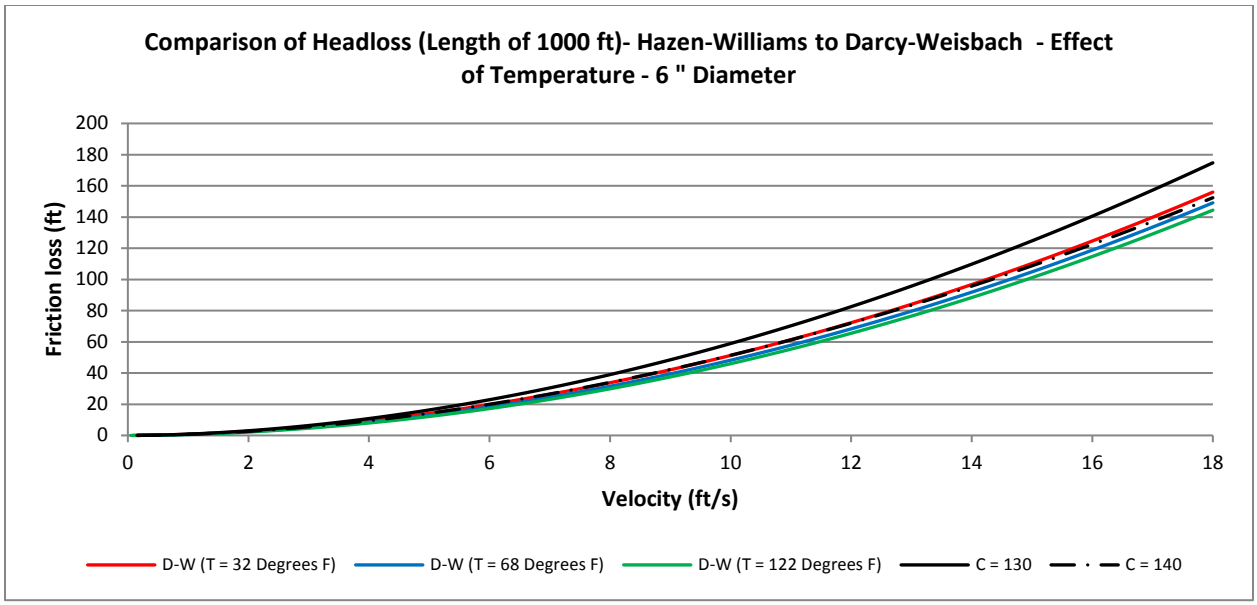

Figure 2.9: System Curve – Comparison of Hazen-Williams Equation to Darcy-Weisbach – 6-in. Diameter

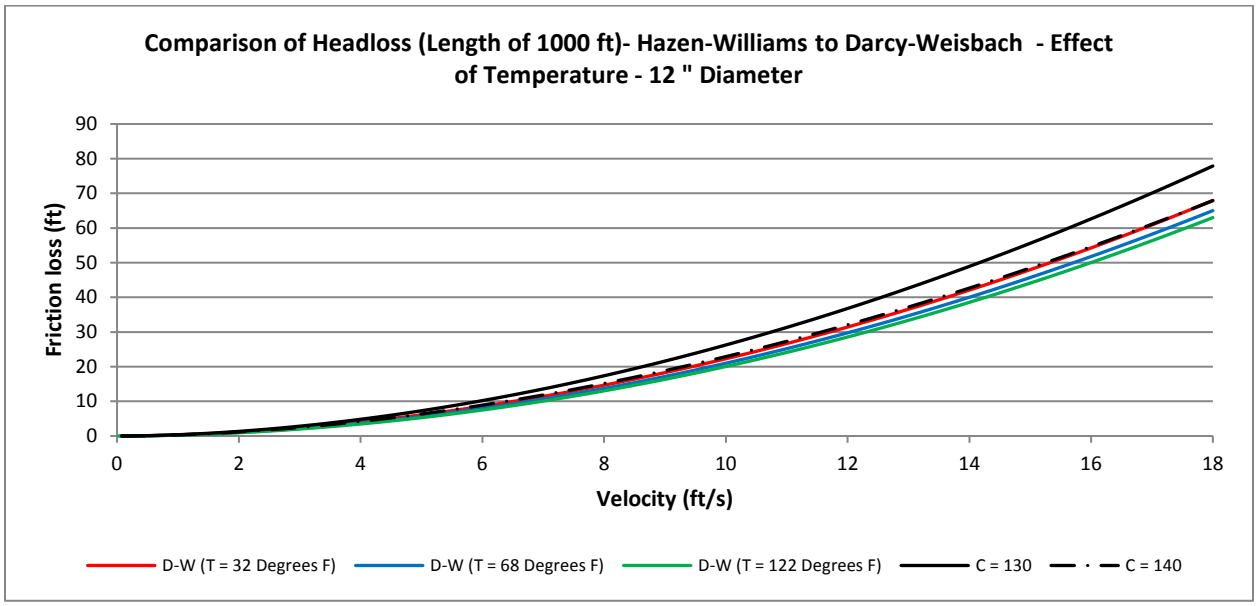

Figure 2.10: System Curve – Comparison of Hazen-Williams Equation to Darcy-Weisbach – 12-in. Diameter

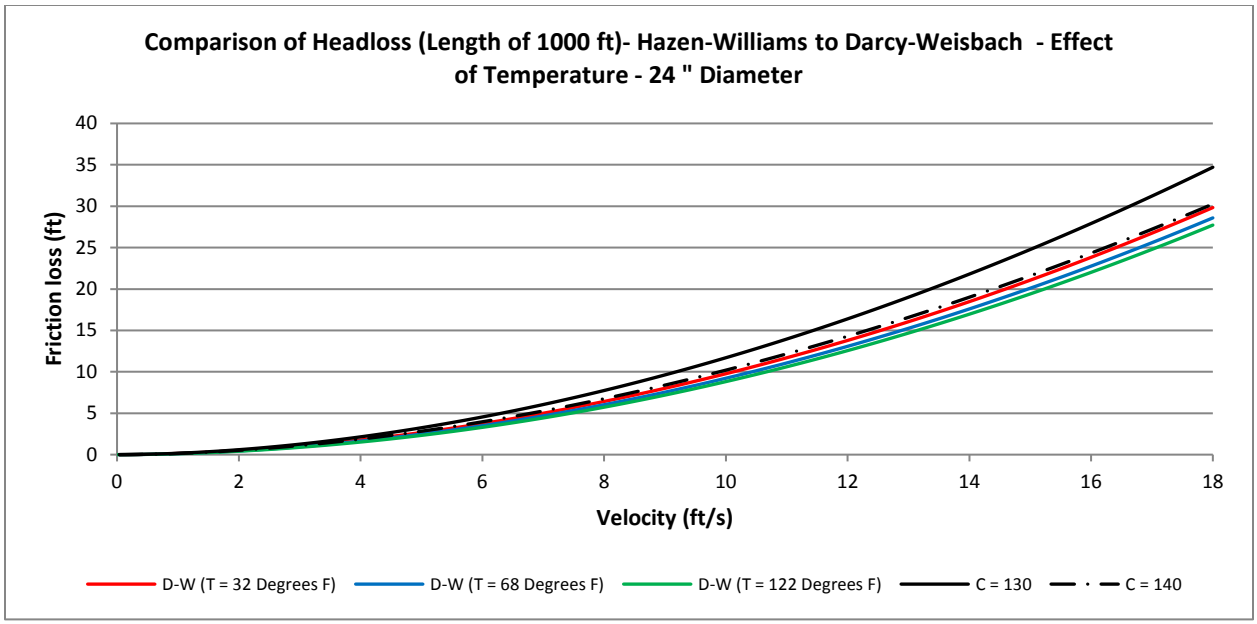

Figure 2.11: System Curve – Comparison of Hazen-Williams Equation to Darcy-Weisbach – 24-in. Diameter

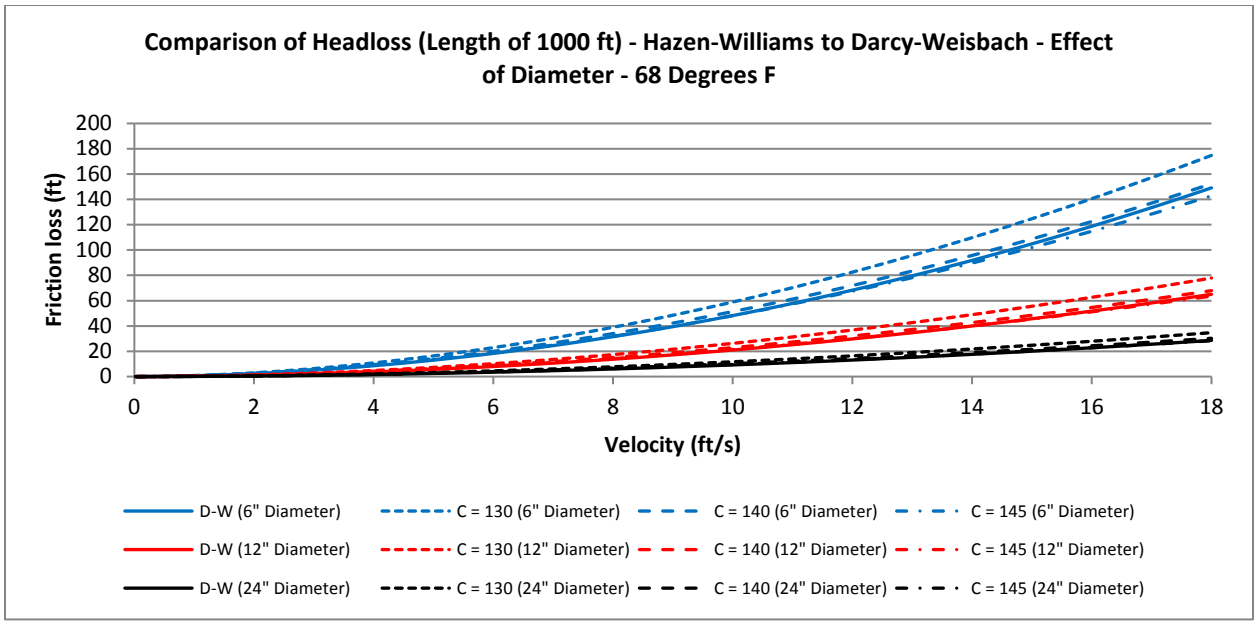

Figure 2.12: System Curve – Comparison of Hazen-Williams Equation to Darcy-Weisbach – Effect of Diameter and C Factor

As shown in the figures above, the error in calculating head loss using the Hazen-Williams equation as compared to the Darcy-Weisbach with Colebrook-White can be significant, but is acceptable for short pipeline lengths because the relative error in calculating head loss is minimal. Considering both the Darcy-

Weisbach and Hazen-Williams equations, the Darcy-Weisbach equation is more rationally based and has received wide acceptance. However, when specific experimental data are available, the Hazen-Williams equation can provide reasonable results.

2.6 Sensitivity to Surface Roughness

Both the Darcy-Weisbach and Hazen-Williams equations were analyzed to determine the sensitivity of each equation to increases in surface roughness or *C* factor, as well as a decrease in diameter. Based upon continuity, a decrease in diameter results in an increase in velocity for the same discharge and, therefore, increases head loss. Tables 2.7 and 2.8 present the sensitivity to surface roughness for pipelines using both the Darcy-Weisbach and Hazen-Williams equations, respectively. A 12-in. (304.8 mm) diameter cement mortar lined steel pipe conveying water at 68˚F (20˚C) at a discharge of 2.36 cfs (0.07 cms) was considered for this comparison. A discharge of 2.36 cfs (0.07 cms) was selected because it results in a velocity of 3 ft/s (0.91 m/s) in a 12 in. (304.8 mm) diameter pipe. Table 2.7 shows that a 50% increase in absolute surface roughness results in a 17.4% increase in head loss, whereas decreasing the diameter by the apparent increase in surface roughness and maintaining k_s for new pipe provides a 2.7% increase in head loss. This indicates that determining the Darcy friction factor is more sensitive to a change in surface roughness and that the surface roughness is the most important factor in calculating head loss.

Table 2.7: Sensitivity to Surface Roughness – Darcy-Weisbach Equation

Item	New Pipe	50% Increase in k_s	Diameter Decrease Corresponding to Increase in k_s
D (in.)	12	12	11.94
k_s (in.)	0.02	0.03	0.02
V (ft/s)	3	3	3.03
v (ft^2/s) T (68˚F)	1.09E-05	1.09E-05	1.09E-05
R_e	2.75E+05	2.75E+05	2.74E+05
f	0.023	0.025	0.023
L (ft)	10,000	10,000	10,000
h_l (ft)	32.2	35.6	33.1
% increase in h_l		10.3%	2.6%

Table 2.8 presents the results of a similar analysis conducted using the Hazen-Williams equation. For this analysis, it was assumed that a 12-in. diameter pipeline is conveying 2.36 cfs (0.07 cms) and the *C* factor was reduced by 10%. However, a 10% reduction in pipe diameter resulted in a 1.2-in. (30.5 mm)

decrease in diameter, which is unreasonable. Therefore, it was desired to determine the decrease in pipe diameter corresponding to the head loss calculated for a 10% reduction in *C* factor. The results determined that a 4% decrease in diameter resulted in the equivalent head loss from a 10% reduction in *C* factor. In this case, a 4% reduction in pipe diameter, or approximately 0.5 in. (12.7 mm), is still unreasonable, but shows that the head-loss calculation is more sensitive to changes in the *C* factor.

Table 2.8: Sensitivity of Hazen-Williams Equation

Item	New Pipe	10% Decrease in *C*	4% Diameter Reduction
D (in.)	12	12	11.52
C	140	126	140
V (ft/s)	3	3	3.3
L (ft)	10,000	10,000	10,000
h_l (ft)	24.7	30.0	30.1
% increase in h_l		21.5%	22.0%

As shown in Tables 2.7 and 2.8, the effect of flow area reduction is much less significant than increased surface roughness for a 12-in. diameter pipe and may be ignored except in extreme cases where the pipe inside diameter has been significantly reduced or where calculations of the actual velocity are more important. However, the effect of flow area reduction becomes increasingly important as diameter decreases.

2.7 Modern Pipeline Materials

Although a number of pipe materials, along with their corresponding k_s or *C* factors, were presented in Tables 2.4 and 2.6, many of the materials presented Table 2.4 are not used for modern municipal pipelines. The most common pressure pipe materials used for municipal service include concrete, ductile or steel pipe with cement mortar lining for both raw and finished water, ductile or steel pipe with epoxy lining for wastewater service; and HDPE, PVC, fiberglass, for either water or wastewater service. Historically, unlined cast iron pipe was the most popular pipe material for water systems but has been superseded with cement mortar lined ductile iron pipe more than 40 years ago.

Application of any equation to calculate friction loss can only produce accurate results if the correct roughness factor is applied for hydraulic calculations. Fluid mechanics textbooks along with pipe design manuals were reviewed in order to compile a list of recommended roughness values based upon pipe

material. Pipe manufacturers' literature and industry organization design guides were reviewed to compare the recommended roughness values identified against those values listed in Tables 2.4 and 2.6. The information obtained from pipe manufacturers' literature and industry organization design guides for modern pipe materials are summarized in the following sections. As one would expect, these values varied from manufacturer or association and in many cases were provided with little to no guidance or recommendations for their application.

2.7.1 Ductile Iron Pipe

The Ductile Iron Pipe Research Association (DIPRA) recommends using the Hazen-Williams equation with a *C* factor of 140 for all cement mortar lined ductile iron pipe, regardless of diameter or velocity range and suggests that this value is an average and can be applied for future as well as aged pipe conditions. American Water Works Association (AWWA) Manual M41, *Ductile-Iron Pipe and Fittings* applies the DIPRA recommendation of 140 for *C* (AWWA 2009). As presented above, the *C* factor does vary with diameter, so one should be cautious when applying this value for all diameters.

Saint-Gobain, a ductile iron pipe manufacturer recommends a k_s value of 0.03 mm (0.0012 in.) for cement mortar lined ductile iron pipe in their design literature. This value is significantly different from the k_s value of 0.0024 mm (9.45E-5 in.) listed for cement-lined cast iron in Table 2.4.

2.7.2 Steel Pipe

Cement mortar lined steel pipe will perform the same hydraulically as cement mortar lined ductile iron pipe. AWWA Manual M11, *Steel Pipe – A Guide for Design and Installation* for steel pipe design (AWWA 1989) offers a relationship between *C* factors and pipe diameters for water service:

$C = 140 + 0.17D$ (new mortar-lined steel pipe, US Customary Units, *D* in in.)

$C = 130 + 0.16D$ (for long-term considerations of lining deterioration, slime buildup, US Customary Units, *D* in in.)

The above equation(s) predict that the *C* factor varies linearly with diameter. Figure 2.13 combines the change in *C* factor based upon Equation 2.8 and includes the predictions using the above AWWA

equations. As shown in Figure 2.13, this relationship is not necessarily linear. This approach is, however, better than applying a single roughness value for all pipe diameters. It is interesting to note that the *C* factor for new pipe starts at 140 and increases linearly based upon diameter. As identified above, ductile iron and steel pipelines frequently utilize cement mortar linings; however, AWWA and DIPRA provide different recommendations for the roughness factors even though the lining material is the same hydraulically.

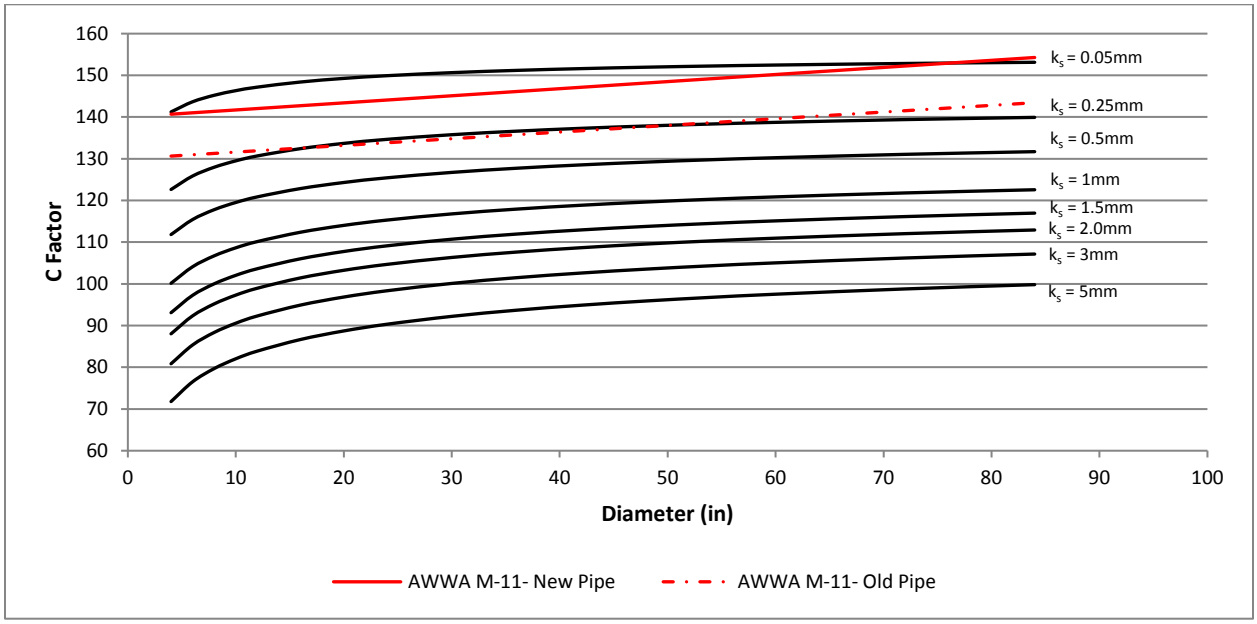

Figure 2.13: Comparison of C Factor Computed from k_s and AWWA Equations (water at 68°F and a velocity of 3 ft/s)

2.7.3 PVC

AWWA Manual M23, PVC Pipe – Design and Installation (AWWA 2002) recommends a k_s value of 0.0015 mm for PVC pipe. AWWA M23 also indicates that several researchers have determined that Hazen-Williams C factors can range from 155 to 165 for aged and new pipe conditions, respectively. However, M23 recommends applying a C factor of 150 to provide a conservative value for PVC-pipe design to account for degradation of the pipe.

2.7.4 HDPE

The Plastic Pipe Institute recommends applying a k_s value of 0.0015 mm (9.91E-5 in.) or a Hazen-Williams C factor of 150 to 155 for HDPE pipe. Because of its flexibility, buried HDPE pipe can deform

slightly under earth and other loads providing a slight elliptical shape. This elliptical deformation slightly reduces the pipe flow area. Calculations have shown that a vertical deformation of 7% results in a flow reduction of approximately 1%. Generally this phenomenon is negligible as it relates to pipe capacity.

2.7.5 Linings

Pipe manufacturers' literature did not provide much information on either the absolute roughness (k_s) or *C* factors for pipes with lining systems. In 2008, Utah State conducted a flow test on a 48-in. diameter polyurethane-lined steel pipe. The flow test determined both the friction factor and *C* factor for velocities ranging from 2.2 to 16.8 ft/s (0.67 to 5.12 m/s). The calculated *C* factor and friction factor (*f*) were determined to be 149 and 0.0105, respectively. Although the friction factor was reported, the corresponding k_s value was not identified. Utilizing the reported results, a k_s value of 0.015 mm (9.91E-5 in.) was calculated for the polyurethane lining, which is larger than what would be expected referring to Table 2.4.

As presented above, pipe manufacturers generally do not provide much information regarding the hydraulic properties of the pipe/lining system; most hydraulic-related guidance is identified in handbooks or other reference material. Therefore, engineers must rely on experience and general tables summarizing the hydraulic roughness of each pipe material. Most of the existing estimates of flow resistance factors are based on data gathered during the 1960s and 1970s. Since then, pipeline technology has changed considerably and under- or over-estimates of pipe roughness can result in the incorrect sizing of pumps and pipelines.

Although not considered as part of the scope of this research, it would be very useful to measure and provide revised absolute pipe roughness values for all modern pipe materials and manufacturing practices. Farshad and Rieke (2006) recently measured the absolute surface roughness of several modern pipe materials and linings using different surface profiling instruments and provided values for absolute roughness as indicated in Table 2.9.

Table 2.9: Absolute Roughness (k_s) Values (Farshad and Rieke 2006)

Material	k_s	
	(in.)	(mm)
Internally plastic coated	0.0002	0.005
Honed base carbon steel	0.000492	0.0125
Electropolished-bare Cr-13	0.00118	0.030
Cement lining	0.0013	0.033
Bare carbon steel	0.00138	0.036
Fiberglass lining	0.0015	0.038
Bare Cr-13	0.0021	0.055

2.8 Additional Sources of Losses

The pipe roughness factors presented in Tables 2.4, 2.6, and 2.9 should be used for clean water in new pipe. Joint deflections and the type of service water could also provide additional headloss increasing the hydraulic roughness factors presented above.

2.8.1 Joint Deflections

It is generally assumed pipelines are constructed straight along line and grade between fittings or bends. However, it is common to have slight deviations, or deflections along the pipeline. Push on joint pipe can typically tolerate a maximum deflection between 2 to 5 degrees, depending on pipe diameter and type of pipe joint. These minor deflections provide additional head loss that is generally not accounted for in hydraulic calculations. Geography or installation location (urban or rural) could provide additional head loss that is not typically accounted for during hydraulic sizing and design of pipelines. Jones et al. (2006) recommend reducing the C factor by 5 units for pipes installed in hilly regions to account for joint deflections. Overall, the literature does not provide guidance for changes in k_s due to joint deflections.

2.8.2 Service Water

Biologically active water such as raw water, recycled water, and wastewater will form biofilms that attach to the pipe wall and can dramatically increase head loss. Biofilms and Biofouling can occur due to any combination of bacteria, algae, fungi, and invertebrate organisms in raw water; bacteria and biological nutrients in recycled water; and bacteria, biological nutrients, sediments, and grease in wastewater. The increase in head loss due to biofouling is generally not included in current design practice, but should be

considered because it can effect performance causing a reduction in capacity, inefficient pump operation, a decrease in power generation (hydropower systems), and ultimately greater operational costs.

Although numerous tables showing typical surface roughness values for various pipe materials, linings, or coatings for newly-installed pipe conveying clean water were found in the literature; little information on in-service hydraulic roughness factors have been collected for different types of service water (raw, finished, recycled, or wastewater). Values quoted in standard references were derived from a very limited amount of data, which in some cases were published decades earlier. A majority of these data were collected on unlined cast-iron pipelines conveying either raw or finished water.

Thort's Water Supply (Johnson et al. 2009) recommends using the following absolute roughness (k_s) values for design purposes to allow for the deterioration of the pipeline, regardless of pipeline material:

- pipelines conveying raw water; 1.5 – 3 mm
- treated water trunk mains; 0.3 – 1.0 mm
- distribution systems; 0.5 – 1.5 mm

Tables for the Hydraulic Design of Pipes and Sewers (H.R. Wallingford and D.I.H Barr 2006) recommends the following values of k_s for wastewater forcemains (rising mains) in normal condition, regardless of pipe material:

- Mean velocity 1.0 m/s; k_s = 0.3 mm
- Mean velocity 1.5 m/s; k_s = 0.15 mm
- Mean velocity 2.0 m/s; k_s = 0.06 mm

Biofilms (Figures 2.14 and 2.15) are aggregations of microorganisms bound by a polymeric matrix that forms on surfaces in contact with water (Lambert et al. 2009). Picologlou et al. (1980) proposed that the head loss due to biofilm development was mainly caused by two physical mechanisms, 1) filaments that increase the roughness of biofilms and oscillate in the flow which increase drag, and 2) the biofilm viscoelastic properties which allow them to deform and absorb energy (Lambert et al. 2009).

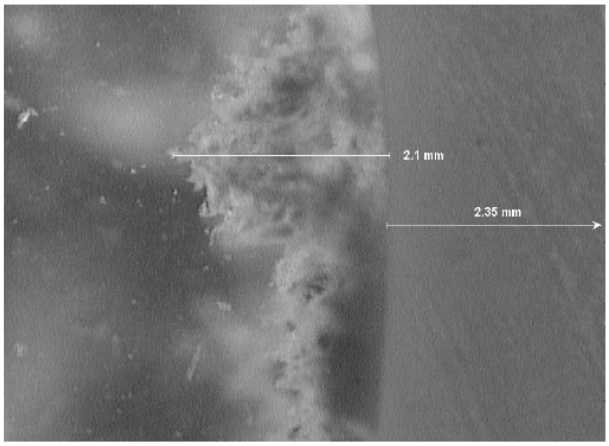

Figure 2.14: Biofilm on Interior of Pipe (Lambert et al. 2009)

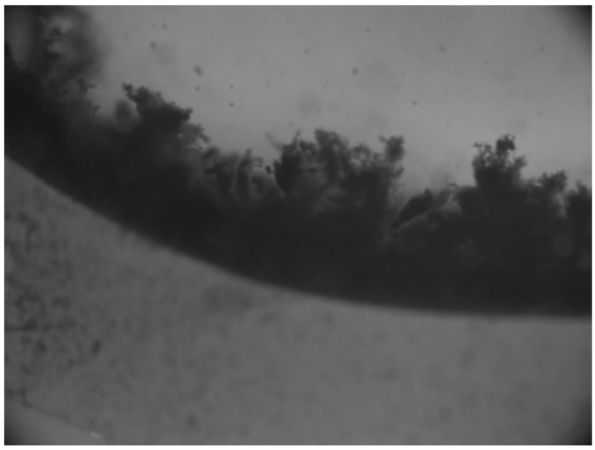

Figure 2.15: A Biofilm 2.6-mm Thick in a 25-mm Diameter Unplasticized Polyvinyl Chloride (uPVC) Pipe (Lambert et al. 2009)

Biofilm formation and development are functions of the water-quality characteristics. Groundwater is generally subject to anaerobic conditions, but could contain iron bacteria or other anaerobic bacteria. Depending on its location, surface waters can be high in biological activity. Surface waters located in Midwestern United States are subject to a number of biological inputs such as runoff from farm fields and effluent from wastewater treatment plants. However, surface waters located in mountainous areas are subject to cooler temperatures and snow melt, minimizing potential biological activity but would be more susceptible to seasonal variations. Therefore, geography and service water type could be factors in predicting biofilm development and hydraulic roughness.

A major indicator of biofilm growth is the dissolved organic carbon (DOC) concentration in the service water. Since biofilms attach to all pipe materials, actual pipe material may be irrelevant in these cases and selecting a certain pipe material because of smooth pipe wall characteristics applied to these types of water may not be warranted. Researchers have determined that the roughness due to biofilms is related to velocity and shear stress, indicating that a maximum velocity or shear stress may cause the biofilm to detach from the pipe wall.

Lambert et al. (2009) conducted an experiment growing biofilms at three different velocities in 25-mm diameter PVC pipe to determine the effect that velocity had on biofilm development and the resulting

change in headloss. Velocities selected were 0.3, 0.7, and 1.0 m/s (1.0, 2.3, and 3.3 ft/s) so only the growth factor varied between the pipes was velocity. It was determined that biofilms grown under higher velocities were less rough than those grown under lower velocities and that the calculated absolute roughness was approximately the same for different pipe diameters implying that biofilm growth is relatively independent of pipe diameter and very dependent on velocity.

Lambert et al. (2009) compared the measured velocity profiles against the theoretical velocity profiles and determined that the von Kármán (k) constant was significantly lower in biofouled pipe than the 0.40 generally accepted for pipes. In addition, a trend of decreasing k_s with increasing velocity was noted in the results. Therefore, equations such as the Colebrook-White, which assumed k = 0.40, may not be valid for biofouled pipes. It should be noted that this research was applied to a very small data set with low R_e (< 25,000) and requires additional study to determine its applicability to friction factor estimates of raw water pipelines. However, these results may provide the concept to develop an accurate equation to estimate biofilm roughness.

In 2004, HR Wallingford (Lauchlan et al. 2005) completed a two-year project on flow resistance in wastewater force mains. Data collected from twenty-three working systems owned by Thames Water and United Utilities across the United Kingdom enabled researchers to develop new recommended values for the hydraulic roughness of wastewater pumping mains. Researchers at HR Wallingford suggested that the pipe roughness in wastewater force mains is influenced by the thickness of the biological slime layer that builds up on the interior of pipes. This, in turn, can depend on the size and surface texture of pipes and on the flow velocity of the sewage travelling through them. They identified that flow velocity was the main factor affecting flow resistance in wastewater force mains with hydraulic roughness decreasing as flow velocity increases and developed an equation to estimate k_s based on flow velocity and is presented as Equation 2.15.

$$k_s = 0.446V^{-2.34} \tag{2.15}$$

where V = m/s. A relationship for Velocity in ft/s, or Hazen Williams C factors, were not determined as part of the study. A chart showing the test results, along with Equation 2.15 (average trend line), and the upper and lower bounds representing the 95% confidence envelope are presented in Figure 2.16. Although Equation 2.15 predicts the roughness coefficient to within a 95% confidence level, there is substantial variance in k_s between the lower to upper bounds.

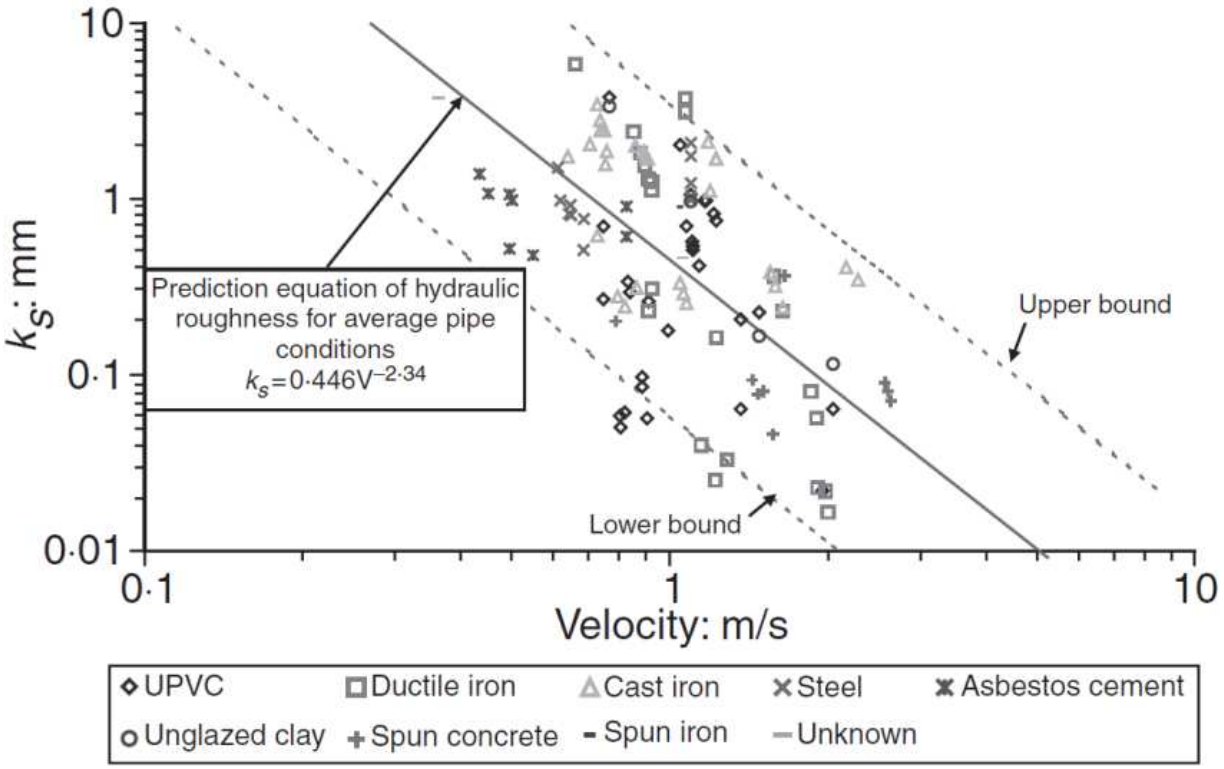

Figure 2.16: Wastewater Pipeline Test Results Compared to Equation (1.1) (Lauchlan et al. 2005)

HR Wallingford attempted to relate the calculated shear stress and k_s for the pipe, but determined that there was no clear correlation between shear stress and k_s. One of the recommendations within the study included conducting further tests over a wider range of velocities and pipe sizes for each pipe material in order to investigate the variation of k_s with pipe size and material.

Although Raw Water, Recycled Water, and Wastewater are subjected to biofilm formation, municipal wastewater forcemains are the focus of this research. Finished water and recycled water are typically associated with distribution systems, which are networked to promote better water quality and

service reliability; whereas wastewater forcemains are typically single-thread pipelines in which operational data can be obtained and applied to reduce potential errors in the analysis and results.

In addition to biofilms, wastewater pipelines are subjected to sediment and loose deposits including organic and inorganic material. Therefore, forcemains must be designed to be self-cleaning in order to prevent solids deposition which could cause increased sulfide production leading to corrosion and odor issues; loss of capacity through a reduction of cross sectional area; or even blockage at low points or at the toe of an adversely sloped pipe leading to costly removal.

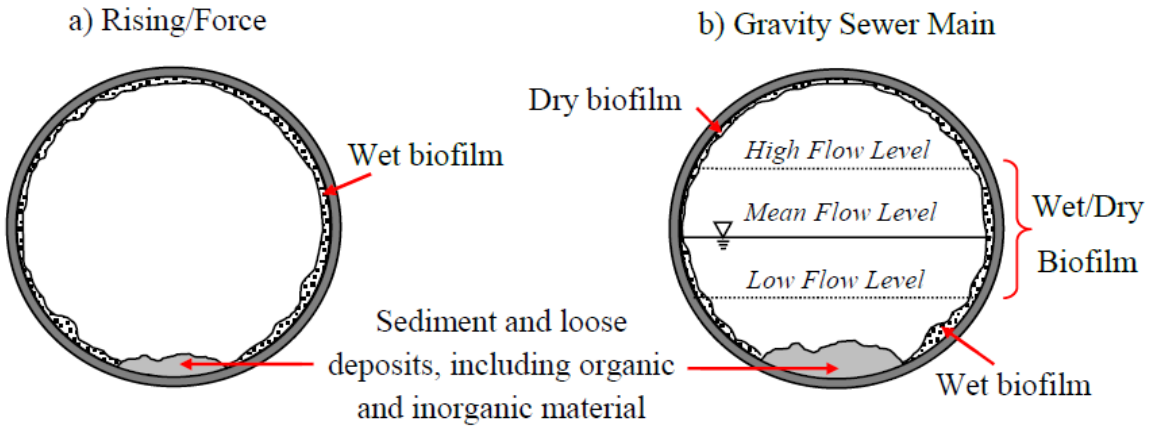

Figure 2.17: Typically fouled water and wastewater pipes, including a) rising/force wastewater main, and b) traditional gravity fed wastewater main (Cowle 2015).

2.9 Roughness Equation Modifications

As presented in Section 2.8.2, biofouling effects pipeline hydraulics and may not conform to the conventional theory of roughness equations. Therefore, modification of the friction factor equations and the Hazen-Williams equation is required to account for the variable roughness associated with biofouled pipelines. Bratland (2009) suggested utilizing a dimensionless surface structure uniformity factor (u_s) to define how the surface imperfections show similarity with each other in terms of shape and size. The more uniform the surface, the more abrupt the transition between smooth and rough flow becomes (Bratland 2009). Bratland suggested Equation 2.16 to calculate f, as a better representation of the pipe surface

roughness (using both k_s and u_s). Bratland indicated that setting u_s = 1 provides a value of f that approximates the Colebrook-White equation:

$$\frac{1}{\sqrt{f}} = -\frac{2}{u_s}\log\left[\left(\frac{1.547}{R_e\sqrt{f}}\right)^{0.9445u_s} + \left(\frac{k_s}{3.7d}\right)^{u_s}\right] \quad (2.16)$$

Bratland indicated that u_s has to be measured, but does not provide guidance on how to determine this factor. However, utilizing the uniformity coefficient concept could help describe biofilms and their effect on pipe roughness and should be evaluated in more detail utilizing actual head-loss data to see if an expression can be determined to define the biofilm influence on the roughness coefficients.

2.10 Aging of Pipelines

As demonstrated, friction is a very important factor in determining a pipeline's capacity. The challenge in calculating friction losses is due to the uncertainty in selecting a value for the pipe roughness (k_s for Darcy-Weisbach and C factor for Hazen-Williams). There are several sources that provide reliable pipe roughness values for new pipe. However, there is little information or guidance to selecting or applying roughness factors for future or aging pipe conditions. In general, an allowance must be added to new pipe values to account for deterioration in service as a result of deposits, erosion, corrosion, biofilms (slimes and biological growths), and other potential fouling (Miller 1990).

Experience of similar systems is the best guide to selecting roughness values and potential deterioration allowances for pipe aging. Pipes conveying water pose a particular problem because of a wide variation of pH, dissolved gases, and chemical composition of the water. Some waters could be high in nutrients or biological growth and could form biofilms that would attach to the pipe wall (Miller 1990).

All values of k_s (absolute roughness) identified in Table 2.4 are recommended for new pipe conveying clean water. As a pipe ages, it is subject to the water chemistry of the service water. Most pipelines that have been in service for several years will suffer a reduction in carrying capacity due to corrosion or biofilms, encrustations, or grease that may attach to the pipe wall. The rate of deterioration is

dependent on the chemical constituents of the water and the pipe material. Therefore, it is necessary to consider the future pipe condition when designing a pipeline.

Colebrook and White showed by a simple application of their transitional friction factor equation, that a 25% reduction in carrying capacity would be experienced in 20-in. diameter pipe if roughness was increased from k_s = 0.254 to 2.54 mm (0.1 to 1 in.). However, the corresponding reduction in cross-sectional area would be about 2%. Therefore, a reduction in pipe capacity is affected more by an increase in surface roughness as the pipe ages. By analyzing the data from unlined cast-iron pipes, Colebrook and White determined that the roughness increased uniformly with age and could be best expressed by Equation 2.17.

$$k_t = k_s + \alpha t \tag{2.17}$$

where k_t = the absolute roughness after t years; k_s = the absolute roughness of the new pipe surface; α = the growth factor (mm/year); and t = time in years. The growth factor is difficult to predict and must be field-determined for each system because water quality and pipe material influence this value. Numerous researchers have shown a similar equation for aging pipe roughness for cast-iron pipes. Lamont studied the records of sixty old cast-iron pipes and suggested a relationship between the growth factor and the Langelier Saturation Index (LSI), which depends on the pH, alkalinity, and the calcium content of the water (Bhave and Gupta 2006). Hudson (1966) studied several distribution system pipes (finished water) in seven cities located in the US and concluded that softening of water results in deposits and loss of carrying capacity and is a major factor in determining carrying capacity. Figure 2.18 presents a summary of the C factor trend data based upon pipe age and shows the variation in C factors from each city. This shows that geography, or more importantly, the water quality plays a significant role in aging hydraulic roughness factors. It should also be noted that Hudson performed the tests and calculated the composite C factor for the entire pipeline, including all minor losses. The head loss associated with the pipeline appurtenances (minor losses) should be determined in order to calculate the roughness coefficient accurately. In addition, Hudson did not identify pipe materials for each test. Although pipe materials were

not identified, it is assumed that a majority of the pipes tested were unlined cast-iron pipes given the time period of the study and age of pipes tested.

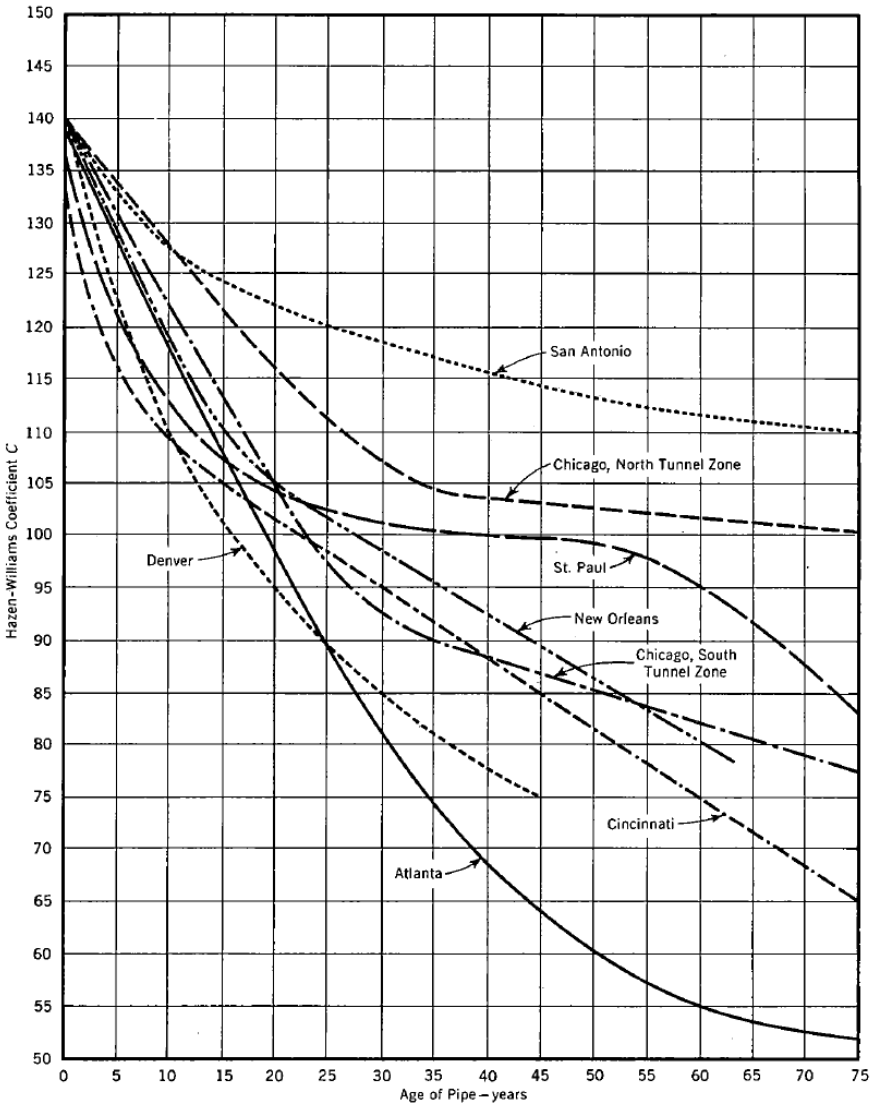

Figure 2.18: Trend Curves of Head Loss Tests – Finished Water (Hudson 1966)

Hudson did not provide the test data indicating pipeline parameters, testing velocity, or change in discharge over time, but did provide a summary of changes in treatment processes over time with the most severe changes in *C* factors occurring at times where treatment plant operations or processes were changed. Walski et al. (1988) proposed an equation to estimate the *C* factor of unlined metal pipe based upon age and quality of the water, but is only applicable to unlined iron-based pipe. The literature does not provide documentation for aging roughness factors of modern pipe materials.

Lamont (1954) reported that in hydraulically smooth non-ferrous pipes or spun-lined pipes carrying clean water, little or no age effect is to be expected and an allowance of 5% should be sufficient. He also recommended allowing a 25% reduction in capacity for spun-lined and concrete pipes carrying raw water subject to biofouling. Allowing for a 25% reduction in capacity due to biofouling could oversize the pipe; therefore, analyzing roughness factors due to biofouling and pipe aging is required to obtain a better understanding of how service water effects pipe roughness in order to provide a more accurate prediction of pipe roughness factors.

3 Data Collection and Analysis Methodology

The following sections provide general information on data collection and analysis methodology developed for this research.

3.1 Data Collection

Data collected for this research was obtained from municipal utilities. Additional data from previous studies, academic research, reports, and published papers were used to supplement and support research findings. In order to reduce analysis uncertainty, data collection efforts focused on single thread forcemains and did not consider systems with multiple lift stations pumping into a common forcemain system. The following information was obtained from each utility:

- Pump station asbuilt drawings
- Pipeline plan and profile asbuilt drawings
- Operational data
    - discharge
    - wet well level
    - pressure(s) or HGL elevation(s)
- Pump curve (if applicable); and
- Repairs or failures associated with the pipeline.

The elevation of pumps, wet well floor, and pressure sensors locations were obtained from pump station asbuilt drawings. Pipeline plan and profile drawings were used to determine the date the system was constructed; pipeline diameter, material, pressure rating, length; and to identify the number and type of fittings and appurtenances along the pipeline. Pipeline plan and profile drawings were also used to define the shape of the pipeline profile to determine if it undulates or was installed along a uniform gradient. Information regarding miscellaneous operational features such as chemical feed systems were also be noted. Supervisory Control and Data Acquisition (SCADA) systems were used to obtain operational data for each

system from the utility owner. SCADA systems monitor and record any inputs programmed into the system and can include items such as pressure, flowrate, pumps off/on, wet well level, valves open/closed, or chemical concentrations.

Operational data required to calculate headloss includes the discharge and hydraulic grade line at two known points. Hydraulic grade line could be determined from either pressure or water-surface elevations such as in a wet well or storage tank. Typically, the discharge is measured from flow meters and a pressure or level transducer is used to measure and monitor pressure or water surface levels. The advantage to utilizing SCADA data is that historic records can be obtained and analyzed taking into account different flowrates or operating conditions. In addition, analysis of multiple records can be used to determine or identify potential data errors with the monitoring devices, which could in turn potentially reduce errors in calculations.

Although the use of data obtained from SCADA systems provides multiple data sets, the accuracy of data is reliant upon the accuracy of the existing pressure sensors and flow meters. Therefore, potential discrepancies or errors identified from a review of the data were discussed with the utility in order to determine reliability of the data. Depending on the system, data could be checked against other components within the same system to determine the accuracy. For example, a forcemain discharging to a treatment plant or other similar process can utilize the treatment plant process or other secondary data source to verify the discharge; or the measured change in wet well levels could be used to determine the volume or average flowrate conveyed during a pump cycle.

Frequency of calibration and maintenance of these sensors was discussed with each utility representative and potential time periods where SCADA system errors could exist due to faulty sensors were noted and not considered for the analysis. In general, it was determined that these control and monitoring sensors were field verified and calibrated annually. It was assumed that the flow meters, level, and pressure transducers were calibrated and that data logged by the SCADA system are accurate.

Several utilities requested to remain confidential. Therefore, the state and project name has been provided to reference the data set. However, the name of utility was withheld. Source water quality was not considered for this research.

3.2 Development of System Attributes

3.2.1 Pipeline Attributes

Pipeline material and nominal diameter were noted from the pipeline plan and profile asbuilt drawings. Interior diameter was determined from manufacturers' catalogs and cut sheets based upon the pipeline pressure class identified on the asbuilt drawings. If the pipe pressure class was not identified on the asbuilts, the pressure class was assumed to be approximately 1.5 times the maximum calculated steady state hydraulic grade line for pipeline. With the exception of concrete pipe, where the interior diameter is generally equivalent to its nominal diameter, the interior diameter varies from the nominal diameter based upon material type. In some cases such as HDPE, the interior diameter (ID) can be much smaller than the nominal diameter; on the other hand, the ID is typically larger than the nominal diameter for ductile iron pipe. Therefore it is important to utilize the actual pipe ID for hydraulic calculations. A summary of pipeline materials and corresponding interior diameter utilized as part of this research are provided as Appendix C.

Using the pipeline plan and profile drawings, horizontal station and elevation were recorded at changes in slope along the pipeline. The actual length of the pipeline is the sum of each segment length accounting for changes in slope and elevation along the pipeline and was used in all hydraulic analyses. The actual length was compared to the horizontal station length to determine how horizontal station length relates to actual pipeline length and shape of the pipeline profile.

3.2.1.1 Minor losses

Minor losses are secondary energy losses that occur due to the turbulent interaction with pipe fittings and appurtenances. The minor loss associated with a fitting is based upon a minor loss coefficient

(K-Factor) multiplied by the velocity head in the pipe. Therefore, the total energy loss associated with minor losses is based upon the sum of all K-Factors as presented in Equation 3.1.

$$h_{lm} = \Sigma K \frac{V^2}{2g} \tag{3.1}$$

Where h_{lm} = minor headloss; ΣK = sum of minor loss coefficients; V = velocity; g = acceleration due to gravity.

3.2.1.2 Fittings and Appurtenances

The number and type of fittings and appurtenances were cataloged from the pipeline asbuilt drawings. Minor loss coefficients (*k*-factors) were selected based upon industry standards from the following sources, which provide the most complete database of minor loss coefficients in order to standardize the method of evaluating losses associated with fitting and appurtenances:

- *Internal Flow Systems*, Second Edition (Miller 1990);
- *Handbook of Hydraulic Resistance*, Third Edition (Idelchik 2001);
- *Pipe Flow: A Practical and Comprehensive Guide* (Rennels and Hudson 2012); and
- *Flow of Fluids Through Valves, Fittings and Pipe, TP-410 Metric* (Crane Valve 1999).

K-Factors and corresponding source selected for this research are summarized in Table 3.1. For bends, the r/d ratio corresponds to the ratio of the bend radius to diameter. Total losses associated with fittings and appurtenances along each pipeline were calculated from Equation 3.1 and subtracted from the total head loss to determine the head loss associated with pipe friction.

Table 3.1: Minor Loss Coefficients

Item	K-Factor
Entrance - Sharp (I)	0.50
Exit (I)	1.00
Tee - Through Flow (Dead Branch) (M)	0.04
Tee - Branch Flow (Dead Run) (M)	1.10
Reducer (M)	0.04
Butterfly Valve (C)	0.30
Ball Valve (C)	0.04
Gate Valve (C)	0.10
Plug Valve (C)	0.22
Venturi Flowmeter (R)	0.20
Bends - Short Radius (r/d = 1) (C)	
15º	0.13
30º	0.15
45º	0.18
60º	0.20
75º	0.22
90º	0.24
Bends - Long Radius (r/d = 2) (C)	
15º	0.07
30º	0.08
45º	0.10
60º	0.11
75º	0.13
90º	0.14
Bends - Mitered (C)	
15º	0.05
30º	0.10
45º	0.18
60º	0.30
75º	0.48
90º	0.72

(C) - Crane; (M) - Miller; (I) - Idelchik; (R) - Rennels

3.2.1.3 Joint Deflections

Joint deflections are described in Section 2.8.1. Asbuilt drawings generally do not indicate minor joint deflections. The shape of the pipeline profile may suggest that the joints were deflected during construction, but there is no way to be certain. Therefore, losses associated with joint deflections could not be evaluated and were assumed to be incorporated into the friction loss.

3.2.1.4 Other Minor Losses

Sedimentation and/or air buildup along the pipeline reduces available flow area and increases headloss. The actual loss associated with these items would be difficult to predict without knowing the severity of the impact, or headloss data at a specific location. Therefore, these items cannot be assessed as

part of this research but their potential impact to system operations will be discussed in more detail in Chapter 6.

3.2.2 Lift Stations

Depending on lift station configuration, capacity, and number of pumps, the total headloss for a lift station typically ranges from 3- to 7 ft. The headloss for a small package type lift station will be approximately 3 ft, while a large pump station may be closer to 7 ft. In order to standardize the approach for analyzing each system, the headloss through each lift station was not individually calculated and the total headloss through small and large lift stations were assumed to be 3 ft and 5 ft, respectively. The difference between 3 and 5 ft of headloss is minimal and will not significantly affect the hydraulic calculations. Pump curves were obtained for each lift station which did not monitor and record the pump station discharge pressure.

3.3 Hydraulic Analysis of Research Data

The hydraulic analysis serves to correlate trends in pipe roughness for wastewater forcemains based upon pipe diameter, material, and age. Pipe material, age, diameter, length, and minor losses were determined from the pipeline plan and profile drawings, as described above. Due to the difficulty of measuring the actual inside diameter of the pipe; inside diameter was obtained using pipe manufacturers' catalogs and cut sheets based upon the pressure class noted on the plan and profile drawings.

Utilizing the pressure or hydraulic grade lines, inside diameter, pipe length, and discharge obtained from both the SCADA data and pipeline plan and profile drawings, the total head loss of the system was calculated by rearranging the Energy Equation as shown in Equation 3.2:

$$h_l = \frac{P_2}{\gamma} - \frac{P_1}{\gamma} + \frac{V_2^2}{2g} - \frac{V_1^2}{2g} + Z_2 - Z_1 \tag{3.2}$$

where h_l = head loss; P = pressure; γ = unit weight of the fluid; V = velocity; g = acceleration due to gravity; and Z = elevation. P/γ is known as the pressure head (ft, m); $V^2/2g$ is known as the velocity head

(ft, m); and Z is the elevation head (ft, m). Subscripts 1 and 2 denote the upstream and downstream locations, respectively.

Both the Darcy-Weisbach friction factor and the Hazen-Williams C factor were calculated using pipe friction head loss (total head loss minus minor losses), discharge, inside diameter, and pipe length as identified in Equations 3.3 and 3.4, respectively. Absolute roughness (k_s) was calculated by rearranging the Colebrook-White equation as identified in Equation 3.5:

$$f = \frac{h_l D 2g}{LV^2} \tag{3.3}$$

$$C = \left[\frac{k_u Q^{1.852} L}{h_l D^{4..87}}\right]^{\left(1/1.85\right)} \tag{3.4}$$

$$k_s = 3.7D\left[10^{\left(\frac{-1}{2\sqrt{f}}\right)} - \frac{2.51}{R_e\sqrt{f}}\right] \tag{3.5}$$

The shear stress and shear velocity were evaluated to determine the effects of biofilms and biofouling on these parameters. The shear stress (τ_o) was calculated using Equation 3.6:

$$\tau_o = \gamma h_f \frac{D}{4L} = \frac{\rho f V^2}{8} = \rho U_*^2 \tag{3.6}$$

where γ = unit weight of the fluid; h_f = head loss due to friction; D = diameter; L = pipe length; and U_* is the friction velocity, also known as the shear velocity, which is calculated from Equation 3.7:

$$U_{*=}\sqrt{\frac{\tau_o}{\rho}} = V\sqrt{\frac{f}{8}} \tag{3.7}$$

3.4 Review and Application of SCADA Data

Duration and time interval of the SCADA data measurements were noted from review of the entire data set for each forcemain system. In general, the data fields provided from each utility included the date/time of the measurement; wet well level; discharge pressure, or wet well water surface level; flowrate; and in some instances pump off/on identifying which pump(s) were operational during the pumping cycle.

Wastewater forcemains tend to be single tread pipelines discharging to either a manhole and gravity sewer; lift station wet well; or a wastewater treatment plant. As a result, the downstream HGL is known and can be considered constant at a constant discharge. Therefore, total headloss of the system was estimated using the SCADA data measurements applied to one the following methods:

1) *Flow and discharge pressure provided* - Headloss is the difference between the pump station discharge pressure (HGL) and the downstream HGL. Absolute roughness and C factor are calculated using the headloss, flowrate, and pipeline attributes.
2) *Flow and wet well level provided (discharge pressure not monitored)* – Pump station discharge pressure is estimated using the pump curve along with the wetwell level, flowrate, and elevation of the pump station discharge pipe. Total dynamic head of the system at a given flowrate and wet well level was used to estimate the discharge pressure along the pump station discharge piping. Headloss represents the difference between the pump station discharge pressure (HGL) and the downstream HGL. Absolute roughness and C factor are calculated using the headloss, flowrate, and pipeline attributes.
3) *Pump runtime status and wet well level provided (discharge pressure and flow not monitored)* -Duration of the pump cycle was determined from the pump runtime status. Average discharge during the pump cycle can be estimated from the change in wet well volume displaced during a pump down cycle and could be applied to the pump curve as described in 2) to estimate the discharge pressure. This method also requires monitoring the time to fill the wet well when the pumps are off to determine the average inflow rate into the wet well.

Although Method 3) could produce acceptable results, it requires small time steps recorded by the SCADA system and could introduce too much potential error for the purposes of this research. Therefore, this method of data collection and analysis was not be pursued further and data collection efforts were focused on systems where the flowrate and wet well level or discharge pressures are monitored.

An inherent problem with utilizing SCADA data for this type of analysis is potential errors associated with inaccurate data logging if the sensors are not calibrated or malfunction. Fieldwork was not

performed to verify sensor measurements. Therefore, in order to minimize potential errors associated with SCADA sensor measurements, the flowrate, discharge pressure, and water levels used in the calculations were averaged over each pumping cycle selected.

A potential issue with using pump curves to estimate discharge pressure is that the pumps are assumed to operate along their factory performance curve. Pump performance could not be verified as part of this research. However, this was discussed with utility representatives to identify potential past performance issues with the system being analyzed.

Analysis of each forcemain system included ten sets of calculations. Ten calculations for each forcemain system were selected in order to compare the results to the system being analyzed and to ensure reliable results. The ten pumping cycles used in the calculations were selected at random. However, prior to averaging the data over the pumping cycle and applying it to calculations, the data was screened to ensure that the measured parameters were fairly uniform, consistent with other pumping cycles, and that the flowrate was reasonably close the design discharge of the system. An uncertainty analysis, presented in Section 5.3, was conducted on the data and calculation results in order to validate the use of the data as well as determine sensitivity to calculation parameters.

3.5 Standardization of Calculations

Assumptions used in data collection and the hydraulic analysis include:

- Lift Station asbuilt drawings are accurate;
- Forcemain attributes obtained from record drawings are accurate;
- Pipes provide circular cross section;
- Forcemain remains completely full;
- Forcemain provides complete cross section area; sedimentation, air locking, or other obstructions are not present;
- Valves located along the pipeline are fully open;
- Pipelines are installed along constant slope between grade breaks;

- Pumps are operating along their curves with no degradation of the impeller;
- SCADA measurements are correct;
- Constant Temperature 20 °C (68 °F); and
- Wastewater viscosity is equivalent to clean water viscosity of water.

A Microsoft Excel spreadsheet was developed to standardize the analyses and calculations based upon the methodology described in Section 3.3. All forcemain systems analyzed were single thread pipelines which allowed for direct computation of the absolute roughness and C factor. This research did not consider systems with multiple pump stations discharging to a common forcemain header system. However, some systems did contain multiple pipe diameter segments in series. Since absolute roughness and other pipeline properties could not be directly calculated for each pipe segment in series without headloss data for each segment, a macro was developed in Microsoft Excel using Solver to simultaneously vary values of k_s for each pipe segment until the calculated headloss equaled the headloss measured from the SCADA data.

Constraints established for the macro included assuming k_s in a larger diameter segment was greater than or equal to k_s within the smaller diameter segment. This assumption was made based upon the findings of Lambert et al. (2009) who determined the thickness of biofilms within a pipeline reduced with increased velocity. Therefore, a thicker biofilm would likely be associated with a larger k_s value due to the lower velocity of the larger diameter pipe segment. Since Solver could generate multiple solutions, the application of the macro was performed several times with different starting values to ensure convergence on a consistent result for a given system.

4 Wastewater Lift Station / Forcemain Systems

4.1 General

Wastewater lift stations are pump stations designed to convey raw sewage from a lower to higher elevation through a pipeline, commonly referred as a forcemain or rising main. Lift Stations receive sewage from the sanitary sewer system. Sewage is collected in a wet well, which provides a storage volume to buffer against variable influent flows. Lift station pumps are controlled based upon the wet well level and are driven by either constant speed motors or variable frequency drives (VFD). Constant speed pumps operate between the maximum and minimum water surface levels in the wet well; whereas, VFDs are generally programmed to vary the speed of the pump to match the influent flow and maintain the desired wet well level.

Although there are several guidelines, such as the Recommended Standards for Wastewater Facilities (Wastewater Committee of the Great Lakes 2014), commonly referred to as "10 States Standards", which identifies the minimum recommended velocity of a forcemain, there is little information in literature regarding hydraulic design of forcemains. Forcemains typically convey raw sewage, grit, and grease. These items must be considered during the design process and self-cleansing velocities should be provided to minimize accumulation of grit. Raw wastewater is biologically active; as a consequence, biological growth attaches to the wall of the forcemain. Oversized forcemains with low velocities can potentially experience operational problems such as sedimentation, air or grease buildup, septic conditions, and odors. Air can accumulate at high points along the pipeline and hydrogen sulfide generation can result in corrosion of the forcemain (if air pockets are present) or downstream sewers and structures. These items are discussed in more detail in Chapter 6.

Forcemains represent approximately 7.5% of the U.S. wastewater network with an approximate length of 60,000 miles (Thomson 2010). In percentage terms, gravity sewers are a much greater length. However, a wastewater forcemain failure can create much greater operational and environmental problems

than failure in a gravity line. It is very unusual to find dual force mains or alternative routing. If a key force main is out of commission, the entire wastewater system comes to a stop (Thomson 2010).

According to the Water Environment Research Foundation's (WERF) Inspection Guidelines for Wastewater Force Mains, the primary material for force mains in the United States is ferrous materials (cast iron, ductile iron, and steel) at over 60% with concrete (RCP, PCCP) being the next highest percentage at over 15% (Thomson 2010). Figure 4.1 provides a breakdown of the force main material makeup from the WERF Report.

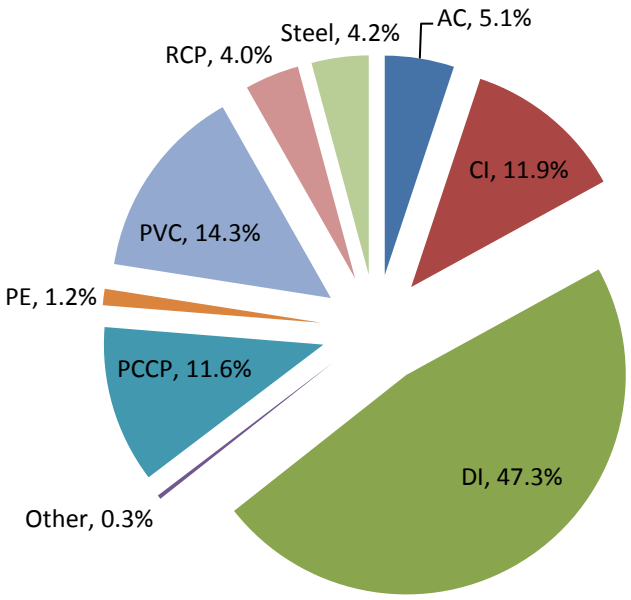

Figure 4.1: Forcemain material breakdown (Thomson 2010)

4.2 Composition of Wastewater

Composition of wastewater refers to the actual amounts of physical, chemical, and biological constituents present in wastewater. Wastewater composition varies widely from community to community and depends on the water quality of the municipal water supply, the type of residential community, the number and type of commercial and industrial connections, and the wastewater collection system. Typical values for constituents found in untreated (raw) wastewater in the United States are presented in Table 4.1.

Table 4.1: Typical Composition of Untreated Domestic Wastewater

Constituent	Concentration Range (mg/l)			
	Weak	Medium	Strong	U.S. Average
Solids, total (TS)	350	720	1200	
Dissolved, total (TDS)	250	500	850	
Fixed	145	300	525	
Volatile	105	200	325	
Suspended solids (SS)	100	220	350	
Fixed	20	55	75	
Volatile	80	165	275	
Settleable solids	5	10	20	
BOD_5 at 20° C	110	220	400	181
Total organic carbon (TOC)	80	160	290	102
Chemical oxygen demand (COD)	250	500	1000	417
Nitrogen (total as N)	20	40	85	34
Organic	8	15	35	13
Free ammonia	12	25	50	20
Nitrites	0	0	0	
Nitrates	0	0	0	0.6
Phosphorus (total as P)	4	8	15	9.4
Organic	1	3	5	2.6
Inorganic	3	5	10	6.8
Chlorides	30	50	100	
Sulfate	20	30	50	
Alkalinity (as $CaCO_3$)	50	100	200	211
Grease	50	100	150	
Total coliform (CFU 100 mL^{-1})	10^6-10^7	10^7-10^8	10^8-10^9	
Volatile organic compounds (VOCs)	<100	100-400	>400	

[1] Adapted from Metcalf and Eddy (1991) and Kienow 1989

As with wastewater flows, concentration of the individual constituents found in wastewater will vary depending on the time of day, day of the month, and month of the year (Kienow 1989). Variation in biochemical oxygen demand (BOD) concentration with time must be considered when assessing hydrogen sulfide generation. Variation of suspended solids, temperature, BOD, and dissolved oxygen (DO) are discussed in the following chapters. Flow hydrodynamics and nutrient availability of wastewater were beyond the scope of this research and were therefore not considered.

Literature recommends clean water viscosities for raw wastewater hydraulic calculations. Standard of practice is to assume wastewater viscosity is equivalent to clean water viscosity. Hager (2010), in Wastewater Hydraulics: Theory and Practice indicates that clean water viscosity is related to the temperature of the sewage.

4.3 Data Collection

This section describes the data collected and analyzed for this research. A total of 415 data points obtained from 68 forcemain systems ranging from 3- to 66 inches (76.2- to 1676.4 mm) in diameter were evaluated as part of this research. Data sets were named Research Data, HR Wallingford, and Papers and Reports. The Research Data set includes operational data collected from municipalities for lift station / forcemain systems across the United States and provided 270 data points. H.R. Wallingford includes 126 data points presented in Report SR 641 - Flow resistance of wastewater pumping mains: improved design through better data. Papers and Reports include data for 19 forcemain systems obtained from professional papers and reports. Each data set is described in more detail in the following sections.

4.3.1 Research Data - Descriptions of Systems

The Research Data set includes 20 forcemains located in Colorado, California, Georgia, and Idaho. In several instances, the utility owner requested to not be identified as part of the research. Therefore, the state and system name will be used to identify the system and Owner's names will be excluded. General attributes of each system including the pipeline length, diameter, material, age, and minor losses are summarized in Table 4.2. Pipeline profiles for each forcemain system are presented in Appendix D.2. It should be noted that Middle Trib, Mid Monument, Norris Lake, LS 03, and LS 15 contained up to three pipe segments of different diameters in series. In addition, the Mid Monument forcemain discharges into the Middle Trib forcemain immediately downstream of the Middle Trib lift station. The Middle Trib and Mid Monument systems are programmed to prevent simultaneous operation; therefore, they were included in the data set.

Table 4.2: Summary of Forcemain Characteristics Collected for this Research

Location	System Name	Pipe Material	Pipe Age (yr)	Nominal Diameter (in)	Internal Diameter (in)	(1) P&P Station Pipe Length (ft)	(2) Calculated Pipe Length (ft)	Change in Length (2) – (1) (ft)	% Increase in Length (Actual Length vs Station Length)	Maximum – Minimum Elevation along Pipeline (ft)	Σ K (Minor Loss Coefficients)	Σ K / 100 ft
Colorado	Janitell	PVC	13	4	4.00	783.7	783.8	0.1	0.014%	11.4	3.74	0.48
Colorado	Kettle Creek	DIP	27	12	12.52	5,860.4	5,872.3	11.9	0.202%	95.0	4.06	0.07
Colorado	Big Valley	DIP	35	4	4.10	413.5	415.9	2.4	0.573%	39.6	1.37	0.33
California	South River	RCP	8	66	66.00	42,796.3	42,960.4	164.1	0.382%	66.5	8.83	0.02
California	Natomas	RCP	4	60	60.00	47,114.7	47,166.5	51.8	0.110%	75.2	13.64	0.03
Colorado	Chapel Hills	PVC	32	8	8.28	5,500.0	5,508.4	8.4	0.153%	125.7	3.06	0.06
Colorado	Drennan	PVC	20	10	9.98	4,612.0	4,613.3	1.3	0.028%	55.0	4.40	0.10
Colorado	Black Squirrel	PVC	27	8	8.28	2,185.4	2,186.6	1.2	0.055%	46.2	4.88	0.22
Colorado	Middle Trib	PVC	5	12	12.08	6,128.5	6,144.7	16.2	0.263%	66.1	3.84	0.06
		PVC	25	8	8.28	2,400.0	2,400.9	0.9	0.036%	64.3	1.40	0.06
Colorado	Mid Monument	DIP	14	16	16.60	3,901.0	3,912.9	11.9	0.304%	49.9	6.52	0.17
		PVC	5	12	12.08	6,128.5	6,144.7	16.2	0.263%	66.1	3.84	0.06
		PVC	25	8	8.28	2,400.0	2,400.9	0.9	0.036%	64.3	1.40	0.06
Colorado	Sand Creek	HDPE	11	36	31.51	19,195.2	19,225.1	30.0	0.156%	112.3	14.36	0.08
Georgia	Norris Lake	DIP	2	16	16.60	17,785.0	17,807.5	22.5	0.126%	224.0	3.36	0.020
		DIP	2	12	12.50	1,860.0	1,861.1	1.1	0.062%	51.0	1.64	0.09
Georgia	Rock Quarry	DIP	19	14	14.60	6,085.0	6,090.4	5.4	0.089%	172.5	2.32	0.04
Georgia	Dacula	DIP	22	16	16.60	7,688.0	7,692.8	4.8	0.062%	140.9	1.99	0.03
Colorado	TRM	RCP	17	42	42.00	6,078.3	6,087.4	9.1	0.149%	37.5	4.01	0.07
Colorado	TRP	RCP	7	42	42.00	7,876.4	7,887.4	11.0	0.140%	37.3	5.25	0.07
Idaho	LS 03	HDPE	9	16	14.01	1,105.0	1,109.4	4.4	0.400%	14.0	0.74	0.07
		HDPE	9	18	15.75	1,660.0	1,660.0	0.0	0.000%	5.5	0.04	0.00
		PVC	28	12	12.08	1,659.3	1,660.2	0.9	0.052%	8.5	1.61	0.10
Idaho	LS 06	PVC	15	18	17.53	12,980.1	12,988.2	8.1	0.062%	29.4	18.00	0.14
Idaho	LS 15	DIP	15	16	16.30	6,186.5	6,186.6	0.1	0.002%	12.3	1.77	0.03
		DIP	15	20	20.80	923.9	930.0	6.1	0.653%	9.6	1.76	0.19
Colorado	Jimmy Camp	PVC	15	12	11.20	12,229.1	12,238.1	9.1	0.074%	132.0	9.05	0.07
								Average	0.16%	-----	6.34	0.10

From Table 4.2, the actual pipeline length was found to be an average of 0.16% longer than the horizontal station length identified on the plan and profile drawings. Also, sum of minor loss coefficients was found to range from 1.4 to 18.0, with an average of 6.34 or 0.10/100 ft. An attempt was made to characterize the forcemains based upon the difference between the maximum and minimum elevations along the pipeline profile and the difference between the actual pipeline and horizontal station length, but there does not to appear to be any obvious correlation. A better way to characterize the pipeline may be based upon the shape of the pipeline or number of undulations; however, a review of the forcemain profiles presented in Appendix D.2 did not provide any useful correlations. These items were noted in an effort to define general pipeline attributes that could be used during the planning process of a new pipeline.

4.3.2 HR Wallingford

A study similar to the current research was undertaken by HR Wallingford and detailed in Report SR641 - Flow resistance of wastewater pumping mains: improved design through better data (Lauchlan et al. 2004). A summary of Report SR 641 was published in the Proceedings of the ICE-Water Management under a technical paper titled Flow Resistance of Wastewater Pumping Mains by Lauchlan et al. (2005). The study conducted a minimum of four field tests for 23 forcemain systems owned by Thames Water and United Utilities across the United Kingdom providing 126 data points.

Researchers at HR Wallingford suggested that the pipe roughness in wastewater forcemains is influenced by the thickness of the biological slime layer that builds up on the interior of pipes; which may depend on the size and surface texture of pipes and on the flow velocity of the sewage travelling through them. The flow velocity was determined to be the main factor affecting flow resistance in wastewater forcemains with hydraulic roughness decreasing as flow velocity increases. Systems analyzed included pipe sizes ranging from 3 to approximately 40 inches in diameter; pipe material included cast iron (CI), ductile iron (DI), asbestos cement (AC), polyethylene (PE), steel, clay, and PVC; and the average velocity ranged from approximately 1.44 ft/s (0.44 m/s) to 7.31 ft/s (2.23 m/s). A summary of general system attributes along with the field test method is provided in Table 4.3.

Table 4.3: Summary of HR Wallingford System Information (Report SR 641)

Utility	Pumping main	Pipe Material	Internal Diameter (m)	Pipe length (m)	Flow (l/s)	Average Velocity (m/s)	Σ K	Test Method
United Utilities	Hebden Green	CI	0.1605	382	24.9	1.23	6.69	UM
United Utilities	Heskin Lane	CI	0.1602	215	47.4	2.23	4.14	UM
United Utilities	Highway Lane	CI	0.1124	620	15.2	1.05	4.99	UM
United Utilities	The Dell	CI	0.0808	233	8.3	0.91	5.97	UM
United Utilities	Church St	DIP	0.2054	620	42.9	1.15	10.85	UM
United Utilities	Lea Gate (old main)	DIP	0.9626	3600	738	1.00	----	UU
Thames Water	Dene Hollow	AC	0.1319	2800	7.3	0.48	7.25	MT
Thames Water	Bishopstone	CI	0.1312	1286	11.7	0.79	6.39	M
Thames Water	Stadhampton	CI	0.102	780	6.1	0.74	5.1	M
Thames Water	Bradfield Farm	DIP	0.1574	980	22.4	0.92	4.85	M / MT
Thames Water	Cheddington south end	DIP	0.1448	1700	33.7	1.67	8.45	MT
Thames Water	Lea Gate (new main)	DIP	1.0106	3600	738	0.88	14.47	MR
Thames Water	Rissington	DIP	0.2472	570	51	0.93	9.8	TW
Thames Water	Freckleton	HDPE	0.5818	2450	320	0.91	14.27	MR
Thames Water	Nether Winchendon	HDPE	0.101	904	8.9	1.14	8.25	M
Thames Water	Fairmile	Steel	0.1518	788	22	1.1	4.3	M
Thames Water	Whitchurch Hill	Steel	0.1071	1440	6.2	0.64	9.8	M
Thames Water	Bibury	UPVC	0.1276	1100	12.1	0.88	9	MT
Thames Water	Garsington	UPVC	0.1032	950	6.8	0.82	4.1	M
Thames Water	Great Coxwell	UPVC	0.1276	1445	15.6	1.05	3.15	MT

* CI – Cast Iron; DIP- Ductile Iron Pipe; AC – Asbestos Cement; HDPE - High Density Polyethylene; Steel; UPVC – Polyvinyl Chloride

Descriptions of the Test Methodology obtained from SR 641 are provided below:

M – The pressure head and the inflow and outflow rates were measured continuously during the test.

MT – The pressure head was measured continuously. The inflow and outflow rates were calculated from the timing the rate of rise and fall of the wet well during the test.

MR - The pressure head was measured continuously. The flowrate was monitored at the treatment works or pumping station and an average flowrate for the test was estimated.

TW – Test data for pump down test provided by Thames Water. The inflow and outflow rates were calculated from timing the rate of rise and fall of the wet well during the test. Static head levels were estimated from the levels of the pumping station and the outflow location. The average pumping head measured on site was used.

UM - Test data for pump down test provided by United Utilities. The inflow and outflow rates were calculated from timing the rate of rise and fall of the wet well during the test. Static head levels were estimated from the levels of the pumping station and the outflow location. The average pumping head measured on site was used.

UU- Hydraulic roughness data was provided by United Utilities. Not enough information was provided to enable recalculation of the hydraulic roughness value. The data was not included in the analysis.

Field data and resulting calculations for all systems including the length of the pipeline, temperature of water, total K-Factors, total system headloss, and calculated friction factor were obtained from Report SR 641. Pipeline profiles were not included as part of the study. The year the project was constructed was provided for a small number of the pipelines included in the data set. Report SR 641 also included data from previous papers; these data are not summarized in Table 4.3 but are described in Chapter 5 Hydraulic Analysis and Results. It should be noted that Report SR 641 indicated that it was not possible to measure the forcemain length at several of the sites and that forcemain lengths were estimated based upon available records. The effect of pipe length was evaluated as part of the uncertainty analysis (Section 5.3.2).

4.3.3 Papers and Reports

A literature review was performed to identify professional papers and reports providing forcemain operational data that could be included as part of the current research. The literature review identified a paper titled "*C-Factor Testing as a Condition Assessment Tool for Wastewater Force Mains*" by Johannessen et al. (2014) and a lift station evaluation report for an unnamed utility in Colorado.

Johannessen et al. (2014) reported hydraulic testing results for 14 forcemains. Neither the location nor utility owner of the forcemains were identified in the paper. However, sufficient information was provided in the paper to perform the hydraulic analyses as part of the current research. Two of the forcemain results were not included in the analysis because 1) neither flowrate nor velocity of the test were included and 2) the pipeline utilized different diameters in series; and the paper did not identify the length of each pipe segment. Summary data from the paper, excluding the pipelines that could not be analyzed, are provided in Table 4.4. Johannessen et al. (2014) reported the flowrate and velocity of each system, which was used to back calculate the interior diameter. The resulting interior diameters are an average of 2% smaller than the ones listed in literature, this is more than likely due to rounding of the flow and velocity values presented in the paper.

Table 4.4: Johannessen et al. (2014) Data Summary

Pipe Material	Nominal Diameter (in)	Interior Diameter (in) [1]	Pipe Length (ft)	Flowrate (mgd)	Velocity V (ft/s)	C factor
DIP	24	24.17	14,610	3.5	1.7	77.0
ACP	4	4.50	1,370	0.1	1.4	57.0
ACP/DIP	16	15.88	11,250	1.6	1.8	79.0
CCP	30	29.52	9,400	4.3	1.4	82.0
CIP	18	17.48	450	1.4	1.3	74.0
DIP	8	8.17	8,300	1.2	5.1	119.0
DIP	20	19.82	1,930	3.6	2.6	108.0
DIP	20	20.13	8,360	3.0	2.1	101.0
DIP	24	23.82	8,070	4.0	2	96.0
DIP	24	24.22	7,240	6.0	2.9	82.0
DIP	6	6.28	640	0.5	3.6	119.0
PVC	12	12.10	3,280	1.6	3.1	95.0
PVC	18	18.00	4,630	2.4	2.1	87.0
RCP	48	47.91	2,150	25.9	3.2	104.0

[1] Calculated from reported flowrate and velocity

Data obtained from a lift station evaluation report for an unnamed utility is summarized in Table 4.5.

Table 4.5: Lift Station Report – System Attribute Summary (Unnamed Utility)

System Name	Pipe Material	Age (yr)	Nominal Diameter (in)	Interior Diameter (in)	Pipe Length (ft)	Velocity (ft/s)
LS 4	CIP	18	4	4.30	507	2.1
LS 9	DIP	20	10	10.50	3,760	3.0
LS 16	DIP	24	6	6.30	4,725	1.9
LS 12	DIP	26	4	4.20	620	3.1
LS 15	DIP	31	4	4.20	818	2.4

4.4 Lift Station / Forcemain System Operation

Lift station pumping cycles vary depending on influent flowrate, wet well storage volume, and capacity of the pumps. SCADA data obtained for each system was used to determine the average duration the pump(s) operated during a pump cycle and time pumps were off prior to the start of the next pump cycle. This analysis was performed to characterize the pump cycle(s). A summary of the type of pump drive; duration of data analyzed; average pump runtime; average time pump is off between pump cycles; total number of pumping cycles; SCADA time interval reading; average station discharge pressure; and minimum and maximum wet well levels are provided in Table 4.6. Average pump runtime was found to vary between 1 and 16 minutes with pumps remaining idle between 2 and 70 minutes between pump cycles.

Table 4.6: System and Operational Summary

System Name	Pump Drive Type	Duration of Data Analyzed (Days)	SCADA Time Interval Reading (Seconds)	Average Station Discharge Pressure (psi)	Minimum / Maximum Wet Well Level (ft)	Approximate Active Wet Well Volume[4] (ft^3)	Average Pump Runtime (min)	Average Time Between Pump Cycles, Pumps off (min)
Black Squirrel	Constant	153.3	30	48.5	3.2 / 5.5	145.3	2.3	16.9
Drennan	Constant	168.3	30	41.8	2.0 / 3.5	113.5	1.4	70.4
Janitell	Constant	168.3	30	17.8	2.0 / 3.0	46.0	16.9	55.2
Kettle Creek	Constant	168.3	30	44.6	4.0 / 5.5	213.0	4.7	5.2
Mid Monument [1]	Constant	183.0	30	65.2	3.3 / 5.7	309.0	2.2	21.7
Chapel Hills	Constant	168.3	30	61.5	2.5 / 4.5	176.0	3.0	65.8
Big Valley	Constant	153.3	30	22.2	2.0 / 3.0	66.5	2.1	23.9
Middle Trib [1]	Constant	183.0	30	70.4	2.6 / 5.7	319.3	3.2	8.5
Sand Creek [2 3]	VFD	546.0	300	66.2	----	----	----	----
Natomas [2 3]	VFD	2735.8	1,800	10.8	----	----	----	----
South River [2 3]	VFD	1471.1	1,800	17.6	----	----	----	----
TRM [2 3]	VFD	365.0	300	14.8	----	----	----	----
TRP [2 3]	VFD	365.0	300	14.8	----	----	----	----
Norris Lake [2]	Constant	1.0	15	115.6	----	----	9.0	27.9
Dacula	Constant	1.0	15	84.0	2.0 / 3.5	185.0	4.1	12.0
Rock Quarry	Constant	1.0	15	85.6	1.3 / 3.0	185.0	6.0	62.6
LS 03	Constant	118.4	60	52.5	5.0 / 5.5	39.3	1.1	2.5
LS 06	Constant	118.4	60	43.9	1.0 / 3.0	570.0	5.7	4.4
LS 15	Constant	118.4	60	31.0	3.0 / 4.0	100.5	4.4	2.3
Jimmy Camp	Constant	47.0	10	88.7	3.5 / 5.8	300.0	1.8	11.7

[1] ECO2 Chemical Feed System; [2] Discharge pressure measured in SCADA system; [3] Wet well level not provided for analysis; [4] Active volume between Min/Max levels

5 Hydraulic Analysis and Results

5.1 Hydraulic Analysis Methodology

5.1.1 Research Data

Hydraulic analyses of the Research Data set were performed using the SCADA Operational Data and System Characteristics (Table 4.2). Due the volume of data collected as part of the Research Data set, analysis was limited to ten sets of calculations for each forcemain system to ensure consistent results. Depending on the data provided for each system, either Methods 1 or 2 (Section 3.4) were utilized to perform the hydraulic analysis of the pumping cycle. Pump cycles were selected at random; the data was screened to ensure that the measurements were fairly consistent over the pumping cycle.

In order to minimize potential errors associated with inaccurate SCADA sensor measurements, flowrate, discharge pressure and/or water levels used in the analysis were averaged over each pumping cycle and applied to the hydraulic calculations. Velocity was calculated using the average flow rate over the pumping cycle and internal diameter of the forcemain. The velocity was used to calculate the headloss associated with minor losses. Equation 4.1 was used to calculate the total headloss; friction headloss was determined by subtracting the minor losses from the total headloss. The following parameters were calculated from the friction headloss:

- Darcy-Weisbach friction factor Equation 3.2;
- Absolute roughness from Equation 3.4;
- Hazen-Williams C factor from Equation 3.3;
- Shear stress (τ_o) from Equation 3.6; and
- Friction velocity (U_*) from Equation 3.7.

Wastewater temperatures were not measured or recorded by the owners and therefore was assumed to be 20 °C (68.0 °F) for all systems. The effect of temperature on the hydraulic calculations is evaluated

in Section 5.3.1. Hydraulic calculation results for the Research Data Set forcemain systems are presented in Appendix D.1.

5.1.2 HR Wallingford Data

General information for the systems analyzed as part of the HR Wallingford Report SR 641 (Lauchlan et al. 2014) are summarized in Table 4.3. Report SR 641 identified the water temperature, sum of the K-Factors, total system headloss, calculated friction factor, and k_s. However, the shear stress, friction velocity, and C factor were not evaluated as part of the study. These parameters were calculated using the methodology identified above and Section 3.3.

Report SR 641 also included data from previous papers; these data were not included in Table 4.3 but were included as part of the hydraulic analysis. Data associated with the previous papers include the velocity, diameter, and k_s. Reynolds Number and friction factor were determined assuming a temperature of 20 °C (68.0 °F). Friction factors were converted to a C factor, and shear stress and shear velocity were determined from the results. Data from previous papers referenced in SR 641 were denoted as "HR Wallingford – Previous Studies" in charts comparing the results. Results of the calculations performed using the HR Wallingford data are presented in Appendix D.3

5.1.3 Papers and Reports

5.1.3.1 Johannessen et al. (2014)

Johannessen et al. (2014) included the C factor, flowrate, velocity, pipe length, nominal diameter and material (Table 4.4). Interior diameter was determined using the flow rate and velocity and verified against manufacturers engineering data for each pipe material. In some cases the calculated interior diameter was different than published manufacturer information, likely due to rounding of the actual values reported in the paper. C factor was converted to a Darcy friction factor using Equation 2.12 and k_s was calculated from Equation 3.5. The variance in interior diameter did not significantly affect the calculated k_s values. Shear stress and shear velocity were determined from Equations 3.6 and 3.7, respectively. Analysis results are summarized in Appendix D.4.

5.1.3.2 Unnamed Utility Lift Station Report

The unnamed lift station evaluation report compared the actual pump performance to the factory pump performance curves. The Unnamed Utility Lift Station Report identified the forcemain attributes for each lift station system and concluded that a majority of the pumps were operating along or very close to the pump factory performance curves. Utilizing the results from the pump performance testing along with the pipeline attributes; hydraulic parameters were calculated based upon the methodology provided in Section 3.3. Results of the analysis are summarized in Appendix D.4.

5.2 Hydraulic Analysis Results

The results of the hydraulic analyses were used to identify, screen, and evaluate trends associated with friction factor, k_s, C factor, pipe age, Bratland Uniformity Factor, and shear stress.

5.2.1 Hydraulic Roughness Parameters

5.2.1.1 Friction Factor and Absolute Roughness (k_s)

Reynolds Number and corresponding friction factor calculated from the Research Data set were plotted on a Moody Diagram as shown in Figure 5.1. The Hydraulically smooth curve is defined by Equation 2.3 and the dashed line represents the boundary between the transition zone and rough turbulent flow, with rough turbulent flow occurring above the boundary line. Moody proposed that this boundary be approximately 1% above friction factor for infinite Reynolds Number defined by $R_e=1600/(k_s/d)$ (McGovern 2011). This relationship along with the Colebrook-White equation was used to determine the friction factor corresponding to this boundary. Results show a majority of the data points above the boundary line in the fully rough turbulent flow zone.

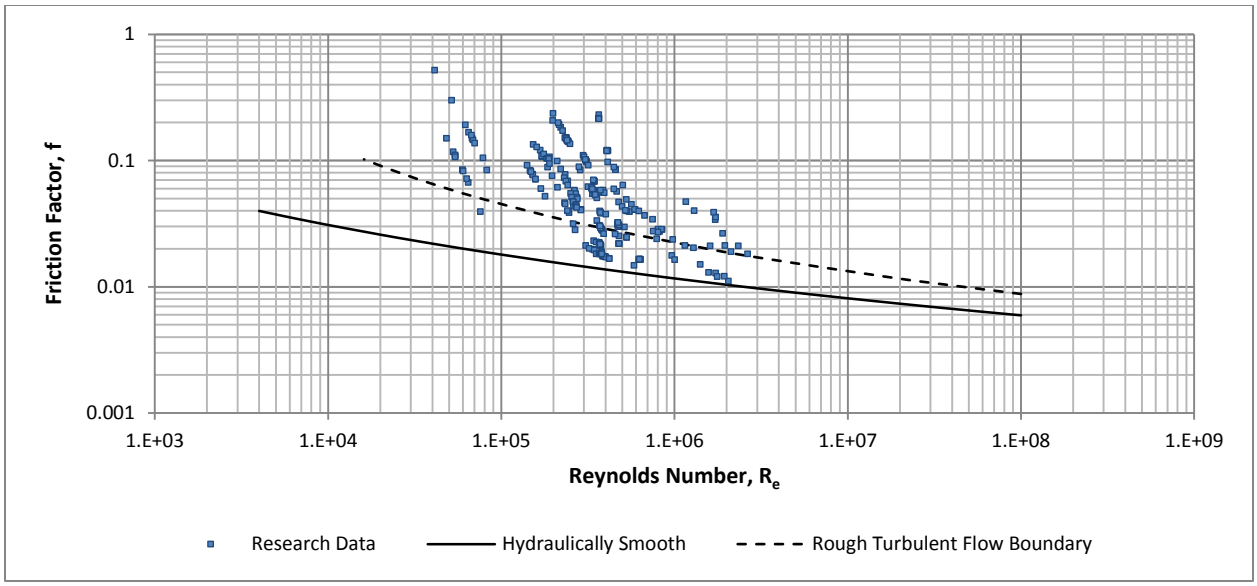

Figure 5.1: Friction factor for Research Data

As shown in Figure 5.2, results were screened by forcemain system to evaluate the change in friction factor for each system since the diameter is constant for each system. Friction factors show a trend of decreasing *f* with increased R_e and are generally grouped together with the exception of Janitell and Big Valley, which are plotted to the left of the main group. Results show that forcemains conveying wastewater do not follow the traditional Moody diagram plot for systems with similar relative roughness (k_s/d).

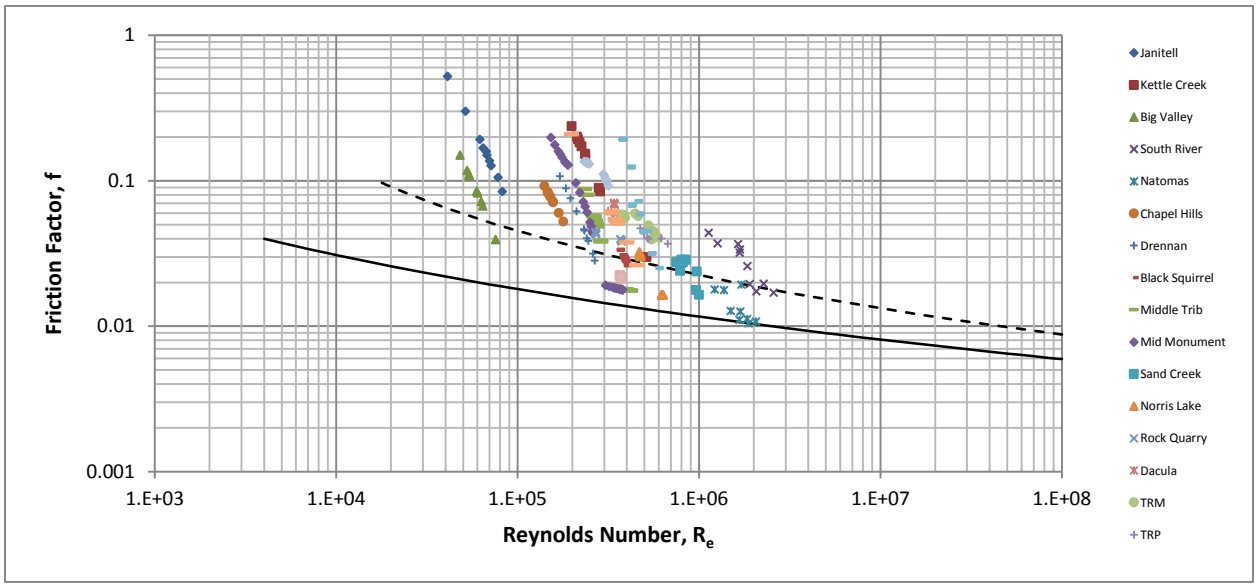

Figure 5.2: Friction factor for Research Data (by Forcemain System)

Friction factors (*f*) calculated for the entire data set are presented by forcemain system in Figure 5.3. Although the results follow a similar trend showing *f* decreasing with increased R_e, the data is primarily clustered into two groups with a R_e value of approximately 1.5E05 as a division line. Steep slopes are associated with the results with several data points approaching the smooth line curve. All data were screened against diameter and material as shown in Figure 5.4 and Figure 5.5, respectively.

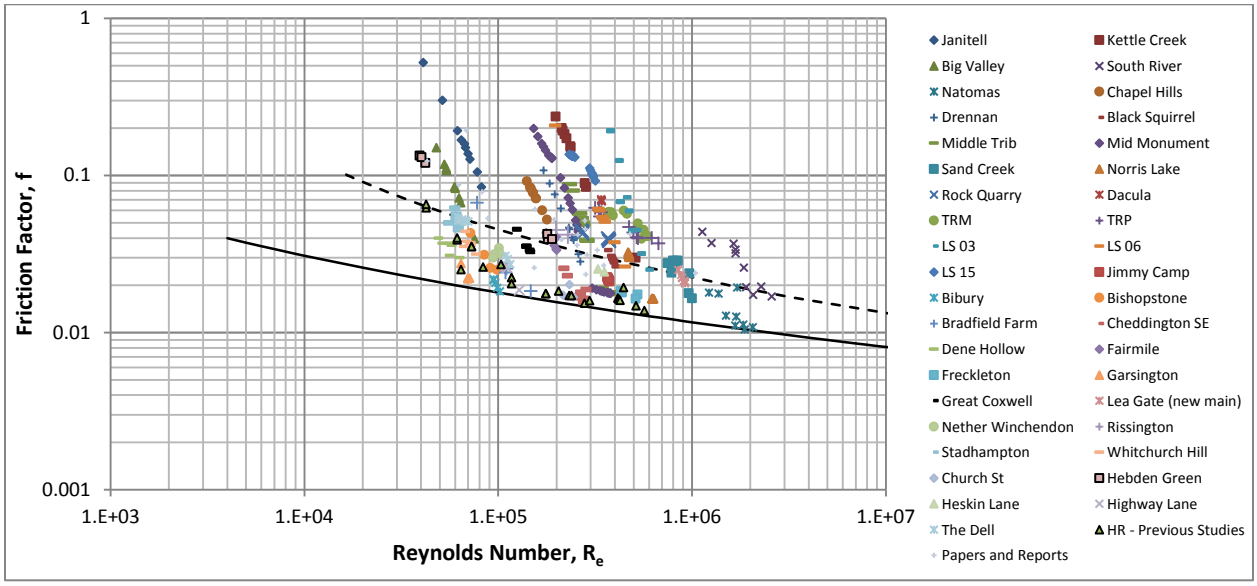

Figure 5.3: Friction factor for All Data (by Forcemain System)

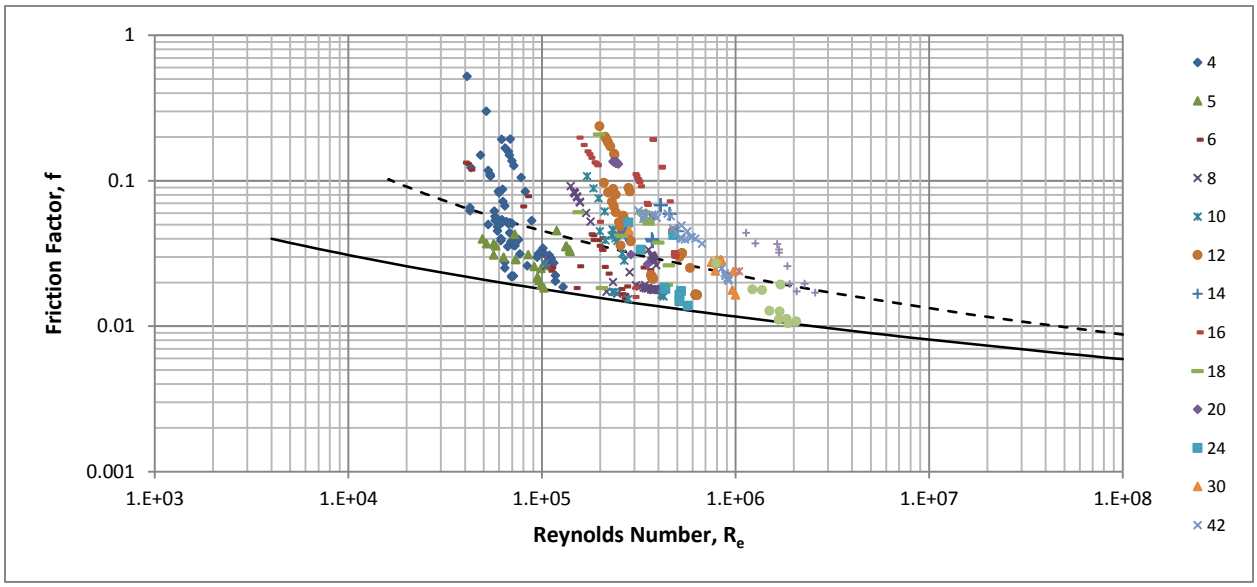

Figure 5.4: Friction factor for All Data (by Pipe Diameter)

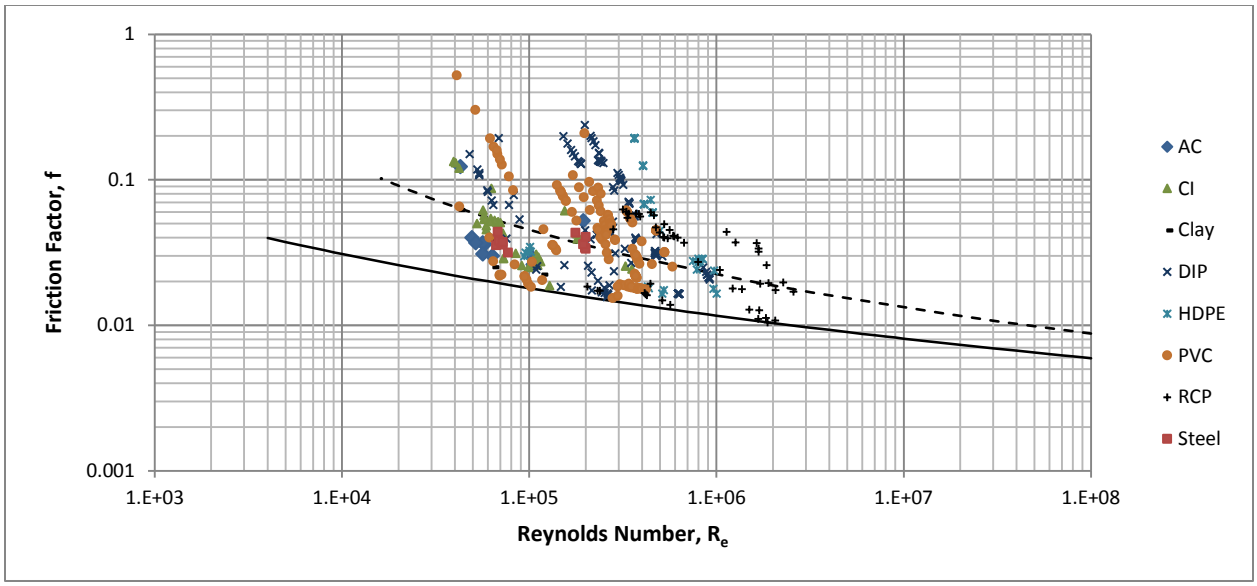

Figure 5.5: Friction factor for All Data (by Pipe Material)

From Figures 5.4 and 5.5, neither the diameter nor the pipe material appear to influence friction factor. The left data cluster shown in Figure 5.4 is composed primarily 4 and 5 in. (101.6 and 127 mm) diameter pipe, with 6 in. (152.4 mm) diameter appearing in both clusters, and diameters larger than 6 in. (152.4 mm) within the right data cluster.

From the Colebrook-White equation, variables influencing friction factor are k_s, D, and R_e. Since R_e is a function of (V, D, ν), where D is constant (for each system), and the kinematic viscosity (ν) was assumed to be constant for each system, then friction factor becomes a function of k_s and velocity. Since the diameter is constant, the sharp reduction in f with increasing R_e indicates a strong influence on velocity. To evaluate this observation, absolute roughness (k_s) was plotted against the corresponding velocity (by forcemain system) as shown in Figure 5.6. The results show that k_s decreases as flow velocity increases for wastewater forcemains, which does not agree with Nikuradse's findings that k_s is fairly uniform (clean water). These results suggest that friction factor and k_s are significantly affected by wastewater biofilms and that k_s is a function of velocity.

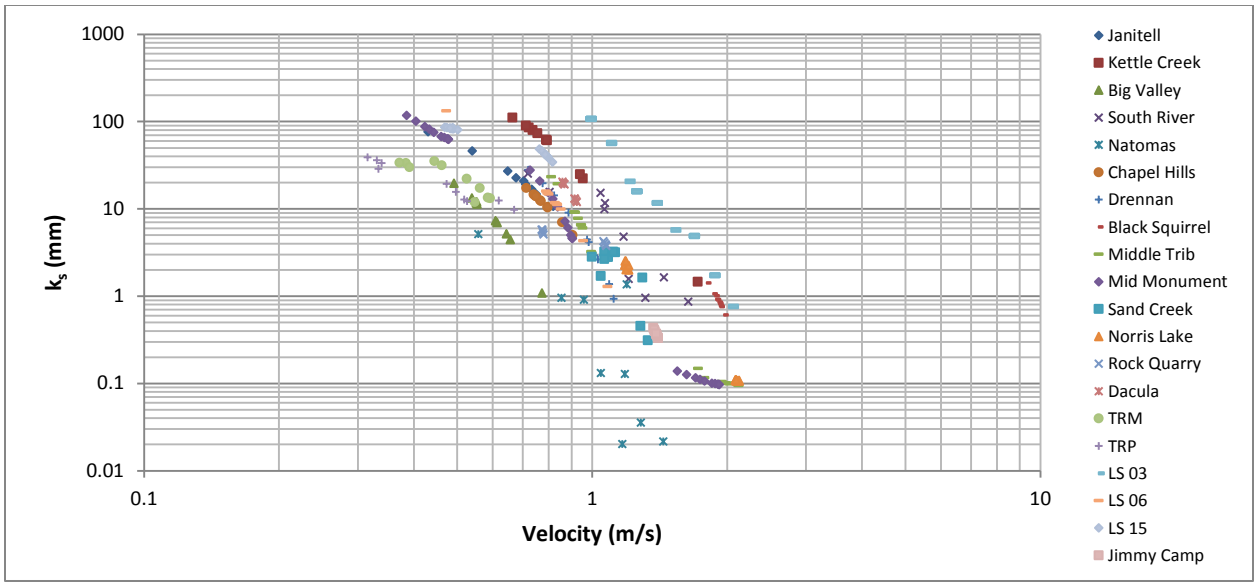

Figure 5.6: k_s versus velocity for Research Data (by Forcemain System)

Figure 5.7 provides a plot of k_s versus velocity for all data. The same trend of decreasing k_s with increasing velocity is observed; however, the additional data sources add a considerable amount of scatter. There appears to be a trend line with additional potential trend lines to the right and left of the core trend line. It is also noted that a majority of lift station / forcemain systems evaluated for this research are operating at velocities less than 1 m/s (3.3 ft/s), below the minimum recommended scour velocity.

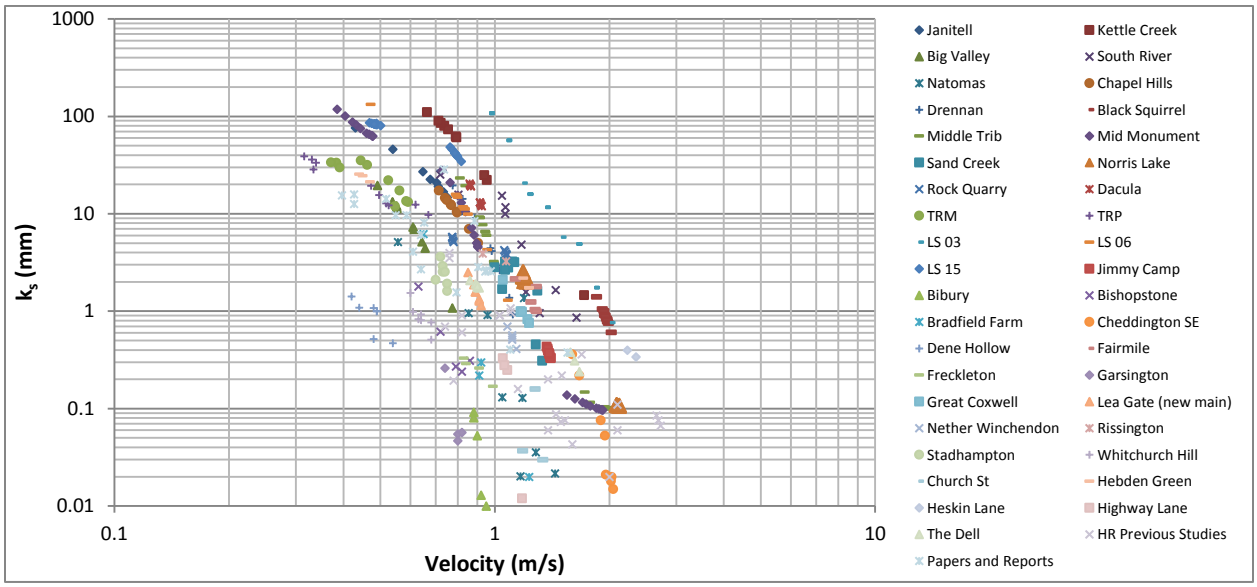

Figure 5.7: k_s versus velocity for All Data (by Forcemain System)

The entire data set was used to quantify the effect of diameter and material on k_s. Figure 5.8 presents the results screened against pipe diameter and Figure 5.9 presents the results screened against pipe material along with typical values of k_s for clean water in new pipe. Results do not indicate any observable trends associated with pipe diameter or material. A majority of the data associated with PVC pipe closely follows the core trend line; however, data for other pipe materials are plotted on either side of the trend line.

As shown in Figure 5.9, a number of data points are approaching the typical k_s value for clean water and new pipe including a few k_s data points plotted below the typical clean water, new pipe k_s value. A majority of the data points approaching the new pipe k_s values and a large portion of the data plotted far left of the core trend line were obtained from Report SR 641. Specific information on these systems were not available. Possible explanations for the variance in results could be that 1) the composition of wastewater in the UK is different than that of the United States, 2) These forcemain systems could be combined wastewater and stormwater systems or have a large volume of clean water reporting to the system, 3) Source water chemistry may have a significant effect on k_s, 4) Sedimentation may be occurring in lower velocity forcemains, or 5) air locking could be occurring within the system. The potential for sedimentation or air locking is presented in Sections 6.1.1 and 6.1.2.

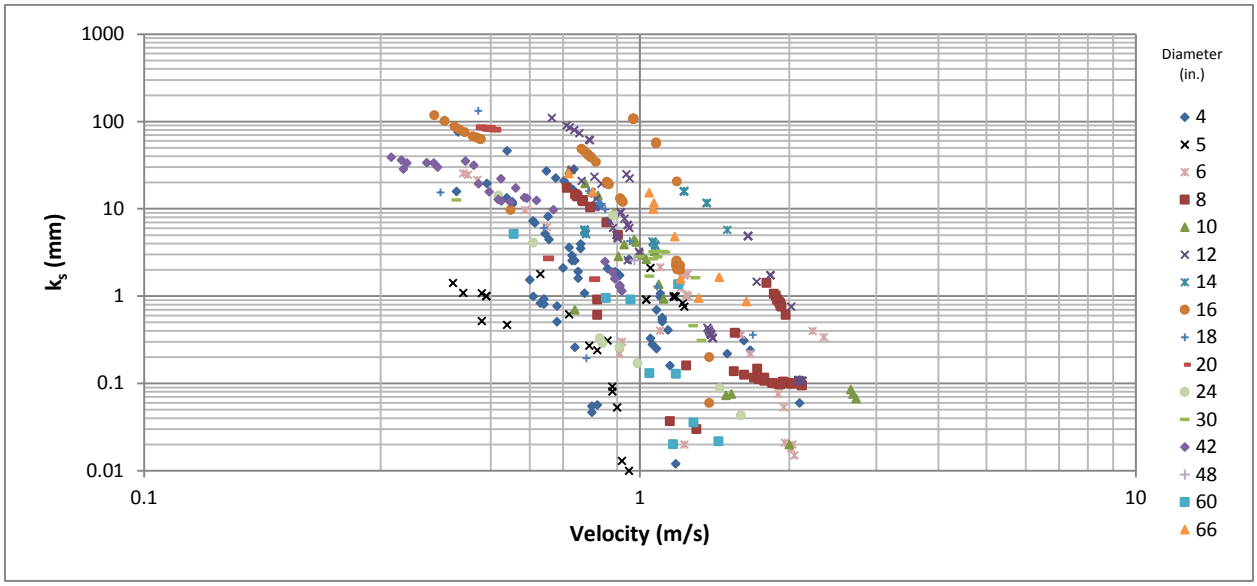

Figure 5.8: k_s versus velocity for All Data (by Pipe Diameter)

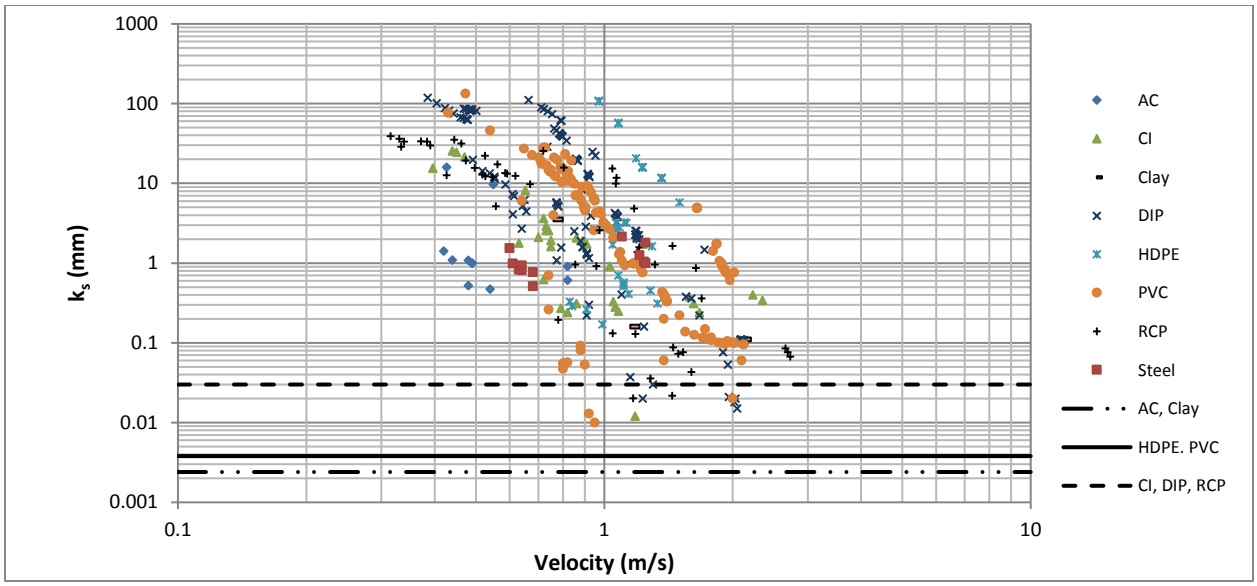

Figure 5.9: k_s versus velocity for All Data (by Pipe Material)

5.2.1.2 C-Factor

As described in Section 2.4, utilization of the Hazen-Williams equation assumes a constant C factor for the calculation of headloss. Larger C factors represent a smoother pipe wall (higher carrying capacity) and smaller C factors describe a hydraulically rougher pipe. From a purely theoretical standpoint, C factor should vary with the flow velocity under turbulent conditions. Equation 2.11 can be used to adjust the C factor for different velocities; however, Walski determined that the effect of this correction is usually minimal with a two-fold velocity increase correlating to an apparent 5% decrease in the roughness factor. This is usually within the error for the roughness estimate; therefore, the C factor is usually held as a constant for systems with constant pipe diameter and material (Walski 1984).

Field data has shown that C factors are not constant with changes in diameter for similar materials. Walski provides typical values of C factors for different pipe material and diameters in *Water Distribution Modelling* (Walski 2001). A summary of the C factors relevant to the current research are provided in Table 5.1.

Table 5.1: Typical C-Factors for New Pipe Carrying Clean Water (Walski 2001)

Type of Pipe	C-Factors for Pipe Diameter				
	3 in.	6 in.	12 in	24 in.	48 in.
Cement Mortar Lined – CI, DIP, Steel	137	142	145	148	148
Asbestos Cement	147	149	150	152	152
HDPE, PVC	147	149	150	152	153
RCP	---	145	147	150	150

C factors calculated from the Research Data Set were plotted against velocity to determine if trends similar to the friction factor and k_s results from the previous section could be identified. Figure 5.10 and Figure 5.11 provide the calculation results of C factor against velocity for the Research Data Set and the entire data set, respectively. Velocity in ft/s was selected since Hazen-Williams is applied predominately in the United States using U.S. Customary Units.

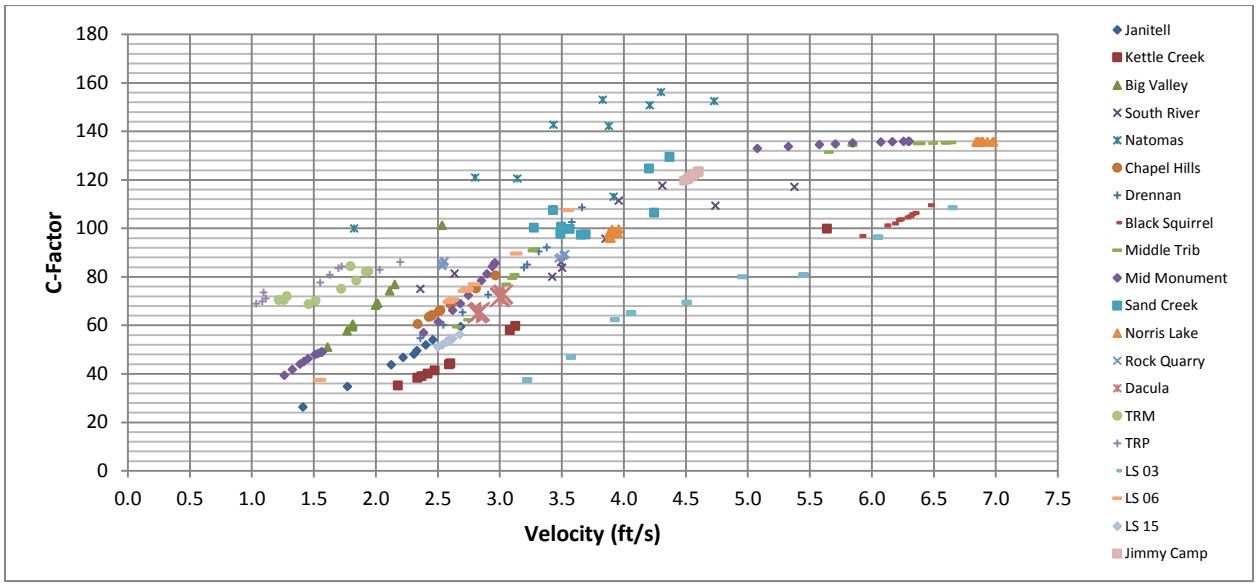

Figure 5.10: C factor versus Velocity for Research Data (by Forcemain)

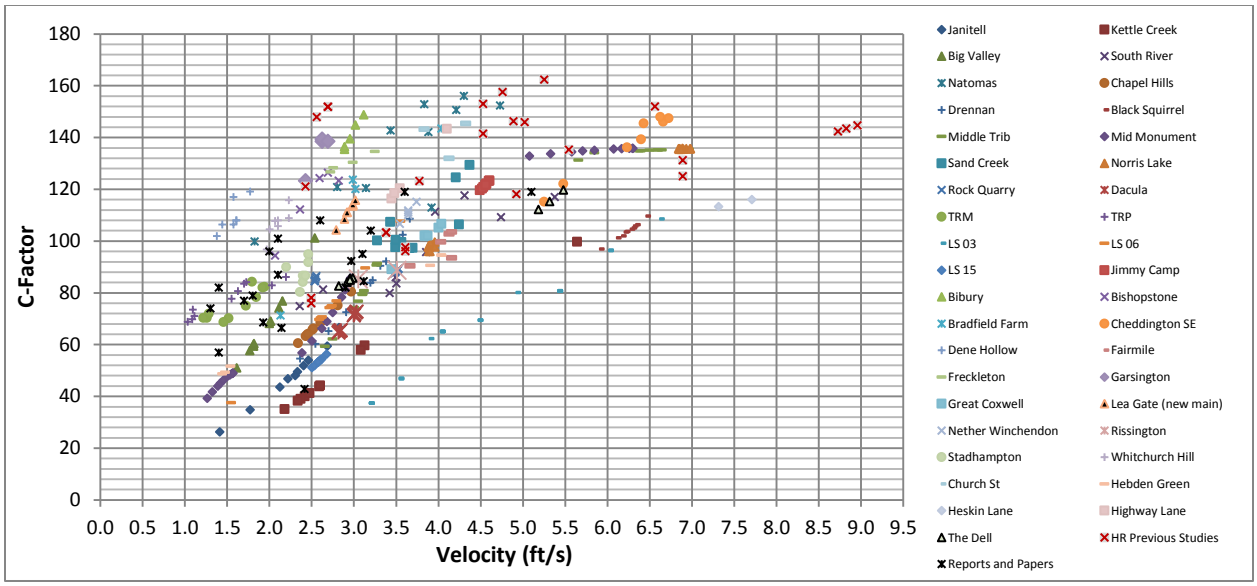

Figure 5.11: C factor versus Velocity for All Data (by Forcemain)

Although the results presented in Figures 5.10 and 5.11 show significant scatter, clear evidence exists that the C factor is a function of velocity with the C factor increasing with increased velocity. A core trend line similar to the k_s findings does exist with a general rise in C factor between velocities ranging between 2.5 ft/s and 4.5 ft/s (0.8 m/s and 1.4 m/s). The slope of the line above 4.5 ft/s (1.4 m/s) appears to stabilize, possibly indicating a potential tendency towards its clean water C factor. If this is the case, then the biofilm layer may be shearing from the pipe wall, resulting in increased hydraulic efficiency. The chart also shows two distinct trend lines located both to the left and right of the core trend line. Several factors could influence these results including pipe material, diameter, sedimentation, air buildup in the pipeline, or even the profile of the pipeline.

C factor results were screened against pipe material and diameter. Figure 5.12 presents the results screened against pipe diameter. Figure 5.13 shows the results screened against pipe material along with the average clean water C factor for the pipe materials related to this research. Average C factors were obtained from Table 2.6 and were shown to determine if the calculated C factors were trending towards the clean water C factor at higher velocities.

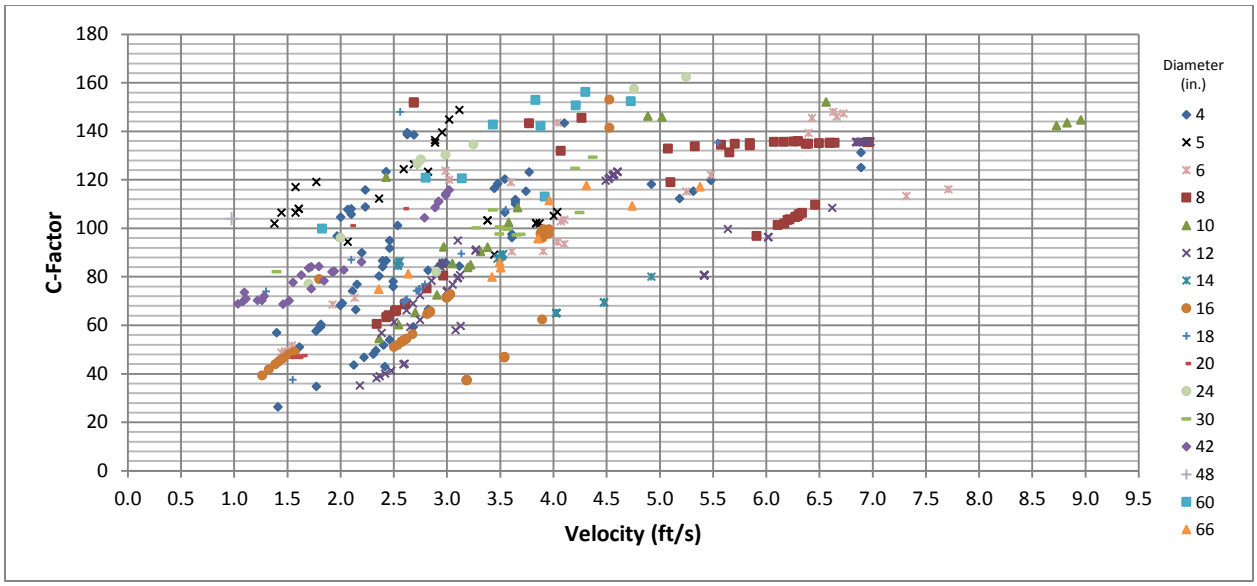

Figure 5.12: C factor versus Velocity for All Data (by Diameter)

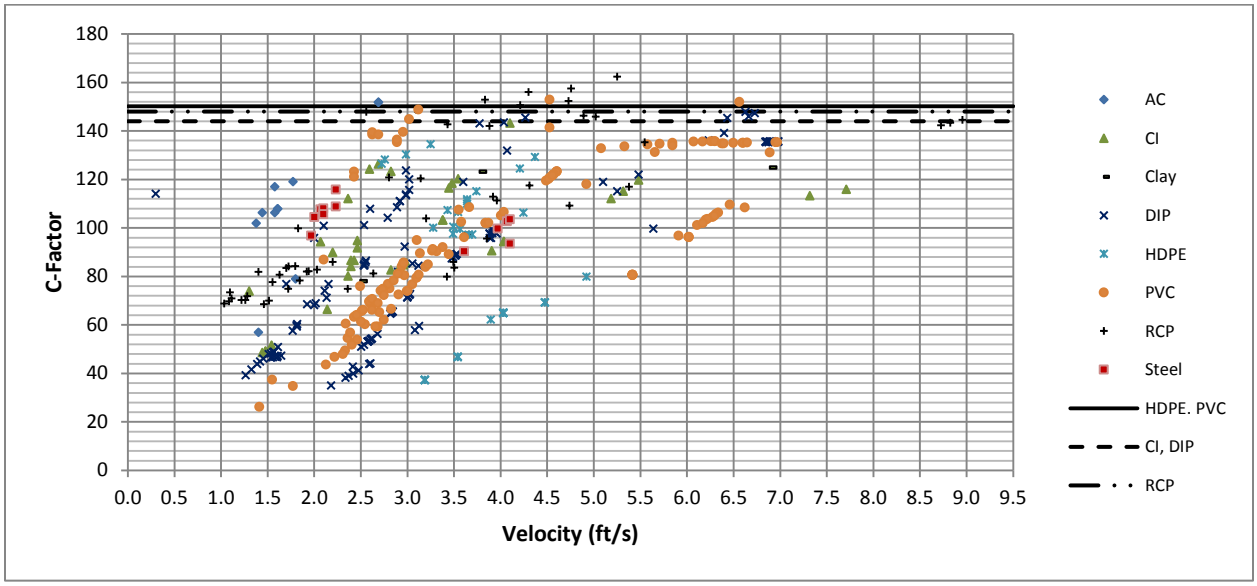

Figure 5.13: C factor versus Velocity for All Data (by Material)

Results show that C factor is not significantly affected by diameter. The results suggest a dominate trendline associated with PVC pipe; however, other pipe materials are located on both sides of this trend line. These results seem to indicate that neither diameter nor material affect the C factor and that velocity is the dominant factor for determining C factor.

In practice, C factors less than 80 are considered to be unreliable for clean water systems; however, the C factors presented in the figures above were determined from operational data and published research.

Results show that approximately 60% of forcemain systems evaluated are operating at C factors less than 100. If the original design assumed higher C factors, then the pumps are likely operating to the left of the design point which requires a longer pump runtime and increased power utilization during a pumping cycle. These items are evaluated in more detail in Section 6.2.

Since the results presented above indicate C factor is primarily a function of velocity, and that material nor diameter appear to affect the C factor, the calculated C factor results for LS 03 are presented in Figure 5.14. LS 03 was selected because the system utilizes three different pipe interior diameters (14 in., 15.75 in. and 12.08 in.) and materials (HDPE and PVC) in series. Results were determined using the Macro described in Section 3.5 and show a direct relationship between velocity and C factor.

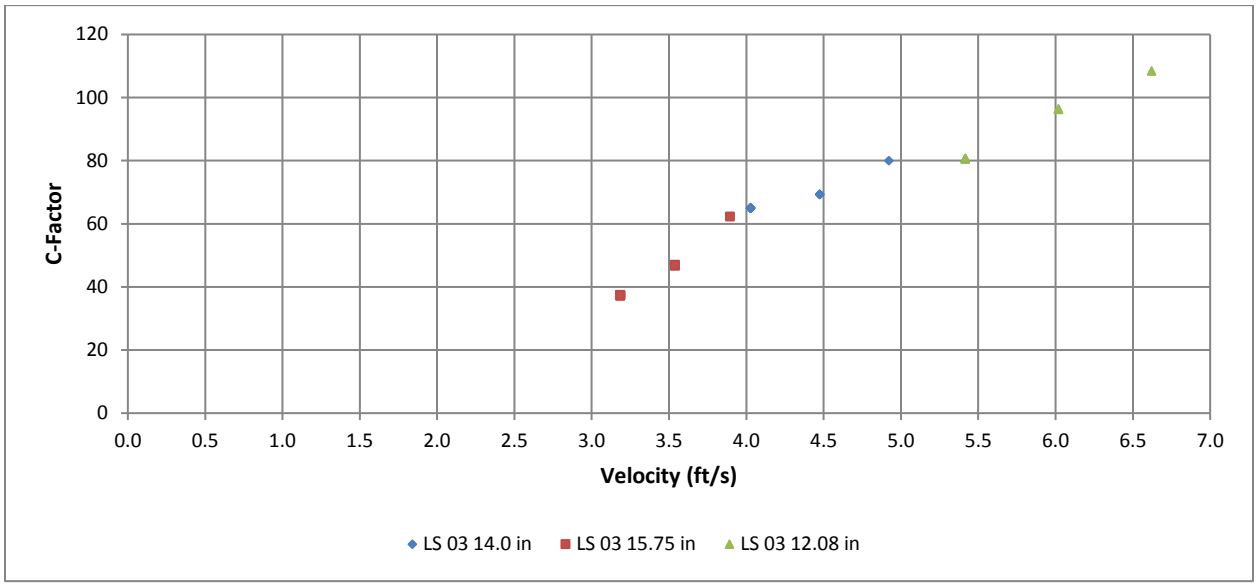

Figure 5.14: C factor versus Velocity for LS 03 (by Pipe Interior Diameter)

5.2.2 Effect of Pipe Age

Results were screened against pipe age to determine if pipe age influences k_s and C factor. Pipe age was only available for the Research Data set. Figure 5.15 presents k_s versus velocity and Figure 5.16 shows C factor versus velocity, both screened against pipe age. From the figures, pipe age does not appear to influence the roughness parameters, confirming that velocity is the dominant factor for wastewater forcemains.

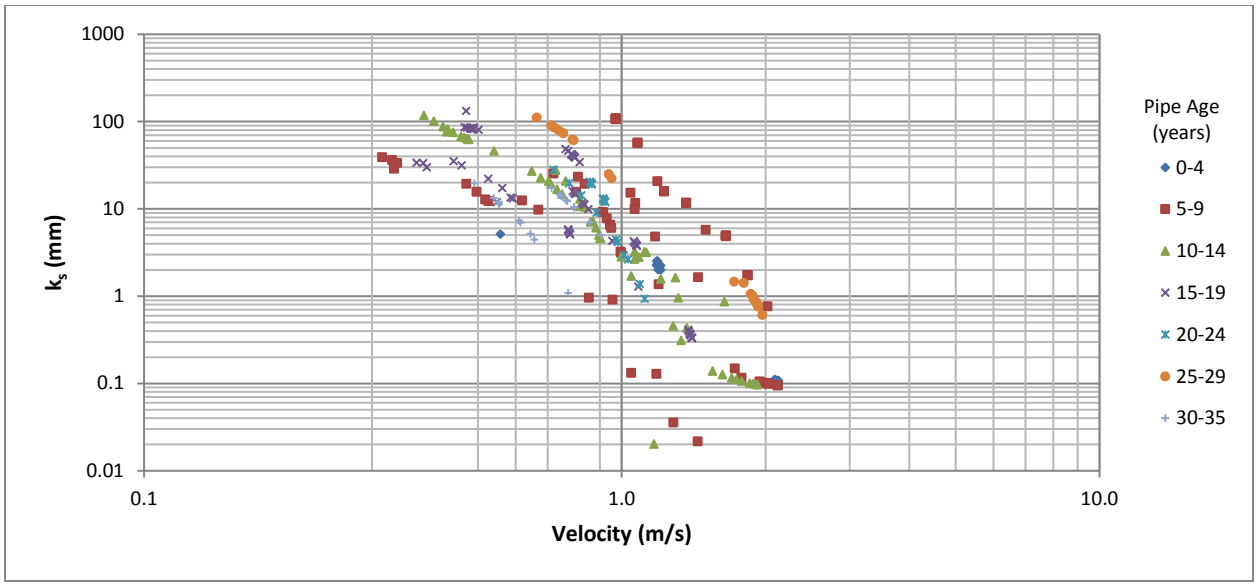

Figure 5.15: k_s versus Velocity for Research Data (by Pipe Age in Years)

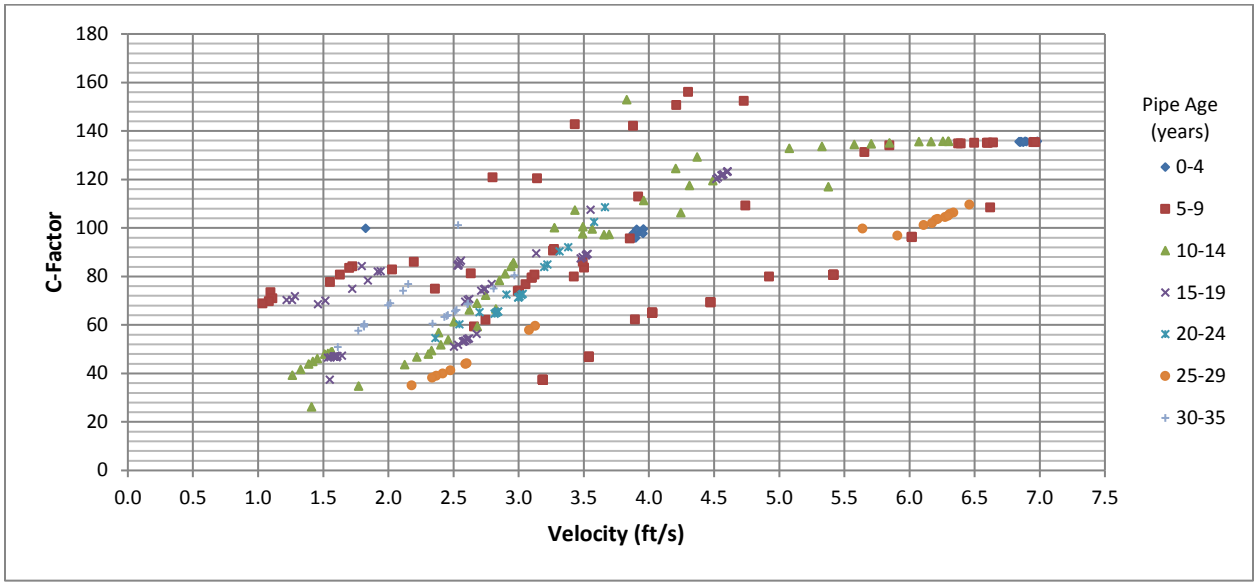

Figure 5.16: C factor versus Velocity for Research Data (by Pipe Age in Years)

5.2.3 Effect of Biofilms on Pipeline Hydraulics

The traditional approach of adopting the Colebrook-White equation to simulate pipeline hydraulics has been proven to be inadequate in evaluating the frictional resistance of biofouled pipelines (Schultz 2000; Schultz and Swain 1999; Barton 2006; Lambert et al. 2009; Cowle 2015). However, under certain situations this is proven not to be the case, namely at the polar extremes of the Moody diagram (i.e. very

low and very high flow), where traditional approaches are valid irrespective of the presence of a biofilm (Picologlou et al. 1980; Lambert et al. 2009; Cowle 2015). Lambert et al. (2009) documented that a 25 mm (1 in.) diameter biofouled pipe followed a smooth pipe law frictional relationship at $R_e < 5x10^3$. This is attributable to the larger boundary layer associated with such conditions and thus the onset of hydraulically smooth flow. Similarly, at the other extreme, high detachment inducing shear forces are likely to limit the extent of biofilm growth. Such situations are generally uncommon within most forcemains (Cowle 2015),

Therefore, traditional practices can lead to under- or over- estimated pipeline flow capacities, which result in unforeseen efficiency issues. For example, if the flow capacity of a pipeline is underestimated (i.e. undersized), it may fail to achieve the design velocity required for self-cleansing and as a result, the likelihood of future fouling and fouling issues will increase. Furthermore, if a pipeline is oversized (i.e. overestimated) it could add unnecessarily to the cost of the project, both financially and environmentally (i.e. in terms of the projects carbon footprint) (Cowle et al. 2012).

Velocity profiles in biofouled pipelines were first investigated by Lambert (2009) using raw water and also by Cowle (2015) using a synthetic wastewater. Lambert plotted the theoretical velocity profile by using the Nikuradse (1933) formula for artificial rough pipe presented in Equation 5.1.

$$\frac{u}{u_*} = \frac{1}{k} ln \frac{y}{k_s} + B \tag{5.1}$$

Where u is the velocity at distance y from the wall; u_* is the friction or shear velocity (Equation 3.7); k_s is absolute roughness; and B is the Nikuradse roughness function (generally taken as 8.48 for conventional surfaces). Theoretical velocity profiles along with Lambert's (2009) biofouled pipe data are shown in Figure 5.17.

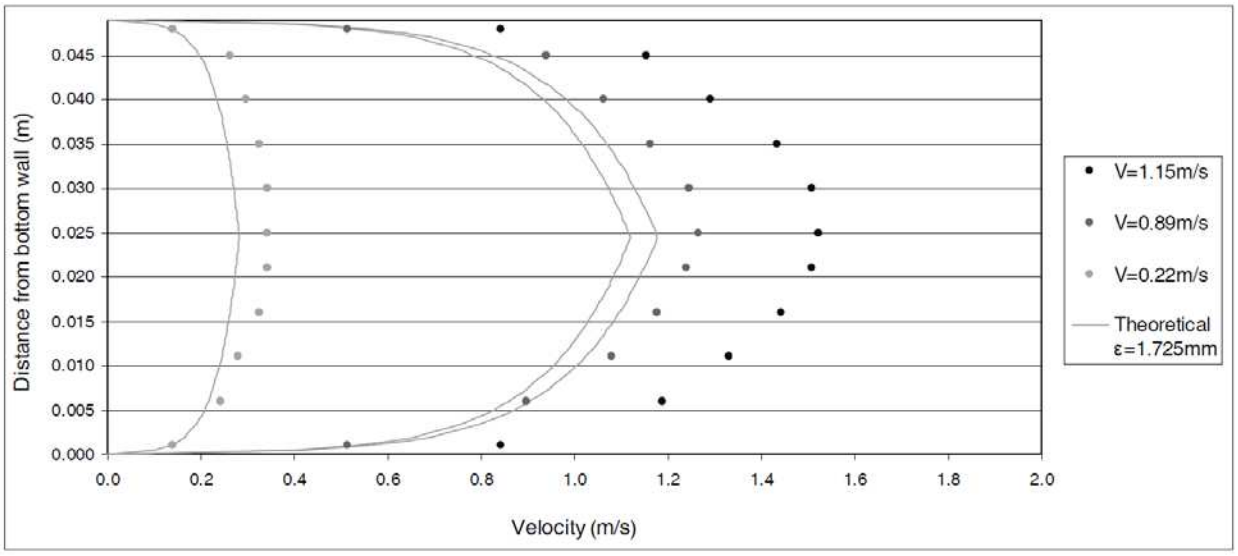

Figure 5.17: Expected Velocity Profiles k_s = 1.725 mm (Lambert et al. 2009)

Lambert et al. (2009) determined that the von Kármán constant of biofouled surfaces was non-universal and lower than the conventional value of $\kappa = 0.40$. From Figure 5.17, the theoretical velocities near the center of the pipe were too low and too high near the pipe walls. Lambert (2009) utilized linear regression to determine the κ and B values to match the measured data and are presented in Table 5.2.

Table 5.2: Values of κ and B for observed velocity profiles (Lambert et al. 2009)

Velocity Profile (m/s)	κ	B
1.15	0.3569	12.25
0.89	0.3106	8.85
0.22	0.2821	9.6

Results show that the von Kármán constant is significantly lower in the biofouled pipe than the 0.40 generally accepted for pipes. In addition, the results also show that both κ and B decrease with increasing velocity. This suggests that the equations used to calculate and predict headloss in pipes such as the Colebrook-White, which assume $\kappa = 0.40$, are not valid for biofouled pipes (Lambert et al. 2009). Figure 5.18 shows that the velocity profiles using the above variable values of k and B closely match the measured data.

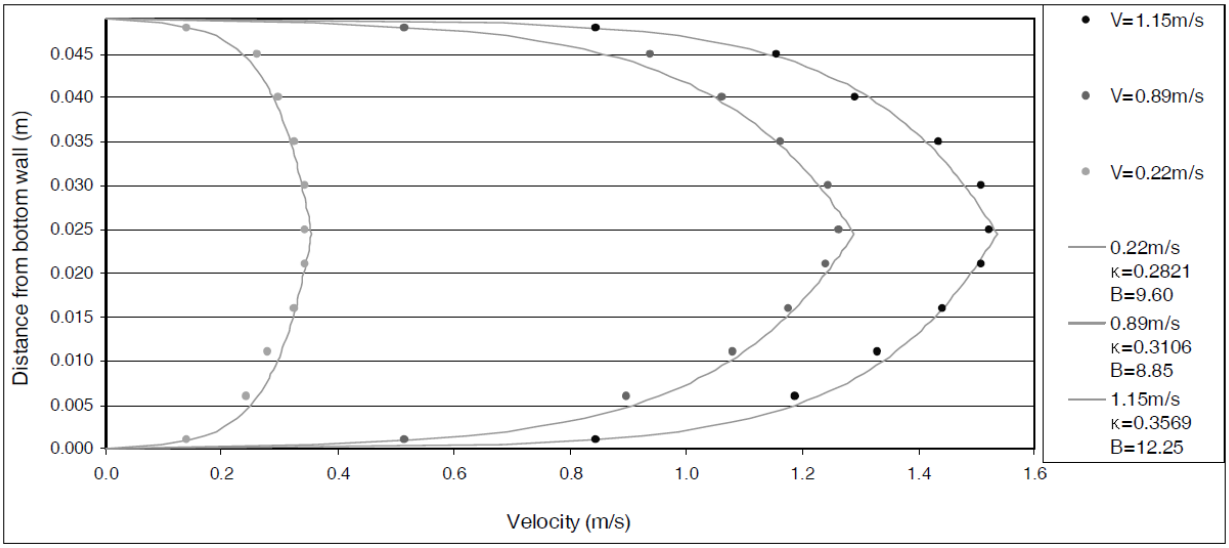

Figure 5.18: Observed and theoretical velocity profiles using κ, B found by linear regression (Lambert et al. 2009)

Cowle assumed the typical von Kármán constant was 0.42; most literature identifies this value as 0.40. Lambert et al. (2009) expressed the non-universal κ as a function of R_e and was confirmed by Cowle (2015) using a synthetic wastewater. Both relationships are presented in Equations 5.2 and 5.3, and Figure 5.19:

$$\kappa=1.00\times10^{-6}R_e+0.26 \quad \text{(Lambert)} \tag{5.2}$$

$$\kappa=9.443\times10^{-7}R_e+0.302 \quad \text{(Cowle)} \tag{5.3}$$

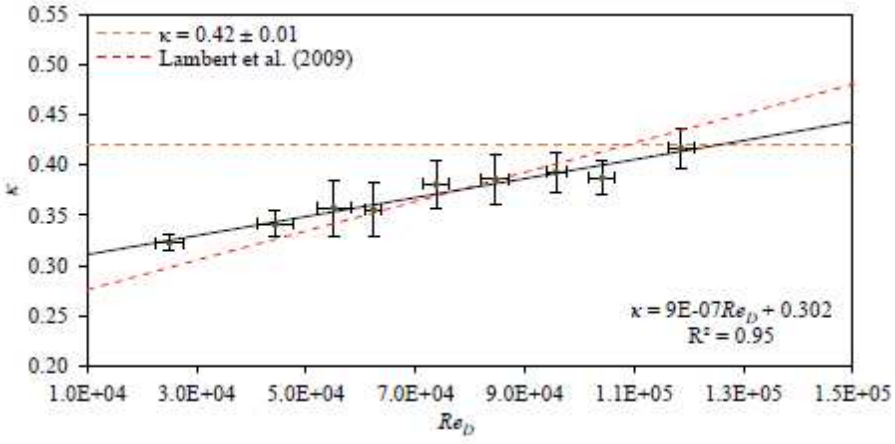

Figure 5.19: Influence of R_e on κ for the combined data from $R_e = 5.98\text{x}10^4$ to $1.00\text{x}10^5$ (Cowle 2015)

Cowle (2015) determined that B also varied linearly with R_e as shown in Equation 5.4.

$$B = -1.964 \times 10^{-5} R_e + 6.001 \tag{5.4}$$

The Colebrook-White equation was derived from a logarithmic velocity distribution (Matthew 1990; Lambert et al. 2009; Cowle 2015) based upon the universal κ. The von Kármán constant is integrated in to the logarithmic multiplier, which is traditionally given as either -0.88 or -2.00 determining the logarithmic form of the equation (Cowle 2015). Using the Colebrook-White equation (Equation 2.5a) along with the experimental observations, Lambert et al. (2009) determined that Equation 2.5a overestimated the value of k_s when applied to biofouled pipes. To correct this error Lambert (2009) altered the dimensionless constant multiplier for *D* from 3.70 to 0.85. The modified Colebrook-White equation proposed by Lambert et al. (2009) is presented as Equation 5.5.

$$\frac{1}{\sqrt{f}} = -\frac{1}{\sqrt{8}k} \ln\left(\frac{k_s}{0.85D} + \frac{2.51}{R_e\sqrt{f}}\right) \tag{5.5}$$

Lambert (2009) applied the modified Colebrook-White equation curves to the observed data from both the River Murray and Myponga systems evaluated by Lambert. Both systems included 50 mm (1 in.) and 25 mm (2 in.) diameter pipes with biofilms grown at 0.3 m/s for 600 hours. Biofilms on both pipes for each system were grown at the same velocity and should be expected to produce a similar trend in κ (Lambert et al 2009). Results are presented in Figures 5.20 and 5.21 and show the modified Colebrook-White curve is in good agreement with the rising limb of the friction factor data until the critical shear is reached. Lambert et al. (2009) indicated that on the limited evidence, the modified Colebrook-White equation may be a start at understanding how biofilms grown under the same velocity behave when the flow conditions are varied. More research will be required to measure velocity profiles in biofouled pipes with various source waters, diameters, and velocities, to determine if a common trend in κ holds between them.

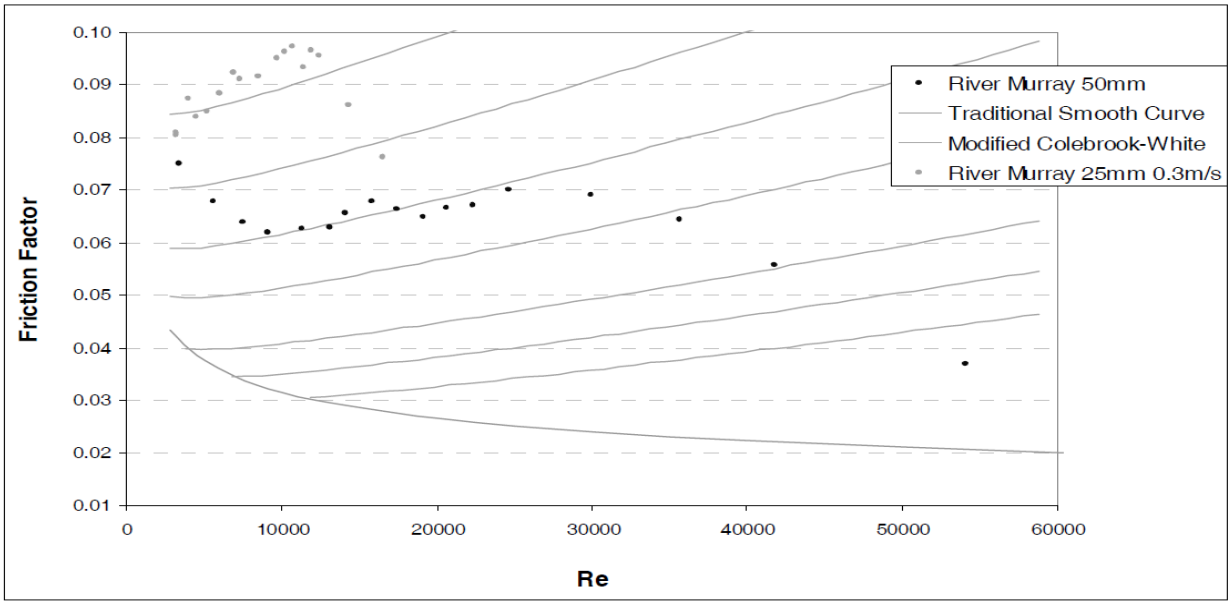

Figure 5.20: Modified Colebrook-White curves with observed River Murray data (Lambert et al. 2009)

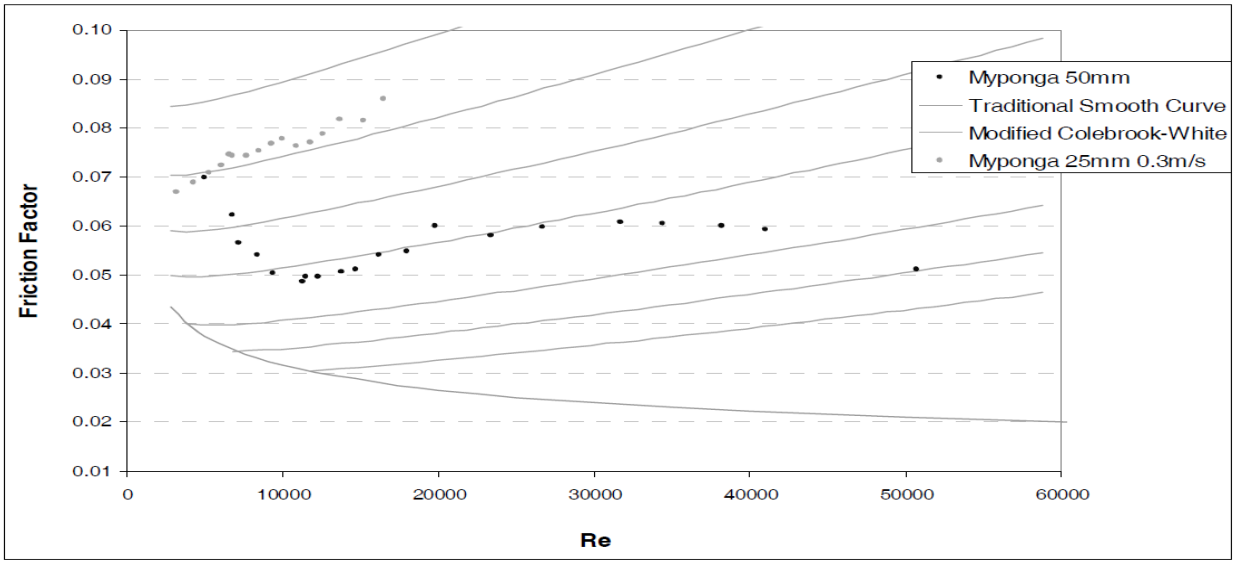

Figure 5.21: Modified Colebrook-White curves with observed Myponga data (Lambert et al. 2009)

Cowle (2015) performed a similar experiment incubating a synthetic wastewater within in a 0.10 m (4 in.) diameter HDPE pipe for approximately 450 hours at Reynolds Numbers of 5.98×10^4 (V=0.58 m/s), 7.82×10^4 (V=0.76 m/s), and 1.00×10^5 (V=0.96 m/s). Figures 5.22 and 5.23 show the modified Colebrook-White curves along with the observed data for Reynolds Number test cases of 5.98×10^4 and 1.00×10^5; where λ = friction factor, *f*.

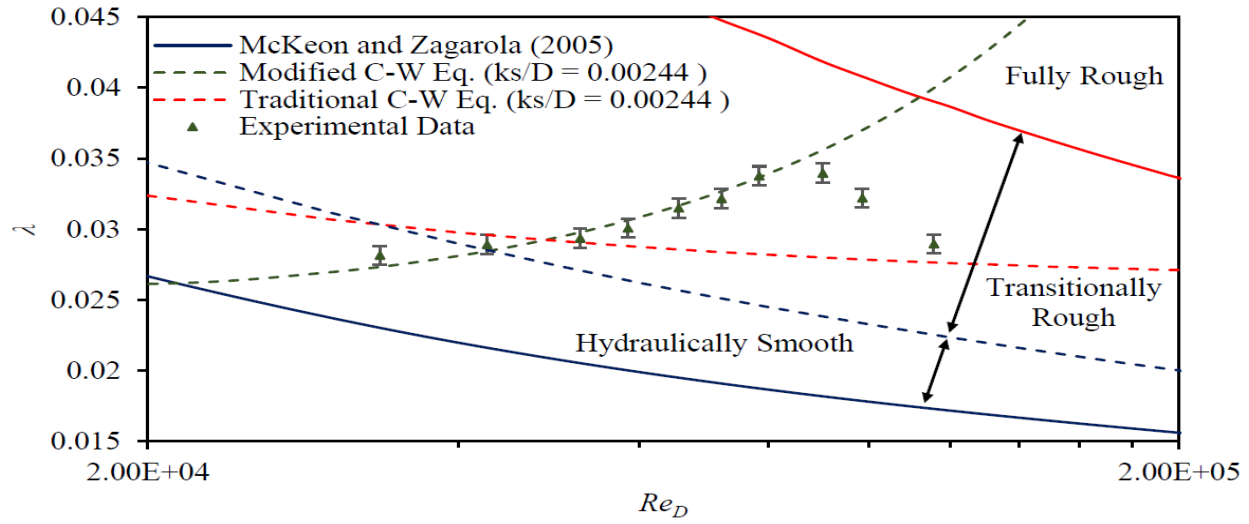

Figure 5.22: Modified Colebrook-White curves with observed data for the biofilm incubated at R_e = $5.98x10^4$ (Cowle 2015)

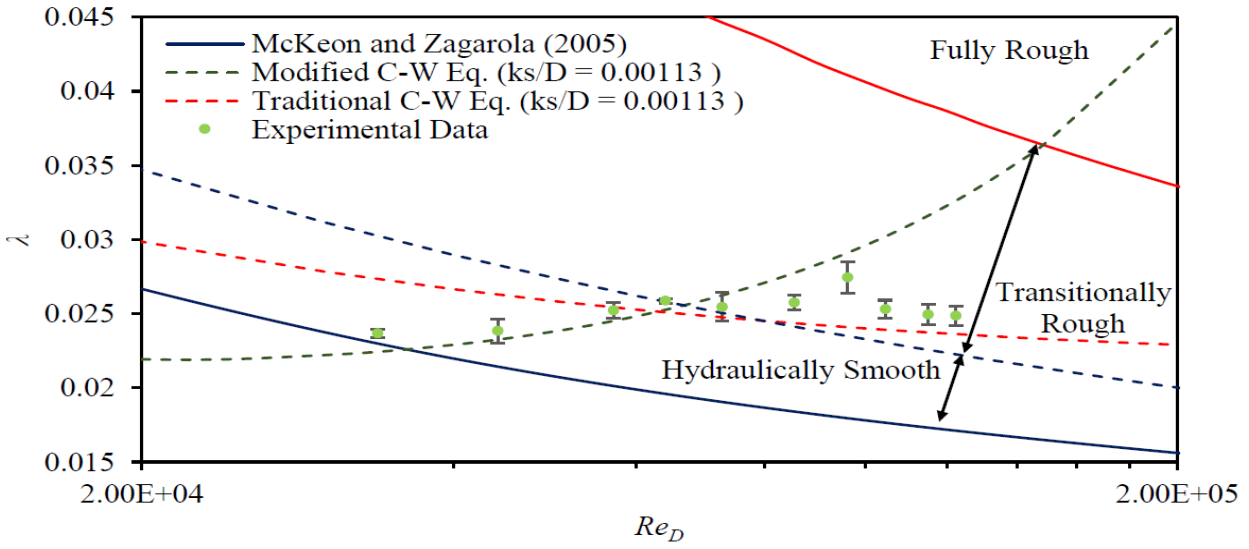

Figure 5.23: Modified Colebrook-White curves with observed data for the biofilm incubated at R_e = $1.00x10^5$ (Cowle 2015)

Figures 5.22 and 5.23 show that the modified Colebrook-White curve is in good agreement with the rising limb of the friction factor data until critical shear is achieved. Cowle (2015) determined that the friction data is independent from the mean-velocity data and supports a non-universal κ, and in particular, the data is in agreement of the values of κ determined from R_e using Equation 5.3.

The observed drop in friction factor is due to the biofilm shearing from the pipe wall at these higher velocities. Only the biofilms grown at 0.3 m/s (1 ft/s) were sheared off at the range of velocities tested;

suggesting these biofilms had lower strength than those grown at higher velocities. Although the biofilms sheared off at different velocities in the two 0.3 m/s (1 ft/s) growth velocity pipes, the pipe wall shear stresses at which this occurred were calculated to be nearly identical, at 3.0 N/m^2 (Lambert et al. 2009).

It should be noted that Lambert et al. (2009) and Cowle (2015) assessed a relatively small range of environmental and hydrodynamic conditions including 25 mm, 50 mm, and 100 mm diameter pipes; with biofilms incubated at velocities of 0.22 m/s, 0.89 m/s, and 1.15 m/s (Lambert et al. 2009) and 0.58 m/s, 0.76 m/s, and 0.96 m/s (Cowle 2015). Since the roughness characteristics of biofilms are highly dependent upon the hydrodynamic conditions they are subjected to, further experimentation is required to confirm the validity or obtain a refined equation for use under a range of environmental conditions and flow regimes (Lambert et al. 2009). Results also show that the pipeline velocity during incubation has the greatest effect on friction factor. As expected, the critical shear is different for each system and is dependent on the pipe velocity during incubation. The results presented by Lambert and Cowle Indicate that biofouling affects the structure of turbulent flow in similar ways despite utilizing different types of water.

Equation 5.3 along with Equation 5.5 (Modified Colebrook-White equation) were applied to the Research dataset to identify data subjected to lower Reynolds Numbers and to quantify the change in k_s using the Modified Colebrook-White equation. Considering that κ varies with R_e, the calculated values for k_s were plotted against velocity along with data points found to have values of $\kappa < 0.4$ Figure 5.24 presents the results screened by system with data points associated with $\kappa < 0.4$ identified with a circle around the data point. Figure 5.25 shows the results for k_s versus velocity by data source and Figure 5.26 provides the results screened by diameter.

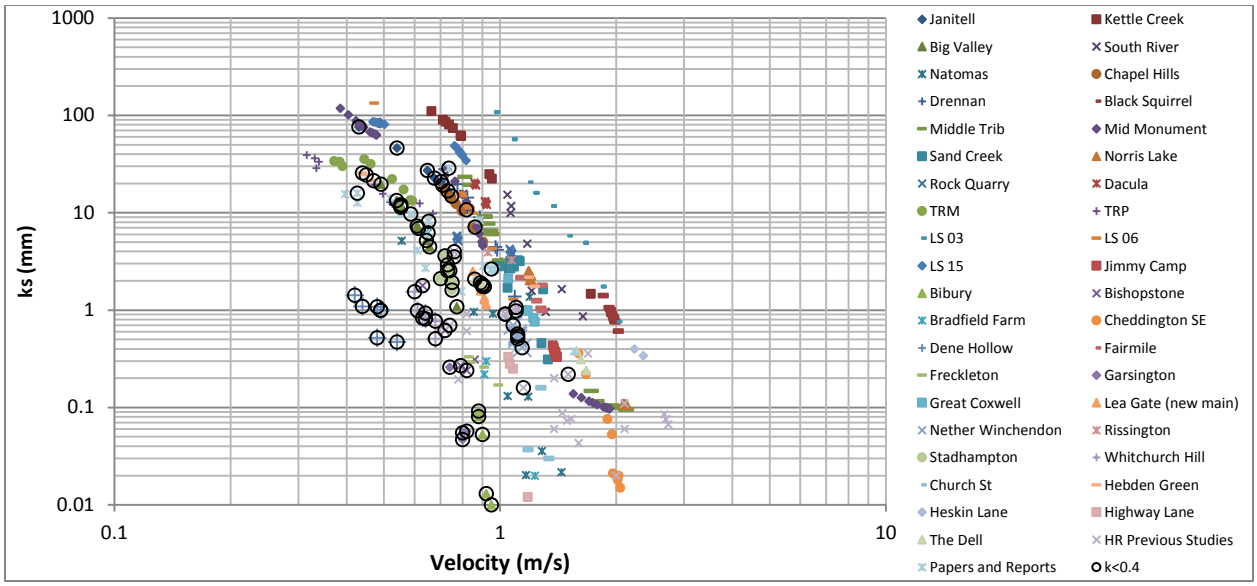

Figure 5.24: k_s vs Velocity (by System)

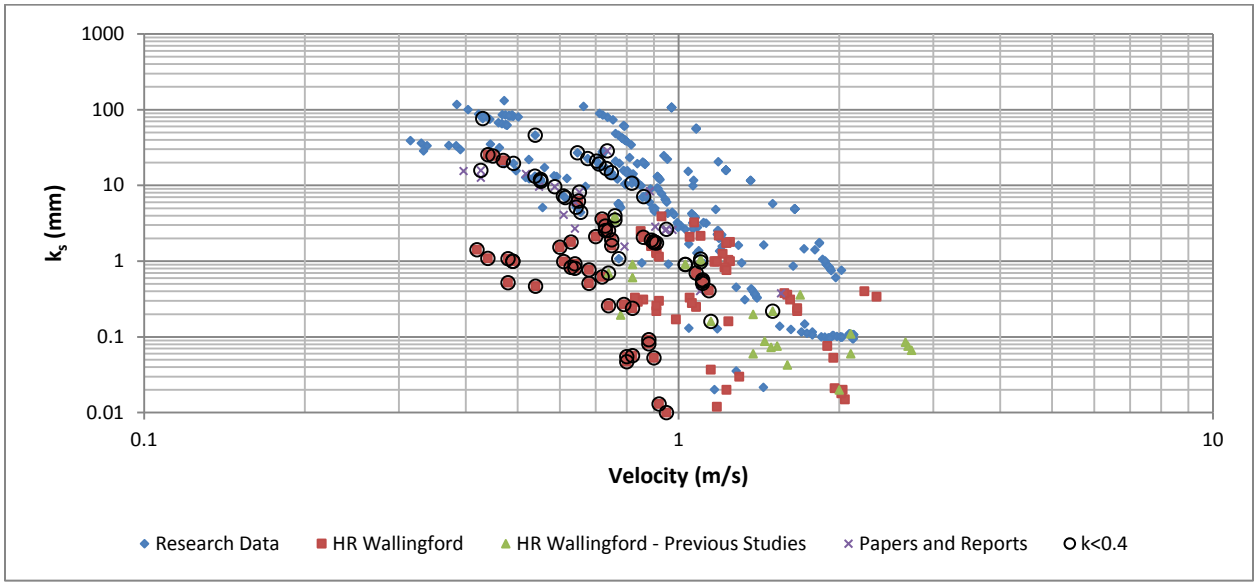

Figure 5.25: k_s vs Velocity (by Data Source)

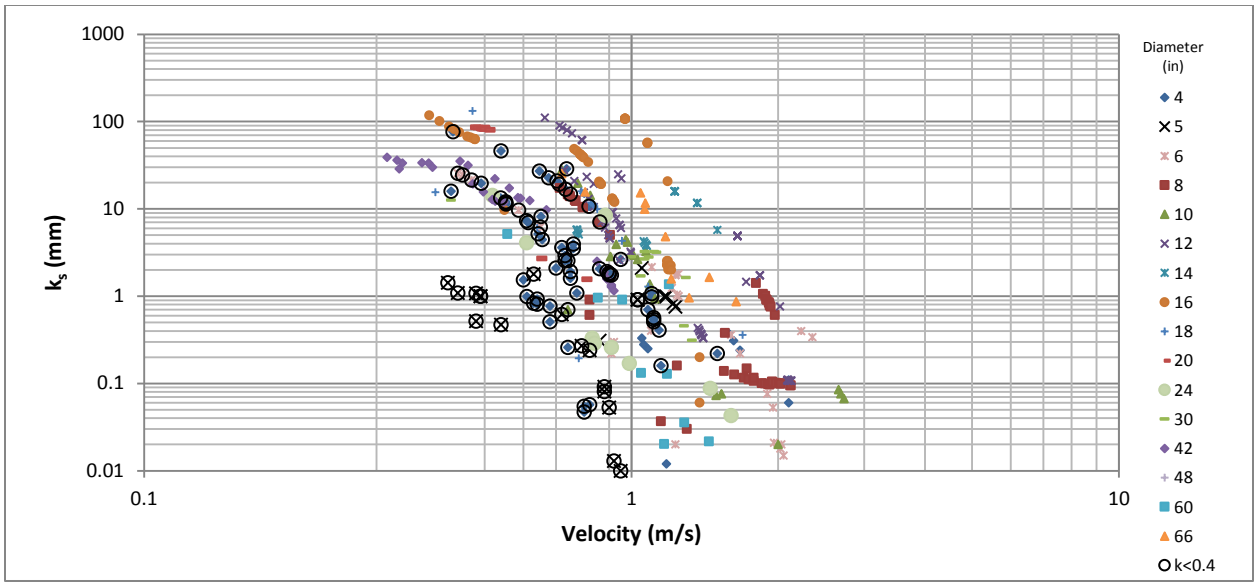

Figure 5.26: k_s vs Velocity (by Diameter (inches))

As shown in Figure 5.25, a majority of the data points where $\kappa < 0.4$ are part of the HR Wallingford data set. As expected, data points corresponding to $\kappa < 0.4$ were found for diameters less than 8 in. (203.2 mm) (Figure 5.26) since smaller diameters tend to promote lower R_e. Values for k_s calculated from the Colebrook-White equation along with the corresponding k_s calculated from the modified Colebrook-White Equation are presented in Figure 5.27. The change in k_s resulting from the two equations is shown in Figure 5.28, the data for Hebden Green and LS 15 are not shown because the modified k_s value for these systems decreased more than 10 mm and the chart was truncated for clarity of the remaining results.

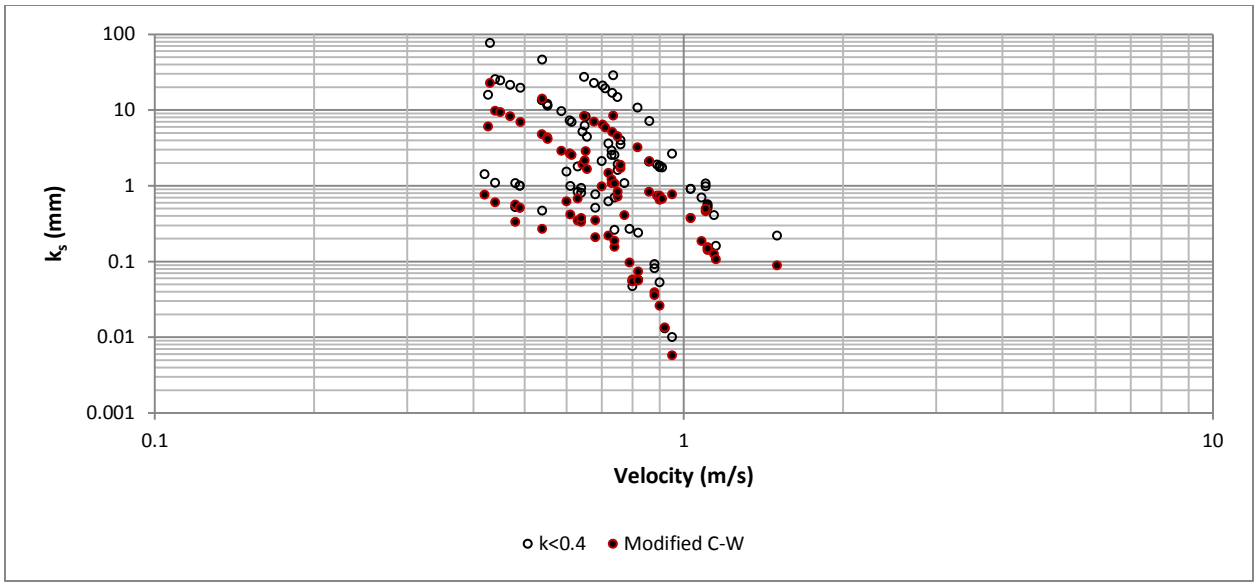

Figure 5.27: k_s vs Velocity Comparing the Influence of Modified Colebrook-White Equation

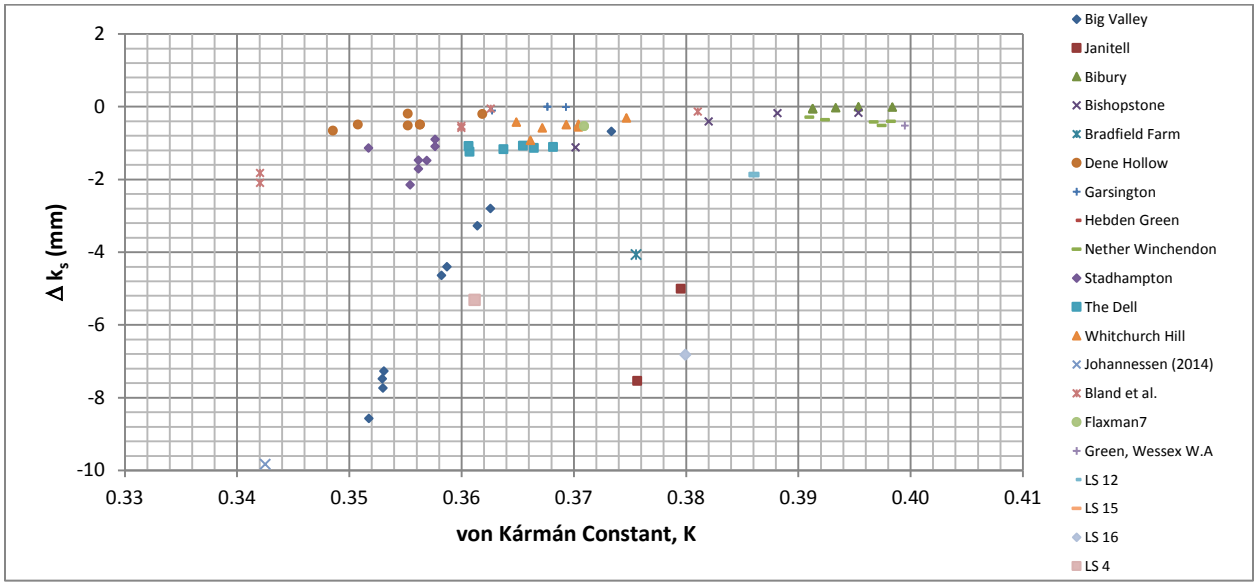

Figure 5.28: Difference in k_s from Colebrook-White Equation compared to Modified Colebrook-White (by System)

In principle, Equation 5.5 is recommended for use in simulating pipelines at the pseudo-equilibrium biofouling stage. However, the equation assumes that k_s is a constant value. Section 5.2.1.1 demonstrated that k_s appears to be a function of velocity for wastewater forcemains.

From Equation 5.3, the Reynolds Number corresponding to κ=0.4 is approximately 1.04×10^5. From the results presented above, it is assumed that the friction factor can be calculated from the standard

Colebrook-White equation when $R_e \geq 1.04x10^5$. Therefore, a Reynolds Number of $1.04x10^5$ was used to determine the forcemain velocity where the standard form of the Colebrook-White equation could be applied considering that the minimum recommended forcemain diameter is 4 in. (101.6 mm). Standard wastewater was assumed to be approximately 70°F (21.1°C); therefore, the velocity was computed for water temperatures 65°F (18.3°C), 70°F (21.1°C) and 75°F (23.9°C) to evaluate the variance in velocities required to maintain the equivalent R_e. Results are presented in Figure 5.29 and show that a velocity of approximately 3.2 ft/s is required for a 4 in. (101.6 mm) diameter pipe; the velocity decreases sharply until a diameter of approximately 20 in. (508 mm). As one would expect, larger velocities are required for a smaller diameters to maintain the equivalent Reynolds Number because the hydraulic radius is smaller. The effect of ±5 °F provides approximately a ±7% change in required velocity to maintain the threshold R_e.

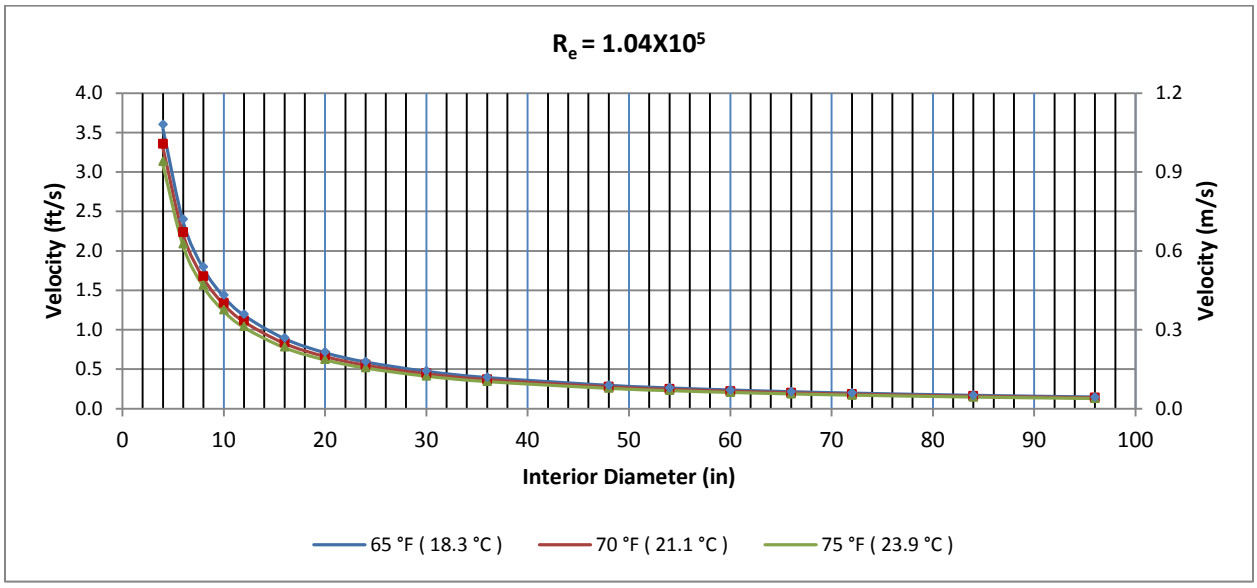

Figure 5.29: Velocity at R_e $1.04x10^5$ (65 °F, 70 °F and 75 °F)

Although the findings from Lambert (2009) and Cowle (2015) show that κ is not constant for biofouled pipes when $R_e < 1.04x10^5$ are significant, the minimum recommended forcemain velocity is generally taken as 3 ft/s (0.9 m/s) to prevent sedimentation. Therefore, forcemains 6 in. (152.4 mm) and greater in diameter should generally operate above the threshold R_e. From Figure 5.29, the threshold velocity for a 4 in. (101.6 mm) diameter forcemain is approximately 3- to 3.5 ft/s (0.91- to 1.1 m/s). The velocity in a 4 in. (101.6 mm) diameter forcemain should therefore be greater than 3.5 ft/s (1.1 m/s) to

ensure that it is operating above the threshold R_e. In general, a properly design forcemain should utilize velocities greater than 3 – 3.5 ft/s (0.91 – 1.1 m/s); therefore, the standard Colebrook-White equation should be used to calculate friction factor.

5.2.4 Bratland – Uniformity Factor

As described in Section 2.9, Bratland (2009) suggested utilizing a dimensionless surface structure uniformity factor (u_s) to define how surface imperfections show similarity with each other in terms of shape and size. The more uniform the surface, the more abrupt the transition between smooth and rough flow becomes (Bratland 2009). Bratland suggested Equation 2.16 to calculate *f*, as a better representation of the pipe surface roughness (using both k_s and u_s). Using Equation 2.16 and k_s from the Colebrook-White equation, the uniformity coefficient (u_s) was calculated for all data using a solver macro in MS Excel. The modified Colebrook-White equation developed by Lambert was used for k_s when $R_e < 1.04x10^5$. Results were plotted against R_e, velocity, k_s, U*, and τ_o to evaluate potential trends associated with u_s. As shown in Figures 5.30 to 5.34, no observable trends were identified from either the R_e or Velocity. These figures also indicate data points where κ was found to be less than 0.40.

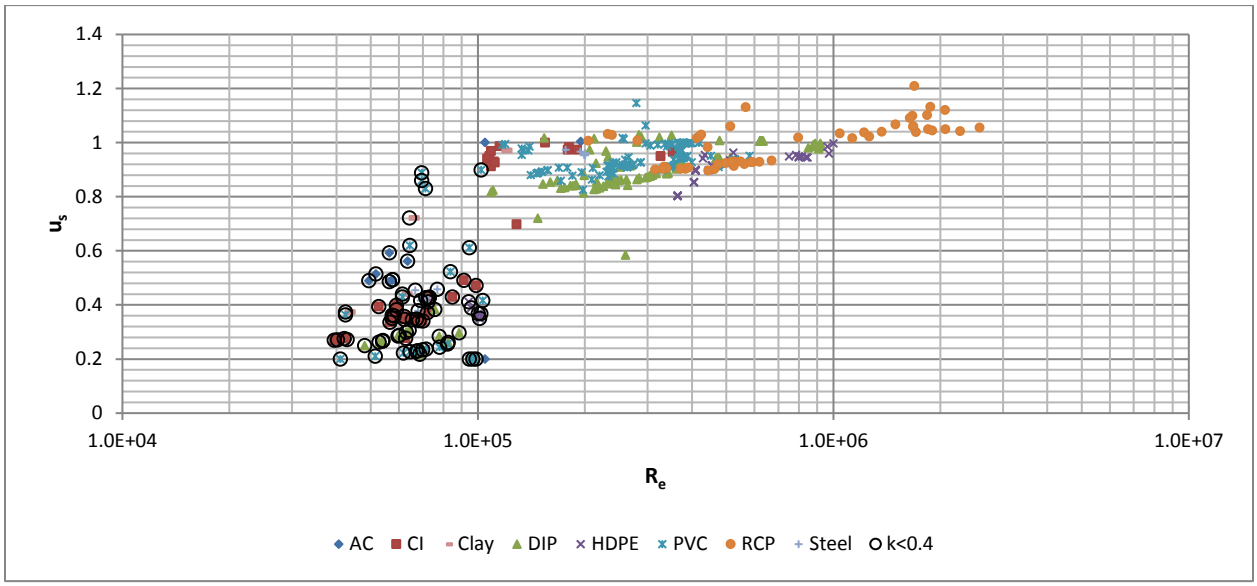

Figure 5.30: u_s versus R_e (by Material)

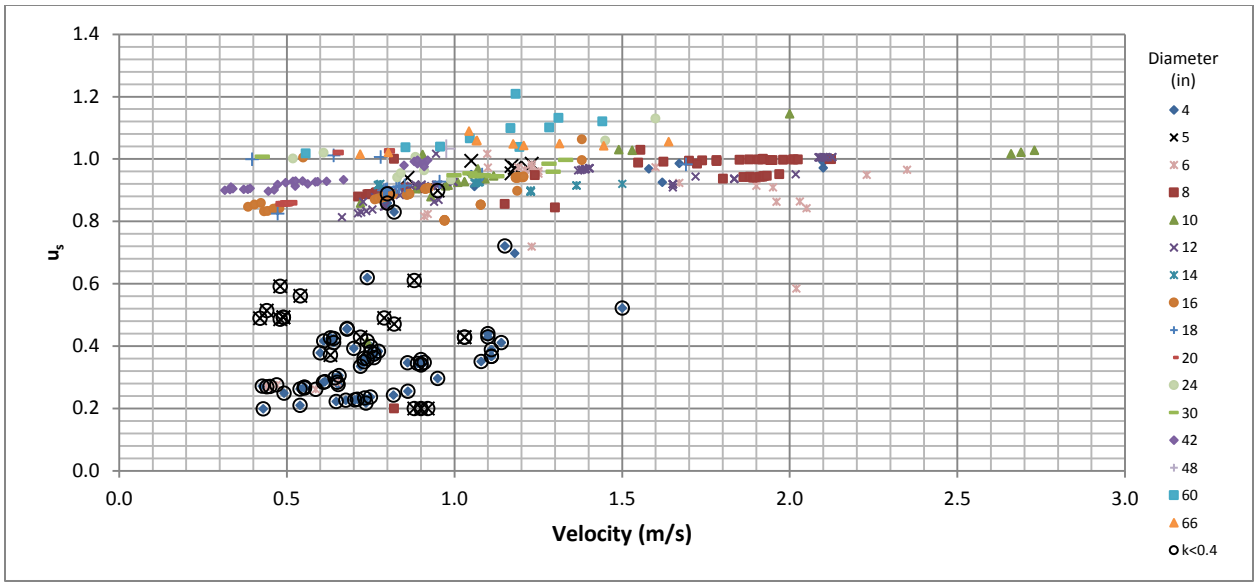

Figure 5.31: u_s versus Velocity (by Diameter)

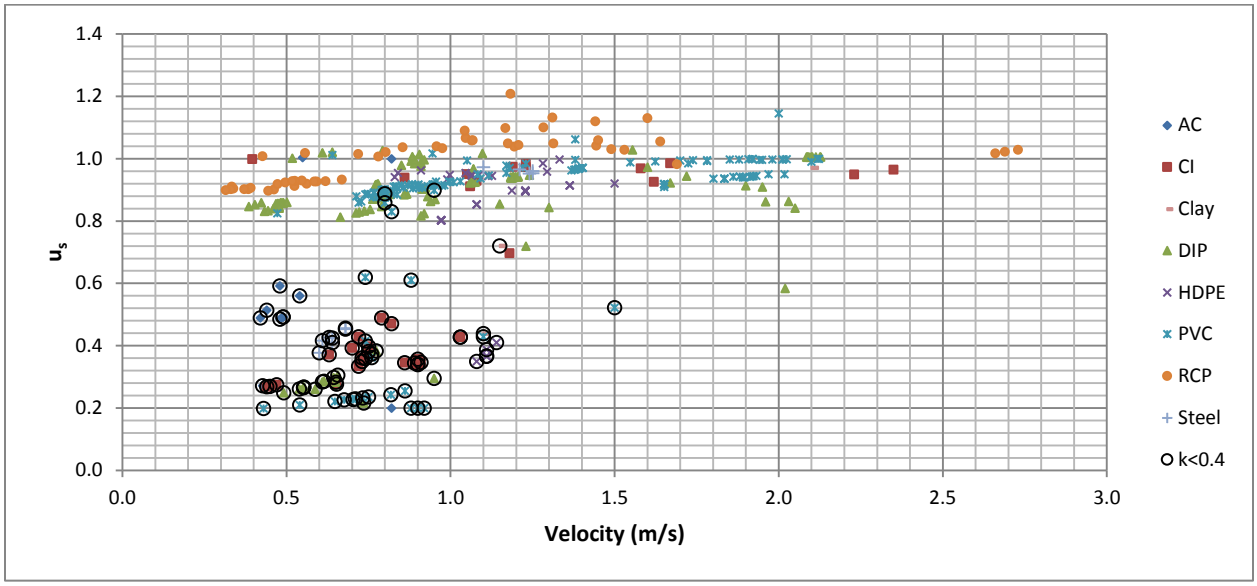

Figure 5.32: u_s versus Velocity (by Material)

It was anticipated that u_s values closer to 1 would be associated with larger diameters; however, no correlations were observed based upon either diameter or material. The results of u_s plotted against k_s, by data source are shown in Figure 5.33. From Figure 5.33, two trends lines were observed; one for u_s approximately equal to 1 and the other with a downward slope with increasing k_s. A majority of the data scatter is associated with the HR Wallingford Data and k_s values for a von Kármán constant less than 0.40. In some cases, k_s determined from the modified Colebrook-White equation shifted the data points towards

the trendline(s), but a majority of the data remained outside the trendline. Although not included as part of this research, u_s versus k_s results were screened against both diameter and material, but observable correlations could not be identified.

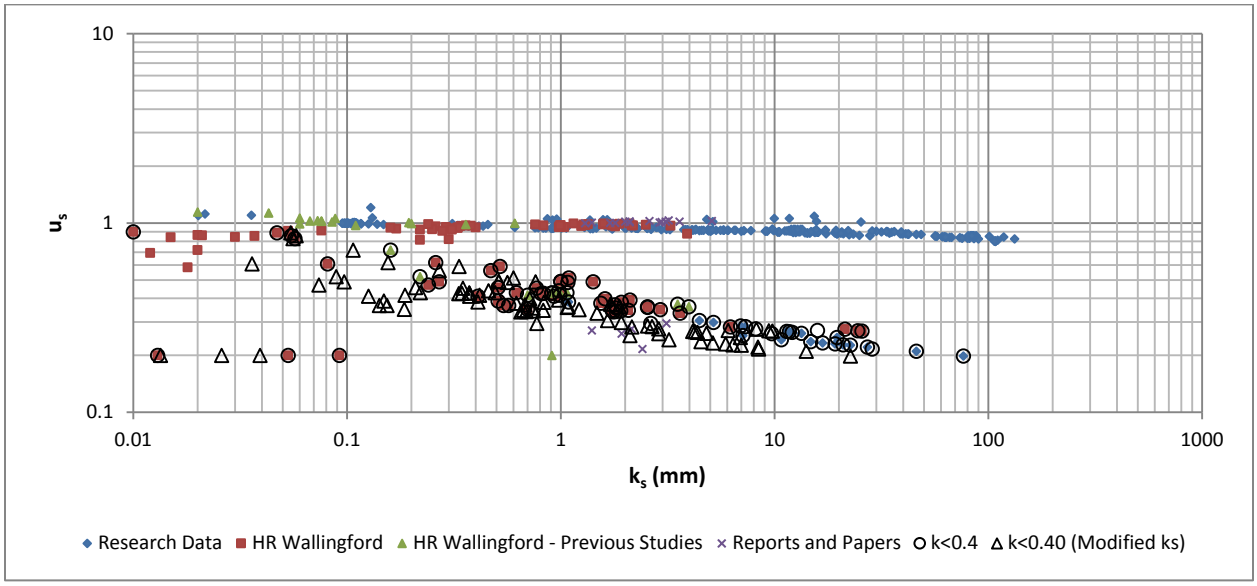

Figure 5.33: u_s versus k_s (by Data Source)

Considering that a majority of the data scatter provided in Figure 5.33 resulted from k_s values corresponding to $\kappa<0.40$ and the fact that the results for k_s varied between the Colebrook-White and modified Colebrook-White equations, the entire data set excluding data points associated with $\kappa<0.4$ were plotted as shown in Figure 5.34. Removing the data associated with lower R_e and $\kappa<0.4$ does provide a well-defined trendline; however, no useful correlations can be developed to determine u_s based upon k_s for use in determining friction factor. Additional trends associated with skin friction and shear stress were also evaluated but did not provide any correlations with u_s and therefore were not presented as part of this research.

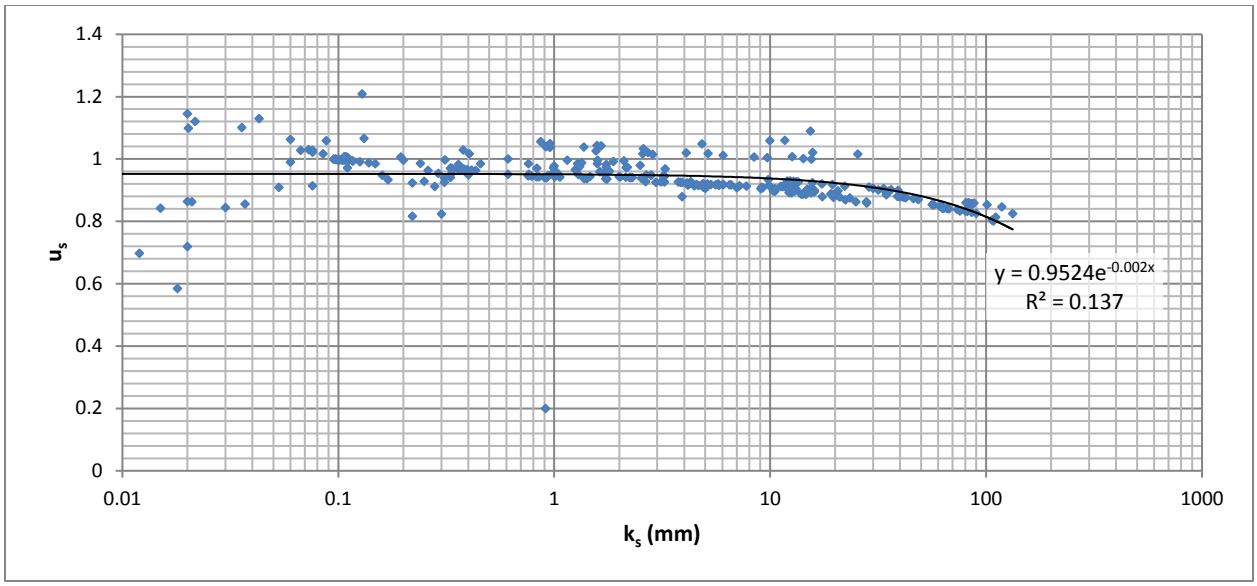

Figure 5.34: u_s versus k_s (κ<0.4 data removed)

Although u_s is an interesting concept for dealing with biofouled pipelines, the modified Colebrook-White equation developed by Bratland (2009) does not provide a useful correlation for pipelines conveying wastewater and therefore is not recommended for use in designing wastewater forcemains.

5.2.5 Effect of Shear Stress

Shear stress (τ_o) for all data was calculated from Equation 4.5, repeated below:

$$\tau_o = \gamma h_f \frac{D}{4L} = \frac{\rho f V^2}{8} = \rho U_*^2 \tag{4.5}$$

As shown above, τ_o is a function of velocity and friction factor (f). Since f is determined from Colebrook-White and k_s appears to be a function of velocity for wastewater pipelines (Section 5.2.1.1); it stands to reason that τ_o should be related to velocity. Calculated shear stress was plotted against R_e, velocity, and k_s to evaluate potential trends associated with the data. Figure 5.35 provides shear stress versus R_e; Figures 5.36 and 5.37 provide shear stress versus velocity, screened against material and diameter, respectively; and Figures 5.38 and 5.39 provide shear stress versus velocity k_s, screened against material and diameter, respectively.

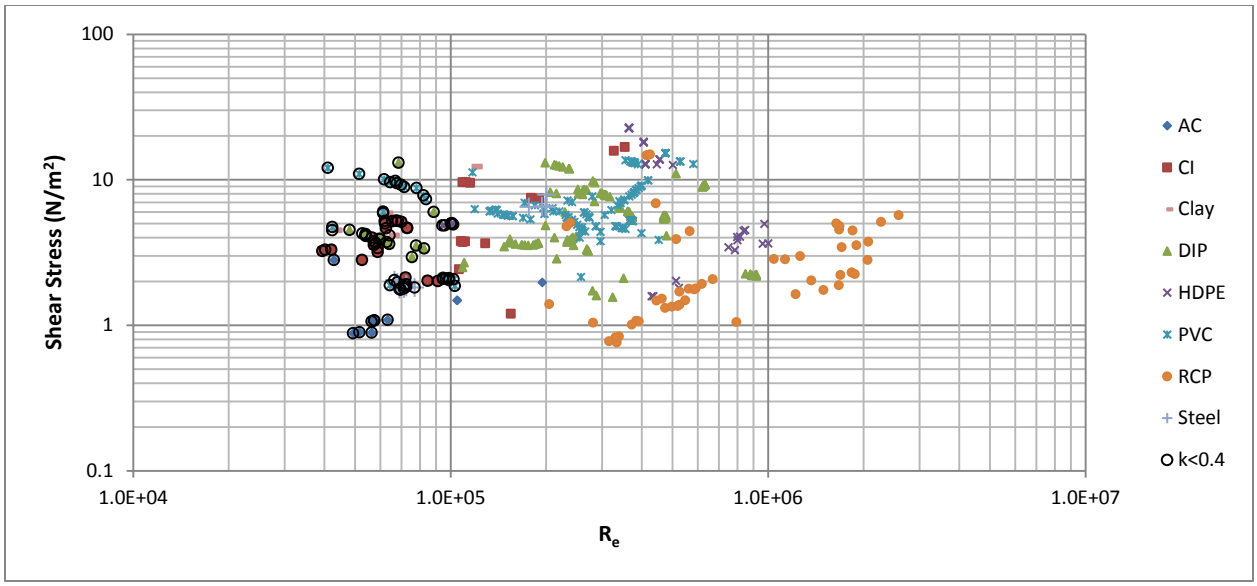

Figure 5.35: Shear Stress vs. R_e (by Pipe Material)

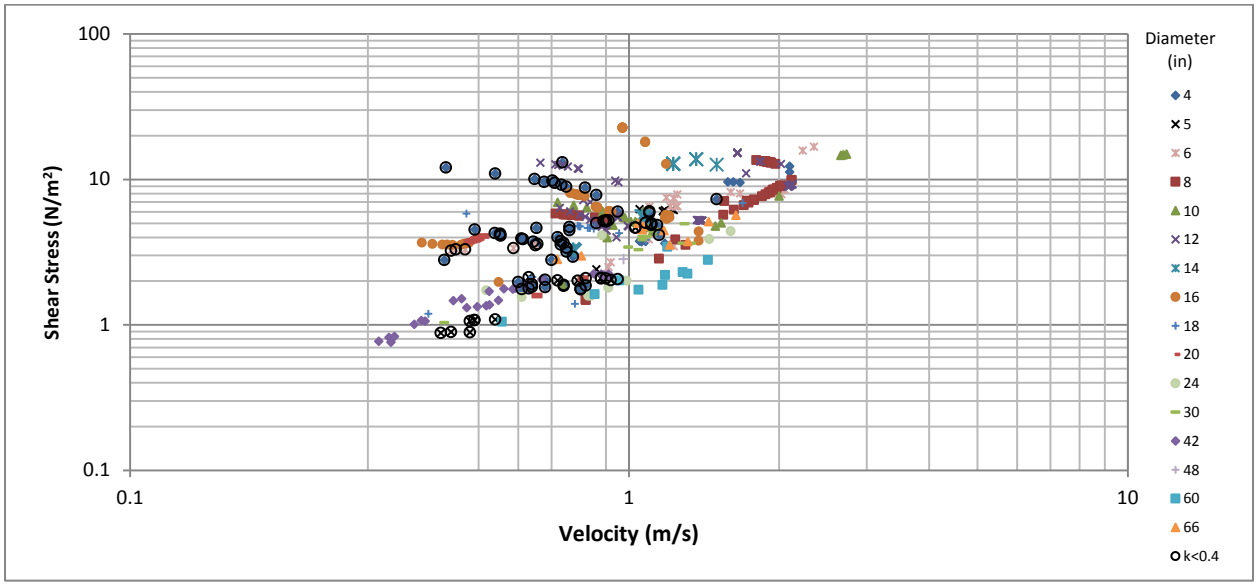

Figure 5.36: Shear Stress vs Velocity (by Pipe Diameter)

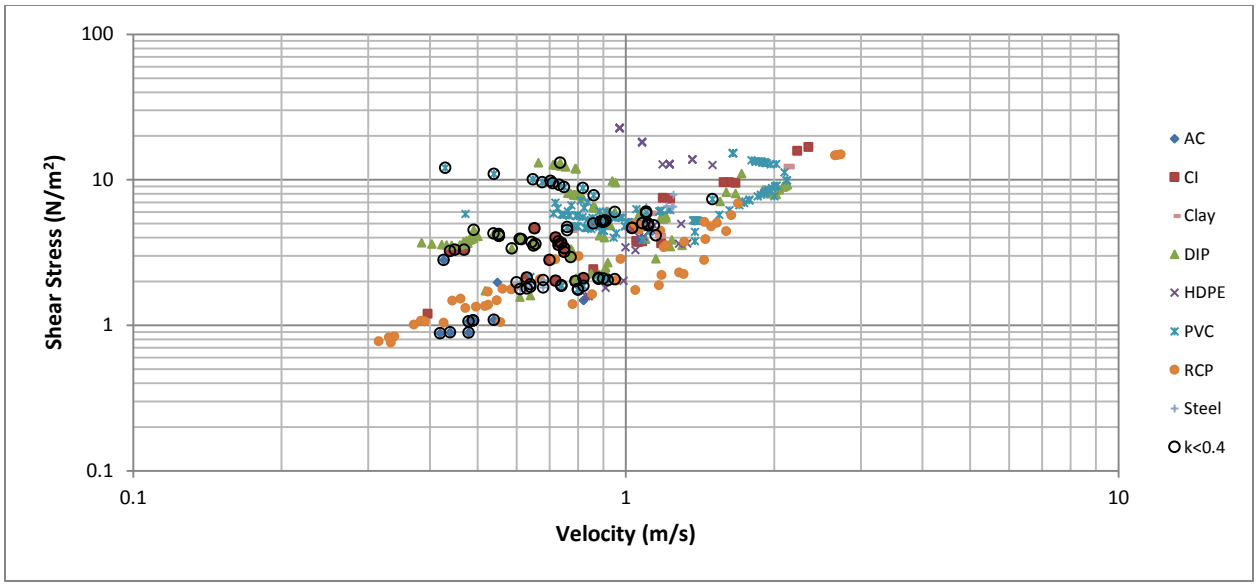

Figure 5.37: Shear Stress vs Velocity (by Pipe Material)

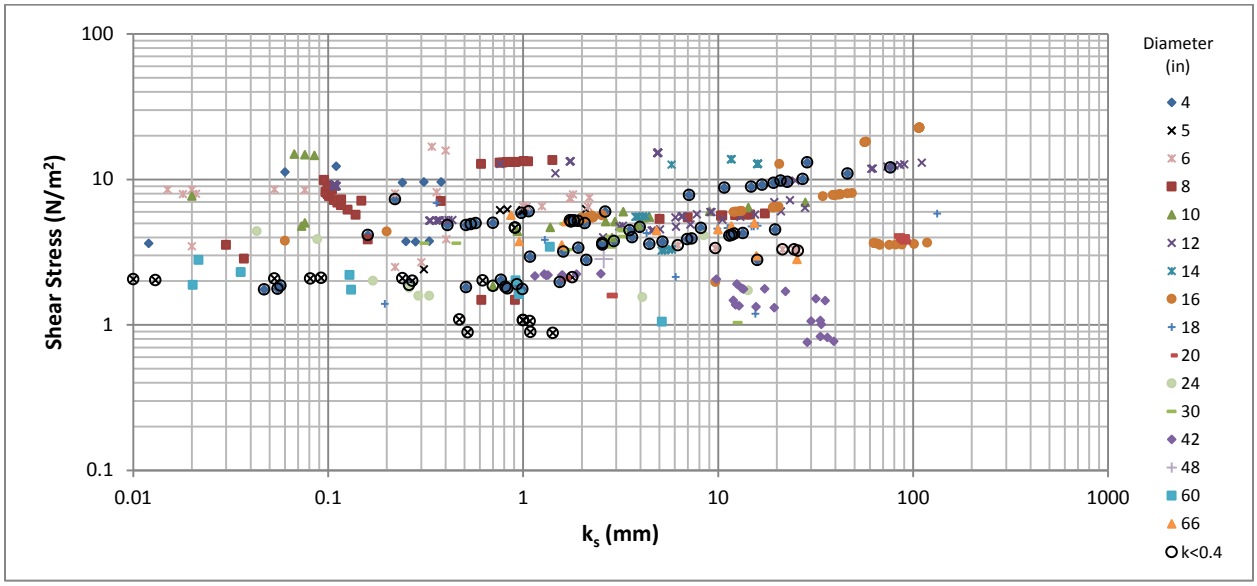

Figure 5.38: Shear Stress vs k_s (by Pipe Diameter)

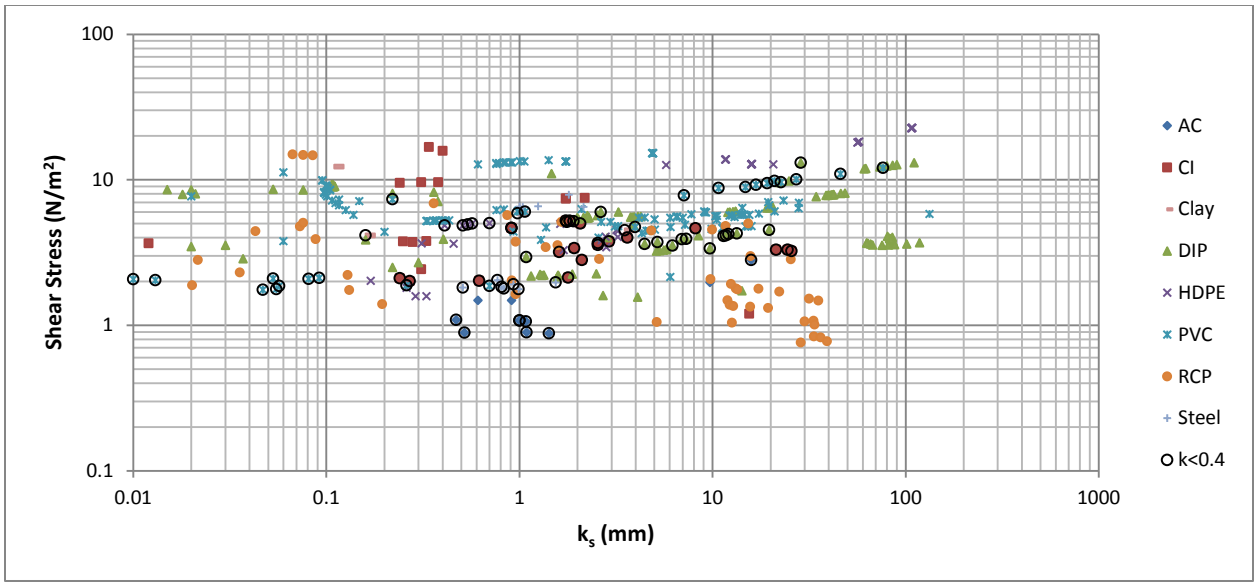

Figure 5.39: Shear Stress vs k_s (by Pipe Material)

Based upon a review of Figures 5.35 to 5.39, no apparent correlation could be identified between shear stress and R_e, velocity, or k_s. Lysne (1969) suggested wastewater biofilms tend to shear from the pipe wall at shear stresses greater than 3.83 N/m^2; Lambert et al. (2009) determined a shear stress of 3.0 N/m^2 was required to shear raw water biofilms from the pipe wall. Shear stress was then plotted against k_s (screened by velocity) as shown in Figure 5.40. No correlations were observed between shear stress and k_s. However, the data show that larger shear stress and lower k_s values are associated with greater velocities.

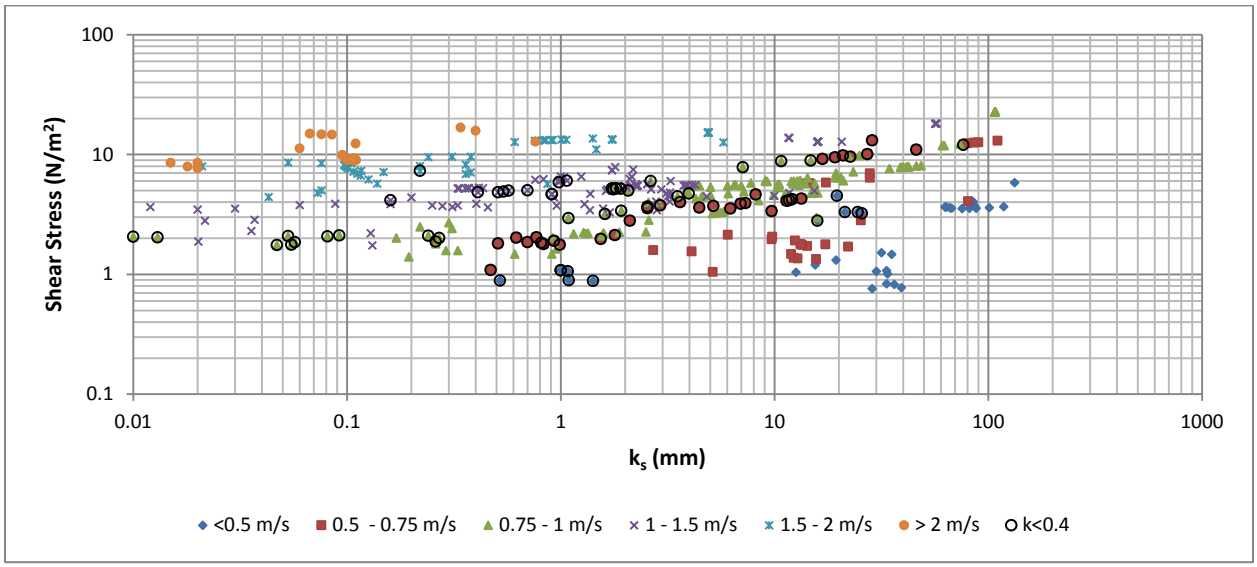

Figure 5.40: Shear Stress vs k_s (by Velocity)

Figures 5.36 and 5.37 show a general trend of increased shear stress with increasing velocity; however, significant scatter is observed away from the apparent trend line. In some cases, data outside the core trend line appears to show decreasing shear stress with increased velocity. A possible explanation of the observed scatter could do with the sensitivity of τ_o based upon its input variables which will be evaluated further in Sections 5.3 and 8.2.

5.3 Uncertainty Analysis

Potential errors associated with the hydraulic calculations performed in Section 5.2 could result from inaccurate as built drawings or operational data. In order to quantify these potential errors, an uncertainty analysis was conducted to evaluate the sensitivity of k_s, C factor, R_e, f, and τ_o based upon a change in the following parameters:

- Temperature;
- Pipe Length;
- Internal Diameter;
- Flowrate; and
- Headloss

Research Dataset results were included in the uncertainty analysis, the remaining datasets were not included since they were collected from various sources and could not be directly verified. Uncertainty analysis was conducted by varying each parameter identified above, all other inputs were maintained from the hydraulic analysis unless the input evaluated is used to determine another value used in the calculations. For example, varying the flowrate causes a change in velocity, which in turns effects f, R_e, k_s, C factor, and τ_o; while a change in temperature influences R_e and k_s. Key results for each parameter are identified in the following sections and a summary of all results are provided in Section 5.3.6.

5.3.1 Temperature

As described in Section 3, wastewater temperature was not field measured and was assumed to be 68 °F (20 °C) for all calculations. The assumed temperature was varied by ±20 °F (±11.12 °C) to evaluate

the effect of temperature on the hydraulic calculations. Reynolds Number is the only parameter directly affected by a change in temperature; k_s is indirectly affected by changes in temperature through changes in Reynolds Number.

Results of the analysis cannot be expressed in simplistic terms such as a maximum or minimum change in k_s due to the change in temperature because of varying pipe sizes and flow conditions within each system. Therefore, results are presented based upon the calculated change in k_s and the corresponding % change in k_s as a function of velocity. Results are presented in Figure 5.41 and show that a larger overall change in k_s is experienced at lower velocities. However, the change in k_s (expressed in terms of percentage) at lower velocities is negligible since large k_s values were determined at lower velocities. The change in k_s was also found to be negligible at higher velocities, but since the k_s values are typically much smaller, the overall percentage change in k_s is larger.

Although not presented here, the change in temperature resulted in a ±30% change in R_e; the resulting change in k_s was determined to average approximately ±0.02 mm (7.87E-4 in.). Therefore, it was concluded that the effect of temperature on the hydraulic calculations was minimal.

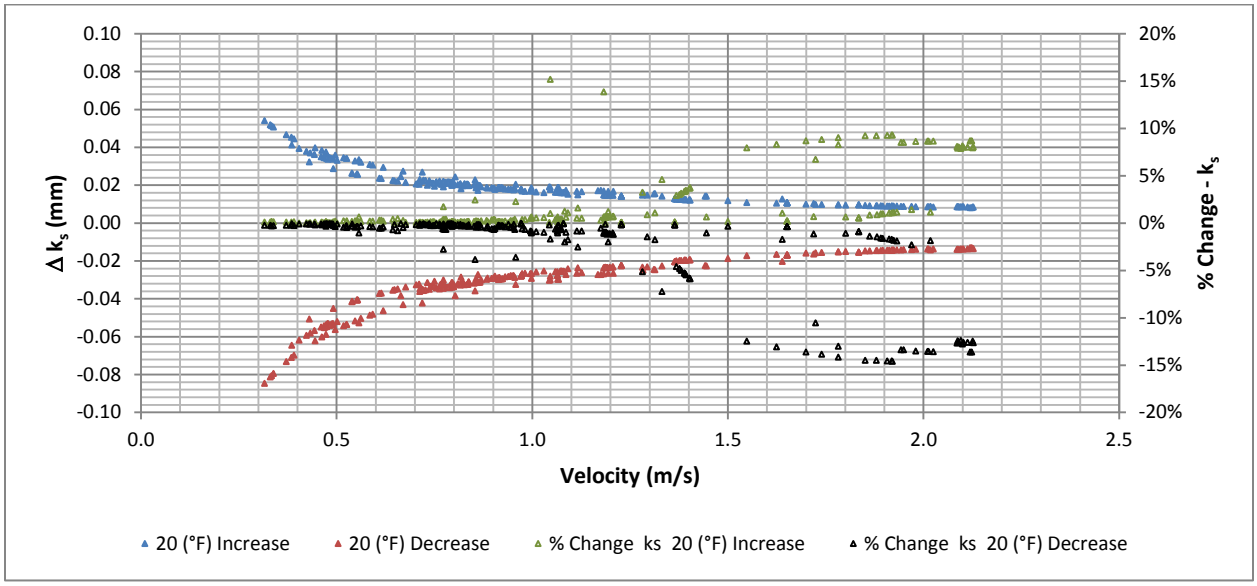

Figure 5.41: Change in k_s Due to Temperature

5.3.2 Pipeline Length

As previously described, the pipeline length was determined from utility asbuilt drawings and was not independently measured or verified. Actual length of each pipeline was calculated from the asbuilt drawings taking into account changes in slope along each pipe segment. As shown in Table 4.2, the difference between the asbuilt station length and the calculated length varied from 0.0 to 0.65 %. This variance is due to the frequency of undulation and utility crossings.

In order to assess the effect of pipeline length on *f*, k_s, and τ_o, a ±1% change in length was selected for the uncertainty analysis. A 1% change in length was determined to be reasonable since the maximum change in length due to undulation was determined to be 0.65%. Although a 1% change in length was used for the analysis, the assumption may not be appropriate for systems with very long pipelines. For example, a 1% change for the Natomas System (actual length of 47,167 ft) results in a change of approximately 500 ft (152.4 mm), which is excessive. Nonetheless, a 1% change in length was applied to each system in order to standardize the analysis.

The resulting change in k_s was determined to range from -1.66 mm to 1.69 mm (-0.65 in. to 0.67 in.), with an average change of approximately 3%. Figure 5.42 shows that the variance increases for larger k_s values since larger k_s values are generally associated with lower velocities. Figure 5.43 confirmed that the change in k_s is minimized with increased velocity.

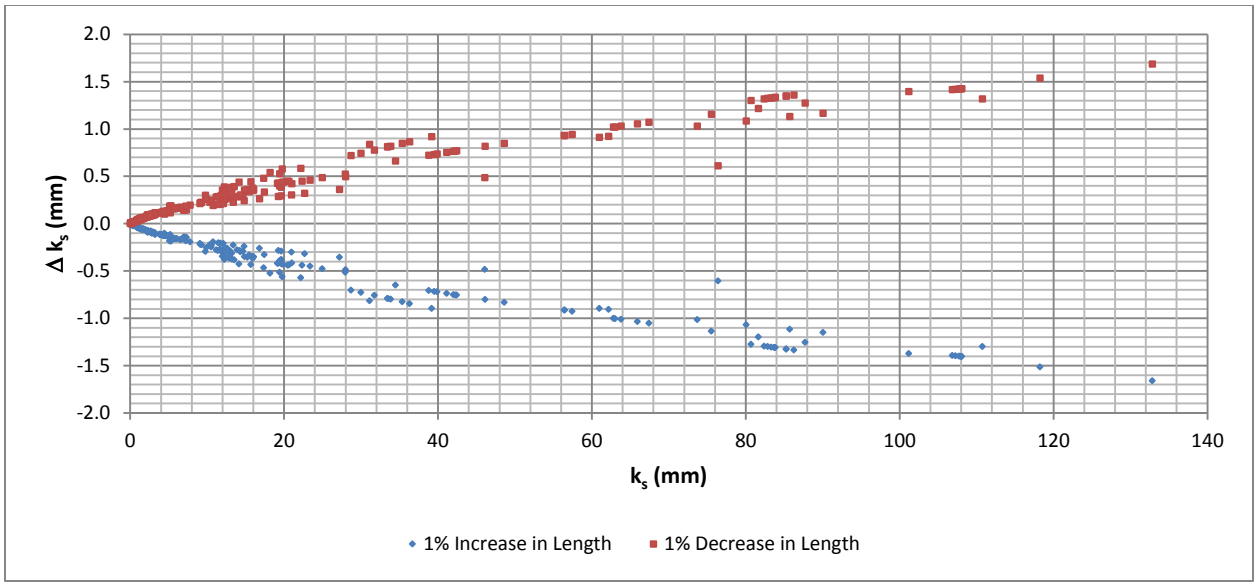

Figure 5.42: Change in k_s from change in pipeline length

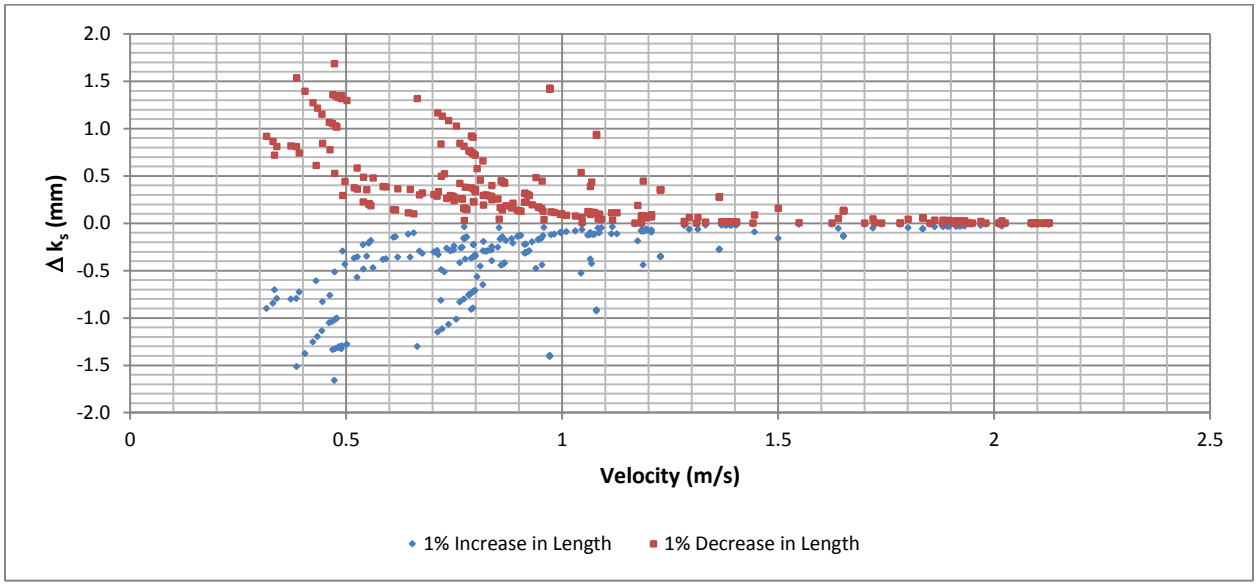

Figure 5.43: Change in k_s from change in pipeline length (velocity)

The resulting change in C factor was determined to be ±1 which corresponds to approximately a 0.5% change. As shown in Figure 5.44, the change in C factor increases with increased velocity. C factor increases with increased pipeline length because a larger C factor indicates increased hydraulic efficiency. Overall, the change in C factor due to a 1% change in pipe length is negligible.

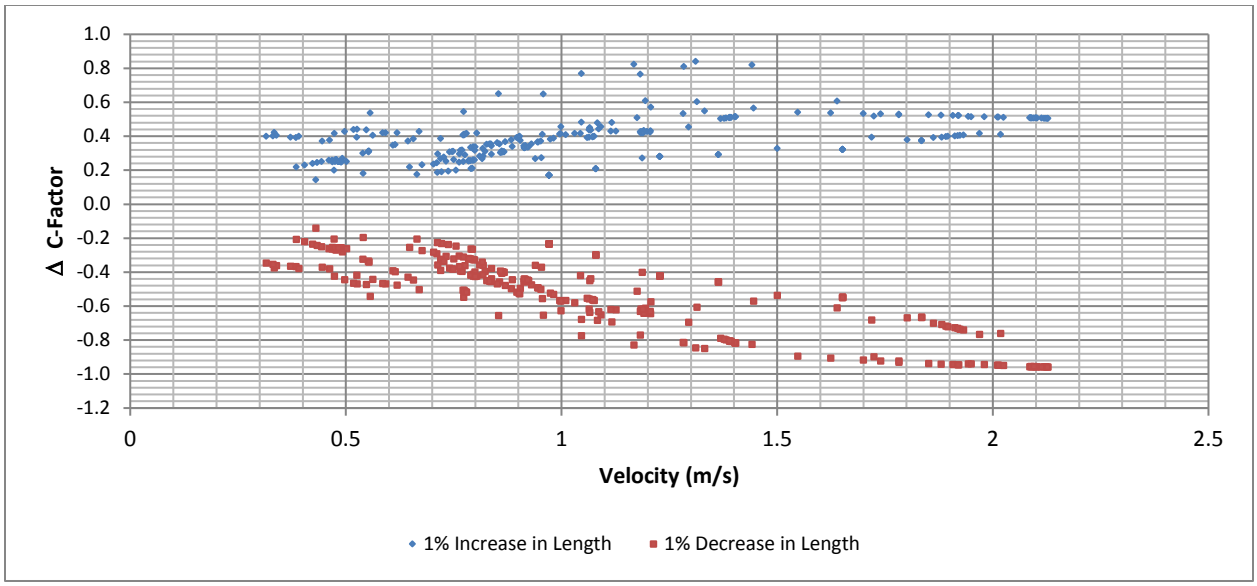

Figure 5.44: Change in C factor due to change in pipeline length

5.3.3 Internal Diameter

Nominal pipe size and material were identified from utility asbuilt drawings. Internal diameters were determined from manufacturers' catalogs and were not field measured or verified. A change in diameter directly affects the friction factor (or C factor) and consequently k_s and τ_o. A 0.25 in. (6 mm) change in diameter was selected to assess the effect of diameter on f, k_s, and τ_o. A 0.25 in. (6 mm) change provides a minimal change in diameter and was determined to be reasonable since pipe interior diameters of cementitious and ferrous pipes could change over its service life due to scaling or corrosion.

Changes in k_s were found to range from -16.5 mm to 17.7 mm (-0.65 in. to 0.7 in.), with and average change of approximately 16%, due to result of a ±0.25 in. (6 mm) change in internal diameter. Change in C factor ranges from -26 to 41, with an average change of approximately 10%. Trends associated with the results could not be readily evaluated since each system provides a different diameter under different flow conditions. The calculated change and percent change in k_s by pipe diameter is presented in Figure 5.45. As one would expect, a 0.25 in. (6 mm) change impacts the calculated k_s value for small diameter pipes as compared to larger diameters. A similar result is shown in Figure 5.46 for C factor.

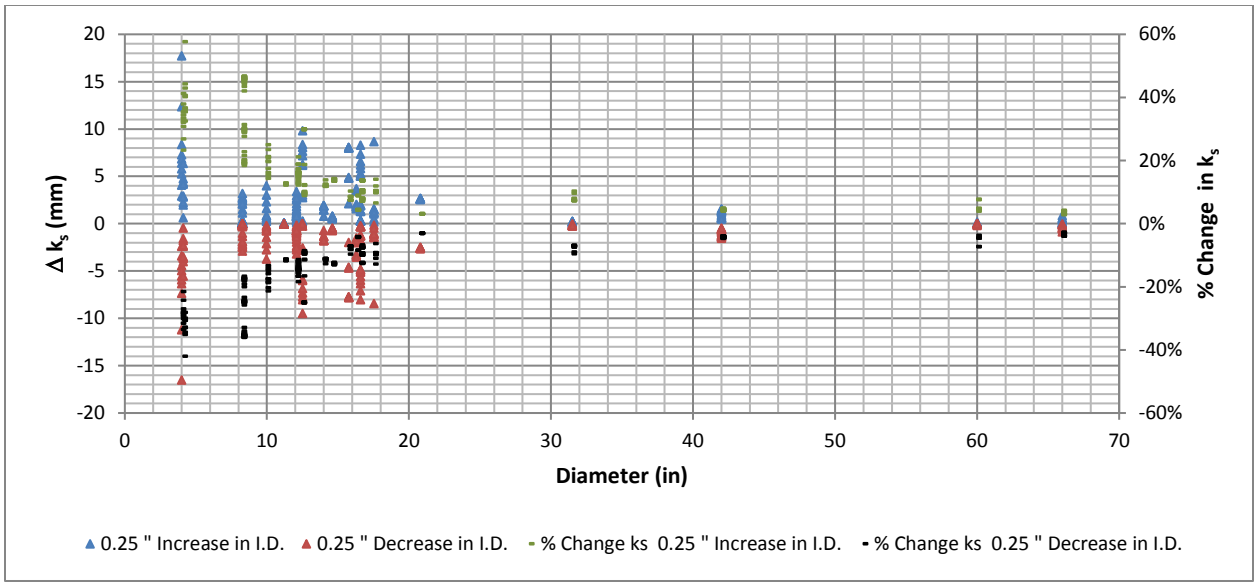

Figure 5.45: Change in k_s due to ±0.25 in. Change in Diameter

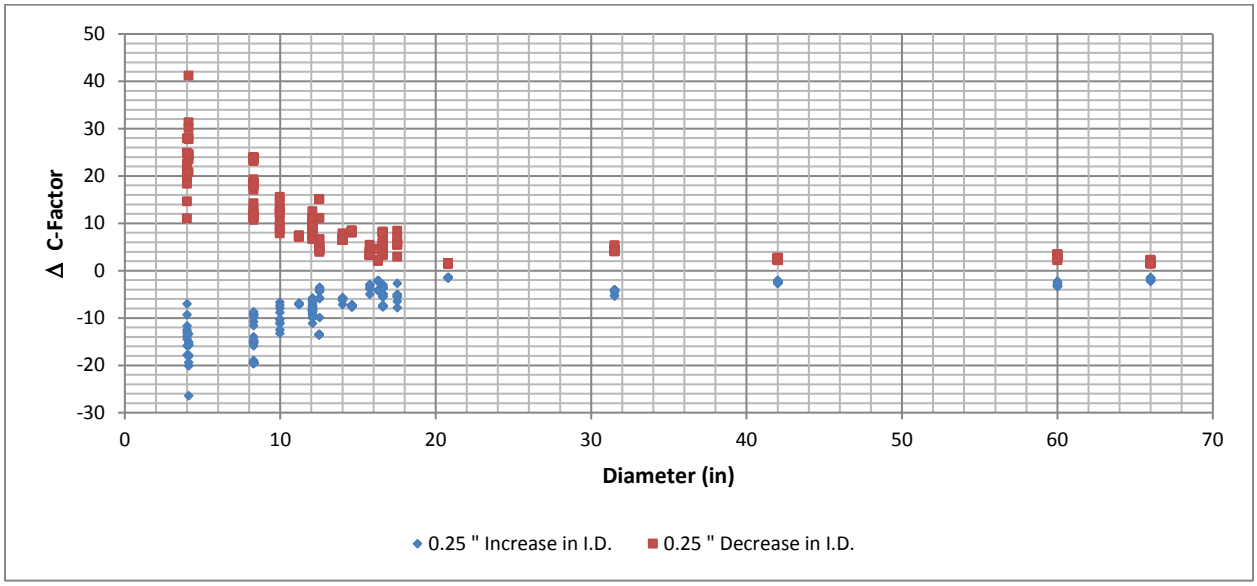

Figure 5.46: Change in C factor due to ±0.25 in. Change in Diameter

5.3.4 Flowrate

Wastewater flows are typically measured using electromagnetic flowmeters (mag meters). Reported accuracy of mag meters ranges from ±0.25% to ±0.50% depending on the manufacturer and model of the mag meter (www.badgermeter.com). The uncertainty analysis assumed a ±1 % change in the average flow to account for the variance in flow measurements averaged over the pump cycle which provides a

conservative estimate for the change in flow. Results are presented in Table 5.3 (Section 5.3.6) and show that a 1% change in flowrate provides negligible change in friction factor; -3.3 mm to 3.4 mm (-0.13 in. to 0.13 in.) change in k_s; and -1.6 to 1.6 change in C factor. Figure 5.47 compares the change in k_s resulting from a 1% change in Flowrate for each calculated value of k_s. A similar comparison for C factor is provided in Figure 5.48. Results show that the change in k_s and C factor resulting in a 1% change in flowrate are minimal.

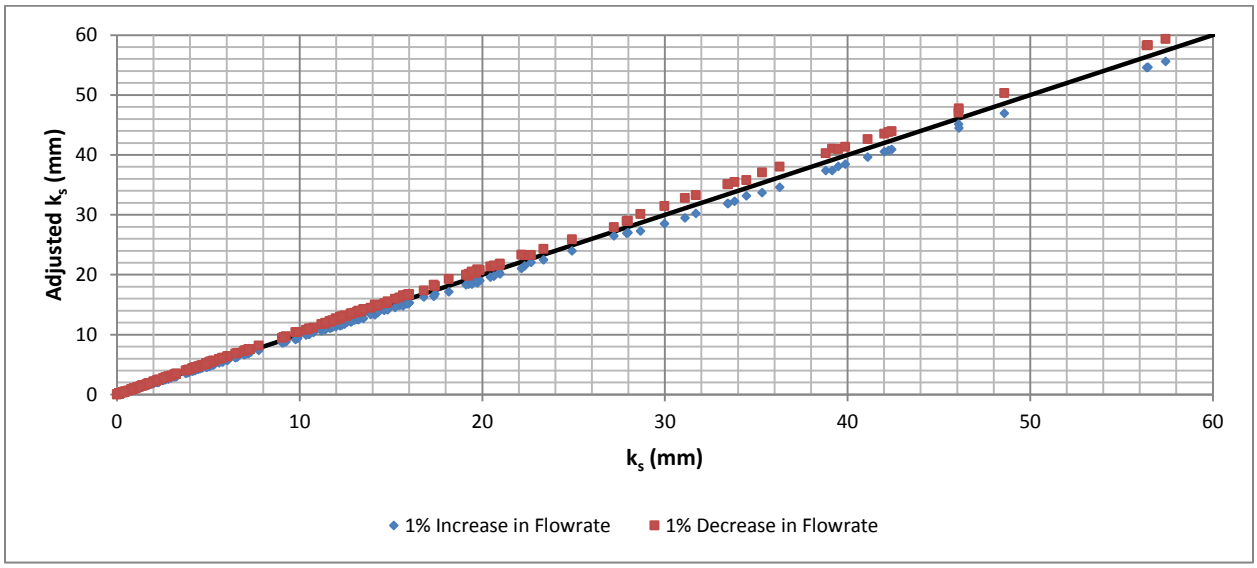

Figure 5.47: Change in k_s due to 1% change in Flowrate

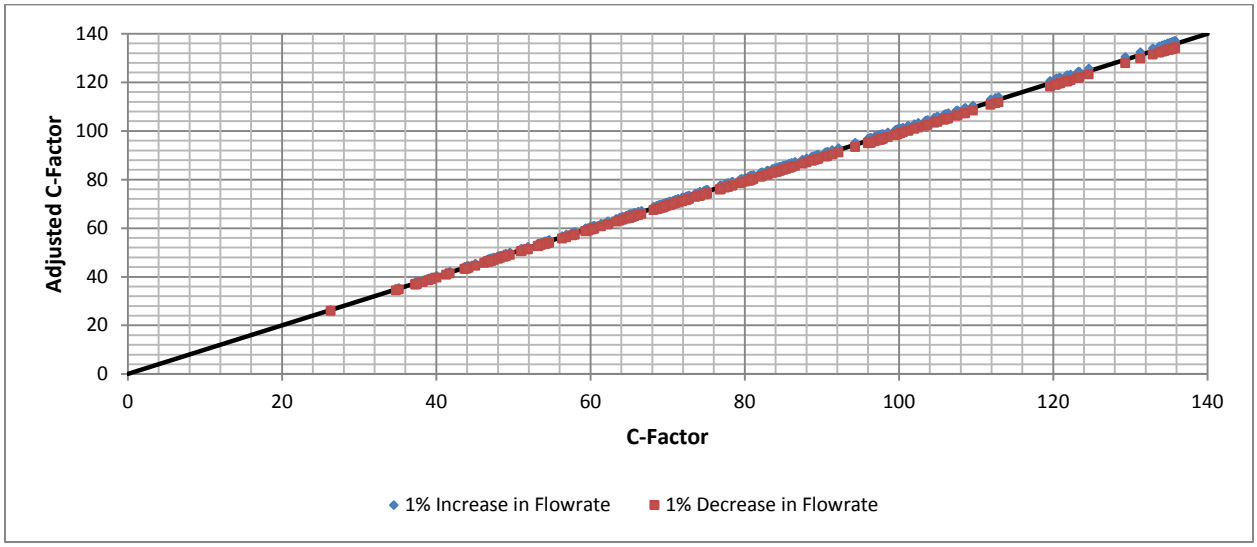

Figure 5.48: Change in C factor due to 1% Change in Flowrate

5.3.5 Headloss

Friction headloss was calculated from the difference between the estimated HGL at both the discharge of the lift station (upstream) and downstream forcemain discharge location. The upstream HGL was estimated using the elevation of the discharge piping and either the discharge pressure or TDH of the pump (adjusted using the wet well level during the pumping cycle). Possible errors associated with the headloss estimate are due to inaccurate SCADA measurements from faulty sensors (flow and pressure); or incorrect system data such as asbuilt records or pump curves. As demonstrated in Section 6.5, a 1% change in flowrate minimally affected the estimation of k_s and C factor. Therefore, for this analysis, the change in headloss was assumed to result from inaccurate pressure sensor measurements or wear of pump impellors.

The Research Dataset included six forcemain systems (Sand Creek, Natomas, South River, TRM, TRP, and Norris Lake) where the lift station discharge pressure was reported from the SCADA data. Inaccurate discharge pressure readings directly affect the calculated headloss of the system. Currently, there is no universally adopted convention for specifying the accuracy of pressure sensors. Accuracy of pressure sensors is based upon stability and accuracy requirements of its intended application. Pressure sensors are generally selected based upon specifications such as Total Error Band (TEB) and integrated amplification, compensation and calibration. Since a general industry standard for pressure sensor accuracy is not available, the uncertainty analysis was performed assuming a ±2.5% change headloss. A change in headloss can also be used to simulate pump impeller wear. Decreased pump performance occurs as the pump impeller wears. The change in Total Dynamic Head (TDH) of a pump varies depending on the shape of the pump curve.

The uncertainty analysis adjusted the friction headloss for each forcemain by ±2.5% to determine the effect of headloss on k_s, C factor, and shear stress. Results are summarized in Table 5.3 (Section 5.3.6) and show a -5.4% to 6.1% change in k_s, approximately a 1.4% change in C factor, and a change of approximately 1.7% in shear stress.

5.3.6 Discussion and Results

Uncertainty analysis results are summarized in Table 5.3. Changes in Internal diameter resulted in the largest change in k_s and C factor, followed by changes in headloss, flowrate, pipe length, and temperature. A ±0.25 in. (0.01 mm) change in internal diameter significantly affected k_s and C factor. Changes to the remaining factors resulted in minimal affects to k_s and C factor. Results show that changes to each of these parameters affect the average change in different ways. As one would expect a change to internal diameter would result in the greatest change to the roughness result since the velocity is related to the flowrate divided by the pipe area; and the pipe area is function of the square of the diameter.

It should be noted that the uncertainty analysis was a desktop exercise since field data was not collected as part of this research. Therefore, a simplified approach was developed which considered a constant change for each parameter and did not consider the dimension of the parameter. For example, a 0.25 in. (0.01 mm) change in diameter provides a greater impact for a smaller diameter. This analysis evaluated the resulting change in k_s and C factor due to a change in each parameter identified above independently; although not evaluated as part of this analysis, changes, or errors, in measurements to several of the parameters would compound the potential error in determining k_s and C factor. Results show the importance of collecting accurate information of the system prior to performing hydraulic calculations.

Table 5.3: Summary of Uncertainty Analysis Results

Item		Change (calculated value - original value)									
		Parameter									
		Temperature		Pipe Length		Internal Diameter		Flowrate		Headloss	
		± 20 °F		± 1.00%		± 0.25-in.		± 1.00%		± 2.50%	
		Increase	Decrease	Increase	Decrease	Increase	Decrease	Increase	Decrease	Increase	Decrease
R_e	Min	----	----	----	----	-2.4E+04	2.8E+03	4.1E+02	-2.6E+04	----	----
	Max	----	----	----	----	-2.8E+03	2.7E+04	2.6E+04	-4.1E+02	----	----
	Avg	----	----	----	----	-1.2E+04	1.3E+04	4.5E+03	-4.5E+03	----	----
	% Change	-30.44%	27.30%	----	----	-11.11%	14.29%	1.00%	-1.00%	----	----
f	Min	----	----	-0.01	0.00	0.00	-0.07	-0.01	0.00	-0.01	-0.01
	Max	----	----	0.00	0.01	0.07	0.00	0.00	0.01	0.01	0.01
	Avg	----	----	0.00	0.00	0.00	0.00	0.00	0.00	0.00	0.00
	% Change	----	----	----	----	----	----	----	----	----	----
k_s (mm)	Min	0.01	-0.08	-1.66	0.00	0.00	-16.50	-3.30	0.01	-4.09	-3.29
	Max	0.05	-0.01	0.00	1.69	17.73	0.00	-0.01	3.39	3.26	4.28
	Avg	0.02	-0.03	-0.36	0.36	1.88	-1.76	-0.71	0.73	-0.57	0.61
	% Change	1.49%	-2.33%	-2.96%	3.07%	16.62%	-14.42%	-5.78%	6.16%	-5.43%	6.08%
C factor	Min	----	----	0.14	-0.96	-26.41	1.45	0.26	-1.58	-2.07	0.36
	Max	----	----	0.84	-0.14	-1.41	41.25	1.56	-0.26	-0.35	2.15
	Avg	----	----	0.38	-0.52	-7.78	9.41	0.77	-0.90	-1.18	1.08
	% Change	----	----	0.47%	-0.61%	-9.50%	11.69%	0.93%	-1.07%	-1.40%	1.30%
τ_o (N/m^2)	Min	----	----	-0.23	0.01	0.01	-1.51	----	----	-0.56	-0.33
	Max	----	----	-0.01	0.23	1.51	-0.01	----	----	0.33	0.58
	Avg	----	----	-0.07	0.07	0.31	-0.31	----	----	-0.12	0.12
	% Change	----	----	-0.99%	1.01%	3.97%	-3.98%	----	----	-1.67%	1.78%

6 Lift Station and Forcemain Operation and Maintenance

6.1 Forcemain Operation

Forcemains are very reliable when they are properly designed and maintained (EPA 2000). Issues associated with the operation and maintenance of wastewater forcemains primarily include sedimentation, air buildup, and corrosion. Accumulation of fats, oils, and grease (FOGs) are also potential operational issues; however, most utilities require grease traps within the sanitary sewer system, which minimize potential impacts from FOGs, and therefore will not be discussed further.

Wastewater lift station pumps generally operate intermittently with the frequency of pumping cycles. Sedimentation, air buildup, and corrosion generally occur at lower velocities and are often interrelated. Sedimentation is problematic because both organic and coarse non-cohesive materials could be present in wastewater. Deposition of organic material could turn anaerobic in forcemains with a long detention or high hydraulic retention time (HRT). Although it is rare, mobilization of anaerobic organic deposits from a forcemain could potentially disrupt wastewater treatment plant operations when, or if, mobilized. Sedimentation of granular material could lead to accumulation of material and degradation of hydraulic capacity if the forcemain is not capable of transporting the material.

Air locking and corrosion can occur when the sewage turns anaerobic during periods of idle and low velocities. Improper placement, functionality, or lack of air release valves can lead to air buildup, or even air locking within the forcemain. Hydrogen sulfide released into air pockets can lead to pipe corrosion.

This chapter is intended to provide a brief introduction and define the methodology associated with estimating sediment transport, air clearing, and hydrogen sulfide within forcemains. Results will be used to identify potential operational issues associated with these items and develop forcemain design recommendations. These topics are further evaluated in Chapter 8. The frequency of pumping cycles related to HRT is evaluated in Section 6.2 to determine if correlations can be identified between forcemain hydraulic performance and pumping cycles.

6.1.1 Sedimentation and Sediment Transport

Wastewater forcemains have to cope with a particularly challenging task: they have to ensure that solids contained in the wastewater (sand, gravel, organics) are readily transported along with the wastewater. Both organic and non-cohesive (sand and gravel) materials could be present in the sewage. Sand and gravel could be introduced into sewer systems through cracks or holes in sewer pipes or from roadway surfaces in the case of combined sanitary /stormwater systems.

Forcemains must be designed to be self-cleaning to prevent deposition of solids which could cause increased sulfide production leading to corrosion and odor issues; loss of capacity through a reduction of cross sectional area; or even blockage at low points or at the toe of an adversely sloped pipe leading to costly removal.

Sedimentation occurs when the forcemain velocity is not capable of transporting the material. TM 5-814-2 (Army 1985) indicates that a velocity greater than 2 ft/s (0.6 m/s) is required to maintain organic solids in suspension and that solids will settle at velocities less than 1.0 ft/s (0.3 m/s) and when wastewater pumps are idle. However, a velocity of 2.5 to 3.5 ft/s (0.8 to 1.1 m/s) is generally adequate to re-suspend and flush the solids from the line (Army 1985).

Wastewater pumps are typically non-clog pumps with the capability of passing up to a 6 in. solid (or larger), depending on the size of the pump. Most utilities require pumps to be able to pass a minimum 3 in. solid to minimize clogging of the pumps. Even though the pumps are capable of passing large diameter solids, the forcemain may not have sufficient velocity to transport larger solids, leading to solids accumulation, capacity reduction, or potential clogging of the forcemain.

Sediment can be transported in forcemains through either suspended load and/or bed load, which vary depending on the flow conditions (velocity), fluid properties, and characteristics of the solids. Suspended load conveys particles in homogeneous or heterogeneous suspensions. Homogeneous suspensions occur when velocity is turbulent and high enough to keep the solids uniformly suspended and moving along with the fluid. As velocity slows, a heterogeneous suspension develops as heavier particles

slow down and begins to settle in the pipe. If operating velocity is too low, heterogeneous flow can lead to solids deposition (Copeland 2013).

Under a sliding bed condition (bed load, or bed motion), particles will settle to the bottom of the pipe and slide or roll along at a slower, uniform rate or in discontinuous movements. At very low velocities with large particles, a stationary bed occurs, in which the lower part remains deposited, but some particles may move along the surface. The point of transition from heterogeneous flow to a sliding bed is called the deposition velocity or re-suspension velocity (also sometimes referred to as the "saltation regime"). Intermediate conditions can occur in suspensions of varying particle characteristics (i.e. size, shape, density, etc.) (Copeland 2013).

Based upon the findings presented in Chapter 5, a number of forcemains within the Research Data Set such as TRP and TRM, and 6 other forcemains were consistently operating at a velocities less than 3 ft/s (0.9 m/s). With the exception of TRP and TRM, these lift stations are operated intermittently based upon the influent flow rate reporting to the station. TRP and TRM are controlled using VFDs, but are consistently operating at velocities less than 2.3 ft/s (0.7 m/s). Therefore, sedimentation is likely occurring within these forcemains. Since the velocity is less than 3.5 ft/s (1.2 m/s), re-suspension of the material is not likely to occur; which will ultimately reduce capacity over time and increase operating costs.

Forcemains tend to undulate as the pipeline follows the ground topography. Forcemain profiles for the systems collected and analyzed as part of this research are provided in Appendix D.2. The profiles show that a majority of the pipelines undulate and many sections of the forcemains contain steep adverse slopes, or even vertical sections, which affect the transport of granular particles.

Utilizing the results from the hydraulic analysis (Chapter 5), the maximum theoretical particle size transported in a horizontal pipeline was estimated for each system within the Research Dataset. Other data sets were not evaluated since plan and profile drawings were not available for these forcemains. Sediment size characteristics for sewers located in the U.S. were not found in the literature. However, Butler (1996) presented typical sewer sediment characteristics found in sewers located in the U.K. (Table 6.1).

Table 6.1: Wastewater Solids Characteristics (U.K. Data)

Sediment Class	Normal Transport Mode	Median Size, d_{50} (mm)		
		Low	Medium	High
Sanitary Solids	Suspension	0.01	0.04	0.06
Grit	Bedload	0.30	0.75	1.00

A particles threshold of movement can be defined by the Shields Diagram, presented as Figure 6.1. Shields diagram empirically shows how the dimensionless critical shear stress is a function of the particle Reynolds number. A simplified approach for estimating the critical particle diameter for movement and predicting the associated critical velocities necessary for grit transport is presented in the following sections. Several factors including cohesion may affect the results and are not accounted for in the methodology presented below. Cohesion increases the required shear stress that the flow needs to exert on the deposited bed in order to initiate movement of particles in the surface layer. In laboratory tests, erosion of synthetic cohesive particles has been observed to occur at bed shear stresses of 2.5 N/m^2 (organic material) and 6-7 N/m^2 (granular, consolidated deposits) (Butler 2003).

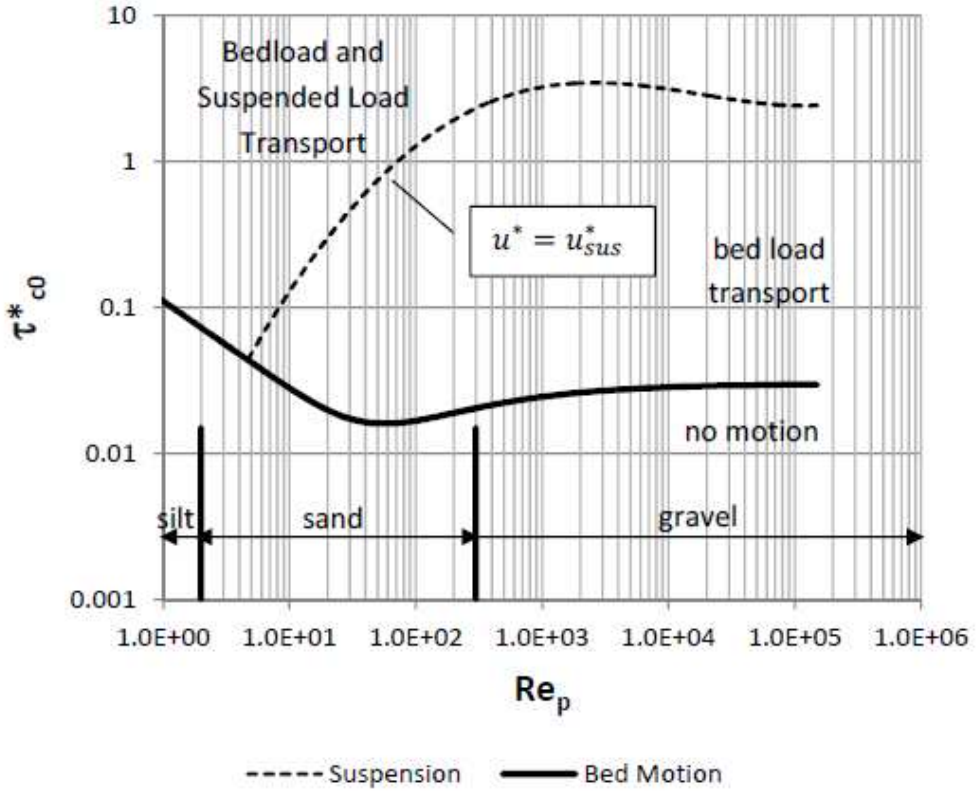

Figure 6.1: Critical Shields Number for Particle Movement (Axworthy 2014)

6.1.1.1 Movement by Suspension

Particle movement in suspension occurs when the shear velocity (U*) of the pipe flow is greater than suspension shear velocity (U^*_{sus}), or ($U^* > U^*_{sus}$). The shear velocity is calculated from Equation 3.7 and the shear velocity for particle suspension (U^*_{sus}) is calculated from Equation 6.1.

$$U^*_{sus} = \sqrt{\tau^*_{sus}(G-1)gd_s} \tag{6.1}$$

Where τ^*_{sus} is the dimensionless shear stress for particle suspension; G is the specific gravity of the particle; g is the gravitational constant (ft/s^2, m/s^2); and d_s is the particle size (ft, m). The dimensionless shear stress for particle suspension is determined from Equation 6.2.

$$\tau^*_{sus} = R_f^2 \tag{6.2}$$

where R_f (Dietrich 1982) is determined from Equation 6.3.

$$R_f = exp\left(-b_1 + b_2 ln(R_{ep}) - b_3\left(ln(R_{ep})\right)^2 - b_4\left(ln(R_{ep})\right)^2 + b_5\left(ln(R_{ep})\right)^2\right) \tag{6.3}$$

The Dietrich Equation coefficients are identified in Table 6.2 and the Particle Reynolds Number (R_{ep}) is determined from Equation 6.4.

Table 6.2: Dietrich Equation Coefficients

Coefficient	Value
b_1	2.891394
b_2	0.952960
b_3	0.056835
b_4	0.002892
b_5	0.000245

$$R_{ep} = \frac{d_s\sqrt{(G-1)gd_s}}{\upsilon} \tag{6.4}$$

The maximum particle size conveyed under sediment suspension was estimated for each system using Microsoft Excel. Since transport through suspension occurs when $U^* > U^*_{sus}$; a macro was developed to determine the maximum theoretical value of d_s when $U^* = U^*_{sus}$ assuming U* was 95% of U^*_{sus}. This approach was utilized to ensure $U^* > U^*_{sus}$.

The maximum theoretical particle size that can be transported through suspension for each forcemain system is shown in Figure 6.2. The theoretical particle size transported was found to range from 0.22 mm to 0.82 mm, which are classified as medium to coarse sand particles. Although the results provide significant scatter, there does appear to be a general trend of increased suspended particle size transported with increasing velocity.

Since sediment suspension occurs when $U^* > U^*_{sus}$ and U* is a function of τ, the results for d_s were compared to the calculated values of τ and U*. Results for τ were presented in Section 5.2.5 and show a general trend of increased τ with increased velocity. Figure 6.3 provides U* plotted against Velocity and shows the same general pattern as Figure 6.2, with a general trend of increasing U* as a function of velocity. This topic will be reviewed further in Section 8.2.

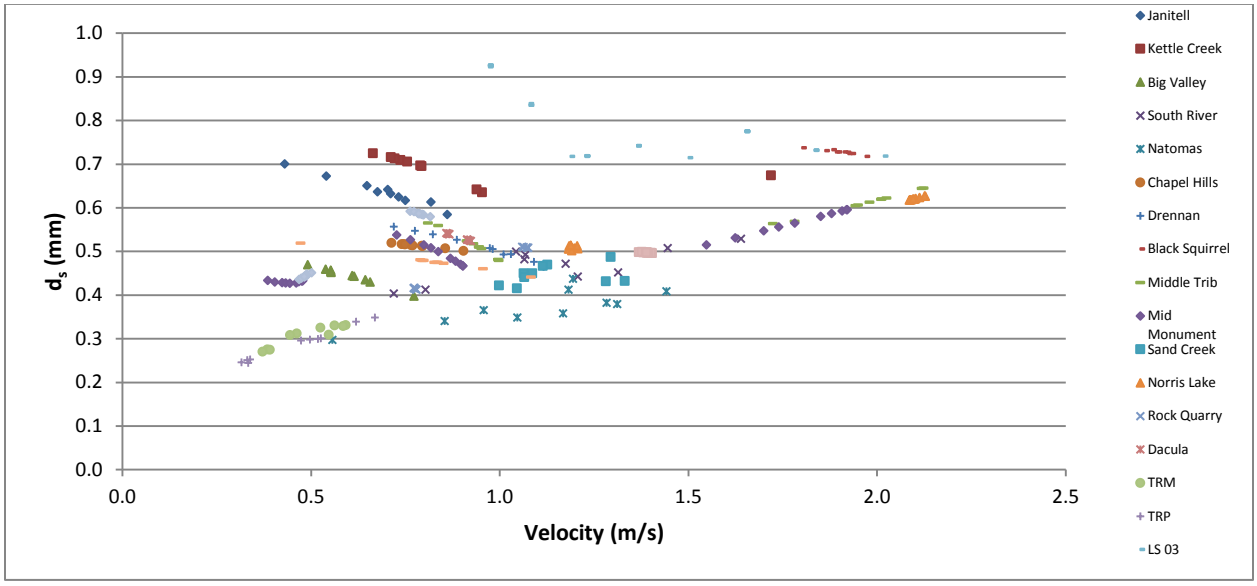

Figure 6.2: Maximum Theoretical Particle Size Transported Through Suspension

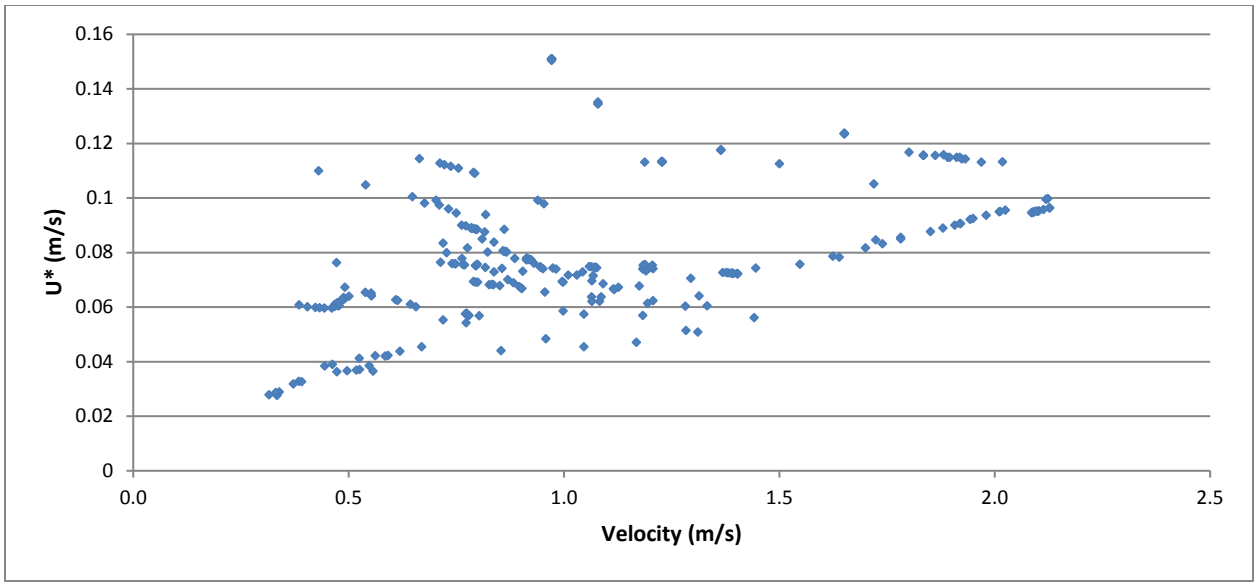

Figure 6.3: Friction Velocity (U*) versus Velocity for Particle Suspension

6.1.1.2 Bed Motion

As shown in Figure 6.1, bed motion of a specific particle size occurs when the $U^* \leq U^*_{sus}$ and when the dimensionless shields parameter (τ^*) is greater than or equal to the critical shields parameter (τ^*_c). The shields parameter is a function of the hydraulic conditions in the forcemain and the diameter of the particle and is provided as Equation 6.5. Critical shields parameter, as defined by Parker (2008), is provided as Equation 6.6.

$$\tau^* = \frac{(U^*)^2}{(G-1)gd_s} \tag{6.5}$$

$$\tau^*_c = \tau^*_{c\,O} \cos\alpha \left(1 + \frac{\tan\alpha}{\mu_c}\right) \tag{6.6}$$

where $\tau^*_{c\,O}$ is the critical shields number for a horizontal pipe; α is the angle of the forcemain with respect to the horizontal (adverse angle measured counterclockwise and positive); μ_c is the tangent of the angle of repose (tan ϕ) for the particle. Approximate values for angle of repose are summarized in Table 6.3. Equation 6.6 accounts for the downward gravitational force exerted on a particle when resting on an inclined forcemain (Axworthy 2014). The critical shields parameter is determined from Equation 6.7.

$$\tau_{c\,O}^{*} = 0.5\left(0.22R_{ep}^{-0.6} + 0.06(10)^{\left(-7.7R_{ep}^{-0.6}\right)}\right) \quad (6.7)$$

Table 6.3: Approximate Angle of Repose Values by Particle Size (Julien 1997)

Class Name	d_s, mm / (in)	Angle of Repose, ϕ
Sand	> 0.25 (0.01)	30
	> 0.5 (0.02)	31
	> 1 (0.04)	32
Gravel	> 2 (0.08)	33
	> 4 (0.16)	35
	> 8 (0.31)	36
	> 16 (0.63)	38
	> 32 (1.26)	40
Cobble	> 64 (2.52)	41
	> 128 (5.04)	42
	> 256 (10.08)	42

Bed motion of large particles can cause erosion of the pipe invert as shown in Figure 6.4.

Figure 6.4: Erosion of Forcemain Invert Due to Sliding Bed Conditions (Copeland 2013)

The maximum particle size conveyed under bed motion was calculated for each system in the Research Dataset using Microsoft Excel. Since transport through bed motion occurs when $U^* \leq U_{sus}^*$ and when the dimensionless shields parameter (τ^*) is greater than or equal to the critical shields parameter (τ_c^*)

($\tau^* \geq \tau_c^*$); a macro was developed to determine the maximum theoretical d_s assuming $\tau^* = 0.95\tau_c^*$ to ensure particle transport through bed motion.

The maximum theoretical particle size that can be transported through bed motion for each forcemain system is presented in Figure 6.5 and shows a general trend of increased particle size transported through bed motion with increasing velocity; which follows the same general pattern observed in Figure 6.3. From Figure 6.5, the theoretical particle size transported was calculated to be less than 50 mm (2 in), which is classified as gravel. As with suspended particles, bed motion is determined by the friction velocity, U*. The particle size transported through bed motion as a function of U* is presented in Figure 6.6.

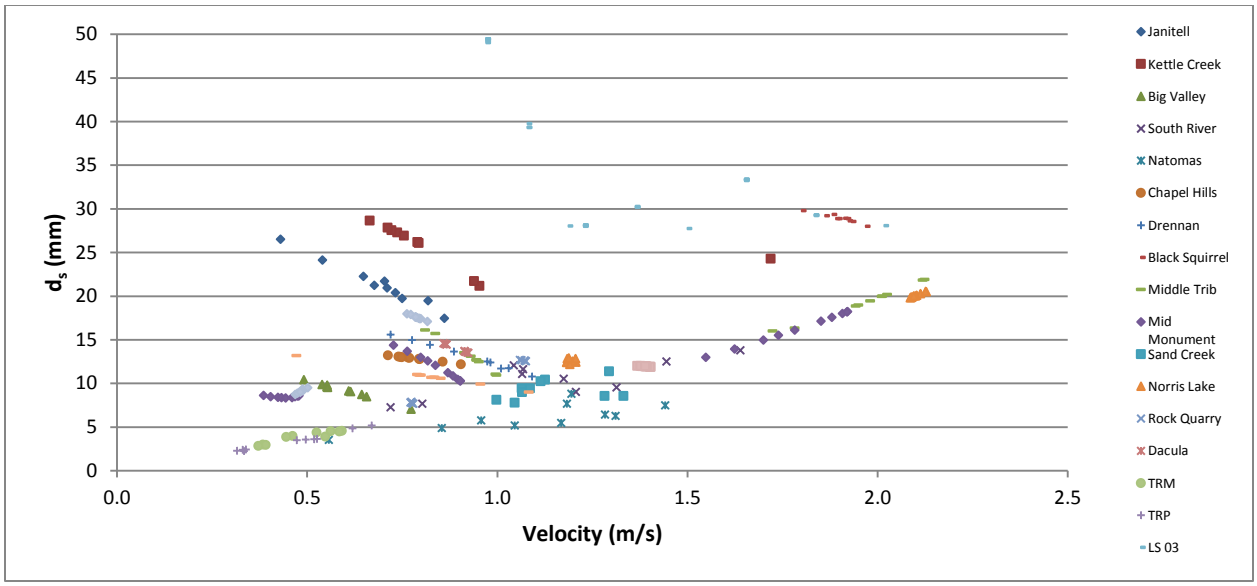

Figure 6.5: Maximum theoretical particle size transported through bed motion (by system)

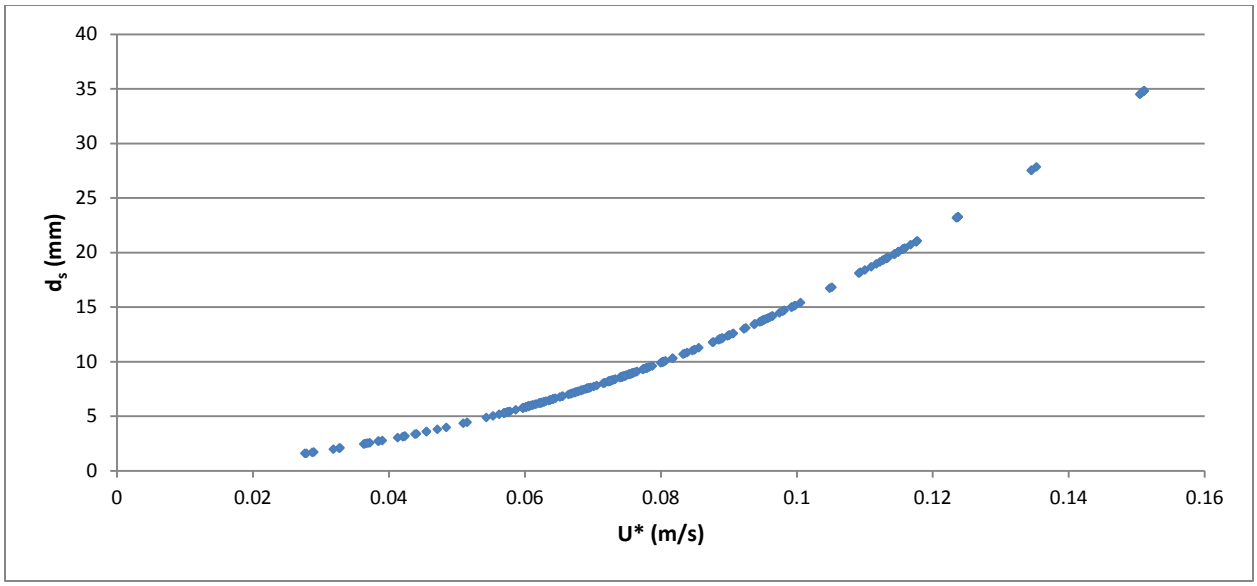

Figure 6.6: Maximum particle size transported through bed motion as a function of shear velocity

The largest particle transported through bed motion was calculated for various adverse angles. Although the results are not presented here, the maximum particle size that could be transported decreases as the adverse angle increased. The particle size reaches a minimum at an adverse angle approximately equal to the particles angle of repose. Results suggest that vertical deflections in wastewater forcemains should not exceed the angle of repose of the material being transported through bed motion. Axworthy (2014) reached a similar conclusion and Hashimoto et al, (1980) reported that compared to the horizontal case, flow up an incline tends to require higher throughput velocities in order to avoid deposition.

In an experimental investigation carried out at Queen's University, Wilson & Tse (1984) evaluated the transport of four particle sizes between 1 mm and 6 mm at angles of inclination up to 40 degrees from the horizontal. Wilson & Tse (1984) plotted the change in deposited velocity (Δ_D) against the angle of inclination, presented as Figure 6.7. Results show that the change in depositional velocity reaches a maximum at an angle of approximately 30 degrees and continues to 40 degrees. For the materials tested this maximum velocity was approximately 50 percent larger than that required to move a deposit in a horizontal pipe. This large difference is clearly a matter of importance for both design and operation of pipelines with inclined sections (Wilson 2006).

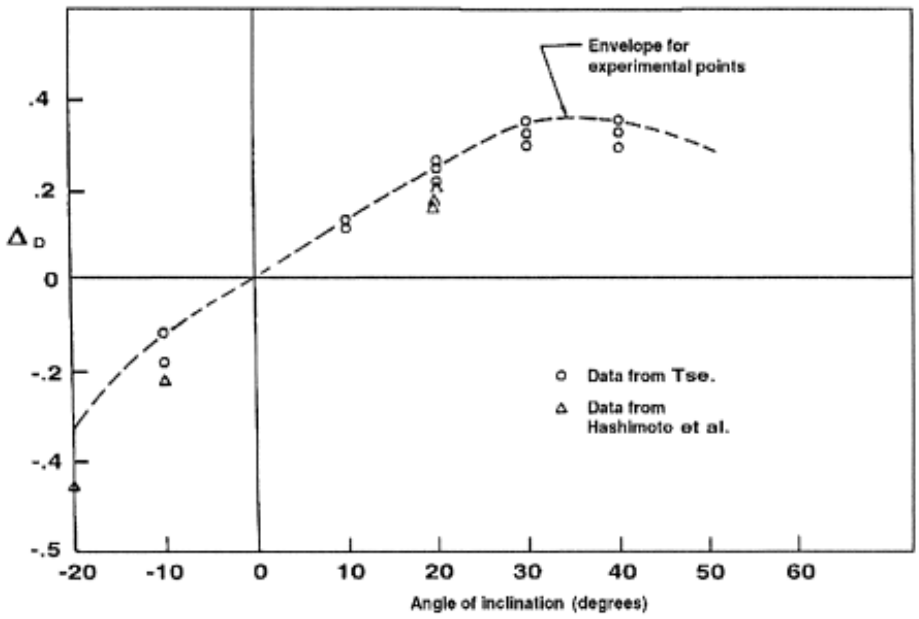

Figure 6.7: Change in Deposition Velocity from Angle of Inclination (Wilson & Tse 1984)

May (2001) evaluated self-cleaning velocities required to convey sand and gravel particles through inverted sewer siphons and determined that the maximum velocity required to prevent deposition occurred at an adverse angle between approximately 30 and 37.5 degrees. Results are consistent with results presented above and confirms that the maximum adverse angle of deflection along a forcemain transporting coarse particles should not exceed the particles angle of repose. Pipeline angles greater than the angle of repose could further decrease the ability to transport particles through bed motion. Therefore, the maximum adverse angle along a forcemain may be limited to 30 degrees (from horizontal) unless the diameter along the rising limb is decreased to increase velocity to provide an equivalent transport capacity.

Relationships for bed motion transport in pipelines subjected to biofilms could not be found in the literature. This condition should be further studied to determine how biofilms affect the incipient motion of particles and bed motion transport in forcemains. From the above analysis, sand was determined to be the maximum particle size transported through suspension and gravels are typically transported through bed motion. Both of these items are evaluated further in Section 8.2.

6.1.1.3 Vertical Pipes

In order for sediment to be transported in a vertical pipe, the particle must be suspended in the pipe flow ($U^* > U^*_{sus}$) and the average velocity in the pipe must exceed the fall velocity (ω_o) of the particle. Fall velocity (ω_o) of a particle is determined from Equation 6.8:

$$\omega_o = \left(\frac{4}{3}(G-1)\frac{g d_s}{C_D}\right)^{0.5} \tag{6.8}$$

Where C_D is the particle drag coefficient calculated from Equation 6.9, which is best suited for natural sands and gravels with $R_{ep} < 10^4$ (Julien 1995). Turton and Levenspiel (1986) proposed Equation 6.10 to estimate the particle drag coefficient of a sphere for $R_{ep} < 3x10^5$.

$$C_D = \frac{24}{R_{e\,p}} + 1.5 \tag{6.9}$$

$$C_D = \frac{24}{R_{e\,p}}\left(1 + 0.173R_{ep}^{0.657}\right) + \frac{0.413}{1+1.63x10^4 R_{ep}^{-1.09}} \tag{6.10}$$

Fall velocity was computed for particle sizes ranging from 0.125 mm to 64 mm. Equations 6.9 and 6.10 were both evaluated in order to compare the fall velocity for both spherical and natural particles. Analysis was performed assuming a water temperature of 18 °C (64.4 °F) and particle specific gravity, G, of 2.65. Results are presented in Table 6.4 and Figure 6.8.

Table 6.4: Comparison of C_D and Fall Velocity Based on Particle Size

d_s (mm)	d_s (in)	R_{ep}	C_D (Julien) [1]	C_D (Turton) [2]	ω_o (m/s) (Julien) [1]	ω_o (m/s) (Turton) [2]
0.125	0.005	5.467E+00	5.89	6.71	0.02	0.02
0.25	0.010	1.546E+01	3.05	3.18	0.04	0.04
0.5	0.020	4.373E+01	2.05	1.69	0.07	0.08
1	0.039	1.237E+02	1.69	0.99	0.11	0.15
2	0.079	3.499E+02	1.57	0.64	0.17	0.26
4	0.157	9.896E+02	1.52	0.46	0.24	0.44
8	0.315	2.799E+03	1.51	0.39	0.34	0.67
16	0.630	7.917E+03	1.50	0.41	0.48	0.92
32	1.260	2.239E+04	1.50	0.45	0.68	1.23
64	2.520	6.333E+04	1.50	0.47	0.96	1.71
80	3.150	8.851E+04	1.50	0.47	1.07	1.91

[1] Natural Particles; [2] Spheres

Wilson (2006) presented Equation 6.11 to approximate the settling velocity of a sphere. Figure 6.8 presents the results of Wilson's equation plotted along with the results from Table 6.4.

$$V_{ts} = 1.73\sqrt{g d_s (G-1)} \tag{6.11}$$

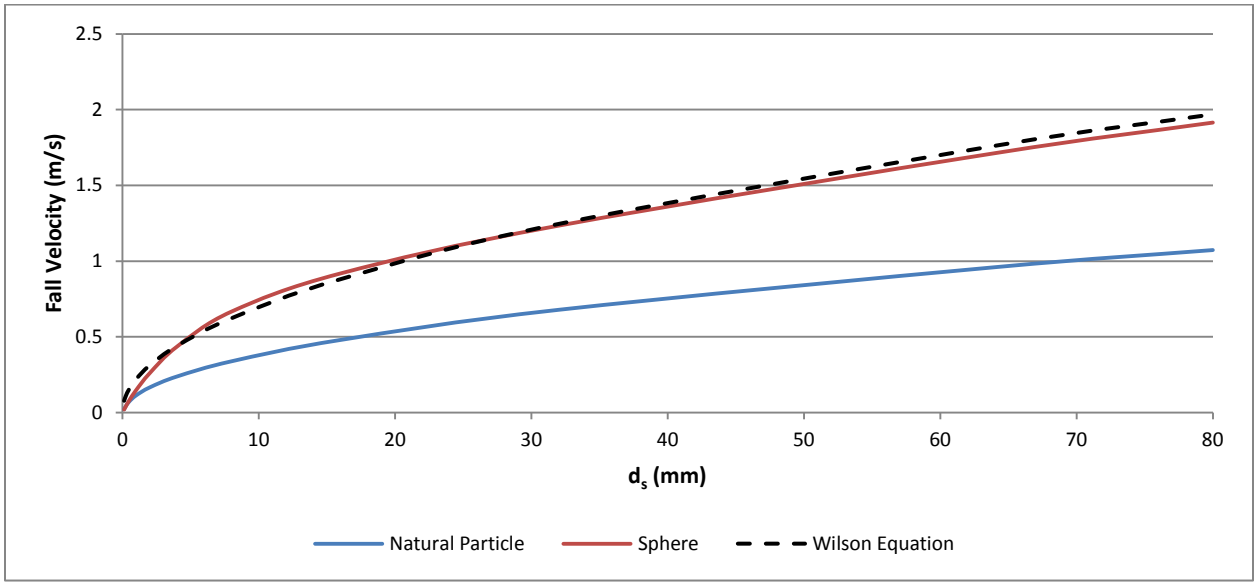

Figure 6.8: Comparison of Fall Velocity Based on Particle Size

From Figure 6.8, Equation 6.11 provides good agreement with the terminal settling velocity of a sphere and is easier to apply than Equations 6.8 and 6.10. The results provided in Table 6.4 show that the fall velocity of natural particles is approximately ½ of the fall velocity of a sphere.

As shown in Appendix D.2, the TRM, TRP, LS 15, LS 03, Natomas and South River forcemains contain vertical sections. Based upon the data collected for these systems, the maximum particle size (assuming a sphere) that can be transported through the vertical risers varies from 0.5 in. (12.7 mm) to less than a 2 in. (50.8 mm), depending on the pipe diameter and flowrate of the system.

In order to transport solids in a vertical riser, continuous flow at a velocity greater than the fall velocity must be provided over a duration long enough to travel the length of the riser section. However, unnecessarily high velocity could cause excessive pipe wear and energy losses. For design purposes, it is recommended to determine the settling velocity based upon a sphere because it provides the most

conservative approach. The diameter of the riser section can then be sized to provide a velocity greater than the settling velocity of the design particle.

6.1.2 Air in Forcemains

This section provides a brief introduction to the causes, mitigation, and transport of air within forcemains. The presence, or accumulation of air/gas within a forcemain can reduce its capacity and may cause corrosion of metallic and concrete pipe materials. Air can be introduced into a forcemain through a number of ways including:

- Initial filling of the pipeline during commissioning;
- As pressure drops and/or temperature rises, dissolved air comes out of solution;
- Cascading of sewage in to lift station wet well and subsequent pumping;
- Entrainment due to vortices in pump suction /intake piping due to insufficient submergence;
- Hydraulic jump – the flow within the pipe system may change from pressurized to gravity at high points. A hydraulic jump could form in a downward sloping pipe due to air accumulation even if the forcemain remains pressurized;
- Forcemain filling and emptying due to repairs or topographic features of the forcemain such as where the forcemain discharge elevation is below a high point along the forcemain;
- Gas formation due to biological activity;
- Surge events – negative pressures within the pipeline during a hydraulic transient event can cause air to enter the pipeline through pipe joints or vacuum valves; and
- Due to cyclic operation of a lift station system, sections of the forcemain may drain at the end of the pumping cycle.

In addition to capacity reduction, anaerobic conditions through biological processes within the biofilm can lead to high hydrogen sulfide development that can cause odors or corrosion of the pipe lining. This is major concern in forcemains with low velocities and long Hydraulic Retention Times (HRT). As illustrated in Figure 6.9, air transport in pipes can occur under several different patterns in vertical and

horizontal pipes. The transition from one flow pattern to another is a function of a number of different variables including: the gas and liquid mass flow rates, the properties of the fluid, and the pipe diameter and angle of inclination to the horizontal (Escarameia 2006).

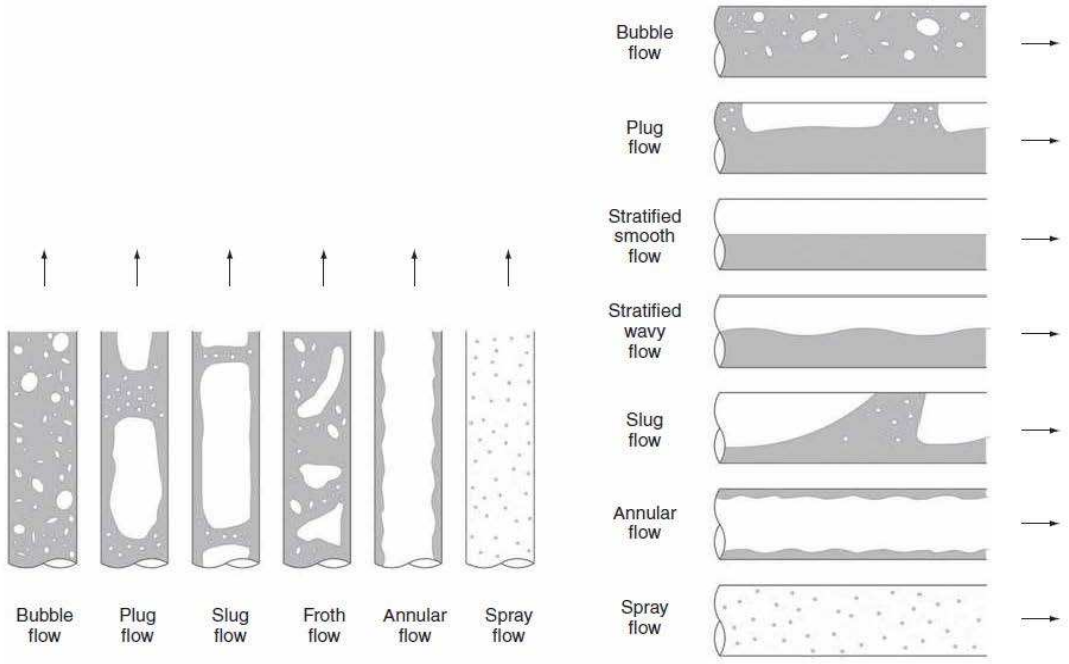

Figure 6.9: Flow patterns in vertical and horizontal pipes (air is represented in white) (Escarameia 2006)

Due to the intermittent operation of wastewater pumps, forcemains can accumulate gas in elevated sections of a pipeline. If gas accumulation is present along the top of a downward sloping segment, a hydraulic jump will develop at the tail end of the gas volume ejecting bubbles from the large pocket. The pumping action of the hydraulic jump transports part of the ejected gas down to the bottom of the declining section (Pothof 2008). Wisner et al. (1975) suggested that the hydraulic removal of air from pipelines may take place due to either sweeping or generation and entrainment. Sweeping is the bodily removal of the whole air pocket. Removal by generation and entrainment occur at the downstream end of the hydraulic jump as shown in Figure 6.10. Generation refers to the process at the downstream end of a hydraulic jump, while entrainment is used to describe the movement within the liquid of these newly generated bubbles (Escarameia 2006). The sweeping condition corresponds to full bore pipe flow whereas generation and entrainment occurs under partially filled conditions.

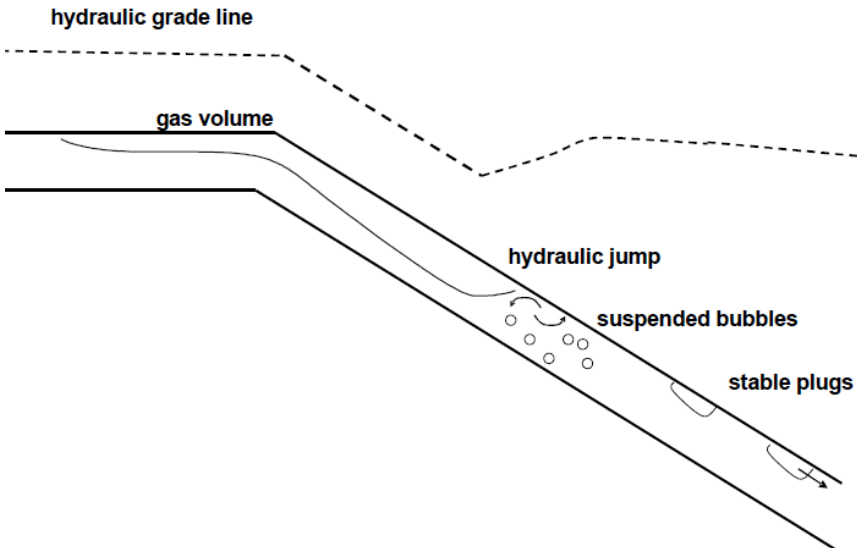

Figure 6.10: Schematic overview of downward gas transport by flowing water (Pothof 2008)

As shown in Figure 6.10, large air pockets accumulated along highpoints reduce the effective pipe cross sectional area and throttles the flow resulting in free surface flow conditions, which causes an increase in energy loss. Certain turbulent conditions of the downstream hydraulic jump may enable to break up large air pockets into smaller air bubbles which can be transported downstream provided the velocity is adequate for conveyance. The velocity required to convey gas along downward sloping pipelines is called the clearing velocity. Although several researchers have developed equations to predict the clearing velocity, there is no generally accepted formula for predicting transport of air in pipelines.

Critical clearing velocity for a given pipe slope has been taken by several researchers as proportional to $(gD)^{0.5}$, where g is acceleration due to gravity and D is pipe diameter (Escarameia 2006). Kent (1952) performed experiments in both 33 mm and 102 mm stationary and downward sloped pipes (15° and 60°). The length of the downward sloped pipe was 5.5 m for the 102 mm diameter pipe. Although Kent (1952) determined an equation for the clearing velocity, Mosvell (1976) provided a better fit to Kent's (1952) data and is provided as Equation 6.12.

$$\frac{V_c}{\sqrt{gD}} = 0.55 + 0.5\sqrt{sin\theta} \tag{6.12}$$

Where V_c is the clearing velocity; g is acceleration due to gravity; D is diameter; and θ is angle from horizontal. Wisner (1975) focused on stable air volumes instead of the clearing velocity and developed Equation 6.13. Experiments were performed in a 245 mm diameter pipe at a fixed downward angle of 18°.

$$\frac{V_c}{\sqrt{gD}} = 0.825 + 0.25\sqrt{sin\theta} \tag{6.13}$$

Escarameia et al. (2006) performed experiments in a 150 mm diameter pipe with gas pockets up to 5 Liters and downward slopes up to 22.5°. Escarameia et al. (2006) proposed Equation 6.14 for the clearing velocity.

$$\frac{V_c}{\sqrt{gD}} = 0.61 + 0.56\sqrt{sin\theta} \tag{6.14}$$

Clearing velocity was evaluated using the above equations for pipe diameters ranging from 6 to 66 in. in. and downward slopes ranging from horizontal to vertical. Figure 6.11 presents the clearing velocity as a function of diameter for horizontal and 45° downward sloping angles. Results show that the Wisner's equation provides the most conservative clearing velocity for horizontal conditions and Equation 6.14, developed by Escarameia et al. (2006) provides the most conservative clearing velocity for a 45° downward angle. Results also indicate that the required clearing velocity increases with diameter.

Figure 6.12 presents the effect of downward angle on the clearing velocity for 12 in., 24 in., and 48 in. (304.8 mm, 609.6 mm, and 1219.2 mm) diameters. Results show that both Kent / Mosvell and Escarameia follow a similar trend whereas, the results from Wisner appear to require greater clearing velocities for horizontal pipes; it should be noted that Wisner's research focused on air clearing in horizontal pipes. Equation 6.14, developed by Escarameia et al. (2006) provides the most conservative clearing velocity for downward angles greater than 30°.

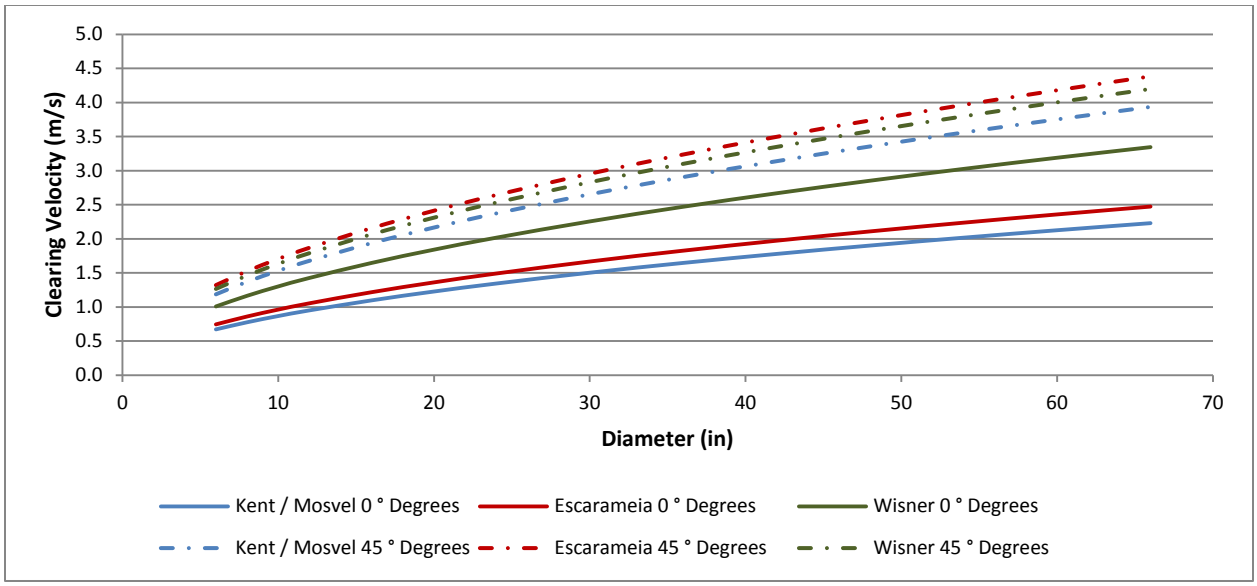

Figure 6.11: Clearing Velocity versus Diameter – by Downward Angle

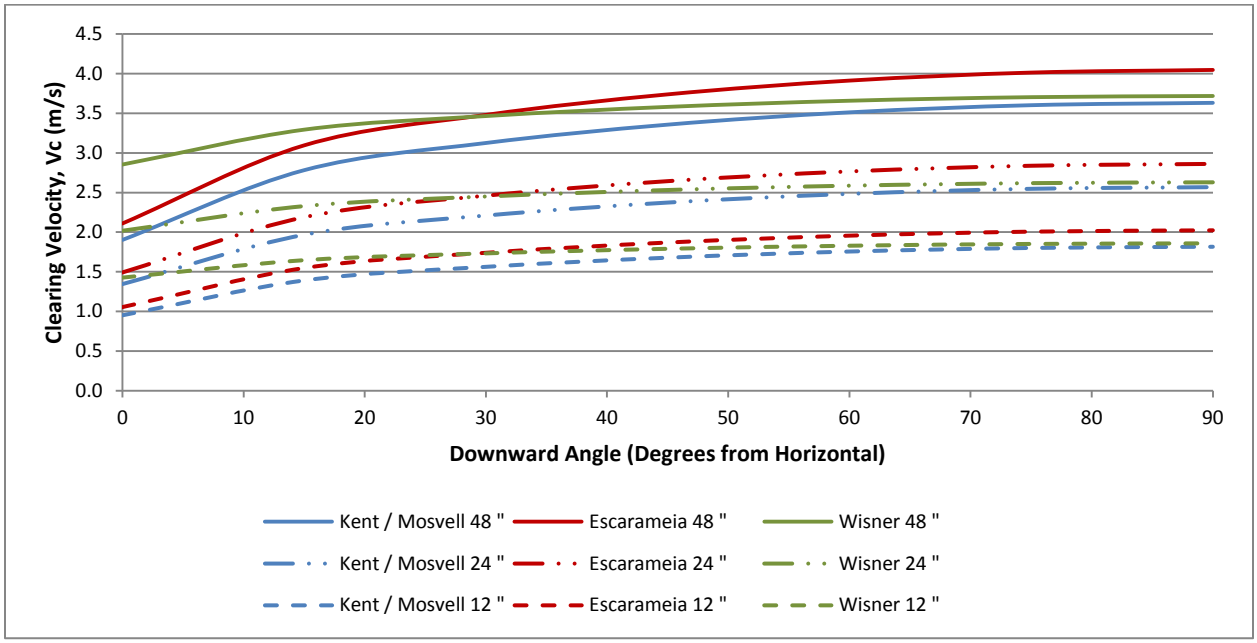

Figure 6.12: Clearing Velocity versus Downward Angle – by Diameter

Lubbers (2007) performed experiments on 110 mm, 220mm, and 500 mm (4.3 in., 8.7 in., and 19.7 in.) diameter pipes at downward sloping angles ranging from 5° to 30° and 90°. Lubbers determined the clearing velocity is at maximum for downward slopes of approximately 10° and that the clearing velocity decreases with diameter. These results are in sharp contrast with the results presented above. Lubbers' results are for stable plugs downstream of the hydraulic jump whereas the other clearing velocities are for

large individual gas pockets. Experimental observations indicated that gas pockets can accumulate along a control section located at the transition between pipes with sub- and supercritical flows, forcing free surface flow conditions below pockets (Lubbers & Clemens 2005).

Based upon the above analysis, Equation 7.14 developed by Escarameia (2006) is recommended because it provides the most conservative estimate for clearing velocity. Results show that a sufficiently high fluid velocity should be used for air/gas removal from a pipeline. Additional mitigation measures to manage air in pipelines include limiting the number of undulations and length along the falling limb of the pipeline; reducing the diameter along the downward sloping pipe segment to increase the velocity; or removing air mechanically through air release valves.

Although air can be removed from wastewater forcemains using air release valves, maintenance of sewage air release valves can be difficult; slime buildup can render them inoperable, and improper placement will prevent air purging from the system. In addition, the results from Lubbers suggest that an air valve located at the high point of a gradual sloped pipeline would be ineffective because air could become trapped along the sloping portion of the pipeline.

Air pockets can decrease capacity significantly which causes increased power consumption. Pozos (2007) indicated that investigations on a variety of water pipelines throughout the world have revealed that entrapped air can reduce their efficiency by as much as 30%. Most pipeline systems are commonly operated with air volumes that diminish system flow efficiencies by 15 to 20%. Pockets of compressed air present enormous obstacles for pumping fluids. Entrapped air increases head pressure by 20% and will force pumps to perform 20% harder, and thus demand 20% more electrical energy to overcome the restrictions. In addition, Escarameia et al. (2005) stated that although limited reliable data was collected, test results appear to show that for the same flow conditions, the hydraulic gradient associated with flow with an air pocket is 25 to 35% larger than associated with water alone.

Increased headloss associated with air pockets could explain some of the variability in the calculated absolute roughness and C factors results presented in Chapter 5. Air clearing is evaluated further in Section 8.2.5.

Information presented above shows that the management of air within wastewater forcemains is critical. Air or gas pockets can cause a significant decrease in capacity, increased headloss, and extra power consumption. The presence of gas pockets are often a preliminary indicator of a potential failure location through corrosion (metallic and cementitious pipes). Leak detection technologies can identify potential trouble spots along the pipeline that may grow over time and lead to failure. Pothof (2011) indicated that these gas pockets are responsible for an estimated annual CO_2 release of 10,000 tons in the Netherlands, equivalent to the electric power consumption of 5,400 households.

Air release valves should generally be provided at high points along the pipelines for the release of air during filling as well as normal operation of the pipeline. Based upon field inspections of 500 miles of forcemains, Pure Technologies reported that 72% of air pockets are not at known high points (Dettmer 2014), which agree with the findings reported by Lubbers & Clemens (2005). Therefore, it is important to be able to clear air pockets from forcemains since air valves may not be typically provided at these locations. Future forcemain design practice should consider adequate velocities to remove air pockets in order to decrease the reliance on air valves in the event that they become inoperable.

6.1.3 Sulfide Generation

This section provides a brief introduction to hydrogen sulfide generation and the problems associated with hydrogen sulfide in forcemains. As presented in the previous section, gas pockets can develop in forcemains resulting in potential cross sectional flow area reduction and can promote the corrosion of any cement or ferrous pipe material with which they are in contact.

Sulfide related problems are a major concern when designing and operating wastewater collection systems. The major problems related to buildup of sulfide in sewers include corrosion of sewer structures, odor nuisance and health impacts on sewer workers (EPA 1974). These problems are directly associated with gaseous hydrogen sulfide (H_2S). When H_2S is in contact with sewer surfaces exposed to the sewer atmosphere, this gas can be absorbed and oxidized to sulfuric acid by aerobic and autotrophic Thiobacillus

bacteria. Typical H_2S concentration in a sewer atmosphere varied from 0.2 to 300 ppm (Yongsiri 2004, Mak 2011).

Hydrogen sulfide (H_2S) gas is generated within the anaerobic slime layer formed on submerged pipe walls. H_2S releases from the slime layer and rises into the pipe atmosphere and is oxidized by bacteria on the unsubmerged portion of the pipe in the presence of moisture, forming sulfuric acid (H_2SO_4) which corrodes metallic and cementitious based pipe. This phenomenon has been reported to occur worldwide (Pozos 2015, EPA 1991, Sand and Bock 1984, Schafer et al. 1990). Entrained air pockets are a major source of oxygen and major contributors to this type of corrosion (Zloczower 2010). It is well known that most of the gas in a pocket is air and not H_2S (Pozos 2012). However, under certain conditions, if the concentration of H_2S is high and the pockets persist long enough they can damage the line by corrosion (Islander et al. 1991).

The Water Environment Research Foundation (WERF) Inspection Guidelines for Wastewater Force Mains (Thomson 2010) indicates that approximately 50% of ferrous forcemain failures are due to either internal of external corrosion. Hydrogen sulfide and corrosion in wastewater systems are affected by dissolved sulfides, pH, BOD and temperature, dissolved oxygen, and velocity. However, H_2S in the water phase can be transferred to the air phase and therefore can only cause corrosion if air pockets exist within the forcemain.

Once hydrogen sulfide leaves the dissolved phase and enters the gas phase, it can cause odor and corrosion. Hydrogen sulfide gas is a colorless but extremely odorous gas that can be detected by the human sense of smell in concentrations as low as 0.00047 ppm. It is also very hazardous to humans in high concentrations and can cause a number of health-related problems, including death (Kienow 1989). A summary of H_2S concentrations, associated impacts, and health effects are provided in Table 6.5 and examples of corrosion in wastewater pipelines is presented in Figures 7.13 and 7.14.

Table 6.5: H_2S Levels, Impacts, and Health Effects (Kienow 1989)

Hydrogen Sulfide Concentration (ppm)[1]	Impacts and Health Effects
<0.0021	Olfactory detection Threshold
0.00047	Olfactory recognition Threshold
0.5 to 30	Strong odor
10 to 50	Headache, nausea, and eye, nose, and throat irritation
50 to 300	Eye and respiratory injury
300 to 500	Life threatening (pulmonary edema)
>700	Immediate death

[1] 1 ppm ≈ 1 mg/l

Figure 6.13: Forcemain Failure Due to H_2S Attack (Copeland 2013b)

Figure 6.14: Hydrogen Sulfide Corrosion of Concrete Pipe (Dawalt)

Anaerobic conditions develop when the dissolved oxygen concentration reaches zero; therefore, the formation of sulfide is a function of the oxygen demand of the sewage plus the oxygen demand of slimes along the wall of the forcemain. The principal driving force for corrosion in wastewater systems is biogenic sulfuric acid production which is produced from hydrogen sulfide gas. Although sulfide is formed within the forcemain during normal operation, sulfuric acid cannot form unless the pipeline contains an air pocket. Therefore, limiting air pockets will reduce corrosion potential within the pipeline; however, discharge of the wastewater to a downstream structure could induce turbulence and release sulfide and cause corrosion of the structure and downstream sewer pipe.

American Society of Civil Engineers (ASCE) Manual of Practice No. 69 - Sulfide in Wastewater Collection and Treatment Systems (Kienow 1989) identifies Equation 6.15 for estimating the hydrogen sulfide concentration in forcemains.

$$\frac{d[S]}{dt} = 0.0131 \frac{(1+0.12D)}{D} [BOD_5](1.07)^{T-20} \quad (6.15)$$

where d[S]/dt = sulfide production rate (mg/l-hr); d[S] = sulfide concentration (mg/l); dt = detention time in forcemain (hr) = (pipeline length/ velocity); D = diameter (ft); BOD_5= 5 Day Biochemical Oxygen Demand (mg/l); and T = wastewater temperature (°C).

Although the literature does not provide a threshold value of H_2S concentration in a sewage system before giving rise to concern about corrosion, there are two main studies referenced on the subject. One was a paper produced by the Los Angeles County Sanitation Districts which demonstrated that a H_2S gas concentration of 2 ppm or less did not allow the growth of Thiobacillus and therefore prevented serious pipe damage. Once Thiobacillus bacteria colonize, significant pipe damage can occur. Another study from South Africa identified that Thiobacillus bacteria could exist in concentrations between 2 to 5 ppm. This tends to make one believe that Thiobacillus bacteria become substrate-limited at H_2S gas concentrations below 2 ppm. Thus, 2 ppm would be a good number to use for continuous concrete pipe exposure in a sewer environment without producing sulfuric acid (Kienow 1989).

The problem with this approach is that the hydrogen sulfide gas concentration in a sewer is never constant. In addition, recent studies on the effect of the Clean Water Act on sulfide production in domestic wastewater show that sulfide concentrations are rising dramatically as a result of regulation (Kienow 1989).

The rate of hydrogen sulfide production is influenced by both the surface area of the pipe in contact with the sewage and the period of contact. Boon (1992) determined that the frequency of pumping cycles did not have an effect on the rate of sulfide production and that travel time was a major factor. Corrosion rates depend on the sulfide concentration in the forcemain, rate of release of H_2S, and the pipeline material. Predicting corrosion rates are beyond the scope of this research. However, several equations are provided in the literature to estimate the corrosion rate and are detailed in ASCE Manual of Practice No. 69 - Sulfide in Wastewater Collection and Treatment Systems (Kienow 1989).

Sulfide concentration was estimated using Equation 6.15 for various input parameters to determine its sensitivity to diameter, detention time, BOD, and temperature. Typical BOD_5 (20°C) concentrations in

the United States range from 400 mg/l to 110 mg/l with an average of 181 mg/l (Kienow 1989). Effect of diameter was evaluated assuming a BOD_5 concentration of 181 mg/l, wastewater temperature of 20°C (68°F), and detention time of 1 hr. The results are presented in Figure 6.15 and show that the diameter has a significant effect on sulfide concentration.

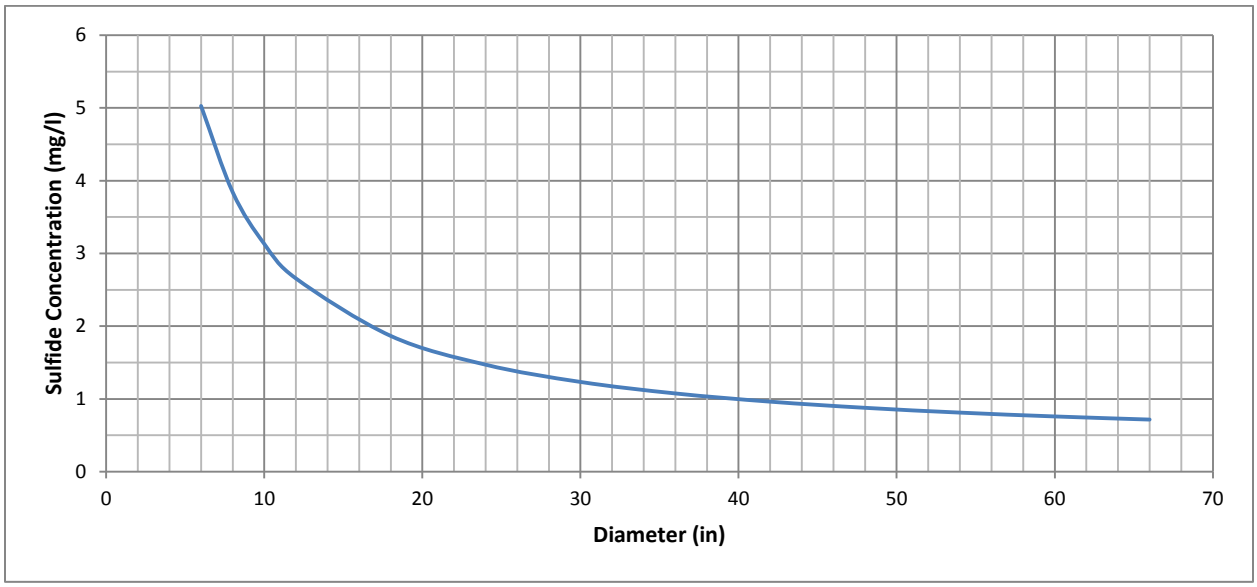

Figure 6.15: Sulfide Concentration: 181 mg/l BOD_5, 20°C, 1 hr Detention Time

The effect of BOD_5 concentration and temperature on sulfide concentration are presented in Figure 6.16 and Figure 6.17, respectively. As shown in Equation 6.15, the Sulfide concentration is proportional to the BOD_5 concentration and temperature. Therefore, as one would expect, sulfide concentration increases with both BOD_5 concentration and temperature.

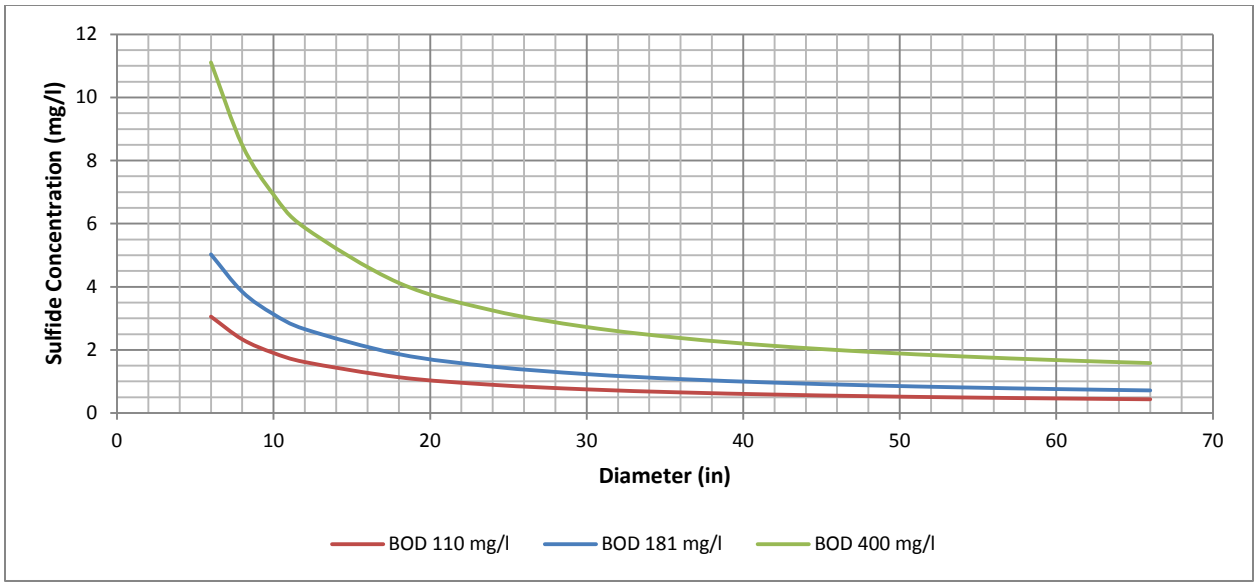

Figure 6.16: Sulfide Concentration: 20°C, 1 hr Detention Time – Effect of BOD_5

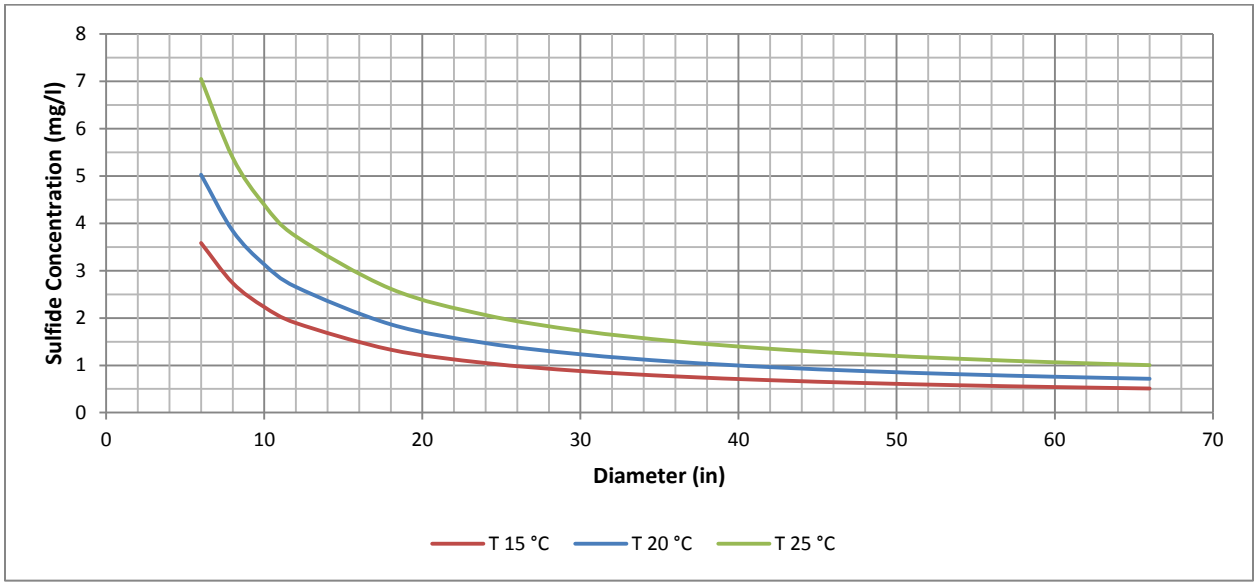

Figure 6.17: Sulfide Concentration: 181 mg/l BOD_5, 1 hr Detention Time

Sulfide concentration is also proportional to the detention time. Figure 6.18 presents the sulfide concentration based upon detention time for 6 in., 12 in. and 24 in. (152.4 mm, 304.8 mm, and 609.6 mm) diameters. Results show that detention time has a significant effect on sulfide concentration.

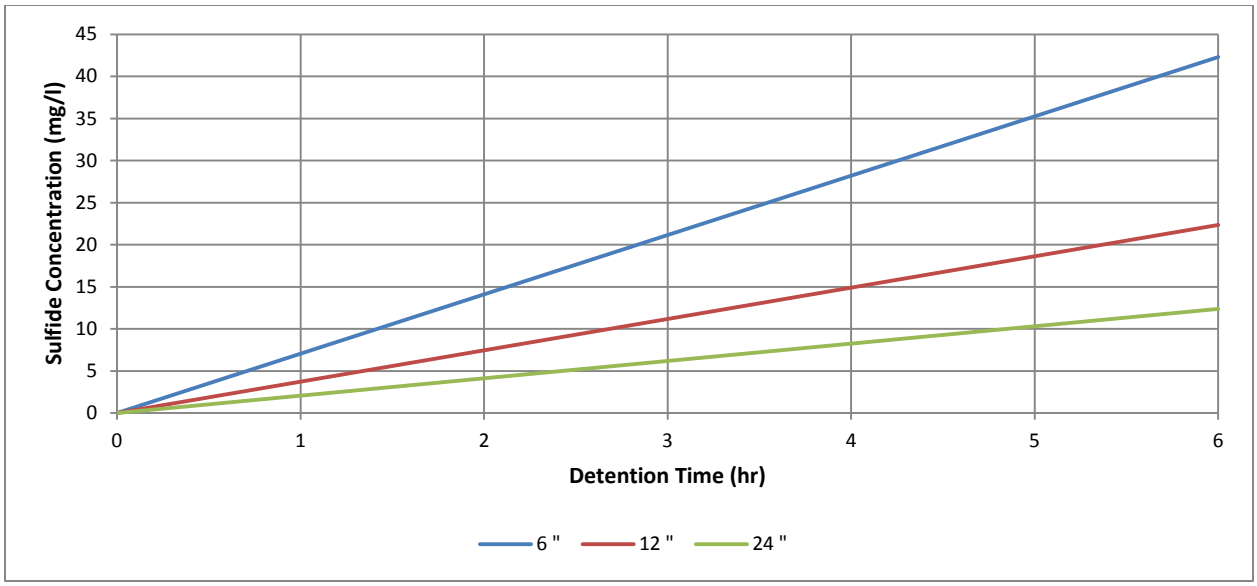

Figure 6.18: Sulfide Concentration by Diameter and Detention Time: 181 mg/l BOD_5, 20°C

When sizing a forcemain system, both the diameter and corresponding detention time should be considered. Results presented above show that the sulfide concentration increases as diameter decreases. However, conveying the same discharge through a smaller diameter pipe increases the velocity, which in turn reduces detention time. The effect of detention time was evaluated for a system conveying 2.36 cfs (0.07 cms) through a 1,000 ft long pipeline. Both 12 in. (304.8 mm) and 10 in. (254 mm) diameters were considered assuming a BOD_5 concentration of 181 mg/l at 20°C (68°C). Results are summarized in Table 6.6 and show that although the sulfide production rate (d[S]/dt) is higher for the 10 in. (254 mm) diameter system, the resulting decrease in detention time more than offsets this increase and reduces the estimated sulfide concentration. This suggests that an oversized forcemain, especially long forcemains, could produce very high sulfide concentrations.

Table 6.6: Comparison of Sulfide Concentration (d[S]) in 10 in. and 12 in. Diameter Pipe

Diameter (in)	12	10
Velocity (ft/s)	3.0	4.32
dt (hr)	0.0926	0.0643
d[S]/dt (mg/l-hr)	2.66	3.13
d[S] (mg/l)	0.25	0.20

Sulfide related problems are a major concern when designing and operating wastewater collection systems. Major problems related to buildup of sulfide in sewers include corrosion of sewer structures, odor

nuisance and health impacts on sewer workers (EPA 1974). Corrosion due to hydrogen sulfide is a major economic problem in sewer networks both because of renovation costs and the costs of preventive measures. The effect of sulfide concentration is discussed further in Section 6.2.1.

6.1.4 Operational Costs

As noted above, a majority of the pumps evaluated were found to be operating to the left of the design point, indicating that more head was required to overcome friction losses within the system than was originally designed. Shifting the pump operating point to the left usually causes a decrease in discharge and operating efficiency which causes the pump to run longer during each pumping cycle; this combined with a reduction in efficiency increases operational costs.

Pump operating points were compared to the design point to evaluate the potential increase in annual operating costs. Average flow at each operating point along with the average time the pumps were operational and remaining idle (Table 6.8) were used to determine the average annual operational costs. The average flow and pump cycle information were used since this analysis was not intended to be an energy audit of each system, but to merely provide an estimate of the change in annual estimated operational costs associated with the increased friction due to the pipe biofilm.

Assuming that the volume pumped remained the same for both operating conditions; the time the pumps were operating at the design point during each pumping cycle was determined by dividing the average volume pump per cycle by the design flow of the pump. The number of annual pumping cycles were determined from the revised pump operating time assuming that the time the pumps remained idle was the same. This was determined to be a valid assumption since the average inflow rate would be the same in both cases.

Operational costs were calculated by multiplying the brake horsepower (BHP) (converted to kW) by the operating time/cycle and the number of cycles assuming an electrical rate of $0.09/ kw-hr. The results are summarized in Table 6.7 and show the change in operating costs is nearly insignificant when comparing the average pump operating point to the design point of the pump.

Table 6.7: Comparison of Calculated Annual Operating Costs at Average Flow and Pump Design Point

System	Average Flow Operating Point					Annual Pump Runtime (days)	Design Point Annual Operating Cost	Change in Operating Cost	Operating Cost Increase (%)
	Flow (gpm)	TDH (ft)	η (%)	BHP	Annual Operating Cost				
Janitell	88.3	55.0	30.8	4.0	$ 547	85.4	$ 377	$ 170	45.2%
Kettle Creek	997.6	105.5	81.6	32.6	$ 9,153	174.3	$ 8,647	$ 506	5.9%
Big Valley	80.8	53.7	42.4	2.6	$ 124	29.8	$ 117	$ 7	5.7%
Chapel Hills	431.3	142.0	57.0	27.2	$ 700	16.0	$ 637	$ 62	9.8%
Drennan	751.9	100.1	71.4	26.6	$ 301	7.0	$ 300	$ 1	0.4%
Black Squirrel	1,045.4	116.7	70.4	43.8	$ 3,058	43.3	$ 2,959	$ 99	3.3%
Middle Trib	1,083.0	158.9	66.1	65.7	$ 10,560	99.7	$ 10,439	$ 121	1.2%
Mid Monument	984.0	156.9	54.0	72.3	$ 3,957	34.0	$ 3,759	$ 198	5.3%
Rock Quarry PS	1,120.8	210.7	64.4	92.6	$ 4,745	31.8	$ 3,664	$ 1,082	29.5%
Dacula	1,970.3	200.4	69.7	143.2	$ 21,608	93.7	$ 19,167	$ 2,441	12.7%
LS 03	2,042.5	115.9	75.7	79.1	$ 14,338	112.5	$ 14,580	$ (242)	-1.7%
LS 06	2,033.9	104.3	76.0	70.6	$ 23,419	206.0	$ 23,595	$ (176)	-0.7%
LS 15	1,682.0	75.9	76.9	41.9	$ 16,280	241.0	$ 16,132	$ 148	0.9%
Jimmy Camp	1,400.0	205.1	73.3	99.0	$ 7,783	48.8	$ 7,582	$ 201	2.7%

η – Efficiency; BHP - Brake Horsepower

6.1.5 Forcemain Cleaning

Although forcemain cleaning is beyond the scope of this research; it does warrant a brief discussion. Forcemain cleaning may be desired to remove sediment deposition, grease, or air blocking in order to restore hydraulic capacity. Numerous technologies are available for forcemain cleaning and generally include either mechanical cleaning or the use of a pipeline pig. Forcemain cleaning may only provide a temporary improvement without correcting the problems that lead to its degraded condition. Ice pigging is a promising new technology that pumps a supercooled water solution forming a solid ice plug (pig) inside the pipe that melts as it travels along the pipe eliminating the need for launching or receiving ports.

6.2 Lift Station Operation

6.2.1 Pumping Cycles

The approach described in Section 4.4 was used to calculate the average pump runtime and time between pump cycles for 2 hr increments over each 24-hr period starting at time 0:00 for lift stations with constant speed pumps (Table 4.6). Two hour increments were selected because some pumps cycled less than once per hr; computational limitations resulting in large files; and it was determined that 2 hr time blocks generally provided adequate results suitable for this research. Since the results are presented as an average over 2 hr increments, the sum of the average run time per cycle and time between pump cycles multiplied by the number of cycles equals 120 minutes. Therefore, the average number of cycles per hour is determined by dividing the number of cycles by 2.

Results provide insight into the frequency and duration of pumping cycles, as well as, average operational conditions of the lift stations included in this research. Results were used to determine if any correlations can be made between the calculated roughness parameters and the pump operational data. Each systems response to inflow is clearly observed in Figures 6.19 to 6.33. As one would expect, the longest time between pumping cycles occurs between 0200 and 0400 with a sharp increase in pump cycles between 0400 and 0800, corresponding to morning peaks.

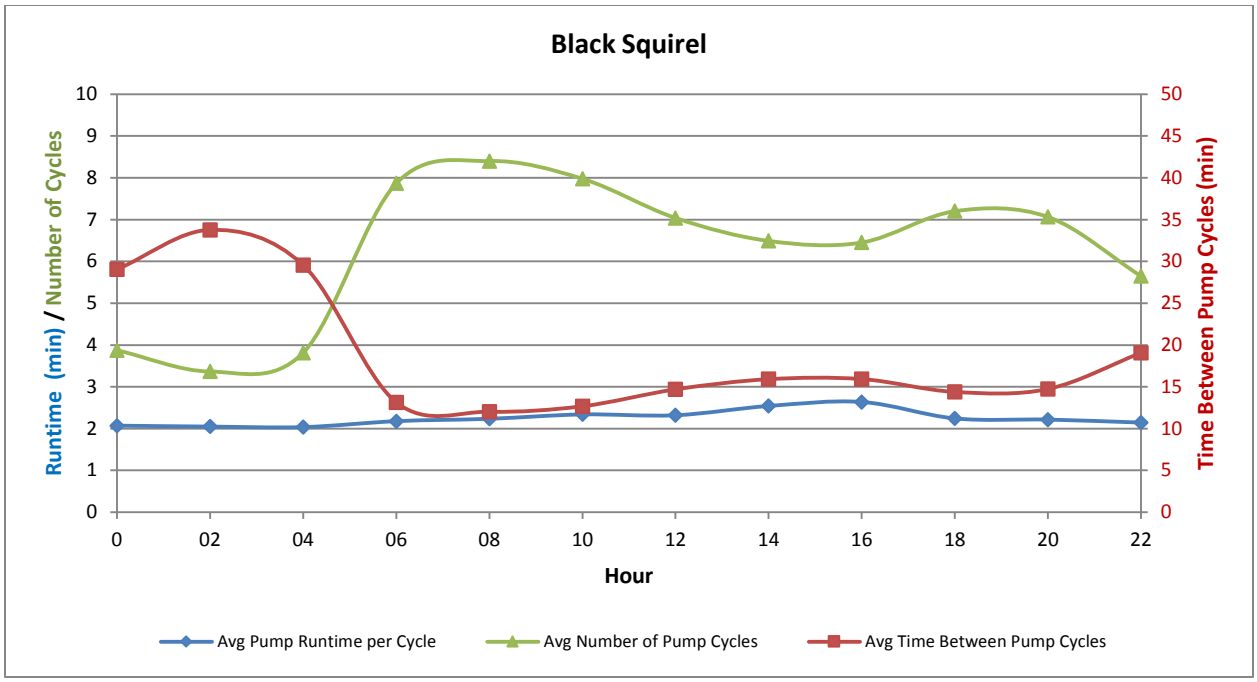

Figure 6.19: Pumping Cycles – Black Squirrel

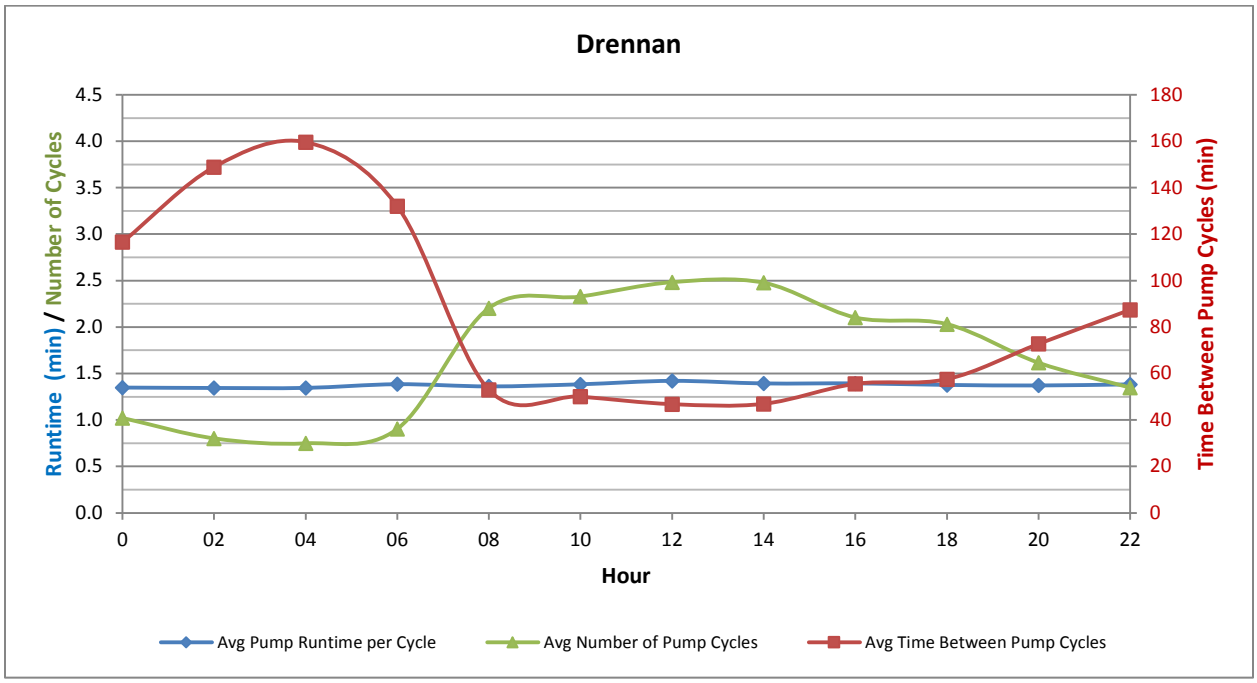

Figure 6.20: Pumping Cycles – Drennan

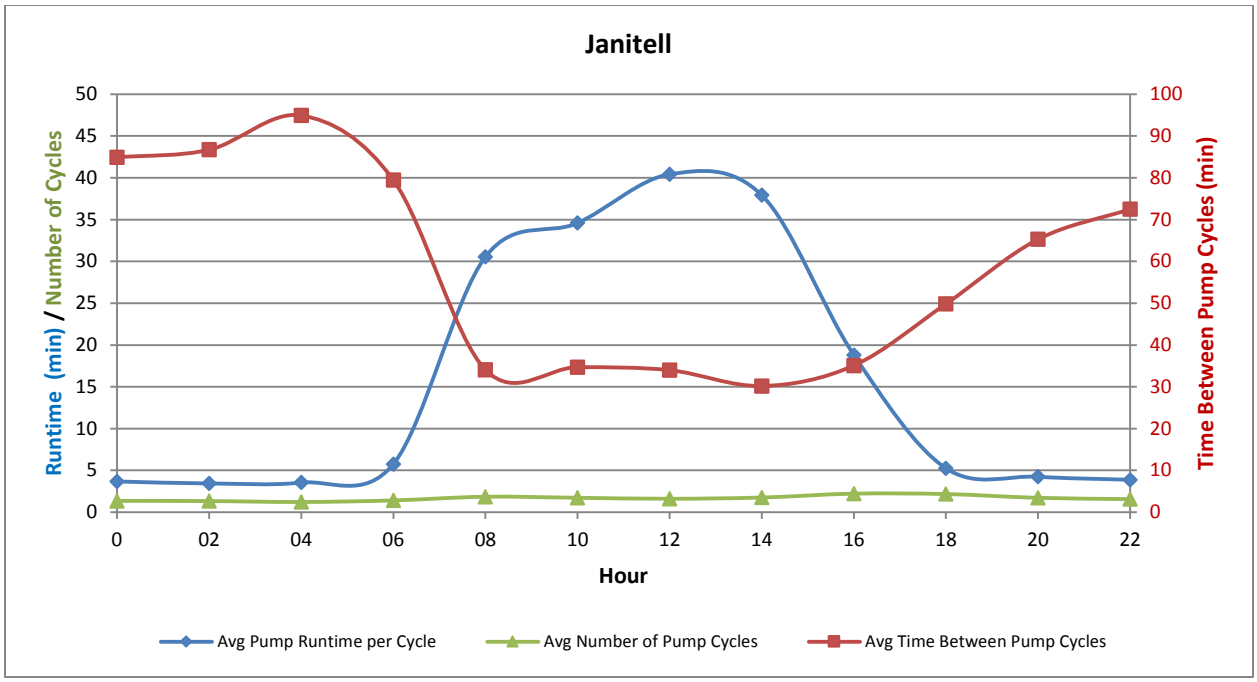

Figure 6.21: Pumping Cycles – Janitell

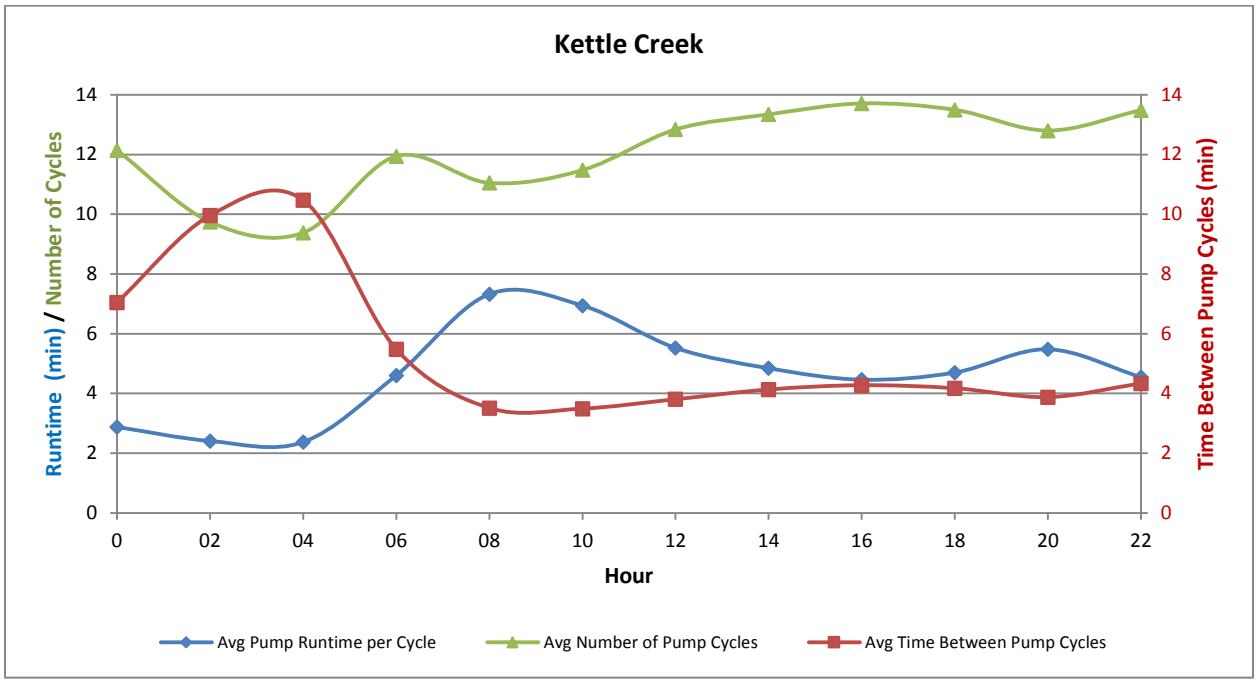

Figure 6.22: Pumping Cycles – Kettle Creek

Figure 6.23: Pumping Cycles – Mid Monument

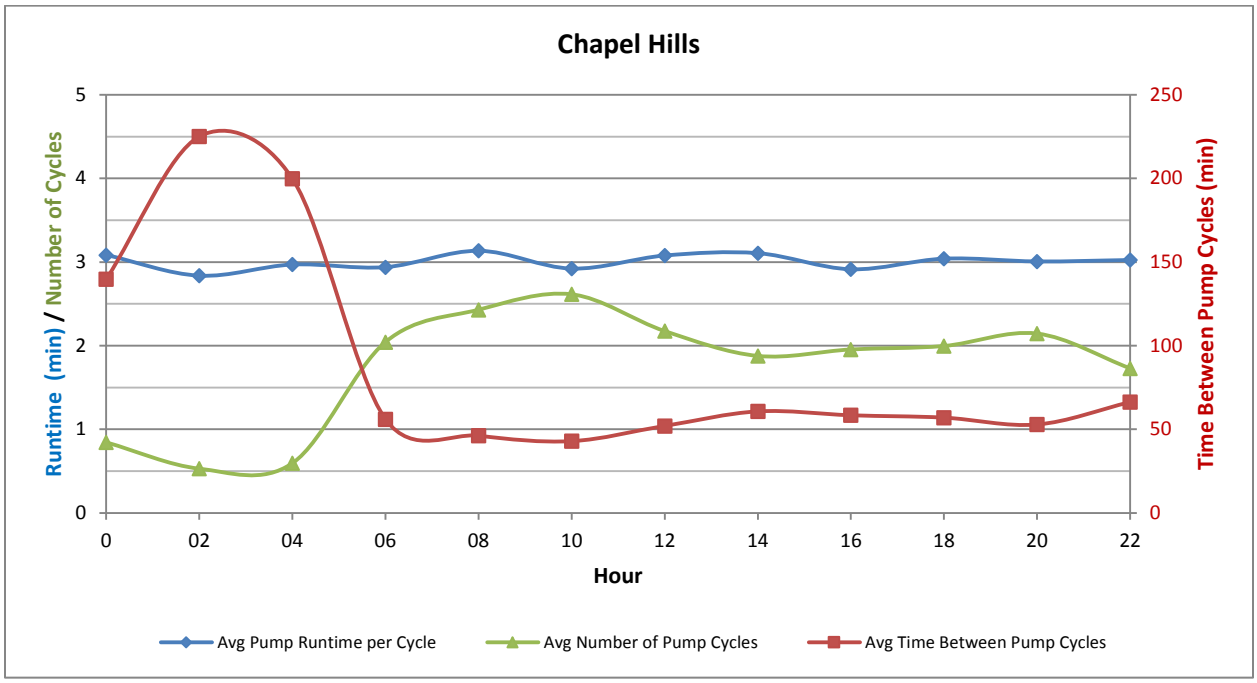

Figure 6.24: Pumping Cycles – Chapel Hills

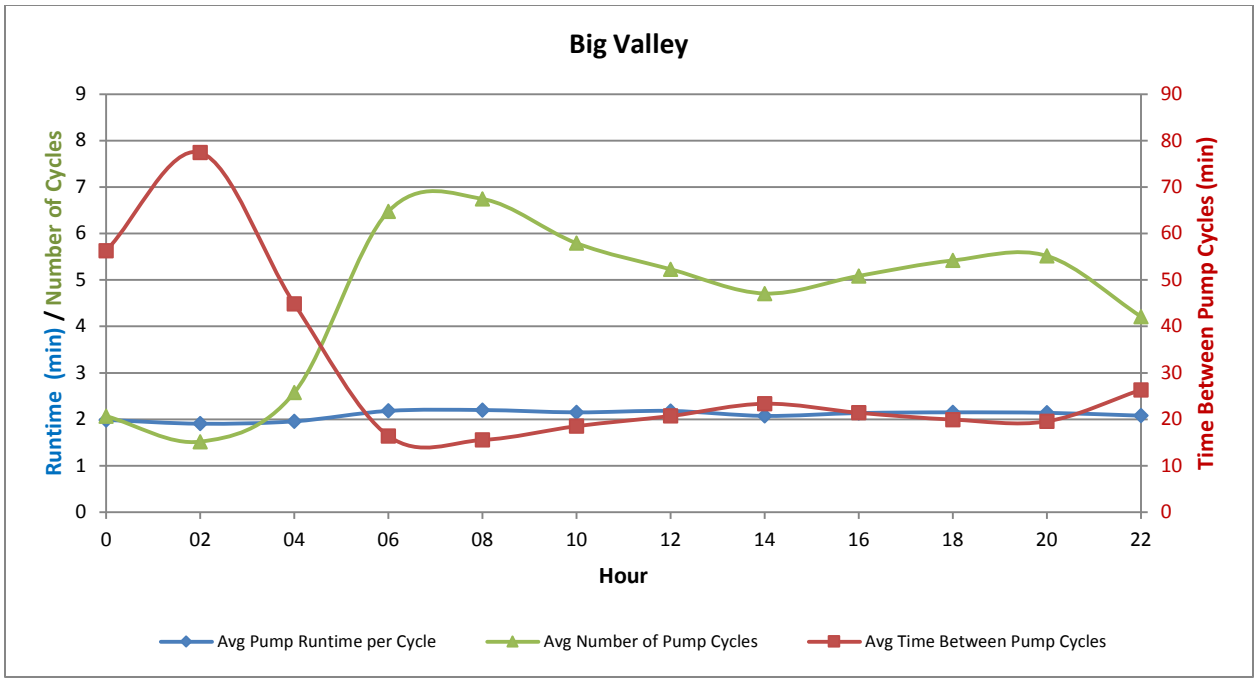

Figure 6.25: Pumping Cycles – Big Valley

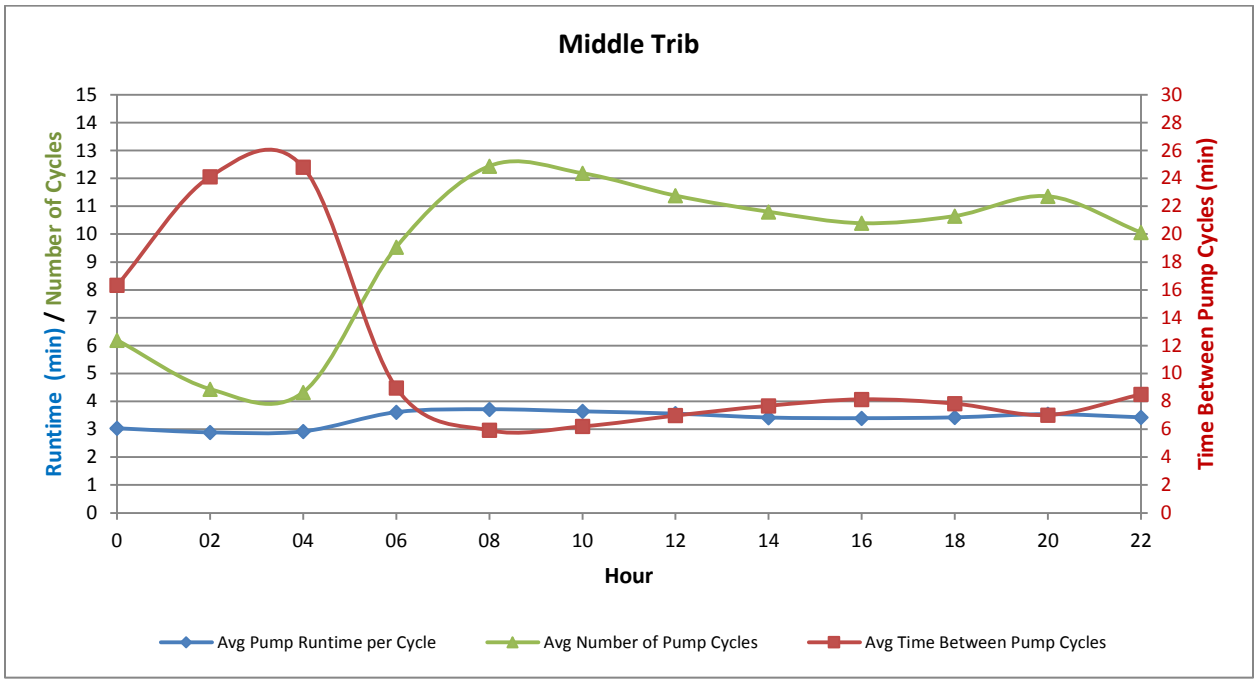

Figure 6.26: Pumping Cycles – Middle Trib

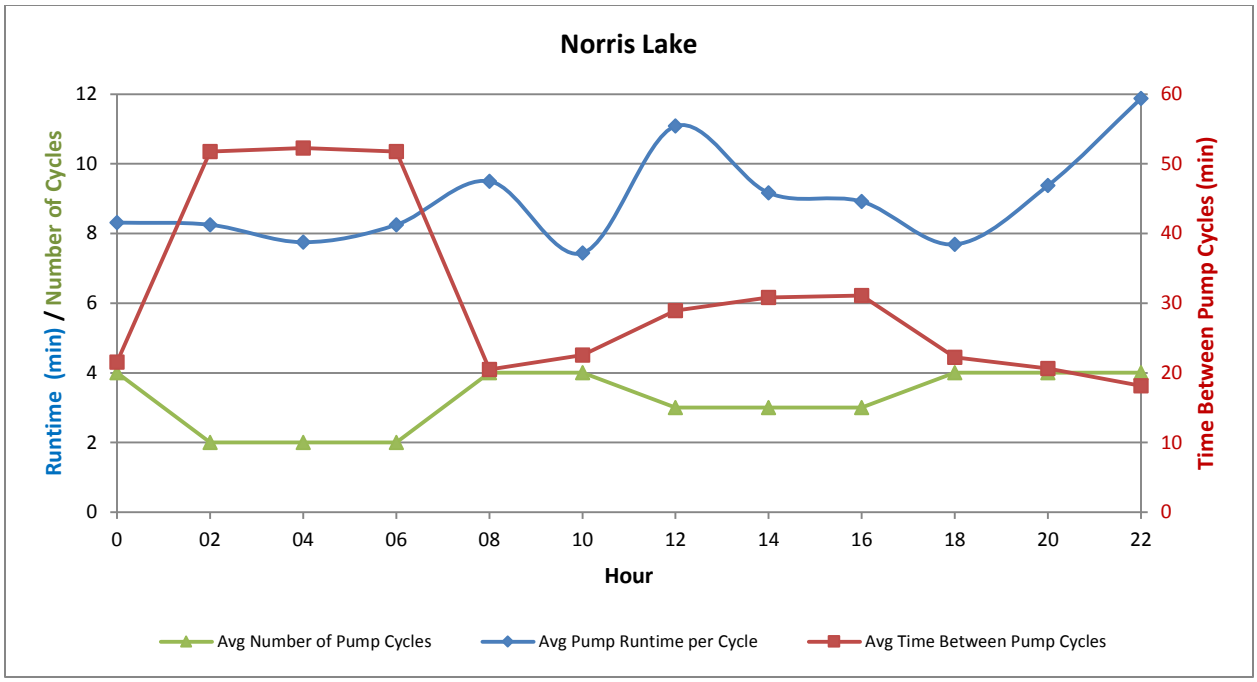

Figure 6.27: Pumping Cycles – Norris Lake

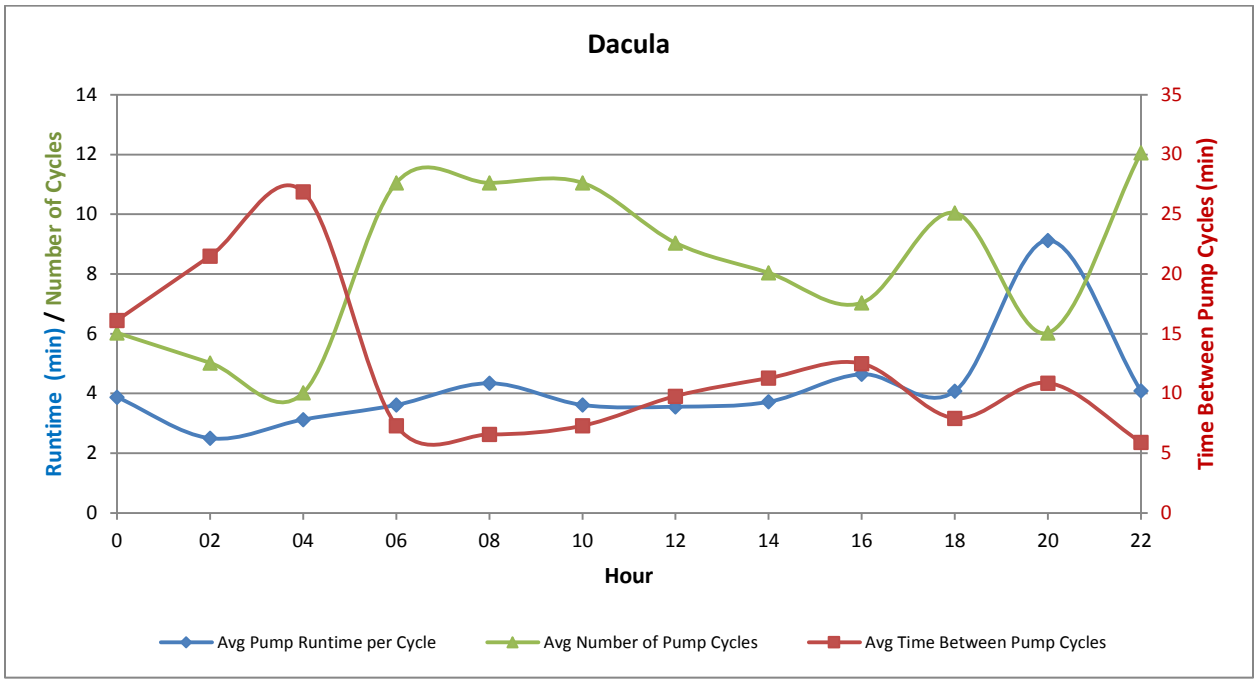

Figure 6.28: Pumping Cycles – Dacula

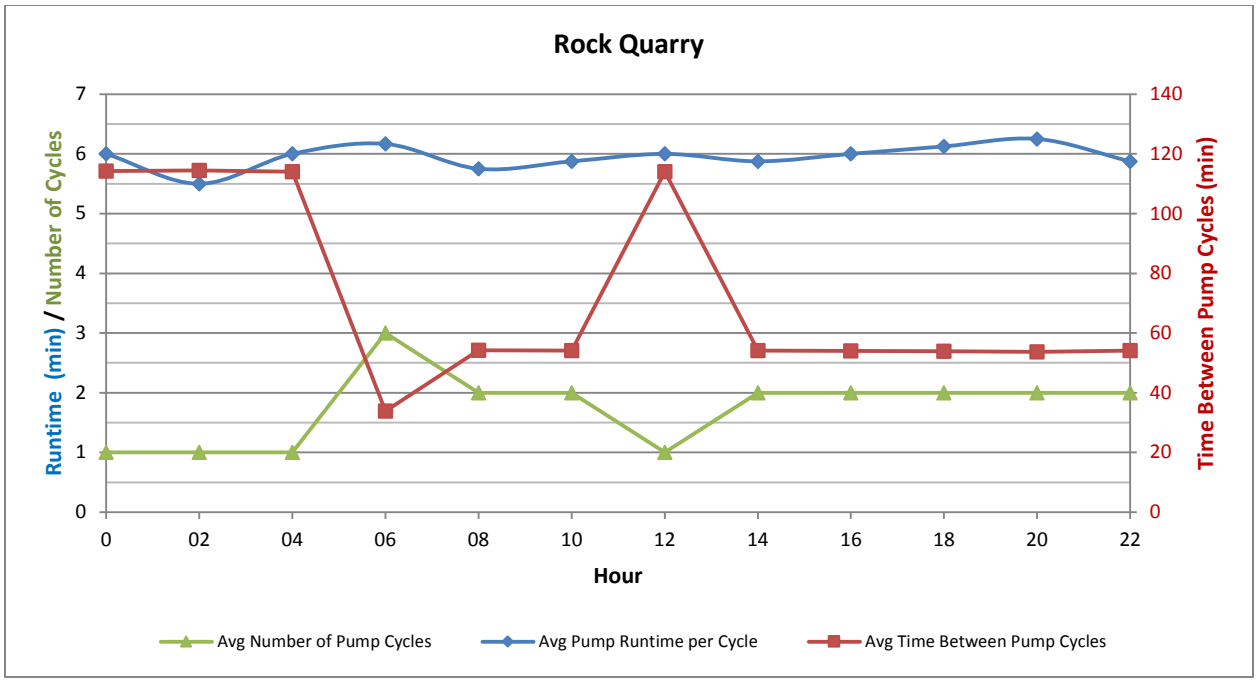

Figure 6.29: Pumping Cycles – Rock Quarry

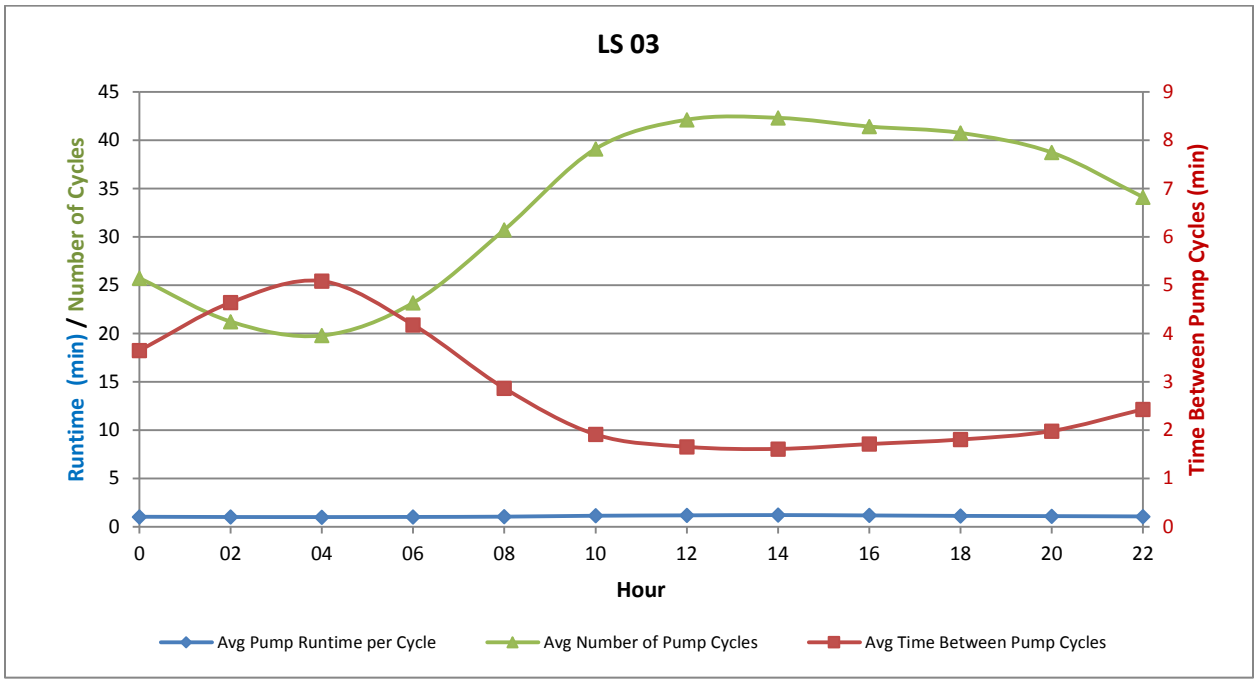

Figure 6.30: Pumping Cycles – LS 03

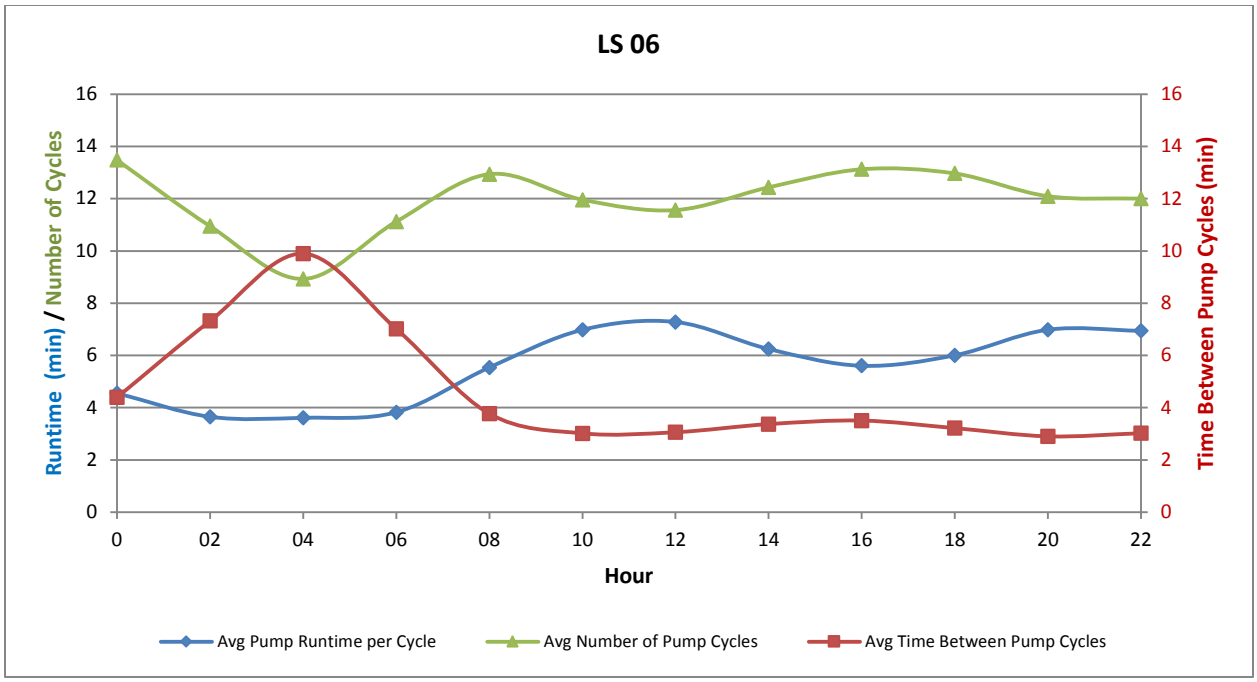

Figure 6.31: Pumping Cycles – LS 06

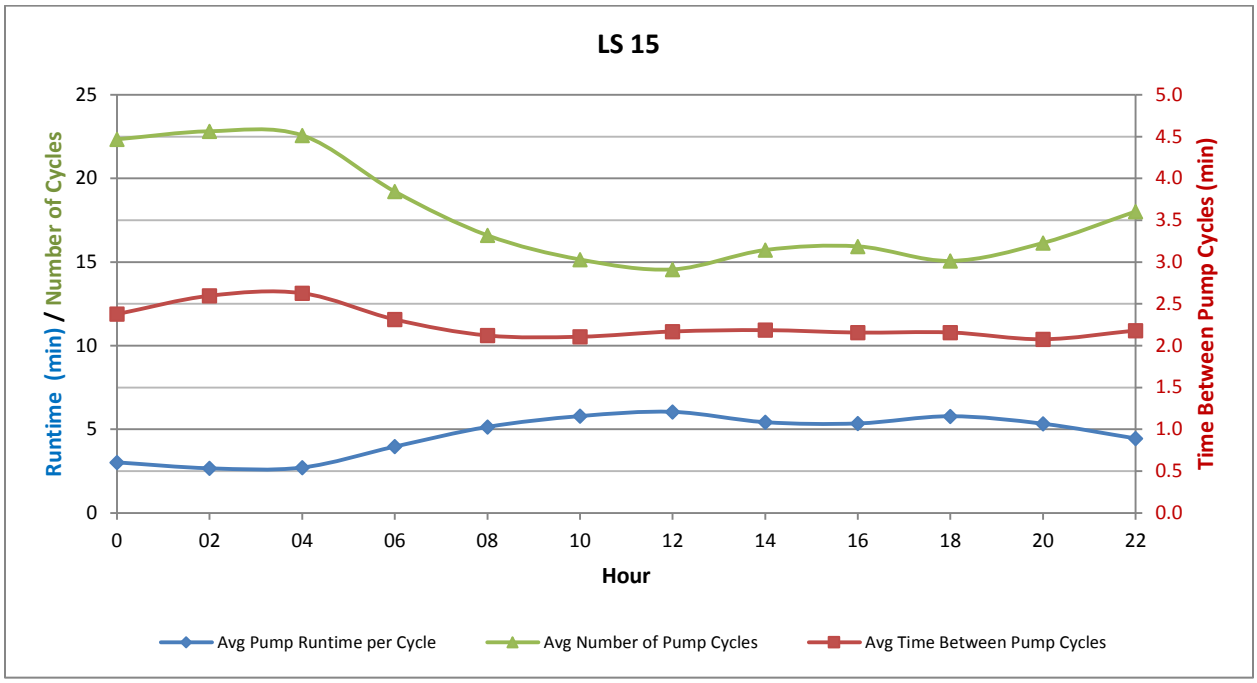

Figure 6.32: Pumping Cycles – LS 15

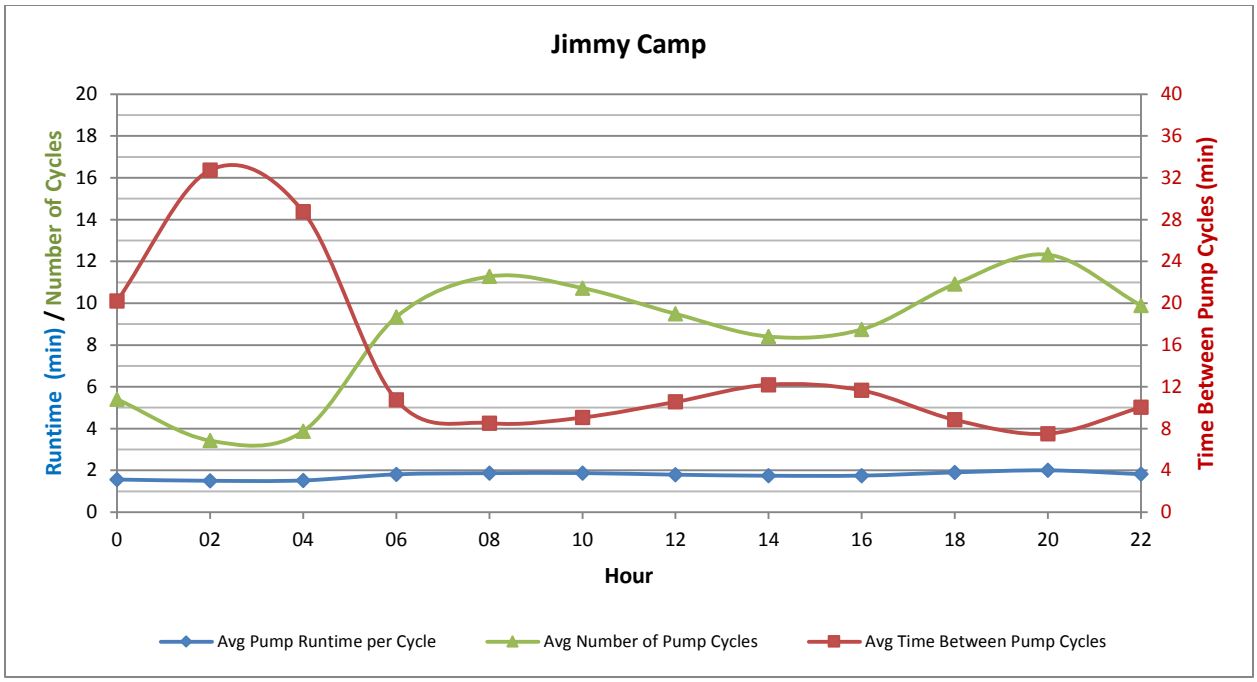

Figure 6.33: Pumping Cycles – Jimmy Camp

As presented in Table 4.6 and Figures 6.19 to 6.33, average pump runtime varied between 1 and 16 minutes with pumps remaining idle between 2 and 70 minutes between pumping cycles. The number of cycles represents the number of pump starts over the 2 hr time increment. The maximum number of starts that a pump can sustain per hour is related to the size of the motor and generally decreases with larger motor sizes.

The average number of pump cycles over the 2 hr interval ranged from 1 to 15 for most lift stations. The exception was LS 03 which operates approximately 1 minute per cycle, with 2.5 minutes of idle time, providing 20 to 45 cycles over each two hour period. Frequent pump cycling is due to a narrow wet well operational band of 0.5 ft (0.15 m).

The time between pump cycles was determined to be approximately 60 minutes or greater for Drennan, Janitell, Chapel Hills, and Rock Quarry lift stations indicating that there is a small volume of flow reporting to these stations. As shown in Table 4.6, the wet well storage band ranges from 0.5 ft to 3.1 ft (0.15 m to 0.94 m) with a per foot volume ranging from 46 ft^3/ft to 285 ft^3/ft (1.3 m^3/m to 8.1 m^3/m).

Although not presented, calculated k_s values were compared to the time of day, and time of year the data was collected and the pump cycle information presented above. No correlations were observed between k_s and operational time of day, year, pumping duration, or time between pumping cycles. Another factor evaluated was the Hydraulic Retention Time (HRT) (also known as Hydraulic Residence Time), which is the average time that the sewage takes to travel the length of the forcemain and is determined by dividing the volume of the pipeline by the flowrate.

Understanding the frequency of operation and the volume of sewage pumped in relation to the HRT could help develop a method for optimizing forcemain design. Utilizing the pump cycle information and discharge during a pump cycle, the HRT was calculated for each operational point evaluated as part of this research. In addition to the HRT, the volume of wastewater pumped during the pump cycle and the corresponding percentage of the total forcemain volume were calculated.

Pumping cycles of each lift station utilizing constant speed pumps were evaluated. Average flowrate calculated from the operational data presented were used to determine the average time that the pumps were operating; average time pumps were idle; percentage of forcemain volume pumped per cycle; number of cycles to pump the volume of the forcemain; and time it takes to pump the entire forcemain volume.

This analysis provides a more realistic methodology to determine the time it takes to pump the entire volume of the forcemain as compared to the HRT calculation since it takes into account the time duration the pumps are operating as well as sitting idle. Results are presented in Appendix E.1. Appendix E.2 presents the results graphically showing the time the pumps are operating, idle, and the number of pump cycles required to convey the entire volume of the forcemain represented by the dashed line. The average pumping cycle results are summarized in Table 6.8.

Table 6.8: Summary of Average Pumping Cycles

System Name	Forcemain Volume (ft^3)	Average Flowrate (cfs)	Average Time Pumps Operating (min)	Average Time Pumps Off (min)	% of Forcemain Volume Pumped per Cycle	Number of Cycles to Pump Forcemain Volume	Time to Pump Forcemain Volume (hr)	Annual Pump Operating Time (days)
Janitell	68.4	0.2	16.9	55.2	291%	0.3	1.2	85.4
Kettle Creek	5020.4	2.2	4.7	5.2	12%	8.0	1.4	174.3
Big Valley	38.1	0.2	2.1	23.9	60%	1.7	0.5	29.8
Chapel Hills	2059.8	1.0	3.0	65.8	8%	11.9	12.7	16.0
Drennan	2504.1	1.7	1.4	70.4	6%	18.0	21.6	7.0
Black Squirrel	817.6	2.3	2.3	16.9	39%	2.6	0.7	43.3
Middle Trib	5788.3	2.4	3.2	8.5	8%	12.6	2.4	99.7
Mid Monument	11669.2	2.2	2.2	21.7	3%	39.8	15.6	34.0
Rock Quarry	7080.8	3.0	6.0	62.6	15%	6.7	7.0	31.8
Norris Lake	29560.9	5.9	9.0	27.9	11%	9.3	5.7	89.5
Dacula	11561.9	4.4	4.1	12.0	9%	10.6	2.8	93.7
LS 03	4755.0	4.6	1.1	2.5	6%	15.7	0.9	112.5
LS 06	21769.1	4.5	5.7	4.4	7%	14.1	2.4	206.0
LS 15	15946.1	3.7	4.4	2.3	6%	16.0	1.8	241.0
Jimmy Camp	8373.0	3.1	1.8	11.7	4%	24.7	5.5	48.8

Results show:

- Although the Janitell pumps sit idle for approximately 55 minutes, the entire forcemain volume is conveyed each pumping cycle. The remaining systems convey approximately 4% to 60% of the forcemain volume per cycle, with a number of systems pumping less than 10% of the volume per cycle.
- Drennan, Mid Monument, and Chapel Hills require 21.6 hrs, 15.6 hrs, and 12.7 hrs, respectively, to pump the forcemain volume. As a result, the wastewater in these forcemains is likely turning septic. Mid Monument discharges directly to the Middle Trib forcemain which is equipped with an ECO2 odor control system, so odor is not likely an issue within this system, but could be an issue for Drennan and Chapel Hills

- Other systems pump the entire forcemain volume in less than 6 hours, which may be acceptable to prevent anaerobic conditions and odors.
- Annual operational time of the pumps is a function of the pump capacity as well as the inflow volume reporting to the lift station and ranges from 7 and 241 days with Drennan operating the least at approximately 7 days per year.

As demonstrated above, the time to pump entire forcemain volume (Table 6.8) provides a better measure of the time it takes to convey the entire volume of the forcemain since it takes into account the time duration the pumps operate and sit idle before the next pumping cycle begins.

Results were also compared to the calculated k_s for each system; neither the time to clear the forcemain nor number or duration of pumping cycles appears to affect k_s. No correlations between the operational data and calculated values of k_s were observed; therefore, k_s is primarily a function of velocity for wastewater pipelines. However, k_s likely varies linearly along the pipeline due to oxygen depletion and formation of sulfide within the slime layer. Evaluation of this topic is beyond the scope of the current research but should be evaluated in future research.

Although k_s was found to be independent of the number and duration of pumping cycles, as well as, the time required to convey the entire forcemain volume, the time to pump the forcemain volume is an important factor to evaluate in order to determine if the wastewater will turn septic during transport. A very long forcemain clearing time will promote anaerobic conditions and sulfide development within the pipeline. The time for wastewater to turn septic depends on several factors including the age of the wastewater; general wastewater characteristics; concentration of dissolved oxygen, sulfate, BOD, and temperature.

Stuetz (2001) performed an experiment to determine the sulfide concentration in raw wastewater, outside sewers, and within a rising main over time. Composition of the sewage used for the two experiments was similar. However, the rising main included well-developed populations of sulfur metabolizing microorganisms present in biofilm.

Stuetz (2001) reported that the establishment of anaerobic conditions in domestic wastewater is not necessarily followed by rapid septicity development. In crude sewage outside sewers, the speed of septicity development remain relatively slow long after it has become anaerobic. Figure 6.34 shows that the change in hydrogen sulfide concentrations in typical sewage is relatively slow during the first 24 hours. However, sulfide develops more rapidly in forcemains. Figure 6.35 shows the change in dissolved sulfide concentrations rapidly rises over time in forcemains (Stuetz 2001).

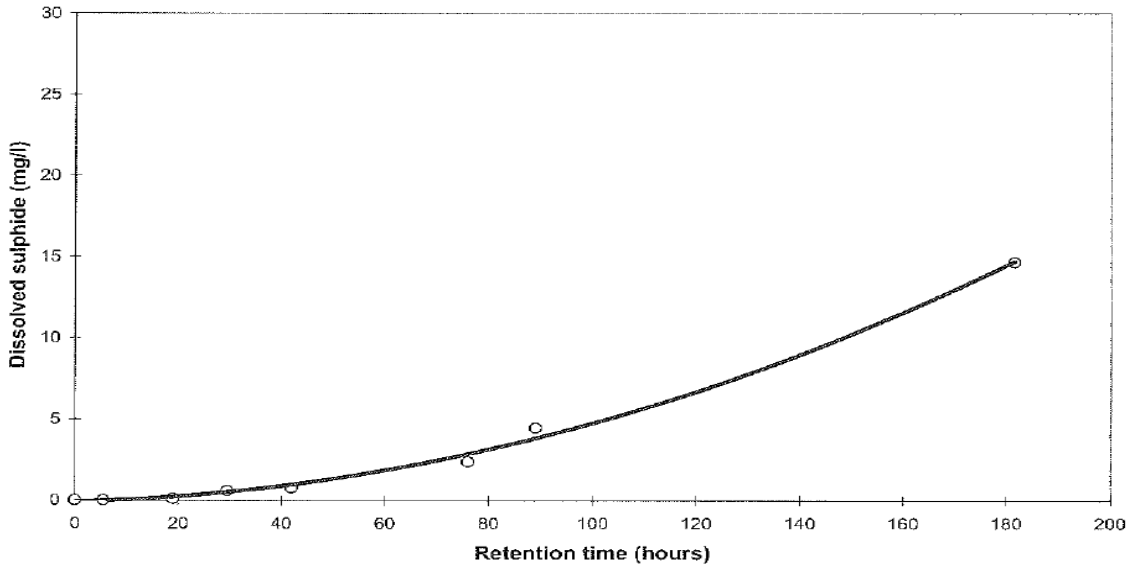

Figure 6.34: Sulfide Generation in Crude Sewage Outside Sewers (Stuetz 2001)

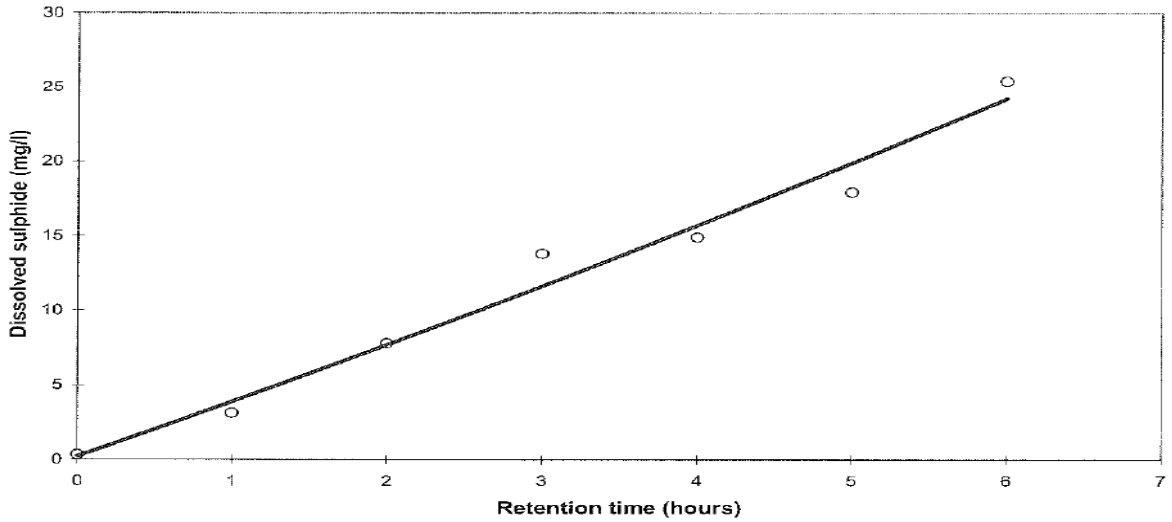

Figure 6.35: Sulfide Generation in a Rising Main (Stuetz 2001)

High concentrations of sulfide can lead to corrosion of metallic and cementitious based pipe materials. Therefore, it is desirable to limit the amount of sulfide produced in forcemains. ASCE Manual of Practice (MOP) No. 60 (MOP 60) (Kienow 1989) indicates that sulfide generation is likely to be minimal for forcemains less than 200 ft (61 m) long. Systems with the greatest potential for sulfide generation are long forcemains (thousands of feet to several miles) and those where velocity is inadequate to transport organic solids (Kienow 1989). Discussion on velocity required for particle transport was provided in Section 6.1.1 and is further evaluated in Section 8.2.

Given the information identified above, the sulfide concentration remains relatively low within raw wastewater. However, the sulfide concentration rises sharply in forcemains which have an established biofilm. High sulfide concentrations can lead to odor issues. Sulfide production rates are greater in forcemains as compared to raw wastewater. Therefore, from an operational standpoint it would be desirable to decrease HRT in the forcemain and provide additional storage in the wet well. In addition, it may be easier to mitigate odor related issues in the wet well as compared to the forcemain.

All of these factors indicate that properly designed forcemains should consider the time to pump the forcemain volume of as well as maintaining a sufficient velocity to transport particles (organic and granular) and air. Optimal pipe sizing is discussed in Chapter 8.

6.2.2 Pump Operation Points

As identified in Chapter 3, pump factory performance curves were provided by the Owner of each system. Pump design points for systems utilizing constant speed pumps are summarized in Table 6.9. Pumps controlled with VFDs were not included since pump curves were not obtained for these systems. Norris Lake utilizes constant speed pumps but was not included in the table below since the discharge pressure of the station is monitored and was used for hydraulic calculations. The maximum solid size that each pump can pass ranges from 1.5 in. to 5 in. Transport of solids is discussed in more detail in Sections 6.1.1 and 8.2.

Table 6.9: Summary of Pump Nameplate Duty Points

System	Number of Duty Pumps	Pump Design Point			BHP (hp)	Max Sphere Size [1] (in)
		Flow (gpm)	TDH (ft)	Efficiency (%)		
Janitell	1	139.6	43.8	39.0	4.0	1.5
Kettle Creek	3	1,130.0	92.0	79.8	32.9	3.0
Big Valley	1	100.0	53.0	45.0	3.0	1.5
Chapel Hills	1	500.0	141.0	62.5	28.5	3.0
Drennan	1	740.0	100.0	71.6	26.1	3.0
Black Squirrel	1	1,120.0	113.0	71.0	45.1	3.0
Middle Trib	1	1,041.0	456.0	65.0	184.6	3.0
Mid Monument	1	1,170.0	155.0	57.0	80.4	3.0
Rock Quarry PS	1	1,650.0	186.0	75.8	102.3	3.0
Dacula	1	2,615.0	184.0	77.0	157.9	3.0
LS 03	1	1,957.0	120.0	76.0	78.1	3.0
LS 06	1	2,400.0	100.0	79.1	76.7	5.0
LS 15	1	1,800.0	72.0	77.0	42.5	3.0
Jimmy Camp	1	1,450.0	203.0	74.8	99.5	3.0

[1] Maximum size particle pump can pass

Equations defining the pump head capacity curve and efficiency from the factory pump performance curve were developed for each pump using M.S. Excel. These equations were used to calculate the pump operating point at each flow measured by the SCADA system and analyzed as part of the hydraulic analysis (Chapter 5) and were compared to the design point of the pump to evaluate the performance of each system.

In most cases it was determined that the pump(s) were operating to the left of the design point indicating that more head was required to overcome friction losses within the system as compared to the original design. This is consistent with the findings of the hydraulic analysis. Pump operating points were plotted along with the pump performance curve for each system and are presented in Figures 6.36 to 6.49. The following results were observed:

- Dacula, Rock Quarry, Chapel Hills, Janitell and Kettle Creek were operating to the left of the design point.
- Big Valley, Chapel Hills, Middle Trib and Mid Monument were operating close to the design point, but the efficiency at the operational point(s) is relatively low compared to the best efficiency point of the pump.

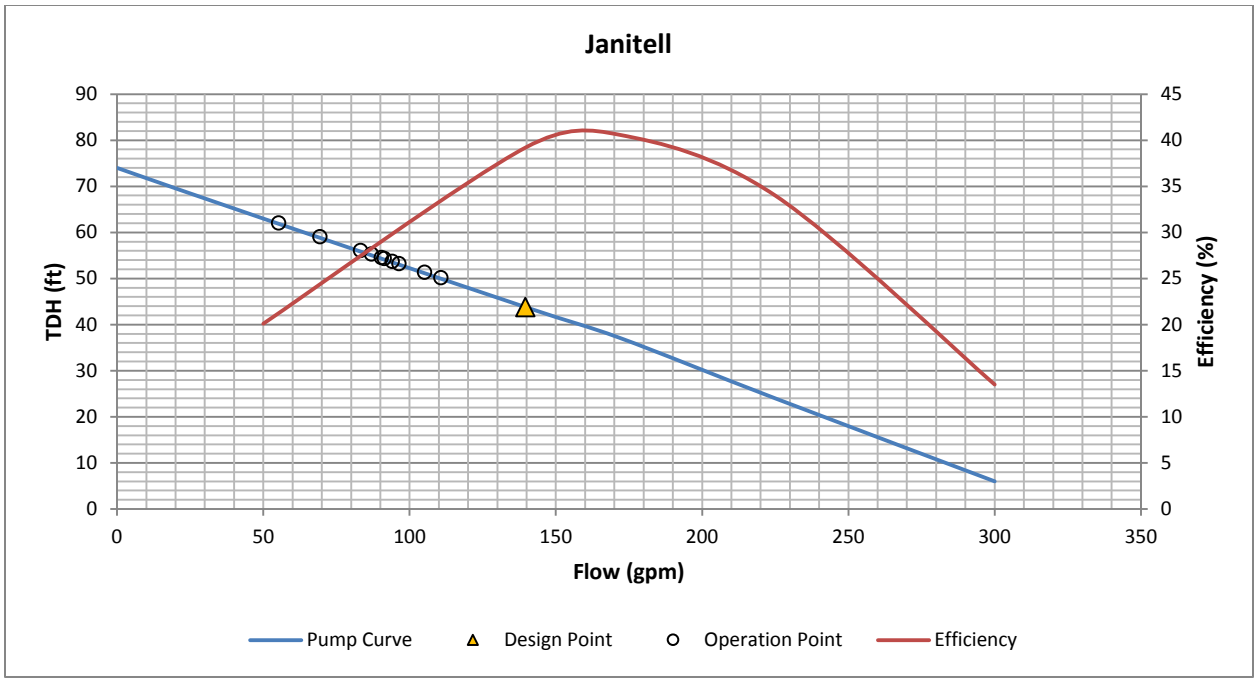

Figure 6.36: Pump Operational Points – Janitell

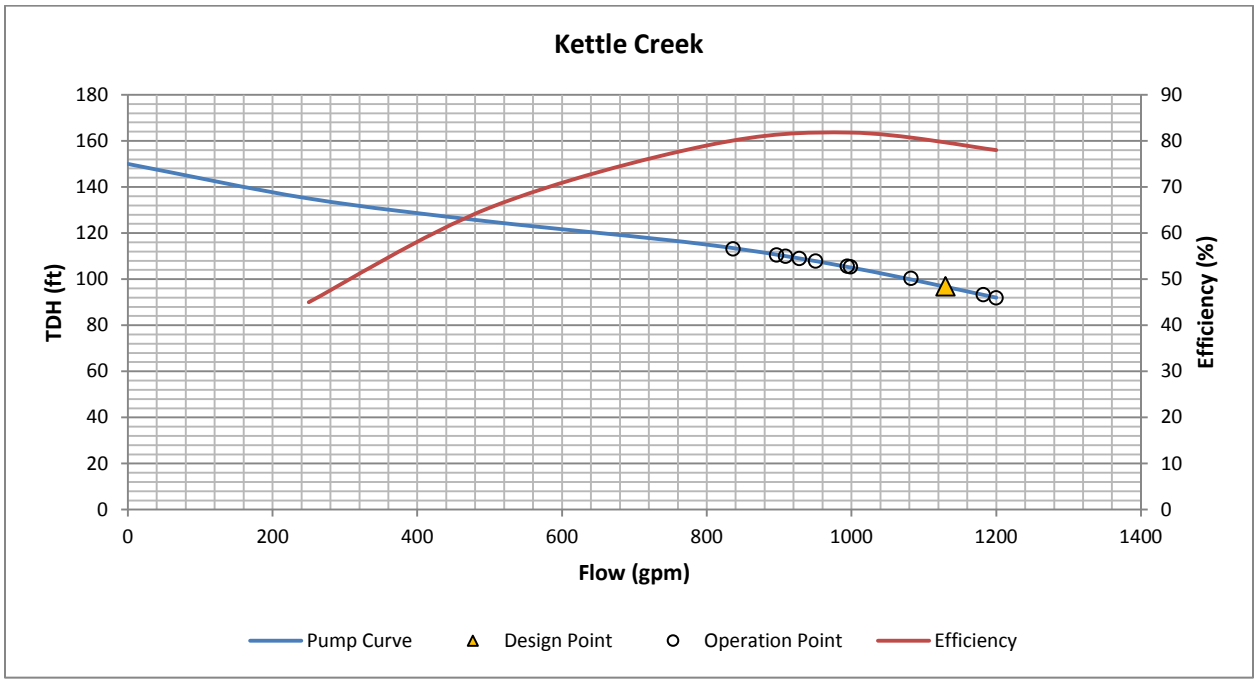

Figure 6.37: Pump Operational Points – Kettle Creek

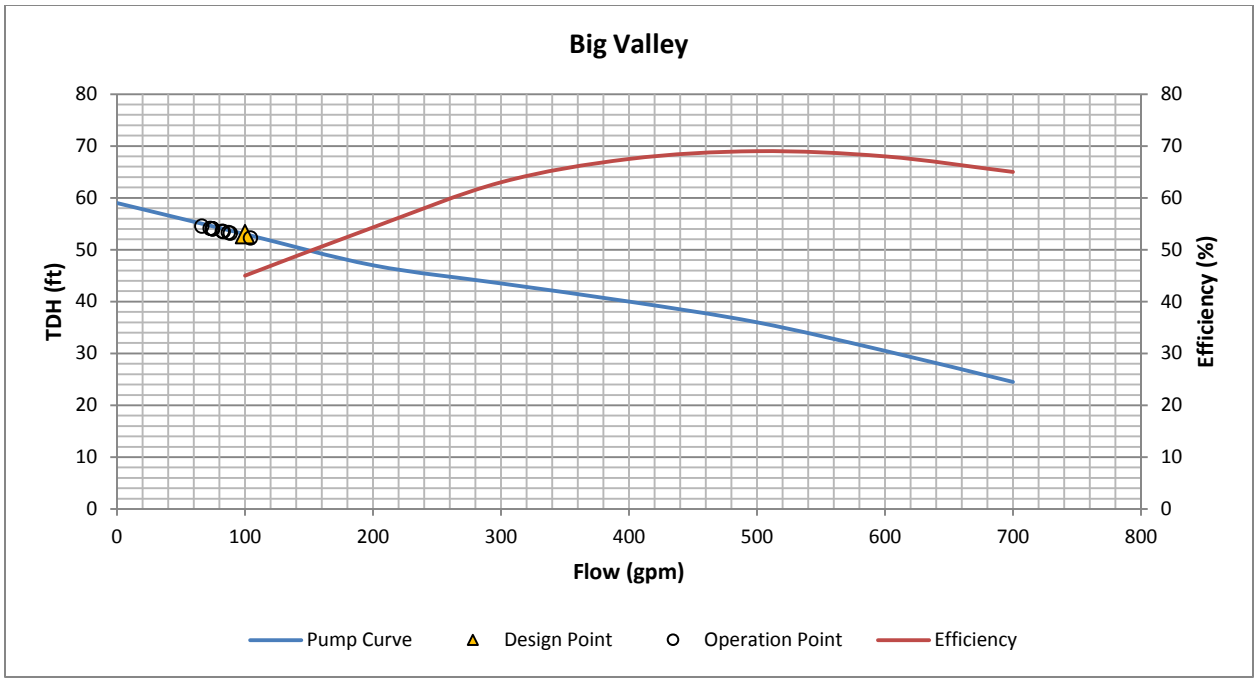

Figure 6.38: Pump Operational Points – Big Valley

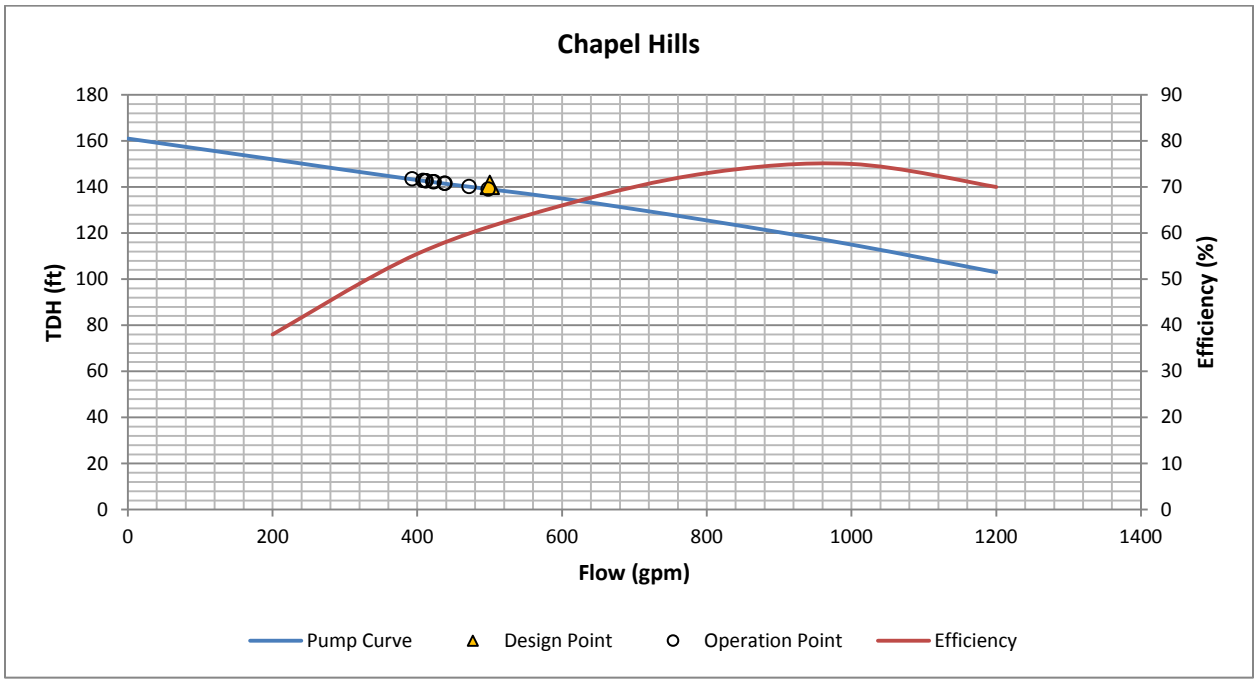

Figure 6.39: Pump Operational Points – Chapel Hills

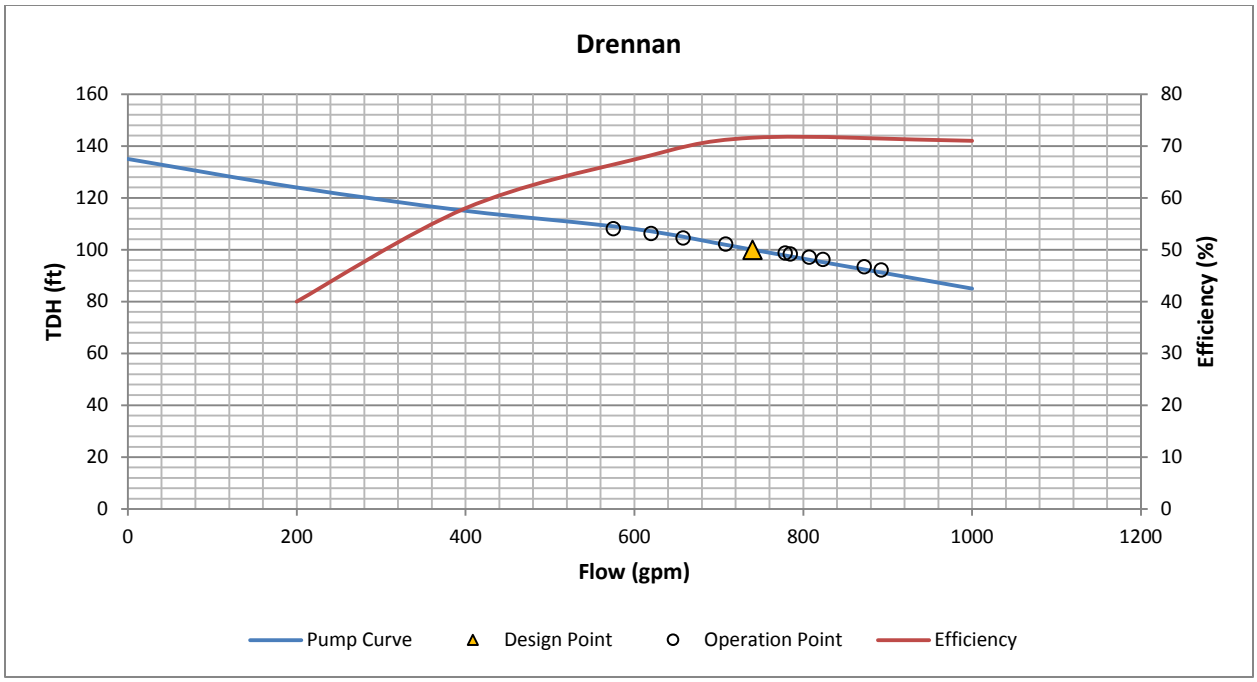

Figure 6.40: Pump Operational Points – Drennan

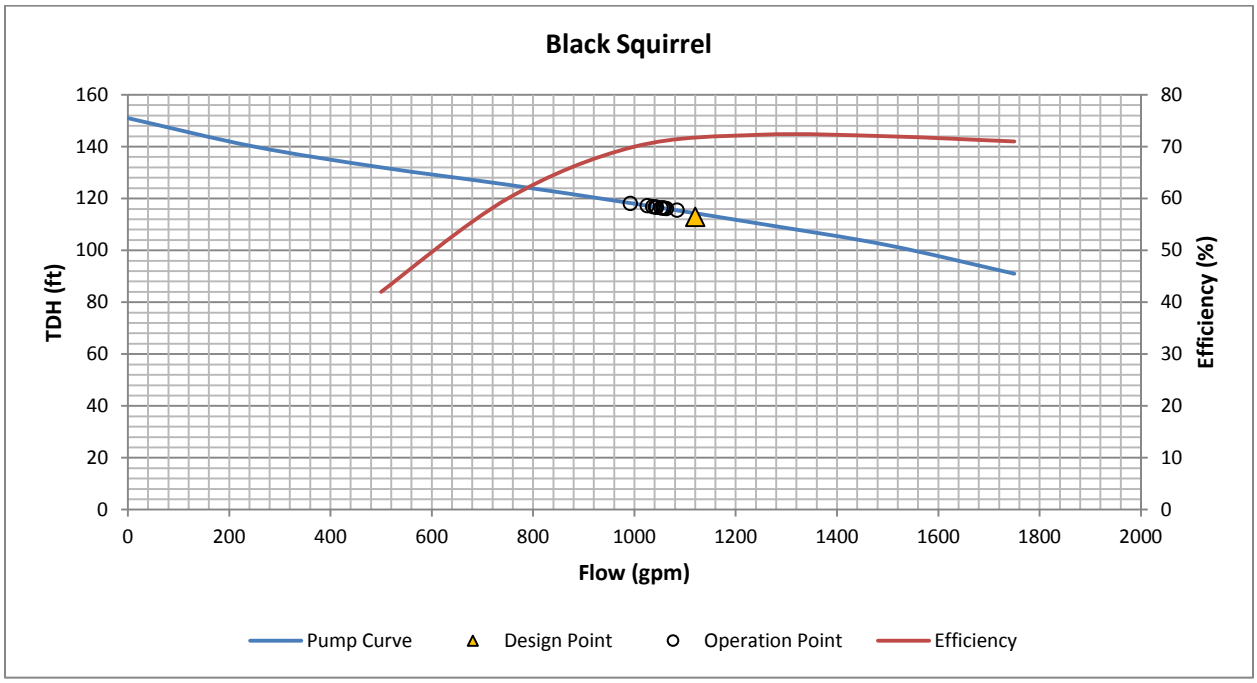

Figure 6.41: Pump Operational Points – Black Squirrel

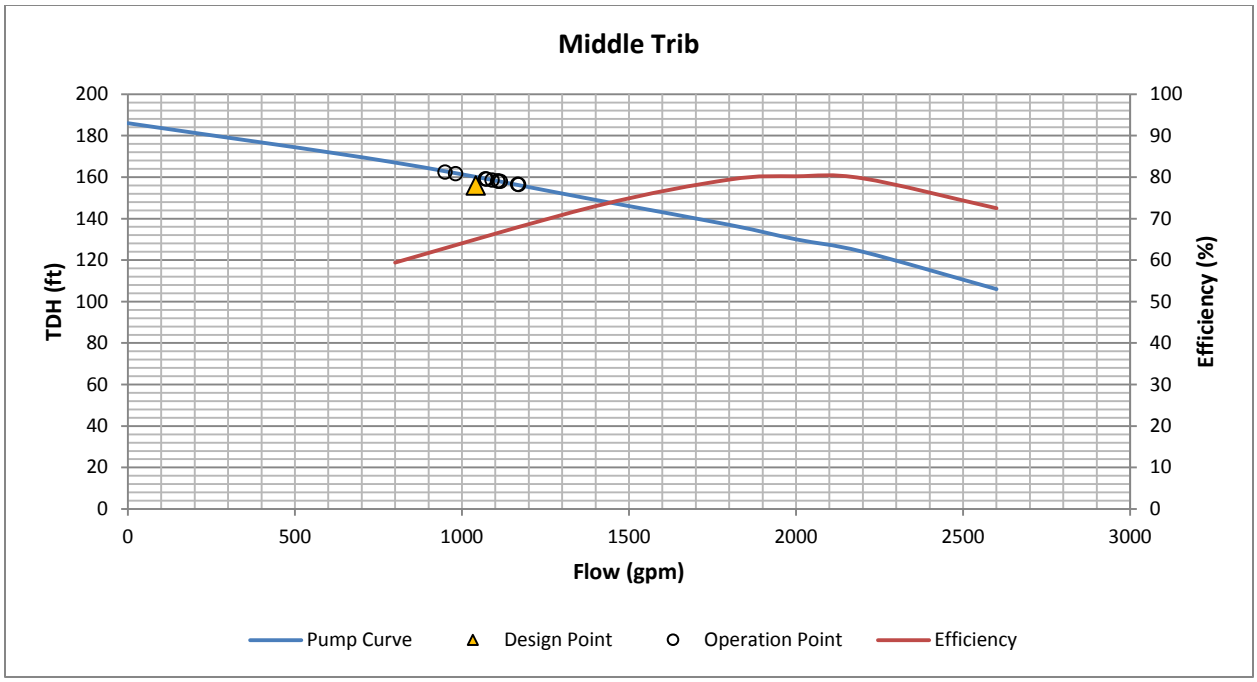

Figure 6.42: Pump Operational Points – Middle Trib

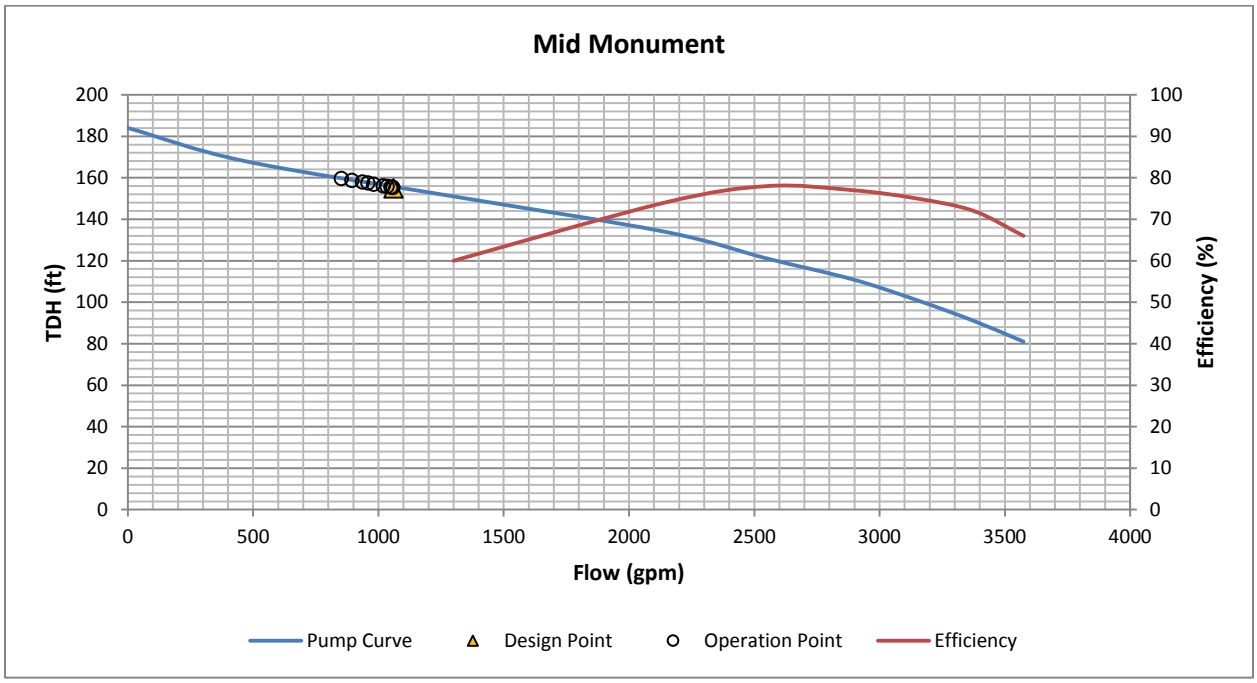

Figure 6.43: Pump Operational Points – Mid Monument

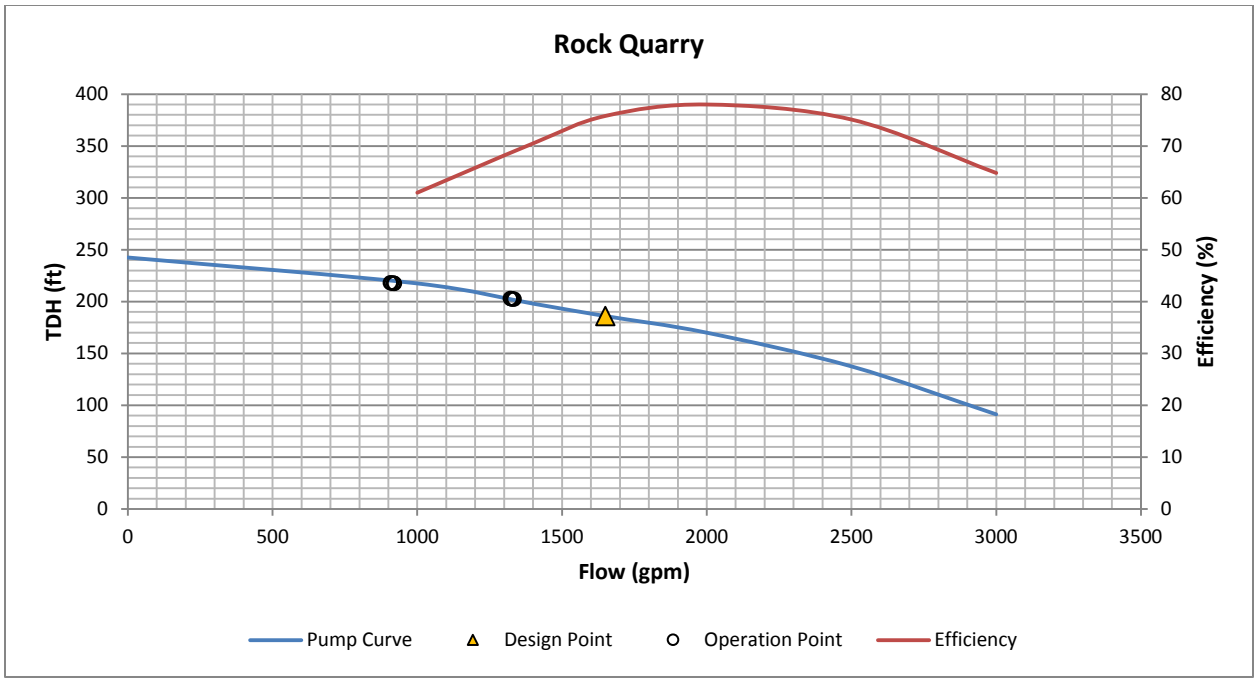

Figure 6.44: Pump Operational Points – Rock Quarry

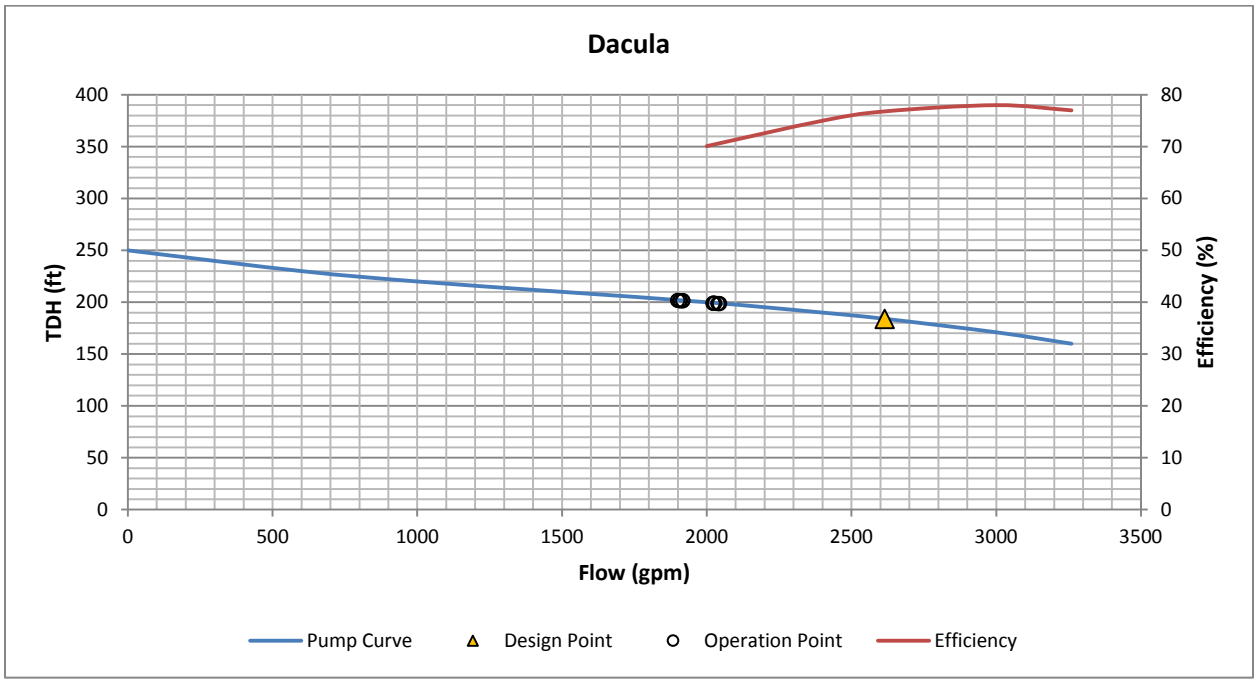

Figure 6.45: Pump Operational Points – Dacula

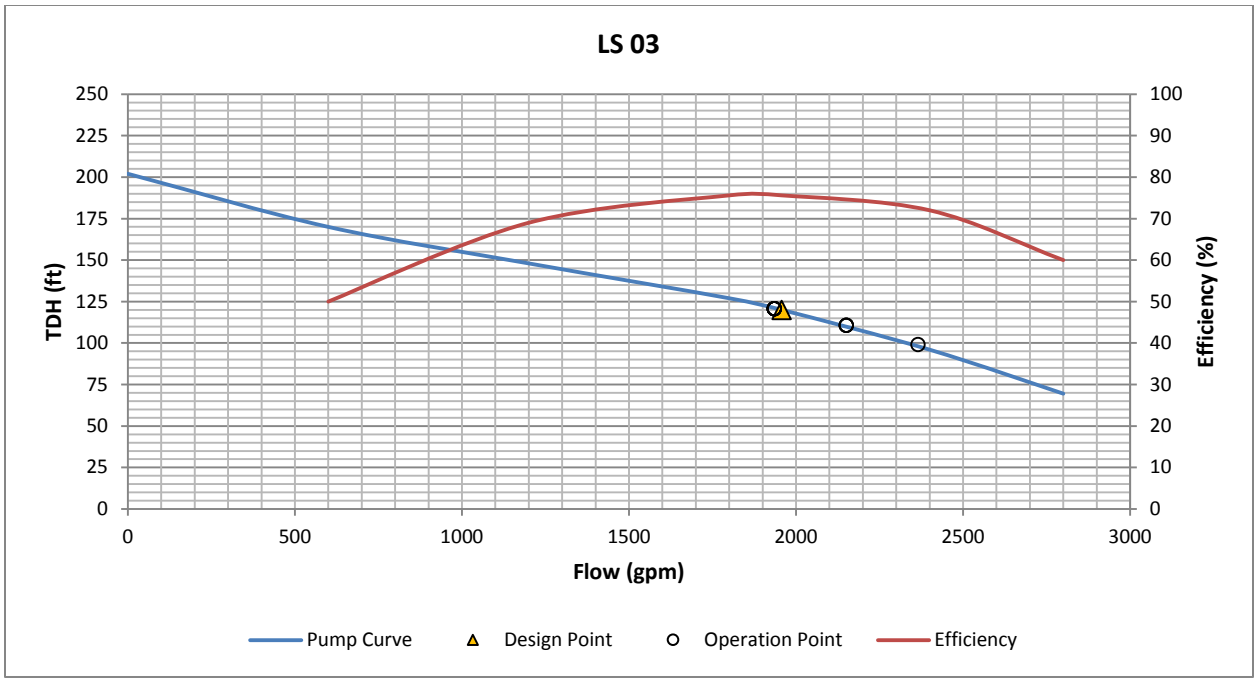

Figure 6.46: Pump Operational Points – LS 03

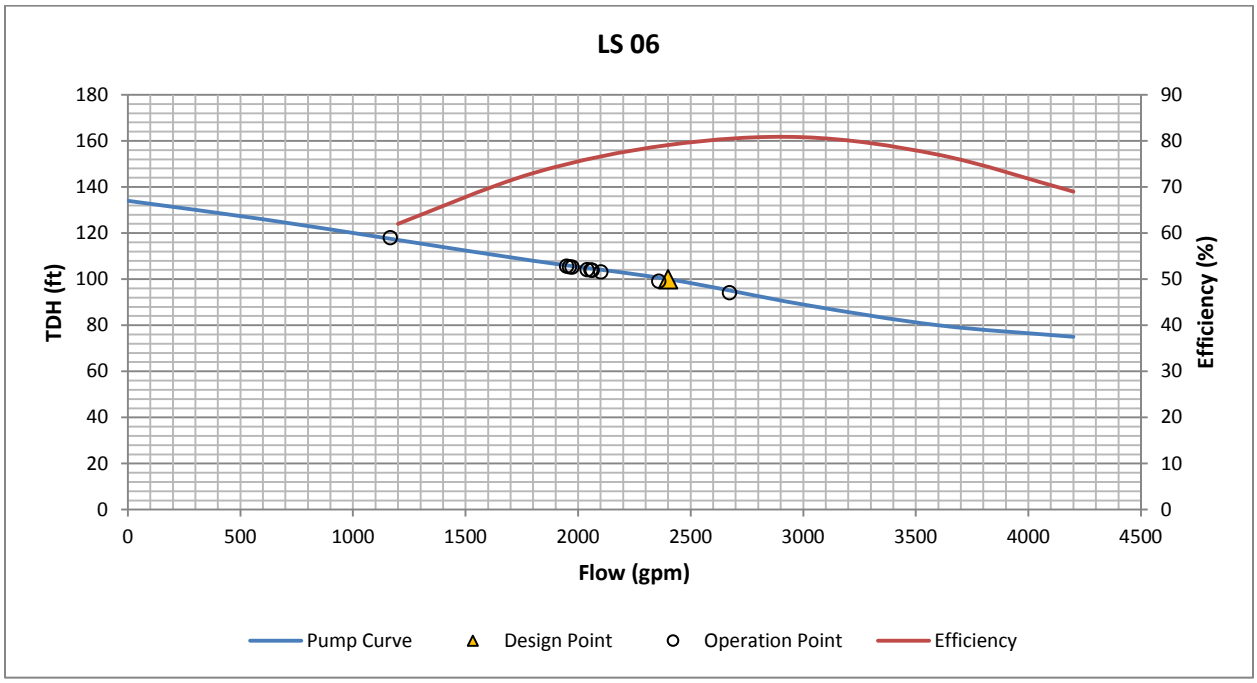

Figure 6.47: Pump Operational Points – LS 06

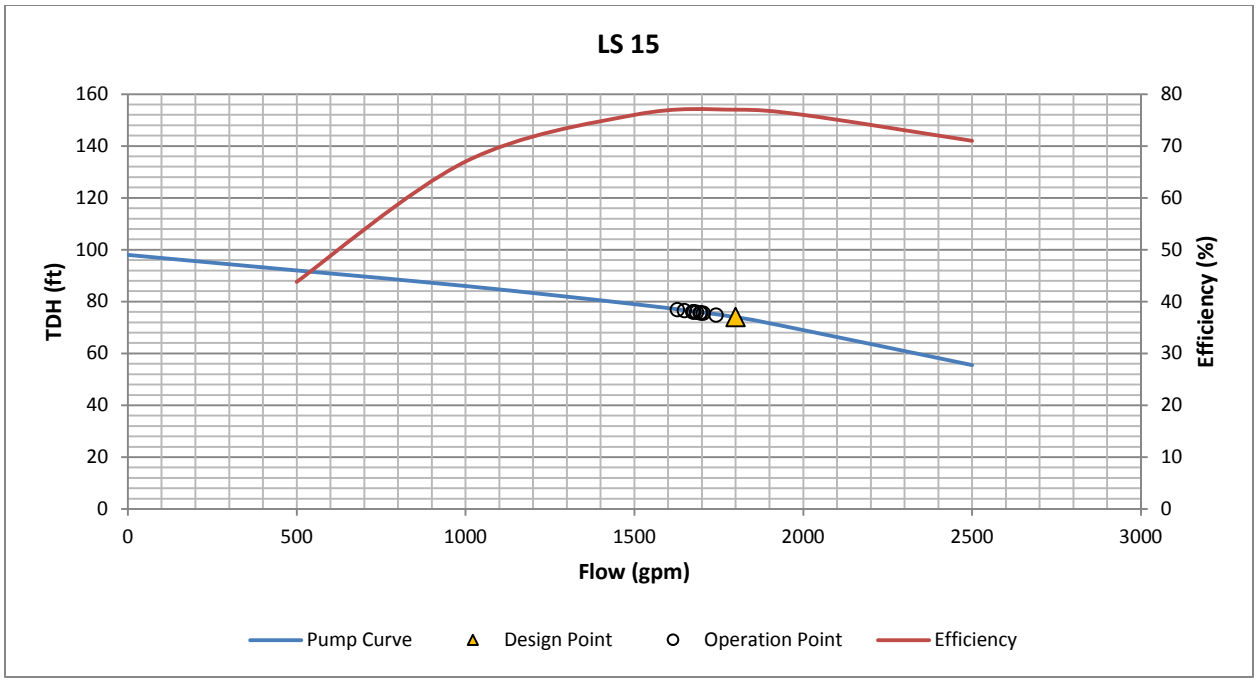

Figure 6.48: Pump Operational Points – LS 15

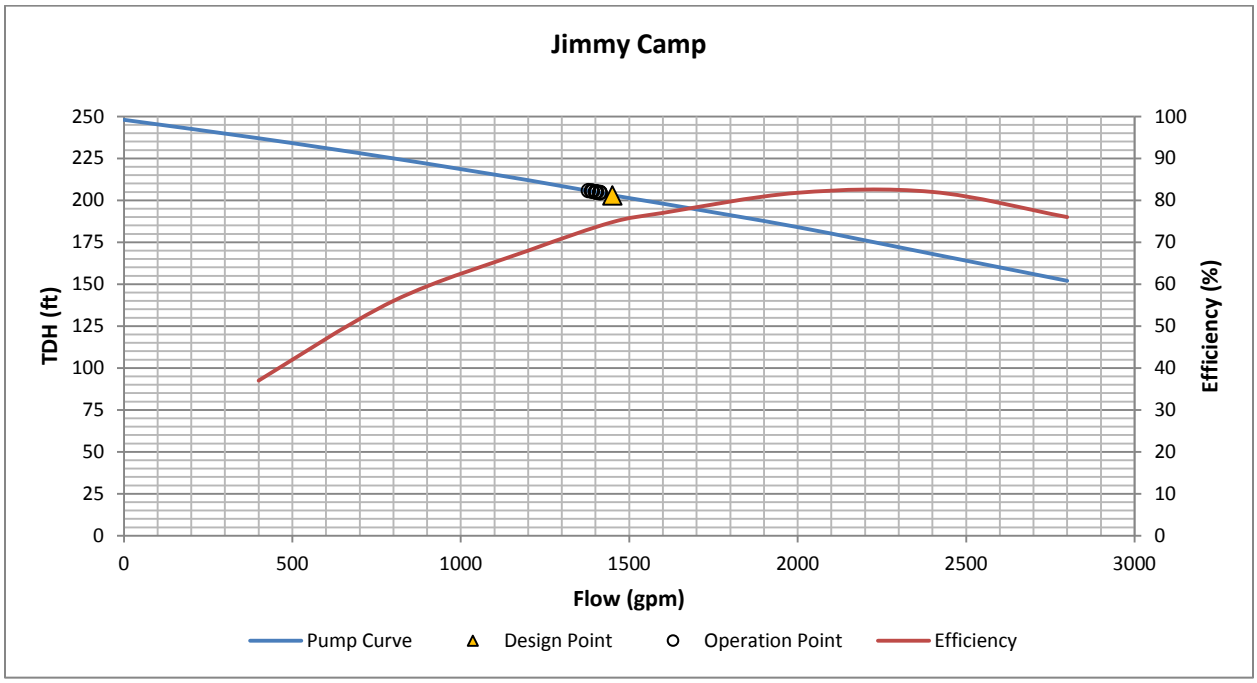

Figure 6.49: Pump Operational Points – Jimmy Camp

7 Prediction of Roughness Factors

7.1 Introduction

As shown in Chapter 5, absolute roughness (k_s) and C factor were found to vary with the velocity. Both the Colebrook-White and Hazen-Williams equations utilize constant k_s and C factors in determining headloss. Therefore, these equations require modification to calculate headloss based upon the findings of this research. The following sections describe the methodology used to evaluate the data and develop predictive equations for both k_s and C factor based upon velocity.

7.2 Data Analysis and Curve Fitting

All data collected as part of this research were evaluated and screened in order to develop predictive equations for k_s and C factor based upon velocity. CurveExpert Professional 2.3.0 and Microsoft Excel were used to analyze the data and develop predictive equations for both k_s and C factor. The following sections detail the data analysis, assumptions, and curve fitting methodology.

7.2.1 Absolute Roughness

All calculated values for k_s evaluated as part of this research are presented in Figure 7.1. The Research Dataset (data collected as part of this research) is shown as blue data points; the red data points represent the H.R. Wallingford Data; and data collected from previous studies and reports are shown in green. Also presented in Figure 7.1 are the k_s data points corresponding to $R_e < 1.04 \times 10^5$ which, as demonstrated in Section 5.2.3, lead to erroneous values of k_s since the von Kármán constant was found to be less than 0.4. Lastly, the predicative equation developed by H.R. Wallingford (Chapter 3) to estimate k_s from velocity is also shown in Figure 7.1.

From Figure 7.1, the predictive equation developed by H.R. Wallingford does not provide a good fit of the dataset. In addition, a large number of data points from the H.R. Wallingford data is subjected to values of k_s where $\kappa<0.4$. Since these data points produce erroneous values of k_s, they were removed from the data set. The remaining data along with the H.R. Wallingford predictive equation line are presented in

Figure 7.2. The HR Wallingford predictive line was provided to illustrate that the remaining data provides much larger values of k_s as compared to the HR Wallingford data and to highlight that the HR Wallingford data set included several data points where the von Kármán constant was less than 0.4.

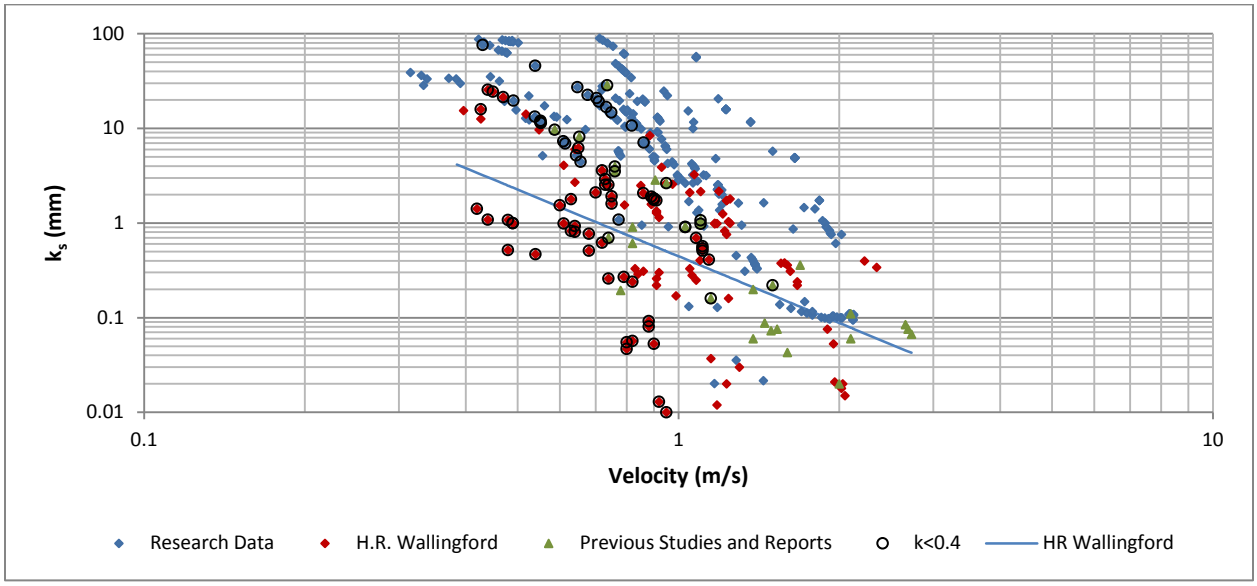

Figure 7.1: Summary of k_s results

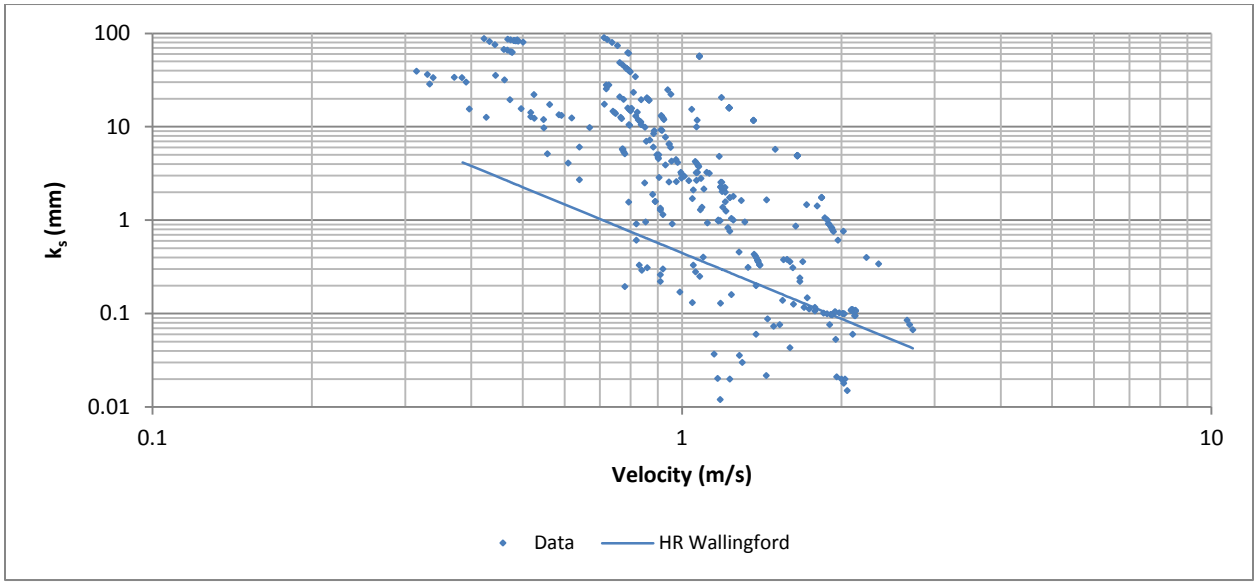

Figure 7.2: k_s Data excluding values where R_e<1.04E5

The data were screened to determine the best fit line. Three predictive lines were developed and are presented in Figure 7.3. First a predictive equation was developed for the entire dataset (excluding $R_e<1.04x10^5$). Second, data associated with k_s values greater than 30 mm (1.2 in.) were removed since it

is impractical to use an equivalent sand roughness value greater than 30 mm (1.2 in.) without adjusting for a reduced interior diameter. 30 mm (1.2 in.) was selected as a reasonable value for the upper threshold of k_s based upon experience. Third, data points identified by a red circle were considered outliers to the dataset. Although these potential outliers provide a linear relationship with a similar slope and shape as the remainder of the dataset, the data points are shifted to the right suggesting higher headloss, which could be the result of an obstruction, sedimentation, or potential air locking and therefore were removed.

Predictive lines were developed in MS Excel as a power function which provided the best overall fit to the data. Several nonlinear functions were evaluated; however, the power function provided the best overall fit to the data given the log - log scale. A summary of these best fit lines and goodness of fit are presented in Figure 7.3 and Table 7.1.

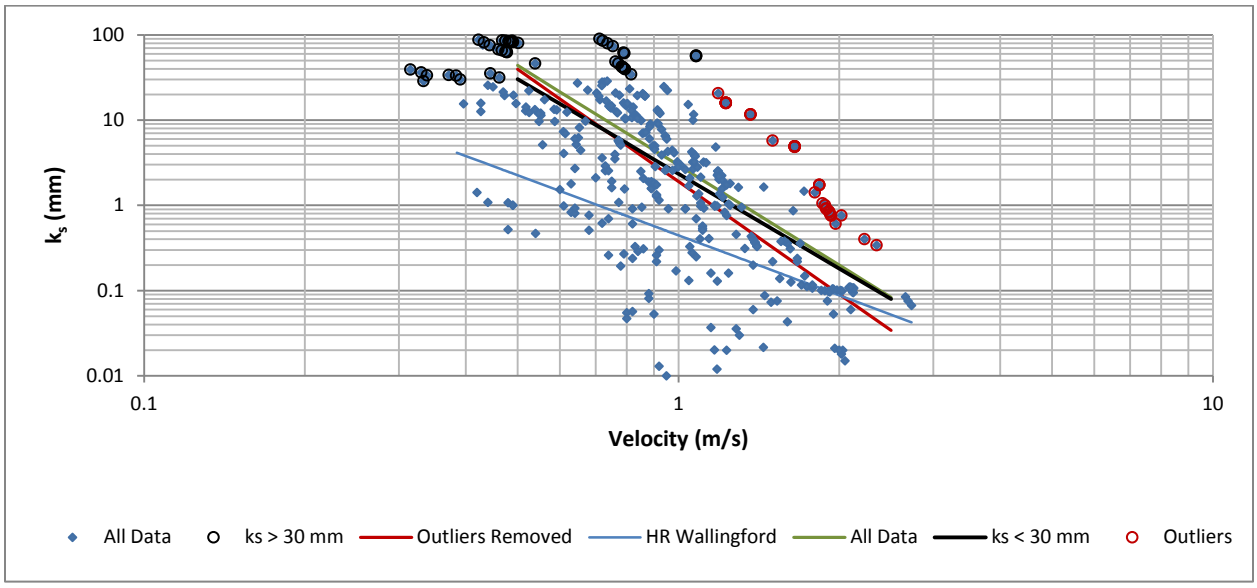

Figure 7.3: Comparison of Best Fit Lines - k_s

Table 7.1: Summary of Predictive Equations and Goodness of Fit - k_s

Data Set	# of Data points	Equation	R^2	SSE	MSE	Standard Deviation
All data excluding R_e<1.04x10^5	332	$k_s=2.95V^{-3.890}$	0.5614	150.9	0.457	1.03
k_s<30 mm	276	$k_s=2.35V^{-3.693}$	0.4741	113.9	0.414	0.89
Outliers Removed	243	$k_s=1.897V^{-4.379}$	0.6118	79.11	0.327	0.92

SSE – Sum of the squared error; MSE – Mean square error

Predictive equations representing the best fit lines shown in Figure 7.3 appear to provide a reasonable fit to the data; however, the outliers removed line (red) appears to best represent the data and crosses the HR Wallingford line at approximately 2 m/s (6.6 ft/s) where there is a concentration of data points. The slope along the other lines developed is flatter and crosses 0.1 mm (0.004 in.) at approximately 2.5 m/s (0.76 ft/s). The predictive line developed by HR Wallingford line was included to show its dependence on data points where $\kappa<0.4$ ($R_e<1.04x10^5$) and to illustrate that the predicted k_s values determined as part of this research are approximately an order of magnitude larger than the HR Wallingford line for velocities less than 1 m/s (3.3 ft/s).

Calculated errors comparing the predicted value of k_s to the actual value are presented in Figure 7.4. Error associated with the predictive equation is less than approximately 2 mm (0.079 in.) for velocities greater than 1 m/s (3.3 ft/s) which is generally considered the minimum recommended forcemain velocity. The large error associated with lower velocities may provide an indicator that selecting 30 mm (1.2 in.) as the upper limit may not be appropriate.

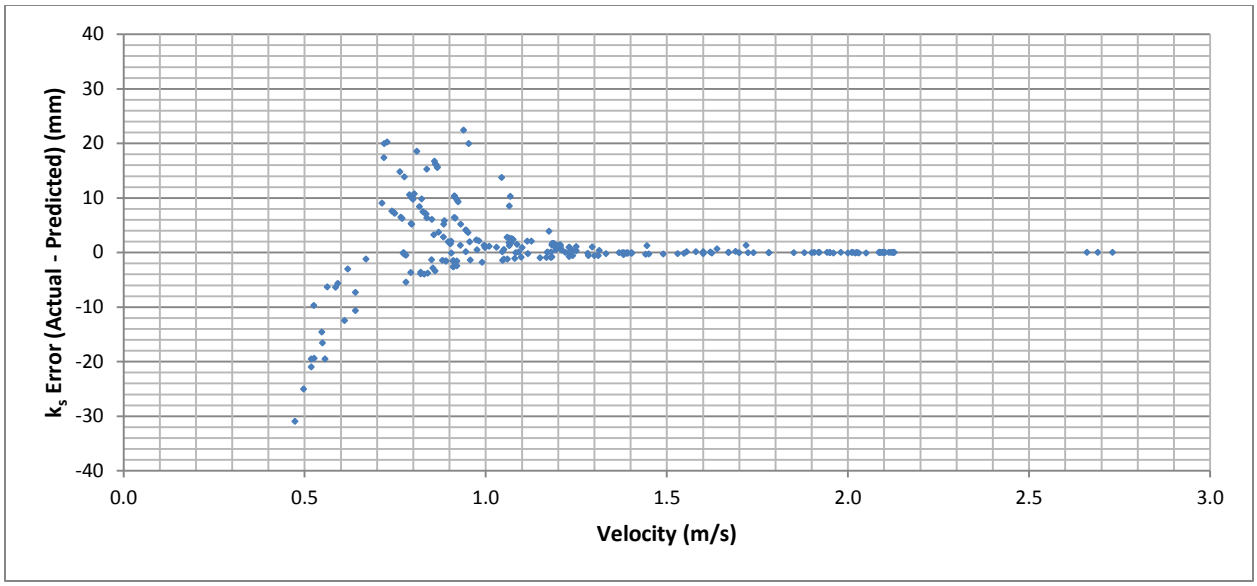

Figure 7.4: Error of Predictive Equation (k_s)

Given the predicted line is a power function, k_s will continue to decrease with increased velocity. A practical maximum velocity must therefore be selected. This is explored further in Section 7.2.3.

7.2.2 C-Factor

The procedure identified above to evaluate k_s data was applied to the C factor results. C factor data plotted by data source along identifying data points associated with R_e<1.04E5 are shown in Figure 7.5.

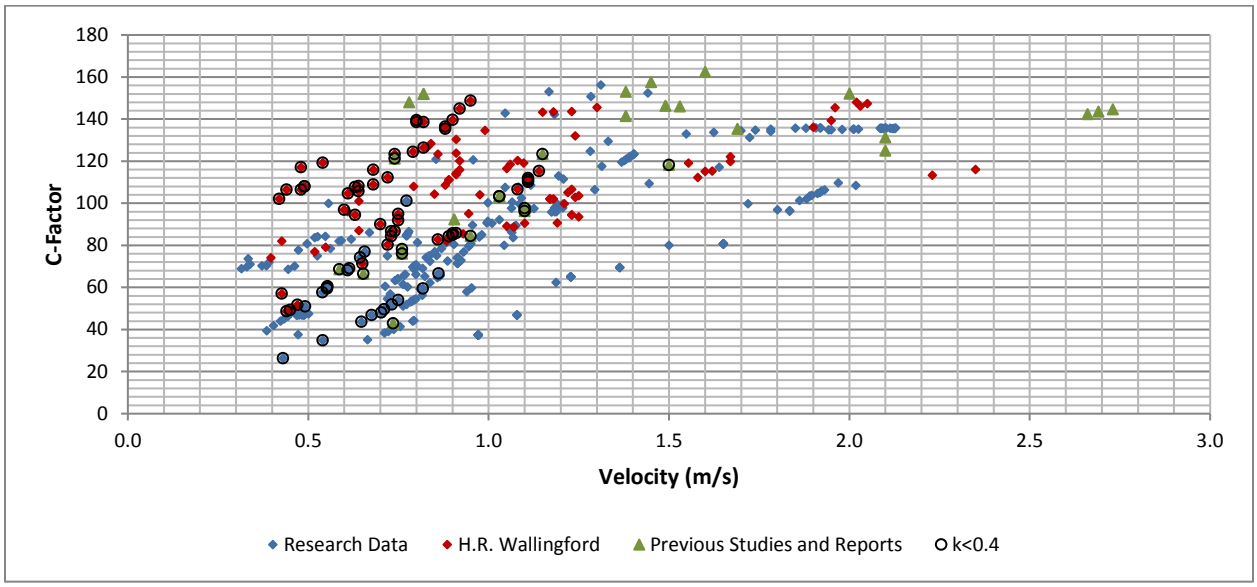

Figure 7.5: Summary of C factor Results

To be consistent with the approach utilized for k_s, three predictive lines for C factors were developed and are presented in Figure 7.6. First a predictive equation was developed for the entire dataset (excluding R_e<1.04x10^5). Second, the C factor data points equivalent to k_s values greater than 30 mm (1.2 in.) were removed since it is impractical to use an equivalent sand roughness value greater than 30 mm (1.2 in.) without adjusting for a reduced interior diameter. Third, the outlier data points identified by a red circle were removed. Although these data points provide a linear relationship, the data points are shifted to the right of the main trend line suggesting higher headloss which could be the result of an obstruction, sedimentation, or potential air locking.

Regression and predictive lines were developed using *CurveExpert Professional*. Several nonlinear functions were evaluated; however, the Weibull function provided the best overall fit. A summary of the best fit lines and goodness of fit are presented in Table 7.2.

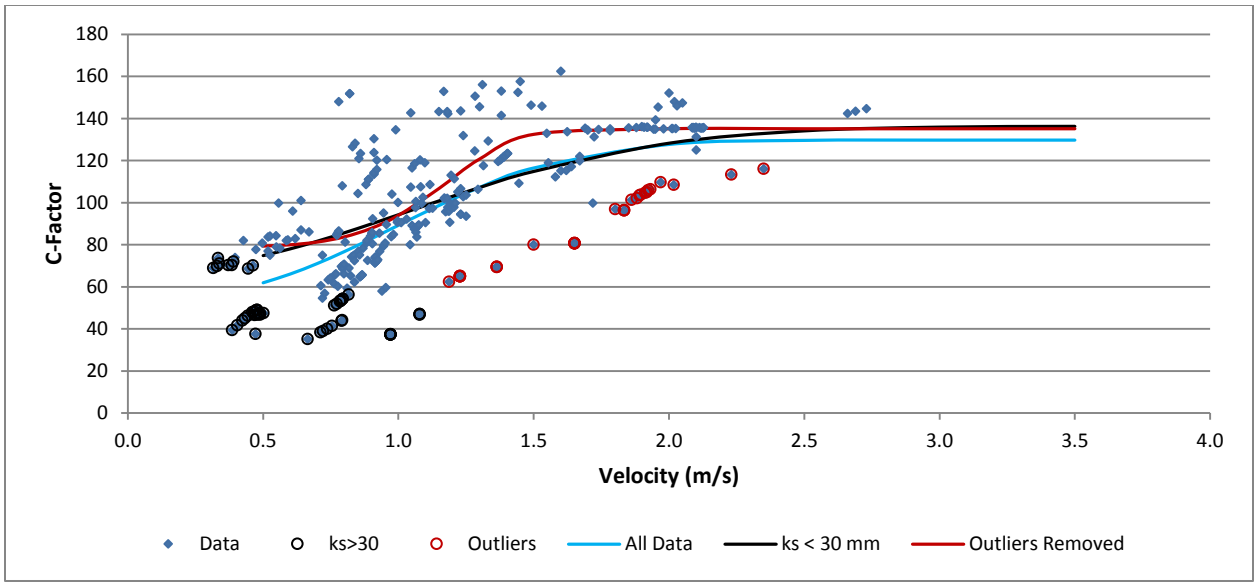

Figure 7.6: Comparison of Best Fit Lines – C factor

Table 7.2: Summary of Predictive Equations and Goodness of Fit – C factor

Equation	Data Set	# of Data points	Equation	R^2	Standard Error
1	All data excluding R_e<1.04x10^5	332	$C = 129.72 - 75.56e^{-0.6236V^{2.53}}$	0.4847	22.97
2	k_s<30 mm	276	$C = 136.32 - 68.89e^{-0.4930V^{2.12}}$	0.3808	21.34
3	Outliers Removed	243	$C = 135.11 - 56.12e^{-0.310V^{5.64}}$	0.5784	17.90

From Figure 7.6, the outliers removed line (red) appears to best represent the data. Calculated errors comparing the predicted value of C factor to the actual value are presented in Figure 7.7. Results show considerable scatter in the calculated error suggesting that other factors such as diameter should also be considered in developing the predictive equation.

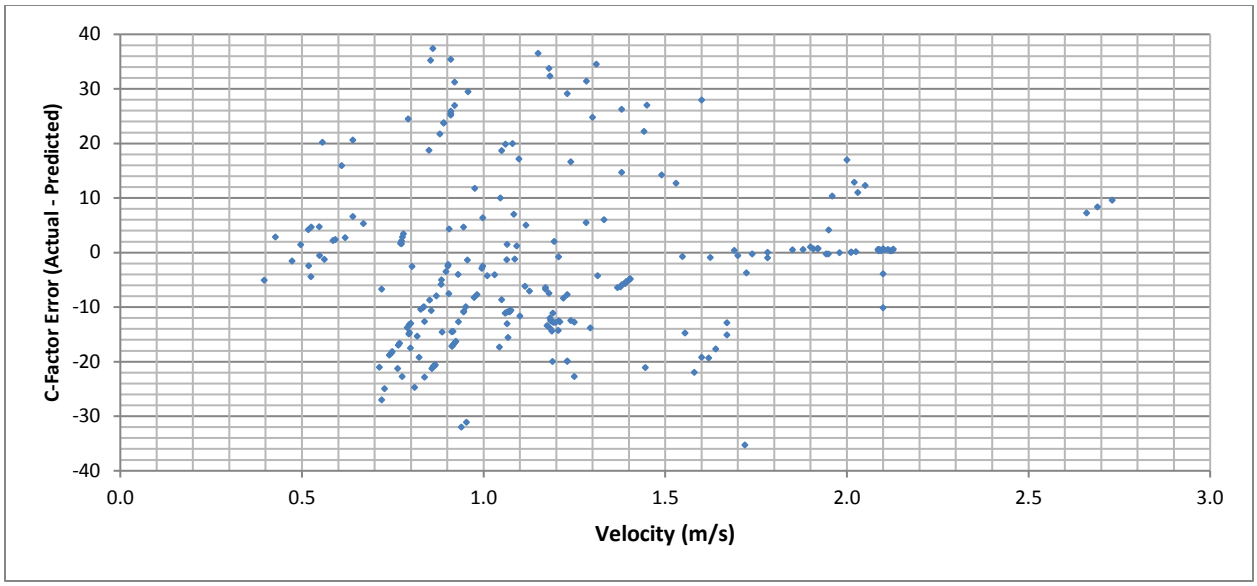

Figure 7.7: Error of Predictive Equation (C factor)

7.2.3 Final Curve Fitting

7.2.3.1 Estimation of k_s

As presented in Section 7.2.1, k_s values greater than 30 mm (1.2 in.) were removed from the dataset since it was assumed to be impractical to have an equivalent sand roughness height greater than 30 mm (1.2 in.) without reducing the diameter. This assumed maximum k_s value is likely too large; however, the data collected and evaluated does not support reducing this assumed threshold. Future studies should further evaluate this in more detail to confirm or refine this assumption.

Figure 7.8 presents all calculated values of k_s by pipe material and also includes the suggested clean water, new pipe absolute roughness values published in the literature. A majority of these data points are well above the clean water, new pipe absolute roughness. Some calculated values of k_s were found to be below the new pipe, clean water published value of k_s. A cluster of data between 1.5 and 2 m/s (4.9 ft/s and 6.6 ft/s) approaches a k_s value of 0.1 mm (0.004 in.). A number of data points are below 0.1 mm (0.004 in.) at velocities approximately 2 m/s (6.6 ft/s) and there are approximately 3 data points near 2.7 m/s (8.9 ft/s).

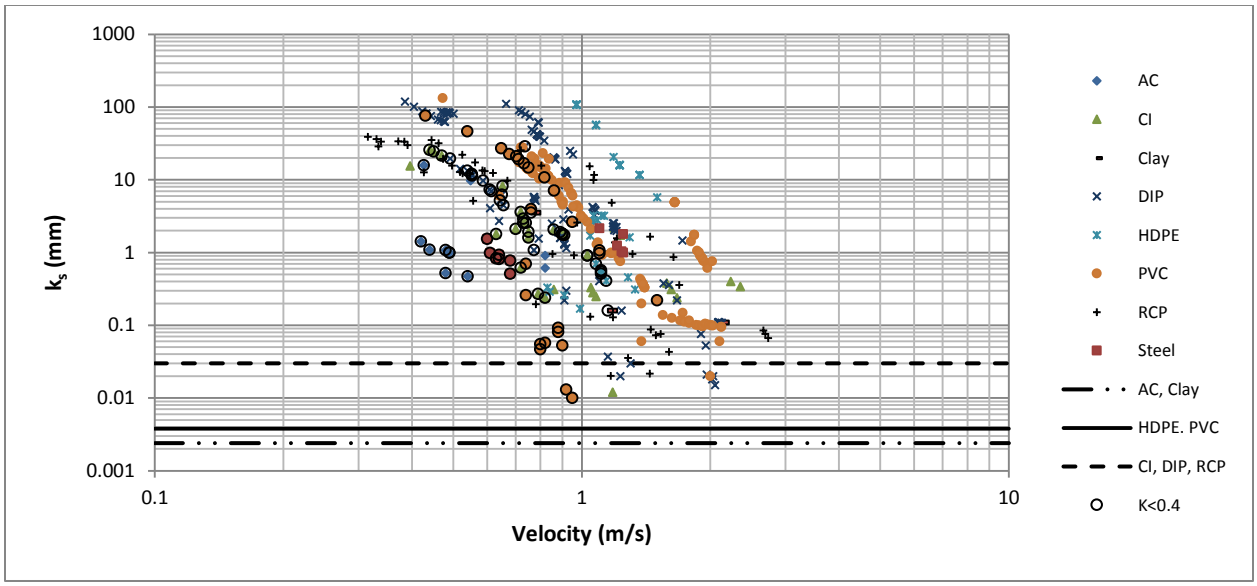

Figure 7.8: k_s Results by Material with New Pipe (Clean Water) Published k_s Values

Predictive equation (outliers removed) developed in section 7.2.1 provides a reasonable fit to the dataset. However, this linear relationship would continue indefinitely providing smaller values of k_s as velocity increases. In practice, this relationship cannot continue beyond the published values of k_s for clean water new pipe. Therefore, a practical lower limit should be established for application of the predictive equation. Intuitively, the slope of the predictive equation should decrease as it approaches the clean water, new pipe k_s value. An equation to define this line could not be readily developed since there are very few data points for velocities greater than 2 m/s (6.6 ft/s).

As shown in Section 7.2.2, C factor results suggest an approximate constant C factor for velocities greater than 2 m/s (6.6 ft/s). Given the limited number of data points greater than 2 m/s (6.6 ft/s), this near constant C factor was used to calculate equivalent k_s values for velocities ranging from 2 (6.6 ft/s) to 4 m/s (13.1 ft/s). Equivalent k_s values were plotted to develop a trendline in MS Excel resulting in Equation 7.1.

$$k_s = 0.1364V^{-0.546} \tag{7.1}$$

where k_s is absolute roughness in mm and V is velocity in m/s. The two predictive equations developed for k_s are shown along with the trimmed dataset (outliers and values for κ<0.4 removed) in Figure

7.9, the goodness of fit is presented in Table 7.1, the two predictive equations intersect at approximately 2 m/s (6.6 ft/s).

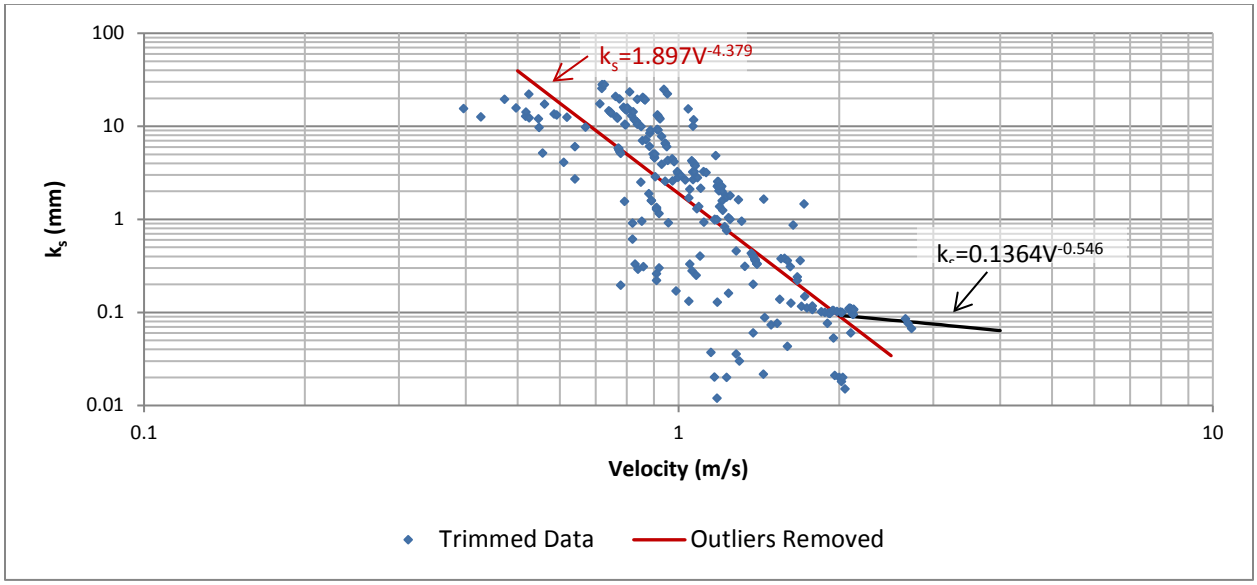

Figure 7.9: Predictive Equations (k_s)

Based upon the above analysis, the recommended application of the predictive equations to calculate k_s are summarized in Table 7.3.

Table 7.3: Summary and Limits of Equations to Estimate k_s

Equation k_s (mm)	Limits
$k_s = 30$	V < 0.54 (m/s)
$k_s = 1.897V^{-4.379}$	0.54 ≤ V ≤ 1.98 (m/s)
$k_s = 0.1364V^{-0.546}$	1.98 < V ≤ 4.0 (m/s)

7.2.3.2 Comparison of Predictive Equations

Headloss was calculated using both the Hazen-Williams and Darcy-Weisbach equations along with the predictive equations identified above in order to compare and verify the accuracy of the predictive equations. Predictive equations for k_s were substituted into the Swamee-Jain equation assuming a water temperature of 70 °F (21.1 °C). Equation 3 in Table 7.2 was substituted in to the Hazen-Williams equation. Headloss was calculated using 6 in., 12 in. and 24 in. (152.4 mm, 304.8 mm, and 609.6 mm) diameters at a pipe length of 16,404 ft (5,000 m), results are shown in Figure 7.10.

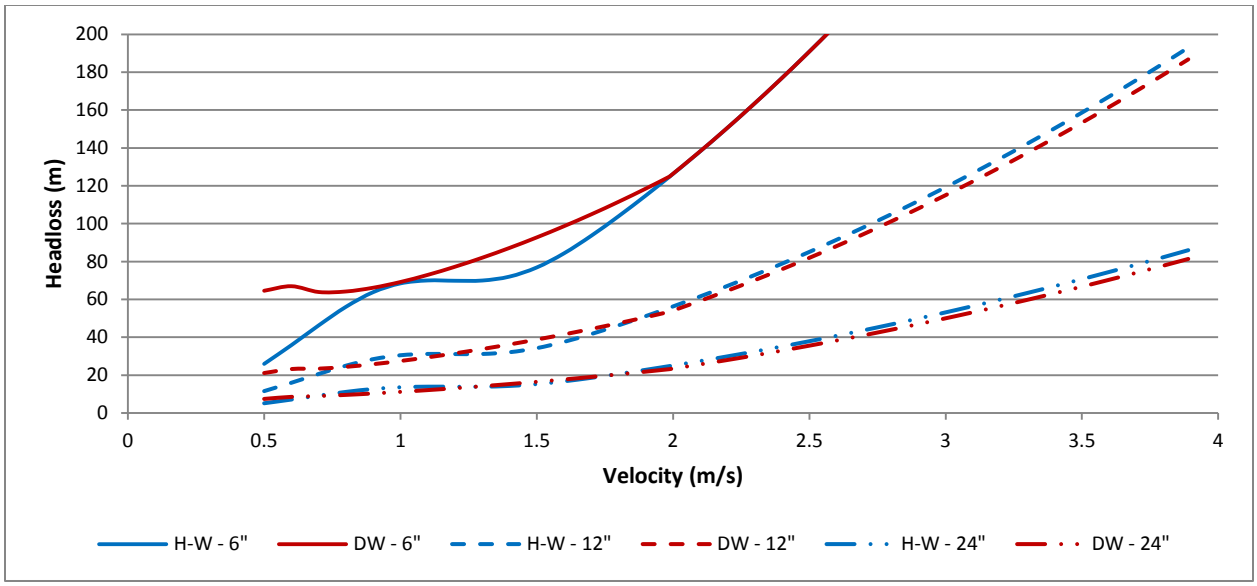

Figure 7.10: Comparison of Headloss using Predictive Equations

Results show a substantial gap between the calculated headloss from 1m/s (3.3 ft/s) to 2 m/s (6.6 ft/s) for a 6 in. (152.4 mm) diameter pipe; this gap narrows as diameter increases. Also noted is a rise in headloss using the Darcy-Weisbach equation for velocities less than 0.7 m/s (2.3 ft/s). This rise in headloss further indicates that the assumed maximum k_s value of 30 mm (1.2 in.) may not be appropriate for smaller diameters; which is logical from an application standpoint since an equivalent sand roughness of 30 mm (1.2 in.) provides a diameter reduction of nearly 40% (6 in. diameter). In addition, the Hazen-Williams headloss curve for a 6 in. (152.4 mm) diameter pipe shows a flat, or constant headloss between 1.15 m/s (3.8 ft/s) and 1.4 m/s (4.6 ft/s). The actual headloss should not be constant within this region and is not consistent with the results observed in the hydraulic analysis. Although there is a sharp transition in headloss for Darcy-Weisbach using a 6 in. (152.4 mm) diameter at approximately 1.9 m/s (0.58 ft/s), the headloss calculated from both methods correlates well for velocities greater than 1.9 m/s (0.58 ft/s). Headloss determined by Hazen-Williams for the 12 in. and 24 in. (304.6 mm and 609.6 mm) diameters are 4% and 7%, greater than the Darcy-Weisbach, respectively.

Headloss calculated from either equation should produce similar results. Results presented above suggest that the Hazen-Williams predictive equation should also account for diameter since there is a substantial deviation for smaller diameters between 1 m/s (3.3 ft/s) – 2 m/s (6.6 ft/s) and the relative error

increases with larger diameters. Considering the deviation in headloss results using the two equations, the k_s predictive equation was used to calculate the equivalent C factor for a number of diameters assuming a 16,404 ft (5,000 m) long pipe and water temperature of 70 °F (21.1 °C). Results are presented in Figure 7.11 and suggest that the Hazen-Williams predictive equation should include both velocity and diameter as dependent variables in determining C factor.

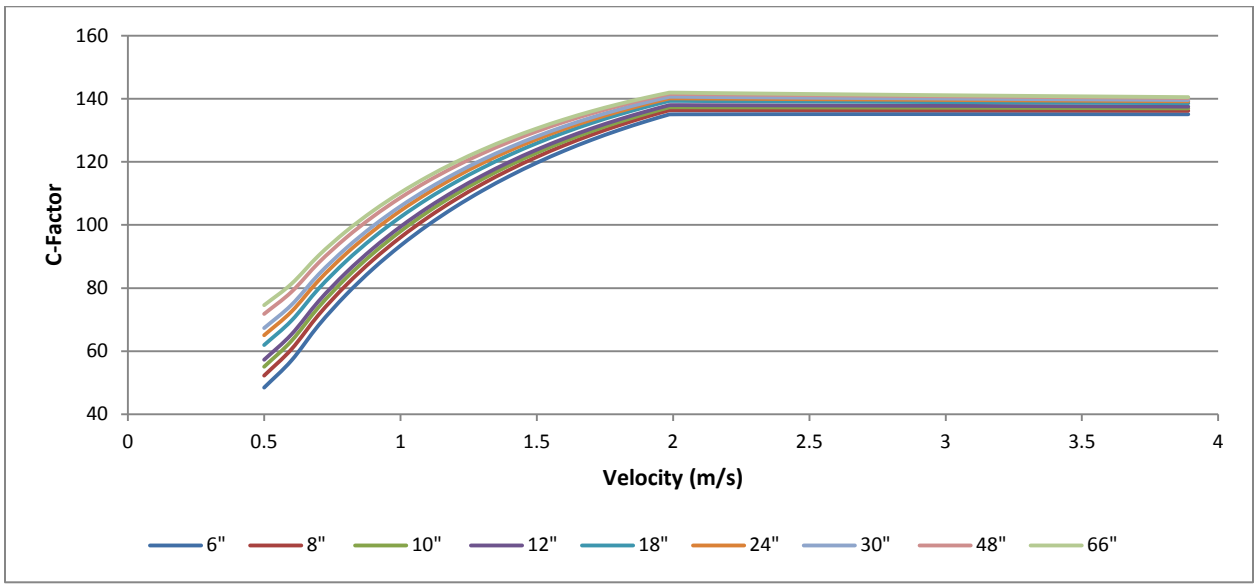

Figure 7.11: Equivalent C factor Relationship by Diameter

An attempt to develop a single predictive equation to estimate C factor using a multi-variable nonlinear regression produced unfavorable results. Therefore, a new approach was developed; *CurveExpert Professional* was used to evaluate and develop an equation to define the results for each diameter presented in Figure 7.11. The Weibull Model was found to best represent the data and takes form of Equation 7.2 where y is the C factor and x is the velocity (m/s):

$$y = a - be^{-cx^d} \tag{7.2}$$

The Weibull Model parameters determined by *CurveExpert Professional* are provided in Table 7.4.

Table 7.4: Summary of Weibull Model Parameters – C factor Equation Development

Diameter (in)	a	b	c	d
6	135.65	112.16	0.963	1.876
8	136.81	108.75	0.967	1.883
10	137.62	106.14	0.97	1.889
12	138.22	104.04	0.973	1.893
18	139.36	99.46	0.978	1.904
24	140.03	96.3	0.982	1.912
30	140.46	93.89	0.985	1.919
48	141.17	88.96	0.992	1.933
66	141.48	85.72	0.996	1.943
Average			0.978	1.906

Each parameter was plotted against diameter using Microsoft Excel to identify and screen critical relationships between parameters. Due to the relative ranges of each parameter, both the a and b parameters are presented in Figure 7.12 and the c and d parameters in Figure 7.13. The figures also provide the trendline and corresponding R^2 values for each parameter.

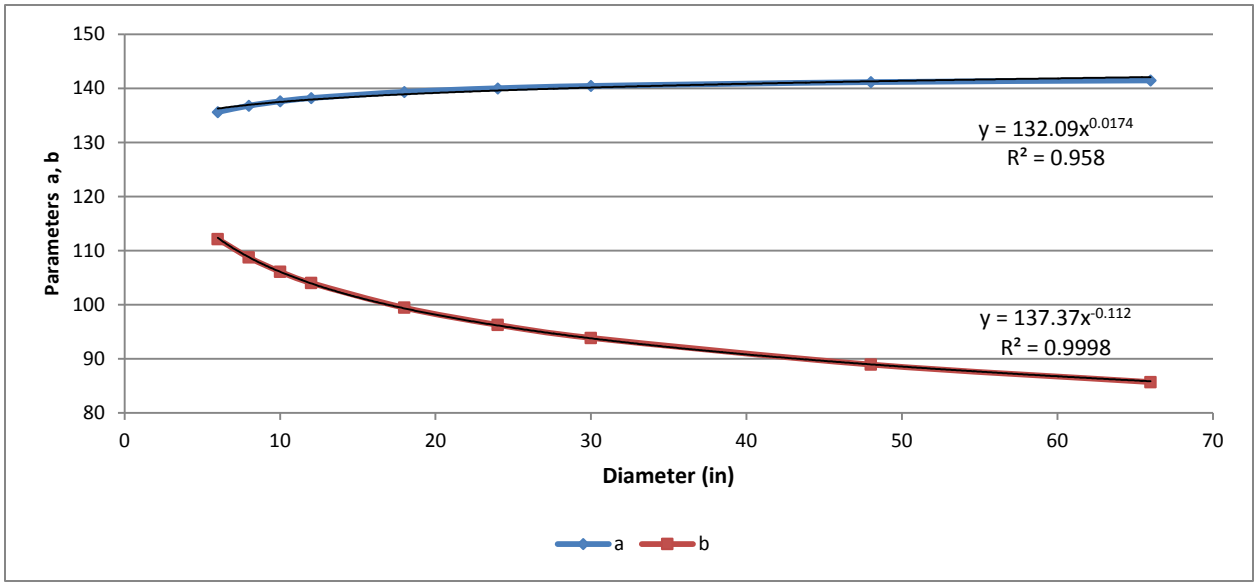

Figure 7.12: Parameters a and b – C factor (Metric)

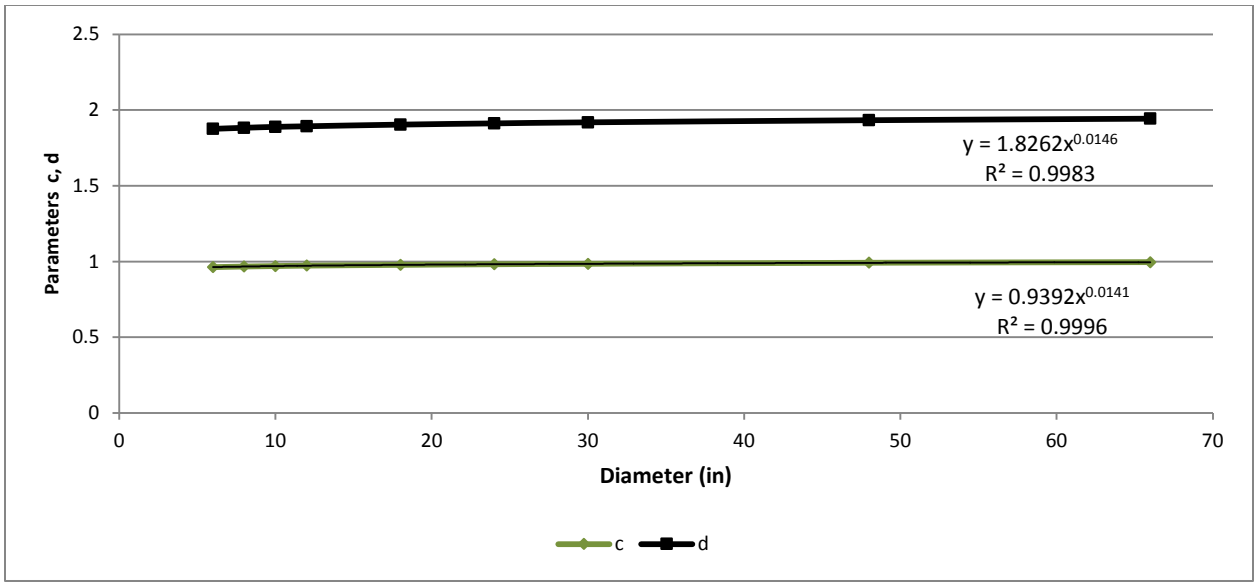

Figure 7.13: Parameters c and d – C factor (Metric)

Both the a and b parameters vary significantly with diameter. However, the c and d parameters are nearly constant. Therefore, the impact of the c and d parameters on the Weibull Model was evaluated by comparing the average of these parameters to the actual values for the exponential portion of the model (e^{-cx^d}). The results are presented in Figure 7.14 for a 6 in. diameter pipe and show that utilizing the average for the c and d parameters provides nearly identical results.

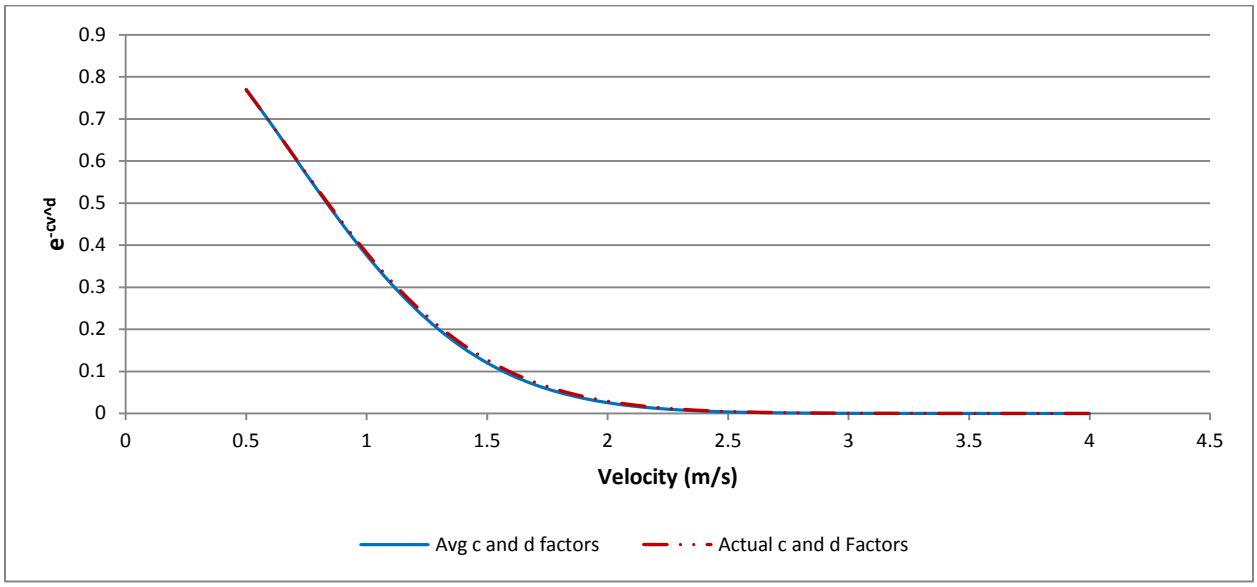

Figure 7.14: Comparison of Average and Actual c and d parameters on e^{-cx^d}

C factors were calculated for both 6 in. and 66 in. diameter pipe using the trendlines developed for the a and b parameters (Figure 7.12) and both the actual and average values for c and d in order to verify that that using the average values did not significantly affect C factor. These two diameters represent the minimum and maximum diameter evaluated as part of this research. Results along with the calculated error comparing the actual against the average c and d parameters are shown in Figure 7.15. Using the average c and d parameters provided calculated C factors with less than 0.8% error indicating that it is acceptable to apply the average c and d parameters to the exponential portion of the predictive equation.

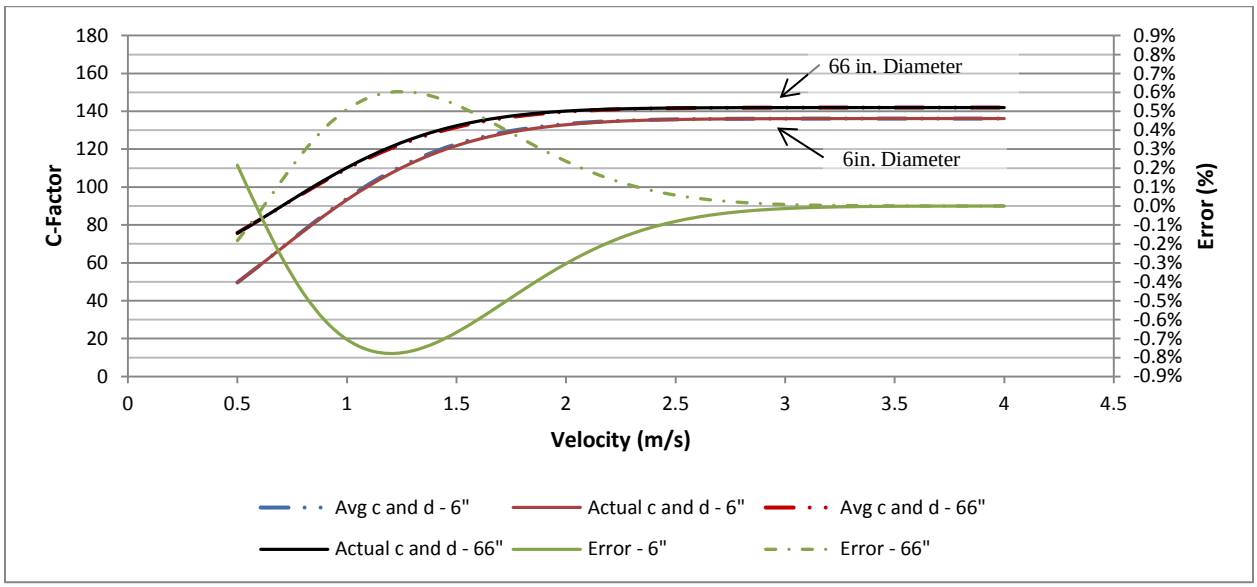

Figure 7.15: Comparison of C factors Calculated from Actual and Average c and d parameters

Combining the trendlines for the a and b parameters as well as the average values for the c and d parameters to Equation 7.2 results in Equation 7.3 to determine C factor based upon both velocity and pipe diameter:

$$C_{Factor} = a - be^{-cV^d} \tag{7.3}$$

Where a $= 132.09\phi^{0.0174}$; $b = 137.37\phi^{-0.112}$; c = 0.978 ; d = 1.906; ϕ is diameter in inches; and V is velocity in m/s.

A comparison of the headloss determined from both the Hazen-Williams equation and Equation 7.3; and the Darcy-Weisbach equation using the equation(s) presented in Table 7.3 is provided in Figure 7.16 for 6 in., 12 in., and 24 in. (152.4 mm, 304.8 mm, and 609.6 mm) diameters. The error associated with calculated headloss using the predictive equation(s) was determined to be less than 5%. Results show that a slight gap for the headloss curves between 1.15 m/s (3.78 ft/s) and 1.75 m/s (5.74 ft/s) still remains for 6 in. (152.4 mm) diameter pipe but is greatly reduced as compared to Figure 7.10; however, the remainder of the headloss curve matches very well. In addition, the headloss curves for the larger diameters provide nearly identical results. The headloss curve associated with Hazen-Williams was noted to be a smooth curve whereas the Darcy-Weisbach provides a rise in headloss for velocities less than 0.7 m/s, which further indicates that that the assumed maximum k_s value of 30 mm (1.2 in.) may not be appropriate for smaller diameter pipe. These predictive equations should be used to estimate roughness factors for pipelines conveying wastewater based upon the velocity in the pipe. Although not detailed here; a similar analysis was conducted for U.S Customary Units. Results are presented in Appendix F and the predictive equation is provided in Section 7.3.1.2.

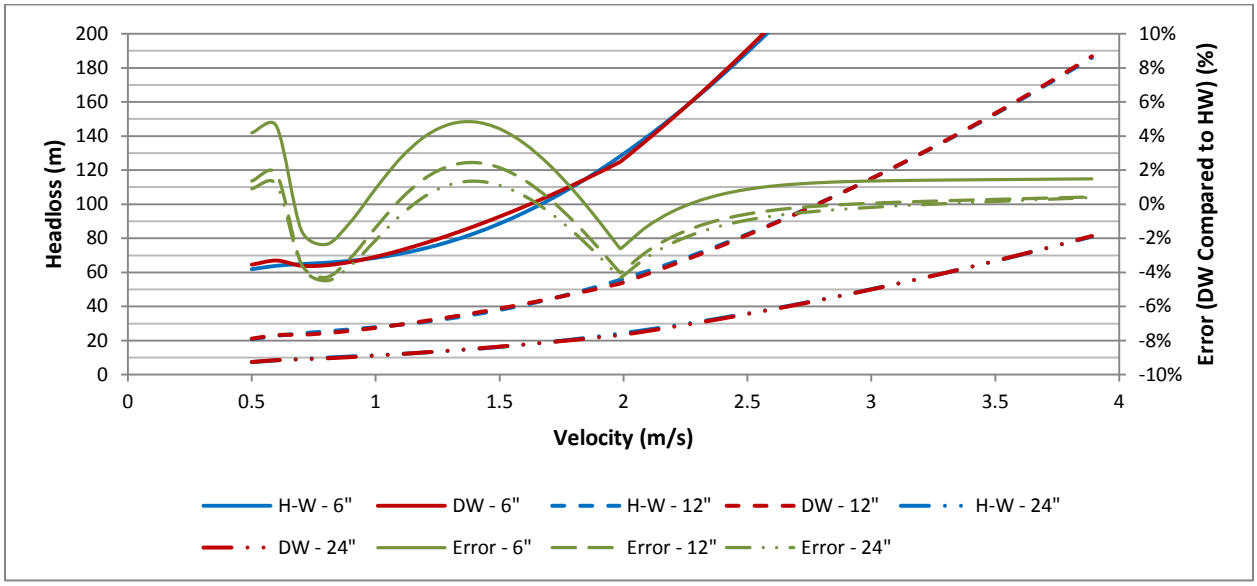

Figure 7.16: Comparison of Headloss Calculated from Hazen-Williams and Darcy-Weisbach Equations for 6 in., 12 in. and 24 in. Diameters

The above analysis determined the minimum velocity corresponding to a k_s value of 30 mm (1.2 in.) is approximately 0.54 m/s (1.77 ft/s). Since the C factor is a function of both velocity and diameter, the minimum recommended C factor corresponding to a velocity of 0.54 m/s (1.77 ft/s) was determined and plotted against diameter as presented in Figure 7.17 and can be calculated from Equation 7.4.

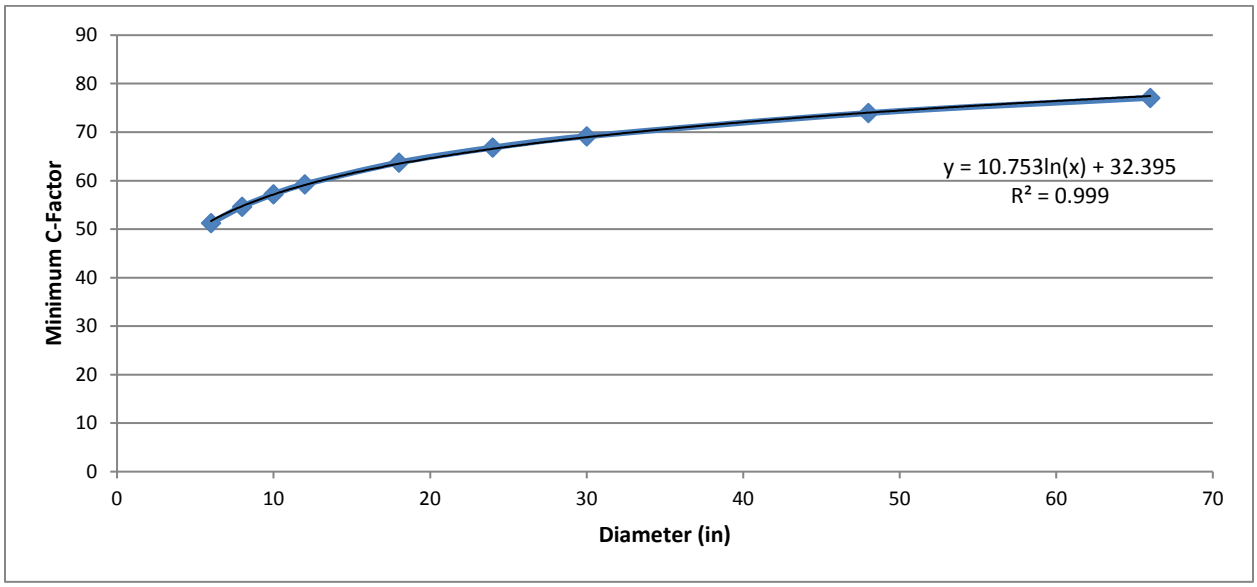

Figure 7.17: Minimum Applied C factor by Diameter

$$C_{Factor\ (\mathrm{Min})} = 10.753ln(\phi) + 32.395 \quad (7.4)$$

where ϕ is diameter (in)

7.2.3.2.1 Temperature Effects on Equivalent C-Factors

Equations 7.2 and 7.3 were developed assuming a wastewater temperature of 70 °F. Equivalent C factors were also evaluated assuming temperatures of 50 °F and 60 °F (10 °C and 15.6 °C). Analysis shows that the equivalent C factors were reduced approximately 0.54% for every 10 °F (5.56 °C) reduction in temperature. Equation 7.5 provides a simple correction factor (C_T) to be applied to Equation 7.3 to adjust the C factor (C factor * C_T) based upon wastewater temperature.

$$C_T = [1 - 5x10^{-4} * (70 - T(°\mathrm{F}))] \quad (7.5)$$

It should be noted that this analysis was performed assuming an average wastewater temperature of 70 °F (21.1 °C) and therefore should be verified in future research.

7.3 Summary of Results and Recommendations

This section summarizes the predictive equations developed to estimate absolute roughness (k_s) and C factor, based upon velocity. These equations should be substituted in the Colebrook-White / Darcy-Weisbach and Hazen-Williams equations to calculate headloss in wastewater forcemains.

7.3.1 Final Predictive Equations

A summary of the recommended predictive equations for both Darcy-Weisbach and Hazen-Williams equations in both Metric and US Customary units are provided below.

7.3.1.1 Absolute Roughness - k_s

Table 7.5: Summary of Predictive Equation and Limits - k_s (Metric Units)

Equation k_s (mm)	Limits	Equation No.
$k_s = 30$	V < 0.54 (m/s)	(7.6a)
$k_s = 1.897V^{-4.379}$	0.54 ≤ V ≤ 1.98 (m/s)	(7.6b)
$k_s = 0.1364V^{-0.546}$	1.98 < V ≤ 4.0 (m/s)	(7.6c)

Table 7.6: Summary of Predictive Equation and Limits - k_s (U.S. Customary Units)

Equation k_s (in)	Limits	Equation No.
$k_s = 1.18$	V < 1.77 (ft/s)	(7.7a)
$k_s = 13.571V^{-4.379}$	1.77 ≤ V ≤ 6.50 (ft/s)	(7.7b)
$k_s = 0.0103V^{-0.546}$	6.50 < V ≤ 13.12 (ft/s)	(7.7c)

7.3.1.2 C-Factor

Equations 7.8 (Metric) and 7.9 (US Customary) estimate C factor based upon velocity and diameter. The minimum C factor to be applied to hydraulic calculations for velocities less than 0.54 m/s (1.77 ft/s) is calculated from Equation 7.4. Equations 7.8 and 7.9 were developed assuming a wastewater temperature of 70 °F (21.1 °C), Equation 7.5 is used to adjust the C factor for wastewater temperatures other than 70 °F (21.1 °C).

Table 7.7: Summary of Predictive Equations and Limits: C factor

C-Factor Equation	Limits	Equation No.
Metric Units		
$C_{Factor} = 132.1\phi^{0.0174} - 137.37\phi^{-0.112}e^{-0.908V^{1.906}}$	0.54 ≤ V ≤ 4 (m/s)	(7.8)
US Customary Units		
$C_{Factor} = 132.1\phi^{0.0175} - 137.29\phi^{-0.112}e^{-0.102V^{1.907}}$	1.77 ≤ V ≤ 13.12 (ft/s)	(7.9)

Where: ϕ is diameter in inches; V is velocity m/s, (ft/s)

8 Implementation of Results

8.1 Economic Forcemain Sizing

The hydraulic analyses performed in Chapter 5 determined that the hydraulic roughness parameters (absolute roughens and C factor) varied with velocity for wastewater forcemains. As velocity increases, the absolute roughness was found to decrease, and similarly, the C factor increases with higher velocity. Results indicate that the hydraulic efficiency of forcemains improve with increased velocity. Although hydraulic efficiency improves, the system experiences higher headloss with increased velocity since headloss is a function of square of the velocity.

Economic factors such as operational and capital costs should be considered when sizing forcemain systems. A significant portion of operational costs are associated with energy usage. Capital costs associated with the lift station depend on the number, type, and size of the pumps; the forcemain cost is a function of the pipe material, diameter, and length. All of these items are inter-related. In general, the forcemain capital cost decreases as diameter decreases; however, decreasing the diameter increases velocity, which in turn, increases pump sizing and operational costs associated with energy.

Sewage lift stations are generally designed for a yearly maximum flow; however, the average flow may be considerably less. Larsen (2016) indicates that due to the nonlinear relation between energy consumption and flow velocity in turbulent flows, the power consumption will be at its minimum if the flow is distributed as close as possible to the yearly average.

The following sections review and evaluate the methodology for economic sizing of pipelines and discusses several economic factors to be considered during design and how they are inter-related. This analysis is not intended to be a market study and utilizes general cost curves for estimating capital costs since local or geographical factors such as economies, material costs, energy costs, or labor rates can significantly affect operational and construction costs. Operational costs vary depending on the frequency

and duration of pump operation. Equation 8.1 can be used to estimate the pump runtime where Q_{in} is the inflow (gpm) and Q_p is the pump flowrate (gpm)

$$t = 760 \frac{Q_{in}}{Q_p}_{ts} \tag{8.1}$$

Additionally, the rate structure of electrical utilities can also affect energy costs. For example, electrical utilities could offer discounts for energy usage during off peak hours or may provide surcharges for usage during peak consumption time periods. Frequency and duration also affect the energy usage as smaller lift stations tend to run periodically while larger stations could run more frequently or even continuously. Frequency of operation within smaller stations depends on the size of the pumps and the inflow rate reporting to the station. Table 6.8 shows that the smaller lift stations evaluated as part of this research operate between 7 to 241 days annually.

Annual costs associated with pumping water were determined for velocities ranging from 1.64 ft/s (0.5 m/s) to 13.1 ft/s (4 m/s) and diameters ranging from 6 in. (152.4 mm) to 18 in. (457.2 mm). Energy costs were determined from the water horsepower due to constant pumping (365 days annually) assuming an electrical rate of \$0.07/kw-hr which is the average industrial rate for Colorado (http://www.electricitylocal.com/). Water horsepower was determined from the flowrate and friction loss; the friction loss was calculated using the Hazen-Williams Equation along with Equation 9.6 to estimate the C factor assuming a 5,000 ft (1,524 m) long pipeline for velocities ranging from 1.64 ft/s (0.5 m/s) to 13.1 ft/s (4 m/s). Results are presented in

Figure 8.1 and show that velocity has a significant effect on annual pumping costs assuming continuous pumping. The actual annual duration of pump runtime will affect the annual operation cost and ultimately the economic diameter of the forcemain and will be evaluated in the following section.

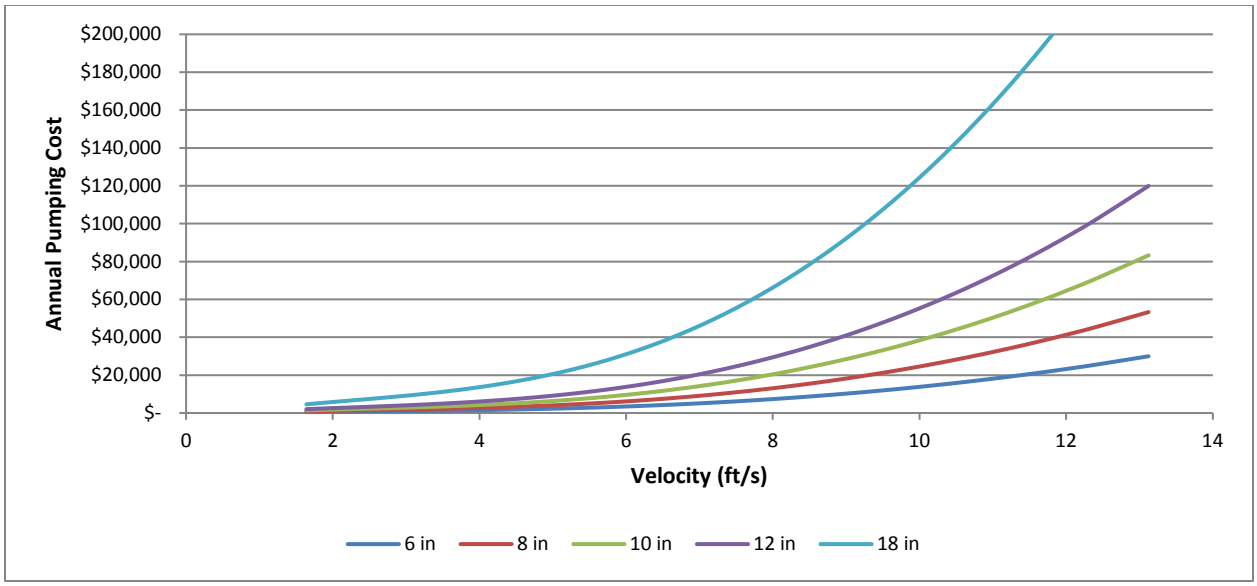

Figure 8.1: Example of Annual Pumping Cost with Respect to Diameter

8.1.1 Pipeline Economic Analysis

As presented above, velocity has a significant effect on pumping costs. Other factors that can affect the economic sizing of forcemains include pipe length, annual duration of pump runtime, energy costs, capital costs of the pipeline and pump station, and project financing terms. Although the project financing terms (interest rate and payback period) can affect economic sizing, these parameters are a function of local economic factors and will not be evaluated as part of this research.

Economic analysis of a system evaluates the project life cycle costs (LCC) based upon the system configuration. The system is optimized when the LCC is a minimum. Several methods such as the Capitalization; Annuity; or Present Value Methods can be used to estimate the LCC. The Capitalization Method converts recurring costs to capital costs; the Annuity Method converts capital costs to recurring costs; and the Present Value Method determines the net present worth of the system. Present Value Method is the most common and will be utilized for this analysis based upon the methodology identified in Hydraulics of Pipelines by Tullis (1989). The present worth (PW) is determined from Equation 8.2.

$$PW = \frac{inital\ cost}{(1+n)^i} \tag{8.2}$$

Where: *n* is the years of useful life; and *i* is the interest rate. The most economical diameter is the diameter that produces the lowest present worth considering the annual operational cost of pumping and capital cost for the pump station and pipeline. The process includes calculating the total annual costs for a given flowrate considering various pipe diameters. Total annual cost is the present worth of the capital costs (pump station and pipeline), annual operational costs, and any other costs to be included. The minimum total cost results in the most economic system over its life cycle. Requirements and procedure for optimal diameter analysis is identified in Table 8.1.

Table 8.1: Procedure of Optimal Pipe Diameter Selection

#	Item	Calculation
1	Total Cost of Installed Pipeline ($)	Unit cost of pipe ($/ft) * length
2	Annual Cost of Pipeline ($/yr)	Present Worth of pipeline
3	Required Pump Head (ft)	Determine system head on pump (total dynamic head)
4	Required Pump HP	Pump BHP
5	Required Electrical Power (kW)	Convert pump hp to kW (BHP * 0.7457 = kW)
6	Annual Power Cost of Pumping ($/yr)	Cost of power usage ($/kW-hr * total hrs operating annually)
7	Cost of Pumping Station ($)	Total Capital $ of Pump Station
8	Annual Cost of Pump Station ($/yr)	Present Worth of Pump Station Capital Cost
9	Total Annual Pumping Cost ($/yr)	(6 + 8)
10	Total Annual Cost ($/yr)	(2 + 9)

Required Pump Head is the total headloss (friction and minor loses) plus the static head of the system. The required pump horsepower (hp) represents the brake horsepower (BHP) of the pump and is determined from the discharge, pump head, and pump efficiency. Microsoft Excel was used to develop a spreadsheet to determine the optimal diameter using the methodology presented above. The following sections will evaluate the sensitivity of economic sizing to energy costs, pump runtime, pipe length, system static head, and pipeline capital costs given the following design parameters:

- Static head of 50 ft (15.2 m);
- Electrical unit rate of $0.07 / kw-hr; constant rate; no demand charges or future increases considered;
- Pipe unit cost of $8 / ft / in-diameter: assumed to be constant over entire length;
- Pipe length of 10,000 ft (3,048 m);
- Pumps are 75% efficient and operate an average of 12 hrs/day over the year;

- Pump Station capital costs amortized over 20 years and pipeline amortized over 30 years; both at a 7% interest rate;
- Headloss determined from the Hazen-Williams equation using Equation 7.8 (Section 7.3.1.2) to estimate the C factor; and
- Minor losses were assumed to be 5% of friction losses.

Although not presented as part of the sensitivity analysis below, the effect of pump station cost was found to be insignificant to the economic sizing of the pipe. Pump station costs vary depending on several factors, of which the most important include the type and number of pumps, number of redundant pumps, depth of the structure, and volume of wet well storage. As a general rule of thumb, pump station unit cost ($/station hp) decreases with increased hp, or station size. A power function was developed to estimate the station cost based upon its total required hp assuming a cost of $15,000 /hp for small (1 hp) stations and $2,000 /hp for large (3,000 hp) stations. The resulting power function is $Station\ Cost\ (\$) = 15{,}000(hp)^{0.7483}$. This cost model is not intended to provide a complete estimate of pump station capital cost but provides relative costs for comparison purposes based upon the station horsepower.

Pipeline economic sizing was first performed using the above assumptions given flowrates of 500 gpm (0.03 cms), 2,000 gpm (0.13 cms), 5,000 gpm (0.32 cms), 10,000 gpm (0.63 cms), 20,000 gpm (1.26 cms), and 50,000 gpm (3.15 cms) in order to provide a baseline for the sensitivity analysis below. Results for the 5,000 gpm (0.32 cms) case are presented graphically in Figure 8.2 with the optimal diameter identified by the arrow. Calculations are also summarized in Table 8.2 to show the methodology and results of the calculations. Analysis was performed for interior diameters of 1-inch increments; however, only results near the optimal diameter (some diameter results omitted for brevity) to illustrate the relative change in results near the optimal diameter.

The relative change in total annual cost is relatively minor for diameters ± 3 in. (76.2 mm) from the optimal diameter. Therefore, a slightly smaller diameter could be selected to increase operational velocity without significantly impacting the total annual cost. This is illustrated graphically in Figure 8.2,

with a nearly flat spot in curve adjacent to the optimal diameter. Figure 8.2 also shows that the velocity falls quickly with increasing diameter.

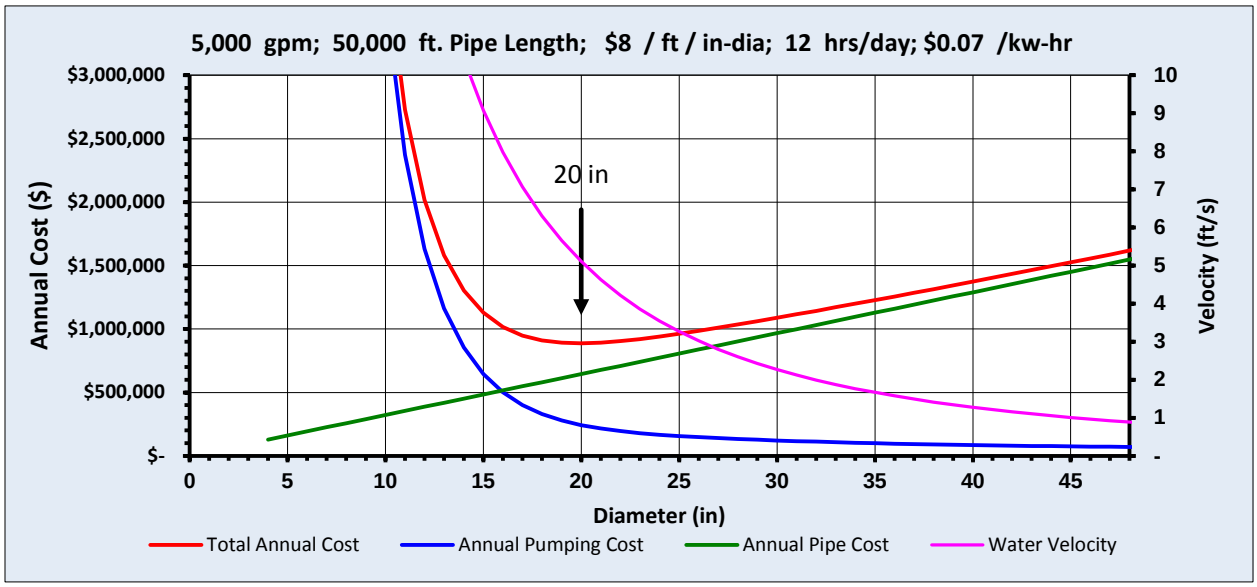

Figure 8.2: Example of Optimal Diameter Calculation

Table 8.2: Example of Optimal Diameter Calculation Results for 5,000 gpm and 10,000 ft long pipeline

	17 in.	19 in.	20 in.	21 in.	25 in.
Total Cost of Installed Pipeline ($)	$ 1,360,000	$ 1,520,000	$ 1,600,000	$ 1,680,000	$ 2,000,000
Annual Cost of Pipeline ($/yr)	$ 109,598	$ 122,491	$ 128,938	$ 135,385	$ 161,173
Required Pump Head (ft)	136.8	103.7	94.1	87.1	72.4
Required Pump HP	230.5	174.7	158.5	146.8	121.9
Required Electrical Power (kW)	171.9	130.3	118.2	109.5	90.9
Annual Power Cost of Pumping ($/yr)	$ 52,707	$ 39,942	$ 36,245	$ 33,571	$ 27,880
Cost of Pumping Station ($)	$ 879,267	$ 714,499	$ 664,415	$ 627,382	$ 545,963
Annual Cost of Pump Station ($/yr)	$ 82,997	$ 67,444	$ 62,716	$ 59,220	$ 51,535
Total Annual Pumping Cost ($/yr)	$ 135,703	$ 107,386	$ 98,962	$ 92,792	$ 79,415
Total Annual Cost ($/yr)	$ 245,301	$ 229,877	$ 227,900	$ 228,177	$ 240,588
Velocity (ft/s)	7.1	5.7	5.1	4.6	3.3

Results of the base economic analysis are summarized in Table 8.3 and show that the velocity at the most economical diameter (10,000 ft pipeline) also increases with diameter and flowrate. As demonstrated above, the optimal diameter selected can vary a few inches to either increase operational velocity or facilitate selection of a standard size pipe diameter without significantly impacting the total annual cost.

Table 8.3: Economic Sizing for different flowrates with 10,000 ft long pipe at 50 ft static head

Flowrate (gpm)	Optimal Diameter (in)	Velocity (ft/s)	Required Pump Head (ft)	Headloss (ft)	Annual Pumping Costs	Pumping Cost % of Total
500	7	4.2	181.5	131.5	$ 6,991	10%
2,000	13	4.8	120.0	70.0	$ 18,492	13%
5,000	20	5.1	94.1	44.1	$ 36,245	16%
10,000	28	5.2	80.0	30.0	$ 61,666	18%
20,000	39	5.4	70.9	20.9	$ 109,283	22%
50,000	60	5.7	63.4	13.4	$ 244,329	27%

8.1.2 Effect of Energy Costs

The effect of the energy unit cost was evaluated for the base case evaluated above. Unit rates for energy were varied in $0.01 increments from $0.05 / kw-hr to $0.10 / kw-hr. The results presented in Figure 8.3 and Table 8.4 show that the economic diameter is not significantly affected for small flowrates. It is also noted that the optimal diameter increases slightly as the discharge and energy rate increase. This suggests that the present worth of a larger diameter pipeline is less than the annual operational cost associated with the higher energy rates.

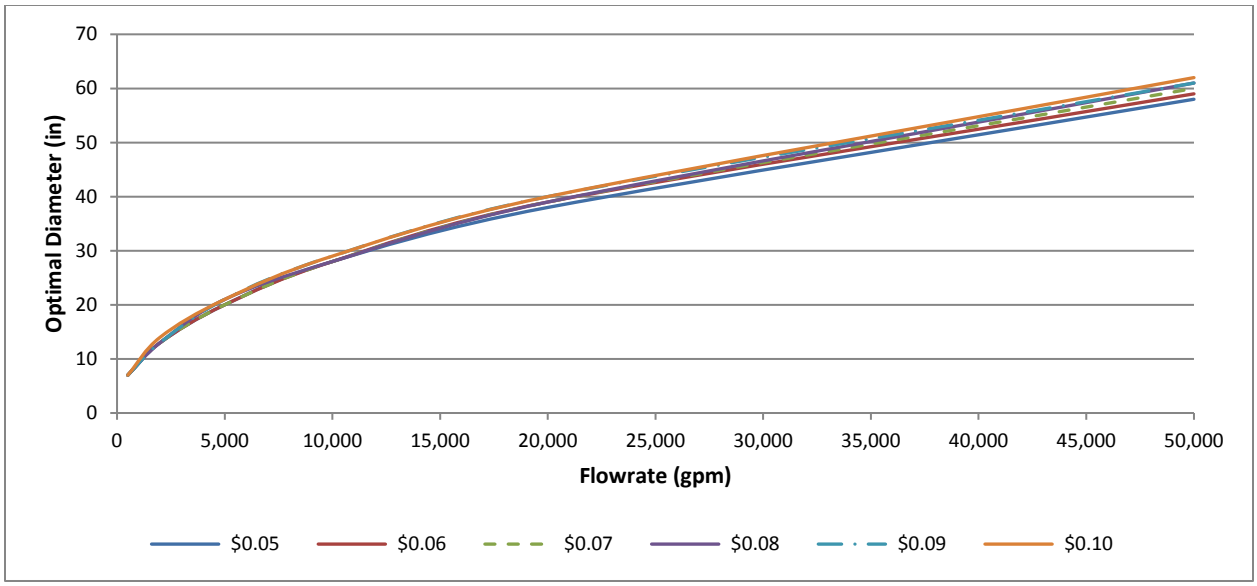

Figure 8.3: Effect of Energy Cost on Optimal Diameter – 10,000 ft long pipe

Table 8.4: Effect of Energy Cost on Optimal Diameter – 10,000 ft long pipe

Flowrate (gpm)	Optimal Diameter (in) / (Velocity (ft/s))					
	$ 0.05/kw-hr	$ 0.06/kw-hr	$ 0.07/kw-hr	$ 0.08/kw-hr	$ 0.09/kw-hr	$ 0.10/kw-hr
500	7 / (4.2)	7 / (4.2)	7 / (4.2)	7 / (4.2)	7 / (4.2)	7 / (4.2)
2,000	13 / (4.8)	13 / (4.8)	13 / (4.8)	13 / (4.8)	13 / (4.8)	14 / (4.2)
5,000	20 / (5.1)	20 / (5.1)	20 / (5.1)	21 / (4.6)	21 / (4.6)	21 / (4.6)
10,000	28 / (5.2)	28 / (5.2)	28 / (5.2)	28 / (5.2)	29 / (4.9)	29 / (4.9)
20,000	38 / (5.7)	39 / (5.4)	39 / (5.4)	39 / (5.4)	40 / (5.1)	40 / (5.1)
50,000	58 / (6.1)	59 / (5.9)	60 / (5.7)	61 / (5.5)	61 / (5.5)	62 / (5.3)

8.1.3 Effect of Pipe Length

The effect of length was evaluated for pipe lengths ranging from 500 ft to 50,000 ft and flowrates ranging from 500 gpm to 50,000 gpm (0.03 cms to 3.15 cms) with all other assumptions identified above remaining the same. As shown in Table 8.5, the effect of length on optimal diameter is minimal, with optimal diameters decreasing slightly as pipe length increases.

Table 8.5: Effect of Length on Optimal Diameter – Various Flowrates

Flowrate (gpm)	Optimal Diameter (in) / (Velocity (ft/s))					
	500 ft	1,000 ft	5,000 ft	10,000 ft	20,000 ft	50,000 ft
500	7 / (4.2)	7 / (4.2)	7 / (4.2)	7 / (4.2)	7 / (4.2)	7 / (4.2)
2,000	14 / (4.2)	13 / (4.8)	13 / (4.8)	13 / (4.8)	13 / (4.8)	13 / (4.8)
5,000	21 / (4.6)	21 / (4.6)	20 / (5.1)	20 / (5.1)	20 / (5.1)	20 / (5.1)
10,000	28 / (5.2)	28 / (5.2)	28 / (5.2)	28 / (5.2)	28 / (5.2)	28 / (5.2)
20,000	39 / (5.4)	39 / (5.4)	39 / (5.4)	39 / (5.4)	39 / (5.4)	38 / (5.7)
50,000	60 / (5.7)	60 / (5.7)	60 / (5.7)	60 / (5.7)	60 / (5.7)	59 / (5.9)

8.1.4 Effect of Static Head

The effect of static head on optimal diameter was evaluated for static heads ranging from 25 ft (7.6 m) to 200 ft (61 m) in 25 ft (7.6 m) increments. Analysis was completed for pipe lengths of 1,000, 10,000 and 20,000 ft (304.8, 3,048, and 6,096 m) and the assumptions identified above. Results are summarized in Tables 8.6, 8.7, and 8.8. Overall, the effect of static head on optimal diameter was found to be minimal. The optimal diameter was found to decrease by one 1 in. (25.1 mm) for a change in static head of approximately 175 ft (55.3 m) for flows less than 10,000 gpm (0.63 cms). For flows larger than 10,000 gpm (0.63 cms), the effect of increased static head reduced the diameter an additional inch as compared to flows less than 10,000 gpm (0.63 cms).

Table 8.6: Effect of Pump Static Head on Optimal Diameter – 1,000 ft long Pipe

Static Head	Optimal Diameter (in) / (Velocity (ft/s))					
(ft)	500 gpm	2,000 gpm	5,000 gpm	10,000 gpm	20,000 gpm	50,000 gpm
25	7 / (4.2)	14 / (4.2)	21 / (4.6)	29 / (4.9)	40 / (5.1)	61 / (5.5)
50	7 / (4.2)	13 / (4.8)	21 / (4.6)	28 / (5.2)	39 / (5.4)	60 / (5.7)
75	7 / (4.2)	13 / (4.8)	20 / (5.1)	28 / (5.2)	39 / (5.4)	60 / (5.7)
100	7 / (4.2)	13 / (4.8)	20 / (5.1)	28 / (5.2)	39 / (5.4)	60 / (5.7)
125	7 / (4.2)	13 / (4.8)	20 / (5.1)	28 / (5.2)	39 / (5.4)	59 / (5.9)
150	7 / (4.2)	13 / (4.8)	20 / (5.1)	28 / (5.2)	38 / (5.7)	59 / (5.9)
175	7 / (4.2)	13 / (4.8)	20 / (5.1)	28 / (5.2)	38 / (5.7)	59 / (5.9)
200	7 / (4.2)	13 / (4.8)	20 / (5.1)	28 / (5.2)	38 / (5.7)	59 / (5.9)

Table 8.7: Effect of Pump Static Head on Optimal Diameter – 10,000 ft long Pipe

Static Head	Optimal Diameter (in) / (Velocity (ft/s))					
(ft)	500 gpm	2,000 gpm	5,000 gpm	10,000 gpm	20,000 gpm	50,000 gpm
25	7 / (4.2)	13 / (4.8)	21 / (4.6)	28 / (5.2)	39 / (5.4)	61 / (5.5)
50	7 / (4.2)	13 / (4.8)	20 / (5.1)	28 / (5.2)	39 / (5.4)	60 / (5.7)
75	7 / (4.2)	13 / (4.8)	20 / (5.1)	28 / (5.2)	39 / (5.4)	60 / (5.7)
100	7 / (4.2)	13 / (4.8)	20 / (5.1)	28 / (5.2)	39 / (5.4)	59 / (5.9)
125	7 / (4.2)	13 / (4.8)	20 / (5.1)	28 / (5.2)	38 / (5.7)	59 / (5.9)
150	7 / (4.2)	13 / (4.8)	20 / (5.1)	28 / (5.2)	38 / (5.7)	59 / (5.9)
175	7 / (4.2)	13 / (4.8)	20 / (5.1)	28 / (5.2)	38 / (5.7)	59 / (5.9)
200	7 / (4.2)	13 / (4.8)	20 / (5.1)	28 / (5.2)	38 / (5.7)	59 / (5.9)

Table 8.8: Effect of Pump Static Head on Optimal Diameter – 20,000 ft long Pipe

Static Head	Optimal Diameter (in) / (Velocity (ft/s))					
(ft)	500 gpm	2,000 gpm	5,000 gpm	10,000 gpm	20,000 gpm	50,000 gpm
25	7 / (4.2)	13 / (4.8)	20 / (5.1)	28 / (5.2)	39 / (5.4)	60 / (5.7)
50	7 / (4.2)	13 / (4.8)	20 / (5.1)	28 / (5.2)	39 / (5.4)	60 / (5.7)
75	7 / (4.2)	13 / (4.8)	20 / (5.1)	28 / (5.2)	39 / (5.4)	59 / (5.9)
100	7 / (4.2)	13 / (4.8)	20 / (5.1)	28 / (5.2)	38 / (5.7)	59 / (5.9)
125	7 / (4.2)	13 / (4.8)	20 / (5.1)	28 / (5.2)	38 / (5.7)	59 / (5.9)
150	7 / (4.2)	13 / (4.8)	20 / (5.1)	28 / (5.2)	38 / (5.7)	59 / (5.9)
175	7 / (4.2)	13 / (4.8)	20 / (5.1)	28 / (5.2)	38 / (5.7)	59 / (5.9)
200	7 / (4.2)	13 / (4.8)	20 / (5.1)	28 / (5.2)	38 / (5.7)	59 / (5.9)

8.1.5 Effect of Pump Runtime

The effect of pump runtime (hrs /day) was evaluated at various flowrates utilizing the assumptions identified above. Evaluation considered pipe lengths of 1,000 ft (304.8 m), 10,000 ft (3,048 m), and 20,000 ft (6,096 m) to determine if runtime was inter-related to the pipe length. Results are presented in Tables 8.9, 8.10, and 8.11. Consistent with the previous sections, the pipe length does not significantly affect the optimal diameter. Also noted from the results below is that a minimal change in optimal diameter is due to pump runtime for flowrates approximately 2,000 gpm (0.13 cms) and less. For flows greater the 2,000 gpm (0.13 cms), the optimal diameter increases with an increase in pump runtime with approximately a 10 in.

(254 mm) diameter change in optimal diameter at 50,000 gpm (3.15 cms). This suggests that the present worth of a larger diameter pipeline is less than the annual operational cost associated with the higher energy rates.

Table 8.9: Effect of Pump Runtime on Optimal Diameter – 1,000 ft long Pipe

Pump Runtime (hrs/day)	Optimal Diameter (in) / (Velocity (ft/s))					
	500 gpm	2,000 gpm	5,000 gpm	10,000 gpm	20,000 gpm	50,000 gpm
2	7 / (4.2)	13 / (4.8)	19 / (5.7)	26 / (6.0)	36 / (6.3)	55 / (6.8)
4	7 / (4.2)	13 / (4.8)	20 / (5.1)	27 / (5.6)	37 / (6.0)	56 / (6.5)
6	7 / (4.2)	13 / (4.8)	20 / (5.1)	27 / (5.6)	38 / (5.7)	57 / (6.3)
8	7 / (4.2)	13 / (4.8)	20 / (5.1)	28 / (5.2)	38 / (5.4)	58 / (6.1)
10	7 / (4.2)	13 / (4.8)	20 / (5.1)	28 / (5.2)	39 / (5.4)	59 / (5.9)
12	7 / (4.2)	13 / (4.8)	21 / (4.6)	28 / (5.2)	39 / (5.4)	60 / (5.7)
14	7 / (4.2)	14 / (4.2)	21 / (4.6)	29 / (4.9)	40 / (5.1)	61 / (5.5)
16	7 / (4.2)	14 / (4.2)	21 / (4.6)	29 / (4.9)	40 / (5.1)	62 / (5.3)
18	7 / (4.2)	14 / (4.2)	21 / (4.6)	29 / (4.9)	41 / (4.9)	63 / (5.1)
20	7 / (4.2)	14 / (4.2)	21 / (4.6)	30 / (4.5)	41 / (4.9)	63 / (5.1)
22	7 / (4.2)	14 / (4.2)	22 / (4.2)	30 / (4.5)	41 / (4.9)	64 / (5.0)
24	7 / (4.2)	14 / (4.2)	22 / (4.2)	30 / (4.5)	42 / (4.6)	64 / (5.0)

Table 8.10: Effect of Pump Runtime on Optimal Diameter – 10,000 ft long Pipe

Pump Runtime (hrs/day)	Optimal Diameter (in) / (Velocity (ft/s))					
	500 gpm	2,000 gpm	5,000 gpm	10,000 gpm	20,000 gpm	50,000 gpm
2	7 / (4.2)	12 / (5.7)	19 / (5.7)	26 / (6.0)	36 / (6.3)	54 / (7.0)
4	7 / (4.2)	13 / (4.8)	19 / (5.7)	27 / (5.6)	37 / (6.0)	56 / (6.5)
6	7 / (4.2)	13 / (4.8)	20 / (5.1)	27 / (5.6)	37 / (6.0)	57 / (6.3)
8	7 / (4.2)	13 / (4.8)	20 / (5.1)	27 / (5.6)	38 / (5.4)	58 / (6.1)
10	7 / (4.2)	13 / (4.8)	20 / (5.1)	28 / (5.2)	38 / (5.4)	59 / (5.9)
12	7 / (4.2)	13 / (4.8)	20 / (5.1)	28 / (5.2)	39 / (5.4)	60 / (5.7)
14	7 / (4.2)	13 / (4.8)	21 / (4.6)	29 / (4.9)	40 / (5.1)	61 / (5.5)
16	7 / (4.2)	14 / (4.2)	21 / (4.6)	29 / (4.9)	40 / (5.1)	62 / (5.3)
18	7 / (4.2)	14 / (4.2)	21 / (4.6)	29 / (4.9)	40 / (5.1)	62 / (5.3)
20	7 / (4.2)	14 / (4.2)	21 / (4.6)	29 / (4.9)	41 / (4.9)	63 / (5.1)
22	7 / (4.2)	14 / (4.2)	21 / (4.6)	30 / (4.5)	41 / (4.9)	64 / (5.0)
24	7 / (4.2)	14 / (4.2)	22 / (4.2)	30 / (4.5)	42 / (4.6)	64 / (5.0)

Table 8.11: Effect of Pump Runtime on Optimal Diameter – 20,000 ft long Pipe

Pump Runtime (hrs/day)	Optimal Diameter (in) / (Velocity (ft/s))					
	500 gpm	2,000 gpm	5,000 gpm	10,000 gpm	20,000 gpm	50,000 gpm
2	6 / (5.7)	12 / (5.7)	19 / (5.7)	26 / (6.0)	35 / (6.7)	54 / (7.0)
4	6 / (5.7)	12 / (5.7)	19 / (5.7)	26 / (6.0)	36 / (6.3)	55 / (6.8)
6	7 / (4.2)	13 / (4.8)	19 / (5.7)	27 / (5.6)	37 / (6.0)	57 / (6.3)
8	7 / (4.2)	13 / (4.8)	20 / (5.1)	27 / (5.6)	38 / (5.4)	58 / (6.1)
10	7 / (4.2)	13 / (4.8)	20 / (5.1)	28 / (5.2)	38 / (5.4)	59 / (5.9)
12	7 / (4.2)	13 / (4.8)	20 / (5.1)	28 / (5.2)	39 / (5.4)	60 / (5.7)
14	7 / (4.2)	13 / (4.8)	20 / (5.1)	28 / (5.2)	39 / (5.4)	61 / (5.5)
16	7 / (4.2)	13 / (4.8)	21 / (4.6)	29 / (4.9)	40 / (5.1)	61 / (5.5)
18	7 / (4.2)	14 / (4.2)	21 / (4.6)	29 / (4.9)	40 / (5.1)	62 / (5.3)
20	7 / (4.2)	14 / (4.2)	21 / (4.6)	29 / (4.9)	41 / (4.9)	63 / (5.1)
22	7 / (4.2)	14 / (4.2)	21 / (4.6)	30 / (4.5)	41 / (4.9)	64 / (5.0)
24	7 / (4.2)	14 / (4.2)	21 / (4.6)	30 / (4.5)	42 / (4.6)	64 / (5.0)

The results provided in Table 8.10 for a 10,000 ft (3,048 m) pipe length are shown graphically in Figure 8.4.

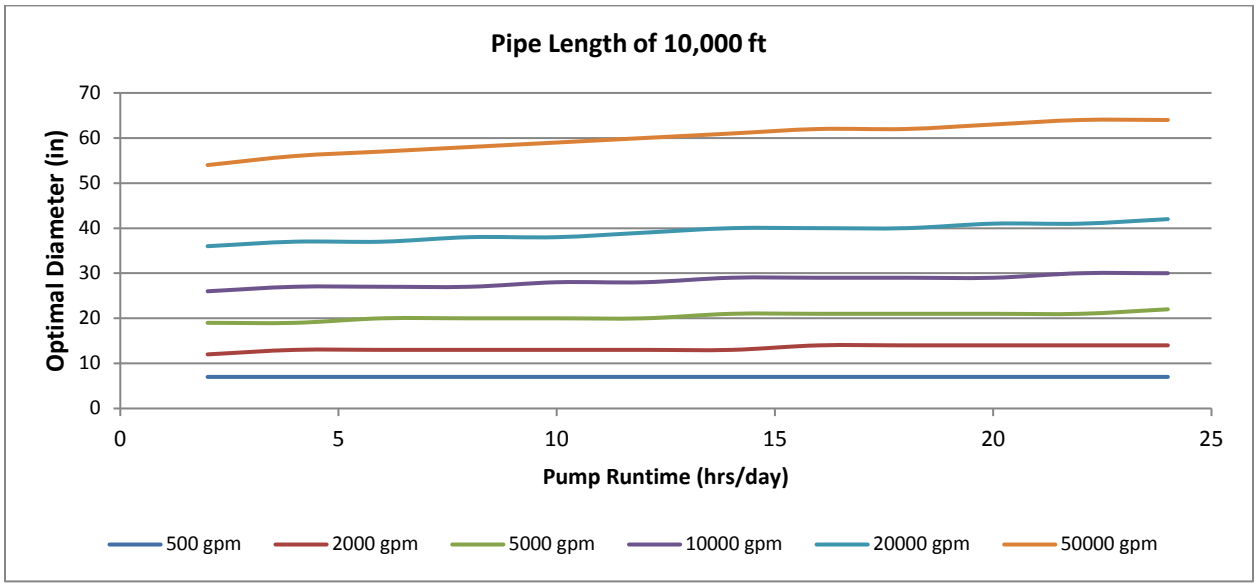

Figure 8.4: Effect of Pump Runtime on Optimal Diameter – 10,000 ft long pipe

8.1.6 Effect of Pipe Costs

Cost of the pipe (materials and installation) is often one of the largest single expenditure of a project. Several factors must be considered in arriving at the most economical type and diameter of the pipe. Initial cost and life expectancy of a pipeline vary with the material and requirements for linings or protective coatings (Tullis 1989). Although these factors should be considered when evaluating pipe

economics, they are beyond the scope of this research. A general rule of thumb for pipeline installation cost ranges from $6 to $10 / foot / in.-diameter depending on the pipe material, linings / coatings, length, installation depth, geotechnical conditions, and the number or type of crossings.

Effect of pipe cost was evaluated in $0.50/ ft/ in.-dia. increments from $6 - $10/ ft/ in.-dia. Evaluation considered pipe lengths of 1,000 ft (304.8 m), 10,000 ft (3,048 m), and 20,000 ft (6,096 m) and the remaining assumptions identified above. Results presented in Tables 8.12 to 8.14 show that the pipe cost does not significantly affect the optimal diameter.

Table 8.12: Effect of Pipe Cost on Optimal Diameter – 1,000 ft long Pipe

Pipe Cost ($ / ft/ in-dia)	Optimal Diameter (in) / (Velocity (ft/s))					
	500 gpm	2,000 gpm	5,000 gpm	10,000 gpm	20,000 gpm	50,000 gpm
6.0	8 / (3.2)	15 / (3.6)	23 / (3.9)	32 / (4.0)	44 / (4.2)	68 / (4.4)
6.5	8 / (3.2)	15 / (3.6)	23 / (3.9)	31 / (4.3)	43 / (4.4)	67 / (4.5)
7.0	8 / (3.2)	15 / (3.6)	22 / (4.2)	31 / (4.3)	43 / (4.4)	66 / (4.7)
7.5	8 / (3.2)	14 / (4.2)	22 / (4.2)	30 / (4.5)	42 / (4.6)	65 / (4.8)
8.0	7 / (4.2)	14 / (4.2)	22 / (4.2)	30 / (4.5)	42 / (4.6)	64 / (5.0)
8.5	7 / (4.2)	14 / (4.2)	22 / (4.2)	30 / (4.5)	41 / (4.9)	64 / (5.0)
9.0	7 / (4.2)	14 / (4.2)	21 / (4.6)	30 / (4.5)	41 / (4.9)	63 / (5.1)
9.5	7 / (4.2)	14 / (4.2)	21 / (4.6)	29 / (4.9)	41 / (4.9)	63 / (5.1)
10.0	7 / (4.2)	14 / (4.2)	21 / (4.6)	29 / (4.9)	40 / (5.1)	62 / (5.3)

Table 8.13: Effect of Pipe Cost on Optimal Diameter – 10,000 ft long Pipe

Pipe Cost ($ / ft/ in-dia)	Optimal Diameter (in) / (Velocity (ft/s))					
	500 gpm	2,000 gpm	5,000 gpm	10,000 gpm	20,000 gpm	50,000 gpm
6.0	8 / (3.2)	15 / (3.6)	23 / (3.9)	32 / (4.0)	44 / (4.2)	67 / (4.5)
6.5	8 / (3.2)	15 / (3.6)	22 / (4.2)	31 / (4.3)	43 / (4.4)	67 / (4.5)
7.0	7 / (4.2)	14 / (4.2)	22 / (4.2)	31 / (4.3)	43 / (4.4)	66 / (4.7)
7.5	7 / (4.2)	14 / (4.2)	22 / (4.2)	30 / (4.5)	42 / (4.6)	65 / (4.8)
8.0	7 / (4.2)	14 / (4.2)	22 / (4.2)	30 / (4.5)	42 / (4.6)	64 / (5.0)
8.5	7 / (4.2)	14 / (4.2)	21 / (4.6)	30 / (4.5)	41 / (4.9)	64 / (5.0)
9.0	7 / (4.2)	14 / (4.2)	21 / (4.6)	29 / (4.9)	41 / (4.9)	63 / (5.1)
9.5	7 / (4.2)	14 / (4.2)	21 / (4.6)	29 / (4.9)	40 / (5.1)	63 / (5.1)
10.0	7 / (4.2)	13 / (4.8)	21 / (4.6)	29 / (4.9)	40 / (5.1)	62 / (5.3)

Table 8.14: Effect of Pipe Cost on Optimal Diameter – 20,000 ft long Pipe

Pipe Cost ($ / ft/ in-dia)	Optimal Diameter (in) / (Velocity (ft/s))					
	500 gpm	2,000 gpm	5,000 gpm	10,000 gpm	20,000 gpm	50,000 gpm
6.0	8 / (3.2)	15 / (3.6)	23 / (3.9)	31 / (4.3)	44 / (4.2)	67 / (4.5)
6.5	7 / (4.2)	14 / (4.2)	22 / (4.2)	31 / (4.3)	43 / (4.4)	66 / (4.7)
7.0	7 / (4.2)	14 / (4.2)	22 / (4.2)	31 / (4.3)	42 / (4.6)	66 / (4.7)
7.5	7 / (4.2)	14 / (4.2)	22 / (4.2)	30 / (4.5)	42 / (4.6)	65 / (4.8)
8.0	7 / (4.2)	14 / (4.2)	21 / (4.6)	30 / (4.5)	42 / (4.6)	64 / (5.0)
8.5	7 / (4.2)	14 / (4.2)	21 / (4.6)	30 / (4.5)	41 / (4.9)	64 / (5.0)
9.0	7 / (4.2)	14 / (4.2)	21 / (4.6)	29 / (4.9)	41 / (4.9)	63 / (5.1)
9.5	7 / (4.2)	13 / (4.8)	21 / (4.6)	29 / (4.9)	40 / (5.1)	62 / (5.3)
10.0	7 / (4.2)	13 / (4.8)	21 / (4.6)	29 / (4.9)	40 / (5.1)	62 / (5.3)

8.1.7 Effect of Pump Station Cost

Effect of pump station cost was not evaluated in detail as part of this research. Although not presented, the pump station capital cost was found to be insignificant to optimal diameter sizing of the pipeline.

8.1.8 Effect of Payback Period and Interest Rates

Although the results are not presented here, the effect of payback period and interest rates were also found to be minimal in determining optimal diameter; utilizing actual values in the analyses are important in estimating the present worth of the total project cost. However, changing either the interest rate to finance the project or life cycle duration minimally affected the optimal diameter, resulting in a ± 1 – 2 in. (25.4- 50.8 mm) change in optimal diameter.

8.1.9 Range of Flow for Optimal Diameter

The range of flow corresponding to optimal diameters 6 in. (152.4 mm) to 42 in. (1,079.4 mm) were determined assuming a pipe length of 10,000 ft (3,048 m); energy cost of $0.07 / kw-hr; 12 hrs/day runtime; and 50 ft (15.2 m) static head. Results are shown in Figure 8.5. As one would expect, the range of flow is narrow with smaller diameter pipe and increases with diameter. As identified in Section 8.1.3, the pipe length does not significantly affect the optimal diameter for the assumed inputs. Therefore, this figure can be used as an initial estimate of optimal diameter for a given flowrate.

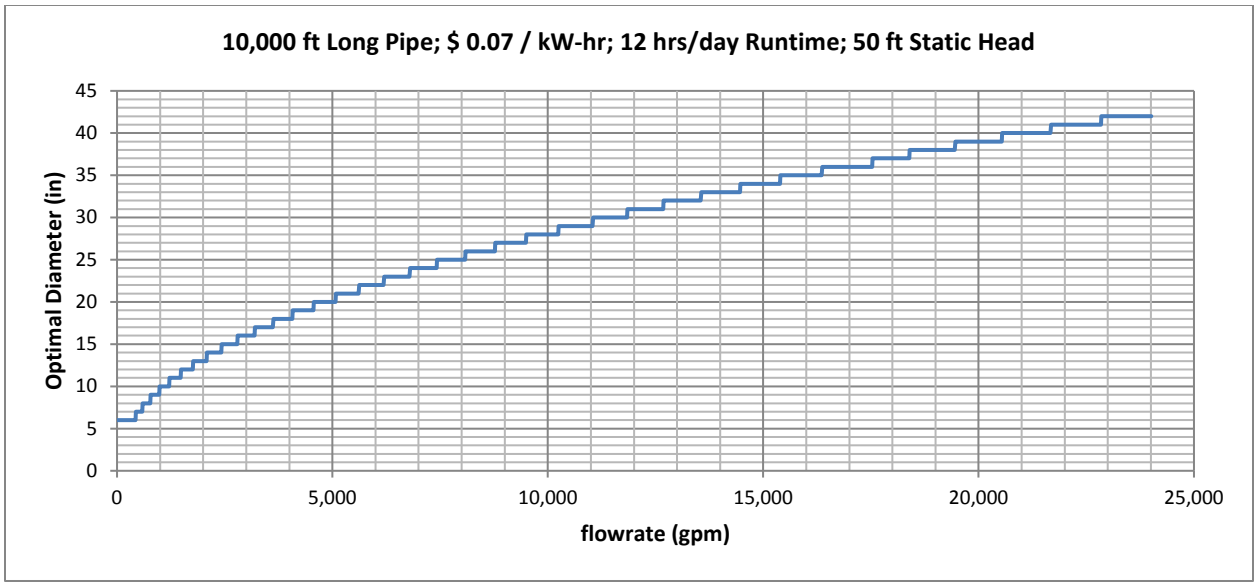

Figure 8.5: Range of Flow for Optimal Diameter – 10,000 ft long pipe

8.1.10 Comparison of Selecting One Diameter Smaller Than Optimal

The results presented in Table 8.3 were compared to the results for a diameter 1 in. (25.4 mm) less than the optimal diameter. The velocity corresponding to the optimal diameter ranged from approximately 4.2 ft/s (1.3 m/s) for a 7 in. (177.8 mm) diameter pipe to 5.5 ft/s (1.7 m/s) for a 6 in. (152.4 mm) diameter pipe. Selecting a pipe size 1 in. (25.4 mm) smaller increases velocity and headloss but only accounted for an increase in annual energy costs of approximately $3,500. This increase is nominal compared to the benefits of increasing the velocity regarding sediment and air transport in the forcemain, especially for diameters less than 24 in. (609.6 mm). The effect of velocity on selecting a 1 in. (25.4 mm) smaller than optimal diameter is presented in Figure 8.6 and Table 8.15.

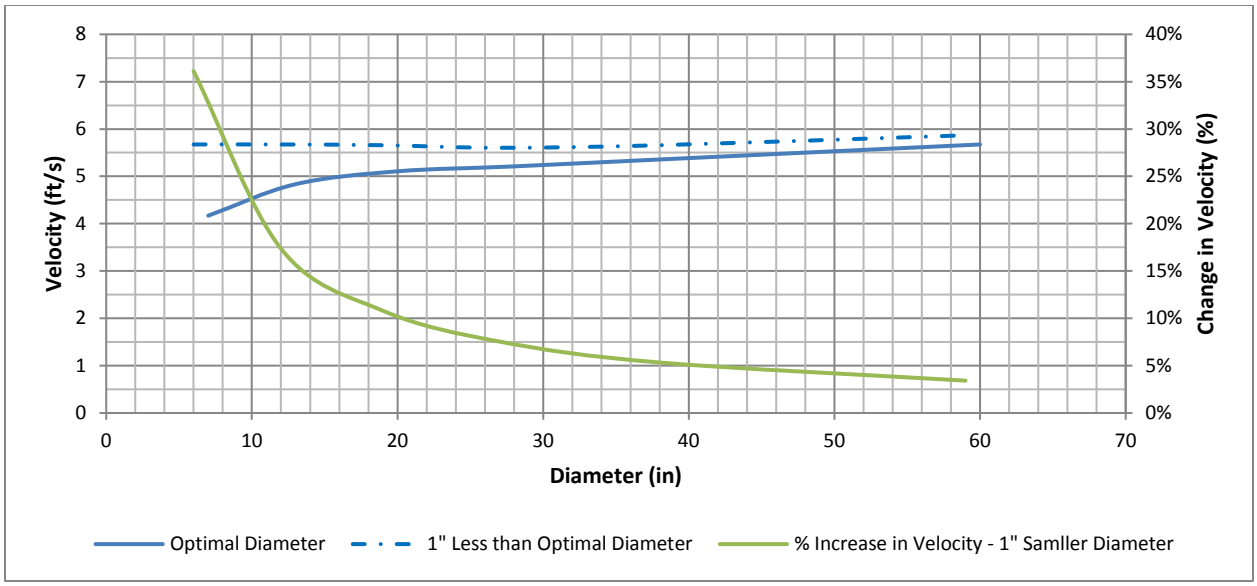

Figure 8.6: Effect of Selecting Diameter 1 in. Smaller than Optimal Diameter – 10,000 ft long pipe

Table 8.15: Change in Velocity and Annual Pumping Costs Resulting from Selecting Diameter 1 in. Smaller than Optimal Diameter

Flowrate (gpm)	500	2000	5000	10000	20000	50000
Optimal Diameter (in)	7	13	20	28	39	60
Velocity (ft/s)	4.17	4.83	5.11	5.21	5.37	5.67
Change from Selecting Diameter 1 in. Smaller than Optimal						
Diameter (in)	6	12	19	27	38	59
Velocity (ft/s)	5.67	5.67	5.66	5.60	5.66	5.87
% Increase Velocity	36%	17%	11%	8%	5%	3%
Increase in Annual Pumping Cost	$ 3,316	$ 3,693	$ 3,697	$ 3,532	$ 3,539	$ 3,769

8.1.11 Summary

This section presented the methodology associated with economic sizing of forcemains. This methodology was used to evaluate the effect of pipeline length, energy costs, pump station capital costs, pipeline capital cost, pump runtime, static head, and project financing terms (interest rate and duration of payback period) on determining the optimal diameter.

Although these parameters are all inter-related; the analysis determined that the optimal diameter is not significantly affected by pump station capital cost, length of pipeline, or static head. It should be noted that the length of pipe significantly affects the pipeline capital costs; however, energy costs associated with pump runtime, velocity (headloss), and electrical usage were determined to have the greatest effect on optimal pipe sizing. Pipeline capital costs are directly related to the diameter and length. Pipeline length

has a greater effect on optimal sizing as diameter (flowrate) increases. Pump runtime had a substantial effect on pipe sizing since operational costs are directly related to the frequency and duration of pumping operations.

Even though several parameters were found to have minimal impact on the optimal diameter, it is important to note that each parameter was evaluated independently. Combining extreme values for each parameter may cause a shift in optimal diameter selection; therefore, it is important to completely define all parameters to ensure an accurate evaluation.

8.2 Forcemain Design and Operational Considerations

This chapter evaluates a forcemains theoretical ability to transport particles and clear air considering the use of the predictive equations to estimate pipe roughness parameters (k_s and C factor) from velocity. Results are compared to current design practice, as well as the research data, to provide recommendations for forcemain sizing.

8.2.1 Design Standards

An internet search was conducted to review forcemain design standards obtained from various utilities, professional organizations, and publications. Design standards from within the United States as well as around the world were reviewed. Numerous organizations cite the Ten State Standards or provide similar requirements. Therefore, a brief summary of the Ten States Standards as well as those that differ from these standards are presented below:

Wastewater Committee of the Great Lakes - Upper Mississippi River Board of State and Provincial Public Health and Environmental Managers. Recommended Standards for Wastewater facilities "Ten States Standards" (2014) – A minimum forcemain diameter of 4-inches. A cleansing velocity of at least 2.0 ft/s (0.6 m/s) should be maintained at design pumping rate and a maximum velocity of 8 ft/s (2.4 m/s) to avoid high headloss.

*Pumping Station Design (*Jones 2006*)* – The lowest velocity for raw wastewater to keep grit moving is 2 ft/s (0.6 m/s) and a daily peak velocity of 3.5 ft/s (1.1 m/s) is desirable to re-suspend settled solids. If

velocities are less than 2.5 ft/s (0.8 m/s), then a daily flush at 4.0 ft/s (1.2 m/s) long enough to sweep out the entire volume is desirable. A lower velocity of 1.6 ft/s (0.5 m/s) can be tolerated if a twice-daily velocity of 3.5 ft/s (1.1 m/s) is attained.

City of Los Angeles – Minimum velocity of 3 ft/s (0.9 m/s) to maintain solids in suspension. The recommended velocity should normally be between 5 ft/s (1.5 m/s) and 7.5 ft/s (2.3 m/s), depending on most economical pipe size given the present worth of the pipeline assuming a 60 year life expectancy. Maximum velocity should not exceed 10 ft/s (3 m/s) during intermittent flow conditions. A Hazen-Williams C factor of 140 shall be used for clean new pipes and 100 for very old pipes.

City of Baton Rouge Conveyance Design Requirements (2012)– maximum velocity of 8 ft/s, with acceptable operating velocities between 5 ft/s (1.5 m/s) and 8 ft/s (2.4 m/s) during typical flow conditions.

Colorado Springs Utilities – Public Force Mains shall be sized, in conjunction with the pumps, to maintain velocities of at least 2 ft/s (0.6 m/s) in the Public Force Main. If a Public Force Main's length is such that the Wastewater within the pipe cannot travel the entire distance from the pump to the discharge manhole in 1 pump cycle, then the velocity during each pump cycle shall be a minimum of 3.5 ft/s (1.1 m/s) to re-suspend solids during pump operations.

Hunter Water Corporation (Australia) Water and Sewer Design Manual (2008) – Recommend determining design velocity from V = -0.3log(0.1/D) where D is pipe diameter (mm) and velocity (m/s) with a maximum velocity of 3 m/s (10 ft/s) to minimize the potential of pipe scour from entrained grit. The equation was developed to provide a shear stress of 0.3 N/m^2 and to control biofilm growth. Application of the equation yields a velocity of 0.95 m/s (3.1 ft/s) for a 6 in. diameter and 1.2 m/s (4 ft/s) for 48 in. diameter. The lowest rate of pumping should be limited to approximately 25% of the maximum rate. Reference is made to "Tables for the Hydraulic Design of Pipes and Sewers" by HR Wallingford and the recommended k_s of 0.3 mm (1 m/s), 0.15 mm (1.5 m/s), and 0.06 mm (2 m/s).

Kildare County Council Requirements for Foul Pumping Stations and Associated Infrastructure (2012) - The diameter of the rising main shall be such that the velocity of the discharge is within the range 0.75 m/s (2.5 ft/s) to 1.8 m/s (5.9 ft/s) to ensure effective self-cleansing. The maximum velocity shall not

exceed 3 m/s. The roughness value (k_s) used for the design of the pumping main shall be shown in calculations, and shall be in accordance with the latest edition of Tables for the Hydraulic Design of Pipes, Sewers and Channels published by HR Wallingford.

San Antonio Water System Lift Station Design Lift Station Design & Construction Guidelines (2012) - Minimum force main size will be 4-inch (except for grinder pumps). Force Mains sized so that flow velocity is between 3 ft/s (0.9 m/s) and 3.5 ft/s (1.1 m/s) (velocities s*l*ightly above 3 ft/s (0.9 m/s) are recommended) with one pump in operation. Maximum flow velocities shall be 4.8 ft/s (1.5 m/s) for two pumps in operation and 6.0 ft/s (1.8 m/s) with three pumps in operation. For lift stations with more than 2 pumps, flow velocities may be as low as 2 ft/s (0.6 m/s) with one pump in operation, but when three or more pumps operate a flow velocity equal to, or greater than 5 ft/s (1.5 m/s) must be generated.

Western Municipal Water District's Sewer Lift Station and Forcemain Guidelines – The minimum and maximum velocity under all operating points shall be 3 ft/s (0.9 m/s) and 7 ft/s (2.1 m/s), respectively. The velocity at design flow point should be between 4 ft/s (1.2 m/s) and 5 ft/s (1.5 m/s).

Washington Suburban Sanitary Commission Pipeline Design Manual – Part Two – Sewer Design Standards (2008) - minimum velocity of 2 ft/s (0.6 m/s) and maximum velocity of 6 ft/s (1.8 m/s). Velocities ranging from 2 ft/s (0.6 m/s) to 3.5 ft/s (1.1 m/s) would be required to re-suspend solids that have settled in the forcemain. This higher velocity is required for profiles which undulate containing multiple high and low points. Relatively small stations with intermittent pumping of one or two pumps generally should be designed for higher minimum velocities in the forcemain, compared to larger stations with having more than three pumps.

Waitakere City Council (Auckland Australia) Code of Practice City Infrastructure and Land Development Section 5.0 Wastewater Drainage (2008) – Darcy-Weisbach absolute roughness, k_s = 1.5 mm (0.06 in.), with a maximum velocity of 4.5 m/s (14.8 ft/s), and maximum rise of 60 m (197 ft). A recommended minimum velocity was not identified.

City of Phoenix Wastewater Lift Station Design Guidance Manual – The force main must be sized to achieve a velocity between 3 ft/s (0.9 m/s) and 7 ft/s (2.1 m/s) for all planned phases of expansion. Either

the Darcy-Weisbach or the Hazen-Williams equation can be used for hydraulic calculations of headloss over a range of flow rates. Both friction and minor losses must be considered during the analysis. System Curves developed assuming C factors of 100 and 120 or equivalent friction factors. The design shall be based on a C factor of 100.

Although the general consensus is that a velocity greater than 2.0 ft/s (0.6 m/s) is required to prevent deposition of solids and a velocity of approximately 3.5 ft/s (1.1 m/s) is required to re-suspend solids that may have settled, these standards are generally not applied consistently by different engineers or from project to project. San Antonio's standards provided velocity guidelines based upon the number of pumps operating. This approach removes potential misinterpretation of the required design velocities. The minimum theoretical velocity required for self-cleansing, sediment transport, air clearing, and the economical diameter will be evaluated and compared to the research data in the following sections.

8.2.2 Sediment Transport – Self Cleansing Velocity

Organic, sand, and gravel particles are present in wastewater systems. Sedimentation of this material in forcemains may increase hydraulic roughness factors, reduce hydraulic capacity, create obstructions at low points, and could cause increased sulfide production leading to corrosion and odor issues. Therefore, wastewater forcemains are best designed to be self-cleaning to prevent the deposition of solids. Self-cleaning properties occur when the critical shear stress is achieved to transport the largest particle.

In the United States, concentration of suspended solids in domestic sewage varies from 100 to 350 mg/L (Metcalf & Eddy, Inc. 2003). Typical sanitary sewage contains about 210 mg/L of suspended mater, of which about 160 mg/L is mineral and 50 mg/L is organic (Tchobanoglous et. al 2003, Bizier 2007).

Past design practices utilized a velocity of 2 ft/s (0.6 m/s) as a general rule of thumb to obtain self-cleaning velocities. The tractive force method was determined to be a better way of assessing the critical velocity in order to obtain self-cleansing velocities for solids transport is sewers and forcemains. Over the last few decades, countries around the world are increasingly using tractive force as the preferred method

for self-cleansing design (Merrit 2009). ASCE and WEF now advocate a transition to the tractive force approach for self-cleansing design (Bizier 2007). Proper application of the tractive force method strongly depends on selection of an appropriate design sediment particle and good, realistic estimates of design minimum flow rates (Bizier 2007).

As wastewater flows over a sediment bed in a sewer, hydrodynamic lift and drag forces are exerted on the bed particles. If these two combined forces do not exceed the restoring forces of the sediment submerged weight, interlocking, and cohesion (if present), then the particles remain stationary. If they exceed the restoring force, then entrainment occurs, resulting in movement of the particles at the flow/sediment boundary. Not all of the particles of a given size at this boundary are dislodged and moved at the same time, as the flow is turbulent and contains short-term fluctuations in velocity (Butler 2003).

Solids with a larger size and a higher specific gravity are more likely to be transported as bedload along the invert of the sewer; whereas solids with a smaller size and a lower specific gravity are transported through suspension. Consequently, if the average shear stress is sufficient to transport a design particle as bedload, then all smaller particles will also be effectively transported, either in suspension or as bedload (Bizier 2007).

Various efforts have been made to identify the tractive forces required to transport various sizes and types of particles is sewer conduits (Medina and Vega 2002, Bizier 2007). Flow conditions are classified as self-cleansing when the actual shear stress (τ) is greater than or equal to a specified critical shear stress (τ_c) at a defined frequency of occurrence (Bizier, 2007). Raths and McCauley (1962) conducted experiments to determine the tractive force required to move sand particles in an 8 in. (205 mm) diameter sewer flowing sewage. Particle sizes ranged from 0.15 to 7.9 mm with a specific gravity of 2.7. Walski et al. (2004) linearized their results Equation 8.3.

$$\tau_c = kd^{0.277} \tag{8.3}$$

Where τ_c is the critical shear stress; k =0.867 for SI units (τ_c in N/m^2) and 0.0181 for US Customary units (τ_c in lb/ft^2). Equation 8.3 applies to discrete granular particles and not to particles embedded within

a cohesive matrix (Merritt 2009). The literature generally identifies a 1 mm particle as grit in wastewater; this value corresponds to the measured grit particle size in UK sewage (Table 6.1) and applying Equation 8.3 yields a critical shear stress of 0.0181 lb/ft^2 (0.867 N/m^2). Critical shear stress associated with standard particle sizes ranging from 0.25 mm (0.01 in.) to 64 mm (2.52 in.) using Equation 8.3 are summarized in Table 8.16.

Table 8.16: Summary of Critical Shear Stress for Standard Particle Sizes

Class Name	Particle Size		Critical Shear Stress [1]	
	mm	inches	N/m^2	lb/ft^2
Sand	0.25	0.01	0.59	0.012
	0.5	0.02	0.72	0.015
	1	0.04	0.87	0.018
Gravel	2	0.08	1.05	0.022
	4	0.16	1.27	0.027
	8	0.31	1.54	0.032
	16	0.63	1.87	0.039
	32	1.26	2.26	0.047
Cobble	64	2.52	2.74	0.057

[1] From Equation 8.3

Methods that address self-cleansing are described in Yao (1974), Hager (1994), Butler et al. (2003), and Walski et al. (2004). Additional sewer self-cleansing aspects are covered in several sources, such as those by Durand (1953), Ota and Nalluri (2003), Saul et al. (2003), and Tait et al. (2003) (Merrit 20009). Recommendations of shear stress for sanitary sewage system range from about 0.03 to 0.08 lb/ft^2 (1.4 to 3.8 N/m^2) as identified in Table 8.17. The low end of the range would be appropriate for sewage containing small sized particles (1 mm) with limited grit load or frequent scouring-velocity occurring. The high end of the range would be appropriate for larger sized grit, higher than normal grit production or cohesiveness of deposits, and less frequent scouring-velocity events. Kienow (1989) suggests that shear stresses of 0.10 lb/ft^2 (4.79 N/m^2) and higher could be appropriate for larger-sized gravel materials found in combined systems and some sanitary systems, with larger shear stresses required to mobilize cohesive particles.

Table 8.17: Recommended Critical Shear Stress to Move Deposits in Sanitary Sewers and Forcemains (Kienow 1989)

Reference	Recommended Shear stress	
	lb/ft^2	N/m^2
Lysne 1969	0.08	3.83
Paintal 1972	0.08	3.83
Schultz 1960	0.03 to 0.04	1.44 to 1.92
Yao 1974	0.03 to 0.04 (<1 mm)	1.44 to 1.92
Yao 1974	0.06 to 0.08 (>1 mm)	2.87 to 3.83
Maguire[1]	0.13	6.2
Bischop[1]	0.05	2.5

[1] Cited in Nalluri and Ghani 1996

All of these shear stresses are higher than would be necessary in clean water because of the cohesive properties of wastewater and the effects of sediment particles in reducing turbulence in the boundary layer (Kienow 1989). May et al. (1996) indicates that cohesion 1) will tend to increase the value of shear stress that the flow needs to exert on the deposited bed in order to initiate movement of particles in the surface layer and 2) may alter the way in which the sediment then moves which affects the sediment transporting capacity of the flow. May et al. (1996) further indicate that experimental research by Nalluri and Alvarez (1992) using synthetic cohesive sediments suggests that the second condition may not be significant; once the structure of a cohesive bed is disrupted, the particles are stripped away and transported by the flow in a similar way to non-cohesive sediments.

The effect of cohesion on shear stress can be large at the threshold of movement. Most information about threshold shear stress for sewer sediments are expressed in terms of the component acting on the bed; this will tend to be higher than the corresponding average shear stress for the pipe as a whole, since the bed will usually be rougher than the pipe wall. Nalluir and Alvarez (1992) concluded that a shear stress of 2.5 N/m^2 (0.05 lb/ft^2) was required for the more mobile fine-grained material on the surface of a deposit and 6 - 7 N/m^2 (0.13 - 0.15 lb/ft^2) for the more granular and consolidated material below (May et al. 1996).

May et al. (1996) concluded that a critical shear stress of 2.0 N/m^2 (0.04 lb/ft^2) was sufficient for a design flow of specified frequency of occurrence; this could correspond to small forcemain systems where the pumps would frequently cycle at the design flow. Yao (1974) recommends a minimum shear stress of

1 - 2 N/m^2 (0.02 - 0.04 lb/ft^2) for sanitary systems and 3-4 N/m^2 (0.06-0.08 lb/ft^2) for combined sewer systems.

A critical shear stress (τ_c) between 1 N/m^2 (0.02 lb/ft^2) and 2 N/m^2 (0.04 lb/ft^2) is typically recommended to prevent the formation of a thick biofilm. However, the Melbourne and Metropolitan Boards of Work (1989) proposed τ_c of 3.4 N/m^2 (0.07 lb/ft^2). In a small diameter pipe (<0.4 m), this value corresponds to a flow velocity about 1 m/s (3.3 ft/s). In a larger pipe with a diameter >1 m, the velocity should exceed 1.2–1.4 m/s (3.9 – 4.6 ft/s) to prevent excessive biofilm growth (Hvitved-Jacobsen 2013). As identified as part of this research, biofilms also affect the roughness of the sewer pipe. Lambert (2009) concluded that biofilms in raw water pipelines sheared from pipe walls when $t_c \geq 3.0$ N/m^2 (0.06 lb/ft^2).

A large range of recommended critical shear stresses were identified above. Other than the findings from Lambert (2009), the critical shear stress guidelines identified above were developed for sanitary sewers providing continuous flow and may be appropriate for larger lift station/forcemain systems which operate continuously. Considering that smaller lift stations operate in cycles where the pump(s) may sit idle for an extended time period, selecting a larger shear stress may be more appropriate to re-mobilize cohesive sediment. In addition, the larger shear stress values should be used for systems subjected to larger particles that may enter the system regardless if the pumps operate continuously. The velocity associated with the critical shear stress can be determined by rearranging Equation 4.5 into Equation 8.4.

$$v_c = \sqrt{\frac{8\tau_c}{\rho f}} \tag{8.4}$$

Where ρ is the density of water; *f* is the friction factor, determined from the Swamee-Jain equation (repeated from Section 2.3). k_s in the Swamee Jain equation was estimated from Equations 7.6a to 7.7c provided in Section 7.2.3.1.

$$f = \frac{0.25}{\left[\log\left(\frac{k_S}{3.7D} + \frac{5.74}{R_e^{0.9}}\right)\right]^2} \tag{2.6}$$

The critical velocity corresponding to shear stresses ranging from 1 N/m^2 (0.02 lb/ft^2) to 7 N/m^2 (0.15 lb/ft^2) were determined assuming a water temperature of 70 °F (21.11 °C). Results are presented in Figure 8.7. Although not presented below, changes in water temperature (density) insignificantly affected critical velocity.

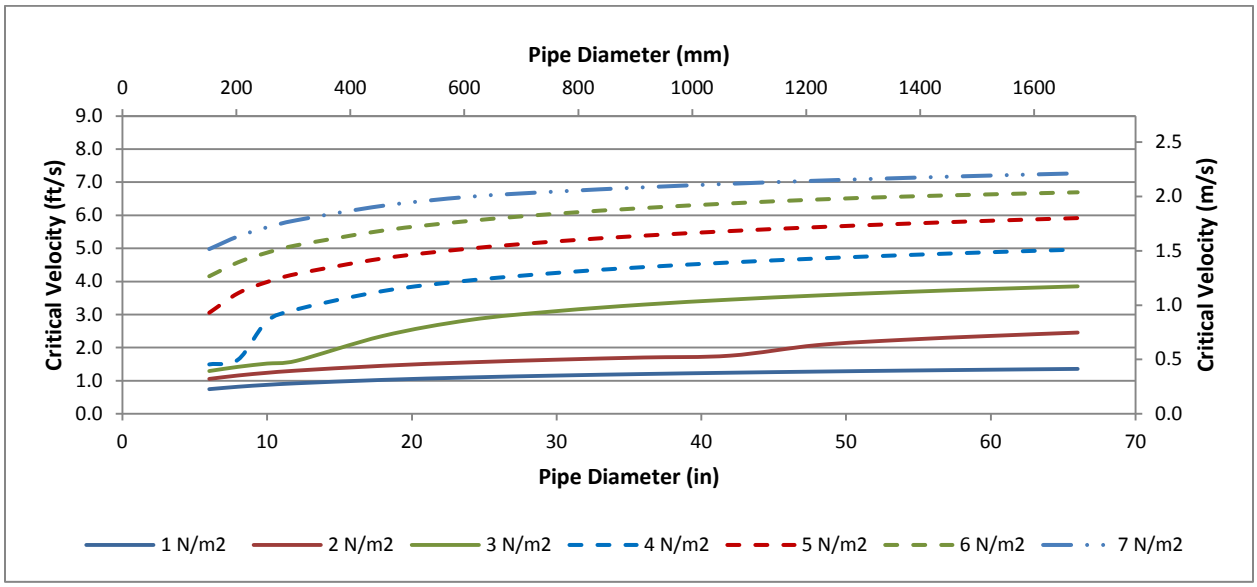

Figure 8.7: Critical Shear Velocity for Shear Stresses Ranging from 1 to 7 N/m^2

The sharp rise in critical velocity observed for shear stresses 2, 3, and 4 N/m^2 (Figure 8.7) occurs at the transition from velocities less than 0.54 m/s (1.8 ft/s) which results in a k_s of 30 mm (1.2 in.). As identified in Section 7.3, the predictive equation for k_s applied an assumed upper limit of 30 mm (1.2 in.) for low velocities (<1.8 ft/s (0.54 m/s)). A rise is not shown for the critical velocities of 1 N/m^2 since the velocity is less than 0.54 m/s (1.8 ft/s), resulting in a constant k_s of 30 mm (1.2 in.). These results imply that the upper roughness limitation assumed in developing the predictive equations may be incorrect. It should be noted that this upper limit was assumed and should be field verified through additional study.

Although the literature did not provide guidance in regards to the time between flushing cycles before cohesion would begin to affect particle transport, cohesion is unlikely to be an issue in forcemain systems since no apparent distinction was observed in the calculated k_s values based upon pump cycle data. In other words, the pump cycle, or time between pumping cycles did not appear to effect k_s. However, this should be field verified through additional study.

General consensus in the literature was that a minimum shear stress of 2 N/m^2 (0.04 lb/ft^2) should be applied to sanitary sewer systems. Shear stress should be increased based upon the type of system as well as expected particle size. Several references identified in Table 8.16 recommend a shear stress of 0.08 lb/ft^2 (3.83 N/m^2) and Bizier (1989) recommends 0.10 lb/ft^2 (4.80 N/m^2) for gravel sized particles. Therefore, to be conservative in design, it may be appropriate to size a forcemain to provide self-cleaning velocities based upon a shear stress of either 0.08 lb/ft^2 (3.83 N/m^2) or 0.10 lb/ft^2 (4.80 N/m^2) to ensure mobilization of all expected particles or cohesive particles. The critical velocity associated with these shear stresses for pipe diameters ranging from 6 in. (152.4 mm) to 66 in. (1,676.4 mm) are presented in Figure 8.8.

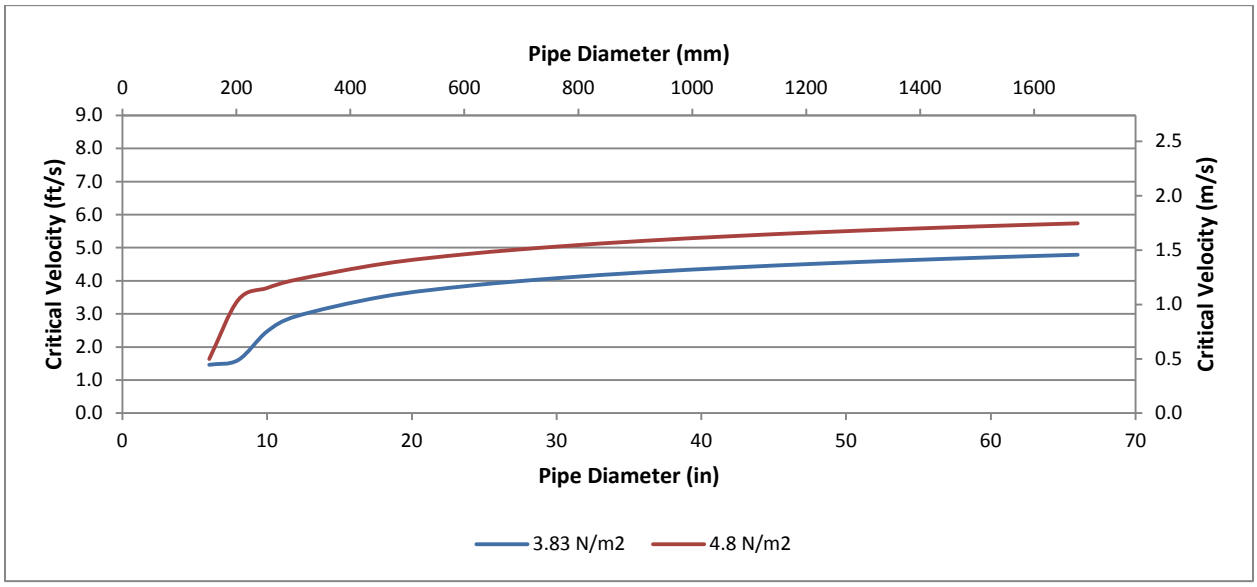

Figure 8.8: Critical Shear Velocity for Shear Stresses of 3.83 and 4.80 N/m^2

Equations to estimate the critical velocity for each shear stress were developed using the trendline function in M.S Excel and are provided in Table 8.18. It should be noted that these equations were developed by removing the data points associated with low velocities where k_s = 30 mm since this value was assumed as an upper limit for k_s values and does not appear to fit the results presented in Figure 8.7.

Table 8.18: Equations to estimate critical velocity based upon diameter for shear stress of 3.83 N/m^2 and 4.80 N/m^2

Critical Shear Velocity Units	τ_c = 3.83 N/m^2	τ_c = 4.80 N/m^2
ft/s	$v_c = 1.161\ln(\phi) + 0.032$	$v_c = 1.021\ln(\phi) + 1.514$
m/s	$v_c = 0.354\ln(\phi) + 0.010$	$v_c = 0.311\ln(\phi) + 0.462$

ϕ is diameter in inches

8.2.2.1 Recommendations

It is crucial to design a forcemain system without permanent solids accumulation. Based upon the expected particle size in the wastewater, the critical shear stress should be used to determine the minimum velocity required to prevent deposition of solids in the forcemain. Particle sizes should be determined based upon the size of the system and whether it is a separate sanitary system or combined sanitary / storm system. The systems geographic location should also be considered when selecting minimum shear stress since systems located in Eastern United States tend to be both older and combined sanitary and storm systems which could allow more infiltration and/or larger particles to enter the system. Defects present in older systems could also allow sediment from cracked pipe or separated joints to enter the sewer system adding to the sediment load.

Although a design particle of 1 mm (0.04 in.) is considered appropriate for typical domestic sewage, the self-cleansing velocity of a forcemain should be selected based upon the design critical shear stress instead of particle size due to potential cohesion of particles and undulation that occurs along a typical forcemain profile. Selecting a design shear stress of 0.08 lb/ft^2 (3.83 N/m^2) or 0.10 lb/ft^2 (4.80 N/m^2) provides a conservative estimate of required velocity to achieve scour and transport of particles found in sewage.

Additional research should be conducted to identify typical particle sizes found in forcemain systems. Research should also evaluate the effect of biofilms and cohesion on particle transport in forcemains.

8.2.3 Sediment Transport - Suspended Sediment

Transport through suspension occurs when ($U^* > U^*_{sus}$). The shear velocity (U^*) is determined from Equation 3.7, and the suspension shear velocity can be determined from Equation 6.1. Following the methodology identified in Section 6.1.1.1, the maximum theoretical particle size (d_s) transported through suspension was estimated assuming $U^* = 0.95U^*_{sus}$. This approach was utilized to ensure movement through suspension since it is unknown how the presence of biofilms or cohesion affects particle transport in wastewater forcemains. The friction factor was determined from the Swamee-Jain equation with k_s determined using the predictive equations identified in Section 7.3.1.1. The methodology is based upon sediment transport theory along a horizontal plane and does not account for cohesion of particles. The theoretical maximum particle size transported through suspension was determined for diameters ranging from 6 in. to 66 in. and velocities ranging from 0.25 m/s (0.8 ft/s) to 4 m/s (13.1 ft/s). Results are presented in Figure 8.9 and show that the maximum particle size transported is limited to sand ranging from 0.2 mm (0.08 in.) to approximately 1 mm (0.04 in.).

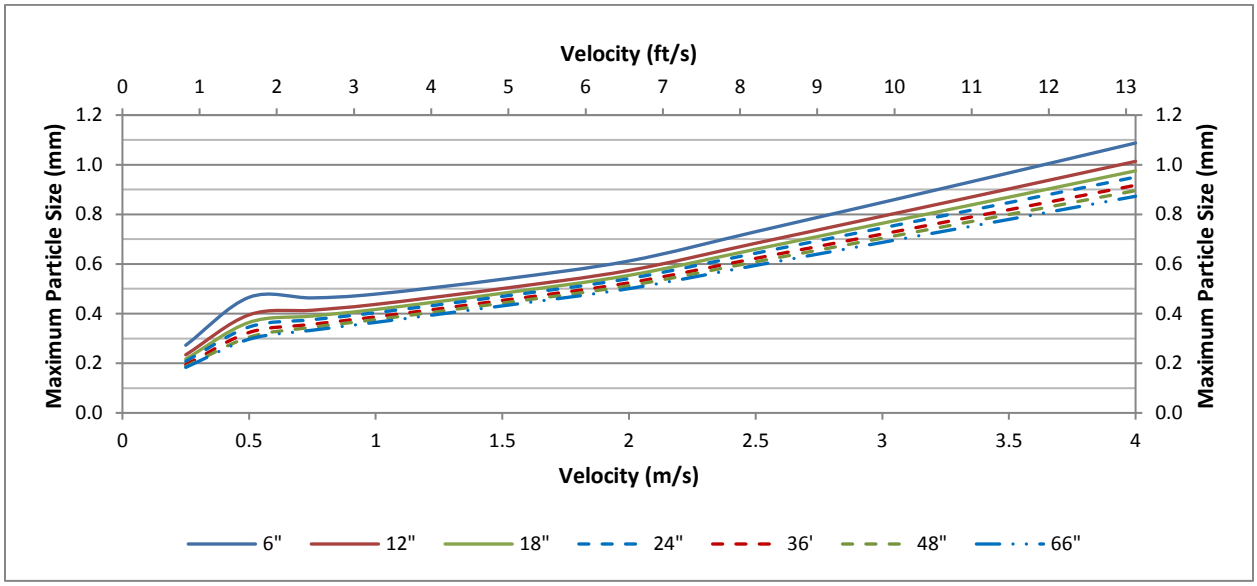

Figure 8.9: Maximum Particle Size Transported Through Suspension – By Diameter

8.2.4 Sediment Transport – Bed Motion

As demonstrated in Section 6.1.1.2, bed motion of a specific particle size occurs when the $U^* \leq U^*_{sus}$ and when the dimensionless shields parameter (τ^*) is greater than or equal to the critical shields parameter (τ^*_c), ($\tau^* \geq \tau^*_{sus}$). The methodology identified in Section 6.1.1.2 along with the predictive equation for k_s was utilized to determine the maximum theoretical particle size that can be transported through bed motion. The maximum particle size in relation to the angle of inclination was also evaluated. It should be noted that this methodology is based upon sediment transport theory and does not account for cohesion of particles.

Figure 8.10 presents the maximum particle size that can be transported by bed motion for diameters ranging from 6 in. to 66 in. and velocities ranging from 0.25 to 4 m/s given a horizontal pipe. Results show that the maximum theoretical particle size transported through bed motion is substantially larger than suspended particle sizes and ranges from approximately 3 mm (0.12 in.) at 0.25 m/s (0.82 ft/s) to 45 mm (1.8 in.) to 72 mm (2.8 in.) at 4 m/s (13.1 ft/s). Since k_s is a constant based on the velocity, the maximum particle size decreases with increasing diameter because the friction factor decreases as Reynolds Number R_e increases; therefore, as diameter increases, R_e increases and friction factor decreases, decreasing the friction velocity, and reducing the particle size transported.

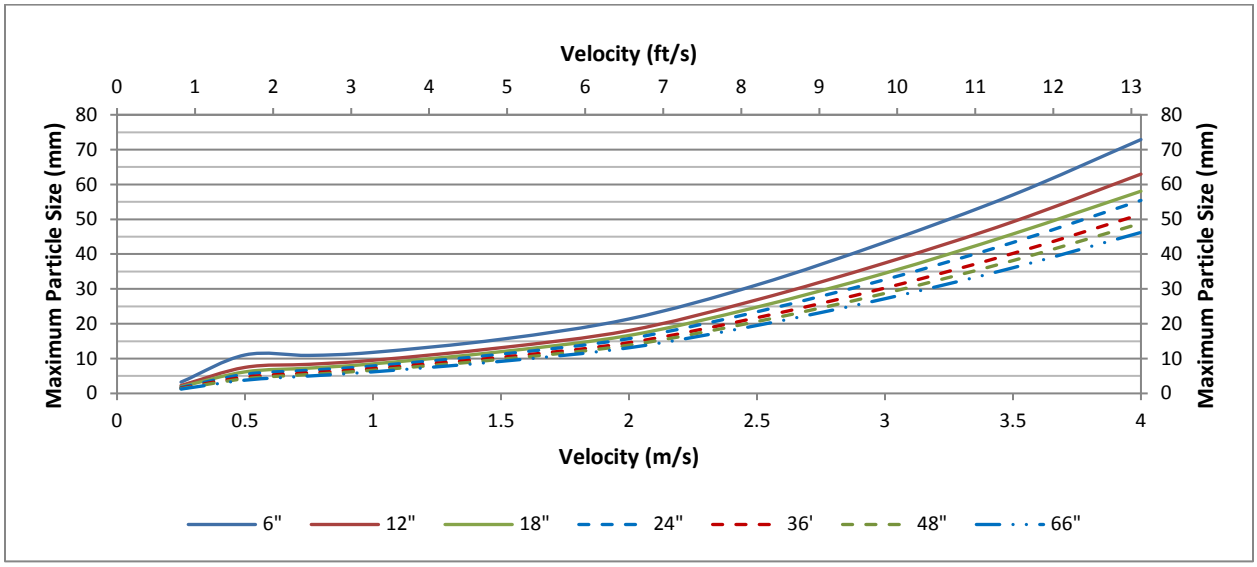

Figure 8.10: Maximum Particle Size Transported Through Bed Motion – Horizontal Pipe – By Diameter

The effect of inclination angle on the maximum particle size transported in 6 in., 24 in. and 48 in. diameter pipe is shown in Figures 8.11 to 8.13. Results show that the maximum particle size transported decreases as diameter increases and with increased inclination angle. The particle size transported was found to be a minimum between inclination angles of approximately 30° to 65°. Results also show that the particle size transported increases for inclination angles greater than 65°.

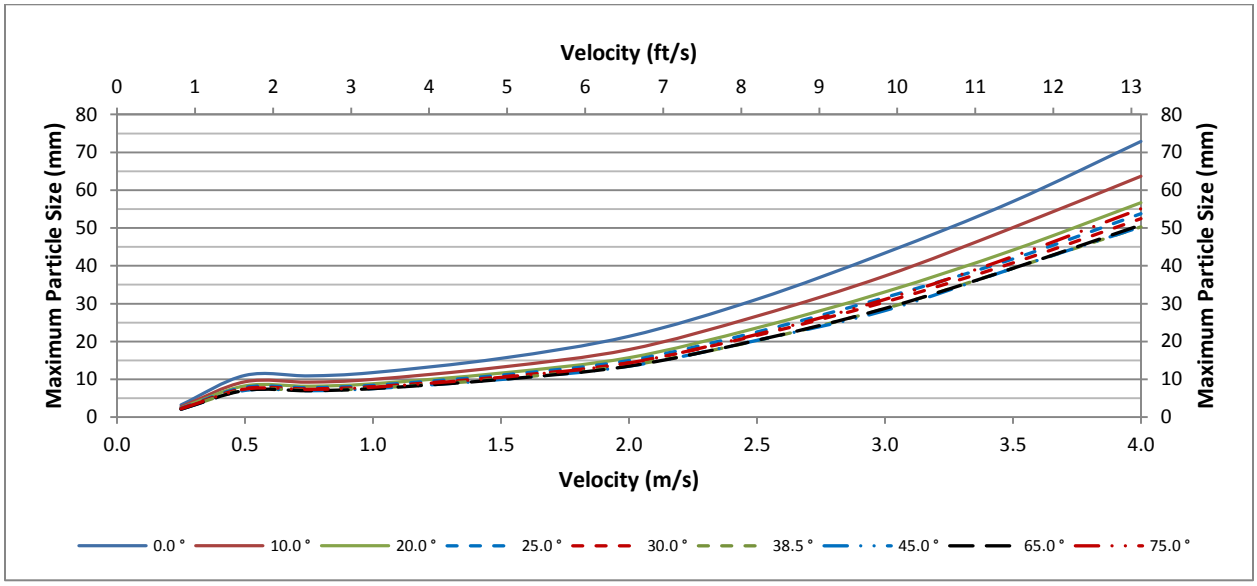

Figure 8.11: Maximum Particle Size Transported Through Bed Motion - By Angle of Inclination – 6 in. Diameter

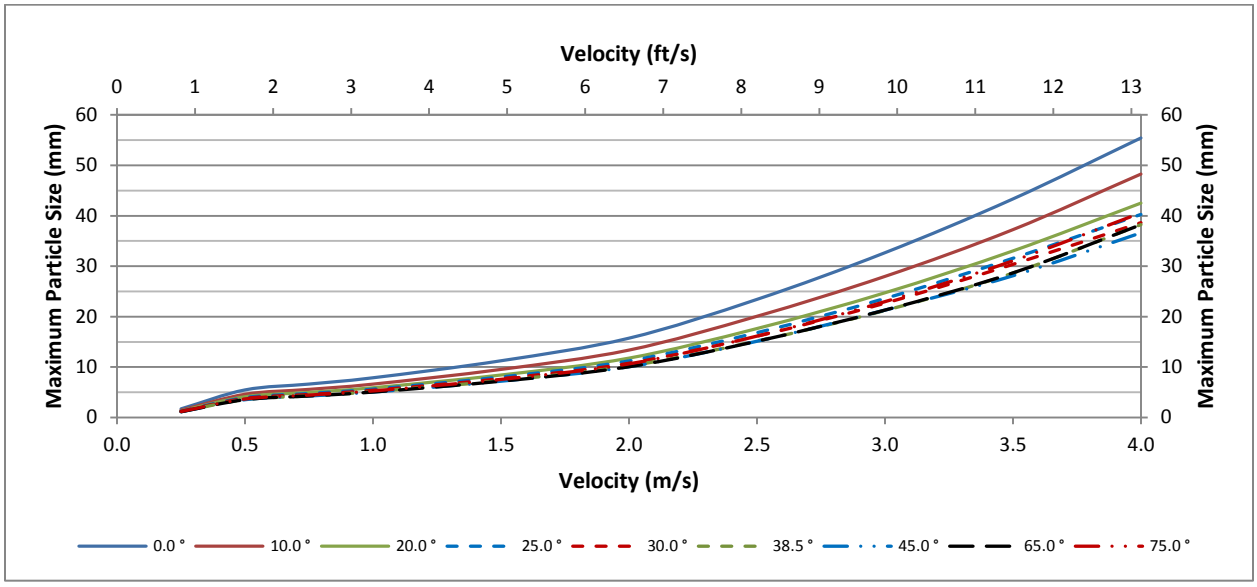

Figure 8.12: Maximum Particle Size Transported Through Bed Motion - By Angle of Inclination – 24 in. Diameter

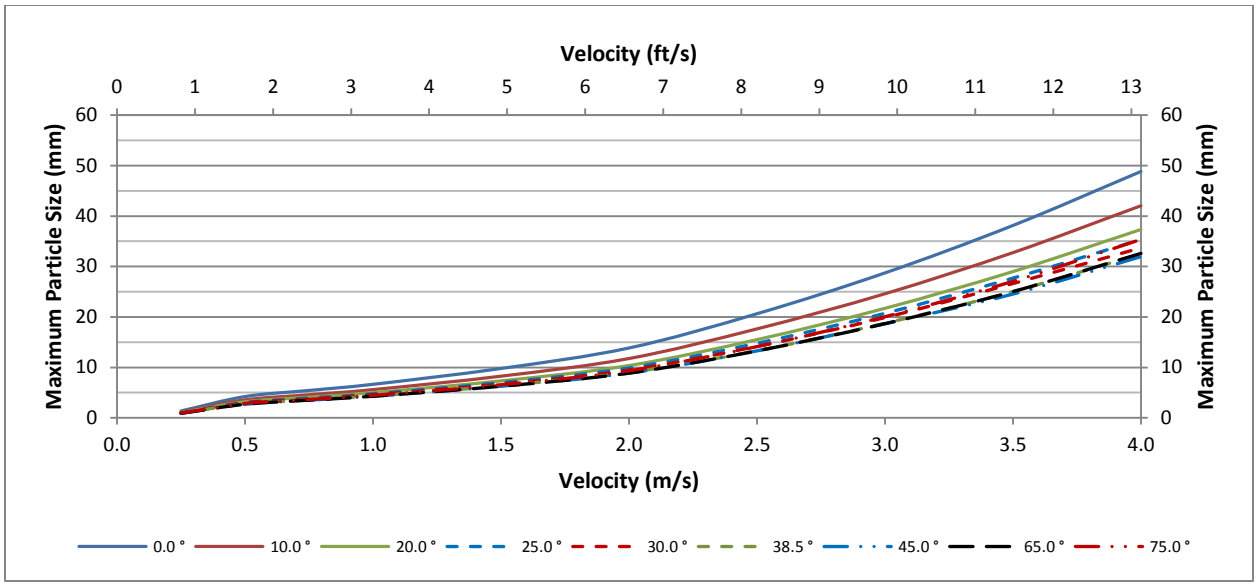

Figure 8.13: Maximum Particle Size Transported Through Bed Motion - By Angle of Inclination – 48 in. Diameter

The effect of inclination angle was further explored by comparing the minimum particle size and corresponding angle of repose against velocity for 6 in., 24 in. and 48 in. diameter pipe. Results are presented in Figures 8.14 to 8.16 and show that the minimum particle size occurred over a range varying from its angle of repose to an angle of approximately 60°. It should be noted that the difference between the minimum particle sizes between these angles was within 0.1 mm (0.004 in.) suggesting that the transport capacity is approximately equivalent. Further, the minimum particle size transported at an inclination angle between its angle of repose and 60° was determined to be approximately 50% of the particle that can be transported in a horizontal pipe. The reduction in particle size transported comparing the minimum particle in an inclined pipe to the particle size transported in a horizontal pipe at the same velocity is shown in Figure 8.17. This reduction in particle size ranges from 45% to 58% depending on the diameter and velocity and identified the importance of considering particle transport in forcemains where the pipeline undulates.

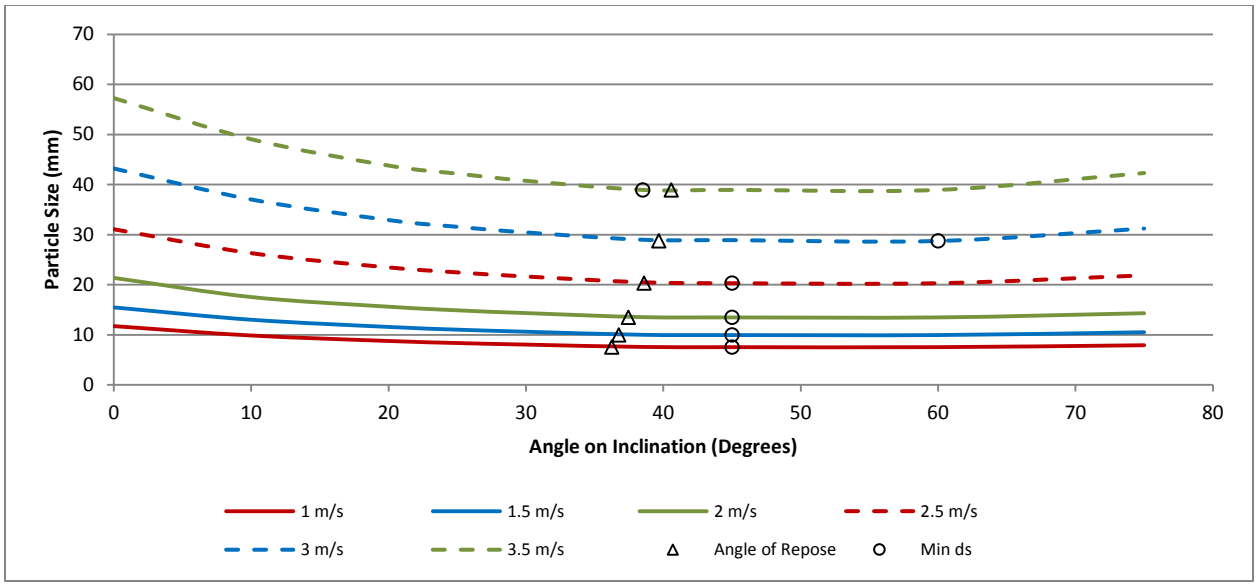

Figure 8.14: Maximum Particle Size Transported Through Bed Motion – 6 in. Diameter - By Velocity (m/s)

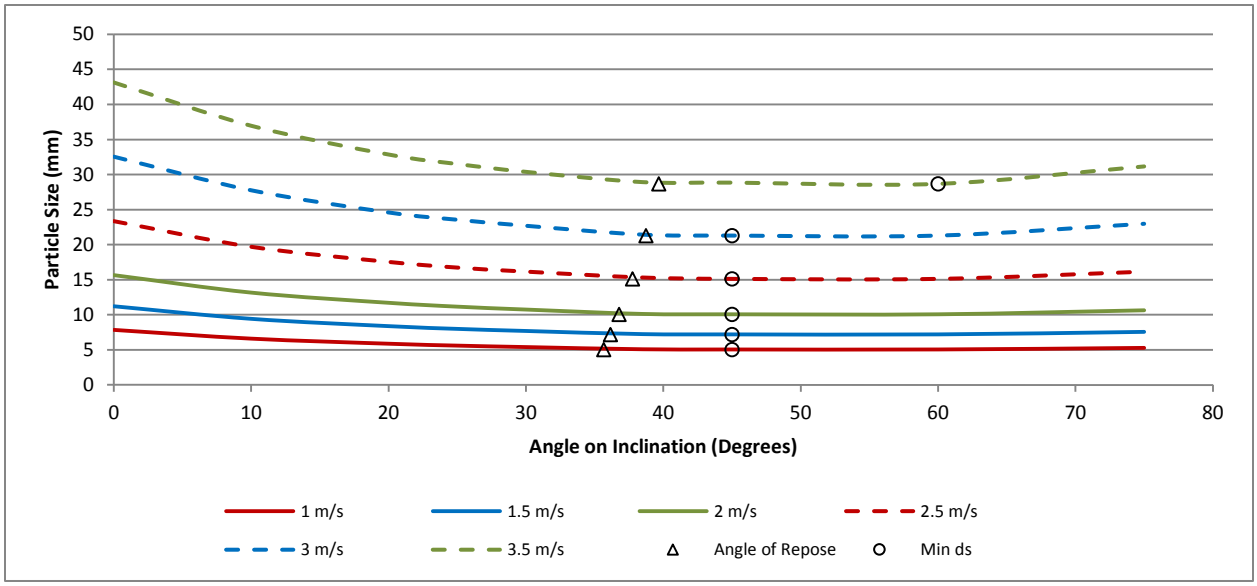

Figure 8.15: Maximum Particle Size Transported Through Bed Motion – 24 in. Diameter - By Velocity (m/s)

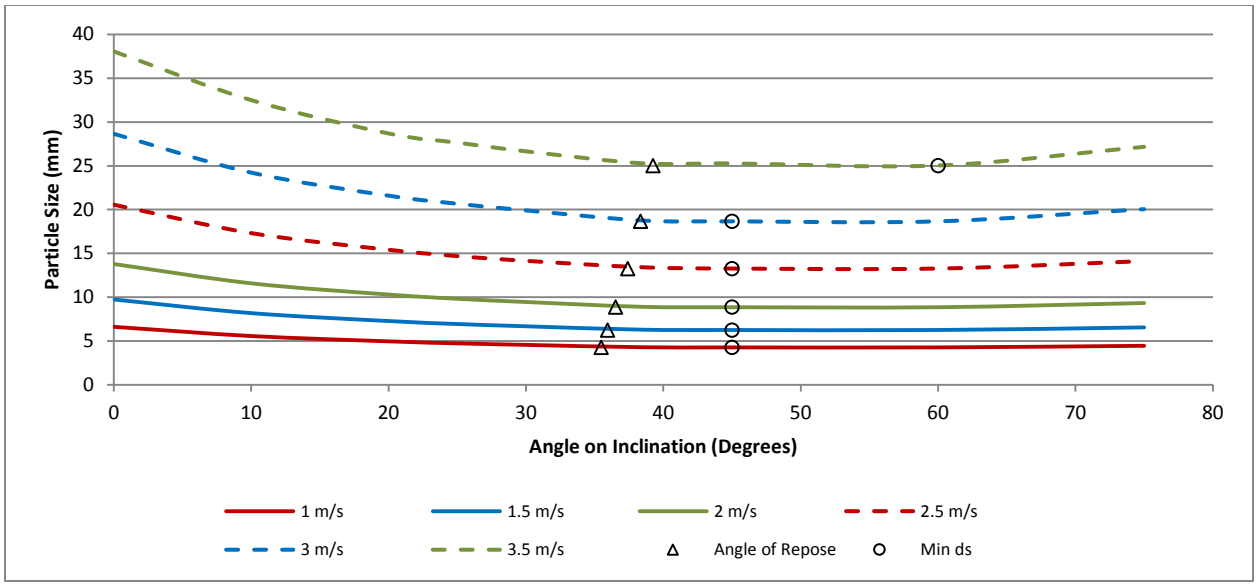

Figure 8.16: Maximum Particle Size Transported Through Bed Motion – 48 in. Diameter - By Velocity (m/s)

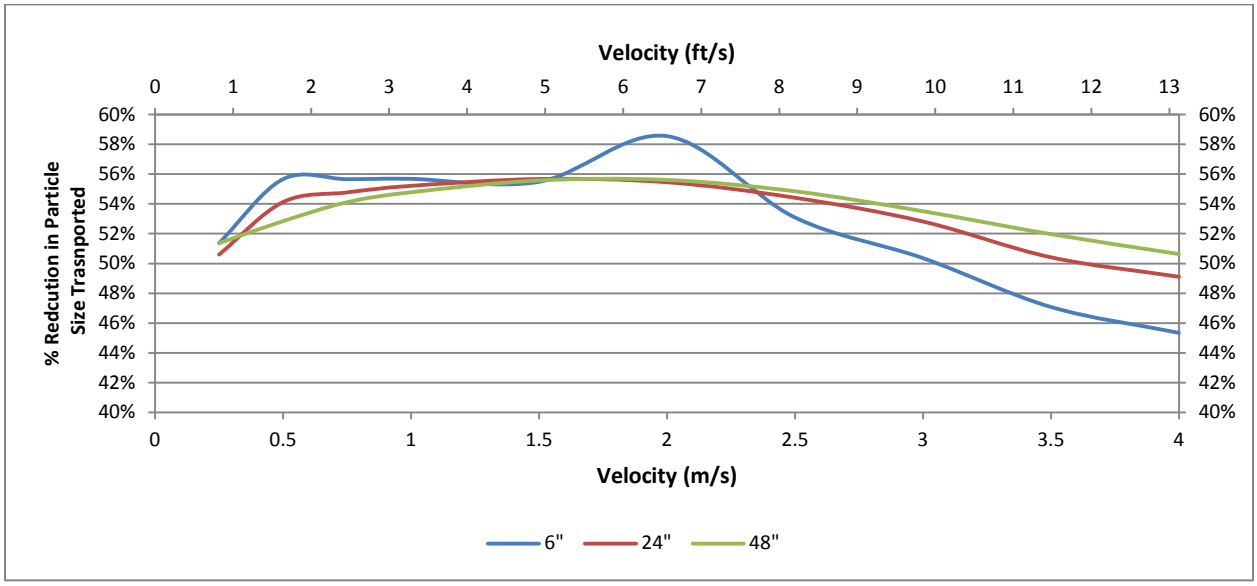

Figure 8.17: Reduction in Particle Size due to Inclined Pipe – Minimum Particle Size Compared to Particle Size Transported in Horizontal Pipe.

Forcemains typically undulate along the pipeline alignment following the natural terrain. Results show that a pipelines capacity to transport large particles is diminished along the rising limbs of a forcemain based upon the angle of inclination. Therefore, in systems where the transport of large particles is required, consideration should be given to the pipeline profile when selecting forcemain diameter. Depending on the required particle size to be transported, it may be necessary to limit deflection angles to a maximum of 30°

from horizontal to minimize the reduction in bed motion transport capacity or it may be necessary to reduce the diameter along the rising limb for angles greater than 30° in order to increase the velocity and thus the particle transport capacity of the pipe.

Effect of both angle of inclination and particle size was further evaluated to determine the required velocity to transport 12.7 mm (0.5 in.), 25 mm (1 in.), 38.1 mm (1.5 in.), and 50 mm (2 in.) sized particles through a system given angles of inclination ranging from 10° to 75°. The results are presented in Figures 8.18 to 8.21 and show that an increase in velocity of approximately 30% is required to transport the particle through a rising limb at a 30° angle. A marginal increase in velocity is required to transport the same particle size through greater angles of inclination.

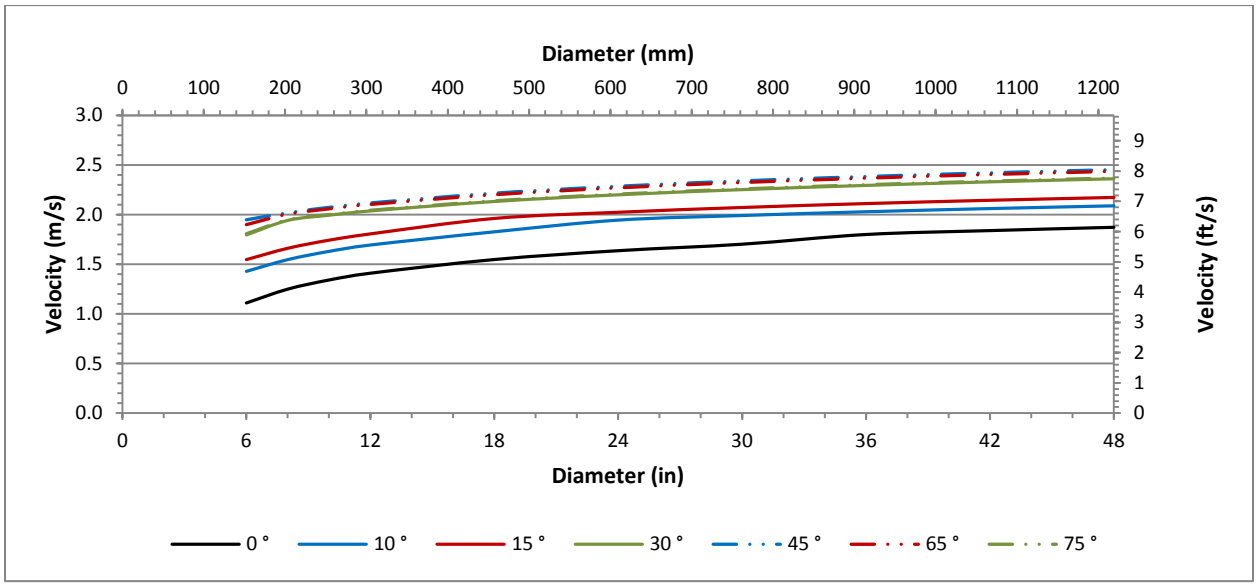

Figure 8.18: Velocity required to Transport 12.7 mm (0.5 in.) Particle Size Through Bed Motion – By Angle of Inclination

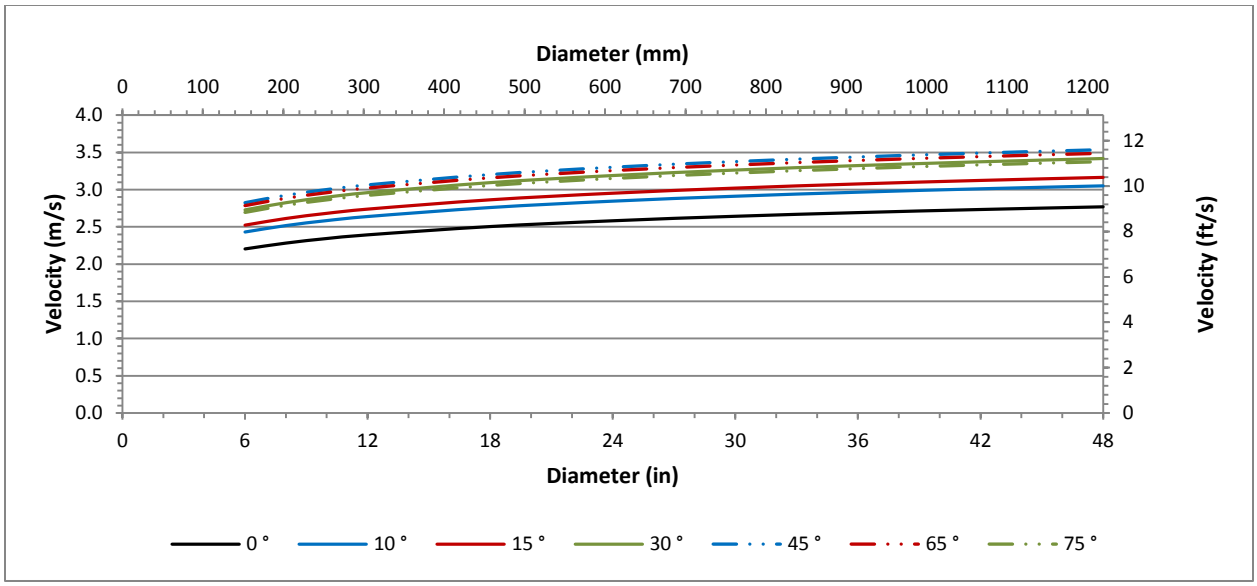

Figure 8.19: Velocity required to Transport 25 mm (1 in.) Particle Size Through Bed Motion – By Angle of Inclination

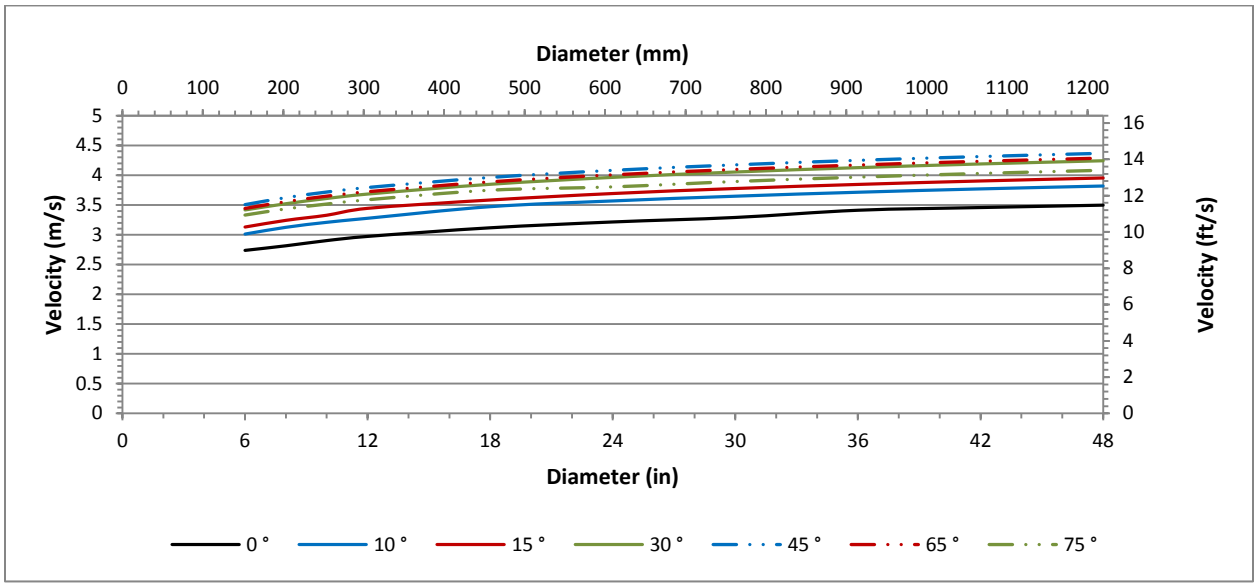

Figure 8.20: Velocity required to Transport 38.1 mm (1.5 in.) Particle Size Through Bed Motion – By Angle of Inclination

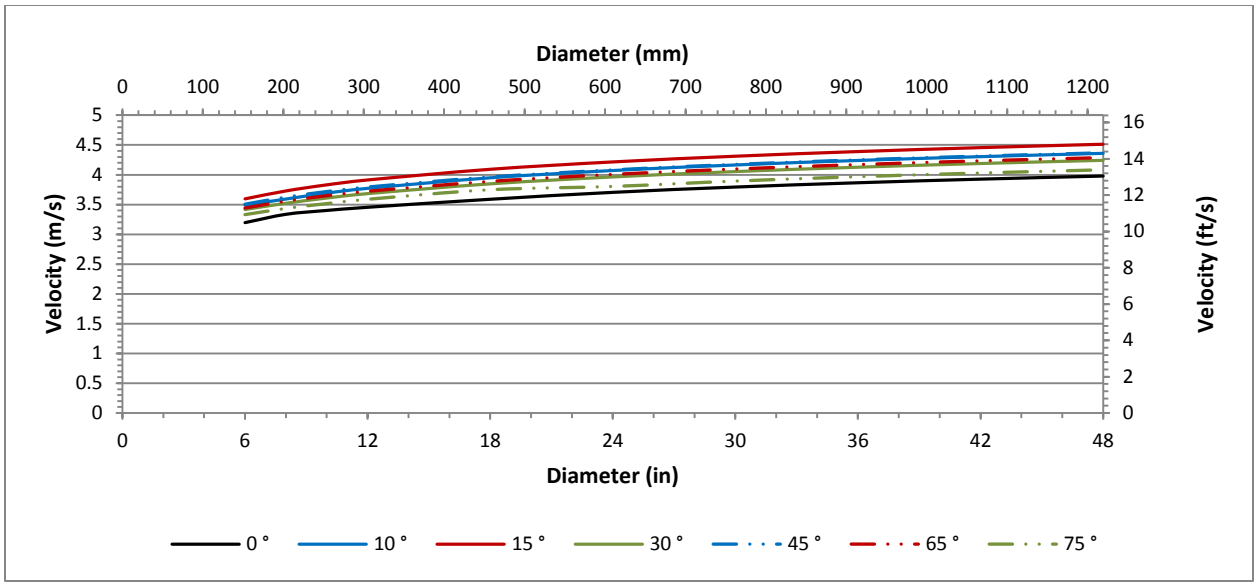

Figure 8.21: Velocity required to Transport 50 mm (2 in.) Particle Size Through Bed Motion – By Angle of Inclination

The required velocity to transport a specific particle size through rising limbs was presented above. The corresponding percent increase in velocity required to transport the particle as compared to the horizontal velocity for each of the above conditions is presented in Figures 8.22 to 8.25. Results show that that the velocity should be increased by a minimum of 20% to transport the particle along rising limbs 30° and greater.

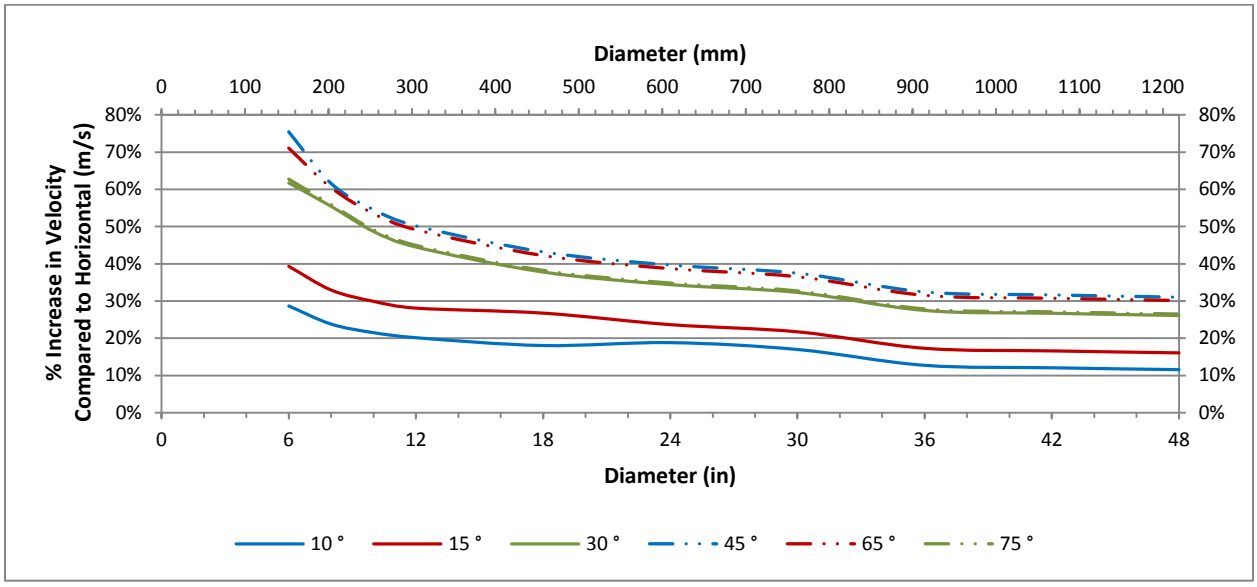

Figure 8.22: Increase in Velocity required to Transport 12.7 mm (0.5 in.) Particle Size as Compared to Horizontal – By Angle of Inclination

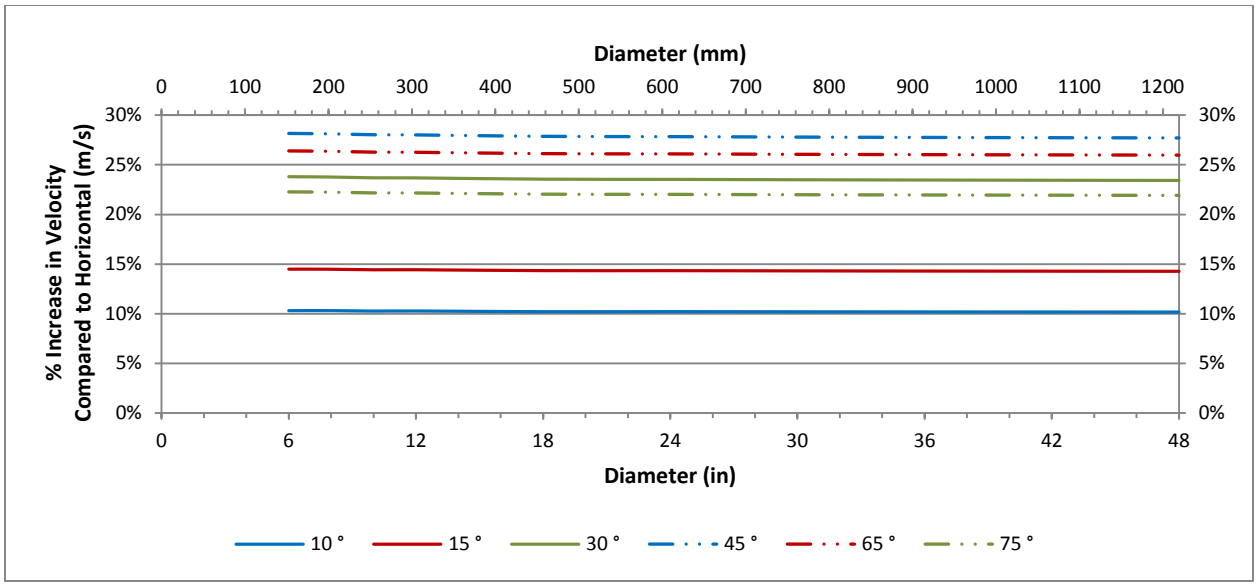

Figure 8.23: Increase in Velocity required to Transport 25 mm (1 in.) Particle Size as Compared to Horizontal – By Angle of Inclination

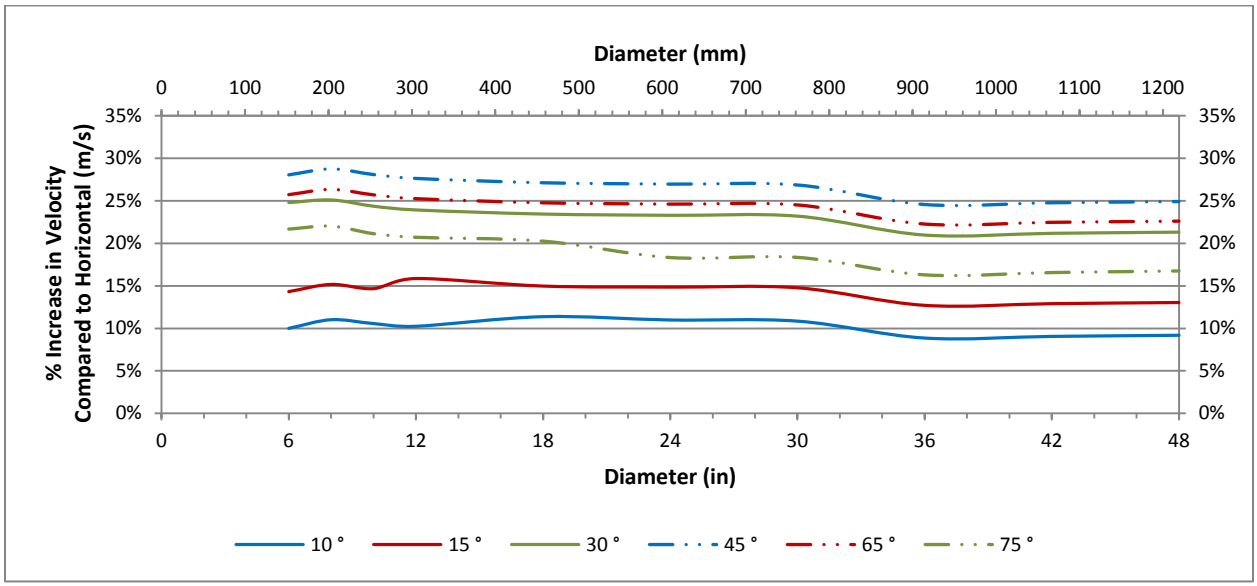

Figure 8.24: Increase in Velocity required to Transport 38.1 mm (1.5 in.) Particle Size as Compared to Horizontal – By Angle of Inclination

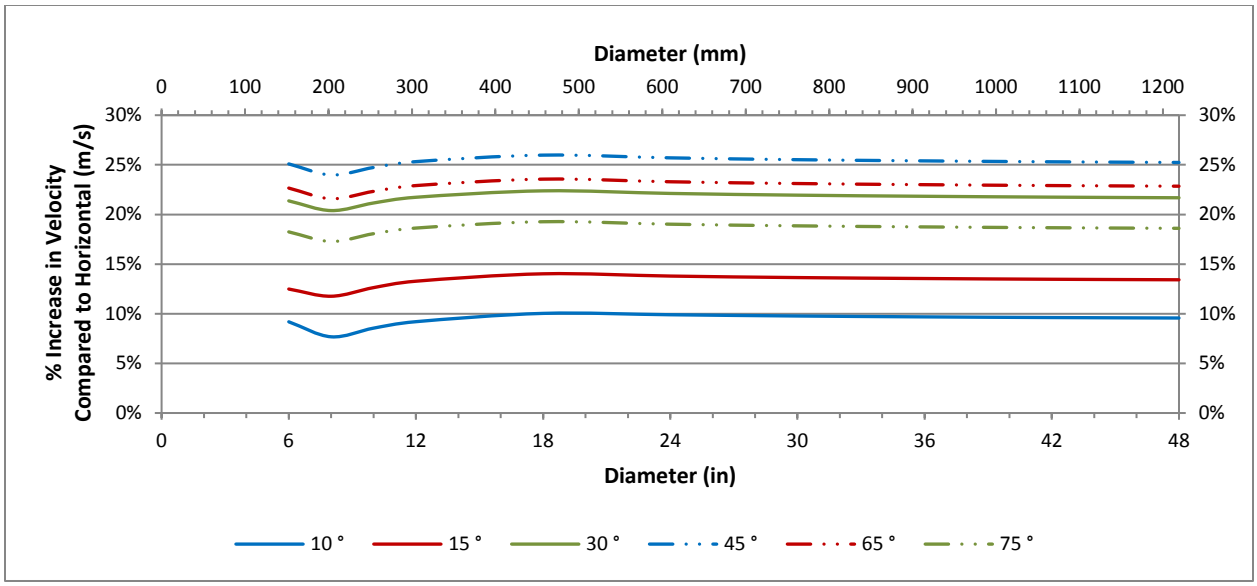

Figure 8.25: Increase in Velocity required to Transport 50 mm (2 in.) Particle Size as Compared to Horizontal – By Angle of Inclination

The above analysis provides a guide to transporting sediment particles through forcemains. Results are based up on the theoretical transport of particles through bed motion and do not consider the effect of cohesion on particle transport. Therefore, if large particles are expected, then a safety factor should be included to ensure that a sufficient velocity is provided to transport the design particle. Forcemains with insufficient transport capacity may accumulate particles at low points or the base of rising limbs, which may develop potential obstructions over time and reduce the overall capacity of the system.

8.2.5 Air Clearing Velocity

Air clearing velocities were evaluated and discussed in Section 6.1.2. Three equations developed by Kent (1952) / Mosevell (1976), Wisner (1975), and Escarameia (2006) were evaluated to estimate the required velocity to clear an air pocket from a downward sloping pipe. All equations produced similar results for downward angles greater than 15°. The Wisner (1975) equation (Equation 6.13) appears to over-estimate clearing velocities as compared to the other methods for larger diameters with downward sloping angles less than 15°. Equation 6.14 developed by Escarameia (2006) is recommended because it provided the most conservative air clearing velocity.

Based upon in-service field inspection of 500 miles of forcemains, Pure Technologies reports that 72% of air pockets are not at known high points (Dettmer 2014). This emphasizes the importance of providing air clearing velocities to remove air from forcemains since air valves would not typically be provided at these locations. Table 8.19 summarizes the air clearing velocities from Escarameia (2006) along with approximate average air clearing velocity from all three methods for 12 in., 24 in. and 48 in. diameter pipe with a downward sloping angle of approximately 45°. Results show that although Equation 6.14 (Escarameia 2006) is the most conservative, the average of all three methods yields similar results, indicating that the Escarameia equation is not overly conservative. It is also observed that the air clearing velocity for a 48 in. diameter pipe is very high at 3.6 m/s which may not be practical under normal operating conditions.

Table 8.19: Clearing Velocity Summary for 45° Downward Sloping Pipe

Diameter (in)	Clearing Velocity	
	Escarameia (2006)	Average [1]
12	1.8 m/s / (5.9 ft/s)	1.7 m/s / (5.6 ft/s)
24	2.6 m/s / (8.5 ft/s)	2.5 m/s / (8.2 ft/s)
48	3.6 m/s / (11.8 ft/s)	3.5 m/s / (11.5 ft/s)

[1] Average of Kent (1952) / Mosevell (1976), Wisner (1975), and Escarameia (2006) Methods

8.2.6 Comparison of Design Velocities

In the previous sections, velocities were determined for the most economical (optimal) diameter, self-cleansing (Tractive Force) design, particle transport through suspension and bed motion; and air clearing. The diameter corresponding to the minimum present worth of the capital and operational costs is the most economical (optimal) diameter of a system. Self-cleansing (Tractive Force) design determines the velocity required to achieve critical shear stress to enable particle transport. Evaluation of bed motion considered the velocity required to transport a maximum particle size along the pipe considering an upwards angle of inclination; particles smaller than this maximum particle size are considered to be transported through either bed motion or suspension. Air clearing velocity is the velocity required to clear an air pocket through the pipe considering a downward sloping angle.

Each of these items should be considered when sizing forcemains to determine the critical parameter that controls the selection of the diameter and design velocity for a given system. Figure 8.26

provides a comparison of the design velocities required for each of these categories in order to identify the critical condition based upon the following assumptions:

- Economic Diameter – Pipe length of 10,000 ft; 12 hrs/day pump runtime; $ 0.07 / kW-hr power cost; 50 ft Static Head;
- Self-Cleansing Velocity – τ_c of 0.10 lb/ft^2 (4.80 N/m^2);
- Bed Motion – Particle sizes of 12.7 mm (0.5 in.) and 25 mm (1 in.) diameter particles at 30° angle of inclination; and
- Air Clearing – 30° downward angle and Equation 6.14.

It should be noted that economic diameter is dependent on the actual system parameters and changes to system attributes and assumptions will affect the selection of the optimal diameter and thus velocity at the design flowrate.

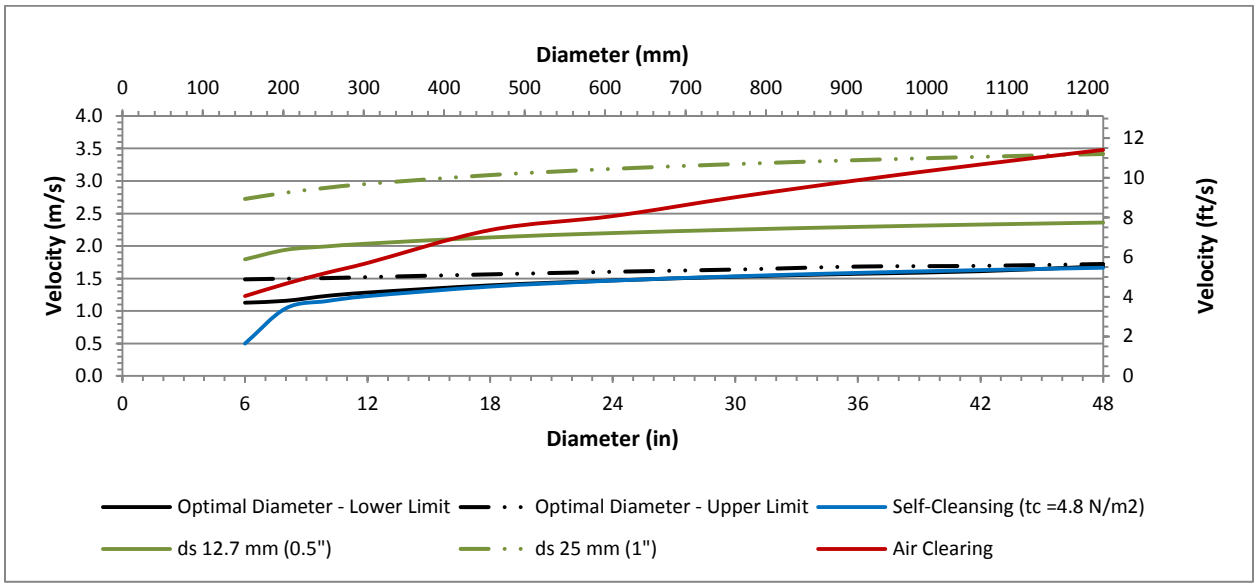

Figure 8.26: Comparison of Design Velocity Considerations

The design velocity associated with either bed motion or the air clearing velocity were found to be the most conservative (>2 m/s) depending on the pipe diameter and selected particle size to be transported. Particle sizes of 12.7 mm (0.5 in.) and 25 mm (1 in.) are large compared to the grit measured in wastewater (Table 6.1) but were assumed to be reasonable particle sizes that could be found in wastewater systems.

Air clearing velocity was determined assuming a 30° downward sloping pipe and the bed motion velocity was determined from a 30° upward sloping pipe. As shown in Section 8.2.4, an upwards sloping pipe reduces the particle size that can be transported by approximately 30 - 50%. Therefore, it is important to minimize the amount of undulation occurring along the pipeline profile, or reduce the diameter along the rising limb to offset this reduction in transport capacity. It should be noted that sedimentation may occur for velocities less than the self-cleansing velocity.

The velocity associated with the economic diameter was provided over the range of optimal flowrates corresponding to each diameter. Results show that the self-cleansing velocity closely follows the velocity associated with the optimal diameter (lower limit); however, bed motion and air clearing velocities are much higher than the optimal diameter velocities.

Figure 8.26 illustrates the importance of evaluating these conditions when selecting a design velocity and diameter. Results show that the optimal diameter may not be the appropriate design diameter based upon the anticipated grit or requirement for air removal. Under these assumptions, the optimal diameter appears to provide velocities greater than self-cleansing velocity and should be selected over the self-cleansing requirements. It should be noted that changing the pump runtime or electrical rates could result in conditions where the self-cleansing velocity is greater than the optimal diameter.

Figure 8.27 presents the forcemain velocity calculated for the data collected as part of this research plotted along with the results of Figure 8.26. Results show that most forcemains greater than 6 in. diameter were operating below both the most economical and self-cleansing velocity recommendations indicating potential poor performance; a number of the smaller diameter forcemains ($\leq$ 6 in.) are operating in between the self-cleansing and optimal diameter velocities; and several forcemains (< 12 in.) appear to have capacity to transport larger particles and clear air. The remaining systems were found to be operating below the self-cleansing velocity indicating potential sedimentation. Performance of the systems operating at low velocities could potentially be improved by replacing pumps with larger capacity units in order to increase the operating velocity.

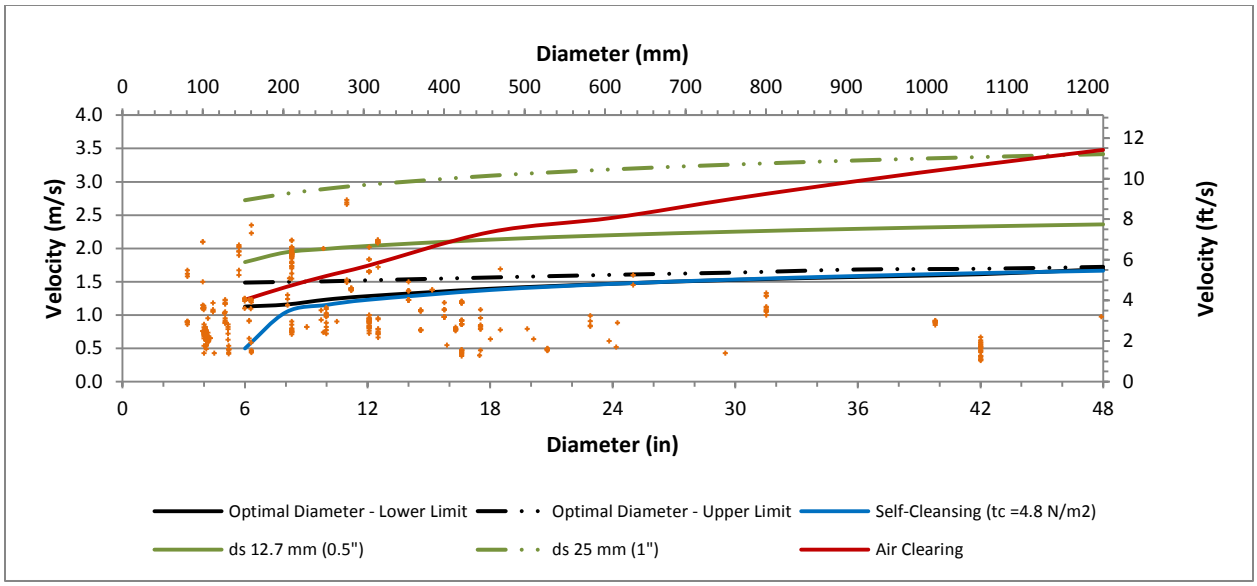

Figure 8.27: Comparison of Design Velocity Considerations and Research Data

As described in Section 8.2.1, many standards recommend a minimum design velocity of 2 ft/s (0.6 m/s) and 3.5 ft/s (1.1 m/s) to re-suspend solids. The results presented above show that a majority of the research data for 6 in. and smaller diameters were found to be operating in between the optimal diameter and self-cleansing velocity indicating that these systems may not be optimized but at least provide the self-cleansing velocity. In addition, a number of systems with forcemain diameters larger than 6 in. were found to be operating below the self-cleansing velocity with several systems operating less than 2 ft/s (0.6 m/s) promoting potential sedimentation.

Based upon these results, selecting a design velocity between 2 ft/s (0.6 m/s) and 3.5 ft/s (1.1 m/s) may not be appropriate and the minimum design velocity should be selected upon either the self-cleansing velocity or economical pipe sizing. Although each system should be evaluated to determine the minimum design velocity based upon the proposed conditions, these results suggest that the minimum forcemain design velocity should be approximately 5 ft/s (1.5 m/s).

It should be noted that operating forcemains at higher velocities increases surge potential. In addition, forcemain discharge structures could be subjected to erosion due to the velocity jet or high turbulence leading to hydrogen sulfide off gassing and subsequent corrosion within these structures. In order to mitigate against potential corrosion or erosion at these structures; the forcemain could discharge

under submerged conditions; the discharge structure could be epoxy lined to resist corrosion; or the forcemain diameter can be enlarged over say the last 10 -20 ft to reduce velocities entering the discharge structure. These mitigation measures are not all encompassing and are merely suggestions. This topic is beyond the scope of this research, site specific constraints or owner requirements may dictate an appropriate mitigation strategy and should evaluated further during the design process.

8.2.7 Effects of Low Velocities in Forcemains

As shown in Section 8.2.6, a large number of systems evaluated as part of this research were found to be operating at low velocities. Low velocities promote grease/ biofilm accumulation, sedimentation, air binding, and hydrogen sulfide buildup. All of these items can lead to reduced asset life and increased life cycle costs. Both sedimentation and air accumulation reduce flow area and increase system losses, which provide increased operating pressures and reduced pumping capacity. In addition, sedimentation can increase microbial activity, Hydrogen Sulfide production can promote corrosive conditions and potential odors. These issues are often inter-related and often compound each other.

Air release valves can be used to exhaust air from a forcemain. However, forcemain design should balance the capital, operational, and maintenance cost of adding an excessive number of air release valves against the capital and operational costs of providing air clearing velocities. It should also be noted that Pure Technologies determined that 72% of air pockets identified through inspection of 500 miles of forcemains were not at known high points. Therefore, utilization of air release valves may not be sufficient to exhaust air/gas accumulation. Potential sedimentation is generally not an issue when providing air clearing velocities; however, the increased velocity could result greater surge conditions, pumping costs, and operational pressures which must be considered during the design process.

A method for addressing forcemains that are operating at low velocities would be to allow the wet well to surcharge and then operate all pumps to increase velocity and “flush” out the forcemain. The pumps should operate over a duration long enough to pump the forcemain volume or as long as can be tolerated.

Numerous technologies can be used to clean the forcemain. A detailed discussion of these technologies is beyond the scope of this research. A brief description of pipeline "pigging" was provided in Section 6.1.4 because it is one of the more utilized technologies to clean forcemains. These technologies utilize a foam plug matching the pipeline interior diameter to push the grit and accumulated material through the pipeline using the system velocity provided by the pumps. Ice pigging is a promising new technology that uses an ice slurry inserted through a small tap or air release valve piping that solidifies inside the forcemain. The ice melts with increased travel along the forcemain and does not require a dedicated recovery point to capture the pig.

It is understood that wastewater pumps deteriorate with time and usage. However, pump performance is generally not measured or monitored. Operation and maintenance practices are often based on rules-of-thumb and qualitative field observations. Hydraulic models are frequently used to design new pumping systems, assessment of existing systems, and develop energy optimization strategies. However, such models generally use original manufacturer specifications for hydraulic performance and energy consumption of pumps without proper consideration of their actual behavior. As a result, many decisions are made without complete or accurate information (Papa 2013).

One common method utilized to determine the condition of the forcemain or pumps is through routine pump station field measurements. Benchmarking and comparing the pump capacity on an annual basis will identify potential degradation to pump capacity. Because these changes could also be attributed to pump wear or pipeline capacity reduction, it is essential to verify that the pumps are in good working order before determining that the forcemain requires cleaning. Pressure sensors located along the discharge side of the pumps can verify problems associated with the poor pump performance or changes to the headloss along the pipeline. The field measured operating points should be compared to the original pump curve to determine the amount of pump degradation.

Air buildup and sedimentation have been demonstrated to be potential issues associated with forcemains. It is likely that a forcemain system subjected to sedimentation will ultimately reach equilibrium with the corresponding reduction in diameter providing the critical shear stress required to transport grit

particles along the deposited bed preventing additional sedimentation from occurring. Both the TRM and TRP forcemains (Table 4.2) are 42 in. diameter; the hydraulic calculations determined that these forcemains were operating at low velocities (< 2 ft/s (0.6 m/s)). An effort was made to estimate the volume of sedimentation that may have accumulated within the forcemain due to the low velocities, however, the results from the analysis were inconclusive. A more detailed analysis collecting operational data along the pipeline would be recommended to determine changes in headloss along the pipeline which may represent specific pipe segments which are subjected to sedimentation. The effect of sedimentation should be evaluated further in future research.

9 Conclusions and Recommendations

Chemical and biological processes within wastewater form biofilms that attach to the forcemain pipe wall and increase headloss. This increase in head loss is generally not accounted for in current design practice of forcemains. There is little information in the literature regarding the effect of wastewater biofilms on the forcemain hydraulics. This research evaluated the hydraulic effect of biofilms on in-service forcemains

Wastewater forcemains have to cope with a particularly challenging task: they have to ensure that solids contained in the wastewater (sand, gravel, organics) are readily transported along with the wastewater. Sedimentation, air buildup, corrosion, and odors are often inter-related and generally occur at lower velocities. To further complicate forcemain design and operation; wastewater lift station pumps generally operate intermittently which requires re-mobilization of any material that may have settled while pumps remain idle. Frequency of pumping cycles are based upon the influent flow rate and could range from a few minutes to several hours between pumping cycles.

Therefore, forcemains must be designed to be self-cleaning in order to prevent solids deposition which could cause increased sulfide production leading to corrosion and odor issues; loss of capacity through a reduction of cross sectional area; or even blockage at low points, or at the toe of an adversely sloped pipe, leading to costly removal. In many instances, forcemains are designed conservatively to account for potential large variations in surface roughness or future flowrates.

The goal of this research is to identify short-comings in current forcemain design practice through expanded evaluation of the findings by HR Wallingford identified in Report *SR 641 - Flow resistance of wastewater pumping mains: improved design through better data* in order to improve hydraulic design methodologies of forcemains. Key objectives to achieve this goal are as follows:

- Evaluate the hydraulic effect of biofilms on absolute roughness (k_s);
- Evaluate the hydraulic effect of biofilms on Hazen-Williams C factor; and

- Estimate critical velocity required for sediment transport, air clearing, self-cleansing and optimal diameters of forcemains, which are not identified in forcemain design standards.

9.1 Main Conclusions of Research

1. A significant finding of this research is that k_s decreases with increasing velocity in a fairly linearized relationship plotted on a log-log scale, suggesting that k_s is a function of velocity and is significantly affected by wastewater biofilms. This result does not agree with Nikuradse's findings that k_s is fairly uniform (clean water). Although results present a fair degree of scatter, a core trend line was observed in the results with groupings of data observed on either side of the core trend line. Possible explanations for deviation from the core trendline include 1) potential errors in system attributes 2) Some forcemain systems could be combined wastewater and stormwater systems or have a large volume of clean water reporting to the system, 3) Source water chemistry may have an effect on the value of k_s, 4) Sedimentation may be occurring in lower velocity forcemains, or 5) off gassing or air locking could be occurring within the system. Results do not present any observable trends associated with pipe diameter, material, or age. Calculated values of k_s ranged from approximately 35 mm to 0.01 mm, with the larger values occurring at velocities less than 1 m/s (3.3 ft/s). The upper range of k_s values are orders of magnitude larger than the standard clean water, new pipe k_s value found in literature. A few calculated k_s results for metallic and cementitious pipe were found to be smoother than standard clean water, new pipe k_s value published in literature. This deviation is likely a result of inaccurate system or operational data. Plastic pipe results for k_s were all larger than the standard clean water, new pipe k_s value published in literature. Results suggest that biofilms effect forcemains in a similar manner regardless of diameter or pipe material and that the traditional methods in determining pipeline capacity are not appropriate for biofouled pipes and will likely over estimate flow capacity. The literature shows that the von Kármán constant (κ) of biofouled surfaces was non-universal and was lower than the conventional value

of 0.40 for $R_e<1.04x10^5$; therefore, the traditional Colebrook-White equation is not applicable for biofouled pipes for $R_e<1.04x10^5$. Although these findings are significant, the minimum recommended forcemain velocity is generally taken as 3 ft/s (0.9 m/s) to prevent sedimentation. Therefore, forcemains should generally operate above the threshold R_e and the standard Colebrook-White equation should be used to calculate friction factor.

2. C factor results ranged from approximately 30 to 150, with lower C factors found at velocities less than 3 ft/s. In general practice, C factors less than 80 are considered to be unreliable for clean water systems; however, the C factors calculated for this research were determined from operational data and published research indicating the results are valid for the systems evaluated. Approximately 60% of forcemain systems evaluated are operating at C factors less than 100, which is much lower than the recommended values published in the literature for clean water, new pipe. Results show that C factor is a function of velocity with the C factor increasing with increased velocity indicating that traditional methods in determining pipeline capacity for biofouled pipes are not appropriate and will likely over estimate flow capacity. A core trend line similar to the k_s findings was identified with a general rise in C factor for velocities between 2.5 ft/s (0.8 m/s) and 4.5 ft/s (1.4 m/s); the slope of the line above 4.5 ft/s (1.4 m/s) appears to tend towards horizontal, indicating a potential tendency towards its clean water, new pipe C factor. If this is the case, then the biofilm is likely shearing from the pipe wall and thus increasing hydraulic efficiency. Results suggest that velocity is the dominant factor for determining C factor and that biofilms effect forcemains in a similar manner regardless of pipe diameter, material, or age. However, a comparison of the C factor results to k_s results show that C factor is dependent upon both velocity and diameter.
3. Results of the hydraulic analysis determined that 44% of the systems evaluated were operating at velocities between 2- and 3.5 ft/s (0.6- and 1.1 m/s) and 16% of systems were operating at velocities less than 2 ft/s (0.6 m/s). The required design velocity for self-cleansing, sediment transport, air clearing, and economical diameter was compared to these results and show that a

majority of the research data for 6 in. (152.4 mm) and smaller diameters were found to be operating in between the optimal diameter and self-cleansing velocity indicating that these systems may not be optimized but at least provide the self-cleansing velocity (Figure 8.27). In addition, a number of systems with forcemain diameters larger than 6 in. (152.4 mm) were found to be operating below the self-cleansing velocity. Considering that the many design standards recommend a minimum design velocity of 2 ft/s (0.6 m/s) and 3.5 ft/s (1.1 m/s) to prevent settling and re-suspend solids; selecting a design velocity between 2 ft/s (0.6 m/s) and 3.5 ft/s (1.1 m/s) may not be appropriate and the minimum design velocity should be selected upon either the self-cleansing velocity or economical pipe sizing. Although each system should be evaluated to determine the correct minimum design velocity based upon the proposed system properties, these results suggest that the minimum forcemain design velocity should be at least 5 ft/s (1.5 m/s).

9.2 Development of Predictive Equations for k_s and C-Factor

Predictive equations were developed to estimate k_s and C factor. All data collected and evaluated as part of this research were considered for the development of the predictive equation(s). However, the following data points were removed from the dataset 1) data points where $R_e < 1.04x10^5$ in biofouled pipes lead to von Kármán constants less than 0.4 and potential erroneous results of k_s. 2) results where k_s was greater than 30 mm (1.2 in.) were also removed since it is impractical to use an equivalent sand roughness value greater than 30 mm (1.2 in.) without adjusting for a reduced interior diameter. 30 mm (1.2 in.) was selected as a reasonable value for the upper threshold of k_s based upon experience. 3) data points shifted far to the right of the core trend line suggest higher headloss which could be the result of an obstruction, sedimentation, or potential air locking and were considered outliers and were also removed. A summary of the recommended predictive equations of both k_s and C factor for both Metric and US Customary Units are provided in Sections 9.2.1 and 9.2.2.

9.2.1 Absolute Roughness - k_s

Table 9.1: Recommended Equation and Limits - k_s (Metric Units)

Equation k_s (mm)	Limits	Equation No.
$k_s = 30$	V < 0.54 (m/s)	(7.6a)
$k_s = 1.897V^{-4.379}$	0.54 ≤ V ≤ 1.98 (m/s)	(7.6b)
$k_s = 0.1364V^{-0.546}$	1.98 < V ≤ 4.0 (m/s)	(7.6c)

Table 9.2: Recommended Equation and Limits - k_s (U.S. Customary Units)

Equation k_s (in)	Limits	Equation No.
$k_s = 1.18$	V < 1.77 (ft/s)	(7.7a)
$k_s = 13.571V^{-4.379}$	1.77 ≤ V ≤ 6.50 (ft/s)	(7.7b)
$k_s = 0.0103V^{-0.546}$	6.50 < V ≤ 13.12 (ft/s)	(7.7c)

9.2.2 C-Factor

Table 9.3: Recommended Equation and Limits: C-Factor

C-Factor Equation	Limits	Equation No.
Metric Units		
$C_{Factor} = 132.1\phi^{0.0174} - 137.37\phi^{-0.112}e^{-0.908V^{1.906}}$	0.54 ≤ V ≤ 4 (m/s)	(7.8)
US Customary Units		
$C_{Factor} = 132.1\phi^{0.0175} - 137.29\phi^{-0.112}e^{-0.102V^{1.907}}$	1.77 ≤ V ≤ 13.12 (ft/s)	(7.9)

Where: ϕ is diameter in inches; V is velocity m/s, (ft/s)

9.3 Forcemain Design Recommendations

1. The hydraulic effect of biofilms on forcemain flow resistance was evaluated and determined that hydraulic roughness parameters (k_s and C factor) varied with forcemain velocity. Although velocity was determined to be the principle factor affecting k_s and C factor; a comparison of the C factor results to k_s results show that C factor is dependent upon both velocity and diameter. Predictive equations developed to estimate k_s and C factor are summarized in Section 7.3 and include Equations 7.6a to 7.9. These equations should be utilized along with the Colebrook-White / Darcy-Weisbach and Hazen-Williams equations to estimate the friction headloss for forcemains.
2. It is crucial to design a forcemain system to be economical and to prevent permanent solids accumulation or air buildup. The most economical (optimal) diameter; self-cleansing (Tractive Force) design; particle transport through suspension and bed motion; and air clearing velocities should be evaluated during the design process to determine the critical parameter that controls

the selection of diameter and design velocity for a given system. Although a design particle of 1 mm (0.04 in.) is considered appropriate for typical domestic sewage, self-cleansing velocities should be selected based upon the design critical shear stress instead of particle size due to potential cohesion of particles and undulation that occurs along a typical forcemain profile. Utilizing a design shear stress of 0.08 lb/ft^2 (3.83 N/m^2) or 0.10 lb/ft^2 (4.80 N/m^2) provides a conservative estimate of the required self-cleansing velocity to achieve scour and transport of particles found in sewage given undulating pipelines and potential cohesive particles. Based upon the findings of this research, the minimum recommended design velocity should be at least 5 ft/s (1.5 m/s); this velocity corresponds to both the optimal diameter and self-cleansing velocity (Figure 8.26).

3. If the design particle is larger than 1 mm (0.04 in.), the forcemain should be designed considering bed motion to ensure transport of the design particle. The maximum upwards deflection should be limited to 30° unless the diameter of the rising limb is reduced to provide the equivalent solids transport capacity.
4. Forcemain design should also consider air clearing velocities to ensure transport of air and to prevent potential pipe corrosion.
5. Pipeline alignment and profile should be evaluated to determine the maximum vertical deflection angle (upwards and/or downwards) as this will affect the forcemains ability to transport sediment or clear air.
6. Although there appears to be numerous benefits for increasing the operating velocity of a forcemain, increased surge potential is a consequence of selecting a higher design velocity.

In many instances, a forcemain diameter could be oversized to provide a future maximum flowrate. Selecting a minimum velocity of 5 ft/s (1.5 m/s) may seem high compared to most design standards. However, based upon continuity, a 40% capacity increase is obtained by increasing the velocity from 5 ft/s (1.5 m/s) to 7 ft /s (2.1 m/s). A 40% capacity increase should be sufficient for most systems and can likely be accomplished by changing pump impellors.

9.4 Limitations and Recommendations for Further Work

1. This research was performed as a desktop analysis of forcemain systems using operational data obtained from SCADA systems, supplemented by data from published reports and technical papers. These results should be confirmed using field data on forcemains under a range of environmental conditions and flow regimes.
2. Hydraulic analyses were performed assuming an average wastewater temperature and clean water viscosity; effect of temperature and viscosity on the roughness parameters should be verified in future research.
3. The assumed maximum k_s value of 30 mm (1.2 in.) is likely too large and may require reduction; however, data collected and evaluated does not support reducing this assumed threshold. Future studies should further evaluate this in more detail to confirm or refine this assumption.
4. Further evaluate pipe material to determine if pipe material influences biofilm growth.
5. Due to the limited number of data points for velocities greater than 6.6 ft/s (2 m/s), additional field data should be collected for forcemains operating at velocities greater than 6.6 ft/s (2 m/s) in order to verify the assumed predicative equation(s) established for velocities between 6.50 ft/s $< V \leq$ 13.1 ft/s (1.98 m/s $< V \leq$ 4.0 m/s).
6. Relationships for bed motion transport in pipelines subjected to biofilms could not be found in the literature. Additional research should be conducted to identify maximum particle sizes found in forcemain systems and the effect of biofilms and cohesion on particle transport in forcemains.
7. Identify critical shear stress based upon cohesive properties and intermittent pump operation to determine the time between pumping cycles before cohesion impacts particle transport.
8. Physical measurements of the biofilm (slime layer) to determine how its structure varies with nutrient loadings, temperature, and source water chemistry. Additional consideration should

be given to daily, seasonal variations, and operational conditions to confirm the assumptions provided in this research.

9. Field measurements to determine the change in biofilm properties along the length of the forcemain.

References

Ackers, P. (1958). Resistance of fluids flowing in channels and pipes. In: Hydraulics Research Paper, No. 1, Her Majesty's Setationary Office, London, UK.

American Water Works Association (AWWA) (1989). Steel Pipe – A Guide for Design and Installation. Manual M11, Third Edition, AWWA, Denver, CO.

American Water Works Association (AWWA) (2002). PVC Pipe – Design and Installation. Manual M23, Second Edition, AWWA, Denver, CO.

American Water Works Association (AWWA) (2009). Ductile-Iron Pipe and Fittings. Manual M41, Third Edition, AWWA, Denver, CO.

Ashley, R. M. (1993). Cohesive sediment erosion and transport in sewers. InProc 5th Annual Seminar Scottish Hydraulics Study Group.

Barr, D. I. H. (1972). New forms of equations for the correlation of pipe resistance data. Technical Note, Institution of Civil Engineers (ICE), ICE Proceedings, Part 2: Research and Theory, 53(2):383–390, DOI: 10.1680/iicep.1972.5434.

Barr, D. I. H. (1981). Solutions of the Colebrook-White function for resistance to uniform turbulent flow. Technical Note, Institution of Civil Engineers (ICE), ICE Proceedings, Part 2: Research and Theory, 71(2):529-535, DOI: 10.1680/iicep.1981.1895.

Bhave, P. R., and Gupta, R. (2006). Analysis of Water Distribution Networks. Alpha Science International Ltd., Oxford, UK.

Bizier, P. (2007). Gravity sanitary sewer design and construction. ASCE.

Boon, A. G. (1995). Septicity in sewers: causes, consequences and containment. Water Science and Technology, 31(7), 237-253.

Bratland, O. (2009). Pipe Flow 1, Single-phase Flow Assurance. Chapter 2: Pipe Friction, Self-published E-book available at drbratland.com, pp. 21–92.

Butler, D., May, R. W. P., & Ackers, J. C. (1996). Sediment transport in sewers Part 1: background. Proceedings of the Institution of Civil Engineers-Water Maritime and Energy, 118(2), 103-112.

Butler, D., May, R., & Ackers, J. (2003). Self-Cleansing Sewer Design Based on Sediment Transport Principles. Journal of Hydraulic Engineering, 129(4), 276-282.

Chadwick, A., Morfett, J., and Borthwick, M. (2004). Hydraulics in Civil and Environmental Engineering. Fourth Edition, Spon Press, Taylor & Francis Group, London, UK.

Chapin, J. (2006). Municipal wastewater pump station design problems and solutions. Proceedings of the Water Environment Federation, 2006(11), 2158-2164.

Chen, N. H. (1979). An explicit equation for friction factor in pipe. Industrial & Engineering Chemistry Fundamentals, 18(3):296–297, DOI: 10.1021/i160071a019.

Chin, D. A. (2000). Water Supply Engineering. Prentice Hall, Upper Saddle River, NJ.

Chiueh, P. T., Lo, S. L., & Liao, P. Y. (1999). A Study of Self-Cleansing Velocity for Sanitary Sewer System Design. Journal of the Chinese institute of Environmental Engineering, 9(4), 285-292.

Christensen, B. A. (2000). Discussion of "Limitations and proper use of the Hazen-Williams equation." ASCE, Journal of Hydraulic Engineering, 126(2):169–170, DOI: 10.1061/(ASCE) 0733-9429(2000)126:2(167).

Churchill, S. W. (1973). Empirical expressions for the shear stress in turbulent flow in commercial pipe. American Institute of Chemical Engineers (AIChE), AIChE Journal, 19(2):375–376, DOI: 10.1002/aic.690190228.

Churchill, S. W. (1977). Friction factor equation spans all fluid flow regimes. Chemical Engineering, 84(24):91–92.

Colebrook, C. F., and White, C. M. (1937). The reduction of carrying capacity of pipes with age. Institution of Civil Engineers (ICE), Journal of the ICE, 7(1):99–118, DOI: 10.1680/ijoti.1937.14682.

Copeland, B., & O'Rourke, S. (2013). Low Velocities in Force Mains—Impacts and Solutions. Proceedings of the Water Environment Federation,2013(15), 2806-2819.

Copeland, B., & O'Rourke, S. (2014). Low Velocities in Force Mains—Impacts and Solutions. Proceedings of the Water Environment Federation,2014(4), 1-12.

Cowle, M., Samaras, V., & Rauen, W. B. (2012). A comparative analysis of the carbon footprint of large diameter concrete and HDPE pipes. Plastic Pipes XVI, Barcelona.

Cowle, M. W., Babatunde, A. O., Rauen, W. B., Bockelmann-Evans, B. N., & Barton, A. F. (2014). Biofilm development in water distribution and drainage systems: dynamics and implications for hydraulic efficiency. Environmental Technology Reviews, 3(1), 31-47.

Cowle, M. (2015). Assessing the impact of biofouling on the hydraulic efficiency of pipelines (Doctoral dissertation, Cardiff University).

Crabtree, R. W. (1989). Sediments in sewers. Water and Environment Journal, 3(6), 569-578.

Dawalt. http://www.slideshare.net/tdawalt/6-things-sewer-professionals-need-to-know-about-hydrogen-sulfide

Departments of the Army and the Air Force (1985) "Sanitary and Industrial Wastewater Collection—Pumping Stations and Force Mains": Army TM 5-814-2, Air Force AFM 88-11, Vol. 2.

Dettmer, A., (2014) Force Main Condition Assessment: New Technologies & Case Studies, Water Environment Association of Texas, CMOM Workshop.

Enfinger, K. L., & Mitchell, P. S. (2010). Tractive Force Design for Self-Cleansing of Sanitary Sewers: Evaluating Design Guidance Based on the Performance of Existing Sewers. Proceedings of the Water Environment Federation, 2010(12), 4970-4979.

Escarameia, M., Lauchlan, C. S., Gahan, C., & Dabrowski, C. (2004). Experimental and numerical studies on movement of air in water pipelines.

Escarameia, M. (2005). Air problems in pipelines: A design manual. HR Wallingford.

Escarameia, M. (2007). Investigating hydraulic removal of air from water pipelines. In Proceedings of the Institution of Civil Engineers-Water Management (Vol. 160, No. 1, pp. 25-34). Thomas Telford Ltd.

EPA. (1974) Process Design Manual for Sulfide Control in Sanitary Sewerage Systems; EPA-625/1-74-005; Washington, D.C.

EPA. (2000). Sewers, Force Main. Technology Fact Sheet.

Fang, X., Xua, Y., and Zhou, Z. (2011). New correlations of single-phase friction factor for turbulent pipe flow and evaluation of existing single-phase friction factor correlations. Nuclear Engineering and Design, 241(3):897–902, DOI: 10.1016/j. nucengdes.2010.12.019.

Farshad, F. F., and Rieke, H. (2006). Surface roughness design values for modern pipes. Society of Petroleum Engineers (SPE), SPE Drilling & Completion, 21(3):212–215, DOI: 10.2118/89040-PA.

Flemming, H. C. (2002). Biofouling in water systems–cases, causes and countermeasures. Applied microbiology and biotechnology, 59(6), 629-640.

Ghanbari, A., Farshad, F. F., and Rieke, H. H. (2011). Newly developed friction factor correlation for pipe flow and flow assurance. Journal of Chemical Engineering and Materials Science, 2(6):83–86.

Haaland, S. E. (1983). Simple and explicit formulas for the skim friction in turbulent pipe flow. American Society of Mechanical Engineers (ASME), Journal of Fluids Engineering, 105:89–90.

Hager, W. H. (2010). Wastewater hydraulics: Theory and practice. Springer Science & Business Media.

Haestad, M., Walski, M. T., Barnard, E. T., Harold, E., Merritt, B. L., Walker, N., & Whitman, E. B. (2004). Wastewater collection system modeling and design. Haestad Press, Waterbury CT.

Hudson, W. D. (1966). Studies of distribution system capacity in Seven Cities. Journal (American Water Works Association), 58(2):157–164, URL: http://www.jstor.org/ stable/41264657.

Idelchik, I. E. (2001). Handbook of Hydraulic Resistance. Third Edition.

Jacobs, K. (2012). How Does My Hydraulic Retention Time Affect Odor and Corrosion? Proceedings of the Water Environment Federation, 2012(16), 956-965.

Islander, R. L., Devinny, J. S., Mansfeld, F., Postyn, A., & Shih, H. (1991). Microbial ecology of crown corrosion in sewers. Journal of Environmental Engineering, 117(6), 751-770.

Jain, A. K. (1976). Accurate explicit equation for friction factor. ASCE, Journal of the Hydraulics Division, 102(5):674–677.

Johannessen, M., & Villalobos, J. L. (2014). C-Factor Testing as a Condition Assessment Tool for Wastewater Force Mains. In Pipelines 2014: From Underground to the Forefront of Innovation and Sustainability (pp. 1402-1411). ASCE.

Johnson, K. M., Ratnayaka, D. D., and Brandt, M. J. (2009). Thort's Water Supply. Sixth Edition, Elsevier Ltd., Burlington, MA.

Jones, G. M., Bosserman, B. E., Sanks, R. L., & Tchobanoglous, G. (Eds.). (2006). Pumping Station Design. Gulf Professional Publishing.

Kienow, K. (1989). Sulfide in Wastewater Collection and Treatment Systems. ASCE Manuals and Reports on Engineering Practice No. 69, ASCE, New York.

Lambert, M. F., Edwards, R. W. J., Howie, S. J., De Gilio, B. B., and Quinn, S. P. (2009). The impact of biofilm development on pipe roughness and velocity profile. In: S. Starrett (Ed.): ASCE, Proceedings of the World Environmental and Water Resources Congress 2009: Great Rivers, Kansas City, MO, May 17-21, pp. 122–134, DOI: 10.1061/41036(342)13.

Lamont, P. A. (1954). A review of pipe-friction data and formulae, with a proposed set of exponential formulae based on the theory of roughness. Institution of Civil Engineers (ICE), ICE Proceedings, Engineering Divisions, Part III, 3(2):248–275, DOI: 10.1680/ipeds.1954.12561.

Lamont, P. A. (1981). Common pipe flow formulas compared with the theory of roughness. Journal (American Water Works Association), 73(5):274–280, URL: http://www.jstor.org/stable/41271185.

Larsen, T., Arensman, M., & Nerup-Jensen, O. (2015). Including Pressure Measurements in Supervision of Energy Efficiency of Wastewater Pump Systems. Journal of Hydraulic Engineering, 142(2), 04015048.

Lauchlan, Christine, Forty, E.J., and May, R. (2004). Flow Resistance of Wastewater Pumping Mains Report SR 641. HR Wallingford.

Lauchlan, C., Forty E.J., & May, R. (2005). Flow resistance of wastewater pumping mains. Proceedings of the Institution of Civil Engineers-Water Management (Vol. 158, No. 2, pp. 81-88). Thomas Telford Ltd.

Liou, C. (1998). Limitations and proper use of the Hazen-Williams equation. ASCE, Journal of Hydraulic Engineering, 124(9):951–954, DOI: 10.1061/(ASCE)0733-9429(1998)124:9(951).

Lubbers, C. L., & Clemens, F. H. L. R. (2005). Air and gas pockets in sewerage pressure mains. Water science and technology, 52(3), 37-44.

Lubbers, C. L., & Clemens, F. H. L. R. (2005). Capacity reduction caused by air intake at wastewater pumping stations.(Experiments of transport of gas in pressurized wastewater mains.) Technical Report, Section of Sanitary Engineering, Faculty of Civil Engineering and Geosciences. Delft University of Technology, The Netherlands.

Lubbers, C. L., & Clemens, F. H. L. R. (2006). Breakdown of air pockets in downwardly inclined sewerage pressure mains. Water science and technology, 54(11-12), 233-240.

Lubbers, C. L. (2007). On gas pockets in wastewater pressure mains and their effect on hydraulic performance (Vol. 11). IOS Press.

Mak, G. (2011). Internal PCCP Force Main Deterioration Analysis and Rehabilitation. ASCE Pipelines Conference 2011.

Manadilli, G. (1997). Replace implicit equations with signomial functions. Chemical Engineering, 104(8):129–132.

May, R. W. P. (1993). Sediment transport in pipes, sewers and deposited beds.

May, R. W., Ackers, J. C., Butler, D., & John, S. (1996). Development of design methodology for self-cleansing sewers. Water Science and Technology, 33(9), 195-205.

May, R. W. (2001). Minimum self-cleansing velocities for inverted sewer siphons. In Proceedings of the Urban Drainage Modelling (UDM) Symposium, part of the World Water Resources & Environmental Resources Congress, edited by RW Brashear and C. Maksimovic, Orlando, Florida, USA.

McGovern, J. (2011). Technical Note: Friction Factor Diagrams for Pipe Flow.

McKeon, B. J., & Smits, A. J. (2002). Static pressure correction in high Reynolds number fully developed turbulent pipe flow. Measurement Science and Technology, 13(10), 1608.

McKeon, B. J., Li, J., Jiang, W., Morrison, J. F., & Smits, A. J. (2003). Pitot probe corrections in fully developed turbulent pipe flow. Measurement science and technology, 14(8), 1449.

Mckeon, B. J., Li, J., Jiang, W., Morrison, J. F., & Smits, A. J. (2004). Further observations on the mean velocity distribution in fully developed pipe flow. Journal of Fluid Mechanics, 501, 135-147.

McKeon, B. J., Zagarola, M. V., & Smits, A. J. (2005). A new friction factor relationship for fully developed pipe flow. Journal of fluid mechanics, 538, 429-443.

Melo, L. F., & Bott, T. R. (1997). Biofouling in water systems. Experimental thermal and fluid science, 14(4), 375-381.

Merritt, L. B. (2009). Tractive Force design for sanitary sewer self-cleansing. Journal of Environmental Engineering, 135(12), 1338-1347.

Metcalf, L., Eddy, H. P., & Tchobanoglous, G. (1991). Wastewater engineering: treatment, disposal, and reuse. McGraw-Hill, New York.

Miller, D. S. (1990). Internal Flow Systems. Second Edition, Gulf Publishing Company.

Molobela, I. P., & Ilunga, F. M. (2012). Impact of bacterial biofilms: the importance of quantitative biofilm studies. Annals of microbiology, 62(2), 461-467.

Momba, M. N., & Makala, N. (2004). Comparing the effect of various pipe materials on biofilm formation in chlorinated and combined chlorine-chloraminated water systems. Water SA, 30(2), 175-182.

Monty, J. P. (2005). Developments in smooth wall turbulent duct flows. University of Melbourne, Department of Mechanical and Manufacturing Engineering.

Moody, L. F. (1944). Friction factors for pipe flow. American Society of Mechanical Engineers (ASME), Transactions of the ASME, 66(8):671–684.

Moody, L. F. (1947). An approximate formula for pipe friction factors. American Society of Mechanical Engineers (ASME), Transactions of the ASME, 69:1005–1006.

Morrison, J. F., McKeon, B. J., Jiang, W., & Smits, A. J. (2004). Scaling of the streamwise velocity component in turbulent pipe flow. Journal of Fluid Mechanics, 508, 99-131.

Murray, D., Carroll, C., & Higgins, M. (2009). Evaluating in-service force mains with air pocket and leak detection technology. In Pipelines 2009: Infrastructure's Hidden Assets (pp. 499-507). ASCE.

Nagib, H. M., & Chauhan, K. A. (2008). Variations of von Kármán coefficient in canonical flows. Physics of Fluids, 20(10), 1518.

Nalluri, C., & Alvarez, E. M. (1992). The influence of cohesion on sediment behaviour. Water science and technology, 25(8), 151-164.

Nalluri, C., & Ghani, A. A. (1996). Design options for self-cleansing storm sewers. Water Science and Technology, 33(9), 215-220.

Nielsen, A., et al. "Simulation of sulfide buildup in wastewater and atmosphere of sewer networks." Water Science & Technology 52.3 (2005): 201-208.

Nielsen, A. H., Vollertsen, J., Jensen, H. S., Wium-Andersen, T., & Hvitved-Jacobsen, T. (2008). Influence of pipe material and surfaces on sulfide related odor and corrosion in sewers. Water research, 42(15), 4206-4214.

Nikora, V. (2010). Hydrodynamics of aquatic ecosystems: an interface between ecology, biomechanics and environmental fluid mechanics. River Research and Applications, 26(4), 367-384.

Nowell, A. R. M. and Church, M. (1979). Turbulent flow in a depth-limited boundary layer. Journal of Geophysical research, 84(C8), pp. 4816-4824.

Ohashi, A., & Harada, H. (1994). Adhesion strength of biofilm developed in an attached-growth reactor. Water Science and Technology, 29(10-11), 281-288.

Österlund, J. M., Johansson, A. V., Nagib, H. M., & Hites, M. H. (2000). A note on the overlap region in turbulent boundary layers. Physics of Fluids (1994-present), 12(1), 1-4.

Papa, F., & Radulj, D. (2013). Canada takes a lead in benchmarking pump energy efficiency. Water 21, 30-33.

Percival, S. L., Knapp, J. S., Wales, D. S., & Edyvean, R. G. J. (1999). The effect of turbulent flow and surface roughness on biofilm formation in drinking water. Journal of industrial Microbiology and Biotechnology, 22(3), 152-159.

Pereira, M. O., Kuehn, M., Wuertz, S., Neu, T., & Melo, L. F. (2002). Effect of flow regime on the architecture of a Pseudomonas fluorescens biofilm.Biotechnology and bioengineering, 78(2), 164-171.

Perkins, S. C. T., Henderson, A. D., Walker, J. M., Sargison, J. E., & Li, X. L. (2014). The influence of bacteria-based biofouling on the wall friction and velocity distribution of hydropower pipes. Australian Journal of Mechanical Engineering, 12(1), 77-88.

Perry, A. E., & Abell, C. J. (1975). Scaling laws for pipe-flow turbulence. Journal of Fluid Mechanics, 67(02), 257-271.

Picologlou, B. F., Characklis, W. G., and Zelver, N. (1980). Biofilm growth and hydraulic performance. ASCE, Journal of the Hydraulics Division, 106(5):733–746.

Pomeroy, R. D. (1990). The problem of hydrogen sulphide in sewers. Clay Pipe Development Association. Ltd., London, 2nd edition (edited by A. G. Boon), 1990, 24.

Pons, M. N., Spanjers, H., Baetens, D., Nowak, O., Gillot, S., Nouwen, J., & Schuttinga, N. (2004). Wastewater characteristics in Europe-A survey. European Water Management Online, 4, 10-p.

Pothof, I., & Clemens, F. H. L. R. (2008). On gas transport in downward slopes of sewerage mains. In 11th International Conference on Urban Drainage. Edinburgh, Scotland. United Kingdom (p. 11).

Pothof, I. W. M., Tukker, M., Kooij, K., & Clemens, F. H. L. R. (2011). Guidelines on capacity reducing gas pockets in wastewater mains. In Proceedings of the 11th International Conference on Computing and Control for the Water Industry, Exeter, UK, 5-9 September, 2011; authors version. Centre for water Systems, University of Exeter.

Pozos-Estrada, O., Fuentes-Mariles, O. A., & Pozos-Estrada, A. (2012). Gas pockets in a wastewater rising main: a case study. Water Science and Technology, 66(10), 2265-2274.

Pozos, O. E. (2007). Investigation on the effects of entrained air in pipelines. Germany: Universität Stuttgart. PhD Thesis http://elib. uni-stuttgart. de/opus/frontdoor.

Pozos, O.E., Fuentes, O., Sanchez, A., De Luna, F., and Rodal, E. (2015). Hydraulic Analysis Of Gas Pockets In Wastewater Rising Mains. 36th IAHR World Congress, Netherlands.

Rennels, D. C., and Hudson, H. M. (2012). Pipe Flow: A Practical and Comprehensive Guide. Wiley.

Reynolds, A. J. (1974). Turbulent flows in engineering. J. Wiley.

Ristenpart, E., & Uhl, M. (1993). Behaviour and pollution of sewer sediments. In Sixth ICUSD Conference, Niagara Falls (pp. 748-753).

Romeo, E., Royo, C., and Monzón, A. (2002). Improved explicit equations for estimation of the friction factor in rough and smooth pipes. Chemical Engineering Journal, 86(3):369–374, DOI: 10.1016/S1385-8947(01)00254-6.

Round, G. F. (1980). An explicit approximation for the friction factor – Reynolds number relation for rough and smooth pipes. The Canadian Journal of Chemical Engineering, 58(1):122–123, DOI: 10.1002/cjce.5450580119.

Saleh, O. A. B., Durst, F., Ünsal, B., Hodgson, A. W., Mischler, S., Rechenberg, B. V., & Virtanen, S. (2005). Fully developed turbulent smooth and rough channel and pipe flows (Doctoral dissertation, PhD thesis, University of Erlangen-Nuremberg, Erlangen, Germany).

Schlichting, H. (1979). Boundary Layer Theory New York., New York.: McGraw-Hill.

Schultz, M. P. and Swain, G. W. (1999). The effect of biofilms on turbulent boundary layers. Journal of Fluids engineering, 121, pp. 1-22.

Schultz, M. P. (2000). Turbulent boundary layers on surfaces covered with filamentous algae. Transactions of the ASME, Journal of Fluids Engineering, 122(2), pp. 357-363.

Schultz, M. and Flack, K. (2005). Outer layer similarity in fully rough turbulent boundary layers. Experiments in fluids, 38(3), pp. 328-340.

Shirazi, R. H. S. M., Campisano, A., Modica, C., & Willems, P. (2014). Modelling the erosive effects of sewer flushing using different sediment transport formulae. Water Science and Technology, 69(6), 1198-1204.

Shockling, M. A., Allen, J. J., & Smits, A. J. (2006). Roughness effects in turbulent pipe flow. Journal of Fluid Mechanics, 564, 267-285.

Simões, M., Pereira, M. O., Sillankorva, S., Azeredo, J., & Vieira, M. J. (2007). The effect of hydrodynamic conditions on the phenotype of Pseudomonas fluorescens biofilms. Biofouling, 23(4), 249-258.

Simões, L. C., Simões, M., & Vieira, M. J. (2010). Adhesion and biofilm formation on polystyrene by drinking water-isolated bacteria. Antonie Van Leeuwenhoek, 98(3), 317-329.

Skipper, G. N., Occiano, V., Sen, S., Wong, P., & Smoczynski, M. (2013). … Excuse Me… My Force Main Has Gas. Proceedings of the Water Environment Federation, 2013(10), 5436-5451.

Sonnad, J. R., and Goudar, C. T. (2006). Turbulent flow friction factor calculation using a mathematically exact alternative to the Colebrook–White equation. ASCE, Journal of Hydraulic Engineering, 132(8):863–867, DOI: 10.1061/(ASCE)0733-9429(2006) 132: 8(863).

Stoodley, P., Dodds, I., Boyle, J. D., & Lappin-Scott, H. M. (1998). Influence of hydrodynamics and nutrients on biofilm structure. Journal of applied microbiology, 85(S1).

Stoodley, P., Lewandowski, Z., Boyle, J. D., & Lappin-Scott, H. M. (1998). Oscillation characteristics of biofilm streamers in turbulent flowing water as related to drag and pressure drop. Biotechnology and bioengineering, 57(5), 536-544.

Stoodley, P., Cargo, R., Rupp, C. J., Wilson, S., & Klapper, I. (2002). Biofilm material properties as related to shear-induced deformation and detachment phenomena. Journal of Industrial Microbiology and Biotechnology, 29(6), 361-367.

Stuetz, R., & Frechen, F. B. (Eds.). (2001). Odours in wastewater treatment: measurement, modelling and control. IWA publishing.

Swamee, P. K., and Jain, A. K. (1976). Explicit equations for pipe-flow problems. ASCE, Journal of the Hydraulics Division, 102(5):657–664.

Tchobanoglous, G., Franklin, L.B., & Stensel, H. D. (2003). Wastewater engineering: treatment and reuse. Edition 4th. Metcalf and Eddy Inc.

Teng, F., Guan, Y. T., & Zhu, W. P. (2008). Effect of biofilm on cast iron pipe corrosion in drinking water distribution system: corrosion scales characterization and microbial community structure investigation. Corrosion science, 50(10), 2816-2823.

Teodósio, J. S., Simões, M., Melo, L. F. and Mergulhão, F. J. (2010). Flow cell hydrodynamics and their effects on E. coli biofilm formation under different nutrient conditions and turbulent flow. Biofouling, 27(1), pp. 1-11.

Thomson, J. C., Morrison, R. S., & Sangster, T. (2010). Inspection Guidelines for Wastewater Force Mains. Water Intelligence Online, 9, 9781843392866.

Travis, Q., and Mays, L. (2007). Relationship between Hazen–William and Colebrook–White roughness values. ASCE, Journal of Hydraulic Engineering, 133(11):1270–1273, DOI: 10.1061/(ASCE)0733-9429(2007)133:11(1270).

Tullis, J. P. (1989). Hydraulics of Pipelines Pumps, Valves, Cavitation, and Transients. John Wiley & Sons, New York, NY.

Vieira, M. J., Melo, L. F., & Pinheiro, M. M. (1993). Biofilm formation: hydrodynamic effects on internal diffusion and structure. Biofouling, 7(1), 67-80.

Vignaga, E. (2012). The effect of biofilm colonization on the stability of non-cohesive sediments (Doctoral dissertation, University of Glasgow).

Wagner, T. B., & Jennifer Steffens, P. E. (2014). What's In The Numbers? A Review and Analysis of More Than 400 Miles of Force Main Inspection and Condition Assessment Data. Proceedings of the Water Environment Federation, 2014(4), 1-10.

Walker, J. M., Sargison, J. E., & Henderson, A. D. (2013). Turbulent boundary-layer structure of flows over freshwater biofilms. Experiments in fluids, 54(12), 1-17.

Walker, J. M. (2014). The application of wall similarity techniques to determine wall shear velocity in smooth and rough wall turbulent boundary layers. Journal of Fluids Engineering, 136(5), 051204.

Walski, T. M. (1984). Analysis of Water Distribution Systems. Van Nostrand Reinhold Company, New York, NY.

Walski, T. M., Barnhart, T. S., Driscoll, J. M., & Yencha, R. M. (1994). Hydraulics of corrosive gas pockets in force mains. Water Environment Research, 66(6), 772-778.

Walski, T. M., Sharp, W. W., and Shields Jr, F. D. (1988). Predicting Internal Roughness in Water Mains. Miscellaneous Paper EL-88-2, U. S. Army Engineer Waterways Experiment Station, Environmental Laboratory, Vicksburg, MS; available from National Technical Information Service, Springfield, VA.

Walski, T. M., Chase, D. V., & Savic, D. A. (2001). Water distribution modeling.

Ward, M., Bott, C., Sparks, J., & Easter, C. (2012). Characterization of Methane Generation and Emissions from a Wastewater Force Main.Proceedings of the Water Environment Federation, 2012(16), 897-925.

Wastewater Committee of the Great Lakes - Upper Mississippi River Board of State and Provincial Public Health and Environmental Managers. (2014). Recommended Standards for Wastewater facilities - Policies for the design, review and approval of plans and specifications for wastewater collection and treatment facilities. New York: Health Research Inc., Health Education Services Division.

White, F. M. (1998). Fluid Mechanics. Fourth Edition, McGraw Hill, New York, NY.

Wilson, K.C, & Tse, J.K.P. (1984). Deposition limit for coarse-particle transport in inclined pipes. Proc. Hydrotransport 9, BHRA Fluid Engineering, Cranfield, UK. pp. 149-169.

Wilson, K. C., Addie, G. R., Sellgren, A., & Clift, R. (2006). Slurry transport using centrifugal pumps. Springer Science & Business Media.

Wood, D. J. (1966). An explicit friction factor relationship. Civil Engineering, 36(12):60–61.

Wosnik, M., Castillo, L., & George, W. K. (2000). A theory for turbulent pipe and channel flows. Journal of Fluid Mechanics, 421, 115-145.

Wu, Y., & Christensen, K. T. (2007). Outer-layer similarity in the presence of a practical rough-wall topography. Physics of Fluids, 19(8), 85108-85108.

Zagarola, M. V. and Smits, A. J. (1998). Mean-flow scaling of turbulent pipe flow. Journal of Fluid Mechanics, 373, pp. 33-79.

Zanoun, E. S., Durst, F., & Nagib, H. (2003). Evaluating the law of the wall in two-dimensional fully developed turbulent channel flows. Physics of Fluids, 15(10), 3079-3089.

Zanoun, E. S., Durst, F., Bayoumy, O., & Al-Salaymeh, A. (2007). Wall skin friction and mean velocity profiles of fully developed turbulent pipe flows.Experimental Thermal and Fluid Science, 32(1), 249-261.

Zigrang, D. J., and Sylvester, N. D. (1982). Explicit approximations to the solution of Colebrook's friction factor equation. American Institute of Chemical Engineers (AIChE), AIChE Journal, 28(3):514–515, DOI: 10.1002/aic.690280323.

Zloczower, N. (2010). Reduction of damage and hindrance to wastewater transmission systems caused by air pockets by deployment of air valves. Pipelines 2010: Climbing New Peaks to Infrastructure Reliability: Renew, Rehab, and Reinvest (pp. 449-462). ASCE.

Additional Reading

Andrewartha, J. M., Sargison, J. E., and Perkins, K. J. (2008). The influence of freshwater biofilms on drag in hydroelectric power schemes. World Scientific and Engineering Academy and Society (WSEAS), *WSEAS Transactions on Fluid Mechanics*, 3(3):201–206.

Blasius, P. R. H. (1913). Das Aehnlichkeitsgesetz bei Reibungsvorgangen in Flüssigkeiten. *Forschungsheft,* 131:1–41.

Bombardelli, F. A., and García, M. H. (2003). Hydraulic design of large-diameter pipes. ASCE, *Journal of Hydraulic Engineering*, 129(11):839–846, DOI: 10.1061/(ASCE)0733-9429(2003)129:11(839).

Chen, J. J. J. (1984). A simple explicit formula for the estimation of pipe friction factor. Technical Note, Institution of Civil Engineers (ICE), *ICE Proceedings, Part 2: Research and Theory*, 77(1):49–55, DOI: 10.1680/iicep.1984.1272.

Chin, D. A. (1999). Water Resources Engineering. Prentice Hall, Upper Saddle River, NJ.

Colebrook, C. F. (1939). Turbulent flow in pipes, with particular reference to the transition region between the smooth and rough pipe laws. Institution of Civil Engineers (ICE), *Journal of the ICE*, 11(4):133–156, DOI: 10.1680/ijoti.1939.13150.

Darcy, H. (1857). Recherches Experimentales Relatives au Mouvement de L'Eau dans les Tuyaux (Experimental Research Relating to the Movement of Water in Pipes). 2 Volumes, Mallet-Bachelier, Paris, France, 268 pp. + atlas.

Genić, S., Aranđelović, I., Kolendić, P., Jarić, M., Budimir, N., and Genić, V. (2011). A review of explicit approximations of Colebrook's equation. Faculty of Mechanical Engineering (FME), *FME Transactions*, 39(2):67–71.

Lamont, P. A. (1969). The choice of the pipe flow laws for practical use. *Water and Water Engineering*, 875(73):55-63.

Larson, T. E. (1955). Report on loss in carrying capacity of water mains. *Journal (American Water Works Association)*, 47(11):1061–1072, URL: http://www.jstor.org/stable /41253654.

Nikuradse, J. (1932). Gesetzmäßigkeit der turbulenten Strömung in glatten Rohren. *Forsch. Arb. Ing.-Wes.*, No. 356.

Poiseuille, J. L. M. (1840a). Recherches expérimentales sur le mouvement des liquides dans les tubes de très petits diamètres – I. Influence de la pression sur la quantité de liquide qui traverse les tubes de très petits diamètres. *C. R. Acad. Sci.*, 11:961–967.

Poiseuille, J. L. M. (1840b). Recherches expérimentales sur le mouvement des liquides dans les tubes de très petits diamètres – II. Influence de la longueur sur la quantité de liquide qui traverse les tubes de très petits diametres; III. Influence du diamètre sur la quantité de liquide qui traverse les tubes de très petits diamètres. *C. R. Acad. Sci*., 11:1041–1048.

Poiseuille, J. L. M. (1846). Recherches expérimentales sur le mouvement des liquides dans les tubes de très-petits diamètres. In: Memoires presentés par divers savants à l'Académie Royale des Sciences de l'Institut de France, IX:433–544.

Prandtl, L. (1935). The mechanics of viscous fluids. In: W.F, D. (Ed.) Aerodynamic Theory III. Springer, Berlin, Germany.

Reynolds, O. (1883). An experimental investigation of the circumstances which determine whether the motion of water shall be direct or sinuous and of the law of resistance in parallel channel. *Philosophical Transactions of the Royal Society*, 174:935–982.

Stanton, T. E., and Pannell, J. R. (1914). Similarity of motion in relation to surface friction of fluids. *Philosophical Transactions of the Royal Society of London, Series A*, 214:199–224, URL: http://www.jstor.org/stable/91017.

Weisbach, J. (1845). Lehrbuch der Ingenieur- und Maschinen-Mechanik, Braunschweig.

APPENDIX A Explicit Friction Factor Equations

Table A.1: Explicit Friction Coefficient Equations

Authors	Explicit Friction Coefficient Equation	Range of Validity		Reported Accuracy Compared to *Colebrook-White*
		R_e	k_s	
Moody (1947)	$f = 0.0055\left[1 + \left(20000\left(\frac{k_s}{D}\right) + \left(\frac{10^6}{R_e}\right)\right)^{1/3}\right]$	$4x10^3 \le R_e \le 10^8$	$0 \le \frac{k_s}{D} \le 0.01$	± 5%
Jain (1976)	$\frac{1}{\sqrt{f}} = -2\log\left[\frac{k_s}{3.715D} + \left(\frac{6.943}{R_e}\right)^{0.9}\right]$	$5x10^3 \le R_e \le 10^7$	$4x10^{-5} \le \frac{k_s}{D} \le 0.05$	±1%
Swamee and Jain (1976)	$f = \frac{0.25}{\left[\log\left(\frac{k_s}{3.7D} + \frac{5.74}{R_e^{0.9}}\right)\right]^2}$	$4x10^3 \le R_e \le 10^8$	$10^{-5} \le \frac{k_s}{D} \le 0.05$	±1%
Churchill (1973)	$\frac{1}{\sqrt{f}} = -2\log\left[\frac{k_s}{3.7D} + \left(\frac{7}{R_e}\right)^{0.9}\right]$	Not Reported	Not Reported	3%
Churchill (1977)	$f = 8\left[\left(\frac{8}{R_e}\right)^{12} + \frac{1}{(A+B)^{1.5}}\right]^{1/12}$ $A = \left\{2.457ln\left[\frac{1}{\left(\frac{7}{R_e}\right)^{0.9} + \left(\frac{0.27k_s}{D}\right)}\right]\right\}^{16}$ $B = \left(\frac{37530}{R_e}\right)^{16}$	$R_e > 0$	Not Reported	± 0.45 %
Chen (1979)	$\frac{1}{\sqrt{f}} = -2\log\left\{\frac{k_s}{3.7065D} - \left(\frac{5.0452}{R_e}\right)\log\left[\left(\frac{\left(k_s/D\right)^{1.1098}}{2.8257}\right) + \left(\frac{5.8506}{R_e^{0.8981}}\right)\right]\right\}$	$4x10^3 \le R_e \le 4x10^8$	$10^{-7} \le \frac{k_s}{D} \le 0.05$	1.2%
Barr (1981)	$\frac{1}{\sqrt{f}} = -2\log\left\{\frac{k_s}{3.7D} + \frac{4.518\log\left(\frac{R_e}{7}\right)}{R_e\left(1 + \frac{R_e^{0.52}}{29}\left(\frac{k_s}{D}\right)^{0.7}\right)}\right\}$	Not Reported	Not Reported	1.2%

Authors	Explicit Friction Coefficient Equation	Range of Validity		Reported Accuracy Compared to *Colebrook-White*
		R_e	k_s	
Haaland (1983)	$\frac{1}{\sqrt{f}} = -1.8\log\left[\left(\frac{k_s}{3.7D}\right)^{1.11} + \frac{6.9}{R_e}\right]$	$4\text{x}10^3 \leq R_e \leq 10^8$	$10^{-6} \leq \frac{k_s}{D} \leq 0.05$	1.2%
Zigrang and Sylvester (1982)	$\frac{1}{\sqrt{f}} = -2\log\left\{\frac{k_s}{3.7D} - \left(\frac{5.02}{R_e}\right)\log\left[\frac{k_s}{3.7D} - \left(\frac{5.02}{R_e}\right)\log\left(\frac{k_s}{3.7D} + \frac{13}{R_e}\right)\right]\right\}$	Not Reported	Not Reported	± 0.33%
Manadilli (1997)	$\frac{1}{\sqrt{f}} = -2\log\left[\frac{k_s}{3.7D} + \frac{95}{R_e^{0.983}} - \frac{96.82}{R_e}\right]$	$5.235\text{x}10^3 \leq R_e \leq 10^8$	$0 \leq \frac{k_s}{D} \leq 0.05$	
Romeo et al. (2002)	$\frac{1}{\sqrt{f}} = -2\log\left[\frac{k_s}{3.7065D} - \frac{5.0272}{R_e}log\left[\frac{k_s}{3.827D} - \frac{4.567}{R_e}\log\left\{\left(\frac{k_s}{7.7918D}\right)^{0.9924} + \left(\frac{5.3326}{208.815 + R_e}\right)^{0.9345}\right\}\right]\right]$	$3\text{x}10^3 \leq R_e \leq 1.5\text{x}10^8$	$0 \leq \frac{k_s}{D} \leq 0.05$	1.2%
Sonnad and Goudar (2006)	$\frac{1}{\sqrt{f}} = 0.8686ln\left[\frac{0.4587R_e}{S^{(S/(S+1))}}\right] \quad S = 0.1240\frac{k_s}{D}R_e + ln(0.4587R_e)$	$4\text{x}10^3 \leq R_e \leq 10^8$	$10^{-6} \leq \frac{k_s}{D} \leq 0.05$	
Wood (1966)	$f = 0.53\frac{k_s}{D} + 0.094\left(\frac{k_s}{D}\right)^{0.225} + 88\left(\frac{k_s}{D}\right)^{0.44} R_e^{-1.62\left(\frac{k_s}{D}\right)^{0.134}}$	$4\text{x}10^3 \leq R_e \leq 5\text{x}10^7$	$10^{-5} \leq \frac{k_s}{D} \leq 0.04$	-4 to 6%
Round (1980)	$\frac{1}{\sqrt{f}} = -1.8\log\left[0.135\left(\frac{k_s}{D}\right) + \frac{6.5}{R_e}\right]$	$4\text{x}10^3 \leq R_e \leq 4\text{x}10^8$	$0 \leq \frac{k_s}{D} \leq 0.05$	
Ghanbari *et al*. (2011)	$f = \left(-1.52\log\left(\left(\frac{k_s}{7.21D}\right)^{1.042} + \left(\frac{2.731}{R_e}\right)^{0.9152}\right)\right)^{-2.169}$	$2.1\text{x}10^3 \leq R_e \leq 10^8$	$0 \leq \frac{k_s}{D} \leq 0.05$	

APPENDIX B Comparison of Explicit Friction Factor Equations

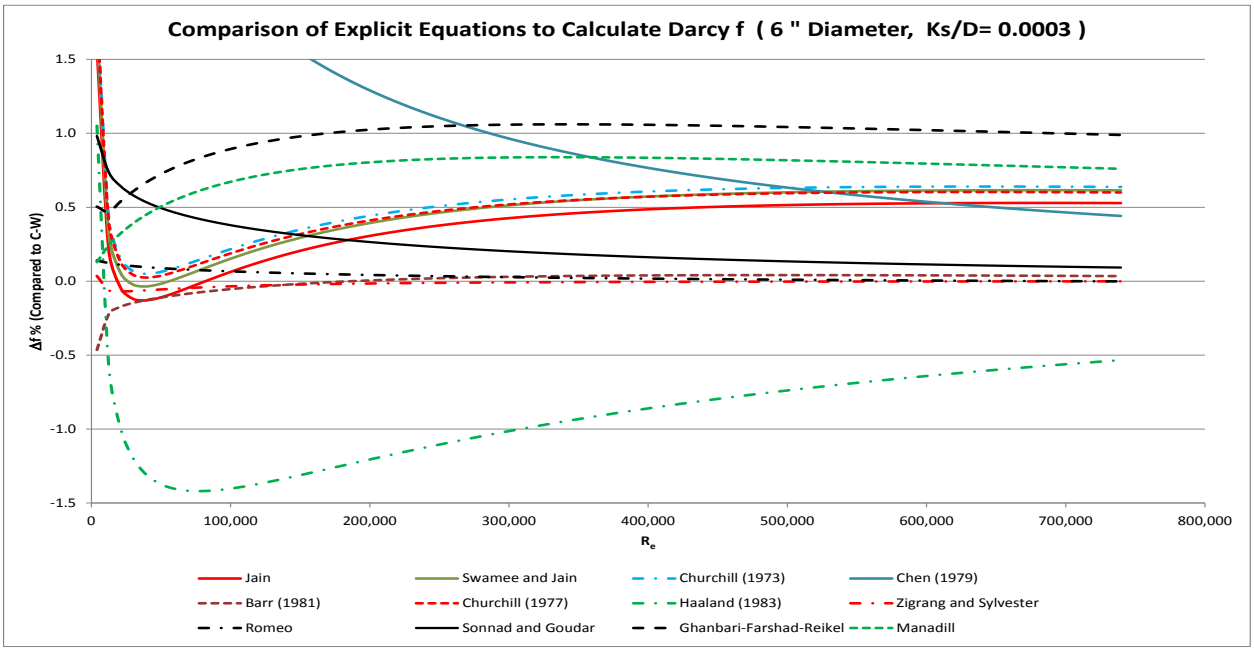

Figure B.1: Comparison of Explicit Equations to Calculate Darcy f (k_s/D = 0.0003)

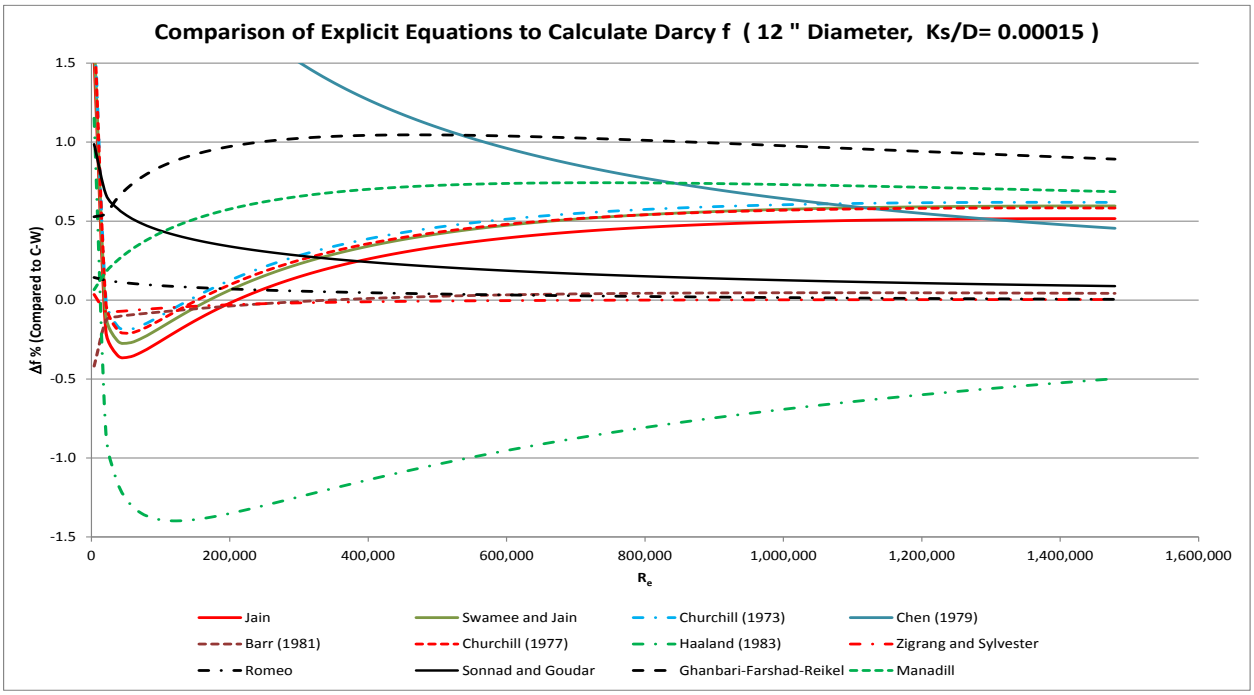

Figure B.2: Comparison of Explicit Equations to Calculate Darcy f (k_s/D = 0.00015)

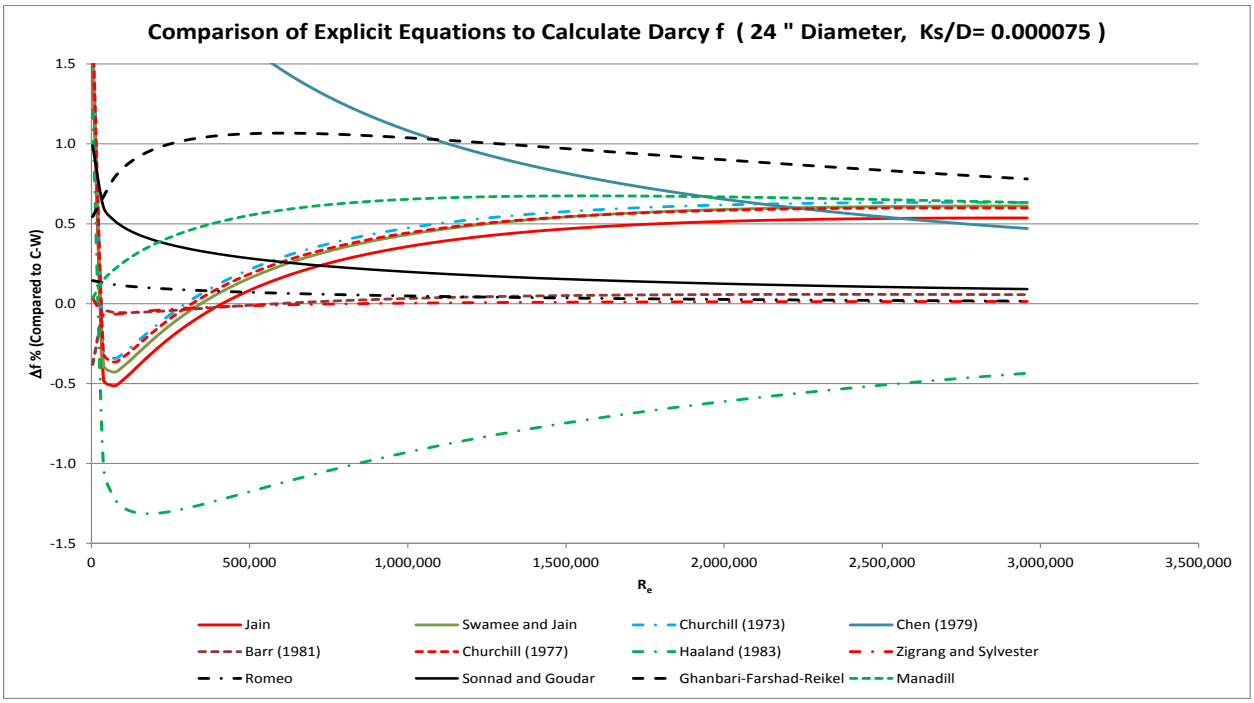

Figure B.3: Comparison of Explicit Equations to Calculate Darcy f (k_s/D = 0.000075)

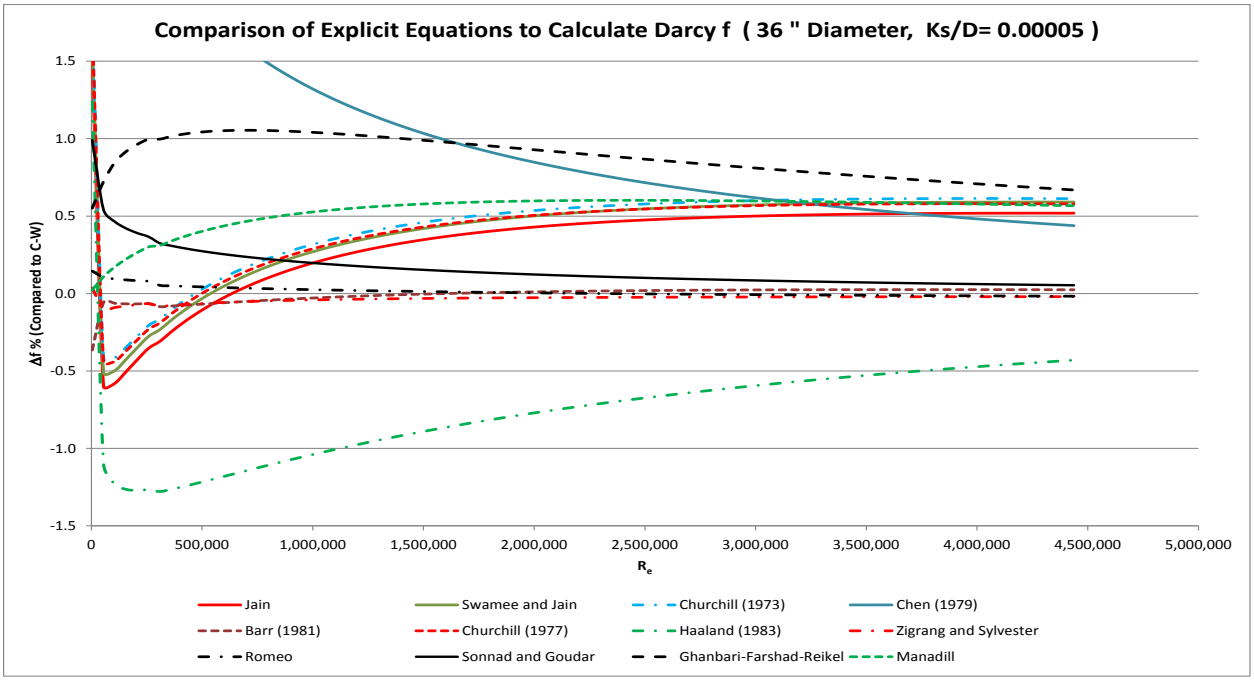

Figure B.4: Comparison of Explicit Equations to Calculate Darcy f (k_s/D = 0.00005)

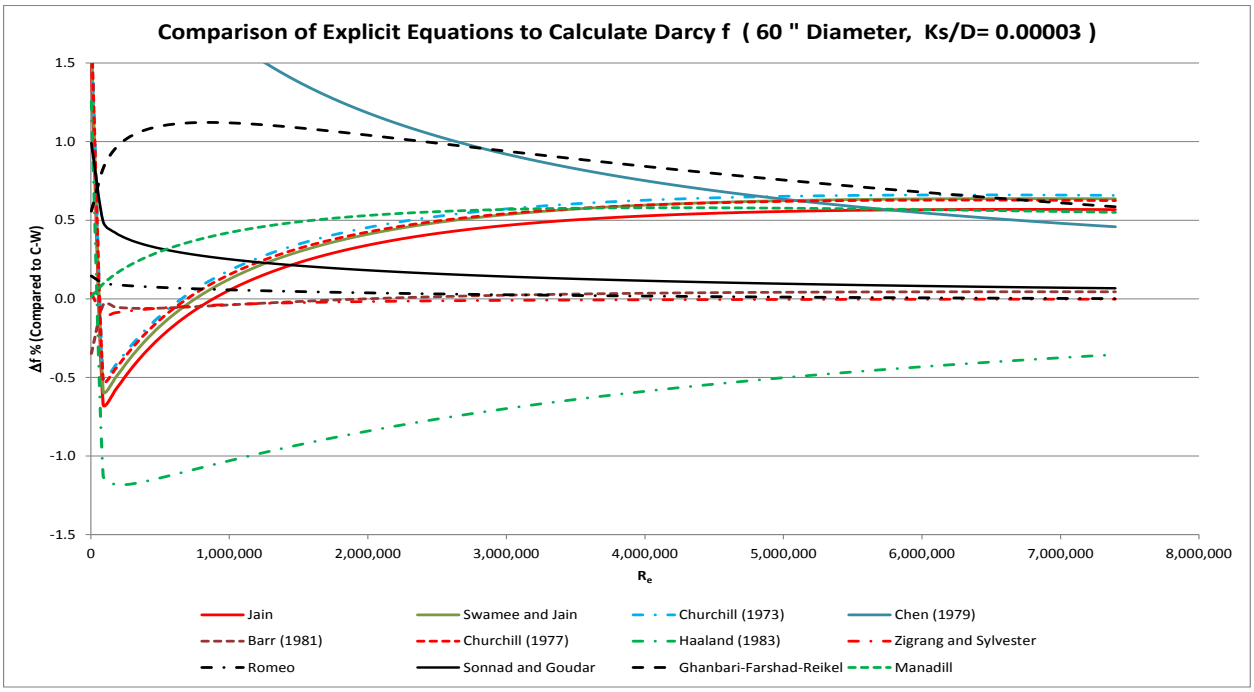

Figure B.5: Comparison of Explicit Equations to Calculate Darcy f (k_s/D = 0.00003)

APPENDIX C Pipe Data

Table C.1: PVC Pipe Data

Nominal Diameter (in)	Internal Diameter (in) Pressure Class (psi) 165 (DR25)	125 (DR32.5)	100 (DR41)
4	4.39	----	----
6	6.31	----	----
8	8.28	----	----
10	10.16	----	----
12	12.08	----	----
14	14	14.3	14.52
16	15.92	16.27	16.51
18	17.85	18.23	18.5
20	19.77	20.19	20.49
24	23.61	24.12	24.48
30	29.29	29.91	30.35
36	35.05	35.8	36.3
42	40.73	41.6	42.18
48	46.49	47.49	4814

http://www.jmeagle.com

AWWA C900/ C905 PVC pipe

Table C.2: Ductile Iron / Cast Iron Pipe Data

			Internal Diameter (in)		
Nominal Diameter (in)	Outside Diameter (in)	Wall Thickness (in)	Interior Diameter (No lining)	Cement Mortar Lining Thickness (in)	Interior Diameter (CML) [5]
3 [1]	3.96	0.25	3.46	0.0625	3.335
4 [1]	4.8	0.25	4.3	0.0625	4.175
6 [1]	6.9	0.25	6.4	0.0625	6.275
8 [1]	9.05	0.25	8.55	0.0625	8.425
10 [1]	11.1	0.26	10.58	0.0625	10.455
12 [1]	13.2	0.28	12.64	0.09375	12.4525
14 [2]	15.3	0.28	14.74	0.09375	14.5525
16 [2]	17.4	0.3	16.8	0.09375	16.6125
18 [2]	19.5	0.31	18.88	0.09375	18.6925
20 [2]	21.6	0.33	20.94	0.09375	20.7525
24 [3]	25.8	0.33	25.14	0.09375	24.9525
30 [4]	32.0	0.34	31.32	0.125	31.07
36 [4]	38.3	0.38	37.54	0.125	37.29
42 [4]	44.5	0.41	43.68	0.125	43.43
48 [4]	50.8	0.46	49.88	0.125	49.63
54 [4]	57.56	0.51	56.54	0.125	56.29
60 [4]	61.61	0.54	60.53	0.125	60.28
64 [4]	65.67	0.56	64.55	0.125	64.3

Adapted from www.uspipe.com

[1] 350 psi Pressure Class
[2] 250 psi Pressure Class
[3] 200 psi Pressure Class
[4] 150 psi Pressure Class
[5] CML – Cement Mortar Lining

Table C.3: HDPE – DIPS PE4710 Pipe Data

Nominal Diameter (in)	Internal Diameter (in) Pressure Class (psi)		
	125 (DR17)	111 (DR19)	100 (DR21)
4	4.202	4.264	4.315
6	6.039	6.130	6.203
8	7.922	8.041	8.136
10	9.716	9.862	9.979
12	11.555	11.727	11.867
14	13.392	13.593	13.755
16	15.229	15.458	15.643
18	17.068	17.325	17.531
20	18.905	19.190	19.419
24	22.582	22.921	23.195
30	28.014	28.430	28.769
36	33.524	34.026	34.433
42	38.950	39.535	40.008
48	44.465	45.131	45.672

Adapted from http://www.jmeagle.com

DIPS - Ductile Iron Pipe Sizes

Table D.1: Research Data – Results of Hydraulic Calculations

Project	Pipe Material	Pipe Length (ft)	I.D. (in)	Velocity		friction factor f	Headloss		Minor loss % of Total	R_e	k_s (in)	k_s (mm)	C-Factor	U* (m/s)	Shear Stress τ_o	
				(ft/s)	(m/s)		$h_{l\ f\ (}$ft)	$h_{l\ total}$ (ft)							(lb/ft²)	(N/m²)
Janitell	PVC	783.8	4.00	2.12	0.65	0.19	31.77	32.03	0.8%	6.18E+04	1.07	27.20	43.7	0.10	0.21	10.09
Janitell	PVC	783.8	4.00	2.33	0.71	0.15	29.84	30.16	1.0%	6.77E+04	0.76	19.23	49.6	0.10	0.20	9.48
Janitell	PVC	783.8	4.00	2.46	0.75	0.13	28.08	28.43	1.2%	7.15E+04	0.58	14.80	54.0	0.09	0.19	8.92
Janitell	PVC	783.8	4.00	2.22	0.68	0.17	30.29	30.58	0.9%	6.45E+04	0.89	22.66	46.8	0.10	0.20	9.62
Janitell	PVC	783.8	4.00	1.77	0.54	0.30	34.54	34.72	0.5%	5.15E+04	1.81	46.07	34.8	0.10	0.23	10.97
Janitell	PVC	783.8	4.00	1.41	0.43	0.52	38.05	38.16	0.3%	4.10E+04	3.01	76.39	26.3	0.11	0.25	12.08
Janitell	PVC	783.8	4.00	2.31	0.70	0.16	30.96	31.27	1.0%	6.70E+04	0.82	20.93	48.1	0.10	0.21	9.83
Janitell	PVC	783.8	4.00	2.40	0.73	0.14	29.02	29.36	1.1%	6.98E+04	0.66	16.80	51.9	0.10	0.19	9.22
Janitell	PVC	783.8	4.00	2.82	0.86	0.08	24.67	25.13	1.8%	8.21E+04	0.28	7.11	66.6	0.09	0.16	7.83
Janitell	PVC	783.8	4.00	2.68	0.82	0.11	27.70	28.12	1.5%	7.80E+04	0.42	10.75	59.4	0.09	0.18	8.80
Kettle Creek	DIP	5872.3	12.52	2.59	0.79	0.15	90.01	90.43	0.5%	2.36E+05	2.45	62.17	43.9	0.11	0.25	11.94
Kettle Creek	DIP	5872.3	12.52	2.18	0.66	0.24	98.60	98.90	0.3%	1.98E+05	4.36	110.73	35.1	0.11	0.27	13.08
Kettle Creek	DIP	5872.3	12.52	2.42	0.74	0.18	93.86	94.23	0.4%	2.20E+05	3.15	80.05	40.0	0.11	0.26	12.45
Kettle Creek	DIP	5872.3	12.52	2.48	0.75	0.17	92.59	92.98	0.4%	2.25E+05	2.90	73.67	41.3	0.11	0.26	12.29
Kettle Creek	DIP	5872.3	12.52	2.37	0.72	0.19	94.79	95.14	0.4%	2.15E+05	3.37	85.71	39.0	0.11	0.26	12.58
Kettle Creek	DIP	5872.3	12.52	2.60	0.79	0.15	89.57	90.00	0.5%	2.37E+05	2.40	60.96	44.2	0.11	0.25	11.89
Kettle Creek	DIP	5872.3	12.52	3.13	0.95	0.08	72.16	72.77	0.8%	2.84E+05	0.88	22.31	59.7	0.10	0.20	9.57
Kettle Creek	DIP	5872.3	12.52	3.08	0.94	0.09	74.12	74.71	0.8%	2.80E+05	0.98	24.92	58.0	0.10	0.21	9.83
Kettle Creek	DIP	5872.3	12.52	5.64	1.72	0.03	83.19	85.19	2.4%	5.13E+05	0.06	1.47	99.8	0.11	0.23	11.04

Project	Pipe Material	Pipe Length (ft)	I.D. (in)	Velocity		friction factor f	Headloss		Minor loss % of Total	R_e	k_s (in)	k_s (mm)	C-Factor	U* (m/s)	Shear Stress τ_o	
				(ft/s)	(m/s)		$h_{l\ f\ (f}$ ft)	$h_{l\ total}$ (ft)							(lb/ft^2)	(N/m^2)
Kettle Creek	DIP	5872.3	12.52	2.34	0.71	0.20	95.72	96.07	0.4%	2.12E+05	3.54	90.01	38.3	0.11	0.27	12.70
Big Valley	DIP	415.9	4.10	1.81	0.55	0.11	6.77	6.84	1.0%	5.39E+04	0.46	11.72	60.0	0.06	0.09	4.15
Big Valley	DIP	415.9	4.10	1.77	0.54	0.12	6.97	7.04	0.9%	5.27E+04	0.53	13.38	57.6	0.07	0.09	4.28
Big Valley	DIP	415.9	4.10	2.15	0.66	0.07	5.89	5.99	1.6%	6.41E+04	0.18	4.45	76.9	0.06	0.08	3.62
Big Valley	DIP	415.9	4.10	2.00	0.61	0.08	6.41	6.50	1.3%	5.95E+04	0.29	7.31	68.2	0.06	0.08	3.93
Big Valley	DIP	415.9	4.10	1.81	0.55	0.11	6.90	6.97	1.0%	5.40E+04	0.48	12.09	59.4	0.07	0.09	4.24
Big Valley	DIP	415.9	4.10	2.11	0.64	0.07	6.08	6.17	1.5%	6.29E+04	0.20	5.19	74.2	0.06	0.08	3.73
Big Valley	DIP	415.9	4.10	2.01	0.61	0.08	6.35	6.44	1.3%	6.00E+04	0.27	6.94	69.1	0.06	0.08	3.90
Big Valley	DIP	415.9	4.10	1.82	0.55	0.11	6.70	6.77	1.0%	5.41E+04	0.45	11.41	60.5	0.06	0.09	4.11
Big Valley	DIP	415.9	4.10	1.61	0.49	0.15	7.38	7.43	0.7%	4.80E+04	0.77	19.63	51.0	0.07	0.09	4.53
Big Valley	DIP	415.9	4.10	2.54	0.77	0.04	4.80	4.94	2.8%	7.55E+04	0.04	1.09	101.2	0.05	0.06	2.95
South River	RCP	42960.4	66.00	3.85	1.17	0.03	46.74	48.78	4.2%	1.85E+06	0.19	4.83	95.7	0.07	0.09	4.47
South River	RCP	42960.4	66.00	2.63	0.80	0.04	31.26	32.21	3.0%	1.26E+06	0.62	15.71	81.3	0.05	0.06	2.99
South River	RCP	42960.4	66.00	5.38	1.64	0.02	59.66	63.62	6.2%	2.58E+06	0.03	0.86	117.1	0.08	0.12	5.70
South River	RCP	42960.4	66.00	3.49	1.06	0.03	47.49	49.16	3.4%	1.68E+06	0.39	9.97	86.0	0.07	0.09	4.54
South River	RCP	42960.4	66.00	3.96	1.21	0.02	37.11	39.26	5.5%	1.90E+06	0.06	1.58	111.4	0.06	0.07	3.55
South River	RCP	42960.4	66.00	4.31	1.31	0.02	39.27	41.82	6.1%	2.07E+06	0.04	0.96	117.6	0.06	0.08	3.76
South River	RCP	42960.4	66.00	2.36	0.72	0.04	29.63	30.40	2.5%	1.13E+06	1.00	25.41	74.9	0.05	0.06	2.83
South River	RCP	42960.4	66.00	4.74	1.44	0.02	53.66	56.74	5.4%	2.27E+06	0.06	1.65	109.3	0.07	0.11	5.13
South River	RCP	42960.4	66.00	3.50	1.07	0.03	50.20	51.88	3.2%	1.68E+06	0.46	11.71	83.7	0.07	0.10	4.80
South River	RCP	42960.4	66.00	3.42	1.04	0.04	52.34	53.95	3.0%	1.64E+06	0.60	15.34	80.0	0.07	0.10	5.00
Natomas	RCP	47166.5	60.00	1.83	0.56	0.03	13.30	14.00	5.0%	7.96E+05	0.20	5.15	99.9	0.03	0.02	1.05
Natomas	RCP	47166.5	60.00	3.14	0.96	0.02	25.63	27.72	7.5%	1.37E+06	0.04	0.91	120.5	0.05	0.04	2.03
Natomas	RCP	47166.5	60.00	3.83	1.17	0.01	23.83	26.94	11.5%	1.67E+06	0.00	0.02	152.9	0.04	0.04	1.89
Natomas	RCP	47166.5	60.00	3.88	1.18	0.01	27.92	31.11	10.2%	1.69E+06	0.01	0.13	142.2	0.05	0.05	2.21
Natomas	RCP	47166.5	60.00	3.43	1.05	0.01	22.09	24.59	10.1%	1.50E+06	0.01	0.13	142.7	0.04	0.04	1.75

Project	Pipe Material	Pipe Length (ft)	I.D. (in)	Velocity		friction factor f	Headloss		Minor loss % of Total	R_e	k_s (in)	k_s (mm)	C-Factor	U* (m/s)	Shear Stress τ_o	
				(ft/s)	(m/s)		$h_{l\ f\ (f}$ ft)	$h_{l\ total}$ (ft)							(lb/ft^2)	(N/m^2)
Natomas	RCP	47166.5	60.00	3.92	1.19	0.02	43.48	46.74	7.0%	1.71E+06	0.05	1.37	113.0	0.06	0.07	3.44
Natomas	RCP	47166.5	60.00	4.21	1.28	0.01	29.18	32.93	11.4%	1.84E+06	0.00	0.04	150.7	0.05	0.05	2.31
Natomas	RCP	47166.5	60.00	4.73	1.44	0.01	35.42	40.16	11.8%	2.06E+06	0.00	0.02	152.4	0.05	0.06	2.80
Natomas	RCP	47166.5	60.00	4.30	1.31	0.01	28.41	32.33	12.1%	1.87E+06	0.00	0.00	156.1	0.05	0.05	2.25
Natomas	RCP	47166.5	60.00	2.80	0.85	0.02	20.62	22.29	7.5%	1.22E+06	0.04	0.96	120.9	0.04	0.03	1.63
Chapel Hills	PVC	5508.4	8.28	2.51	0.77	0.08	61.09	61.39	0.5%	1.51E+05	0.49	12.57	65.7	0.08	0.12	5.71
Chapel Hills	PVC	5508.4	8.28	2.52	0.77	0.08	60.87	61.17	0.5%	1.52E+05	0.48	12.24	66.2	0.08	0.12	5.69
Chapel Hills	PVC	5508.4	8.28	2.61	0.80	0.07	60.24	60.56	0.5%	1.57E+05	0.41	10.34	68.9	0.08	0.12	5.64
Chapel Hills	PVC	5508.4	8.28	2.45	0.75	0.08	61.60	61.88	0.5%	1.47E+05	0.56	14.21	63.8	0.08	0.12	5.76
Chapel Hills	PVC	5508.4	8.28	2.81	0.86	0.06	58.72	59.10	0.6%	1.69E+05	0.28	7.00	75.1	0.07	0.11	5.49
Chapel Hills	PVC	5508.4	8.28	2.43	0.74	0.08	61.60	61.88	0.5%	1.46E+05	0.58	14.63	63.3	0.08	0.12	5.76
Chapel Hills	PVC	5508.4	8.28	2.46	0.75	0.08	61.35	61.63	0.5%	1.48E+05	0.55	13.89	64.2	0.08	0.12	5.74
Chapel Hills	PVC	5508.4	8.28	2.61	0.79	0.07	60.48	60.81	0.5%	1.57E+05	0.41	10.53	68.6	0.08	0.12	5.66
Chapel Hills	PVC	5508.4	8.28	2.34	0.71	0.09	62.45	62.71	0.4%	1.41E+05	0.69	17.41	60.5	0.08	0.12	5.84
Chapel Hills	PVC	5508.4	8.28	2.97	0.90	0.05	57.21	57.63	0.7%	1.78E+05	0.20	5.02	80.5	0.07	0.11	5.35
Drennan	PVC	4613.3	9.98	3.66	1.12	0.03	32.75	33.66	2.7%	2.66E+05	0.04	0.93	108.6	0.07	0.09	4.41
Drennan	PVC	4613.3	9.98	2.36	0.72	0.11	51.71	52.09	0.7%	1.71E+05	1.10	27.99	54.6	0.08	0.15	6.96
Drennan	PVC	4613.3	9.98	3.38	1.03	0.04	38.21	38.99	2.0%	2.45E+05	0.10	2.65	92.2	0.07	0.11	5.14
Drennan	PVC	4613.3	9.98	2.70	0.82	0.08	47.68	48.17	1.0%	1.96E+05	0.56	14.28	65.3	0.08	0.13	6.42
Drennan	PVC	4613.3	9.98	3.58	1.09	0.03	34.92	35.79	2.4%	2.59E+05	0.05	1.38	102.5	0.07	0.10	4.70
Drennan	PVC	4613.3	9.98	2.91	0.89	0.06	44.98	45.56	1.3%	2.11E+05	0.36	9.04	72.6	0.08	0.13	6.05
Drennan	PVC	4613.3	9.98	3.31	1.01	0.04	38.13	38.88	1.9%	2.40E+05	0.12	2.96	90.4	0.07	0.11	5.13
Drennan	PVC	4613.3	9.98	2.54	0.78	0.09	49.58	50.02	0.9%	1.84E+05	0.77	19.63	60.3	0.08	0.14	6.67
Drennan	PVC	4613.3	9.98	3.19	0.97	0.05	40.99	41.69	1.7%	2.32E+05	0.18	4.45	83.9	0.07	0.12	5.52
Drennan	PVC	4613.3	9.98	3.22	0.98	0.05	40.64	41.35	1.7%	2.33E+05	0.16	4.16	84.9	0.07	0.11	5.47
Black Squirrel	PVC	2186.6	8.28	5.91	1.80	0.03	57.76	60.40	4.4%	3.55E+05	0.06	1.41	96.9	0.12	0.28	13.61

Project	Pipe Material	Pipe Length (ft)	I.D. (in)	Velocity		friction factor f	Headloss		Minor loss % of Total	R_e	k_s (in)	k_s (mm)	C-Factor	U* (m/s)	Shear Stress τ_o	
				(ft/s)	(m/s)		$h_{l\ f\ (f}$ ft)	$h_{l\ total}$ (ft)							(lb/ft^2)	(N/m^2)
Black Squirrel	PVC	2186.6	8.28	6.34	1.93	0.03	55.34	58.38	5.2%	3.81E+05	0.03	0.76	106.3	0.11	0.27	13.04
Black Squirrel	PVC	2186.6	8.28	6.11	1.86	0.03	56.60	59.43	4.8%	3.68E+05	0.04	1.06	101.3	0.12	0.28	13.34
Black Squirrel	PVC	2186.6	8.28	6.31	1.92	0.03	55.41	58.43	5.2%	3.80E+05	0.03	0.79	105.8	0.11	0.27	13.06
Black Squirrel	PVC	2186.6	8.28	6.27	1.91	0.03	55.99	58.98	5.1%	3.77E+05	0.03	0.85	104.6	0.11	0.28	13.20
Black Squirrel	PVC	2186.6	8.28	6.29	1.92	0.03	55.94	58.95	5.1%	3.79E+05	0.03	0.83	105.0	0.11	0.28	13.18
Black Squirrel	PVC	2186.6	8.28	6.20	1.89	0.03	55.97	58.89	5.0%	3.73E+05	0.04	0.92	103.4	0.11	0.28	13.19
Black Squirrel	PVC	2186.6	8.28	6.22	1.90	0.03	55.97	58.90	5.0%	3.74E+05	0.04	0.90	103.7	0.11	0.28	13.19
Black Squirrel	PVC	2186.6	8.28	6.46	1.97	0.03	54.22	57.38	5.5%	3.89E+05	0.02	0.61	109.6	0.11	0.27	12.78
Black Squirrel	PVC	2186.6	8.28	6.17	1.88	0.03	56.90	59.79	4.8%	3.71E+05	0.04	1.01	102.0	0.12	0.28	13.41
Middle Trib	PVC	6144.7	12.08	2.66	0.81	0.09	58.92	59.34	0.7%	2.33E+05	0.92	23.35	59.3	0.08	0.15	7.21
Middle Trib	PVC	6144.7	12.08	2.75	0.84	0.08	57.39	57.84	0.8%	2.41E+05	0.76	19.42	62.2	0.08	0.15	7.02
Middle Trib	PVC	6144.7	12.08	2.99	0.91	0.06	48.86	49.40	1.1%	2.63E+05	0.36	9.24	74.0	0.08	0.12	5.98
Middle Trib	PVC	6144.7	12.08	3.00	0.92	0.06	48.89	49.43	1.1%	2.64E+05	0.36	9.11	74.2	0.08	0.12	5.98
Middle Trib	PVC	6144.7	12.08	3.05	0.93	0.05	47.29	47.85	1.2%	2.68E+05	0.31	7.76	76.8	0.08	0.12	5.79
Middle Trib	PVC	6144.7	12.08	3.10	0.94	0.05	45.70	46.27	1.2%	2.72E+05	0.26	6.58	79.4	0.07	0.12	5.59
Middle Trib	PVC	6144.7	12.08	3.10	0.95	0.05	45.56	46.13	1.2%	2.72E+05	0.26	6.49	79.6	0.07	0.12	5.57
Middle Trib	PVC	6144.7	12.08	3.12	0.95	0.05	44.85	45.43	1.3%	2.74E+05	0.24	6.03	80.8	0.07	0.11	5.49
Middle Trib	PVC	6144.7	12.08	3.27	1.00	0.04	39.36	40.00	1.6%	2.87E+05	0.13	3.24	90.7	0.07	0.10	4.82
Middle Trib	PVC	6144.7	12.08	3.27	1.00	0.04	39.03	39.67	1.6%	2.87E+05	0.12	3.12	91.3	0.07	0.10	4.78
Middle Trib	PVC	2400.9	8.28	5.66	1.72	0.02	33.32	34.01	2.0%	3.40E+05	0.01	0.15	131.3	0.08	0.15	7.15
Middle Trib	PVC	2400.9	8.28	5.85	1.78	0.02	34.06	34.80	2.1%	3.52E+05	0.00	0.12	134.1	0.09	0.15	7.31
Middle Trib	PVC	2400.9	8.28	6.37	1.94	0.02	39.56	40.44	2.2%	3.83E+05	0.00	0.10	134.9	0.09	0.18	8.49
Middle Trib	PVC	2400.9	8.28	6.40	1.95	0.02	39.81	40.69	2.2%	3.85E+05	0.00	0.10	134.9	0.09	0.18	8.54

Project	Pipe Material	Pipe Length (ft)	I.D. (in)	Velocity		friction factor f	Headloss		Minor loss % of Total	R_e	k_s (in)	k_s (mm)	C-Factor	U* (m/s)	Shear Stress τ_o	
				(ft/s)	(m/s)		$h_{l\ f\ (f}$ ft)	$h_{l\ total}$ (ft)							(lb/ft^2)	(N/m^2)
Middle Trib	PVC	2400.9	8.28	6.50	1.98	0.02	40.88	41.79	2.2%	3.91E+05	0.00	0.10	135.1	0.09	0.18	8.77
Middle Trib	PVC	2400.9	8.28	6.60	2.01	0.02	41.99	42.93	2.2%	3.97E+05	0.00	0.10	135.2	0.09	0.19	9.01
Middle Trib	PVC	2400.9	8.28	6.60	2.01	0.02	42.06	43.01	2.2%	3.97E+05	0.00	0.10	135.2	0.10	0.19	9.03
Middle Trib	PVC	2400.9	8.28	6.64	2.02	0.02	42.50	43.46	2.2%	4.00E+05	0.00	0.10	135.2	0.10	0.19	9.12
Middle Trib	PVC	2400.9	8.28	6.95	2.12	0.02	46.09	47.14	2.2%	4.18E+05	0.00	0.10	135.5	0.10	0.21	9.89
Middle Trib	PVC	2400.9	8.28	6.97	2.12	0.02	46.27	47.33	2.2%	4.19E+05	0.00	0.10	135.5	0.10	0.21	9.93
Mid Monument	DIP	3912.9	16.60	1.39	0.42	0.16	13.55	13.74	1.4%	1.67E+05	3.45	87.71	43.9	0.06	0.07	3.58
Mid Monument	DIP	3912.9	16.60	1.57	0.48	0.13	13.89	14.14	1.8%	1.89E+05	2.47	62.80	49.0	0.06	0.08	3.67
Mid Monument	DIP	3912.9	16.60	1.26	0.39	0.20	13.98	14.14	1.1%	1.52E+05	4.65	118.22	39.3	0.06	0.08	3.69
Mid Monument	DIP	3912.9	16.60	1.33	0.40	0.18	13.69	13.87	1.3%	1.60E+05	3.98	101.18	41.7	0.06	0.08	3.61
Mid Monument	DIP	3912.9	16.60	1.42	0.43	0.15	13.50	13.70	1.5%	1.71E+05	3.21	81.63	45.0	0.06	0.07	3.56
Mid Monument	DIP	3912.9	16.60	1.45	0.44	0.14	13.45	13.66	1.6%	1.75E+05	2.97	75.52	46.2	0.06	0.07	3.55
Mid Monument	DIP	3912.9	16.60	1.51	0.46	0.13	13.48	13.71	1.7%	1.82E+05	2.65	67.42	48.0	0.06	0.07	3.56
Mid Monument	DIP	3912.9	16.60	1.53	0.47	0.13	13.71	13.94	1.7%	1.85E+05	2.59	65.91	48.3	0.06	0.08	3.62
Mid Monument	DIP	3912.9	16.60	1.56	0.47	0.13	13.82	14.07	1.7%	1.88E+05	2.51	63.76	48.8	0.06	0.08	3.65
Mid Monument	DIP	3912.9	16.60	1.57	0.48	0.13	13.89	14.14	1.8%	1.89E+05	2.48	63.00	49.0	0.06	0.08	3.67
Mid Monument	PVC	6144.7	12.08	2.62	0.80	0.07	46.88	47.29	0.9%	2.30E+05	0.61	15.47	66.2	0.08	0.12	5.74
Mid Monument	PVC	6144.7	12.08	2.96	0.90	0.04	36.43	36.95	1.4%	2.60E+05	0.18	4.56	85.7	0.07	0.09	4.46
Mid Monument	PVC	6144.7	12.08	2.39	0.73	0.10	52.18	52.52	0.6%	2.09E+05	1.10	27.91	56.9	0.08	0.13	6.38
Mid Monument	PVC	6144.7	12.08	2.50	0.76	0.08	49.53	49.90	0.7%	2.20E+05	0.83	20.97	61.4	0.08	0.13	6.06

Project	Pipe Material	Pipe Length (ft)	I.D. (in)	Velocity		friction factor f	Headloss		Minor loss % of Total	R_e	k_s (in)	k_s (mm)	C-Factor	U* (m/s)	Shear Stress τ_o	
				(ft/s)	(m/s)		$h_{l\ f\ (f}$ ft)	$h_{l\ total}$ (ft)							(lb/ft^2)	(N/m^2)
Mid Monument	PVC	6144.7	12.08	2.68	0.82	0.07	45.34	45.77	0.9%	2.35E+05	0.51	13.00	69.0	0.07	0.12	5.55
Mid Monument	PVC	6144.7	12.08	2.75	0.84	0.06	43.38	43.83	1.0%	2.41E+05	0.41	10.51	72.4	0.07	0.11	5.31
Mid Monument	PVC	6144.7	12.08	2.85	0.87	0.05	40.12	40.61	1.2%	2.50E+05	0.28	7.20	78.4	0.07	0.10	4.91
Mid Monument	PVC	6144.7	12.08	2.90	0.88	0.05	38.75	39.25	1.3%	2.54E+05	0.24	6.07	81.1	0.07	0.10	4.74
Mid Monument	PVC	6144.7	12.08	2.94	0.90	0.05	37.21	37.72	1.4%	2.58E+05	0.20	5.03	84.2	0.07	0.10	4.55
Mid Monument	PVC	6144.7	12.08	2.96	0.90	0.04	36.63	37.15	1.4%	2.60E+05	0.18	4.66	85.4	0.07	0.09	4.48
Mid Monument	PVC	2400.9	8.28	5.58	1.70	0.02	31.07	31.75	2.1%	3.36E+05	0.00	0.12	134.5	0.08	0.14	6.67
Mid Monument	PVC	2400.9	8.28	6.30	1.92	0.02	38.23	39.09	2.2%	3.79E+05	0.00	0.10	135.8	0.09	0.17	8.20
Mid Monument	PVC	2400.9	8.28	5.08	1.55	0.02	26.69	27.25	2.1%	3.06E+05	0.01	0.14	132.9	0.08	0.12	5.73
Mid Monument	PVC	2400.9	8.28	5.33	1.62	0.02	28.83	29.45	2.1%	3.21E+05	0.00	0.13	133.7	0.08	0.13	6.19
Mid Monument	PVC	2400.9	8.28	5.71	1.74	0.02	32.27	32.98	2.1%	3.43E+05	0.00	0.11	134.8	0.08	0.14	6.93
Mid Monument	PVC	2400.9	8.28	5.85	1.78	0.02	33.59	34.33	2.2%	3.52E+05	0.00	0.11	135.1	0.08	0.15	7.21
Mid Monument	PVC	2400.9	8.28	6.07	1.85	0.02	35.81	36.61	2.2%	3.65E+05	0.00	0.10	135.6	0.09	0.16	7.69
Mid Monument	PVC	2400.9	8.28	6.17	1.88	0.02	36.81	37.63	2.2%	3.71E+05	0.00	0.10	135.7	0.09	0.16	7.90
Mid Monument	PVC	2400.9	8.28	6.26	1.91	0.02	37.76	38.61	2.2%	3.76E+05	0.00	0.10	135.8	0.09	0.17	8.10
Mid Monument	PVC	2400.9	8.28	6.30	1.92	0.02	38.17	39.03	2.2%	3.79E+05	0.00	0.10	135.8	0.09	0.17	8.19
Sand Creek	HDPE	19225.1	31.51	3.56	1.09	0.03	39.77	42.60	6.6%	8.16E+05	0.11	2.80	99.6	0.06	0.08	4.06
Sand Creek	HDPE	19225.1	31.51	3.43	1.05	0.02	32.26	34.88	7.5%	7.86E+05	0.07	1.70	107.4	0.06	0.07	3.29
Sand Creek	HDPE	19225.1	31.51	3.69	1.13	0.03	44.33	47.38	6.4%	8.46E+05	0.13	3.18	97.4	0.07	0.09	4.52

Project	Pipe Material	Pipe Length (ft)	I.D. (in)	Velocity		friction factor f	Headloss		Minor loss % of Total	R_e	k_s (in)	k_s (mm)	C-Factor	U* (m/s)	Shear Stress τ_o	
				(ft/s)	(m/s)		$h_{l\ f\ (f}$ ft)	$h_{l\ total}$ (ft)							(lb/ft^2)	(N/m^2)
Sand Creek	HDPE	19225.1	31.51	3.49	1.06	0.03	39.75	42.47	6.4%	7.99E+05	0.13	3.23	97.6	0.06	0.08	4.06
Sand Creek	HDPE	19225.1	31.51	3.27	1.00	0.03	33.68	36.07	6.6%	7.50E+05	0.11	2.82	100.2	0.06	0.07	3.44
Sand Creek	HDPE	19225.1	31.51	4.21	1.28	0.02	35.73	39.67	9.9%	9.63E+05	0.02	0.46	124.6	0.06	0.08	3.64
Sand Creek	HDPE	19225.1	31.51	4.37	1.33	0.02	35.81	40.06	10.6%	1.00E+06	0.01	0.31	129.3	0.06	0.08	3.65
Sand Creek	HDPE	19225.1	31.51	3.66	1.11	0.03	43.63	46.61	6.4%	8.37E+05	0.13	3.24	97.2	0.07	0.09	4.45
Sand Creek	HDPE	19225.1	31.51	4.25	1.29	0.02	48.73	52.75	7.6%	9.72E+05	0.06	1.63	106.4	0.07	0.10	4.97
Sand Creek	HDPE	19225.1	31.51	3.49	1.06	0.03	37.73	40.45	6.7%	8.00E+05	0.10	2.67	100.5	0.06	0.08	3.85
Norris Lake	DIP	17807.5	16.60	3.96	1.21	0.03	94.47	95.28	0.9%	4.77E+05	0.08	1.99	99.6	0.07	0.11	5.48
Norris Lake	DIP	17807.5	16.60	3.89	1.19	0.03	95.11	95.89	0.8%	4.69E+05	0.09	2.30	97.6	0.07	0.12	5.52
Norris Lake	DIP	17807.5	16.60	3.91	1.19	0.03	95.39	96.19	0.8%	4.72E+05	0.09	2.23	97.9	0.07	0.12	5.53
Norris Lake	DIP	17807.5	16.60	3.93	1.20	0.03	95.21	96.01	0.8%	4.74E+05	0.08	2.15	98.5	0.07	0.12	5.52
Norris Lake	DIP	17807.5	16.60	3.88	1.18	0.03	94.76	95.54	0.8%	4.69E+05	0.09	2.28	97.6	0.07	0.11	5.50
Norris Lake	DIP	17807.5	16.60	3.88	1.18	0.03	94.18	94.97	0.8%	4.68E+05	0.09	2.26	97.8	0.07	0.11	5.46
Norris Lake	DIP	17807.5	16.60	3.91	1.19	0.03	92.38	93.18	0.9%	4.71E+05	0.08	2.02	99.5	0.07	0.11	5.36
Norris Lake	DIP	17807.5	16.60	3.88	1.18	0.03	97.71	98.49	0.8%	4.68E+05	0.10	2.54	96.0	0.08	0.12	5.67
Norris Lake	DIP	17807.5	16.60	3.95	1.21	0.03	97.75	98.57	0.8%	4.77E+05	0.09	2.25	97.7	0.08	0.12	5.67
Norris Lake	DIP	17807.5	16.60	3.90	1.19	0.03	98.43	99.22	0.8%	4.70E+05	0.10	2.54	96.0	0.08	0.12	5.71
Norris Lake	DIP	1861.1	12.50	6.98	2.13	0.02	22.19	23.43	5.3%	6.34E+05	0.00	0.11	135.7	0.10	0.19	9.27
Norris Lake	DIP	1861.1	12.50	6.86	2.09	0.02	21.51	22.71	5.3%	6.23E+05	0.00	0.11	135.6	0.09	0.19	8.99
Norris Lake	DIP	1861.1	12.50	6.90	2.10	0.02	21.73	22.94	5.3%	6.26E+05	0.00	0.11	135.6	0.10	0.19	9.08
Norris Lake	DIP	1861.1	12.50	6.93	2.11	0.02	21.92	23.15	5.3%	6.30E+05	0.00	0.11	135.7	0.10	0.19	9.16
Norris Lake	DIP	1861.1	12.50	6.85	2.09	0.02	21.46	22.65	5.3%	6.22E+05	0.00	0.11	135.6	0.09	0.19	8.97
Norris Lake	DIP	1861.1	12.50	6.84	2.09	0.02	21.40	22.59	5.3%	6.21E+05	0.00	0.11	135.7	0.09	0.19	8.94
Norris Lake	DIP	1861.1	12.50	6.89	2.10	0.02	21.63	22.84	5.3%	6.26E+05	0.00	0.11	135.8	0.10	0.19	9.04
Norris Lake	DIP	1861.1	12.50	6.85	2.09	0.02	21.50	22.69	5.3%	6.22E+05	0.00	0.11	135.5	0.09	0.19	8.99
Norris Lake	DIP	1861.1	12.50	6.97	2.13	0.02	22.21	23.45	5.3%	6.34E+05	0.00	0.11	135.6	0.10	0.19	9.28

Project	Pipe Material	Pipe Length (ft)	I.D. (in)	Velocity		friction factor f	Headloss		Minor loss % of Total	R_e	k_s (in)	k_s (mm)	C-Factor	U* (m/s)	Shear Stress τ_o	
				(ft/s)	(m/s)		$h_{l\ f\ (f}$ ft)	$h_{l\ total}$ (ft)							(lb/ft^2)	(N/m^2)
Norris Lake	DIP	1861.1	12.50	6.87	2.10	0.02	21.65	22.86	5.3%	6.24E+05	0.00	0.11	135.4	0.10	0.19	9.05
Rock Quarry	DIP	6090.4	14.60	2.54	0.77	0.04	22.34	22.58	1.0%	2.69E+05	0.23	5.79	84.5	0.06	0.07	3.33
Rock Quarry	DIP	6090.4	14.60	2.55	0.78	0.04	21.86	22.09	1.1%	2.70E+05	0.21	5.32	85.9	0.06	0.07	3.26
Rock Quarry	DIP	6090.4	14.60	2.53	0.77	0.04	22.21	22.44	1.0%	2.69E+05	0.23	5.78	84.6	0.06	0.07	3.31
Rock Quarry	DIP	6090.4	14.60	2.54	0.77	0.04	22.06	22.30	1.0%	2.69E+05	0.22	5.59	85.1	0.06	0.07	3.29
Rock Quarry	DIP	6090.4	14.60	2.56	0.78	0.04	21.70	21.93	1.1%	2.71E+05	0.20	5.12	86.5	0.06	0.07	3.24
Rock Quarry	DIP	6090.4	14.60	3.49	1.06	0.04	37.41	37.85	1.2%	3.70E+05	0.16	4.11	88.0	0.07	0.12	5.58
Rock Quarry	DIP	6090.4	14.60	3.53	1.08	0.04	37.10	37.55	1.2%	3.74E+05	0.15	3.76	89.4	0.07	0.12	5.54
Rock Quarry	DIP	6090.4	14.60	3.52	1.07	0.04	37.18	37.62	1.2%	3.73E+05	0.15	3.84	89.0	0.07	0.12	5.55
Rock Quarry	DIP	6090.4	14.60	3.47	1.06	0.04	37.53	37.97	1.1%	3.69E+05	0.17	4.26	87.5	0.07	0.12	5.60
Rock Quarry	DIP	6090.4	14.60	3.52	1.07	0.04	37.35	37.79	1.2%	3.73E+05	0.15	3.92	88.7	0.07	0.12	5.57
Dacula	DIP	7692.8	16.60	3.03	0.92	0.06	44.48	44.76	0.6%	3.66E+05	0.47	11.98	72.8	0.08	0.12	5.97
Dacula	DIP	7692.8	16.60	2.84	0.87	0.07	47.94	48.19	0.5%	3.43E+05	0.76	19.25	65.5	0.08	0.13	6.44
Dacula	DIP	7692.8	16.60	2.84	0.87	0.07	47.81	48.06	0.5%	3.43E+05	0.75	19.12	65.7	0.08	0.13	6.42
Dacula	DIP	7692.8	16.60	3.01	0.92	0.06	44.95	45.22	0.6%	3.63E+05	0.50	12.78	71.8	0.08	0.13	6.04
Dacula	DIP	7692.8	16.60	2.83	0.86	0.07	48.08	48.33	0.5%	3.41E+05	0.78	19.87	65.1	0.08	0.13	6.46
Dacula	DIP	7692.8	16.60	2.83	0.86	0.07	48.06	48.31	0.5%	3.41E+05	0.77	19.68	65.2	0.08	0.13	6.45
Dacula	DIP	7692.8	16.60	3.00	0.91	0.06	45.23	45.51	0.6%	3.62E+05	0.52	13.17	71.4	0.08	0.13	6.07
Dacula	DIP	7692.8	16.60	3.00	0.91	0.06	45.17	45.45	0.6%	3.61E+05	0.52	13.14	71.4	0.08	0.13	6.07
Dacula	DIP	7692.8	16.60	3.02	0.92	0.06	44.70	44.98	0.6%	3.65E+05	0.48	12.30	72.4	0.08	0.13	6.00
Dacula	DIP	7692.8	16.60	2.82	0.86	0.07	48.38	48.63	0.5%	3.40E+05	0.81	20.45	64.6	0.08	0.14	6.50
TRM	RCP	6087.4	42.00	1.52	0.46	0.06	3.54	3.69	3.9%	4.63E+05	1.25	31.70	70.1	0.04	0.03	1.52

Project	Pipe Material	Pipe Length (ft)	I.D. (in)	Velocity		friction factor f	Headloss		Minor loss % of Total	R_e	k_s (in)	k_s (mm)	C-Factor	U* (m/s)	Shear Stress τ_o	
				(ft/s)	(m/s)		$h_{l\ f\ (f}$ ft)	$h_{l\ total}$ (ft)							(lb/ft^2)	(N/m^2)
TRM	RCP	6087.4	42.00	1.26	0.38	0.06	2.50	2.60	3.8%	3.84E+05	1.32	33.43	70.3	0.03	0.02	1.07
TRM	RCP	6087.4	42.00	1.28	0.39	0.06	2.48	2.58	4.0%	3.91E+05	1.18	29.97	72.0	0.03	0.02	1.06
TRM	RCP	6087.4	42.00	1.72	0.52	0.05	3.96	4.15	4.5%	5.26E+05	0.87	22.15	75.0	0.04	0.04	1.70
TRM	RCP	6087.4	42.00	1.22	0.37	0.06	2.35	2.45	3.8%	3.72E+05	1.33	33.82	70.3	0.03	0.02	1.01
TRM	RCP	6087.4	42.00	1.84	0.56	0.05	4.14	4.35	4.9%	5.63E+05	0.68	17.34	78.4	0.04	0.04	1.78
TRM	RCP	6087.4	42.00	1.80	0.55	0.04	3.45	3.65	5.5%	5.48E+05	0.47	11.98	84.3	0.04	0.03	1.48
TRM	RCP	6087.4	42.00	1.94	0.59	0.04	4.17	4.40	5.3%	5.93E+05	0.52	13.22	82.3	0.04	0.04	1.79
TRM	RCP	6087.4	42.00	1.46	0.44	0.06	3.43	3.56	3.7%	4.45E+05	1.39	35.33	68.6	0.04	0.03	1.47
TRM	RCP	6087.4	42.00	1.92	0.59	0.04	4.10	4.33	5.3%	5.86E+05	0.53	13.48	82.0	0.04	0.04	1.76
TRP	RCP	7887.4	42.00	1.09	0.33	0.05	2.30	2.40	4.1%	3.34E+05	1.13	28.67	73.6	0.03	0.02	0.76
TRP	RCP	7887.4	42.00	1.11	0.34	0.06	2.53	2.63	3.8%	3.39E+05	1.32	33.46	71.0	0.03	0.02	0.84
TRP	RCP	7887.4	42.00	1.08	0.33	0.06	2.49	2.58	3.7%	3.31E+05	1.43	36.28	69.8	0.03	0.02	0.82
TRP	RCP	7887.4	42.00	1.55	0.47	0.05	3.97	4.16	4.7%	4.73E+05	0.76	19.42	77.7	0.04	0.03	1.31
TRP	RCP	7887.4	42.00	1.03	0.32	0.06	2.34	2.43	3.6%	3.16E+05	1.54	39.16	68.9	0.03	0.02	0.77
TRP	RCP	7887.4	42.00	1.63	0.50	0.04	4.04	4.26	5.1%	4.97E+05	0.62	15.66	80.7	0.04	0.03	1.34
TRP	RCP	7887.4	42.00	2.03	0.62	0.04	5.79	6.12	5.5%	6.20E+05	0.49	12.46	82.9	0.04	0.04	1.92
TRP	RCP	7887.4	42.00	1.72	0.53	0.04	4.16	4.40	5.5%	5.26E+05	0.48	12.30	84.2	0.04	0.03	1.38
TRP	RCP	7887.4	42.00	1.70	0.52	0.04	4.10	4.33	5.4%	5.19E+05	0.50	12.83	83.6	0.04	0.03	1.36
TRP	RCP	7887.4	42.00	2.20	0.67	0.04	6.24	6.63	5.9%	6.70E+05	0.38	9.78	86.1	0.05	0.04	2.07
LS 03	HDPE	1109.4	14.01	4.92	1.50	0.05	16.11	16.39	1.7%	5.01E+05	0.23	5.76	80.0	0.11	0.26	12.66
LS 03	HDPE	1109.4	14.01	4.47	1.36	0.06	17.61	17.84	1.3%	4.56E+05	0.46	11.73	69.3	0.12	0.29	13.84
LS 03	HDPE	1109.4	14.01	4.03	1.23	0.07	16.33	16.52	1.1%	4.10E+05	0.63	15.99	65.0	0.11	0.27	12.84
LS 03	HDPE	1109.4	14.01	4.03	1.23	0.07	16.29	16.47	1.1%	4.10E+05	0.63	15.89	65.1	0.11	0.27	12.80
LS 03	HDPE	1109.4	14.01	4.47	1.36	0.06	17.56	17.79	1.3%	4.56E+05	0.46	11.65	69.4	0.12	0.29	13.80
LS 03	HDPE	1109.4	14.01	4.03	1.23	0.07	16.33	16.52	1.1%	4.10E+05	0.63	16.00	65.0	0.11	0.27	12.84
LS 03	HDPE	1109.4	14.01	4.03	1.23	0.07	16.31	16.50	1.1%	4.10E+05	0.63	15.95	65.0	0.11	0.27	12.82
LS 03	HDPE	1109.4	14.01	4.47	1.36	0.06	17.56	17.79	1.3%	4.56E+05	0.46	11.65	69.4	0.12	0.29	13.80

Project	Pipe Material	Pipe Length (ft)	I.D. (in)	Velocity		friction factor f	Headloss		Minor loss % of Total	R_e	k_s (in)	k_s (mm)	C-Factor	U* (m/s)	Shear Stress τ_o	
				(ft/s)	(m/s)		$h_{l\ f\ (f}$ ft)	$h_{l\ total}$ (ft)							(lb/ft^2)	(N/m^2)
LS 03	HDPE	1109.4	14.01	4.03	1.23	0.07	16.33	16.51	1.1%	4.10E+05	0.63	15.98	65.0	0.11	0.27	12.83
LS 03	HDPE	1109.4	14.01	4.03	1.23	0.07	16.26	16.45	1.1%	4.10E+05	0.62	15.84	65.1	0.11	0.27	12.78
LS 03	HDPE	1660.0	15.75	3.89	1.19	0.07	21.65	21.66	0.0%	4.46E+05	0.81	20.63	62.3	0.11	0.27	12.79
LS 03	HDPE	1660.0	15.75	3.54	1.08	0.13	30.92	30.93	0.0%	4.05E+05	2.26	57.41	46.7	0.14	0.38	18.26
LS 03	HDPE	1660.0	15.75	3.19	0.97	0.19	38.60	38.60	0.0%	3.65E+05	4.25	108.03	37.3	0.15	0.48	22.79
LS 03	HDPE	1660.0	15.75	3.19	0.97	0.19	38.38	38.39	0.0%	3.65E+05	4.22	107.25	37.4	0.15	0.47	22.67
LS 03	HDPE	1660.0	15.75	3.54	1.08	0.12	30.58	30.59	0.0%	4.05E+05	2.22	56.38	47.0	0.13	0.38	18.06
LS 03	HDPE	1660.0	15.75	3.19	0.97	0.19	38.60	38.61	0.0%	3.65E+05	4.25	108.05	37.3	0.15	0.48	22.79
LS 03	HDPE	1660.0	15.75	3.19	0.97	0.19	38.50	38.51	0.0%	3.65E+05	4.24	107.69	37.3	0.15	0.47	22.74
LS 03	HDPE	1660.0	15.75	3.54	1.08	0.12	30.60	30.61	0.0%	4.05E+05	2.22	56.45	47.0	0.13	0.38	18.07
LS 03	HDPE	1660.0	15.75	3.19	0.97	0.19	38.56	38.57	0.0%	3.65E+05	4.25	107.92	37.3	0.15	0.48	22.77
LS 03	HDPE	1660.0	15.75	3.19	0.97	0.19	38.27	38.28	0.0%	3.65E+05	4.21	106.83	37.5	0.15	0.47	22.60
LS 03	PVC	1660.2	12.08	6.62	2.02	0.03	28.28	29.37	3.7%	5.81E+05	0.03	0.76	108.5	0.11	0.27	12.81
LS 03	PVC	1660.2	12.08	6.02	1.83	0.03	29.57	30.47	3.0%	5.28E+05	0.07	1.75	96.2	0.12	0.28	13.39
LS 03	PVC	1660.2	12.08	5.42	1.65	0.04	33.75	34.49	2.1%	4.75E+05	0.19	4.92	80.6	0.12	0.32	15.29
LS 03	PVC	1660.2	12.08	5.42	1.65	0.04	33.67	34.40	2.1%	4.75E+05	0.19	4.88	80.7	0.12	0.32	15.25
LS 03	PVC	1660.2	12.08	6.02	1.83	0.03	29.49	30.40	3.0%	5.28E+05	0.07	1.74	96.4	0.12	0.28	13.35
LS 03	PVC	1660.2	12.08	5.42	1.65	0.04	33.76	34.49	2.1%	4.75E+05	0.19	4.92	80.6	0.12	0.32	15.29
LS 03	PVC	1660.2	12.08	5.42	1.65	0.04	33.72	34.45	2.1%	4.75E+05	0.19	4.90	80.7	0.12	0.32	15.27
LS 03	PVC	1660.2	12.08	6.02	1.83	0.03	29.50	30.40	3.0%	5.28E+05	0.07	1.74	96.4	0.12	0.28	13.36
LS 03	PVC	1660.2	12.08	5.42	1.65	0.04	33.74	34.47	2.1%	4.75E+05	0.19	4.91	80.6	0.12	0.32	15.28
LS 03	PVC	1660.2	12.08	5.42	1.65	0.04	33.62	34.35	2.1%	4.75E+05	0.19	4.86	80.8	0.12	0.32	15.23
LS 06	PVC	12988.2	17.53	2.71	0.83	0.05	55.37	57.43	3.6%	3.45E+05	0.47	11.81	74.2	0.07	0.10	4.65
LS 06	PVC	12988.2	17.53	2.74	0.84	0.05	55.40	57.50	3.7%	3.49E+05	0.44	11.19	75.0	0.07	0.10	4.65
LS 06	PVC	12988.2	17.53	2.61	0.79	0.06	56.86	58.76	3.2%	3.32E+05	0.60	15.22	70.3	0.07	0.10	4.78
LS 06	PVC	12988.2	17.53	2.79	0.85	0.05	54.74	56.92	3.8%	3.56E+05	0.39	9.90	76.9	0.07	0.10	4.60

Project	Pipe Material	Pipe Length (ft)	I.D. (in)	Velocity		friction factor f	Headloss		Minor loss % of Total	R_e	k_s (in)	k_s (mm)	C-Factor	U* (m/s)	Shear Stress τ_o	
				(ft/s)	(m/s)		$h_{l\ f\ (f}$ ft)	$h_{l\ total}$ (ft)							(lb/ft^2)	(N/m^2)
LS 06	PVC	12988.2	17.53	1.55	0.47	0.21	69.34	70.01	1.0%	1.97E+05	5.23	132.81	37.5	0.08	0.12	5.82
LS 06	PVC	12988.2	17.53	2.59	0.79	0.06	57.18	59.06	3.2%	3.30E+05	0.63	15.91	69.7	0.07	0.10	4.80
LS 06	PVC	12988.2	17.53	2.62	0.80	0.06	56.87	58.79	3.3%	3.34E+05	0.58	14.83	70.7	0.07	0.10	4.78
LS 06	PVC	12988.2	17.53	2.73	0.83	0.05	55.45	57.54	3.6%	3.48E+05	0.45	11.40	74.7	0.07	0.10	4.66
LS 06	PVC	12988.2	17.53	3.55	1.08	0.03	45.91	49.43	7.1%	4.52E+05	0.05	1.29	107.6	0.06	0.08	3.86
LS 06	PVC	12988.2	17.53	3.13	0.96	0.04	51.13	53.88	5.1%	3.99E+05	0.17	4.29	89.6	0.07	0.09	4.29
LS 15	DIP	6186.6	16.30	2.61	0.80	0.10	47.73	47.92	0.4%	3.09E+05	1.55	39.48	54.2	0.09	0.16	7.83
LS 15	DIP	6186.6	16.30	2.62	0.80	0.10	47.67	47.85	0.4%	3.10E+05	1.53	38.80	54.5	0.09	0.16	7.82
LS 15	DIP	6186.6	16.30	2.58	0.79	0.10	48.20	48.38	0.4%	3.05E+05	1.65	42.01	53.3	0.09	0.17	7.90
LS 15	DIP	6186.6	16.30	2.60	0.79	0.10	47.85	48.04	0.4%	3.09E+05	1.57	39.87	54.1	0.09	0.16	7.85
LS 15	DIP	6186.6	16.30	2.59	0.79	0.10	48.06	48.24	0.4%	3.07E+05	1.62	41.11	53.6	0.09	0.16	7.88
LS 15	DIP	6186.6	16.30	2.57	0.78	0.10	48.25	48.43	0.4%	3.05E+05	1.67	42.43	53.1	0.09	0.17	7.91
LS 15	DIP	6186.6	16.30	2.68	0.82	0.09	46.74	46.94	0.4%	3.17E+05	1.36	34.46	56.3	0.09	0.16	7.67
LS 15	DIP	6186.6	16.30	2.50	0.76	0.11	49.34	49.51	0.3%	2.96E+05	1.91	48.59	51.1	0.09	0.17	8.09
LS 15	DIP	6186.6	16.30	2.53	0.77	0.11	49.10	49.28	0.4%	3.00E+05	1.81	46.09	51.9	0.09	0.17	8.05
LS 15	DIP	6186.6	16.30	2.58	0.78	0.10	48.28	48.46	0.4%	3.05E+05	1.66	42.23	53.2	0.09	0.17	7.92
LS 15	DIP	930.0	20.80	1.60	0.49	0.14	2.89	2.96	2.4%	2.42E+05	3.36	85.24	46.7	0.06	0.08	4.03
LS 15	DIP	930.0	20.80	1.61	0.49	0.13	2.85	2.92	2.4%	2.43E+05	3.24	82.39	47.2	0.06	0.08	3.97
LS 15	DIP	930.0	20.80	1.58	0.48	0.13	2.79	2.86	2.4%	2.39E+05	3.29	83.65	47.0	0.06	0.08	3.88
LS 15	DIP	930.0	20.80	1.60	0.49	0.13	2.83	2.90	2.4%	2.42E+05	3.26	82.81	47.1	0.06	0.08	3.94
LS 15	DIP	930.0	20.80	1.59	0.48	0.13	2.81	2.88	2.4%	2.40E+05	3.28	83.30	47.1	0.06	0.08	3.91
LS 15	DIP	930.0	20.80	1.58	0.48	0.13	2.78	2.85	2.4%	2.39E+05	3.30	83.81	47.0	0.06	0.08	3.87
LS 15	DIP	930.0	20.80	1.64	0.50	0.13	2.94	3.02	2.4%	2.49E+05	3.18	80.68	47.4	0.06	0.09	4.10
LS 15	DIP	930.0	20.80	1.54	0.47	0.14	2.68	2.74	2.4%	2.32E+05	3.40	86.24	46.6	0.06	0.08	3.73
LS 15	DIP	930.0	20.80	1.56	0.47	0.14	2.73	2.80	2.4%	2.35E+05	3.36	85.26	46.8	0.06	0.08	3.80
LS 15	DIP	930.0	20.80	1.58	0.48	0.13	2.79	2.86	2.4%	2.39E+05	3.30	83.74	47.0	0.06	0.08	3.88

Project	Pipe Material	Pipe Length (ft)	I.D. (in)	Velocity		friction factor f	Headloss		Minor loss % of Total	R_e	k_s (in)	k_s (mm)	C-Factor	U* (m/s)	Shear Stress τ_o	
				(ft/s)	(m/s)		$h_{l\ f\ (f}$ ft)	$h_{l\ total}$ (ft)							(lb/ft^2)	(N/m^2)
Jimmy Camp	PVC	12238.1	11.20	4.49	1.37	0.02	92.54	95.37	3.0%	3.65E+05	0.02	0.43	119.6	0.07	0.11	5.27
Jimmy Camp	PVC	12238.1	11.20	4.60	1.40	0.02	91.56	94.54	3.2%	3.75E+05	0.01	0.33	123.4	0.07	0.11	5.21
Jimmy Camp	PVC	12238.1	11.20	4.53	1.38	0.02	92.22	95.11	3.0%	3.69E+05	0.02	0.39	120.9	0.07	0.11	5.25
Jimmy Camp	PVC	12238.1	11.20	4.60	1.40	0.02	91.53	94.51	3.1%	3.75E+05	0.01	0.33	123.3	0.07	0.11	5.21
Jimmy Camp	PVC	12238.1	11.20	4.52	1.38	0.02	92.64	95.51	3.0%	3.68E+05	0.02	0.41	120.2	0.07	0.11	5.28
Jimmy Camp	PVC	12238.1	11.20	4.56	1.39	0.02	92.11	95.03	3.1%	3.71E+05	0.01	0.37	121.9	0.07	0.11	5.25
Jimmy Camp	PVC	12238.1	11.20	4.60	1.40	0.02	91.60	94.57	3.1%	3.74E+05	0.01	0.34	123.2	0.07	0.11	5.22
Jimmy Camp	PVC	12238.1	11.20	4.57	1.39	0.02	91.83	94.77	3.1%	3.72E+05	0.01	0.36	122.3	0.07	0.11	5.23
Jimmy Camp	PVC	12238.1	11.20	4.56	1.39	0.02	92.05	94.97	3.1%	3.71E+05	0.01	0.37	121.8	0.07	0.11	5.24
Jimmy Camp	PVC	12238.1	11.20	4.56	1.39	0.02	92.10	95.01	3.1%	3.71E+05	0.01	0.37	121.7	0.07	0.11	5.25

Appendix D.2 - Research Data Pipeline Profiles

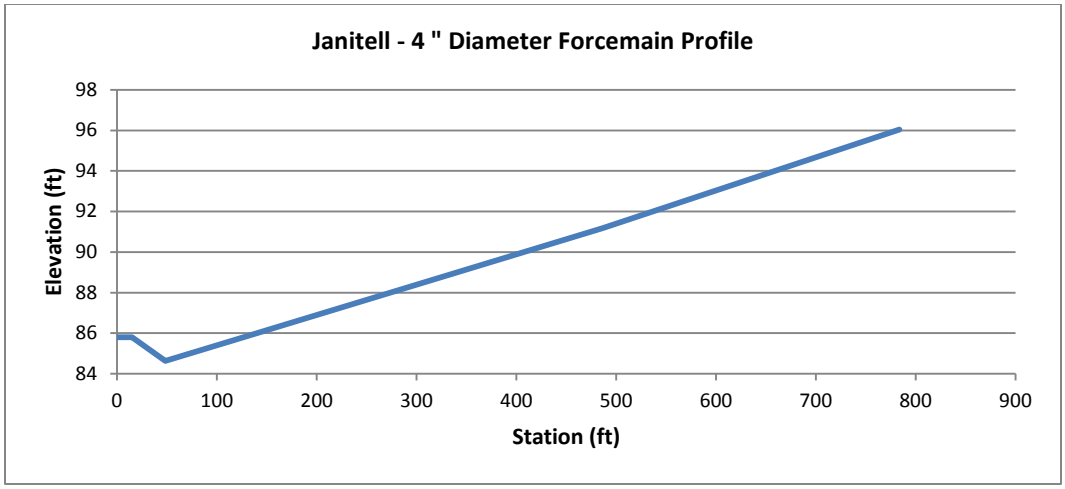

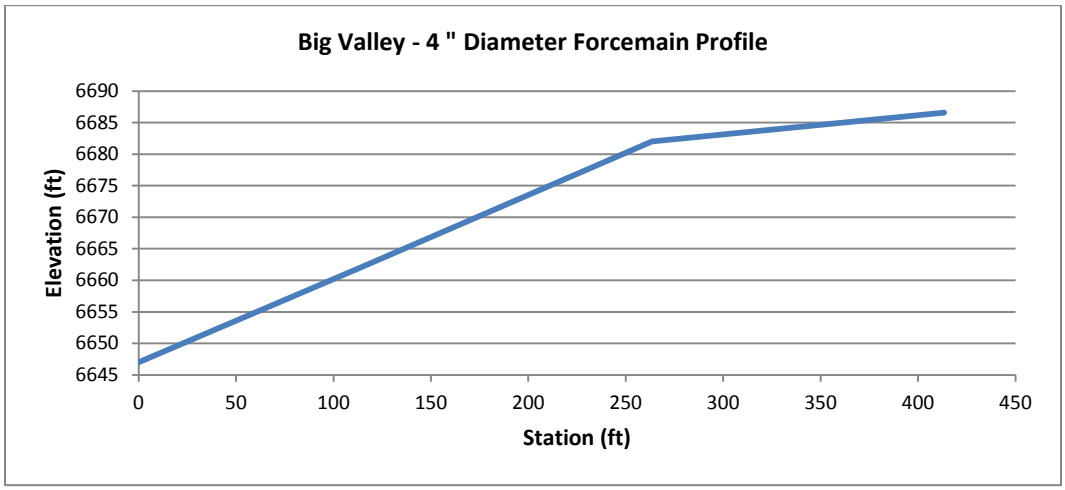

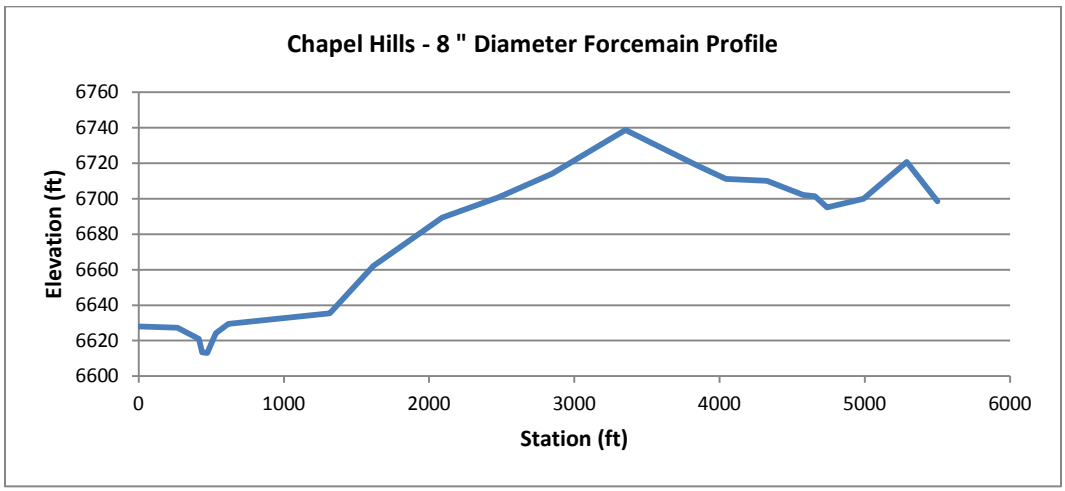

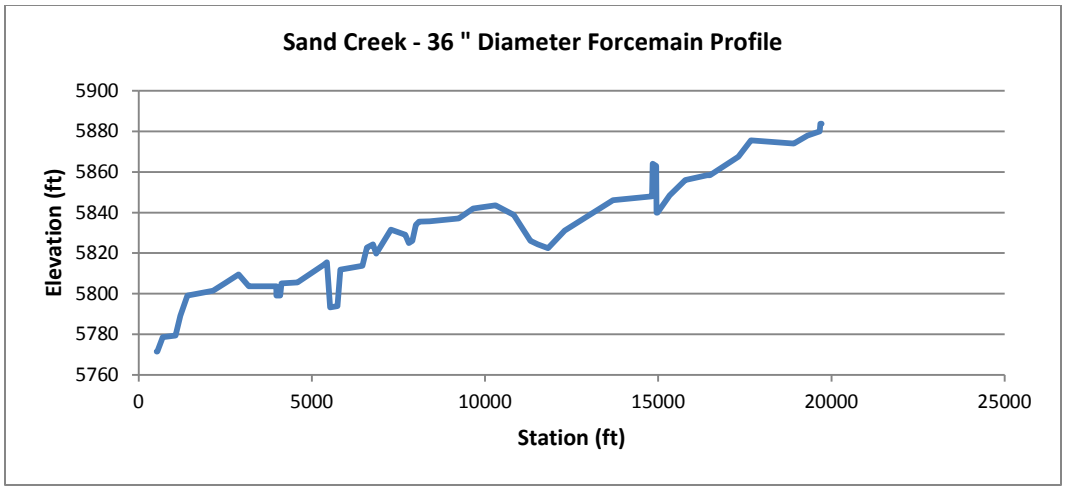
Sand Creek - 36 " Diameter Forcemain Profile
Elevation (ft)
5900
5880
5860
5840
5820
5800
5780
5760
0
5000
10000
15000
20000
25000
Station (ft)

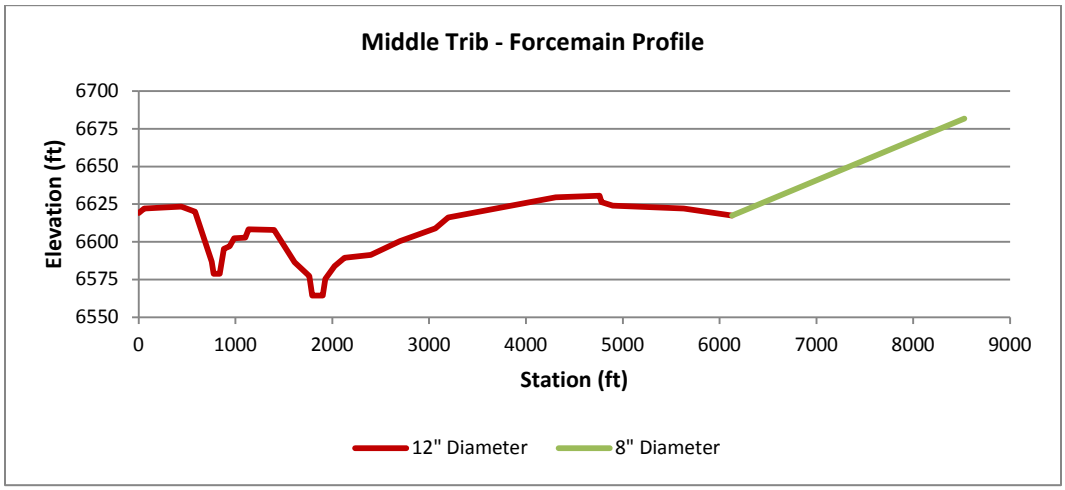
Middle Trib - Forcemain Profile
Elevation (ft)
6700
6675
6650
6625
6600
6575
6550
0
1000
2000
3000
4000
5000
6000
7000
8000
9000
Station (ft)
12" Diameter
8" Diameter

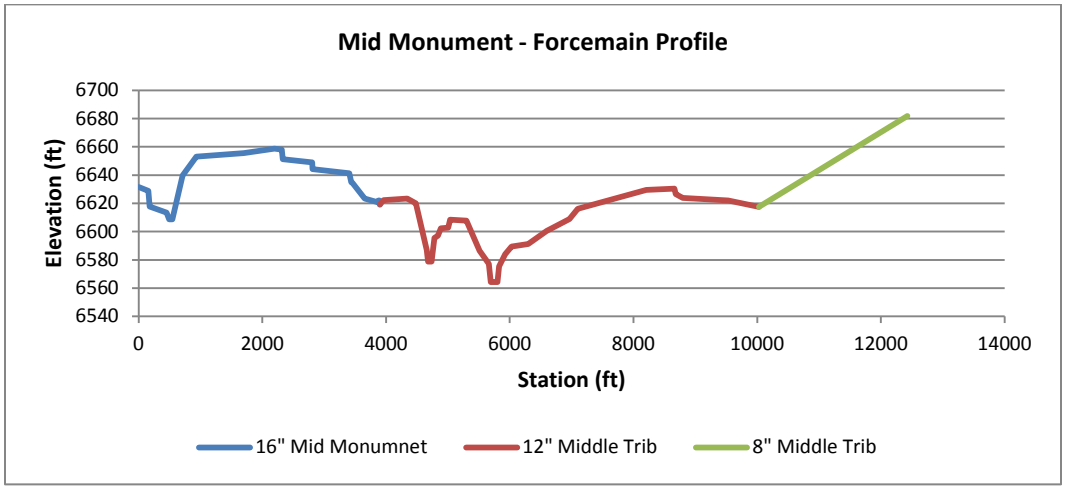
Mid Monument - Forcemain Profile
Elevation (ft)
6700
6680
6660
6640
6620
6600
6580
6560
6540
0
2000
4000
6000
8000
10000
12000
14000
Station (ft)
16" Mid Monumnet
12" Middle Trib
8" Middle Trib

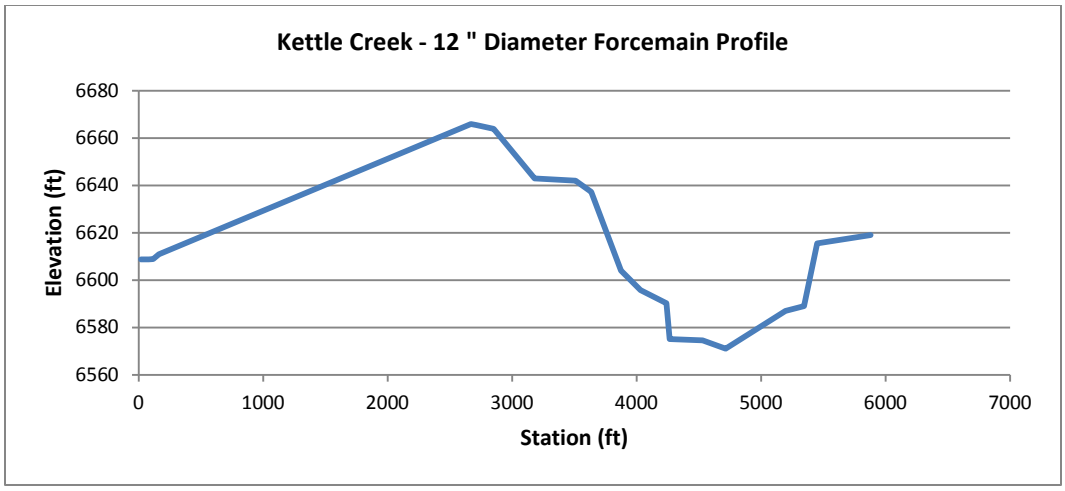
Kettle Creek - 12 " Diameter Forcemain Profile
Elevation (ft)
6680
6660
6640
6620
6600
6580
6560
0
1000
2000
3000
4000
5000
6000
7000
Station (ft)

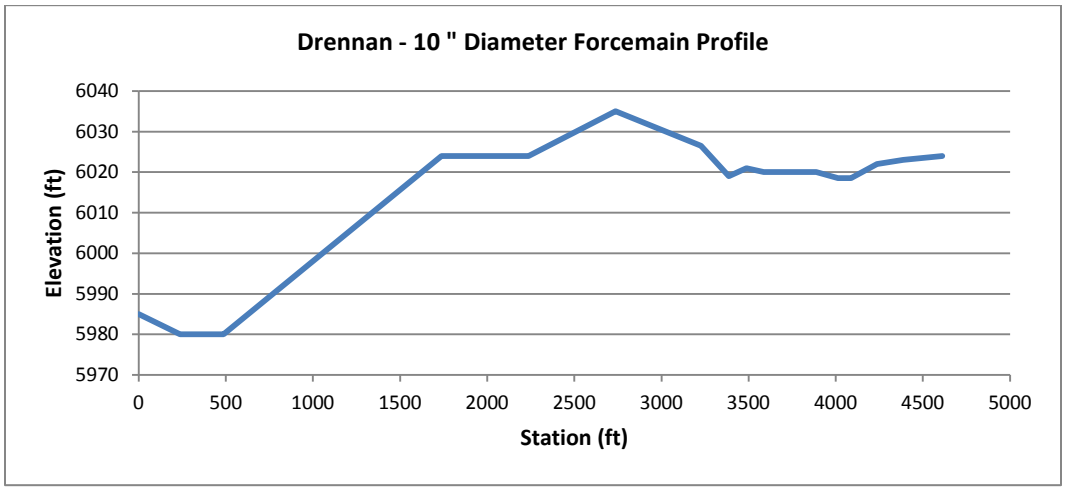
Drennan - 10 " Diameter Forcemain Profile
Elevation (ft)
6040
6030
6020
6010
6000
5990
5980
5970
0
500
1000
1500
2000
2500
3000
3500
4000
4500
5000
Station (ft)

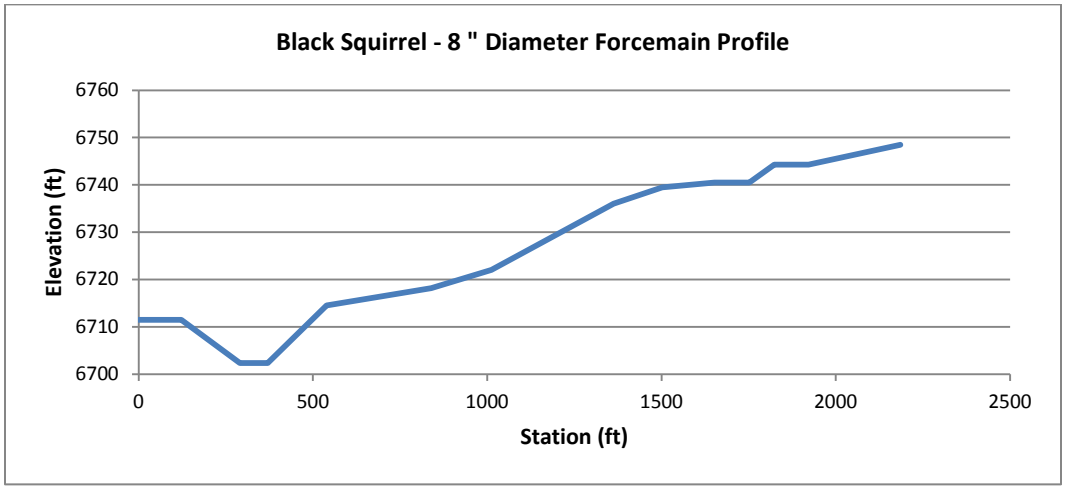
Black Squirrel - 8 " Diameter Forcemain Profile
Elevation (ft)
6760
6750
6740
6730
6720
6710
6700
0
500
1000
1500
2000
2500
Station (ft)

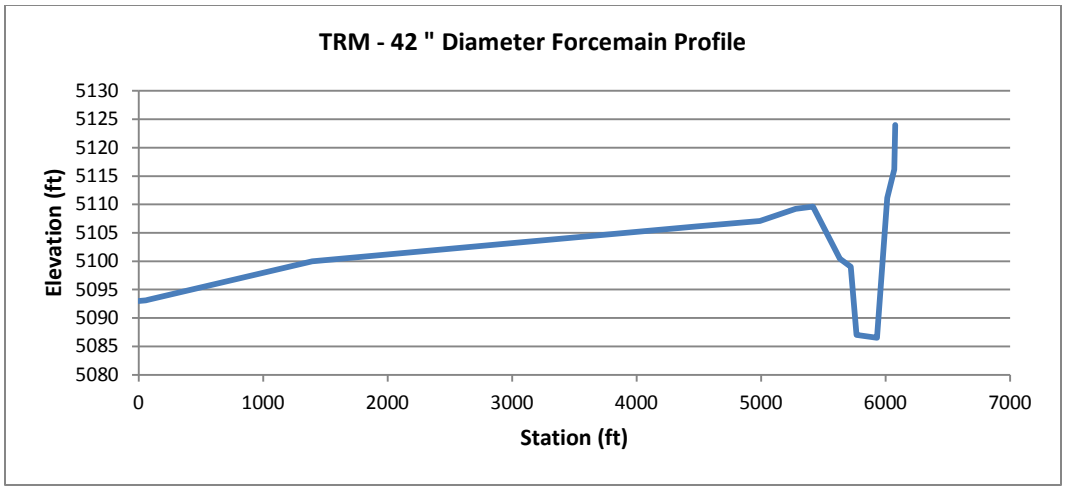
TRM - 42 " Diameter Forcemain Profile
Elevation (ft)
5130
5125
5120
5115
5110
5105
5100
5095
5090
5085
5080
0
1000
2000
3000
4000
5000
6000
7000
Station (ft)

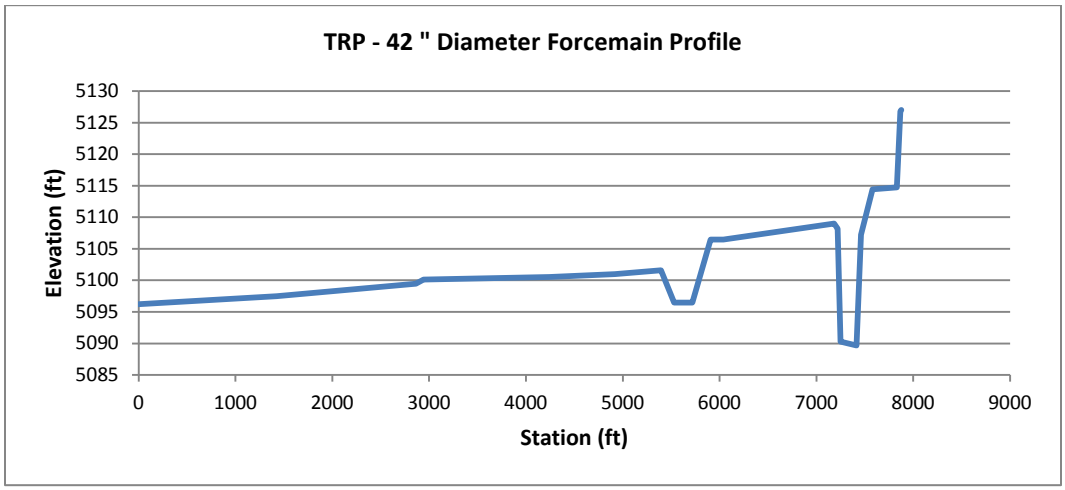
TRP - 42 " Diameter Forcemain Profile
Elevation (ft)
5130
5125
5120
5115
5110
5105
5100
5095
5090
5085
0
1000
2000
3000
4000
5000
6000
7000
8000
9000
Station (ft)

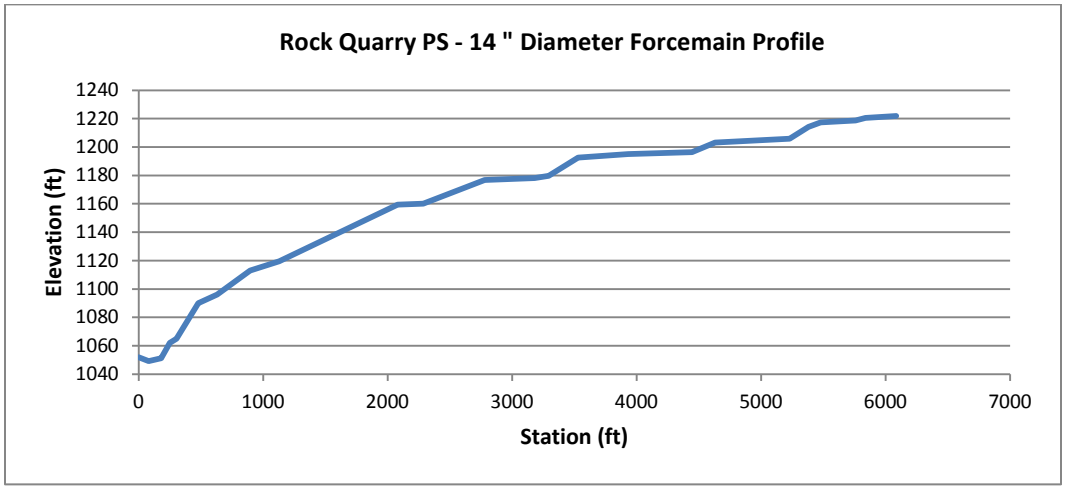
Rock Quarry PS - 14 " Diameter Forcemain Profile
Elevation (ft)
1240
1220
1200
1180
1160
1140
1120
1100
1080
1060
1040
0
1000
2000
3000
4000
5000
6000
7000
Station (ft)

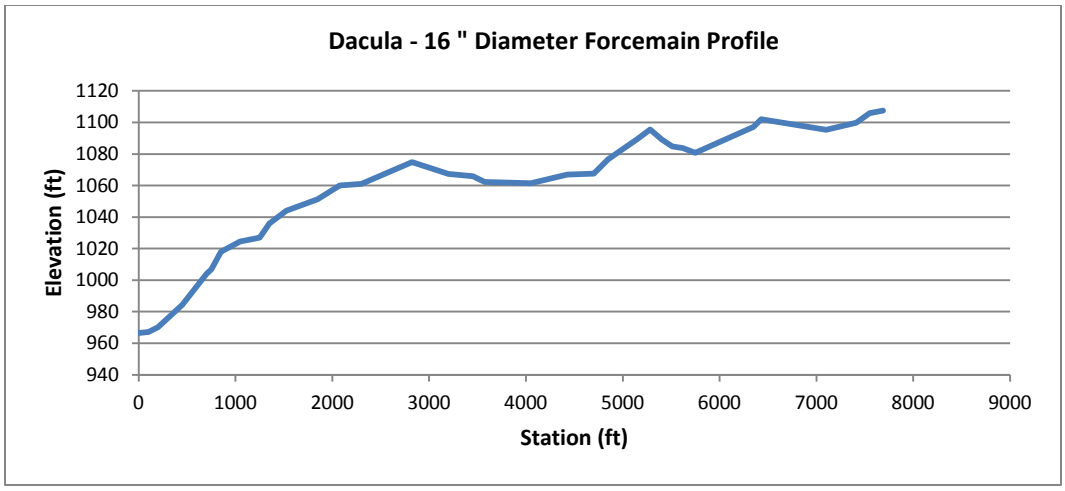
Dacula - 16 " Diameter Forcemain Profile
Elevation (ft)
1120
1100
1080
1060
1040
1020
1000
980
960
940
0
1000
2000
3000
4000
5000
6000
7000
8000
9000
Station (ft)

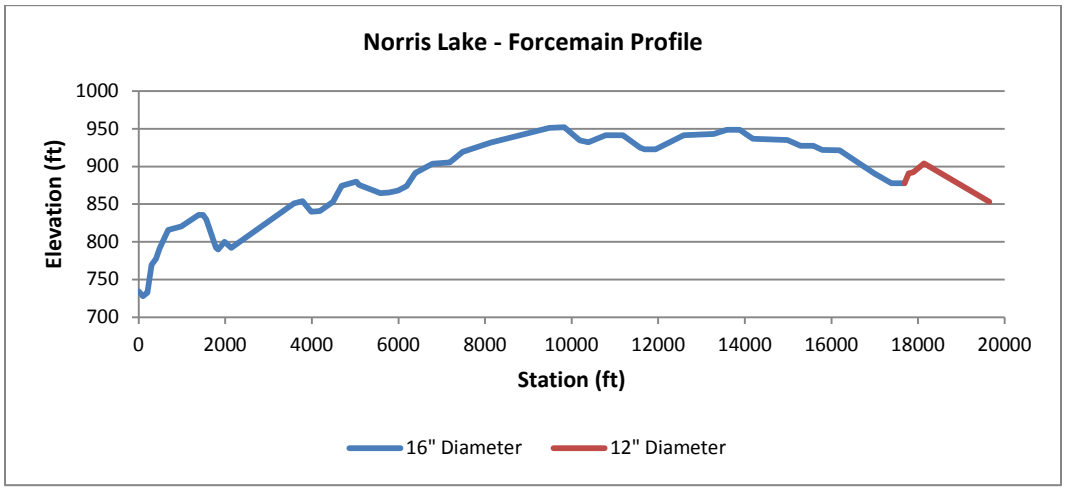
Norris Lake - Forcemain Profile
Elevation (ft)
1000
950
900
850
800
750
700
0
2000
4000
6000
8000
10000
12000
14000
16000
18000
20000
Station (ft)
16" Diameter
12" Diameter

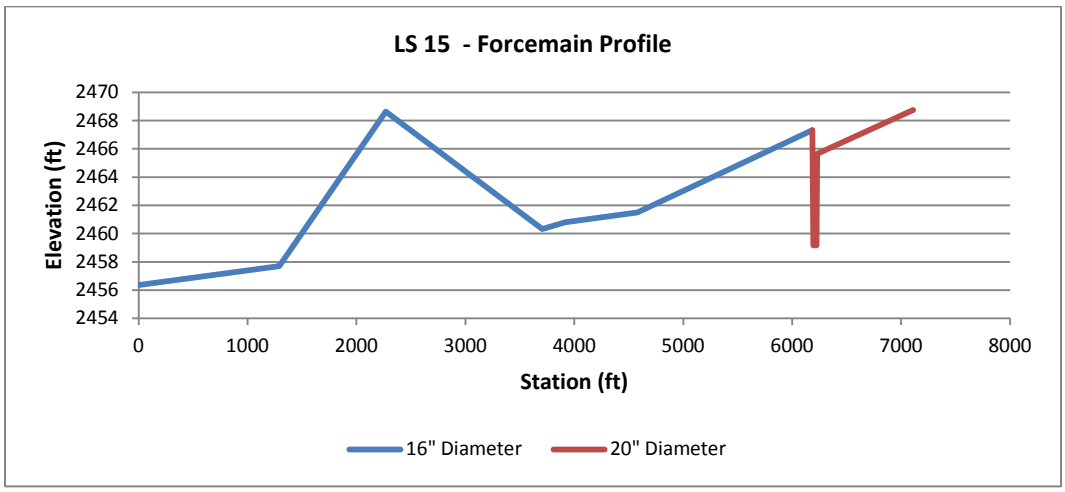
LS 15 - Forcemain Profile
Elevation (ft)
2470
2468
2466
2464
2462
2460
2458
2456
2454
0
1000
2000
3000
4000
5000
6000
7000
8000
Station (ft)
16" Diameter
20" Diameter

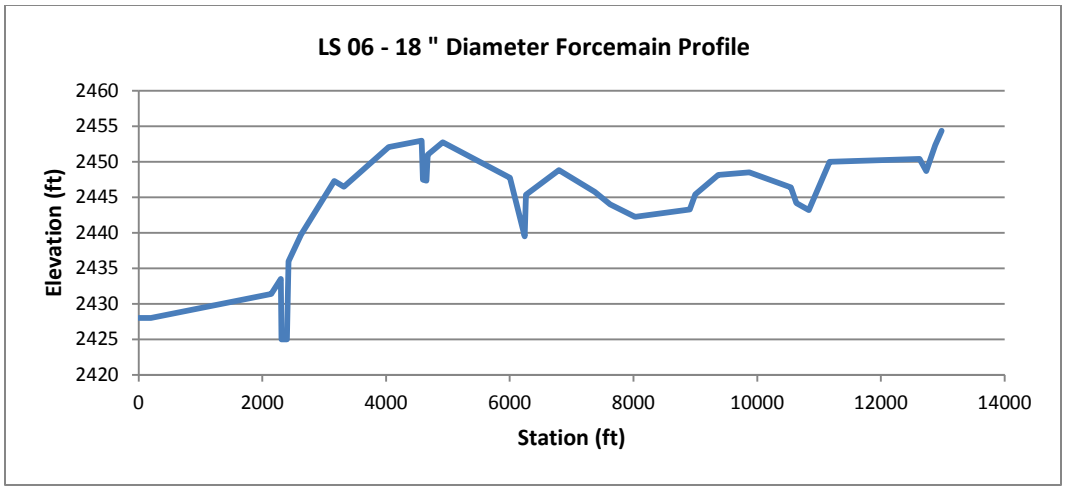
LS 06 - 18 " Diameter Forcemain Profile
Elevation (ft)
2460
2455
2450
2445
2440
2435
2430
2425
2420
0
2000
4000
6000
8000
10000
12000
14000
Station (ft)

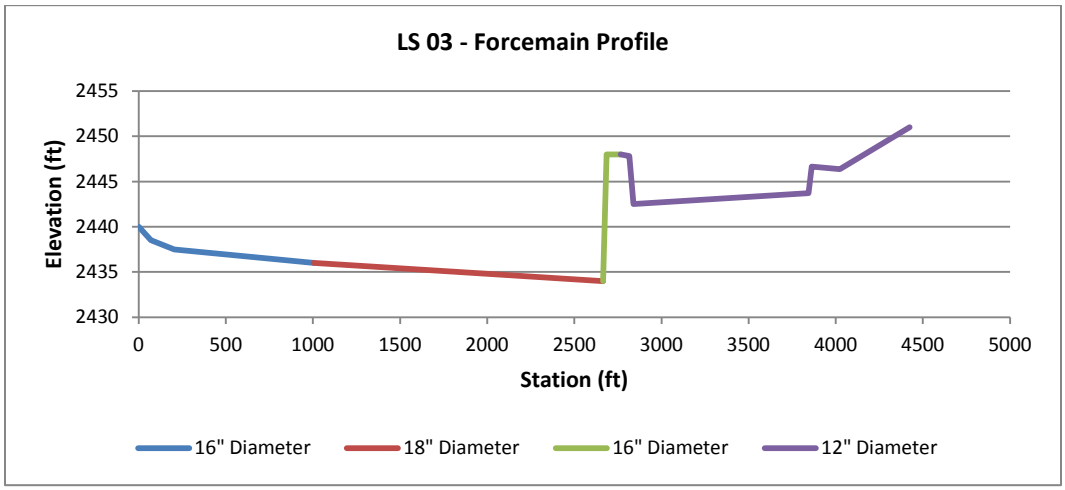
LS 03 - Forcemain Profile
Elevation (ft)
2455
2450
2445
2440
2435
2430
0
500
1000
1500
2000
2500
3000
3500
4000
4500
5000
Station (ft)
16" Diameter
18" Diameter
16" Diameter
12" Diameter

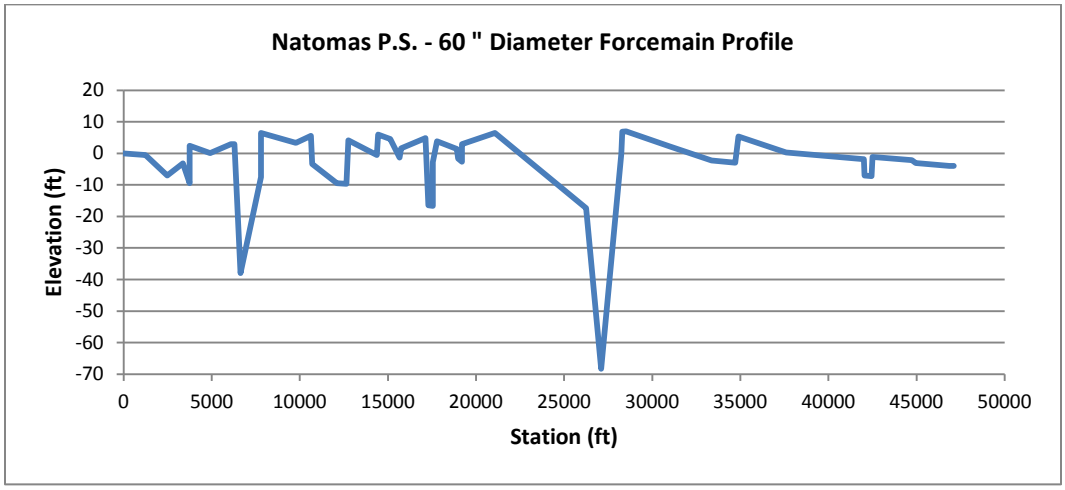
Natomas P.S. - 60 " Diameter Forcemain Profile
Elevation (ft)
20
10
0
-10
-20
-30
-40
-50
-60
-70
0
5000
10000
15000
20000
25000
30000
35000
40000
45000
50000
Station (ft)

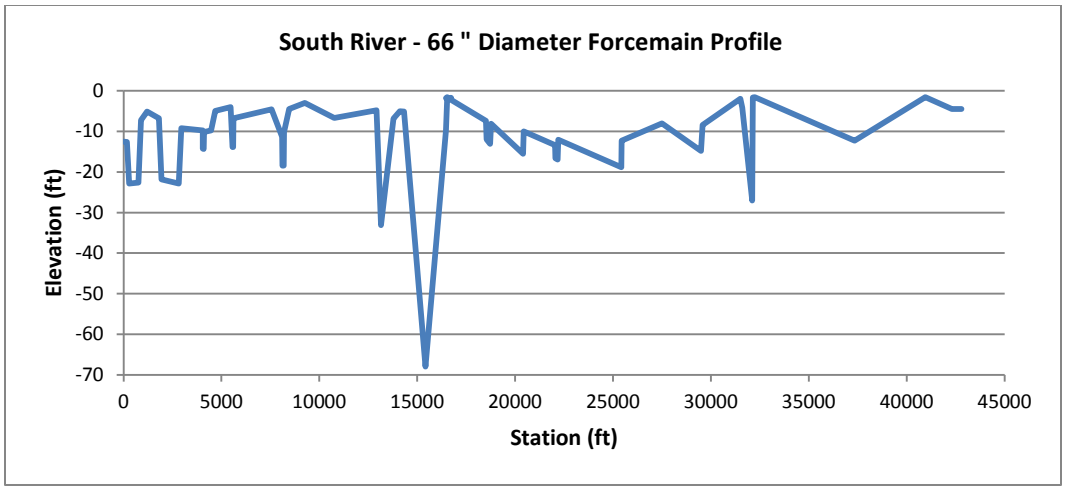
South River - 66 " Diameter Forcemain Profile
Elevation (ft)
0
-10
-20
-30
-40
-50
-60
-70
0
5000
10000
15000
20000
25000
30000
35000
40000
45000
Station (ft)

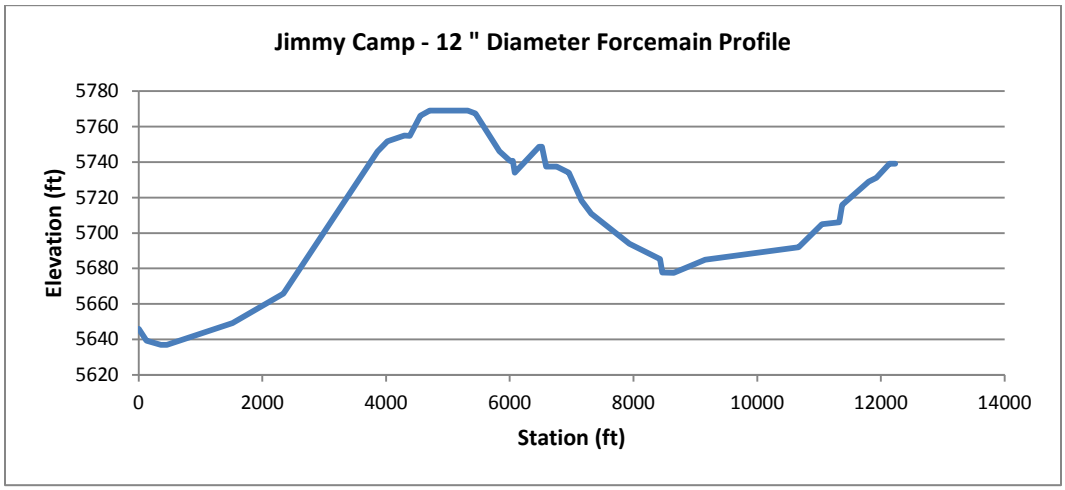
Jimmy Camp - 12 " Diameter Forcemain Profile
Elevation (ft)
5780
5760
5740
5720
5700
5680
5660
5640
5620
0
2000
4000
6000
8000
10000
12000
14000
Station (ft)

Table D.3: HR Wallingford – Results of Hydraulic Calculations

Owner	Project	Pipe Material	Pipe Length (m)	I.D. (in)	Velocity		friction factor, f	$h_{l\,f}$ (ft)	R_e	k_s (in)	k_s (mm)	C-Factor	U* (m/s)	Shear Stress, τ_o	
					(ft/s)	(m/s)								(lb/ft^2)	(N/m^2)
Thames Water	Bibury	PVC	1100	5.024	2.89	0.88	0.0219	24.51	9.5E+04	0.0036	0.092	135.4	0.05	0.04	2.11
Thames Water	Bibury	PVC	1100	5.024	3.02	0.92	0.0193	23.72	9.9E+04	0.0005	0.013	144.9	0.05	0.04	2.04
Thames Water	Bibury	PVC	1100	5.024	2.95	0.90	0.0207	24.28	9.7E+04	0.0021	0.053	139.6	0.05	0.04	2.09
Thames Water	Bibury	PVC	1100	5.024	3.12	0.95	0.0184	23.65	1.0E+05	0.0004	0.010	148.8	0.05	0.04	2.07
Thames Water	Bibury	PVC	1100	5.024	2.89	0.88	0.0216	24.18	9.5E+04	0.0032	0.081	136.5	0.05	0.04	2.08
Thames Water	Bishopstone	CI	1286	5.165	2.59	0.79	0.0258	26.34	9.1E+04	0.0106	0.270	124.4	0.04	0.04	2.01
Thames Water	Bishopstone	CI	1286	5.165	2.07	0.63	0.0430	27.89	7.2E+04	0.0705	1.790	94.4	0.05	0.04	2.13
Thames Water	Bishopstone	CI	1286	5.165	2.36	0.72	0.0312	26.51	8.5E+04	0.0244	0.620	112.2	0.04	0.04	2.02
Thames Water	Bishopstone	CI	1286	5.165	2.69	0.82	0.0250	27.30	9.9E+04	0.0094	0.240	126.4	0.05	0.04	2.10
Thames Water	Bishopstone	CI	1286	5.165	2.82	0.86	0.0262	31.79	1.1E+05	0.0122	0.310	123.3	0.05	0.05	2.42
Thames Water	Bradfield Farm	DIP	980	6.197	3.02	0.92	0.0256	34.45	1.1E+05	0.0118	0.300	120.1	0.05	0.06	2.70
Thames Water	Bradfield Farm	DIP	980	6.197	2.99	0.91	0.0242	34.45	1.1E+05	0.0087	0.220	123.8	0.05	0.05	2.50
Thames Water	Bradfield Farm	DIP	980	6.197	4.04	1.23	0.0184	31.46	1.5E+05	0.0008	0.020	143.5	0.06	0.07	3.47
Thames Water	Bradfield Farm	DIP	980	6.197	2.13	0.65	0.0670	32.25	7.8E+04	0.2445	6.210	71.3	0.06	0.07	3.54
Thames Water	Cheddington SE	DIP	1700	5.701	6.23	1.90	0.0189	133.53	2.7E+05	0.0030	0.076	136.1	0.09	0.18	8.50
Thames Water	Cheddington SE	DIP	1700	5.701	6.40	1.95	0.0181	134.58	2.5E+05	0.0021	0.053	139.3	0.09	0.18	8.59
Thames Water	Cheddington SE	DIP	1700	5.701	6.66	2.03	0.0166	134.12	2.6E+05	0.0008	0.020	146.1	0.09	0.18	8.52
Thames Water	Cheddington SE	DIP	1700	5.701	6.73	2.05	0.0163	134.58	2.6E+05	0.0006	0.015	147.4	0.09	0.18	8.55

Owner	Project	Pipe Material	Pipe Length (m)	I.D. (in)	Velocity		friction factor, f	$h_{l\,f}$ (ft)	R_e	k_s (in)	k_s (mm)	C-Factor	U* (m/s)	Shear Stress, τ_o	
					(ft/s)	(m/s)								(lb/ft^2)	(N/m^2)
Thames Water	Cheddington SE	DIP	1700	5.701	5.25	1.60	0.0257	129.76	2.1E+05	0.0142	0.360	115.2	0.09	0.17	8.22
Thames Water	Cheddington SE	DIP	1700	5.701	6.63	2.02	0.0156	128.05	2.6E+05	0.0007	0.018	148.0	0.09	0.17	7.94
Thames Water	Cheddington SE	DIP	1700	5.701	6.43	1.96	0.0167	125.59	2.5E+05	0.0008	0.021	145.5	0.09	0.17	8.01
Thames Water	Cheddington SE	DIP	1700	5.701	5.48	1.67	0.0231	126.61	2.2E+05	0.0087	0.220	122.1	0.09	0.17	8.04
Thames Water	Dene Hollow	AC	2800	5.193	1.61	0.49	0.0360	30.54	5.8E+04	0.0394	1.000	108.0	0.03	0.02	1.08
Thames Water	Dene Hollow	AC	2800	5.193	1.61	0.49	0.0360	30.54	5.8E+04	0.0394	1.000	108.0	0.03	0.02	1.08
Thames Water	Dene Hollow	AC	2800	5.193	1.38	0.42	0.0400	25.36	4.9E+04	0.0559	1.420	102.0	0.03	0.02	0.88
Thames Water	Dene Hollow	AC	2800	5.193	1.57	0.48	0.0370	30.54	5.6E+04	0.0425	1.080	106.4	0.03	0.02	1.06
Thames Water	Dene Hollow	AC	2800	5.193	1.44	0.44	0.0370	25.36	5.2E+04	0.0429	1.090	106.4	0.03	0.02	0.89
Thames Water	Dene Hollow	AC	2800	5.193	1.77	0.54	0.0300	30.48	6.3E+04	0.0185	0.470	119.2	0.03	0.02	1.09
Thames Water	Dene Hollow	AC	2800	5.193	1.57	0.48	0.0310	25.29	5.6E+04	0.0205	0.520	117.1	0.03	0.02	0.89
Thames Water	Fairmile	Steel	788	5.976	3.61	1.10	0.0431	45.41	1.8E+05	0.0846	2.150	90.4	0.08	0.14	6.52
Thames Water	Fairmile	Steel	788	5.976	4.07	1.24	0.0340	45.18	2.0E+05	0.0409	1.040	102.9	0.08	0.14	6.53
Thames Water	Fairmile	Steel	788	5.976	4.10	1.25	0.0336	45.50	2.0E+05	0.0394	1.000	103.5	0.08	0.14	6.55
Thames Water	Fairmile	Steel	788	5.976	3.97	1.21	0.0360	45.57	1.9E+05	0.0492	1.250	99.8	0.08	0.14	6.57
Thames Water	Fairmile	Steel	788	5.976	4.10	1.25	0.0405	55.02	2.0E+05	0.0709	1.800	93.5	0.09	0.17	7.91
Thames Water	Freckleton	HDPE	2450	22.906	2.99	0.91	0.0175	10.17	5.2E+05	0.0102	0.260	130.4	0.04	0.04	1.81
Thames Water	Freckleton	HDPE	2450	22.906	2.76	0.84	0.0180	8.83	4.3E+05	0.0114	0.290	128.3	0.04	0.03	1.59

Owner	Project	Pipe Material	Pipe Length (m)	I.D. (in)	Velocity		friction factor, f	$h_{l\,f}$ (ft)	R_e	k_s (in)	k_s (mm)	C-Factor	U* (m/s)	Shear Stress, τ_o	
					(ft/s)	(m/s)								(lb/ft^2)	(N/m^2)
Thames Water	Freckleton	HDPE	2450	22.906	2.72	0.83	0.0184	8.86	4.3E+05	0.0130	0.330	126.6	0.04	0.03	1.59
Thames Water	Freckleton	HDPE	2450	22.906	3.25	0.99	0.0165	11.42	5.1E+05	0.0067	0.170	134.6	0.04	0.04	2.02
Thames Water	Garsington	PVC	950	4.063	2.43	0.74	0.0276	23.23	6.4E+04	0.0102	0.260	123.3	0.04	0.04	1.89
Thames Water	Garsington	PVC	950	4.063	2.62	0.80	0.0222	21.75	7.0E+04	0.0022	0.055	138.6	0.04	0.04	1.77
Thames Water	Garsington	PVC	950	4.063	2.62	0.80	0.0220	21.59	7.0E+04	0.0019	0.047	139.5	0.04	0.04	1.75
Thames Water	Garsington	PVC	950	4.063	2.69	0.82	0.0222	22.70	7.1E+04	0.0022	0.057	138.6	0.04	0.04	1.86
Thames Water	Great Coxwell	PVC	1445	5.024	3.44	1.05	0.0456	94.78	1.2E+05	0.0827	2.100	89.2	0.08	0.13	6.28
Thames Water	Great Coxwell	PVC	1445	5.024	3.84	1.17	0.0354	92.19	1.3E+05	0.0386	0.980	102.2	0.08	0.13	6.05
Thames Water	Great Coxwell	PVC	1445	5.024	4.00	1.22	0.0336	94.95	1.4E+05	0.0327	0.830	105.1	0.08	0.13	6.25
Thames Water	Great Coxwell	PVC	1445	5.024	3.84	1.17	0.0356	92.75	1.3E+05	0.0394	1.000	102.0	0.08	0.13	6.08
Thames Water	Great Coxwell	PVC	1445	5.024	4.04	1.23	0.0327	94.39	1.4E+05	0.0299	0.760	106.7	0.08	0.13	6.18
Thames Water	Great Coxwell	PVC	1445	5.024	3.87	1.18	0.0355	93.60	1.3E+05	0.0390	0.990	102.1	0.08	0.13	6.17
Thames Water	Lea Gate (new main)	DIP	3600	39.787	2.89	0.88	0.0232	10.63	8.8E+05	0.0740	1.880	108.6	0.05	0.05	2.25
Thames Water	Lea Gate (new main)	DIP	3600	39.787	2.92	0.89	0.0223	10.56	8.9E+05	0.0622	1.580	111.1	0.05	0.05	2.20
Thames Water	Lea Gate (new main)	DIP	3600	39.787	2.99	0.91	0.0214	10.50	9.1E+05	0.0528	1.340	113.5	0.05	0.05	2.21
Thames Water	Lea Gate (new main)	DIP	3600	39.787	2.99	0.91	0.0213	10.47	9.1E+05	0.0516	1.310	113.8	0.05	0.05	2.20
Thames Water	Lea Gate (new main)	DIP	3600	39.787	2.99	0.91	0.0212	10.47	9.2E+05	0.0504	1.280	114.2	0.05	0.05	2.24
Thames Water	Lea Gate (new main)	DIP	3600	39.787	3.02	0.92	0.0206	10.43	9.2E+05	0.0453	1.150	115.8	0.05	0.05	2.18

Owner	Project	Pipe Material	Pipe Length (m)	I.D. (in)	Velocity		friction factor, f	$h_{l\,f}$ (ft)	R_e	k_s (in)	k_s (mm)	C-Factor	U* (m/s)	Shear Stress, τ_o	
					(ft/s)	(m/s)								(lb/ft^2)	(N/m^2)
Thames Water	Lea Gate (new main)	DIP	3600	39.787	2.79	0.85	0.0250	10.73	8.5E+05	0.0984	2.500	104.3	0.05	0.05	2.26
Thames Water	Lea Gate (new main)	DIP	3600	39.787	2.92	0.89	0.0223	10.56	8.9E+05	0.0626	1.590	111.1	0.05	0.05	2.20
Thames Water	Nether Winchendon	MDPE	904	3.976	3.54	1.08	0.0346	60.14	1.0E+05	0.0276	0.700	106.6	0.07	0.11	5.03
Thames Water	Nether Winchendon	MDPE	904	3.976	3.64	1.11	0.0326	59.84	1.0E+05	0.0224	0.570	110.1	0.07	0.10	5.01
Thames Water	Nether Winchendon	MDPE	904	3.976	3.64	1.11	0.0320	59.15	1.0E+05	0.0213	0.540	111.1	0.07	0.10	4.93
Thames Water	Nether Winchendon	MDPE	904	3.976	3.64	1.11	0.0316	58.30	9.6E+04	0.0201	0.510	111.9	0.07	0.10	4.86
Thames Water	Nether Winchendon	MDPE	904	3.976	3.74	1.14	0.0299	58.50	9.4E+04	0.0161	0.410	115.2	0.07	0.10	4.86
Thames Water	Rissington	DIP	570	9.732	3.51	1.07	0.0420	18.67	2.3E+05	0.1283	3.260	88.7	0.08	0.13	6.00
Thames Water	Rissington	DIP	570	9.732	3.05	0.93	0.0450	14.80	2.0E+05	0.1539	3.910	85.4	0.07	0.10	4.86
Thames Water	Stadhampton	CI	780	4.016	2.20	0.70	0.0501	30.97	5.3E+04	0.0831	2.110	90.0	0.05	0.06	2.81
Thames Water	Stadhampton	CI	780	4.016	2.46	0.75	0.0454	32.35	5.9E+04	0.0634	1.610	94.9	0.06	0.07	3.19
Thames Water	Stadhampton	CI	780	4.016	2.46	0.75	0.0483	34.84	5.9E+04	0.0756	1.920	91.8	0.06	0.07	3.39
Thames Water	Stadhampton	CI	780	4.016	2.39	0.73	0.0537	36.61	5.7E+04	0.1004	2.550	86.7	0.06	0.07	3.57
Thames Water	Stadhampton	CI	780	4.016	2.39	0.73	0.0567	38.48	5.7E+04	0.1150	2.920	84.2	0.06	0.08	3.77
Thames Water	Stadhampton	CI	780	4.016	2.36	0.72	0.0619	40.98	5.7E+04	0.143	3.620	80.3	0.06	0.08	4.01
Thames Water	Stadhampton	CI	780	4.016	2.43	0.74	0.0537	37.93	5.8E+04	0.100	2.550	86.7	0.06	0.08	3.67
Thames Water	Whitchurch Hill	Steel	1440	4.217	2.23	0.68	0.0354	36.45	6.7E+04	0.030	0.770	108.8	0.05	0.04	2.04
Thames Water	Whitchurch Hill	Steel	1440	4.217	1.97	0.60	0.0439	35.79	6.8E+04	0.061	1.540	96.8	0.04	0.04	1.97

Owner	Project	Pipe Material	Pipe Length (m)	I.D. (in)	Velocity		friction factor, f	$h_{l\,f}$ (ft)	R_e	k_s (in)	k_s (mm)	C-Factor	U* (m/s)	Shear Stress, τ_o	
					(ft/s)	(m/s)								(lb/ft^2)	(N/m^2)
Thames Water	Whitchurch Hill	Steel	1440	4.217	2.07	0.63	0.0361	32.48	7.1E+04	0.033	0.830	107.7	0.04	0.04	1.79
Thames Water	Whitchurch Hill	Steel	1440	4.217	2.23	0.68	0.0315	32.38	7.7E+04	0.020	0.510	115.9	0.04	0.04	1.82
Thames Water	Whitchurch Hill	Steel	1440	4.217	2.00	0.61	0.0381	31.73	6.9E+04	0.039	0.990	104.6	0.04	0.04	1.77
Thames Water	Whitchurch Hill	Steel	1440	4.217	2.10	0.64	0.0359	32.94	7.2E+04	0.032	0.810	108.1	0.04	0.04	1.83
Thames Water	Whitchurch Hill	Steel	1440	4.217	2.10	0.64	0.0373	34.05	7.2E+04	0.037	0.930	105.8	0.04	0.04	1.91
United Utilities	Church St	DIP	620	8.087	3.77	1.15	0.0173	11.65	2.2E+05	0.001	0.037	143.2	0.05	0.06	2.86
United Utilities	Church St	DIP	620	8.087	4.27	1.30	0.0168	14.27	2.4E+05	0.001	0.030	145.5	0.06	0.07	3.55
United Utilities	Church St	DIP	620	8.087	4.07	1.24	0.0202	15.55	2.3E+05	0.006	0.160	132.0	0.06	0.08	3.87
United Utilities	Hebden Green	CI	382	6.319	4.04	1.23	0.0393	23.82	1.8E+05	0.069	1.740	94.5	0.09	0.16	7.43
United Utilities	Hebden Green	CI	382	6.319	3.90	1.19	0.0425	23.95	1.8E+05	0.086	2.180	90.6	0.09	0.16	7.51
United Utilities	Hebden Green	CI	382	6.319	4.04	1.23	0.0393	23.82	1.9E+05	0.069	1.740	94.5	0.09	0.16	7.43
United Utilities	Hebden Green	CI	382	6.319	1.44	0.44	0.1340	10.53	3.9E+04	1.009	25.630	48.7	0.06	0.07	3.24
United Utilities	Hebden Green	CI	382	6.319	1.54	0.47	0.1200	10.50	4.2E+04	0.842	21.380	51.7	0.06	0.07	3.31
United Utilities	Hebden Green	CI	382	6.319	1.48	0.45	0.1310	10.53	4.0E+04	0.966	24.540	49.3	0.06	0.07	3.31
United Utilities	Heskin Lane	CI	215	6.307	7.32	2.23	0.0255	28.38	3.3E+05	0.016	0.400	113.4	0.13	0.33	15.83
United Utilities	Heskin Lane	CI	215	6.307	7.71	2.35	0.0244	30.28	3.5E+05	0.013	0.340	116.0	0.13	0.35	16.83
United Utilities	Highway Lane	CI	620	4.425	3.44	1.05	0.0275	27.79	1.1E+05	0.013	0.330	116.5	0.06	0.08	3.78
United Utilities	Highway Lane	CI	620	4.425	3.54	1.08	0.0259	27.72	1.1E+05	0.010	0.250	120.3	0.06	0.08	3.76

Owner	Project	Pipe Material	Pipe Length (m)	I.D. (in)	Velocity		friction factor, f	$h_{l\,f}$ (ft)	R_e	k_s (in)	k_s (mm)	C-Factor	U* (m/s)	Shear Stress, τ_o	
					(ft/s)	(m/s)								(lb/ft^2)	(N/m^2)
United Utilities	Highway Lane	CI	620	4.425	3.48	1.06	0.0266	27.76	1.1E+05	0.011	0.280	118.5	0.06	0.08	3.73
United Utilities	Highway Lane	CI	620	4.425	4.10	1.18	0.0187	23.95	1.3E+05	0.000	0.012	143.3	0.06	0.08	3.65
United Utilities	The Dell	CI	233	3.181	2.99	0.91	0.0507	20.05	6.7E+04	0.069	1.740	85.8	0.07	0.11	5.24
United Utilities	The Dell	CI	233	3.181	2.95	0.90	0.0516	20.05	6.8E+04	0.072	1.820	85.0	0.07	0.11	5.22
United Utilities	The Dell	CI	233	3.181	2.95	0.90	0.0508	20.05	7.0E+04	0.069	1.760	85.7	0.07	0.11	5.14
United Utilities	The Dell	CI	233	3.181	2.82	0.86	0.0542	19.16	6.2E+04	0.081	2.070	82.7	0.07	0.10	5.01
United Utilities	The Dell	CI	233	3.181	2.92	0.89	0.0525	20.08	6.5E+04	0.075	1.910	84.2	0.07	0.11	5.20
United Utilities	The Dell	CI	233	3.181	2.95	0.90	0.0516	20.05	6.2E+04	0.072	1.820	85.0	0.07	0.11	5.22
United Utilities	The Dell	CI	233	3.181	5.48	1.67	0.0273	36.78	1.2E+05	0.009	0.240	119.8	0.10	0.20	9.52
United Utilities	The Dell	CI	233	3.181	5.31	1.62	0.0294	36.97	1.1E+05	0.012	0.310	115.3	0.10	0.20	9.62
United Utilities	The Dell	CI	233	3.181	5.18	1.58	0.0308	37.07	1.1E+05	0.015	0.380	112.2	0.10	0.20	9.61
Previous Study	Bland et al.	Clay	NA	3.937	2.49	0.76	0.0622		4.2E+04	0.139	3.520	78.1	0.07	0.09	4.49
Previous Study	Bland et al.	Clay	NA	3.937	3.61	1.10	0.0390		6.1E+04	0.039	0.980	97.6	0.08	0.12	5.89
Previous Study	Bland et al.	Clay	NA	3.937	3.77	1.15	0.0251		6.4E+04	0.006	0.160	123.3	0.06	0.09	4.15
Previous Study	Bland et al.	Clay	NA	3.937	6.89	2.10	0.0224		1.2E+05	0.004	0.110	125.0	0.11	0.26	12.32
Previous Study	Bland et al.	PVC	NA	3.937	2.49	0.76	0.0655		4.2E+04	0.156	3.970	76.0	0.07	0.10	4.72
Previous Study	Bland et al.	PVC	NA	3.937	3.61	1.10	0.0400		6.1E+04	0.042	1.070	96.2	0.08	0.13	6.05
Previous Study	Bland et al.	PVC	NA	3.937	4.92	1.50	0.0261		8.4E+04	0.009	0.220	118.1	0.09	0.15	7.34

Owner	Project	Pipe Material	Pipe Length (m)	I.D. (in)	Velocity		friction factor, f	$h_{l\,f}$ (ft)	R_e	k_s (in)	k_s (mm)	C-Factor	U* (m/s)	Shear Stress, τ_o	
					(ft/s)	(m/s)								(lb/ft^2)	(N/m^2)
Previous Study	Bland et al.	PVC	NA	3.937	6.89	2.10	0.0205		1.2E+05	0.002	0.060	131.2	0.11	0.24	11.27
Previous Study	Clay6	RCP	NA	25.000	4.76	1.45	0.0149		5.1E+05	0.003	0.088	157.6	0.06	0.08	3.90
Previous Study	Clay6	RCP	NA	25.000	5.25	1.60	0.0138		5.7E+05	0.002	0.043	162.4	0.07	0.09	4.43
Previous Study	Clay6	RCP	NA	18.504	2.56	0.78	0.0184		2.0E+05	0.008	0.195	148.0	0.04	0.03	1.40
Previous Study	Clay6	RCP	NA	18.504	5.54	1.69	0.0194		4.4E+05	0.014	0.360	135.4	0.08	0.14	6.90
Previous Study	Clay6	RCP	NA	10.984	4.89	1.49	0.0172		2.3E+05	0.003	0.073	146.4	0.07	0.10	4.78
Previous Study	Clay6	RCP	NA	10.984	5.02	1.53	0.0173		2.4E+05	0.003	0.076	145.9	0.07	0.11	5.05
Previous Study	Clay6	RCP	NA	10.984	8.73	2.66	0.0166		4.1E+05	0.003	0.085	142.4	0.12	0.31	14.70
Previous Study	Clay6	RCP	NA	10.984	8.83	2.69	0.0164		4.2E+05	0.003	0.076	143.5	0.12	0.31	14.79
Previous Study	Clay6	RCP	NA	10.984	8.96	2.73	0.0161		4.3E+05	0.003	0.067	144.7	0.12	0.31	14.97
Previous Study	Flaxman7	AC	NA	9.016	2.69	0.82	0.0177		1.8E+05	0.024	0.610	151.9	0.04	0.03	1.48
Previous Study	Flaxman7	AC	NA	9.016	2.69	0.82	0.0177		1.8E+05	0.036	0.910	151.9	0.04	0.03	1.48
Previous Study	Flaxman7	CI	NA	5.000	3.38	1.03	0.0353		7.3E+04	0.036	0.910	103.3	0.07	0.10	4.67
Previous Study	Flaxman7	CI	NA	5.000	3.38	1.03	0.0353		7.3E+04	0.036	0.910	103.3	0.07	0.10	4.67
Previous Study	Green, Wessex W.A.	PVC	NA	9.843	2.43	0.74	0.0272		1.0E+05	0.028	0.700	121.2	0.04	0.04	1.86
Previous Study	Green, Wessex W.A.	PVC	NA	9.843	6.56	2.00	0.0154		2.8E+05	0.001	0.020	152.1	0.09	0.16	7.69
Previous Study	HRS8	PVC	NA	15.157	4.53	1.38	0.0160		3.0E+05	0.002	0.060	153.0	0.06	0.08	3.80
Previous Study	HRS8	PVC	NA	15.157	4.53	1.38	0.0185		3.0E+05	0.008	0.200	141.5	0.07	0.09	4.39

Table D.4: Papers and Reports – Results of Hydraulic Calculations

Source	Project	Pipe Material	Pipe Length (ft)	I.D. (in)	Velocity		friction factor f (ft)	$h_{l\,f}$ (ft)	$h_{l\,total}$ (ft)	R_e	k_s (mm)	k_s (in)	C-Factor	U* (m/s)	Shear Stress τ_o	
					(ft/s)	(m/s)									(lb/ft^2)	(N/m^2)
Report	LS 4	CIP	507	4.30	2.14	0.65	0.0874	8.80	9.07	6.27E+04	8.18	0.32	66.5	0.068	0.097	4.649
Report	LS 9	DIP	3760	10.50	2.97	0.90	0.0391	22.98	23.29	2.12E+05	2.86	0.11	92.4	0.063	0.083	3.996
Report	LS 16	DIP	4725	6.30	1.92	0.59	0.0786	40.70	40.84	8.25E+04	9.69	0.38	68.6	0.058	0.071	3.379
Report	LS 12	DIP	620	4.18	3.12	0.95	0.0534	14.34	14.55	8.86E+04	2.64	0.10	84.5	0.078	0.126	6.014
Report	LS 15	DIP	818	4.18	2.41	0.74	0.1939	41.24	41.35	6.86E+04	28.68	1.13	42.9	0.115	0.274	13.104
Johannessen (2014)		DIP	14610	24.17	1.70	0.52	0.0516			2.80E+05	14.23	0.56	77.0	0.042	0.036	1.731
Johannessen (2014)		AC	1370	4.50	1.40	0.43	0.1234			4.29E+04	15.89	0.63	57.0	0.053	0.059	2.806
Johannessen (2014)		AC/DIP	11250	15.88	1.80	0.55	0.0524			1.95E+05	9.70	0.38	79.0	0.044	0.041	1.971
Johannessen (2014)		CCP	9400	29.52	1.40	0.43	0.0457			2.81E+05	12.62	0.50	82.0	0.032	0.022	1.040
Johannessen (2014)		CIP	450	17.48	1.30	0.40	0.0611			1.55E+05	15.50	0.61	74.0	0.035	0.025	1.199
Johannessen (2014)		DIP	8300	8.17	5.10	1.55	0.0235			2.84E+05	0.38	0.01	119.0	0.084	0.148	7.102
Johannessen (2014)		DIP	1930	19.82	2.60	0.79	0.0268			3.51E+05	1.56	0.06	108.0	0.046	0.044	2.102
Johannessen (2014)		DIP	8360	20.13	2.10	0.64	0.0312			2.88E+05	2.71	0.11	101.0	0.040	0.033	1.598
Johannessen (2014)		DIP	8070	23.82	2.00	0.61	0.0336			3.24E+05	4.09	0.16	96.0	0.040	0.033	1.559
Johannessen (2014)		DIP	7240	24.22	2.90	0.88	0.0424			4.78E+05	8.44	0.33	82.0	0.064	0.086	4.138
Johannessen (2014)		DIP	640	6.28	3.60	1.10	0.0259			1.54E+05	0.40	0.02	119.0	0.062	0.081	3.899
Johannessen (2014)		PVC	3280	12.10	3.10	0.94	0.0360			2.55E+05	2.57	0.10	95.0	0.063	0.084	4.012
Johannessen (2014)		PVC	4630	18.00	2.10	0.64	0.0420			2.57E+05	6.05	0.24	87.0	0.046	0.045	2.147
Johannessen (2014)		RCP	2150	47.91	3.20	0.98	0.0240			1.04E+06	2.59	0.10	104.0	0.053	0.059	2.848

APPENDIX E Pump Cycle Results

Table E.1: Research Data Pumping Cycle Results

System	FM Volume (ft^3)	Number of Pumps Operating	Pumping Cycle Date / Time	Average Discharge / Cycle (cfs)	Pump Run Time (min)	Volume Pumped (ft^3)	% of FM Volume Pumped / Cycle	Hydraulic Retention Time (min)	k_s (mm)
Janitell	68.4	1	4/18/2014 8:05	0.19	115.0	1279.3	1870.4%	6.1	27.20
		1	4/18/2014 12:34	0.20	258.5	3154.2	4611.4%	5.6	19.23
		1	4/30/2014 1:06	0.21	4.5	57.9	84.7%	5.3	14.80
		1	5/1/2014 13:49	0.19	187.0	2172.3	3175.9%	5.9	22.66
		1	6/27/2014 19:38	0.15	6.0	55.6	81.3%	7.4	46.07
		1	7/19/2014 21:32	0.12	7.0	51.7	75.6%	9.3	76.39
		1	7/23/2014 8:10	0.20	375.0	4528.1	6620.1%	5.7	20.93
		1	7/28/2014 16:11	0.21	63.5	798.8	1167.8%	5.4	16.80
		1	4/23/2014 9:28	0.25	42.5	628.6	918.9%	4.6	7.11
		1	5/29/2014 13:13	0.23	290.5	4081.0	5966.4%	4.9	10.75
Kettle Creek	5020.4	1	10/1/2014 7:52	2.21	7.0	930.2	18.5%	37.8	62.17
		1	4/16/2014 0:02	1.86	5.5	614.9	12.2%	44.9	110.73
		1	6/15/2014 21:15	2.07	8.5	1054.4	21.0%	40.5	80.05
		1	6/27/2014 19:32	2.12	5.5	698.5	13.9%	39.5	73.67
		1	7/19/2014 21:35	2.02	6.5	789.7	15.7%	41.3	85.71
		1	9/30/2014 8:22	2.22	19.0	2535.5	50.5%	37.6	60.96
		1	10/1/2014 6:50	2.67	6.0	962.3	19.2%	31.3	22.31
		1	5/1/2014 8:37	2.63	5.0	790.1	15.7%	31.8	24.92
		2	6/17/2014 10:53	4.82	8.5	2459.1	49.0%	17.4	1.47
		1	5/18/2014 13:49	2.00	11.5	1377.7	27.4%	41.9	90.01
Big Valley	38.1	1	5/1/2014 0:33	0.17	2.0	19.9	52.2%	3.8	11.72
		1	5/5/2014 12:22	0.16	2.5	24.3	63.8%	3.9	13.38
		1	5/28/2014 23:22	0.20	2.0	23.7	62.1%	3.2	4.45
		1	6/7/2014 14:48	0.18	2.5	27.5	72.1%	3.5	7.31
		1	6/26/2014 8:53	0.17	2.0	19.9	52.3%	3.8	12.09
		1	7/6/2014 14:31	0.19	2.5	29.0	76.2%	3.3	5.19
		1	7/17/2014 10:49	0.18	2.5	27.7	72.7%	3.4	6.94
		1	7/20/2014 16:19	0.17	3.5	34.9	91.6%	3.8	11.41

System	FM Volume (ft^3)	Number of Pumps Operating	Pumping Cycle Date / Time	Average Discharge / Cycle (cfs)	Pump Run Time (min)	Volume Pumped (ft^3)	% of FM Volume Pumped / Cycle	Hydraulic Retention Time (min)	k_s (mm)
		1	9/26/2014 6:41	0.15	3.5	31.0	81.4%	4.3	19.63
		1	8/31/2014 20:49	0.23	2.0	27.9	73.2%	2.7	1.09
Chapel Hills	2059.8	1	4/16/2014 2:11	0.94	2.5	140.8	6.8%	36.6	12.57
		1	4/16/2014 6:11	0.94	3.5	198.1	9.6%	36.4	12.24
		1	4/26/2014 22:13	0.98	3.5	205.0	10.0%	35.2	10.34
		1	5/15/2014 7:04	0.91	3.5	192.1	9.3%	37.5	14.21
		1	6/7/2014 3:21	1.05	3.0	189.0	9.2%	32.7	7.00
		1	8/16/2014 8:41	0.91	2.5	136.2	6.6%	37.8	14.63
		1	9/11/2014 6:25	0.92	5.0	275.5	13.4%	37.4	13.89
		1	10/1/2014 7:29	0.97	4.0	233.8	11.4%	35.2	10.53
		1	9/29/2014 6:48	0.87	5.0	262.4	12.7%	39.2	17.41
		1	6/23/2014 0:13	1.11	3.5	232.9	11.3%	31.0	5.02
Drennan	2504.1	1	10/1/2014 3:23	1.99	1.5	178.9	7.1%	21.0	0.93
		1	4/16/2014 22:34	1.28	1.5	115.3	4.6%	32.6	27.99
		1	9/30/2014 20:01	1.83	1.5	165.1	6.6%	22.8	2.65
		1	9/30/2014 16:18	1.47	1.5	131.9	5.3%	28.5	14.28
		1	9/12/2014 18:21	1.94	1.5	174.9	7.0%	21.5	1.38
		1	5/9/2014 0:15	1.58	1.5	142.0	5.7%	26.5	9.04
		1	5/9/2014 11:05	1.80	1.5	161.8	6.5%	23.2	2.96
		1	5/22/2014 23:15	1.38	1.5	124.3	5.0%	30.2	19.63
		1	9/12/2014 16:37	1.73	1.5	156.1	6.2%	24.1	4.45
		1	8/30/2014 11:24	1.75	1.5	157.3	6.3%	23.9	4.16
Black Squirrel	817.6	1	5/1/2014 0:09	2.21	1.5	198.8	24.3%	6.2	1.41
		1	6/2/2014 13:33	2.37	1.5	213.3	26.1%	5.8	0.76
		1	6/30/2014 22:34	2.28	1.5	205.6	25.1%	6.0	1.06
		1	7/12/2014 19:29	2.36	2.0	283.1	34.6%	5.8	0.79
		1	7/24/2014 20:48	2.35	2.0	281.5	34.4%	5.8	0.85
		1	8/3/2014 21:28	2.35	2.5	353.1	43.2%	5.8	0.83
		1	8/4/2014 17:58	2.32	1.5	208.7	25.5%	5.9	0.92
		1	8/20/2014 13:06	2.33	1.5	209.3	25.6%	5.9	0.90
		1	9/3/2014 2:57	2.42	1.5	217.4	26.6%	5.6	0.61
		1	9/30/2014 1:17	2.31	1.5	207.7	25.4%	5.9	1.01
Middle Trib	4890.6	1	4/30/2014 6:42	2.11	3.5	444.1	9.1%	38.5	23.35

System	FM Volume (ft^3)	Number of Pumps Operating	Pumping Cycle Date / Time	Average Discharge / Cycle (cfs)	Pump Run Time (min)	Volume Pumped (ft^3)	% of FM Volume Pumped / Cycle	Hydraulic Retention Time (min)	k_s (mm)
		1	5/2/2014 19:20	2.19	3.0	393.5	8.0%	37.3	19.42
		1	6/7/2014 10:28	2.38	3.5	500.5	10.2%	34.2	9.24
		1	9/5/2014 12:41	2.39	3.0	430.4	8.8%	34.1	9.11
		1	8/10/2014 0:10	2.43	3.0	437.3	8.9%	33.6	7.76
		1	8/9/2014 22:10	2.47	3.5	518.0	10.6%	33.0	6.58
		1	5/19/2014 19:21	2.47	3.0	444.4	9.1%	33.0	6.49
		1	9/30/2014 18:19	2.48	3.5	521.6	10.7%	32.8	6.03
		1	8/28/2014 12:07	2.60	3.0	467.8	9.6%	31.4	3.24
		1	8/28/2014 6:21	2.61	3.5	547.1	11.2%	31.3	3.12
Middle Trib	1910.9	1	4/30/2014 6:42	2.11	3.5	444.1	23.2%	15.1	0.15
		1	5/2/2014 19:20	2.19	3.0	393.5	20.6%	14.6	0.12
		1	6/7/2014 10:28	2.38	3.5	500.5	26.2%	13.4	0.10
		1	9/5/2014 12:41	2.39	3.0	430.4	22.5%	13.3	0.10
		1	8/10/2014 0:10	2.43	3.0	437.3	22.9%	13.1	0.10
		1	8/9/2014 22:10	2.47	3.5	518.0	27.1%	12.9	0.10
		1	5/19/2014 19:21	2.47	3.0	444.4	23.3%	12.9	0.10
		1	9/30/2014 18:19	2.48	3.5	521.6	27.3%	12.8	0.10
		1	8/28/2014 12:07	2.60	3.0	467.8	24.5%	12.3	0.10
		1	8/28/2014 6:21	2.61	3.5	547.1	28.6%	12.2	0.10
Mid Monument	5880.9	1	4/1/2014 8:21	2.09	3.0	375.4	6.4%	47.0	87.71
		1	9/30/2014 15:24	2.36	2.5	353.4	6.0%	41.6	62.80
		1	8/9/2014 20:06	1.90	2.5	284.8	4.8%	51.6	118.22
		1	5/9/2014 16:27	1.99	2.0	239.1	4.1%	49.2	101.18
		1	6/18/2014 10:05	2.13	2.5	320.0	5.4%	45.9	81.63
		1	6/7/2014 9:12	2.19	3.0	393.5	6.7%	44.8	75.52
		1	6/7/2014 10:24	2.27	3.0	408.7	6.9%	43.2	67.42
		1	5/2/2014 20:19	2.31	3.0	415.0	7.1%	42.5	65.91
		1	4/7/2014 16:30	2.34	2.5	351.0	6.0%	41.9	63.76
		1	4/18/2014 9:15	2.35	2.0	282.5	4.8%	41.6	63.00
Mid Monument	4890.6	1	4/1/2014 8:21	2.09	3.0	375.4	7.7%	39.1	15.47
		1	9/30/2014 15:24	2.36	2.5	353.4	7.2%	34.6	4.56
		1	8/9/2014 20:06	1.90	2.5	284.8	5.8%	42.9	27.91
		1	5/9/2014 16:27	1.99	2.0	239.1	4.9%	40.9	20.97

System	FM Volume (ft^3)	Number of Pumps Operating	Pumping Cycle Date / Time	Average Discharge / Cycle (cfs)	Pump Run Time (min)	Volume Pumped (ft^3)	% of FM Volume Pumped / Cycle	Hydraulic Retention Time (min)	k_s (mm)
		1	6/18/2014 10:05	2.13	2.5	320.0	6.5%	38.2	13.00
		1	6/7/2014 9:12	2.19	3.0	393.5	8.0%	37.3	10.51
		1	6/7/2014 10:24	2.27	3.0	408.7	8.4%	35.9	7.20
		1	5/2/2014 20:19	2.31	3.0	415.0	8.5%	35.4	6.07
		1	4/7/2014 16:30	2.34	2.5	351.0	7.2%	34.8	5.03
		1	4/18/2014 9:15	2.35	2.0	282.5	5.8%	34.6	4.66
Mid Monument	897.7	1	4/1/2014 8:21	2.09	3.0	375.4	41.8%	7.2	0.12
		1	9/30/2014 15:24	2.36	2.5	353.4	39.4%	6.4	0.10
		1	8/9/2014 20:06	1.90	2.5	284.8	31.7%	7.9	0.14
		1	5/9/2014 16:27	1.99	2.0	239.1	26.6%	7.5	0.13
		1	6/18/2014 10:05	2.13	2.5	320.0	35.7%	7.0	0.11
		1	6/7/2014 9:12	2.19	3.0	393.5	43.8%	6.8	0.11
		1	6/7/2014 10:24	2.27	3.0	408.7	45.5%	6.6	0.10
		1	5/2/2014 20:19	2.31	3.0	415.0	46.2%	6.5	0.10
		1	4/7/2014 16:30	2.34	2.5	351.0	39.1%	6.4	0.10
		1	4/18/2014 9:15	2.35	2.0	282.5	31.5%	6.4	0.10
Norris Lake	26763.7	1	5/4/2015 0:02	5.95	5.3	1873.8	7.0%	75.0	1.99
		1	5/4/2015 0:32	5.84	10.0	3506.9	13.1%	76.3	2.30
		1	5/4/2015 1:05	5.88	9.3	3262.1	12.2%	75.9	2.23
		1	5/4/2015 1:43	5.91	8.5	3012.7	11.3%	75.5	2.15
		1	5/4/2015 2:27	5.84	8.5	2977.6	11.1%	76.4	2.28
		1	5/4/2015 6:44	5.83	1.3	466.4	1.7%	76.5	2.26
		1	5/4/2015 7:31	5.87	8.5	2993.8	11.2%	76.0	2.02
		1	5/4/2015 23:58	5.84	7.5	2626.2	9.8%	76.4	2.54
		1	5/4/2015 23:01	5.94	10.8	3833.9	14.3%	75.0	2.25
		1	5/4/2015 22:04	5.86	11.0	3866.1	14.4%	76.1	2.54
Norris Lake	2797.2	1	5/4/2015 0:02	5.95	5.3	1873.8	67.0%	7.8	0.11
		1	5/4/2015 0:32	5.84	10.0	3506.9	125.4%	8.0	0.11
		1	5/4/2015 1:05	5.88	9.3	3262.1	116.6%	7.9	0.11
		1	5/4/2015 1:43	5.91	8.5	3012.7	107.7%	7.9	0.11
		1	5/4/2015 2:27	5.84	8.5	2977.6	106.5%	8.0	0.11
		1	5/4/2015 6:44	5.83	1.3	466.4	16.7%	8.0	0.11
		1	5/4/2015 7:31	5.87	8.5	2993.8	107.0%	7.9	0.11

System	FM Volume (ft^3)	Number of Pumps Operating	Pumping Cycle Date / Time	Average Discharge / Cycle (cfs)	Pump Run Time (min)	Volume Pumped (ft^3)	% of FM Volume Pumped / Cycle	Hydraulic Retention Time (min)	k_s (mm)
		1	5/4/2015 23:58	5.84	7.5	2626.2	93.9%	8.0	0.11
		1	5/4/2015 23:01	5.94	10.8	3833.9	137.1%	7.8	0.11
		1	5/4/2015 22:04	5.86	11.0	3866.1	138.2%	8.0	0.11
Rock Quarry PS	7080.8	1	4/15/2015 0:55	2.95	6.0	1062.3	15.0%	40.0	5.79
		1	4/15/2015 4:56	2.96	6.0	1066.7	15.1%	39.8	5.32
		1	4/15/2015 7:09	2.94	6.8	1191.8	16.8%	40.1	5.78
		1	4/15/2015 10:44	2.95	6.3	1106.6	15.6%	40.0	5.59
		1	4/15/2015 23:20	2.97	6.0	1070.0	15.1%	39.7	5.12
		2	4/15/2015 6:16	4.06	5.8	1399.9	19.8%	29.1	4.11
		2	4/15/2015 7:57	4.10	6.0	1476.9	20.9%	28.8	3.76
		2	4/15/2015 9:47	4.09	5.5	1350.3	19.1%	28.8	3.84
		2	4/15/2015 22:12	4.04	5.8	1393.7	19.7%	29.2	4.26
		2	4/15/2015 3:02	4.09	5.5	1348.7	19.0%	28.9	3.92
Dacula	11561.9	1	5/4/2015 0:06	4.55	3.0	819.8	7.1%	42.3	11.98
		1	5/4/2015 0:17	4.27	6.5	1665.5	14.4%	45.1	19.25
		1	5/4/2015 0:43	4.27	5.8	1473.5	12.7%	45.1	19.12
		1	5/4/2015 3:47	4.52	2.3	610.0	5.3%	42.6	12.78
		1	5/4/2015 5:16	4.25	2.8	700.6	6.1%	45.4	19.87
		1	5/4/2015 5:59	4.25	3.0	765.8	6.6%	45.3	19.68
		1	5/4/2015 6:40	4.50	3.3	878.4	7.6%	42.8	13.17
		1	5/4/2015 8:05	4.50	0.3	90.1	0.8%	42.8	13.14
		1	5/4/2015 23:56	4.54	4.3	1158.2	10.0%	42.4	12.30
		1	5/4/2015 23:06	4.23	2.8	698.1	6.0%	45.5	20.45
LS 03	1187.7	1	1/1/2015 0:11	5.27	1.0	316.1	26.6%	3.8	5.76
		1	1/1/2015 5:55	4.79	1.0	287.4	24.2%	4.1	11.73
		1	1/16/2015 14:30	4.31	1.0	258.7	21.8%	4.6	15.99
		1	1/14/2015 18:22	4.31	2.0	517.3	43.6%	4.6	15.89
		1	4/28/2015 13:32	4.79	1.0	287.4	24.2%	4.1	11.65
		1	3/1/2015 23:23	4.31	1.0	258.7	21.8%	4.6	16.00
		1	2/26/2015 15:53	4.31	1.0	258.7	21.8%	4.6	15.95
		1	2/26/2015 14:01	4.79	1.0	287.4	24.2%	4.1	11.65
		1	2/23/2015 0:16	4.31	1.0	258.7	21.8%	4.6	15.98
		1	2/21/2015 18:17	4.31	1.0	258.7	21.8%	4.6	15.84

System	FM Volume (ft^3)	Number of Pumps Operating	Pumping Cycle Date / Time	Average Discharge / Cycle (cfs)	Pump Run Time (min)	Volume Pumped (ft^3)	% of FM Volume Pumped / Cycle	Hydraulic Retention Time (min)	k_s (mm)
LS 03	2245.9	1	1/1/2015 0:11	5.27	1.0	316.1	14.1%	7.1	20.63
		1	1/1/2015 5:55	4.79	1.0	287.4	12.8%	7.8	57.41
		1	1/16/2015 14:30	4.31	1.0	258.7	11.5%	8.7	108.03
		1	1/14/2015 18:22	4.31	2.0	517.3	23.0%	8.7	107.25
		1	4/28/2015 13:32	4.79	1.0	287.4	12.8%	7.8	56.38
		1	3/1/2015 23:23	4.31	1.0	258.7	11.5%	8.7	108.05
		1	2/26/2015 15:53	4.31	1.0	258.7	11.5%	8.7	107.69
		1	2/26/2015 14:01	4.79	1.0	287.4	12.8%	7.8	56.45
		1	2/23/2015 0:16	4.31	1.0	258.7	11.5%	8.7	107.92
		1	2/21/2015 18:17	4.31	1.0	258.7	11.5%	8.7	106.83
LS 03	1321.4	1	1/1/2015 0:11	5.27	1.0	316.1	23.9%	4.2	0.76
		1	1/1/2015 5:55	4.79	1.0	287.4	21.8%	4.6	1.75
		1	1/16/2015 14:30	4.31	1.0	258.7	19.6%	5.1	4.92
		1	1/14/2015 18:22	4.31	2.0	517.3	39.2%	5.1	4.88
		1	4/28/2015 13:32	4.79	1.0	287.4	21.8%	4.6	1.74
		1	3/1/2015 23:23	4.31	1.0	258.7	19.6%	5.1	4.92
		1	2/26/2015 15:53	4.31	1.0	258.7	19.6%	5.1	4.90
		1	2/26/2015 14:01	4.79	1.0	287.4	21.8%	4.6	1.74
		1	2/23/2015 0:16	4.31	1.0	258.7	19.6%	5.1	4.91
		1	2/21/2015 18:17	4.31	1.0	258.7	19.6%	5.1	4.86
LS 06	21769.1	1	1/1/2015 0:02	4.54	4.0	1090.8	5.0%	79.8	11.81
		1	1/10/2015 18:25	4.60	7.0	1930.2	8.9%	78.9	11.19
		1	1/21/2015 8:40	4.37	8.0	2097.9	9.6%	83.0	15.22
		1	1/31/2015 10:32	4.68	7.0	1965.6	9.0%	77.5	9.90
		1	2/6/2015 0:01	2.60	908.0	141470.2	649.9%	139.7	132.81
		1	2/20/2015 22:58	4.34	6.0	1562.8	7.2%	83.6	15.91
		1	3/1/2015 10:46	4.39	15.0	3955.4	18.2%	82.6	14.83
		1	3/14/2015 19:34	4.58	6.0	1649.1	7.6%	79.2	11.40
		1	1/15/2015 11:39	5.95	11.0	3929.4	18.1%	60.9	1.29
		1	4/23/2015 9:49	5.25	9.0	2837.0	13.0%	69.1	4.29
LS 15	14598.4	1	4/29/2015 9:45	3.78	7.0	1587.8	10.9%	64.4	39.48
		1	4/29/2015 9:12	3.80	7.0	1594.1	10.9%	64.1	38.80
		1	4/29/2015 0:30	3.73	7.0	1568.5	10.7%	65.2	42.01

System	FM Volume (ft^3)	Number of Pumps Operating	Pumping Cycle Date / Time	Average Discharge / Cycle (cfs)	Pump Run Time (min)	Volume Pumped (ft^3)	% of FM Volume Pumped / Cycle	Hydraulic Retention Time (min)	k_s (mm)
		1	4/28/2015 21:21	3.77	11.0	2491.4	17.1%	64.5	39.87
		1	4/22/2015 19:18	3.75	14.0	3151.2	21.6%	64.9	41.11
		1	3/31/2015 20:23	3.73	11.0	2459.2	16.8%	65.3	42.43
		1	3/17/2015 18:10	3.88	9.0	2095.2	14.4%	62.7	34.46
		1	3/1/2015 23:09	3.63	8.0	1740.3	11.9%	67.1	48.59
		1	1/4/2015 21:21	3.67	4.0	881.3	6.0%	66.3	46.09
		1	2/19/2015 17:03	3.73	7.0	1567.5	10.7%	65.2	42.23
LS 15	1347.7	1	4/29/2015 9:45	3.78	7.0	1587.8	117.8%	5.9	85.24
		1	4/29/2015 9:12	3.80	7.0	1594.1	118.3%	5.9	82.39
		1	4/29/2015 0:30	3.73	7.0	1568.5	116.4%	6.0	83.65
		1	4/28/2015 21:21	3.77	11.0	2491.4	184.9%	6.0	82.81
		1	4/22/2015 19:18	3.75	14.0	3151.2	233.8%	6.0	83.30
		1	3/31/2015 20:23	3.73	11.0	2459.2	182.5%	6.0	83.81
		1	3/17/2015 18:10	3.88	9.0	2095.2	155.5%	5.8	80.68
		1	3/1/2015 23:09	3.63	8.0	1740.3	129.1%	6.2	86.24
		1	1/4/2015 21:21	3.67	4.0	881.3	65.4%	6.1	85.26
		1	2/19/2015 17:03	3.73	7.0	1567.5	116.3%	6.0	83.74
Jimmy Camp	8373.0	1	3/29/2014 0:00	3.07	1.0	184.3	2.2%	45.4	0.43
		1	3/17/2015 14:45	3.15	1.5	283.5	3.4%	44.3	0.33
		1	3/18/2015 9:57	3.10	1.8	340.9	4.1%	45.0	0.39
		1	3/28/2015 3:40	3.15	1.3	251.9	3.0%	44.3	0.33
		1	4/4/2015 18:20	3.09	1.8	339.9	4.1%	45.2	0.41
		1	4/5/2015 18:18	3.12	1.8	343.4	4.1%	44.7	0.37
		1	4/16/2015 13:58	3.15	1.8	346.0	4.1%	44.4	0.34
		1	4/17/2015 23:20	3.13	1.5	281.4	3.4%	44.6	0.36
		1	4/23/2015 6:00	3.12	1.3	249.5	3.0%	44.7	0.37
		1	5/1/2015 23:42	3.12	2.2	405.3	4.8%	44.8	0.37

Appendix E.2 Research Data Pumping Cycle Charts

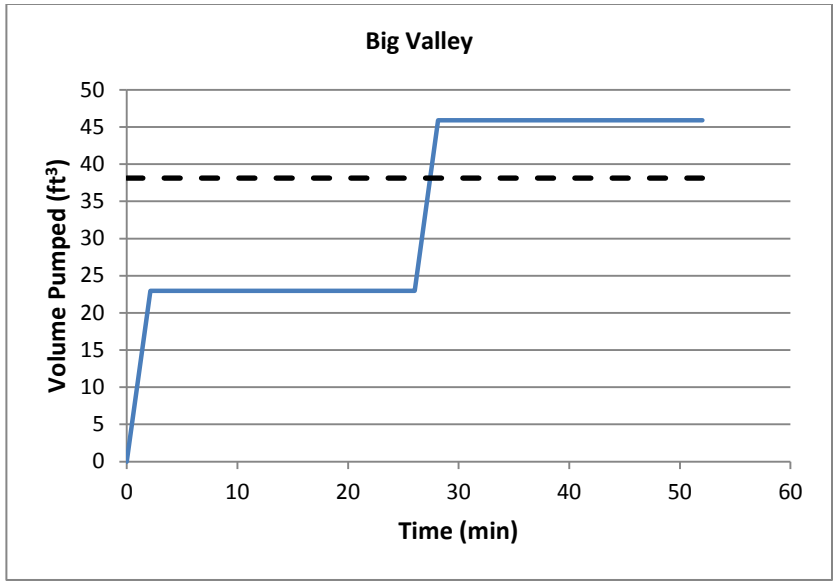

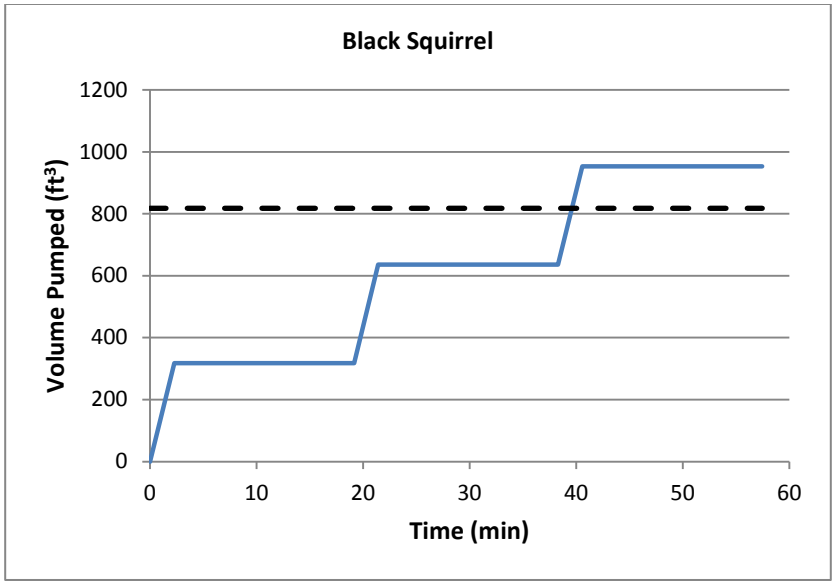

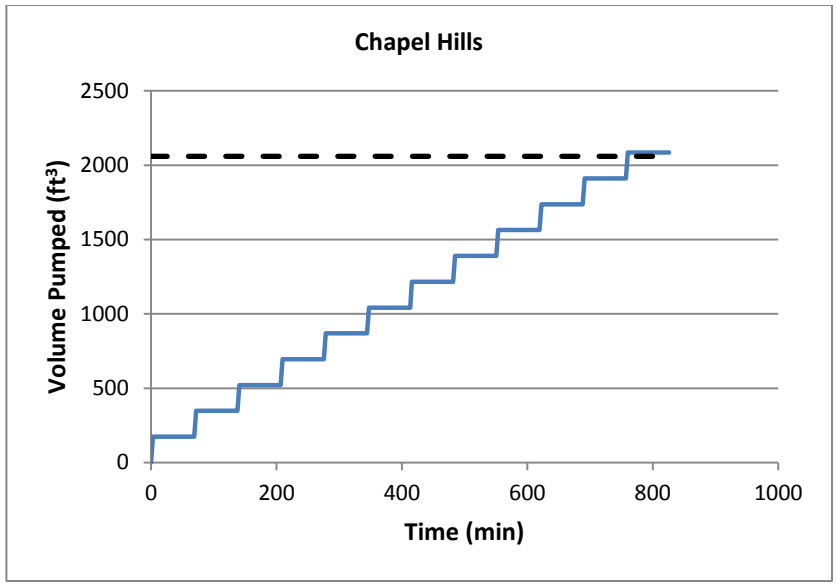
Chapel Hills
Volume Pumped (ft³)
2500
2000
1500
1000
500
0
0
200
400
600
800
1000
Time (min)

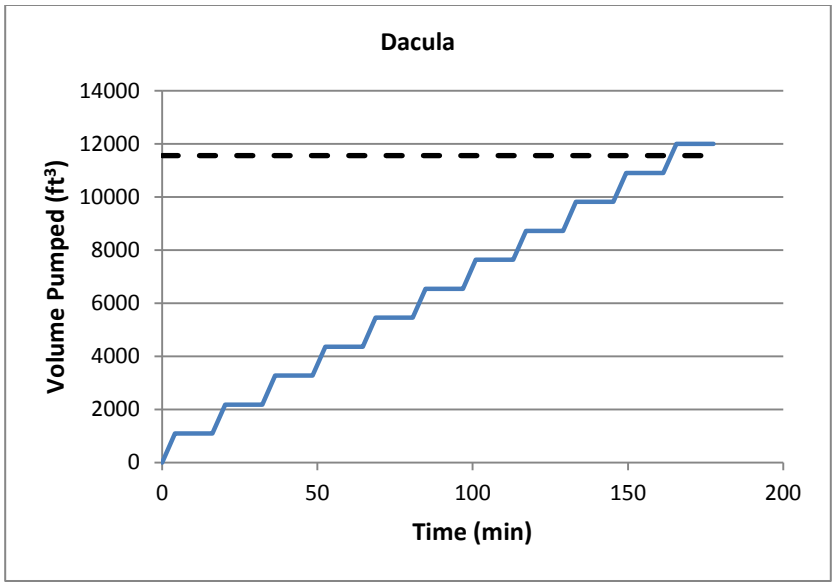
Dacula
Volume Pumped (ft³)
14000
12000
10000
8000
6000
4000
2000
0
0
50
100
150
200
Time (min)

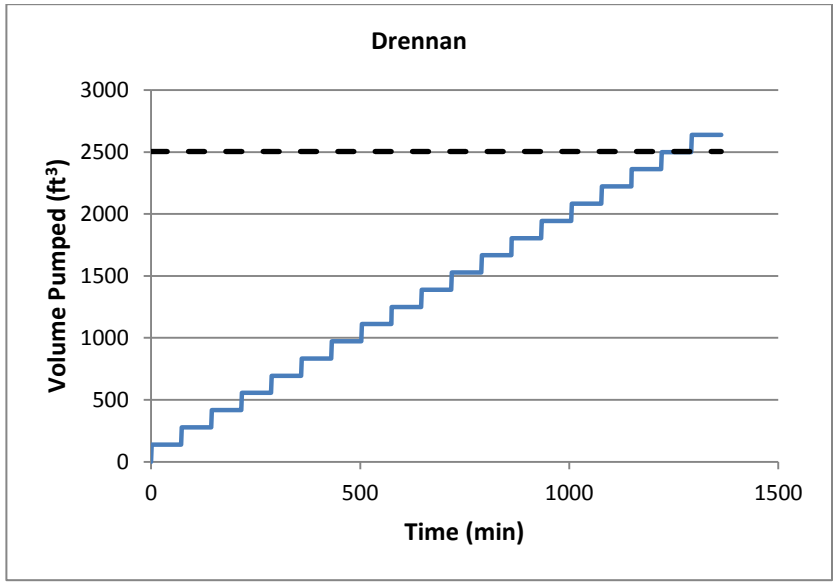
Drennan
Volume Pumped (ft³)
3000
2500
2000
1500
1000
500
0
0
500
1000
1500
Time (min)

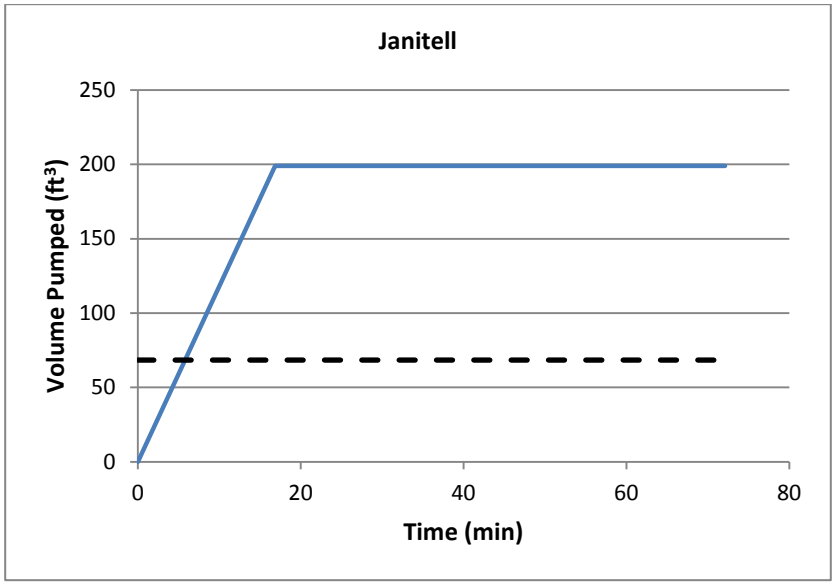
Janitell
Volume Pumped (ft³)
250
200
150
100
50
0
0
20
40
60
80
Time (min)

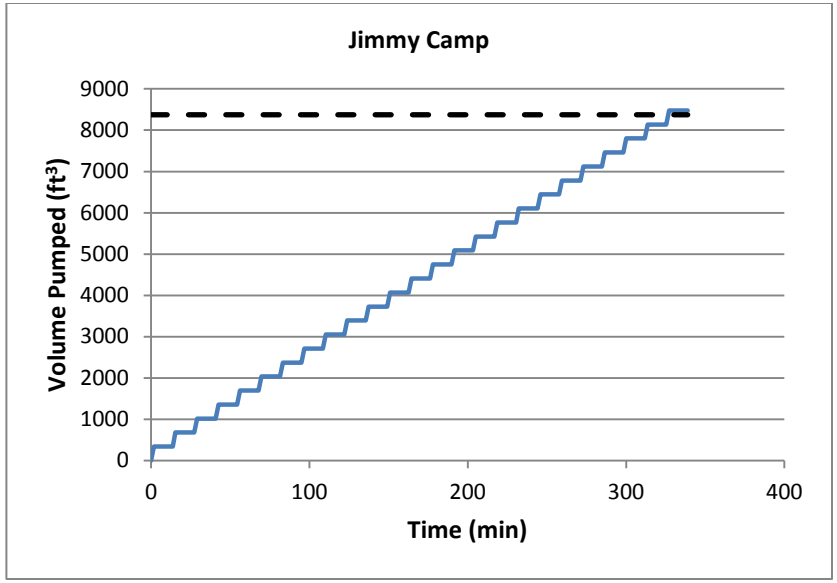
Jimmy Camp
Volume Pumped (ft³)
9000
8000
7000
6000
5000
4000
3000
2000
1000
0
0
100
200
300
400
Time (min)

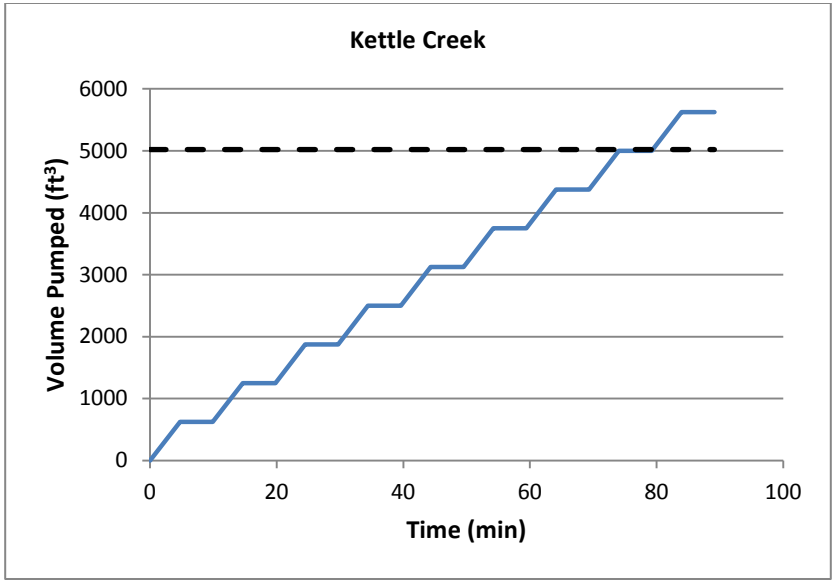
Kettle Creek
Volume Pumped (ft³)
6000
5000
4000
3000
2000
1000
0
0
20
40
60
80
100
Time (min)

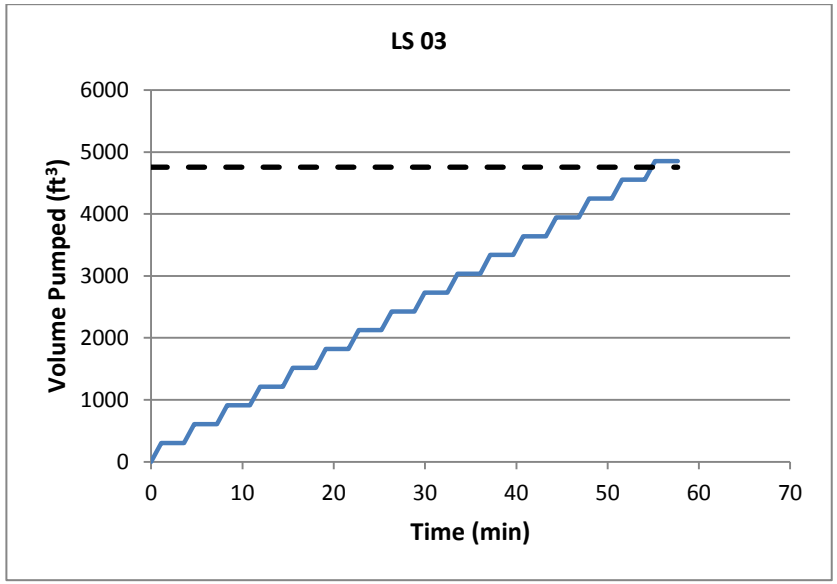
LS 03
Volume Pumped (ft³)
6000
5000
4000
3000
2000
1000
0
0
10
20
30
40
50
60
70
Time (min)

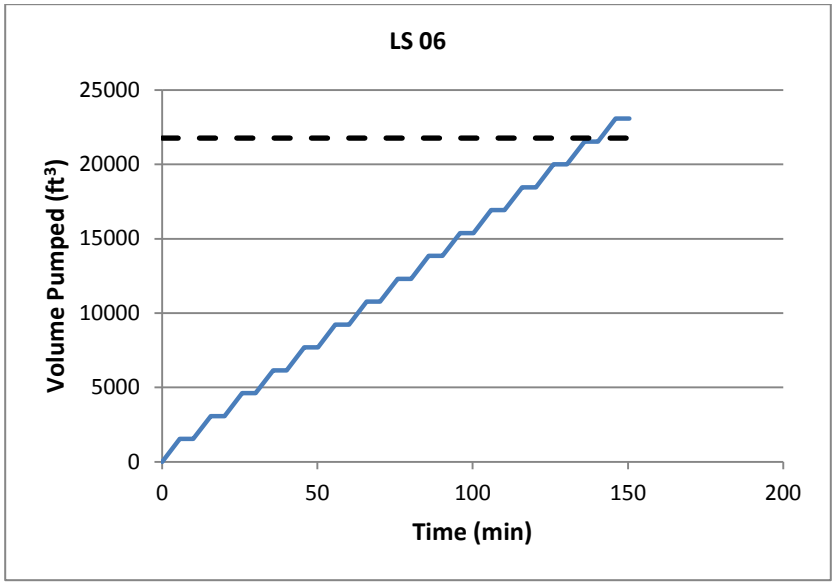
LS 06
Volume Pumped (ft³)
25000
20000
15000
10000
5000
0
0
50
100
150
200
Time (min)

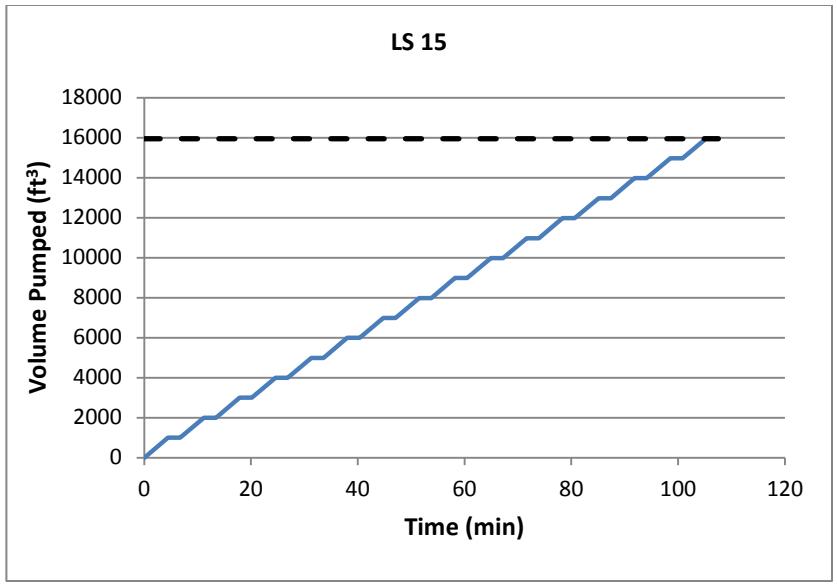
LS 15
Volume Pumped (ft³)
18000
16000
14000
12000
10000
8000
6000
4000
2000
0
0
20
40
60
80
100
120
Time (min)

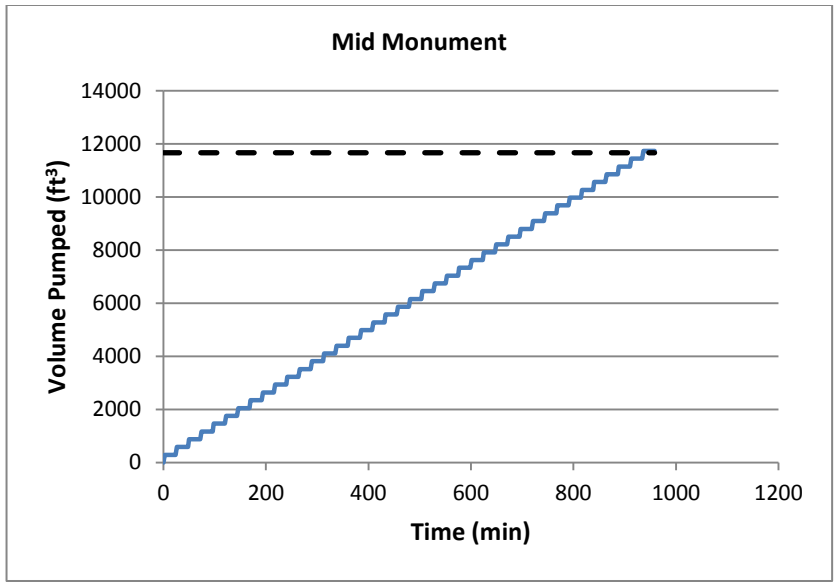
Mid Monument
Volume Pumped (ft³)
14000
12000
10000
8000
6000
4000
2000
0
0
200
400
600
800
1000
1200
Time (min)

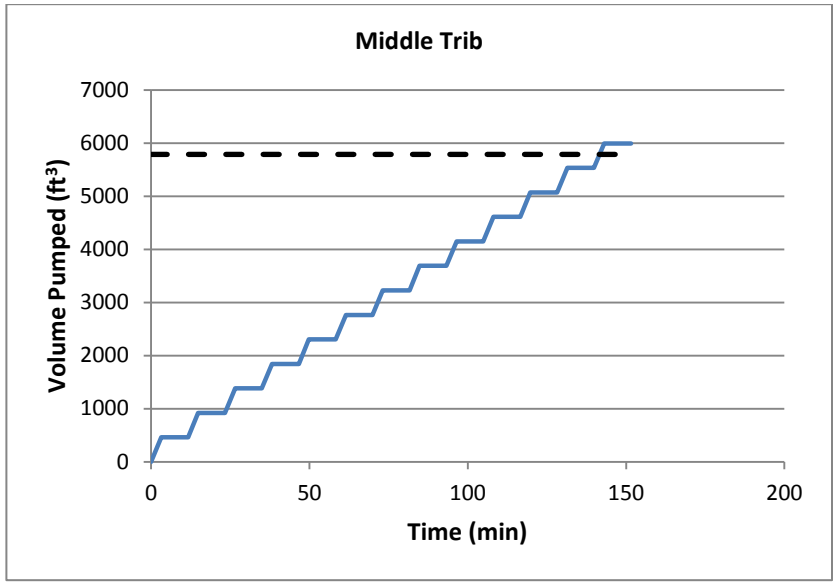
Middle Trib
Volume Pumped (ft³)
7000
6000
5000
4000
3000
2000
1000
0
0
50
100
150
200
Time (min)

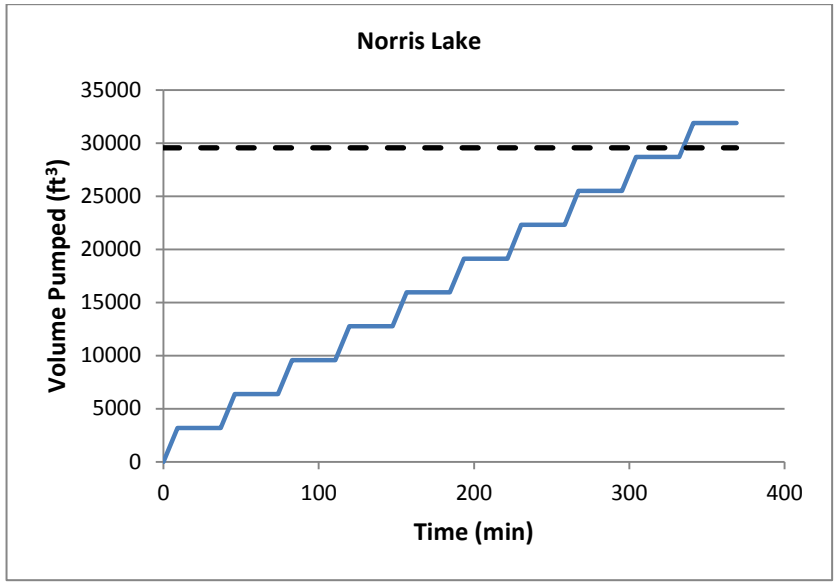
Norris Lake
Volume Pumped (ft³)
35000
30000
25000
20000
15000
10000
5000
0
0
100
200
300
400
Time (min)

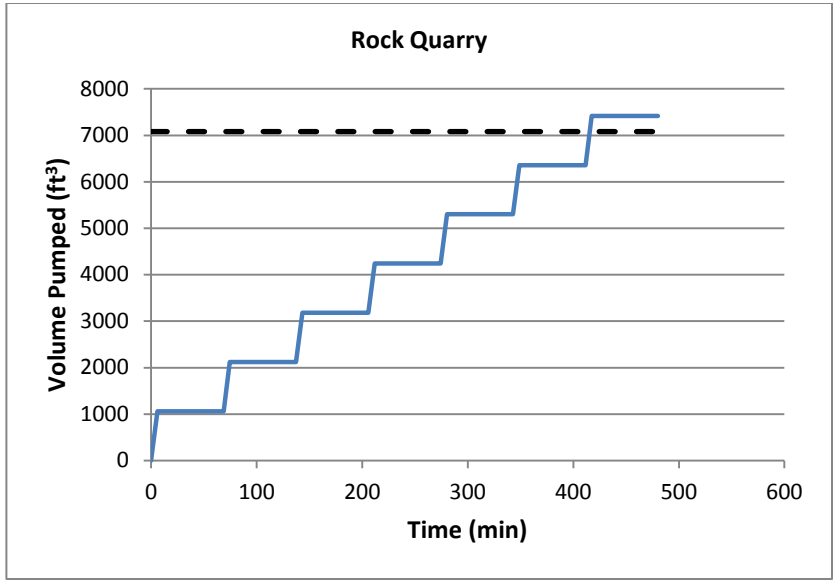
Rock Quarry
Volume Pumped (ft³)
8000
7000
6000
5000
4000
3000
2000
1000
0
0
100
200
300
400
500
600
Time (min)

APPENDIX F C-Factor Predictive Equation (U.S. Customary Units)

This section shows the analysis results for the development of the C factor predictive equation in U.S. Customary Units. The methodology followed was described in Section 9.2.2. The predictive equation(s) were evaluated and developed using the Weibull Model in Curve Expert Professional, as shown in Equation F.1.

$$y = a - be^{-cx^d} \tag{F.1}$$

where y is the C factor and x is the velocity (m/s). The Weibull Model parameters determined by CurveExpert Professional are summarized in Table F.1.

Table F.1: Summary of Weibull Model Parameters

Diameter (in)	a	b	c	d
6	135.64	112.12	0.1035	1.878
8	136.8	108.71	0.1031	1.884
10	137.61	106.1	0.1027	1.89
12	138.21	104	0.1025	1.895
18	139.36	99.42	0.1017	1.906
24	140.02	96.26	0.1012	1.914
30	140.46	93.85	0.1007	1.92
48	141.16	88.93	0.1000	1.934
66	141.48	85.72	0.0991	1.943
Average			0.102	1.907

Each parameter was plotted against diameter using Microsoft Excel to identify and screen critical relationships. Due to the relative values of each parameter, a and b are presented in Figure F.1 and c and d in Figure F.2. The figures also show the trendline and corresponding R^2 values for each parameter.

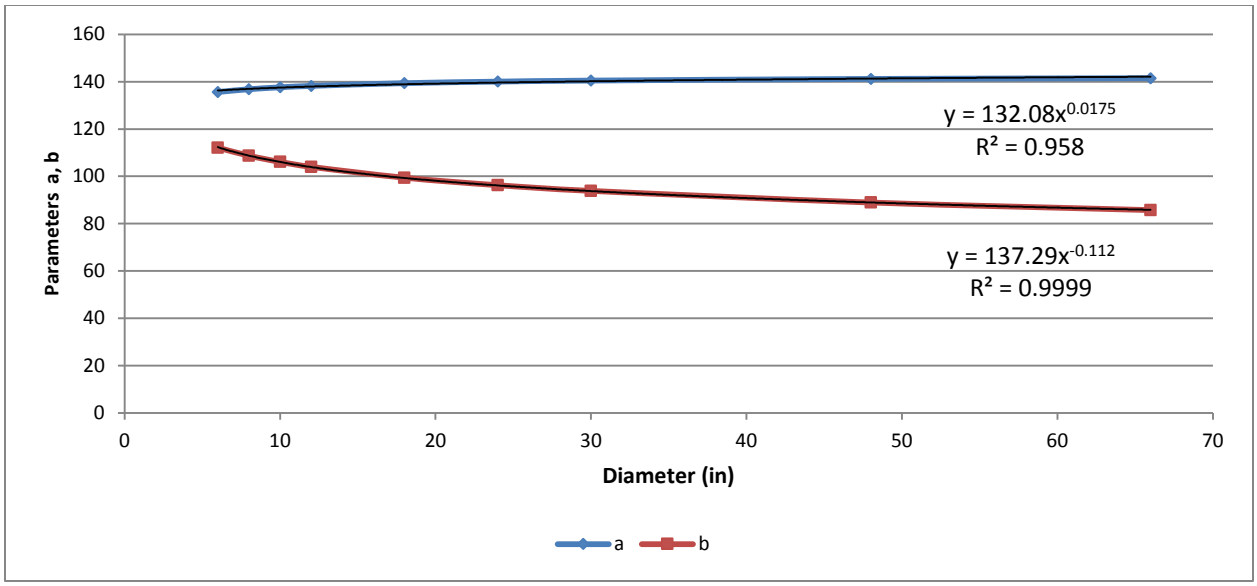

Figure F.1: Parameters a and b

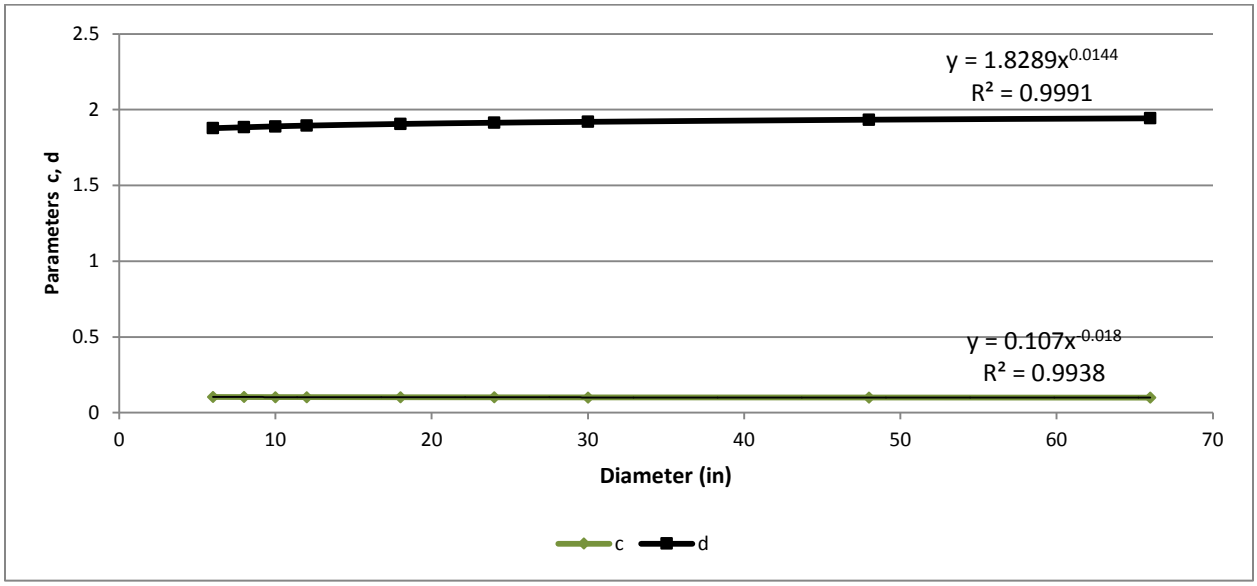

Figure F.2: Parameters c and d

As expected, Both the a and b parameters show a significant deviation with diameter and are nearly identical to the parameters determined under the metric evaluation/ similar to the metric evaluation, the c and d parameters are nearly constant by diameter; however, they vary slightly from the metric evaluation due to the conversion of units required for velocity. The average of the c and d parameters were compared to the actual values for the exponential portion of the model (e^{-cx^d}) in order to verify the assumptions used

in the metric evaluation. The results are presented in Figure F.3 show that utilizing the average for the c and d parameters provides nearly identical results.

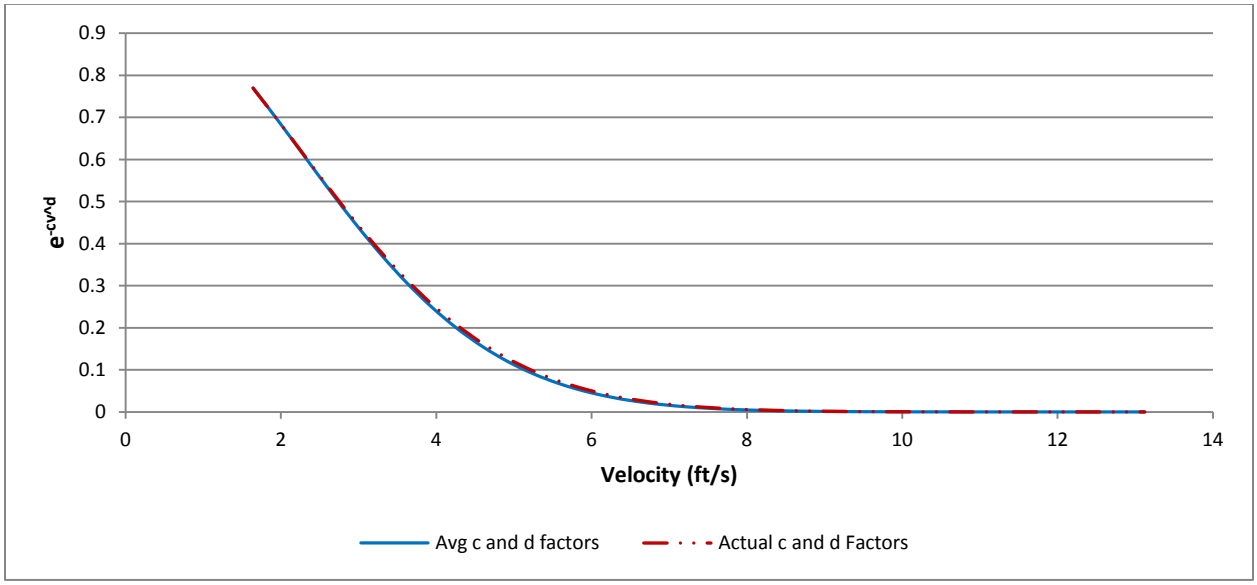

Figure F.3: Comparison of Average c and d parameters on e^{-cx^d}

C factors were calculated for both 6 in. and 66 in. diameter pipe using the trendlines for a and b parameters and both the actual and average values for c and d in order to verify that that using the average values did not significantly affect C factor. These two diameters represent the minimum and maximum diameter evaluated. The results along with the calculated errors comparing the actual against the average c and d parameters are shown in Figure F.4. Using the average c and d parameters provided calculated C factors with an error of less than 1% which indicates that it is acceptable to apply the average c and d parameters to the exponential portion of the predictive equation.

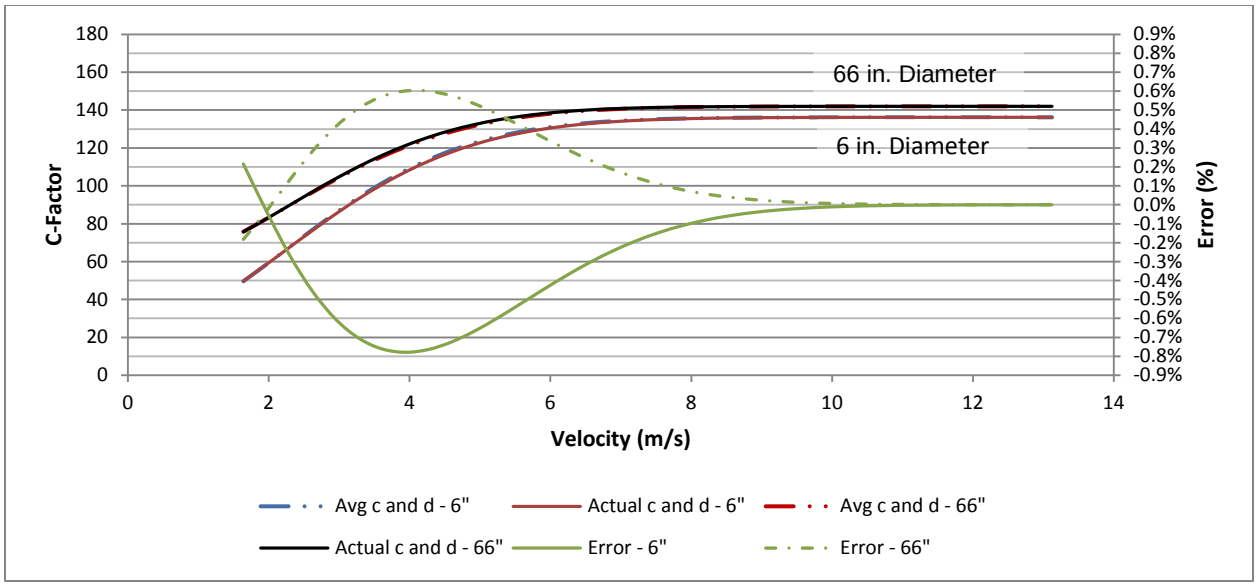

Figure F.4: Comparison of C-Factors Calculated from Actual and Average c and d parameters

Equation F.2 can be used to determine C factor based upon both velocity and pipe diameter:

$$C\ Factor = a - be^{-cV^d} \tag{F.2}$$

Where $a = 132.08\phi^{0.0175}$ (ϕ is diameter in inches); $b = 137.29\phi^{-0.112}$ (ϕ is diameter in inches); c = 0.102; d = 1.907; and V is velocity in ft/s